Ionization, Chemistry, and Dust Formation in the Outflows of Classical Novae and Red Giants

vorgelegt von
Dipl. Phys. Holger Beck
aus Bad Homburg v.d.H.

Vom Fachbereich 4 (Physik)
der Technischen Universität Berlin
zur Erlangung des akademischen Grades

Doktor der Naturwissenschaften (Dr. rer. nat.)

genehmigte Dissertation

Berlin 1993

D 83

Promotionsausschuß:
Vorsitzender : Prof. Dr. P. Zimmermann
Berichter : Prof. Dr. E. Sedlmayr
Priv.-Doz Dr. J.P. Kaufmann

Tag der mündlichen Prüfung : 31. 3. 1993

Hic jam quæritur, unde stellæ in summo æthere, tanta materiæ moles, quæ sufficere potuit ad tantum incendium inflammandum[1]*?*

Johannes Kepler

[1]Nun aber muß gefragt werden, woher der Stern im höchsten Himmel eine so große Menge an Materie bekommt, die ausreichen kann, eine so große Feuersbrunst zu entzünden?

Zusammenfassung

Klassische Novae und Rote Riesen stellen zwei exponierte Vertreter der Klasse staubbildender Objekte im Universum dar. Während Klassische Novae besondere kosmische Laboratorien darstellen, in denen anhand der Beobachtung eines einzelnen Objektes die gesamte Entwicklung von der Enstehung des Staubes bis hin zu seiner Zerstörung verfolgt werden kann, so sind Rote Riesen wegen ihres dominierenden Anteils an der galaktischen Staubinjektionsrate von Bedeutung.

In den thermonuklearen Explosionsereignissen Klassischer Novae bildet sich in der ausgestoßenen Materiehülle massiv Staub. Dies ist zunächst erstaunlich, da das auströmende Gas mit hoher Geschwindigkeit expandiert und zusätzlich einem zeitlich anwachsenden, ionisierenden UV–Strahlungsfeld ausgesetzt ist. Staubbildung in einem vollionisierten Plasma ist jedoch nicht möglich, sodaß die detaillierte zeitliche Entwicklung der Ionisation der verschiedenen Elemente von entscheidender Bedeutung für das Auftreten bzw. Nichtauftreten des Staubes ist und im ersten Teil der Arbeit untersucht wird. Gemeinsam mit der zeitabhängigen Ionisationsgleichung für die Elemente *H, He, C, N, O, Si, Fe, Mg, S, Na* werden die Heiz– und Kühlprozesse in der Novahülle bilanziert. Die Modellrechnungen zeigen, daß die typischen Zeitskalen für die Durchionisation des Kohlenstoffs, dem im Hinblick auf die Staubbildung wichtigsten Element, zwischen 20 und 50 Tagen liegen. Gleichzeitig werden schon in frühen Phasen der Expansion Gastemperaturen unter 2000K erreicht, sodaß die physikalischen Rahmenbedingungen fuer das Einsetzen von Chemie und Staubbildung günstig sind.

Der zweite Schwerpunkt der Arbeit liegt in der Untersuchung der Wechselwirkung von Strahlungsfeld und komplexer Nichtgleichgewichtschemie in den Hüllen sauerstoffeicher Roter Riesen. Im Rahmen einer detaillierten Untersuchung der chemischen Bildungspfade wird die Entstehung der für die Staubbildung relevanten Moleküle diskutiert und die Abhängigkeit der berechneten Molekülkonzentrationen von der Stärke des Strahlungsfeldes untersucht. Es zeigt sich, daß die übliche Annahme chemischen Gleichgewichtes und die daraus abgeleiteten Konsequenzen für die Staubbildung nicht zutreffen. Die Rolle des CO Moleküls für die Chemie in Sternhüllen wird im Lichte dieser Erkenntnisse neu gewichtet.

Im abschließenden Kapitel wird dann im Rahmen einer inhaltlichen und methodischen Synthese der vorangegangenen Untersuchungen Chemie und Staubbildung in den Hüllen Klassischer Novae behandelt. Die Involvierung eines komplexen chemischen Ratennetzwerkes (2000 Reaktionen, 150 Spezies) erlauben nun eine noch detailliertere Analyse der chemischen Reaktionspfade. Entscheidend für die zeitliche Entwicklung der Chemie ist die Besetzungsverteilung des Wasserstoffs, die auf der Basis eines alle Stoss– und Strahlungsübergänge für die ersten drei Niveaus umfassenden zusätzlichen, und in die Chemie integrierten Netzwerkes, und eines vereinfachten Strahlungstransportes, behandelt wird.

Contents

List of Figures

List of Tables

Ordnung um der Ordnung willen beschneidet den Menschen seiner wesentlichen Kraft, der nämlich, die Welt und sich selbst umzuformen. Das Leben schafft Ordnung, aber die Ordnung bringt kein Leben hervor.

A. de Saint-Exupéry

Prologue

Dust is an important and remarkable component of the interstellar medium, as it is deeply involved in the complex cycle of the evolution of matter in the universe. Stars are associated intimately with dust in almost any phase of their evolution. Starbirth currently occurs in dusty molecular clouds in the disc of the Milky Way and the dust grains appear to play a vital role in maintaining the thermal balance of newly formed stars during the initial stage of their evolution. At the end of the stars evolution an important fraction of the placental dust and gas materials is returned gradually to the interstellar medium. To visualize the role of the dust one may consider that:

a) Nearly fifty percent of the heavy elements in the interstellar space are contained in grains of various compositions and shapes. b) These particles dominate the heating and cooling of molecular clouds through photoelectrons and gas–grain collisions. c) They are a dominant source of opacity and clearly determine the spectrum of dust–shrouded objects. d) They serve as the major catalysts for the formation of important interstellar molecules, including the most abundant molecule in space, H_2. e) In interstellar chemistry dust is also involved in the modification, preservation, and the transport of molecules. f) Star formation as well as the formation of planets, which are both processes we substantially benefit from, cannot get along without the presence of small solid particles.

From where do we get the information about the dust?

At first, as an more indirect source of information we can make use of the interaction of the dust with incident photons. Interstellar dust can be observed by its extinction, its spectral features in emission as well as in absorption, and its far–infrared emission[2]. By far the best determined characteristic is the interstellar extinction law (see e.g. [Massa and Savage 1989]). Generally the extinction decreases with increasing wavelength, therefore the near infrared extinction is rather weak. More attention is directed to the optical, where the extinction is approximately given by two curves linear in λ^{-1} and joining at $2.25\mu m^{-1}$. In the ultraviolet wavelength region the most information can be extracted. The most prominent spectral feature is the so called "bump" at a wavelength[3] of 2175Å(for an overview see [Fitzpatrick and Massa 1986] and [Cardelli and Savage 1988]). Obviously only very abundant absorbers like O, C or N can provide such a massive absorption unless a large fraction of the entire amount of the species in question participates in the absorption. If one considers e.g. a mean silicon abundance of 3.3×10^{-5} per hydrogen atom, at least one third

[2]Interstellar dust is emitting up to 20% of the far–infrared radiation of the galaxy.

[3]The bump is also referred to as the 2200Åbump.

of all silicon would be required to produce the bump. Therefore it seems to be more attractive to invoke some kind of carbonaceous material as the cause. From classical Mie theory one infers that scattering by small particles is small compared to absorption and, following this line of arguments, if the bump were produced by small particles, no increased scattering in the corresponding wavelength region would occur. However, observations of Witt et al. (1986) showed evidence for increased scattering in the bump region which would rule out small graphite grains and raise the necessity for other possible absorbers[4]. One possibility, which has found growing attention during the last years, are small polyaromatic hydrocarbons (PAH's)[5], which have been assigned to be responsible for at least 50% of the absorption in the 2200Å bump[6], but although there is a widespread acceptance, the PAH hypothesis suffers from a variety of difficulties[7].

Additional information can be obtained from the infrared emission bands and the associated continuum. About 10% of the total radiated power is released in these emission features, therefore the carrier of the emission surely absorbs a substantial fraction of UV–radiation. Many suggestions have been assigned to the origin of these bands and in this way the formerly unidentified infrared bands have turned into "overidentified" spectral characteristics. Like in the case of the bump, one popular suggestion about the possible nature of the emitters proposes PAHs (for the $3.3, 6.2, 7.7$, and the $11.3\mu m$ features) as the features coincide with the well known bending and stretching modes of these complex aromatic molecules[8] consisting of about 20–100 carbon atoms (and a variable portion of hydrogen). Other theories which try to satisfy both the constraints of fitting the extinction law, and the cosmic abundance restrictions have been proposed:
Duley and Williams (1983, 1986, 1988) have suggested that silicate particles (e.g. Mg_2SiO_4), thinly coated by hydrogenated amorphous carbon, may be responsible for the feature at 2175Å. According to them the bump is produced by OH^- ions in low–coordination sites on – or within the silicate. Alternatively nongraphitic carbonaceous solids of quasi–icosahedral shape (Kroto (1990, 1991, 1992)), the so–called quenched carbonaceous solids (QCC) arising from an electric discharge in a methane–rich hydrocarbon plasma, (Sakata et al. (1984)) or very small (a< 10Å)

[4]It should be noted that the presented picture of interstellar dust, though trying to account for the mainstream ideas and thus presenting the state of the art, is still in the state of flux and a controversially discussed field (an overview is given in *IAU Symposium 135: Interstellar Dust*).

[5]First proposed by Keller and Sedlmayr (1983) for circumstellar shells. For an overview see Léger (1989).

[6]Recent laboratory measurements of Joblin (1992) using a mixture of PAHs claim for a high contribution of PAHs to the 2200Å bump and the total amount of the UV–extinction.

[7]The main arguments against the PAHs as the dominant absorbers have been summarized by Donn et al. (1989) and Draine (1989).

[8]Basically these molecules can be considered as benzene rings with hydrogen atoms attached at the edges, in contrast to graphite which forms infinite sheets of rings linked together in a plane and multiple planes orderly stacked upon another.

amorphous particles (Mathis, (1989)) have been proposed. Greenberg and coworkers ([Greenberg 1986][Greenberg and Hage 1990]) consider a core–mantle model, where silicate cores are covered by an inner mantle of carbon–rich organic refractory material[9] and a second layer consisting of ices in which small graphite and/or silicate particles[10] are trapped.
However, there is hardly any debate about the fact, that the interstellar emission features have their origin in some form of carbonaceous material as the similarity with the band positions of hydrocarbon material is very convincing[11].
Other observational clues to the structure of the interstellar dust may be inferred from the 9.7μm absorption feature which is well fitted by amorphous silicates, and the heavy depletion of some elements like Al, Fe or Si in the ISM, while others, like S or P are not depleted.

More direct information is available from the analysis of comets, meteorites, and interplanetary dust particles (IDPs). The latter can be collected by high altitude aircrafts in the earths stratosphere and have been intensively studied during the last decades[12]. It is commonly assumed that an important subset of these small particles (the normal size lies in the range of 5–50μm) are of interstellar space origin resembling more or less processed interstellar dust (Sandford (1989)). The formation of the IDPs has taken place in the protoplanetary disk by coagulation processes and this accretionary record has been preserved to some extent in the material. The scale size of the building blocks is quite similar to that of interstellar grains, thus the study of IDPs might reveal some insight in the composition of the dust as well as in the physics of grain collisions. Summarizing the information obtained from the laboratory analysis there are several points to mention: a) IDPs are mineralogically heterogeneous and consist of carbonaceous coatings around silicate cores, (Kerridge, (1990)) and b) they show no evidence for the presence of well–ordered graphitic structures.
The carbonaceous chondrites, a class of primitive meteorites, also offer wealth information, mostly connected with isotopic anomalies. Since these anomalies cannot be explained by processes in the solar system, they are attributed to the presence of residual interstellar grains. Although many chondrites are primitive bodies they are not simply collections of presolar grains, but are composed almost entirely of materials that were considerably processed by nebular and parent body processes. However, there is strong evidence that minor components have retained substantial presolar information about the origin and the composition of interstellar dust. The laboratory results derived for the interstellar carbon show the following distribution of chemical structures[13]:

[9] This is the so called "yellow stuff"

[10] The nature of the small particles, however, remains rather uncertain. Greenberg also has raised the possibility of PAHs.

[11] [Duley and Williams 1981]

[12] Often these particles are also referred to as Brownlee particles

[13] The results are adapted from Anders et al. (1989). All values are relative to cosmic abundances.

organic carbon	4×10^{-4}
diamond	7×10^{-4}
graphite/amorphous carbon	2×10^{-4}
SiC	4×10^{-6}

A remarkable detail of these results is that not graphite, but diamond is the dominant form of pure carbon.

The most archaic bodies in the solar system providing insight into the cosmic grains are comets, where a great chance of the preservation of a more or less pristine accumulation of interstellar material is given. The deduction of the composition of bona fide cometary dust used to have to rely on telecope measurements and the analysis of the associated meteors. But recently the return of Halley's comet in 1986 has opened the opportunity of direct measurements of the composition of cometary dust by the mass spectrometers on board of the Vega and Giotto spacecrafts. These in situ studies showed that the mean elemental composition of Halleys dust is in general consistent with that of chondrites. More specific analysis of the submicrometre compositional variability reveal a more heterogeneous and porous structure indicating that the Halley composition is more closely matched by the IDPs (Brownlee and Kissel (1990)).

Although the study of the primitive solar system bodies provide a rather direct access to the dust material, the deduced information about the composition and structure naturally gives a picture of a material which may have undergone several stages of processing during the formation of our solar system.
However, the question of the composition and properties of interplanetary and interstellar dust is only subordinate to the much more fundamental question

Where does the dust come from ?

Many cosmic sources are contributing to the dust in the ISM. Generally dust is produced
I.: by condensation in the winds of evolved stars,
II.: by condensation in the ejecta of novae and supernovae and
III.: by accretion in dark molecular clouds.
Obviously the real birth site of the dust lies in the outflows of evolved stars and novae (and supernovae[14]), since the contribution of the dark clouds is dependent on the presence of formerly condensed grains.
Therefore as a first step the clarification of the nature of cosmic grains must attend to the creation process of dust by nucleation and subsequent growth of small particles in the envelopes of red giants and novae. Both, red giants and novae are

[14]Supernovae are of course expected to form dust with a high contribution of ≈8% to the galactic dust production rate, but unfortunately up to now there is no direct observational evidence for the formation of dust in the fast expanding shells of these objects. A more indirect insight into the possible origin of dust was provided by some isotopic anomalies found in meteorites [Anders *et al.* 1989].

object	type of dust	obs. evidence	dust→ ISM
novae	silicates	10μ, 20μ feature	0.1%
	amorphous carbon	featureless cont. rad.	
	SiC	11.2μ	
	hydrocarbons	3.3μ, 11.3μ	
O–rich giants	silicates	10μ, 20μ features	70%
C–rich giants	amorphous carbon	featureless cont. rad.	20%
	SiC	11.2μ feature	
	PAHs	3.3μ, 6.2μ, 7.7μ, 11.3μ	
Supernovae	?	?	8%
Wolf–Rayets stars	amorphous carbon	featureless cont. rad.	0.5%

Contributions of various galactic sources to the dust injection into the ISM. The types of dust and their spectral signature for which there is observational evidence in the case of the specified objects are indicated. The O–rich giant class has not been subdivided for clarity. The last column displays the relative dust input to the ISM relative to all stars. The data have been taken from Gehrz (1989) and Tielens (1990).

of special interest for the investigations of the cosmic dust formation, but for very different reasons.

The mass loss from red giants is the dominant mechanism for the material injection into the ISM. Comparing the contributions of the different subclasses (M–stars (Miras), OH/IR–stars, M–supergiants, carbon stars) yields that the O–rich stars are clearly outdoing the carbon rich class by a factor of 6–10. This is supported by the IR and CO studies of the gas and dust mass loss rate from these objects, which yield about 0.003–0.01$M_\odot yr^{-1}$ as the total dust injection, which is a fraction of about 10–20% of the total dust production. Most of the dust produced in the stellar outflows is composed of silicates, which are identified by the characteristic 10μ and 20μ features. These particles then may serve as seeds for the subsequent growth in molecular clouds, which can result in the predicted core–mantle structure, where the silicate core is coated by either a thin carbonaceous layer or a mantle of organic refractory material.

Novae, now commonly interpreted as a thermonuclear runaway (TNR) in an accreting hydrogen shell on top of a degenerate C/O– or ONeMg white dwarf in a close binary system, are injecting only a small fraction of the entire dust production in the galaxy (see table). The rate of classical nova events in our galaxy is about 30–50yr^{-1} ([Downes 1986], [Truran 1985b]) and the average mass ejection per nova outburst is about 5–$10\times10^{-5}M_\odot yr^{-1}$ [Gehrz 1988]. The average input of mass to the ISM therefore can be estimated to 1.5–$5\times10^{-3}M_\odot yr^{-1}$, but since only a minor part will condense into grains, the total dust input from classical novae only results

to 10^{-5}–$10^{-4}M_{\odot}yr^{-1}$.
On the other hand, novae do provide us with the possibility to study dust formation as a dynamical process, whereas in almost all other stellar sources, circumstellar dust formation and ejection is observed as a steady state process. Furthermore, as a result of the nuclear burning processes before and during the explosion, novae leave their specific isotopic fingerprint in the ejected material, which then, after transportation to and processing in the ISM, can later be recovered as isotopic anomalies in solar system meteorites. Laboratory analysis of carbonaceous meteoritic material has revealed nova origin for both, the so called C^{α} and the C^{ϵ} component of the carbon. In both cases a significant enrichment of ^{22}Ne, being the decay product of ^{22}Na, was recognized [Kerridge 1990]. The natrium isotope ^{22}Na is effectively synthesized in the TNR and results in a significant overabundance of ^{22}Na in the nova outflow, making classical novae one of the major injectors of this isotope in the galaxy [Wiescher *et al.* 1986] [Weiss and Truran 1990]. These arguments are strengthened by the simultaneous enrichment of the C^{α} component in meteors with ^{13}C and ^{15}N, which are also isotopes produced in excess in nova explosions [Truran 1985b].
A further important fact is that in the envelopes of novae all different types of dust have been identified. Most novae produce amorphous carbon dust[15] and their infrared continuum shows carbon dust emission corresponding to a smooth, featureless blackbody. However, in nova V1370 Aql (1982) SiC emission was observed [Williams and Longmore 1984] and QU Vul shows the condensation of silicates [Greenhouse *et al.* 1988]. Recently the 3.3μm feature was reported to occur in the spectrum of nova V842 Cen [Hyland and MacGregor 1989] supporting the presence of hydrocarbons in the ejecta.

Following the portrayed lines of evidence considering the role of dust in the galaxy, as a natural conclusion, novae and O–rich giants, as two exposed representatives of the class of dustforming objects in the universe, are in the focus of the presented work. The present approach considering the study of dust formation in novae and red giants is of a chemical nature. Dust formation is always part of a complex system of chemical reactions preceding, accompanying and even determining the formation of grains.

In the **1st** chapter the properties of classical novae are reviewed. Starting from historical aspects of the nova phenomenon it is tried to draw a comprehensive picture of the nova system in terms of the model describing the general class of cataclysmic variables, in which classical novae are a subclass. The description of the physical nature of – and the main processes in – the close binary system are intended as a reasonable basis to work on. The dynamical evolution of the spectral and optical appearance of the classical nova outburst is described in the second part of the chapter.

The **2nd part** is devoted to the study of the problem of ionization in expanding

[15](e.g. NQ Vul [Ney and Hatfield 1978], LW Ser [Gehrz *et al.* 1980a], V1668 Cyg [Gehrz *et al.* 1980b])

nova envelopes. The time–dependent course of ionization in the outflowing gaseous material is of central importance in view of its dominant influence on chemistry and dust formation. Incorporating the main processes for ionization and recombination and taking into account the energy balance in the shell, a model is constructed which goes beyond previous approaches. Blackbody radiation fields as well as more realistic fluxes obtained from non–LTE radiative transfer calculations have been used as input radiation fields. These calculations are an important pre–study concerning the possibility of dust formation in nova shells and the chemical and physical state of the environment in which the chemistry and the grain formation will proceed.

The **3$^{\rm rd}$ chapter** is changing the object from classical novae to O–rich giants. For the late–type M–supergiant αOri a chemical model for the inner regions of the stellar envelope including dust formation is constructed, which fully accounts for the oxygen–rich situation. As αOri is known to have a chromosphere releasing substantial amounts of UV radiation, the adequate description of the innermost regions must account for the photoprocesses as an essential part of the modelling. In order to clarify the role of the CO molecule in zones interspersed by UV-photons, the UV–field strength has been treated as an parameter. The chemical results are subjected to a detailed analysis revealing the specific influence of the main molecules for silicon–, carbon– and sulfur–bearing components. Dust formation and chemistry is discussed in comparing several models with different values for the key parameters outflow velocity, particle density, mass loss and temperature profile.

The **4$^{\rm th}$ and last chapter** is based on the preceding investigations of Chap. (2) and Chap. (3). Whereas Chap. (2) is strongly focussed on the ionization structure in nova shells using a semi–analytical method, the 4$^{\rm th}$ chapter addresses the complete complex of chemistry and dust formation, thus including the processes of ionization and recombination in a natural way by solving the the system of chemical rate equations. This approach also extends the chemical study of Chap. (3) in three essential points: firstly a more general chemical model is used, allowing for the adequate description of carbon–rich as well as oxygen–rich situations which both are realized in nova outflows; secondly the changing photospheric temperature, increasing from ≈10,000K to at least 100,000K or more during the epoch of dust formation, demands for a more sophisticated treatment of the photoionization and photodissociation processes and, thirdly, instead of using an artificial cooling law the gas temperature is determined by balancing all relevant heating and cooling processes. The time dependent non–LTE chemistry is outlined in detail and special emphasis is addressed to those molecules which have turned out to be the key species with respect to dust formation.

The **Appendix** is intended to serve as a reference part of the work. The atomic and chemical data used are listed there. Especially the chemical reaction networks for Chap. (3) and Chap. (4) are presented including the thermodynamical data. A brief exposition of the cooling rates for collisionally excited line emission (c.f. Chap. (2)) and the treatment of the hydrogen as a 3–level atom with continuum (c.f. Chap. (4)) are completing this part.

Letzten Endes wird alles, was wir hier auf der Erde tun können, von denselben Gesetzen begrenzt, die den Haushalt der astronomischen Energiequellen regeln. Die umgekehrte Aussage kann aber ebensogut stimmen. Es wäre nicht überraschend, wenn sich herrausstellen würde, daß Ursprung und Schicksal der kosmischen Energie nicht voll verständlich wären, wenn man sie von den Phänomenen des Lebens und des Bewußtseins trennt.

F.J. Dyson

Chapter 1

Properties of Classical Novae

The spectacular increase in luminosity that accompanies the violent ejection of matter during a nova explosion occasionally creating a temporarily naked–eye star for a limited time, where none was known before[1] draws attention to what is simultaneously a class of objects which is one of the most exciting in astrophysics, and also one of the most difficult for interpretation. The explosions of novae have perennially fascinated the imagination of Man – in earlier ages as auguries, portents and signs of divine intervention and later scientifically as a challenge to understanding the sudden explosions by stars, objects which normally evolve in a controlled and stable way. Before going into some details of the nova phenomenon it is useful to give a brief summary of the current state of understanding.

A nova eruption is caused by a thermonuclear explosion in a degenerate layer on the surface of a white dwarf in a close binary system. This layer is produced by continuous accretion of matter by the white dwarf, ejected through the inner Lagrangian point by a companion star which either is a main–sequence object (Classical Novae) or a late–type giant (other Cataclysmic Variables). The mass transfer is triggered by the angular momentum loss caused by either a magnetic stellar wind (period P $>$3hrs.) or gravitational wave radiation (P $<$ 3hrs.). The interaction of the streaming material with the accretion disk leads to an extended zone of increased energy generation, observable as a bright so called *"Hot Spot"*, which is the most luminous energy source of the nova system during the quiescence state. In the nova explosion, which may occur every several hundreds to several thousands of years, a mass of between 10^{-8}M$_\odot$ to 10^{-4}M$_\odot$ is ejected, normally being only a small fraction of the entire mass of the accreted material. The expelled gas is expanding at rather high velocities between a few hundreds to several thousands of kilometers. The ejecta probably contains material from the surface layer of the white dwarf so that the chemical composition of the ejecta, which in most cases is far from a solar composition, reflects the composition of the white dwarf as well as that of the companion. The white dwarf is the core in which nucleosynthesis occured in the precursor state, thus the chemical abundances in the ejecta also give an important piece of information about the evolution of the precursor. A CNO–rich ejecta composition points towards a CO white dwarf, which probably is the core of a $\approx$ 1M$_\odot$ star, whereas ejecta rich in oxygen, neon and magnesium are believed to be a product of a thermonuclear runaway on an ONeMg–white dwarf, which is the core of a more massive

[1]Thus called "*nova stella*" by the early astronomers.

star of $\approx 10M_{\odot}$.
During the first hundred days after the outburst several novae show characteristic infrared emission radiated by heated dust grains which may have formed by a complex series of chemical reactions in the cooling ejecta. The infrared luminosity generated by those small solids in some cases exceeds the optical luminosity and shows that the process of dust formation can proceed very effectively in an environment which otherwise seems to be not very favourable for the proceeding of a complex chemistry. As nova shells are of a peculiar elemental composition comprising rare isotopes of sodium and aluminium as a result of nuclear burning processes in the white dwarf, the dust grain composition is a fingerprint of novae and small traces of these elements have been identified in solar system meteorites.
In addition to the expanding gas there remains a hot and powerful remnant which is physically separated from the ejecta. Immediately after the explosion the luminosity of the central object is fueled by a prolonged shell burning phase on the surface of the white dwarf and is equal to the Eddington luminosity, thus radiation pressure drives off the remaining material during a constant–luminosity burning phase which may last up to one year. Then the remnant begins to cool radiatively upon the cessation of burning and the accretion process is reestablished.
Theoretical studies of the long–term evolution of classical novae have shown that the mass-transfer is not a stationary process, but is substantially higher in the pre– and post–outburst periods and decreases to very low values (hibernation phase) during most of the time between two subsequent outbursts.

1.1 History

In the dynastic chronicles of the old Asean empires China, Korea and Japan references for nearly 100 *"new stars"* are found before 1700 [Yoke 1962] [2]. In Europe, despite the obvious and menacing mutability of the heavens, there was only little vigilance by our ancestors to record those events. Yet until Nova V841 Ophiuchi (1848), the only true classical nova observed in Europe having more than a single surviving western account of its appearance was Nova CK Vulpeculae (1670), which is by far the best documented of ancient novae[3] [Shara *et al.* 1985] .
It was first discovered by Pére Dom Anthelme, a Carthusian monk in France and an account of his discovery was published in 1671 by the *Académie Royale des Sciences*, Paris:

[2] Although the revision of the Catalogue of Lundmark (1921) by comparison of the different Asean sources has shown that some of the nova entries must be attributed to the appearance of comets, most of them can probably be counted as naked–eye novae.

[3] The very low luminosity measured nowadays [Shara *et al.* 1985] points to a very low accretion rate of only $10^{-12} M_{\odot} yr^{-1}$ and can be interpreted in terms of the hibernation scenario, which predicts phases in the long–term evolution of nova systems where the accretion flow nearly completely stops [Prialnik and Shara 1986] .

> *As this person contemplated the Heavens at night, June 20th of the last year, desirous to discover that admirable Star, which hath appear'd and disappear'd twice since the beginning of the century in the Constellation of the Swan (P Cygni); he perceived a Star of the Third Magnitude, which he had never yet observed. He presently signified it to the Company which assembleth in the Library of the King: And divers of that Assembly having beheld the Heavens about the end of June and the beginning of July, took notice, that there was indeed about the Beak of the Swan a New Star of the third magnitude, not to be met with in any Catalogue of Astronomers, although many other neighbouring Stars, that are much smaller, be exactly marked by them.*

A month after this first discovery, CK Vul was found independently by Johannes Hevelius in Gdansk (25 July 1670), who gave the first published account of its appearance. He also followed the decline of CK Vul in late 1670 until it faded from visibility in October of that year. In 1671 CK Vul was recovered by Hevelius and in April it was more brilliant than it had ever been observed before. Giovanni Cassini and Hevelius extensively observed this nova through the late spring and summer of 1671 where it slowly declined until it disappeared in August. A third time of naked–eye visibility is reported (Hevelius) but CK Vul never reached its former splendor, remaining only barely perceptible for two months.

Since 1900 no fewer than 10 classical novae have reached an apparent magnitude m_v=3 or brighter at maximum, bright enough to be conspicuous to the naked eye. Summarizing the nova discoveries in the 20th century the frequency of nova discoveries is distributed as shown in Tab. (1.1). The rate of occurrence for those spectacular events in the galaxy has been estimated [DellaValle and Claudi 1990] to 15 $\pm$ 5 novae yr^{-1}, a rate which is significantly smaller than previously derived results seem to indicate[4]. The recent rate was derived taking into account the rates for the stellar systems M31 (29 $\pm$ 4 novae yr^{-1}), M33 (4 $\pm$ 2 novae yr^{-1}), LMC (2 novae yr^{-1}) and Virgo (160$\pm$80 novae yr^{-1}).

1.2 The Nova System

1.2.1 Orbital Periods

Some years ago one of the peculiarities of the nova period distribution that distinguished classical novae from the other subclasses of cataclysmic variables (CV's) was the restriction of all known novae to above the so called "period–gap" [Vogt 1989].

[4]Former estimates range from a rate of 73 $\pm$ 24 novae yr^{-1} [Liller and Mayer 1987] over a rate of $\approx$ 100 novae yr^{-1} [Allen 1954] to the very high value of 260 novae yr^{-1}, which was reported by Sharov (1972) and seems to be overestimated when compared with the values of M31 and M33.

magnitude interval	nova rate [yr^{-1}]	No. per yr	No. of years
< 1	0.04	0	14
1–2	0.02	1	17
2–3	0.04	2	25
3–4	0.03	3	17
4–5	0.05	4	10
5–6	0.14	5	1
6–7	0.47	6	2
7–8	0.58	8	1

Table 1.1: This table summarizes some information about the discovery statistics of novae. a): Nova rate per year in different magnitude intervals [Duerbeck 1990] (first two columns) and b): number of years in which N novae were discovered [Warner 1990] for the period starting from 1899 and ending with 1986.

This statistically significant gap was located between orbital periods $2.1hrs. \leq P_{\rm orb} \leq 2.8hrs.$. The discovery of the short periods of novae CP Pup (88.5 mins) and GQ Mus (85.5 mins) not only changed the statistics but supported notions that all subclasses of cataclysmic variables are able to interchange[5]. A selection of observed periods of nova systems is given in Tab. (1.2). The frequency with which any cataclysmic variable experiences a classical nova outburst increases with the mass–transfer rate in such a way that in the long period systems the frequency of occurrence is by a factor of 20–35 larger than in the short–period systems, even though there may be 100 times as many short–period systems as there are long–period systems.

1.2.2 Component Masses

The determination of the masses of the two binary components in a nova system is a serious problem, too. In principle the fact that all these systems possess a Roche–lobe filling geometry aids to the derivation of the secondary mass. So, under the additional assumption that the secondary star is on the zero age main–sequence (ZAMS) the mass of the secondary $M_{\rm sec}$ can be directly related to its orbital period

[5]There is strong evidence from polarisation measurements ([Stockman *et al.* 1988] and [Diaz and Steiner 1989]) that GQ Mus and V1500 Cyg evolved from magnetic systems. For CP Pup no circular polarisation could be measured implying that if it has a magnetic field, this must be lower than in the most polars. The photometric measurements of V603 Aql by Schwarzenberg–Czerny and Udalski (1990) showed that also this nova can be classified as an intermediate polar system (IPS). On the basis of a statistical analysis of the periods of novae and IPS they state that about one half of the nova systems are magnetic novae.

Classical Novae	Nova	P_{orb} [d]	t_3 [d]	Δm	Other CV's	type	P_{orb} [d]
GK Per	1901	1.997	13	14.0	RX And	DN	0.212
DI Lac	1910	0.554	–	–	BV Cen	DN	0.610
V1668 Cyg	1978	0.439	23	14.0	WZ Sge	DN	0.056
BT Mon	1939	0.334	–	–	SY Cnc	DN	0.380
V533 Her	1963	0.210	44	14.9	KR Aur	NL	0.163
HR Del	1967	0.214	230	12.5	TT Ari	NL	0.138
T Aur	1891	0.204	80	15.8	V Sge	NL	0.514
DQ Her	1934	0.194	100	14.8	T Crb	RN	227.5
WY Sge	1783	0.154	–	–	U Sco	RN	1.23
RR Pic	1925	0.145	150	12.8	T Pyx	RN	0.143
V1500 Cyg	1975	0.140	39	21.0	V 394 Cra	RN	0.757
V603 Aql	1918	0.139	8	12.0	AM Her	MS	0.129
V Per	1887	0.107	–	–	VV Pup	MS	0.069
CP Pup	1942	0.061	17.0	–	AE Aqr	MS	0.416
GQ Mus	1983	0.059	40	14.5	–	–	–

Table 1.2: Orbital periods P_{orb}, visual amplitudes Δm and time of decrease in optical brightness t_3 of various classical novae. The data for the classical novae are presented in order of decreasing period length. For other classes of cataclysmic variables (DN: Dwarf Nova; NL: Novalike; RN: Recurrent Nova; MS: Magnetic System) only the orbital period is given. The data were taken from Warner (1990) (P_{orb}) and Boyarchuk and Antipova (1990) (Classical Nova) and from the catalogue of Ritter (1990) and the work of Robinson (1983) (CV's).

P

$$M_{\rm sec} = 0.38 \left(\frac{\beta^{1.83}}{\alpha^{1.83}}\right) \cdot P_4^{1.22} \tag{1.1}$$

where the period is in units of 4hrs. and the parameter β is given as

$$\beta = \begin{cases} 1 & : \quad q < 0.52 \\ 1 + 0.066(q - 0.52) & : \quad 0.52 < q < 2 \end{cases} \tag{1.2}$$

and q is the ratio of the secondary and the white dwarf mass M_{WD}. The mass of the white dwarf then can be obtained with the knowledge of the radial velocity amplitude and the inclination of the orbit [Warner 1990] .

However, there are some weak points in this approach.

- the mass–radius relationship used to determine the mass was derived for single stars in LTE[6],

[6]Patterson (1984) has shown that the mass–radius relationship for CV secondaries does not depart very much from the relationship for single stars.

- velocity curves for objects like novae may originate from different locations within the shell.

Masses obtained for novae and nova–like systems are presented in the next table:

Novae	$M_1/M_\odot$	$M_2/M_\odot$	Ref.	Novalike	$M_1/M_\odot$	$M_2/M_\odot$	Ref.
DQ Her	0.45	0.32	4,5,6	PG 1012–03	0.60	0.35	1
T Aur	0.68	0.63	7.8	LX Ser	0.40	0.35	2,3
BT Mon	1.0	0.8	9,10,11	AE Aqr	0.94	0.74	12,13

References

1 :[Williams and Ferguson 1982] 2 :[Young *et al.* 1981]
3 :[Horne 1980] 4 :[Hutchings *et al.* 1981]
5 :[Young and Schneider 1981] 6 :[Young and Schneider 1980]
7 :[Bianchini 1980] 8 :[Walker 1963]
9 :[Robinson *et al.* 1982] 10:[Williams 1983]
11:[Marsh *et al.* 1983] 12:[Patterson 1979]
13:[Chincarini and Walker 1981]

It must be noted that strong selection effects concerning the white dwarf mass in classical novae have to be considered. As the nova frequency is varying strongly as a function of the white dwarf mass [Livio and Soker 1984], those novae observed during the last century are from the high mass end of the distribution. Ritter and Burkert (1986) have shown that there is also a strong tendency to discover preferentially dwarf novae with high white dwarf masses.

1.2.3 Mass Transfer

One of the most important parameters determining the evolution of the close binary system is the rate of mass–transfer $\dot{M}$, which unfortunately is difficult to observe with any reliability. The estimation of $\dot{M}$ from Eq. (1.10) is seriously in error if only a small amount of the kinetical energy of the stream is dissipated in the "Hot Spot". Even if this is not the case the difficulty of estimating the value of R_d is still lasting. Another estimate is based on the measurement of period changes which, under the assumption of the conservation of angular momentum leads to $\dot{M}$ via [Pringle 1975]

$$\dot{M} = \frac{M_{\mathrm{WD}} M_{\mathrm{sec}}}{3(M_{\mathrm{WD}} - M_{\mathrm{sec}})} \times \left[\frac{dP}{dt}\right]^{-1} P \tag{1.3}$$

The long–term data bases required for the application of this method to derive statistical significant $\dot{P}$ are a severe hurdle.
So as an observational result one can state that [Patterson 1984]

- the mean rate of mass transfer in nova systems appears to decrease by three orders of magnitude when going from the longest period systems to the shortest period systems.

- There exists a considerable factor of dispersion (10–100) in the estimated mass-transfer rates at any given orbital period due to
  - uncertainties in the individual estimates,
  - variations in component masses at given orbital period,
  - fluctuations in the mass–transfer rate occuring on timescales which are long compared to the time a system has been monitored.

Thus it is quite conceivable that the mean transfer rate may be quite different from that estimated from the current state of the nova system. It is tempting to suppose that, when averaged over timescales comparable with times between classical nova outbursts, the mass–transfer rate is monotonically related to the orbital period. The relationship of Patterson (1984) suggests a mass–transfer decreasing from

$$\begin{array}{ccccccc} \dot{M} & \approx & 10^{-8.2\pm0.6} & M_\odot yr^{-1} & \Longleftrightarrow & P_{\rm orb} & \approx & 6\text{hrs.} \\ & & & \text{to} & & & & \\ \dot{M} & \approx & 10^{-10\pm0.4} & M_\odot yr^{-1} & \Longleftrightarrow & P_{\rm orb} & \approx & 80\text{min} \end{array}$$

Observations during the outburst seem to indicate that the mass–transfer in the binary system is not significantly altered during this phase. As it is commonly accepted that the secondary fills its Roche lobe any tendency for it to grow in size because of evolutionary processes or for the lobe to shrink because of angular momentum loss will cause a flow of gas through the inner Lagrangian point into the lobe of the white dwarf. As an initiation mechanism for the angular momentum loss the influence of a magnetic stellar wind is proposed [I. Iben Jr. *et al.* 1992] , which carries away angular momentum, thus causing the components to approach each other. For the derivation of a mass-loss law assuming the initiating process to be a magnetic stellar wind one introduces the assumption that the tidal torque in the nova system forces the spin period of the secondary star to be identical with the orbital period (for details see Mestel and Spruit (1987)). The semiempirical formula derived on this basis [I. Iben Jr. *et al.* 1992] reads

$$\dot{M}_{\rm MSW} = \left(\frac{\alpha}{\rho}\right) 1.80 \cdot 10^{-8} M_\odot yr^{-1} M_{\rm sec}^{\epsilon}\, q^{2.2}\, M_{\rm WD} \left(\frac{M_{\rm WD}}{M_{\rm sys}}\right)^{0.2} \times [1.28 - \epsilon/2 - q]^{-1} \tag{1.4}$$

where α, ρ and ϵ are parameters for which the estimates

$$\alpha \approx 1, \quad \rho \approx 1, \quad \epsilon \ll 1 \tag{1.5}$$

are valid. $\dot{M}_{\rm MSW}$ is the magnetic stellar wind induced mass–transfer rate, $M_{\rm sys}$ is the total mass of the system ($M_{\rm WD} + M_{\rm sec}$).

Whereas (1.4) is valid for nova systems with periods longer than $P_{\rm orb} \geq 3hrs.$, in the short period systems with $P_{\rm orb} \leq 2hrs.$, the mass–overflow is triggered by gravitational wave radiation. Under the assumption that gravitational waves are the only source of angular momentum loss between two subsequent outbursts, the rate of mass transfer $M_{\rm GW}$ is given by Cameron and Iben (1986)

$$\dot{M}_{\rm GW} = \frac{M_{\rm sec}}{4\tau_{\rm GW}} \times \left[2(1-q) + \frac{dln R_{\rm sec}}{dln M_{\rm sec}} - \frac{dln R_{\rm RL}}{dln q}\right]^{-1} \tag{1.6}$$

where $R_{\rm sec}$ is the stellar radius and $R_{\rm RL}$ is the radius of the Roche lobe of the secondary star and $\tau_{\rm GW}$ is the hypothetical timescale for two point masses in an initial circular orbit to evolve to contact. By using the more empirical expressions developed by Iben et al. (1992) :

$$\dot{M}_{\rm GW} = 10^{-10.21} M_{\odot} yr^{-1} M_{\rm sec}^{-0.24+4\epsilon} M_{\rm WD} M_{\rm sys}^{-0.76} \times (1.28 - \epsilon/2 - q)^{-1} \tag{1.7}$$

one gets the following values for the mass loss rates:

Nova	$\dot{M}_{\rm MSW}[M_{\odot} yr^{-1}]$	$\dot{M}_{\rm GW}[M_{\odot} yr^{-1}]$
DQ Her	2.7(-8)	1.4(-10)
T Aur	2.3(-8)	4.7(-10)
BT Mon	4.9(-8)	6.9(-10)

1.2.4 Accretion Disk and Hot Spot

A combination of gravitational and centrifugal forces can pull the envelope gas of the secondary towards the white dwarf. The outstreaming material cannot directly move to the white dwarf's surface. Due to its angular momentum it moves in an orbit around the white dwarf forming a centrifugally supported accretion disk in the binary plane. The internal viscosity of the material in the disk causes the gas to spiral inwards via a sequence of Keplerian orbits while the angular momentum is transferred outwards. During the accretion process the binding energy of the infalling material is converted to radiation energy with a total luminosity

$$L_{\rm acc} = G\,\frac{M_{\rm WD}\dot{M}_{\rm acc}}{R_{\rm WD}} \tag{1.8}$$

with $R_{\rm WD}$ being the radius of the white dwarf, G the gravitational constant and $\dot{M}_{\rm acc}$ the accretion rate. Inserting typical values: $R_{\rm WD} \approx 10^9 cm$, $M_{\rm WD} \approx 1 M_{\odot}$ and $\dot{M}_{\rm acc} \approx 10^{-10} M_{\odot} yr^{-1}$ one gets a typical luminosity due to the accretion phenomenon of

$$L_{\rm acc} \approx 10 L_{\odot}\,. \tag{1.9}$$

This clearly dominates the optical appearance of the system during the quiescence phases, as the secondary star typically has a luminosity of $L_{\rm sec} \leq 1 L_{\odot}$[7]. Additionally the optical lightcurve of eclipsing novae shows a prominent hump immediately

[7]Most of the accretion luminosity is emitted in the UV or in shorter wavelength ranges. So the companion may be more prominent than the disk in the near infrared or optical region.

prior to eclipse. This is usually attributed to a region of enhanced anisotropic emission [Robinson 1976] , the so called "bright spot" caused by the collision of the mass transfer stream with the disk[8]. A reasonable estimate positioning the location of the spot near the outer edge of the disk $R_{\rm d}$ implies a total spot luminosity $L_{\rm spot}$ of

$$L_{\rm spot} = \frac{GM_{\rm WD}\dot{M}}{R_{\rm d}} \ll L_{\rm acc} \tag{1.10}$$

which is still smaller than the total accretion luminosity $L_{\rm acc}$. However, the complicated shock structure likely to exist in the zone where the gas flow impacts the outer disk boundary has so far aggravated attempts of a general theoretical modelling and at present there is only some qualitative information about density, temperature and extent of this region based on the models of Bath (1976) , Rees (1976) and more recently Livio et al. (1986) . The interaction between the stream of transferred material originating from the inner Lagrangian point and the accretion disk, responsible for the *Hot Spot* was studied by means of the idealisation of the problem to the framework of a hypersonic flow passing a streaming layer of gas. The 3D–calculations of Livio et al. (1986) show that the results most sensitively depend on the parametrized penetration depth of the gas flow into the accretion disk. The turbulence induced by the stream–disk impact shock can range over a wide fraction of the entire disk, thus in principle giving an explanation of the light variations observed in many CV–systems including classical novae in quiescence [Warner 1976]. The binding energy per unit mass in a circular orbit near the surface of the white dwarf is $\frac{1}{2}(GM_{\rm WD}/R_{\rm WD})$, thus only one half of the accretion luminosity given in Eq.(1.9) is released in a disk extending down to the white dwarf. The other half is still residing as kinetical energy of the gaseous material circulating at distance $R_{\rm WD}$ and has to be released in a thin boundary layer of thickness $R_{\rm b} \ll R_{\rm WD}$, very close to the stellar surface. This boundary layer is the source of the observed hard and soft X–ray emission.

1.2.5 Time Evolution of Close Binaries

As already mentioned before classical novae are members of a wider class of objects known as *cataclysmic variables*. It is a general feature of all these objects that they occur in close binary systems and it is an important goal of the actual investigations to understand what properties of otherwise similar accreting systems lead to such large differences in the observations. This class of objects widely differ in their amplitude and energy release (see Tab. (1.5)) and consists of dwarf novae (U Geminorum stars, Z Camelopardalis stars), recurrent novae, novalike variables and, most interesting for this work, classical novae.

[8]This also may cause rapid optical flickering. In optical light–curves of dwarf-novae and novalikes this is a common observational fact. In old classical novae it is still present but less pronounced.

Class	Amplitude (mag)	Energy (ergs)	Recurrent time
Classical Novae	9 – 14	10^{44}–10^{45}	one eruption
Recurrent novae	7 – 9	10^{43}–10^{44}	10–100 years
(a)U Gem	2 – 6	10^{38}–10^{39}	15–500 days
(b)Z Cam	2 – 5	10^{38}–10^{39}	10–50 days
Novalike	—	—	No eruptions

Table 1.5: Range of visual amplitudes in *mag*, energy output per explosive event in *ergs* and recurrent time for Cataclysmic Variables.

The canonical model for the underlying physical system[9], now universally adopted, is that of a white dwarf and a late–type companion (secondary) which are only little separated. For such a system with masses $M_{\rm WD}$ and $M_{\rm sec}$, characterized by a period P, the binary separation a can be deduced from Keplers third law:

$$4\pi a^3 \;=\; G\,(M_{\rm WD} + M_{\rm sec}) \cdot P^2 \tag{1.11}$$

The circularisation and the synchronisation timescales in all nova systems are sufficiently short [King 1989] that one may assume

a) that the binary orbit is circular and

b) that the secondary co–rotates with the system.

The evaluation of Eq. (1.11), using the mass ratio q and inserting numerical values leads to:

$$a \;=\; 3.53\,\times\,10^{10} M_{\rm WD}^{1/3}\;(1+q)^{1/3}\;P^{2/3}\quad cm \tag{1.12}$$

where $M_{\rm WD}$ is in units of solar masses and P is in hours.
By use of the masses given in Tab. (1.2.2), combined with the orbital periods in Tab. (1.2) one gets typical values for the binary separation:

The recent theoretical studies of Livio et al. (1991) show that there can be substantial changes in the parameters of binary system due to

a) mass–loss from the system during the outburst

b) frictional angular momentum losses in the common envelope phase, when the binary system is rotating in a enclosing shell of gas.

[9]This idea was first proposed by Kraft (1962) (see also [Kraft 1962b] , [Kraft 1964]).

Nova	q	a [10^{10}cm]
DQ Her	0.71	1.08
T Aur	0.92	1.34
BT Mon	0.80	2.07
AE Aqr	0.78	2.33

Table 1.6: Binary separation for several nova systems in units of 10^{10}cm.

The relative change in the binary separation a resulting from mass loss can be calculated by Shara (1986)

$$\left(\frac{\Delta a}{a}\right) = \frac{\Delta M_{\rm ej}}{M_{\rm WD}} \times \left[\frac{1+2\zeta q}{1+q} - \frac{2\zeta}{q(q+1)}\right] \tag{1.13}$$

where $M_{\rm ej}$ represents the total mass ejected in a nova outburst and ζ is the fraction of this mass which could be captured by the secondary[10]. The separation change due to frictional angular momentum loss is more difficult to calculate. The simplified models of MacDonald (1986) have been recently extended by Livio et al. (1991) . They made use of the facts that

- the drag force experienced by the companion is proportional to the geometrical cross–section of the secondary and to the square of the relative velocity (see [Shima *et al.* 1985]),
- from the Roche lobe filling geometry the Roche lobe radius can be computed in terms of the mass ratio q [Eggleton 1983].

The results for the different mechanisms contributing to the change in binary separation obtained by Livio et al. (1991) are briefly summarized in Tab. (1.7).

For both, slow and fast novae the relative change in the binary separation $\Delta a/a$ due to the effects during the explosion increases as a function of the orbital period. But for short orbital period systems Δa is negative, whereas for systems with $P > 8h$ Δa becomes positive. In terms of the orbital period itself this means that the orbital periods of the short period systems decrease while the orbital periods of the long period systems increase. It is important to compare these effects on the binary separation to the corresponding change due to the systematic angular momentum loss as a result of gravitational wave radiation or magnetic breaking. Taking the values in Tab. (1.7) one of the main conclusions that can be carefully drawn from this work is: a classical nova explosion essentially influences the long–term evolution

[10] The maximum value of ζ that can be obtained is represented by the fractional area of the secondary's accretion radius. In the calculation of Livio et al. (1991) it is shown that the assumption of $\zeta = 0$ is a good approximation.

P [hr]	$M_{sec}[M_\odot]$	$\left(\frac{\Delta a}{a}\right)_{\rm fric}$	$\left(\frac{\Delta a}{a}\right)_{\rm ejec}$	$\left(\frac{\Delta a}{a}\right)_{\rm evol}$	$\left(\frac{\Delta a}{a}\right)_{\rm fric} + \left(\frac{\Delta a}{a}\right)_{\rm ejec}$	$\sum\left(\frac{\Delta a}{a}\right)$
2.0	0.220	– 2.4(-5)	+ 5.10(-6)	– 1.6(-5)	– 1.90(-5)	– 3.49(-5)
3.7	0.407	– 1.2(-5)	+ 4.53(-6)	– 8.6(-6)	– 7.47(-6)	– 1.61(-5)
8.0	0.880	– 3.8(-6)	+ 3.52(-6)	– 4.0(-6)	– 2.80(-7)	– 4.28(-6)
12.0	0.750	– 1.8(-6)	+ 3.75(-6)	– 4.7(-6)	+ 1.95(-6)	– 2.75(-6)

Table 1.7: Fractional change in the orbital separation resulting from a nova explosion by mass loss ($(\frac{\Delta a}{a})_{ejec}$) and frictional angular momentum loss ($(\frac{\Delta a}{a})_{fric}$) and the secular evolution between two subsequent outbursts ($(\frac{\Delta a}{a})_{evol}$). The data presented are adapted from Livio et al. (1991) and are calculated for the case of a slow nova, for which a mass loss of $M_{\rm ej} = 7.5 \times 10^{-6} M_\odot$ is assumed. The results for fast novae ($M_{\rm ej} = 4.8 \times 10^{-6} M_\odot$) do not differ significantly from the presented values. The mass of the white dwarf is assumed to be $M_{\rm WD} = 1.25\, M_\odot$. Values given as $a(-b)$ are shorthanded for $a \times 10^{-b}$.

---

of the binary system[11].
The theoretical predictions based on this model are in reasonable agreement with the observations of Schaeffer and Patterson (1983) concerning the old classical nova *BTMon* (see Tab. 1.2) and Stockman et al. (1988) who observed the periodic behaviour of V1500 Cyg.
It should be mentioned that the vast majority of the cataclysmic variables and therefore potentially nova systems contain a white dwarf of rather low mass [Politano and Webbink 1990] having a relatively high mass transfer rate of $\dot{M} > 2 \times 10^{-9} M_\odot yr^{-1}$. As a consequence the resulting thermonuclear runaway in such systems is rather weak. This implies a long duration of the period in which the secondary moves in a gas shell covering the whole system. Since hydrodynamic models of the outburst of classical novae (see next section) do not typically predict the rapid ejection of all the accreted mass on a CO white dwarf, although more mass is ejected if some mechanism for the enrichment of the envelope by heavier elements is assumed to operate, an additional mass loss mechanism is required to explain the observations of the rapid emergence (t$\approx$ 100 days) of the nebular spectrum and of X–rays observed in many classical nova systems ([Williams 1990], [Ögelmann *et al.* 1987]).
At maximum optical luminosity novae have spectral similarities to A or F supergiants and hence have photospheric dimensions of the order of 5×10^{12}cm. Thats why there must be a period for which the Roche lobe filling star is embedded in the nova envelope, experiencing a drag force as it moves through the common envelope

[11] The comparison between the evolutionary effects and that of the explosion is not entirely self–consistent, as the accretion rates used to compute the values of $(\Delta a/a)_{\rm eject}$ and $(\Delta a/a)_{\rm fric}$ are systematically lower than those predicted by the standard models used to compute the long–term evolution by a combined action of magnetic breaking and gravitational wave radiation [McDermott and Taam 1989] .

and thus depositing energy in the expanding nova shell. This energy deposition is rapid enough to induce significant hydrodynamic mass motions and in the case of relatively dense envelopes can eject the bulk of the ejecta [Shankar *et al.* 1991] . This may explain the high mass loss rates observed (up to $10^{-4}\mathrm{M}_{\odot}$) as well as the high ejection velocities.

1.2.6 The Outburst Mechanism

In the previous sections we have set the basic model for a classical nova: a close binary system consisting of a white dwarf and a larger and cooler main–sequence star filling its Roche lobe. Now we take a closer look to the energy generating processes driving the outburst of a classical nova.

During the accretion process the material is falling inwards due to viscous processes. This leads to a deposition of fresh hydrogen–rich material on the surface of the white dwarf. After a long period of quiescence, a time substantially longer than the period of the nova outburst, the accreted layer grows in thickness until the temperature at the bottom is high enough to initiate nuclear burning of hydrogen by the proton–proton chain reactions[12]. Under the conditions of complete degeneracy the energy just produced would be carried away due to the high electron conductivity and the occurrence of a *Thermonuclear Runaway* (TNR) would be prevented. Under the actual conditions present in the white dwarf surface layer this is inefficient[13]. As long as the p–p chain dominates the energy generation, the secular evolution of the shell is slow because the timescale of the nuclear burning is longer than the accretion timescale. When the temperature rises and the energy is provided by the reactions of the CNO–cycle, which has a very strong temperature dependence ($\approx T^{16} - T^{18}$), the nuclear burning timescale shortens and the accreted mass now is depending on the luminosity of the white dwarf.

The intensive studies of the TNR mechanism by Starrfield and coworkers (Starrfield *et al.*1972; 1974a,b,c; 1976; 1978 etc.) have lead to the acceptance of some general features and relations of the TNR mechanism:

- With increasing white dwarf mass it becomes easier to produce a nova outburst. This results from the fact that the radius of a white dwarf is inversely proportional to its mass, so the envelope mass necessary to initiate a TNR decreases with increasing mass of the white dwarf.

- All the observable characteristics of a common classical nova are sensitively linked to the enhancement of the CNO nuclei.

- At the peak of the outburst the β^+ unstable nuclei are the most abundant CNO nuclei (^{13}N, ^{14}O, ^{15}O).

[12]The proton–proton chain starts at about 10 million degrees Kelvin.

[13]As long as the white dwarf's luminosity is below some critical value.

- An important subclass of nova explosions occurs on ONeMg white dwarfs
- the energy production rate $\epsilon_{\rm CNO}$ at maximum due to the abundance of the CNO nuclei $Z_{\rm CNO}$ can be expressed by the simple law:

$$\epsilon_{\rm CNO} = 6 \cdot 10^{15} Z_{\rm CNO} \, erg \, g^{-1} \, s^{-1} \tag{1.14}$$

The progress of the nova outburst evolution in terms of the TNR model can be better reviewed by dividing it into four distinct phases, which correspond to the optical characteristics.

A: The Rise to the Bolometric Maximum

Because of the high temperature dependence of the CNO–cycle this phase will be surpassed very rapidly. When the temperature has grown to 2×10^7K a convective region forms and gradually grows towards the surface as the shell source temperature continues to increase. The energy produced in the interior can now act to increase the surface luminosity thus cooling the TNR zone. Up to this point no sign of the impending outburst has reached the surface. This phase is controlled by the convective turnover timescale [Sparks *et al.* 1990]

$$\tau_{\rm con} = \frac{\Delta R_{\rm s}}{v_{\rm con}} \tag{1.15}$$

where $\Delta R_{\rm s}$ is the thickness of the accreted envelope and $v_{\rm con}$ the velocity of the convective mass elements. At the peak of the TNR this time is about $\tau_{\rm con} \approx 10^2 \, s$. Since the surface layers are very thin ($10^{-8} M_\odot$ or lower) the luminosity can reach $10^5 L_\odot$. At the beginning the expansion velocities are small (1 to 10 km/s), thus the radius has not grown very much from the white dwarf radius, and the effective temperature is $\approx 10^5 K$. Therefore at bolometric maximum novae are luminous ultraviolet or soft X–ray sources.

B: Rise to Visual Maximum

When the peak of energy generation and temperature is reached the shell begins to expand, changing its state from hydrodynamic equilibrium to hydrodynamic expansion. When the luminosity exceeds the Eddington luminosity and the CNO nuclei are overabundant, a shock wave forms and additionally accelerates the material. When the shell reaches its maximum radial extension the visual luminosity also is at maximum. This maximum radius is determined by the expansion cooling of the hot photospheric gas, which gets transparent when the hydrogen starts to recombine ($T \approx 7 - 10 \cdot 10^3 K$); the opacity drops and the effective shell radius moves inwards. From the observations one can deduce an inverse correlation between speed–class and the time needed to rise to maximum brightness: the faster the nova expands the more rapid the visual maximum is reached and the more rapid the visual decline proceeds.

C: The Phase of Constant Bolometric Luminosity

In 1970 multiwavelength observations of Nova FH Ser [Geisel *et al.* 1970] first

showed that the early visual decline was produced by changes in the spectral energy distribution. Following UV observations (e.g. [Gallagher and Code 1974] , [Wu and Kester 1977],[Snijders *et al.* 1984] and infrared studies of classical novae (e.g. [Ney and Hatfield 1978] , [Gehrz *et al.* 1980a]) confirmed the assumption that the optical lightcurve, showing a continuous decrease, is not correlated with the bolometric curve. The physical reason for this behaviour is that the remaining hot gaseous material[14] not being ejected slows down and returns to hydrostatic equilibrium forming an extended envelope similar to that of an asymptotic giant branch star. The peak of the emitted energy then is shifted to the UV and extreme UV when the effective radius of this pseudophotosphere moves inward uncovering the hotter inner layers. Some novae as V1500Cyg and V1668Cyg undergo a Super–Eddington phase in which the material is highly accelerated.
The energy required to drive the high observed mass-loss rates of approximately $10^{-4} M_{\odot} yr^{-1}$ [Bath 1978b] given by:

$$\frac{GM_{\mathrm{WD}}}{R_{\mathrm{WD}}} \cdot \dot{M} \approx 2 \times 10^6 L_{\odot} \tag{1.16}$$

is higher than the observed peak luminosity ($L_{\mathrm{obs}}^{peak} \approx 1 \times 10^5 L_{\odot}$) thus emphasizing the requirement of an enhanced CNO abundance (see Eq. (1.14)).
The subsequent evolution to minimum light can take from 1 to 10 years depending on the speed–class of the nova.

D: The Turn–off Phase

The duration of this period is determined by the timescale needed to burn off the hydrogen on the white dwarf surface. Unfortunately the pure nuclear timescale is several hundreds of years, a period which is not compatible with the observational data. Studies of Nova Muscae 1983 have shown that the phase of constant bolometric luminosity lasts over four years; in the case of Nova Vulpeculae 1984 the constant–bolometric–luminosity phase is estimated to be about one year. Thus the problem arises how the white dwarf can get rid off the envelope material to stop the hydrogen burning process. There are two mechanisms proposed:

a) Bath and Shaviv (1976, 1978) discussed the hypothesis of a nova wind to occur with mass–loss rates about $10^{-6} M_{\odot} yr^{-1}$ initiated by the high white dwarf luminosity which is of the same order as the Eddington luminosity.

b) As a concurring or additional process Shankar et al. (1991) discussed the effects of the so called "common envelope phase". The model is based on the fact that the secondary is moving within the nova envelope. The drag experienced during the orbital motion then leads to an energy deposition in the expanding envelope. This will induce significant hydrodynamic mass motions and the bulk of the material could be ejected on a timescale of at least ≈ 100 days. The predictions made by calculating the mass loss available are of the

[14] In the nova explosion even of fast novae only 10%–50% of the accreted mass is blown away.

order of $10^{-4}\,M_\odot$. The duration of this phase is mainly influenced by the shell density which controls the drag force experienced by the secondary.

However, it is just this stage of the nova binary evolution which will determine the long–term behaviour of the system by the amount of material remaining on the white dwarf.

1.2.7 Abundances in Novae

There are some important implications of the TNR Model on the elemental abundances in classical novae. The recognition of the fact that nova ejecta can exhibit unusual abundances dates back to Payne–Gaposchkin (1957) and has motivated detailed abundance studies for a number of novae. Recent results of abundance determinations are given in Tab. (1.8):

Object	Sun	V1500 Cyg	V1668 Cyg	V693 Cra	V1370 Aql	GQ Mus	PW Vul
Year	–	1975	1978	1981	1982	1983	1984
Ref.	[1]	[2][3]	[4]	[5][6]	[7]	[8]	[9]
H	1.0	1.0	1.0	1.0	1.0	1.0	1.0
He	6.8(-2)	1.5(-1)	1.2(-1)	2.8(-1)	4.5(-1)	2.9(-1)	1.2(-1)
C	4.2(-4)	8.5(-3)	8.0(-3)	1.5(-3)	5.9(-2)	4.9(-3)	1.1(-2)
N	8.7(-5)	5.1(-3)	2.1(-2)	2.1(-2)	2.1(-2)	5.1(-2)	1.7(-2)
O	6.9(-4)	5.5(-3)	1.7(-2)	2.7(-2)	6.5(-2)	4.3(-2)	1.2(-2)
Ne	9.8(-5)	8.7(-4)	7.5(-4)	3.0(-2)	5.3(-1)	6.5(-4)	2.0(-4)
Na	2.3(-6)	–	–	2.5(-4)	–	–	–
Mg	4.0(-5)	–	1.2(-4)	1.1(-3)	5.7(-3)	2.2(-4)	2.3(-5)
Al	3.2(-6)	–	6.7(-5)	4.4(-4)	–	7.6(-5)	–
Si	3.8(-5)	–	2.8(-4)	3.2(-4)	1.3(-4)	3.6(-4)	4.3(-4)
S	1.9(-5)	6.0(-5)	–	–	6.4(-2)	1.8(-4)	–
Fe	3.4(-5)	1.4(-5)	–	–	1.7(-3)	3.1(-5)	3.4(-5)

References

1:[Cameron 1982] 2:[Ferland and Shields 1978] 3:[Lance *et al.* 1988]
4:[Stickland *et al.* 1981] 5:[Williams *et al.* 1985] 6:[Williams 1985]
7:[Snijders *et al.* 1987] 8:[Hassall *et al.* 1989] 9:[Andreä *et al.* 1991]

Table 1.8: Abundances for various recent novae. Values are abundances by number with respect to hydrogen, where $a(-b)$ is shorthanded for $a \times 10^{-b}$. Only those novae are presented for which a rather complete abundance data set exists.

From the collected data several conclusions can be deduced:

a) The heavy element enhancement is a characteristic feature of the classical nova outburst.

b) The helium to hydrogen ratio is significantly higher than solar (the mean value is about five times the solar ratio).

c) Faster novae tend to have higher heavy element enrichments (V1500Cyg, V1370Aql).

d) An important subclass shows large enrichments in neon (e.g. V693 Cra, V1370 Aql).

The occurrence of those significant abundance enhancements must be attributed to the fact that some fraction of the envelope matter was processed in the thermonuclear burning reactions in the core of the white dwarf and has been dredged up from this underlying core to the surface by some still unknown process[15], since the realisation of large carbon and oxygen abundances (also necessary for the CNO cycle in the TNR) requires helium burning which only works at temperatures of $\approx 30 \times 10^6 K$. High He/H ratios are a consequence of the mixing of the accreted H–rich matter with the helium–rich matter on the white dwarf. Similarly the CNO enrichments may be explained by a mixing process penetrating deep into the carbon–oxygen core. The observed overabundances of the carbon–burning products Ne, Na, Mg and Al then can only be understood if the underlying white dwarf is assumed to be oxygen–neon–magnesium rich [Truran and Livio 1986] . These so called "ONeMg–Novae" form an important subclass of the classical novae.
Theoretical estimates of the relative frequency of occurrence of different white dwarf masses in classical nova systems reveal that the mean mass for such systems which are observed in outburst is about 1.14 $M_\odot$ [Politano *et al.* 1990] . So thermonuclear runaways occur on more massive white dwarfs and under the assumption of a constant accretion rate they occur on shorter time intervals. Recent results for the recurrence time t_{rec} and the relative frequencies of occurrence $f^{CN}_{M_{WD}}$ for systems with different white dwarf masses are given in Tab. (1.9).
It should be noted that about one third of the nova events are due to an TNR occuring on an ONeMg–white dwarf. Two examples of this class during the last decade are V693 Cra (see [Snijders 1990]) and V1370 Aql (see [Wiescher *et al.* 1986]).

[15] As concurring processes there was also proposed that

1. mass overflow from the secondary, or

2. transformations of the material during the nuclear reaction cycles working in the runaway

could generate the observed abundance peculiarities.
The influence of the secondary (1.) can be ruled out on the basis of the recent observations showing extremely high Z abundances (V1370 Aql), which could not been produced by a main sequence companion star.
The second possibility is out of discussion because the CNO cycle only rearranges the CNO isotopes but does not create new nuclei.

$M_{WD}/M_\odot$	T_{rec}[yr]	$f^{CN}_{M_{WD}}$
0.6	1.29×10^6	0.103
0.7	7.31×10^5	0.053
0.8	4.16×10^5	0.042
0.9	2.36×10^5	0.040
1.0	1.20×10^5	0.046
1.1	6.39×10^4	0.062
1.2	2.81×10^4	0.100
1.3	9.02×10^3	0.232
1.35	3.98×10^3	0.322

Table 1.9: Relative frequencies of occurrence of classical nova outbursts $f^{CN}_{M_{WD}}$ for binary systems with different white dwarf masses M_{WD} (in units of the solar mass $M_\odot$). The frequencies are normalized to unity and have been calculated by Politano et al. (1990) using the white dwarf distribution function of Politano and Webbink (1990) . The recurrence time scales t_{rec} were taken from Truran (1990) . The last line in the table is the ONeMg nova case, which occur on the most massive white dwarfs.

Another unusual recent outburst was that of the fast recurrent nova U Scorpii (not in the abundance table), where the optical data implied a helium to hydrogen abundance ratio in the ejecta of ≈ 2 (by number). Optical spectra obtained after its return to the quiescence state [Williams *et al.* 1981] predominantly showed HeII lines, indicating that the preoutburst material was probably very rich in helium and this suggests that the secondary star is a highly evolved object in the binary system. For the reproduction of the lightcurve characteristics (see Sect. (1.3)), the expansion velocity and the Super–Eddington luminosity of fast novae substantial enhancements of CNO nuclei above solar values are an indispensible prerequisite.

1.2.8 Nova Contribution to Galactic Nucleosynthesis

The contribution of the classical novae to the galactic heavy element nucleosynthesis can be estimated relying on the following assumptions

- the current rate of nova events is $\approx\ 30\,yr^{-1}$ [Gehrz 1989] [16],
- constancy of the mean outburst rate over the lifetime of the galaxy,
- the average mass ejected per outburst is $\approx\ 10^{-4} - 10^{-5}\,M_\odot$.

[16] In this rate we follow the data used by Gehrz (1989) . This rate is not consistent with the rate used by DellaValle and Claudi (1990) , which was previously mentioned in this chapter.

element	solar mixture	ONeMg–rich mixture	C–O rich mixture
^{22}Na	2.4×10^{-6}	1.8×10^{-4}	4.3×10^{-6}
^{26}Al	1.3×10^{-4}	5.1×10^{-3}	1.0×10^{-4}

Table 1.10: Abundance enhancements of ^{22}Na and ^{26}Al produced in a classical nova event assuming
a) solar mixture
b) ONeMg–rich mixture
c) C-O–rich mixture.
For the model calculations a peak burning temperature of $150 \times 10^6 K$ was assumed. Higher peak burning temperatures lead to a decreased production of the two isotopes.

Thus during the existence of the galaxy about 10^7 solar masses have been ejected by classical novae into the interstellar medium. This is only a small fraction of the entire gas and dust ($\approx 3 \times 10^9\, M_\odot$) and therefore only such nuclei enhanced by a factor of more than 300 can significantly contribute to the enrichment of the heavier elements in interstellar space. These constraints imply that novae can potentially produce important concentrations only of the isotopes of carbon, nitrogen and oxygen ($^{13}C,^{15}N,^{17}O$) which may be enriched by a factor up to 10^3 relative to their solar abundance [Gallagher and Starrfield 1978] .
Probably more significant than the CNO isotopes is the production of the radioactive elements ^{22}Na and ^{26}Al, which have decay times of $\tau_{1/2}^{Na} = 2.6 yr$ and $\tau_{1/2}^{Al} = 7.3 \times 10^5\, yr$, respectively.
Observations with the HEAO 3 γ–ray spectrometer of the 1.809 MeV line emission resulting from the decay of the ^{26}Al isotope ([Mahoney *et al.* 1982] , [Mahoney *et al.* 1984]) have given rise to the prediction that novae are the dominant contributors of ^{26}Al to the Galactic nucleosynthesis. This experimentally based prediction now has been confirmed by the model calculations by Nofar et al. (1991). Also recent calculations of Weiss and Truran (1990) show, that a substantial amount of these isotopes can be produced by novae in which the composition is characterized by high initial enhancements of elements from neon to aluminium as it is shown in Tab. (1.10) presenting the results of Weiss and Truran (1990) .

1.3 Optical and Spectral Appearance

In view of rather large differences between the characteristics of individual novae one can state that on the other hand there is also a great similarity of the different outbursts.

Based on a large collection of data Mc Laughlin (1960) developed his classification system, with which, despite the individual variations of the optical properties during the outburst, the common features can be recognized. Accompanying the optical appearance, the spectral development is closely related to the different nova phases. McLaughlin has established the following phases:

a) prenova

b) initial rise and premaximum

c) premaximum–halt

d) maximum

e) decline

f) transition

g) nebular stage

h) postnova and quiescence

Now we are going to discuss in some detail all these phases collecting the phenomenological data known about classical novae.

1.3.1 Prenova

A complete survey of the Prenova observations, mainly consisting of photographic data, has been done by Robinson (1975) . From his lightcurves one can deduce light variations and also it seems that there is a slight increase in the optical luminosity a few years before eruption[17]. Most prenovae resemble, like their postnovae counterparts, low–amplitude variables. The complete equivalence of pre– and postnova stadium is not assured as long as there are only observations covering just one single spectral region. Generally the time scales on which nova observations were performed do not cover more than a hundred years and thus no statement concerning larger time periods are possible[18]. The existing poor spectroscopic data (V603Aql[19], V533Aql[20], HR Del1967[21]) of novae prior to outburst show a featureless blue con-

[17] For V1500Cyg a brightening of 3^m from 21^m to 18^m has been reported [Wolf 1977] .

[18] CK Vul 1670 and WY Sge 1783 [Shara *et al.* 1984] are the only exceptions.

[19] [Payne–Gaposchkin 1957]

[20] [Stephenson and Herr 1963]

[21] [Stephenson 1967]

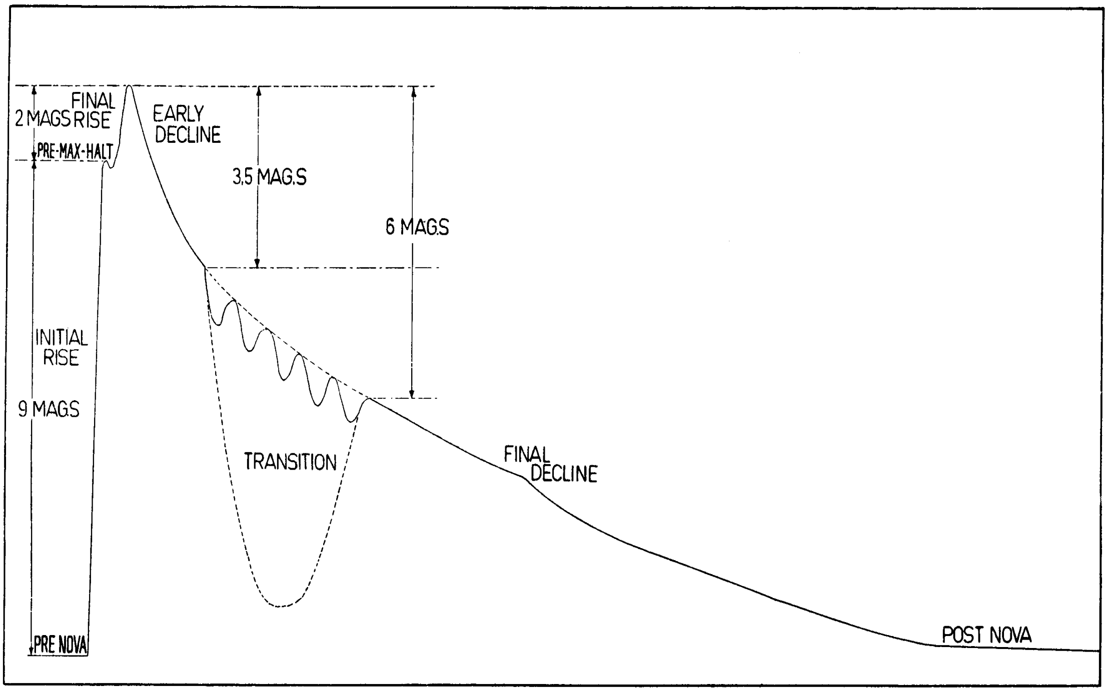

Figure 1.1: Schematic lightcurve of a classical nova displaying the typical phases in the evolution of the optcal appearance (after McLaughlin (1960)).

---

tinuum. The spectra of HR Del, the best resolved, displays an energy distribution similar to that of an O or B star. These features are also present in the postnova stages of all but a few novae ([Payne–Gaposchkin 1957], [Robinson 1976]) and the comparison of these spectra indicates that the accretion disk which might have been disrupted during the outburst re–establishes within a time of ≈ 10 years. This also points to either a relatively low mass of the accretion disk or to the fact that the disruption is not substantial due to a rather high disk mass of 10^{-3}–$10^{-4} M_{\odot}$.
The time between subsequent outbursts and the duration of outburst and quiescence periods were recently determined by Prialnik (1989) on the basis of theoretical hydrodynamic modelling of a complete nova cycle. It turns out that both time periods sensitively depend on the mass of the white dwarf and the amount of mass–overflow as shown in Tab. (1.11)

$\log \dot{M}$ [$M_\odot$/yr]	M_{WD} [$M_\odot$] 0.8	1.2
-10	1300 *2.5(6)*	10 *4.4*
-8	270 *4800*	2.0 *84*

Table 1.11: Outburst and Quiescence periods of Classical Novae for different accretion rates ($\log \dot{M}$) and white dwarf masses M_{WD}. The results in the table for the outburst– (first row) and quiescence periods (second row, italic numbers) are given in years, where $a(b)$ is shorthanded for $a \times 10^b$. (data adopted from Prialnik (1989)).

1.3.2 Initial Rise and Premaximum

The sudden steep rise of the optical luminosity indicating the beginning of a Classical Nova is only rarely observed. The fragmentary data present for the phase of the brightening from the pre–nova stage to the premaximum–halt [Liller *et al.* 1975] , [Samus 1975] , [Alksne and Platais 1975] (all for Nova Cygni 1975[22]) indicate an evolution time for this period in the range of $2 \approx 3$ days, even for slow novae [McLaughlin 1960] . The initial rise is accompanied by a change towards a colour reddening and stops approximately 2^m below maximum. From the spectroscopic data one deduces the following:

- the absorption lines are broad and blueshifted and only one dominant absorption line system is seen,
- a strong and blue continuum is present
- the spectral type is that of a B or A star
- C, N, O absorption lines are very pronounced in comparison with the strength in normal stellar spectrum of this type.

All these facts can be interpreted in terms of a single, expanding and cooling shell with a high velocity dispersion.

1.3.3 Premaximum Halt

In the schematic nova lightcurve (see Fig. (1.1)) one can recognize a brief halt in the rise towards maximum brightness which lasts only for a few days or even hours.

[22] In the case of Nova Cygni 1975 this phase took less than one day.

Naturally this gives only little opportunity for more intensive spectral studies. Fortunately we are in a better situation in the case of slow novae, which had an extended premaximum[23] HR Del we are in the fortunate situation to have spectral information [Sanyal 1974] . During the first brightness plateau of HR Del (about 1.5 month) the typical blue–shifted absorption lines were present indicating an expanding shell with a velocity of $\approx$ 500 km/s. After an increase of optical brightness of about 1.5^m to maximum and the subsequent return of the nova to the former brightness level of the first plateau the lightcurve develops over three month to a second, less pronounced maximum.
During the premaximum halt the variation of the fundamental observation quantities were only small compared to the variations during outburst, thus indicating an also small variation of the underlying energy source (see Tab. (1.12)).

quantity	variation during Premaximum–halt	variation during outburst
luminosity	2	3×10^3
radius	1.6	80
temperature	1.2	$\approx$ 2–10

Table 1.12: Change of fundamental nova quantities during the premaximum–halt compared to the change during outburst.

1.3.4 Maximum and Early Decline

The brightening of classical novae to their maximum optical brightness normally takes only a short time (2–3 days), comparable to the period of the initial rise. The onset of the constant luminosity phase, defined as the physical maximum, must not coincide with the optical maximum. Also the appearance of the principal spectrum, marking the spectroscopic maximum does not necessarily occur simultaneous to the photometric peak. The spectral type of the nova now is close to that of an A or F supergiant[24] and the later the spectral type the lower are the expansion velocities. The principal spectrum displays the following summarized features:

- strong P–Cygni lines, which may be multicomponent, superimposed on a cool continuum,

[23] The premaximum phase of HR Del lasts over five months and sometimes it is considered to be an extended maximum.
[24] See e.g. Nova Cygni 1978 which was analyzed to have a spectral type of F5 Ib [Klare *et al.* 1980] .

Speed class	t_2[d]	$\dot{m}$ (mag d^{-1})	$\overline{M}$	$\overline{\Delta M}$	disc	bulge	M31	LMC
Very fast	$<$ 10	$>$ 0.20	4.4	13.2	38%	24%	17%	56%
Fast	11–25	0.18–0.08	3.7	11.3	33%	30%	44%	44%
Moderately fast	26–80	0.07–0.025	4.4	10.9	15%	36%	31%	0%
Slow	81–150	0.024–0.013	4.1	9.6	5%	9%	7%	0%
Very slow	151–250	0.013–0.008	5.2	9.4	–	–	–	–

Table 1.13: Definition of nova speed class for the classification of light curves. The time t_2 in days denotes the time taken for the nova to diminish by two magnitudes below maximum visual brightness. $\overline{M}$ indicates the absolute magnitude and $\overline{\Delta M}$ describes the mean range of novae at quiescence. The last four columns describe the distribution of the first four speed class novae in different stellar systems.

- the continuum is weakening and getting hotter,
- the spectral lines continuously evolve during the increase of the expansion velocity,
- absorption lines of neutral (e.g. NaI) and single ionized metals (e.g. FeII) are present,
- occurrence of emission lines of hydrogen and metals in low ionization stages (FeII, CaII). Emission of neutral carbon and oxygen is also observed.

When the outburst is developing further the optical lightcurve declines. The optical maximum is occuring at maximum radius and minimum photospheric temperature. The decrease in mass ejection combined with higher particle velocities leads to an inward moving of the photosphere. Thus a hardening of the emitted photon flux, which is reflected by the spectral development and a decline in the optical spectral region is to be observed.
The time development of the principal spectrum reveals

- a fading of the lines of the low ionized species like MgI, OI, CI, SII,
- that lines of higher ionized species appear (NII, NIII, HeII, OIII),
- that hydrogen lines remain strong.

The expansion velocity deduced from the line width of the principal spectrum again shows a correlation to the rate of decline:

$$\log v_{\rm exp} = 3.70 - \frac{1}{2}\log t_3. \qquad (1.17)$$

being a result of the approximate equipartition between the radiation field and the ejected matter.

When the principal spectrum first appears, one major absorption line system is present. This seems to indicate that in the main eruption event one major shell is ejected. More separated absorption components are seen during the decline indicating that subsequently more shells are ejected. Such multicomponent absorption features are more prominent in slow novae, where they may be accompanied by semi–irregular light–variations. A possible explanation for these light variations is that those particles which were not ejected fall back to the energy–generating zone on the white dwarf where they are mixed into the burning material. Thus an enhanced energy production is initiated and also shocks may evolve giving rise to a variation in the energy production and therefore in the observed light.
In fast novae the ratio of kinetical to radiant energy is high and the fast expansion leads to a rapid retraction of the photosphere, parallel to a rapid decline of the optical lightcurve and a transformation to the UV. These novae undergo Super–Eddington phases and for example Nova Cygni 1975 had a luminosity at maximum light that was 100 times the Eddington limit [Ferland *et al.* 1986] and maintained at this Super–Eddington luminosity for about 10 days[25]. This stage of steady hydrogen burning[26] is ceased by enhanced mass–loss due to dynamical friction in the common–envelope phase [MacDonald *et al.* 1985] , where the particles are additionally accelerated.

1.3.5 Continued Decline

When the optical luminosity has fainted by about 2^m most novae undergo a phase where irregular light variations set in (e.g. DQ Her). Mostly the total luminosity has not changed since maximum light. In this period, which starts about 2 days after maximum in fast novae and about 2 weeks after maximum in slow novae, the *diffuse enhanced spectrum appears*. It is characterized by

- diffuse emission and absorption lines of abundant elements like C, N, O, Si and S (in some cases Ne) in their first or second ionization stage, [Rosino *et al.* 1983]
- the velocity of the lines is increasing [Rosino *et al.* 1986] as well as the velocity dispersion,

[25] This estimate of Ferland et al. (1986) is based on the assumption that all the energy was radiated in the optical wavelength range. If a bolometric correction for UV and other non–optical radiation is taken into account the Super–Eddington phase may have lasted for even longer periods.
[26] As shown in section (1.2) the nuclear–burning time scale is of the order of some hundreds of years.

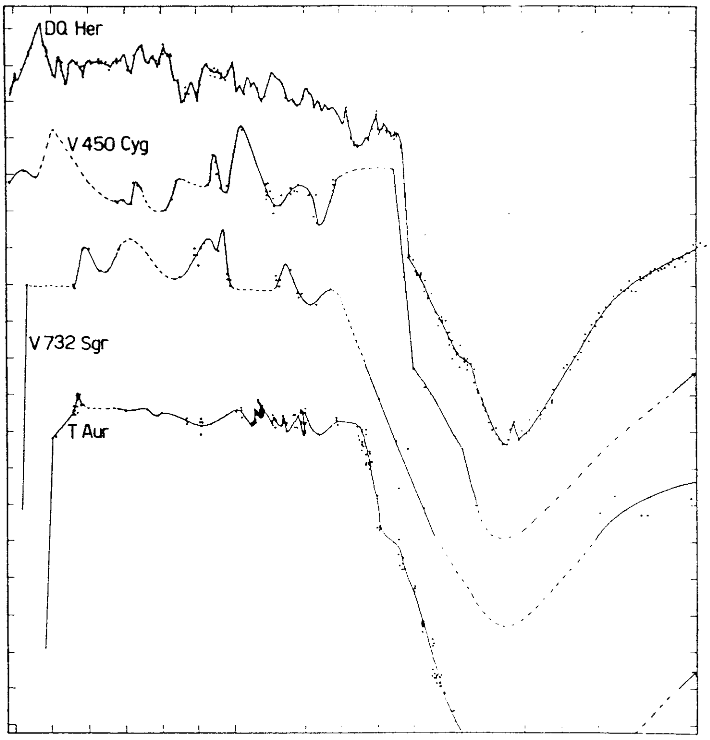

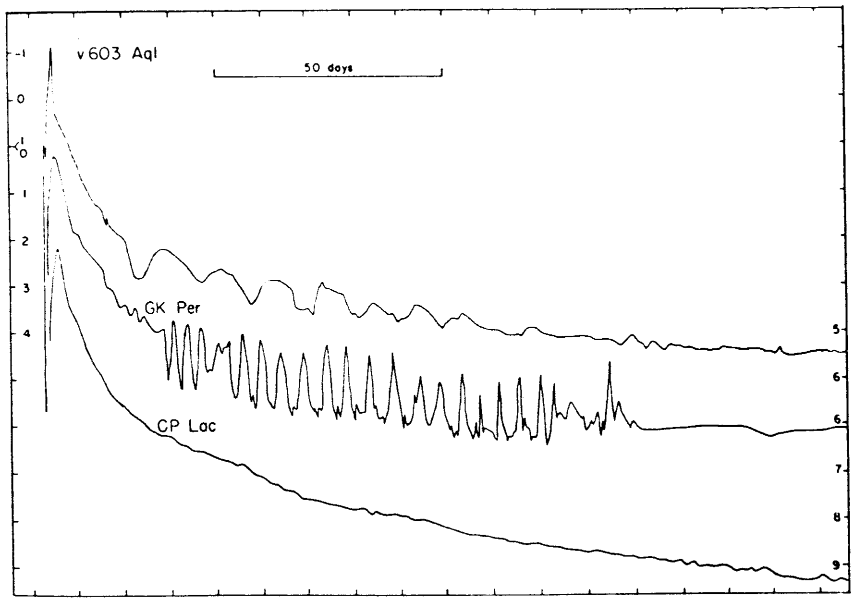

Figure 1.2: Typical nova lightcurves. The pictures are taken from McLaughlin (1960)(lower curve) and Payne–Gaposchkin (1957)(upper curve) . The upper diagram displays some novae of the DQ Herculis type, all showing a deep minimum. The novae are: T Aur (1891), V 450 Cyg (1942), DQ Her (1934) and V 732 Sgr (1936). Ordinate and abscissa are marked in intervals of one day and one magnitude respectively.
The lower diagram shows three typical lightcvurves for fast novae: V 603 Aql (1918), GK Per (1901) and CP Lac (1936).

- the diffuse–enhanced and the principal spectrum are often seen together,
- its duration varies between 16 days for fast novae to 90 days for slow novae [Payne–Gaposchkin 1957]

The thinning out of the ejected material and the decrease in mass–loss now allows the observer to look increasingly deeper into the shell, which has moved nearer to th energy generating layer and therefore is much hotter. The optical depth is reduced and more high energetic photons can penetrate into the expanding envelope material thus higher stages of ionization can be observed. By the higher mean energy of the photons the particles are accelerated up to increasing velocities. The ejected matter now is enriched in processed material, which might be C, N, O for the "normal" CNO–white dwarfs or O, Ne and Mg for underlying ONeMg–white dwarfs.

1.3.6 The Transition Stage

During this period of nova evolution the optical measurements show at least three typical and markedly different types of development;

a) a smooth continuing decline (e.g. DI Lac)

b) quasi–periodic oscillations with typical time scales of 3–15 days (e.g. GK Per)

c) a steep decline with recovering after some weeks to month (e.g DQ Her)

Especially the characteristic of the lightcurve (c) is of significance as it has been attributed to the formation of small solids which absorb the nova photons and reradiate it at longer wavelength[27]. Colour measurements (e.g. [Rosino *et al.* 1983]) have supported this concept and since IR measurements were possible it was confirmed by numerous observations reporting IR excesses for several novae (see Tab. 1.14)
In the proceeding of the evolution of the expanding shell the outer envelope parts thin out and the photospheric radius shrinks so that now the observer can look to increasing depths of the inner system. High stages of ionization appear (NIII, NV) and also, as a sign of the reduced density, forbidden lines appear like those of the highly ionized FeX, SiV and MgVII. The presence of coronal lines indicate very high temperatures (some 10^6K) and electron densities of about 10^8 cm^{-3} and they appear just before dust formation sets in and are observable also during the dust formation phase.

The light variations in this phase are accompanied by the appearance and disappearance of lines. First attempts to clarify the nature of these light variations

[27] Grotrian (1934) has given another possibility in his study of Nova Herculis (1934). The deep decline he interprets in terms of the time development of the photospheric radius and temperature. A more recent work of Bosma (1975) has tried to attribute the deep minimum to an increased absorption H^- ions and H–atoms.

[28] HC: Hydrocarbons

Nova	Year	$\tau_{\rm ir}$	$M_{\rm gas}$	$M_{\rm grain}$	t_3	$t_{\rm dust}$	$v_{\rm exp}$	Dust	Ref.
FH Ser	1970	0.50	–	–	62	60	560	C	abc
V1229 Aql	1970	0.55	–	–	37	–	575	C	acy
V1301 Aql	1975	–	–	–	32	–	$\approx$1000	–	d
V1500 Cyg	1975	3×10^{-5}	8×10^{-4}	–	6	–	1180	–	etc
NQ Vul	1975	1.00	10^{-4}	2×10^{-7}	64	80	750	C	ghc
V4021 Sgr	1977	$\leq$0.56	–	–	–	–	–	–	i
LW Ser	1978	0.70	2×10^{-5}	3.6×10^{-7}	55	75	1250	C	j
V1668 Cyg	1978	0.08	2×10^{-5}	2.5×10^{-8}	30	57	1300	C	jc
V1370 Aql	1982	0.50	7×10^{-6}	2×10^{-5}	10	$\leq$17	2800	C,SiC,SiO_2	klmz
GQ Mus	1983	$\approx$0	–	–	45	–	600	–	no
PW Vul	1984	3×10^{-3}	3.2×10^{-6}	5.1×10^{-10}	100	152	285	C	pc
QU Vul	1984	3×10^{-3}	3×10^{-5}	10^{-8}	40	240	1000	SiO	qrstuv
OS And	1986	–	–	–	–	900	–	–	α
V842Cen	1986	1.00	–	–		36	1200	C,SiO_2,HC [28]	α
V827 Her	1987	0.10	–	–	–	43	1000	C	wx

References

a : [Geisel *et al.* 1970]	b : [Mitchell *et al.* 1985]	c : [van den Bergh and Younger 1987]
d : [Vrba *et al.* 1977]	e : [Ennis *et al.* 1977]	f : [Gallagher and Ney 1976]
g : [Gehrz *et al.* 1980a]	h : [Ney and Hatfield 1978]	i : [Hatfield and Brodzik 1977]
j : [Gehrz *et al.* 1980b]	k : [Bode *et al.* 1984]	l : [Gehrz *et al.* 1984]
m : [Williams and Longmore 1984]	n : [Krautter *et al.* 1984]	o : [Whitelock *et al.* 1984]
p : [Gehrz *et al.* 1988]	q : [Gehrz *et al.* 1985b]	r : [Gehrz *et al.* 1985c]
s : [Gehrz *et al.* 1985a]	t : [Gehrz *et al.* 1986]	u : [Greenhouse *et al.* 1988]
v : [Taylor *et al.* 1987]	w : [Gehrz and Jones 1987]	x : [Greenhouse *et al.* 1987]
y : [Harrison and Gehrz 1988]	z : [Snijders *et al.* 1987]	α : [Gehrz 1990]

Table 1.14: Physical parameters of 15 recent novae. The data were determined by multiwavelength observations. $M_{\rm gas}$ and $M_{\rm grain}$ are given in units of $M_\odot$, t_3 and $t_{\rm dust}$ are given in *days* and $v_{\rm exp}$ is in km/s. The infrared optical depth $\tau_{\rm ir}$ is the ratio of the luminosities in the infrared $L_{\rm ir}$ and in the optical $L_{\rm opt}$.

---

undertaken by Grotrian (1937) have been extended by Mustel (1956) and Phillips and Selby (1977) . They applied a hydrodynamic model assuming radial pulsations of the nova photosphere and in the following we try to explain the light variation in the transition stage within this framework:

- At optical minimum, when the burning layers on the white dwarf surface have dropped into the Sub–Eddington regime, mass ejection is reduced as well as the particle velocities. Now only the most energetic particles can reach escape velocity generating the relatively high velocity observed as well as the small velocity dispersion. The large fraction of those particles which are too slow fall back onto the white dwarf.

- Thus the energy production will raise and more and faster particles are ejected; the mean particle velocity increases and is shifted closer to the escape velocity resulting also in a reduced mean particle velocity in the wind–like flow of ejected material. There are also more particles which do not reach escape velocity, falling back and additionally increase the luminosity to the Eddington limit again. This is the scenario at maximum light during the transitional variations.

- The increased depletion of material caused by the higher energy production limits the duration of this unstable equilibrium period. The whole process is terminated when the system is unable to reach the Eddington luminosity again.

A major objection to this scenario may be that it does not really account for the sudden onset of the variations and as most of the lightcurves are lacking a complete coverage of the transition stage the oscillations may also be due to small bursts which will result in the ejection of a number of thin and quickly dispersing shells. Generally a non–homogeneous [Duerbeck 1987] ring–blob like structure [Mustel and Boyarchuk 1970] is observed. Towards this conjecture points too:

- the existence of multicomponent emission–lines

- the simultaneous presence of a very hot electron gas and newly formed grains.

However, it seems doubtful that the density in such a multishell–structure would be high enough to allow for efficient condensation processes. Alternatively a single main burst will result in the formation of one major thin shell[29] which is dense enough to undergo a phase of chemical evolution and subsequent nucleation.

1.3.7 The Nebular Stage

When the nova has fainted by several magnitudes the nebular stage sets in. The photosphere has become smaller and radiates mainly in the UV and X–ray region. An additional and newly arising observational fact in this phase is the presence of weak long–wavelength bremsstrahlung and recombination radiation. The spectrum is characterized by forbidden lines (OII, OIII, OI, NII and in some cases NeIII). The emission components are numerous reflecting the non–homogeneous spatial structure, where the emission is generated in different cloudlets moving with different radial velocities relative to the observers frame. The shell evolves now into a stage where the physics of gaseous nebulae can be applied and in the fully developed

[29] A thin high density shell expanding into the surrounding thin medium would give rise to Rayleigh–Taylor instabilities and may explain both, the fast disappearance of the shell and the formation of small dense zones for dust formation.

nebular phase at 7^m below maximum the spectrum of the nova resembles that of a planetary nebulae, save for the width of the lines.

Observations of Ögelmann et al. (1984) and Ögelmann et al. (1987) concerning the short–wavelength regions in the case of Nova Muscae 1983 and Nova Vulpeculae 1984 are supporting the constant luminosity model of a hot white dwarf component. The model of a longlasting constant mass loss via optically thick winds as it has been suggested by Bath and Shaviv (1976) and Bath (1978) to be the major ejection mechanism is in conflict with the X–ray measurements, which indicate an upper mass–loss limit for this type of ejection mechanism of $5 \times 10^{-7} M_{\odot}/yr$ after 100 days. Otherwise a stronger wind would lead to a more extended photosphere and therefore lower surface temperatures what does not agree with the observations "Ogelmann et al. (1987) . Thus the material must have been ejected with a substantially higher rate of about $10^{-4} M_{\odot}\, yr^{-1}$. In addition the maximum photospheric temperature derived from the X–ray measurements imply a white dwarf mass of $M_{\mathrm{WD}} \approx 0.7 M_{\odot}$ whereas the observed lifetime of the remnant due to the energy emitted in the UV and X–ray region implies $M_{\mathrm{WD}} \approx 1.4 M_{\odot}$. A further constraint of these observations is that the envelope mass ejected by dynamical friction in the common envelope phase is unsufficient to explain the X–ray observations.
The recent hydrodynamic calculations of Shankar et al. (1991) on the other hand state a high mass loss of $3.6 \times 10^{-4} M_{\odot}/yr$ initiated by the drag forces acting in a common envelope phase. They found that the bulk of the envelope will be ejected on a timescale of $20 \approx 30$ days while the luminosity generated by this process remains constant during this time. subsectionPostnova The photometric and spectroscopic observations of this phase indicate that there is a very hot remnant star and that the nuclear burning has ceased. The accretion disk has been regenerated; the time needed for this reestablishing of the system depends on the mass loss from the secondary and typically is of the order of years. The spectral analysis also reveals that there are noticeable abundance differences in the nova shell. The complete return to the prenova brightness can take decades and light variations during this phase are a common phenomenon.

1.3.8 Novae as Extragalactic Distance Indicators

The study of the observational material has shown that there is a relation between the maximum brightness and the rate of decline, which usually is written in the form [Warner 1990] :

$$M = b_{\mathrm{n}} \log t_{\mathrm{n}} - a_{\mathrm{n}} \tag{1.18}$$

where t_{n}[30] is the time taken to decline to n magnitudes, M is the absolute magnitude at maximum light and a_{n} and b_{n} are parameters. Deviations from (1.18) may occur due to a spread of the white dwarf luminosities before nova outburst. The speed class definition and the typical values of maximum magnitude and magnitude range

[30] For t_{n}, a_{n} and b_{n}, n usually is chosen to be 2 or 3.

for novae are shown in Tab. (1.13).
This empirical relationship between M and $\log t_n$ breaks down for very slow and very fast novae as has been shown by van den Bergh (1975) . For the linear part of the relationship typical values of the parameters a_n and b_n are:

n	a_n	b_n	Ref.
3	-11.3	2.4	[De Vaucouleurs 1978]
3	-10.67±0.30	1.80±0.20	[Pfau 1976]
2	-10.42±0.38	1.76±0.31	[Cohen and Rosenthal 1983]
2	-10.70±0.30	2.41±0.23	[Cohen 1985]

From the theory of nova lightcurves (see [Shara 1981b], [Shara 1981a]) one also has developed a *luminosity–rate of decline relationship*, using B–magnitudes and t_3:

$$\begin{aligned} M_{\mathrm{B}} &= -9.5 + 1.57\log(t_3) - 2.5\log\alpha + 1.79\log\left(\frac{L_{\mathrm{WD}}}{10^{-2}L_\odot}\right) \\ &- 5.72\log\left(\frac{100R_\odot}{R_{\mathrm{phot}}}\right) + 2.86\log\left(\frac{\rho_{\mathrm{phot}}}{3.5\times10^{-13}}\right) \end{aligned} \tag{1.19}$$

where α is the ratio of the luminosity at outburst to the Eddington luminosity. L_{WD} is the luminosity of the white dwarf and R_{phot}, ρ_{phot} are the radius and mass density of the photosphere at maximum, respectively. The physical basis for this relation is that brighter, faster novae erupt on more massive white dwarfs, which have accreted hydrogen–rich envelopes from their binary companion. The Eddington luminosities and hence the observed brightnesses of these objects are therefore higher than in low–mass white dwarfs. Large white dwarf masses are correlated with thermonuclear runaways on low-mass envelopes. Thus the roughly constant envelope ejection rate observed from novae leads to smaller values of t_3 for the brighter and faster novae on massive white dwarfs. Further analysis of the lightcurve data yields another empirical relationship[31], which gets useful in the determination of an extragalactic distance scale [Cohen 1985] : All novae seem to have the same luminosity 15 days after eruption. The mean value of this constant was determined to be

$$\begin{aligned} M(t_{15}) &= -5.74\pm0.60 \quad \text{[Pfau 1976]} \\ M(t_{15}) &= -5.60\pm0.45 \quad \text{[Cohen 1985]} \\ M(t_{15}) &= -5.23\pm0.16 \quad \text{[van den Bergh and Younger 1987]} \end{aligned}$$

and is a result of the minimum spread of absolute magnitudes at about 18 days after visual maximum derivable from the theoretical explanation (1.19).

[31] First reported from Buscombe and De Vaucouleurs (1955) .

Es gehören zwei dazu, die Wahrheit zu entdecken; einer, der sie ausspricht, und einer, der sie versteht.

Khalil Gibran

Chapter 2

Ionization in Nova Shells

2.1 Introduction

Nova outbursts are among the few astronomical events that evolve on a time–scale over which they can be studied directly in contrast to most other phenomena, which require the study of many objects, each at a different stage of evolution, from which then the evolution of a single object must be pieced together. The main matter of concern in this chapter will be the modelling of the time development of the ionization in the outflowing nova gas in view of the importance of the stage of ionization of the gas for the evolution of chemistry and dust formation.

The evolution of the ejecta can be deduced directly from the observations of the emission line spectrum and since different types of lines are seen in the various spectral regions it is important to bring together the observations in the ultraviolet, optical and infrared region for the construction of an accurate picture of the nova shell evolution.

In the spectra of some novae an infrared continuum excess could be detected, indicating dust heating by the strong ultraviolet radiation field emerging from the central nova atmosphere and reemission of the absorbed energy in the infrared spectral region[1]. The existence of dust in nova shells is now confirmed by numerous observations and can be described as a well established phenomenon characterizing one phase in the classical nova event. It seems, however, that dust formation in nova shells depends on some yet unknown intrinsic parameters, since the characteristic infrared excesses were not observed in all objects ([Sanyal 1974], [Gallagher and Ney 1976]).
Some authors ([Gallagher 1977] , [Mitchell and Evans 1984]) have given a criterion for the possibility of dust formation in terms of the decrease of visual brightness $\dot{m}_v$ by estimating the ionization, cooling and nucleation timescales. In several cases, however, the application of this criterion leads to wrong predictions concerning the occurence of grains ([Williams and Longmore 1984] , [Whitelock *et al.* 1984]). This is not too surprising as those criteria are too crude, for such a complex process as dust formation depending on temperature, density, elemental composition, velocity

[1]Observational results can be found in [Ney and Hatfield 1978] ,[Vrba *et al.* 1977] , [Bode and Evans 1981] , [Snijders *et al.* 1987]

and photon field in the nova shell. Thus a more detailed treatment of the time evolution of the ionization and temperature structure in nova shells and a quantitative treatment of the network of chemical reactions operating in the shell is required for a more detailed understanding why and how dust is formed in nova shells.
Gallagher (1977) has pointed out, that molecule and dust formation is not possible in regions where hydrogen is ionized. In these regions all elements of high abundances heavier than H are ionized, too, except perhaps for helium, which is unlikely to play any role in the chemistry of dust formation. The strong Coulomb repulsion between ionized atoms then efficiently suppresses the formation of chemical bonds between elements like H, C, N, O, Si etc. which are probably the main constituents of the dust material. Thus, the observed high efficiency of the dust formation process requires that at least one abundant and also neutral species is involved in the reaction path from atoms to dust which in turn demands that hydrogen is predominantly neutral in the dust-forming region. In this context the important question arises whether carbon is ionized in the HI zone or not, since

- most novae seem to form carbon dust ([Gehrz 1990])
- an ion-neutral chemistry in a CII region has completely different reaction paths, reaction timescales and probably different reaction products than a neutral chemistry in a CI region.

A second indispensible requirement for the efficient formation of chemical bonds is a low gas temperature ($\leq 1000\,K$) since otherwise most chemical bonds would rapidly dissociate again, once they have formed, except for a handfull of small molecules with an extremely high bond energy like CO, N_2, SiO etc., which can be formed and survive at rather high temperatures. Thus a realistic calculation of the temperature in the HI region of a nova shell is required to determine the conditions for the existence of a sufficiently neutral and cool region where molecule and dust formation becomes possible. This will determine the initial conditions being an important prerequisite for the study of the chemistry in nova shells.
Mitchell and Evans (1984) have determined the ionization structure by calculating the Stroemgren spheres and the time scale for the complete ionization of hydrogen and carbon on the basis of the assumptions

- that the expansion of the ionized regions due to the decreasing density in the expanding shell and the increasing effective temperature of the nova pseudoatmosphere is quasi static and
- that the ionization of carbon and hydrogen can be considered as independent from each other.

From their calculations they conclude that carbon in the ejecta becomes ionized within a few days after outburst, so the implication would be unavoidable that the nucleation and growth of carbon grains must originate from a predominantly ionized monomer. However, while their assumptions are essentially satisfactory for hydrogen due to its dominant abundance, for carbon these approximations are too crude since they neglect the enhanced recombination of carbon in the HII zone due to the high density of electrons in this region produced by H ionization. This leads to a strong underestimation of the consumption of photons from the energy interval between the ionization edges of C and H in the HII region and a corresponding severe underestimation of the time required for ionizing carbon in the neutral shell ahead of the HII zone. Rawlings and Williams (1987) in their discussion of the chemistry in novae have refined the calculations of Mitchell and Evans (1984) for the ionization structure by improving the calculations of the number of ionizing quanta, but again assumed independence of the ionization of C and H from each other. Additionally the temperature structure used for their calculations was based on the simplifying assumption of an exponential cooling law.

In this work a more consistent treatment of the ionization and temperature structure in nova shells is presented. These computations are a first part in the investigation of the chemical evolution and the dust formation processes in the expanding shells of classical novae (see Chap. (4)).

Consistent computations of the dynamical evolution of the hydrogen ionization in nova shells for the case of a pure hydrogen shell were already performed by Bosma (1972, 1975a, 1975b)[2].

The treatment of the ionization problem used here is based on a generalization of the methods of Bosma for a mixture of the elements H, He, C, N, O, Na, Fe, Si, Mg and S.

Because the potentials of higher stages of ionization exceed the ionization potential of hydrogen for all elements and, thus, higher ionized atoms can occur only within the HII region, we only consider the first stage of ionization for each element [3].

For the description of the ionization in expanding nova shells it is necessary to recall some basic properties of ionized gases and those processes which govern the ionization state of the matter.

2.1.1 Basic Aspects of Plasmas

Matter can exist in a variety of stable forms which are governed by the physical environment. The normal classification of stable states is that of the solid, liquid and gas. Just as the solid is characterized by a rigid, dense lattice structure; a liquid by a dense non-rigid fluid and a gas by a low density randomized collection of atoms and molecules; so a plasma can be considered as an ionized gas consisting

[2] Bosma (1975b) claims that the deep minimum observed in the lightcurve of several novae (T Aurigae (1892), V450 Cygni (1942), DQ Herculis (1934) and V732 Sagitarii (1936)) can be attributed to the time evolution of the optical depths of the nova shell, which is controlled by recombination of hydrogen in the outer shell parts. Bosma does not take into account the now well established fact of the existence of grains in nova envelopes.

[3] Higher stages of ionization are already observable in early stages of the nova explosion (see section (1.3)).

of electrons, ions and neutral atoms or molecules. Although these states of matter are dominating life on planet earth almost all matter in space can be considered to be a plasma. The plasma state is said to be established when the number of ions and electrons in the gas are sufficiently numerous for their presence to dominate the behaviour of the system. In the context of astrophysics there are a lot of examples

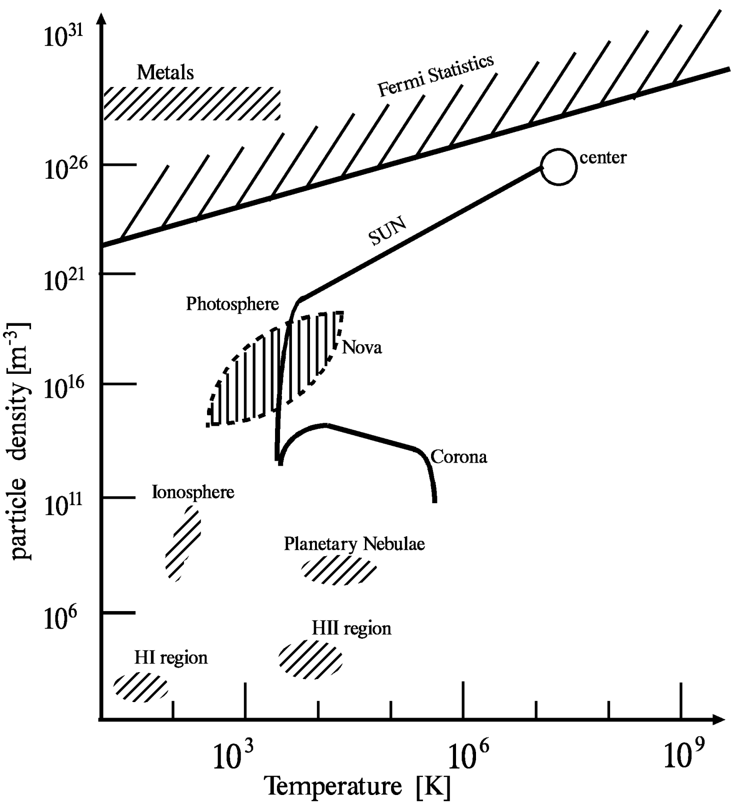

Figure 2.1: Typical astrophysical plasmas characterized by their temperature (Energy) and density. The various regions of the sun are depicted as solid lines for the corona and the photosphere and a light cicrcle for the center. The region covered by the nova shell is represented by a shaded area enclose by a broken line.

for the outstanding role of plasmas in the universe. Our own sun and the stars have surface temperatures in the range from some thousands of degrees to about 70,000 Kelvin, so they are partially to fully ionized in their surface layers and always in their hot fully ionized interiors. Also the space within the stars of a galaxy is filled with a rarified plasma with the average density of about one atom per cubic centimetre. In the neighbourhood of a star a well defined volume, the so called

Stroemgren sphere, with a radius depending on the intensity of the stellar radiation field exists, where the gas is completely ionized. Some typical astrophysical plasmas with their characteristic densities and temperatures are shown in Fig. (2.1). In Classical Novae the plasma state of the matter is deeply involved in various phases of the evolution of the close binary system; in the accretion period as well as in the outburst event and, most interesting for this work, in the ejected gas of the expanding shell. Spectroscopic observations in the early postmaximum phase [Seitter 1990] of the outflowing material show that there are neutral species (OI, NI) as well as ions (FeII, CaII). In later phases of the nova, when the density has substantially decreased one can look increasingly deeper into the inner shell where layers of high temperature are located. Then we see broad lines of ionization stages corresponding to the highest ones observed in normal stellar spectra as NIII and NV.
For the purpose of this work it is advantageous to remember, that the aim is not to develop a complete nova model including the geometrical and hydrodynamic structure of the nova envelope, but instead to look particularly for certain aspects as the time dependent ionization structure preceding the processes of chemistry and dust formation in the gaseous shell. So it is necessary to recall some basic correlations of gases which apply to plasmas as well as to neutral gaseous environments.
Under the conditions of thermodynamic equilibrium at a gaskinetic temperature T the velocity distribution function f(v) of particles of a gas with a speed in the interval v and v+dv is given by the Maxwell–Boltzmann distribution

$$f^{MB}(v) \;=\; \frac{4}{\pi} \cdot \left(\frac{m}{kT}\right)^{\frac{3}{2}} \cdot v^2 \exp\left[-\frac{mv^2}{2kT}\right] \tag{2.1}$$

with m being the mass of the regarded species. The assumption of local thermodynamic equilibrium also allows for a simplified representation of the distribution of the population density of the excited states of atoms[4]. If χ_k is the excitation energy of the k–th state above the ground level and n_0 the number density of atoms in the ground state, the number of atoms in the excited state k is given by

$$n_k \;=\; \frac{g_k}{g_0}\, n_0 \cdot \exp\left(-\frac{\chi_k}{kT}\right) \tag{2.2}$$

where g_0 and g_k are the statistical weights of the ground level and the excited state respectively. Considering a typical nova situation characterized by the values

$$\frac{g_k}{g_0} \approx 1 \quad \chi_k \approx 10eV \quad T_e \approx 10^4 K$$

we get a relation of atoms in the excites state i to atoms in the ground state of approximately 10^{-2}. So, for a good approximation the atoms may be considered as being in the ground level, which greatly simplifies the calculation of the ionization structure [5].

[4]This is important for the calculation of the heating rates by ionization of excited H-levels.

[5]For the calculation of the heating rate in the model calculations of the nova chemistry the non-LTE level population of the H-atom is taken into account

2.2 Ionization and Recombination Processes

In astrophysical environments atoms and molecules are subject to various processes which may alter their state of energy, momentum and their composition. One class of interactions we are especially interested in are those processes which lead to a change in the charge of a particle. A short overview about the processes is given in Fig. (2.2)

2.2.1 Photoionization

Photoionization probably is the most important process for the calculation of the ionization structure in nova shells. Therefore it is desirable to give a short overview of the theoretical description of this process and its implications in the framework of the formulation of the ionization problem in nova shells.
From the theory of the interaction of radiation with matter (see e.g. [Marr 1968]) it is possible to derive expressions which relate the oscillator strength and the integrated absorption cross–section for a narrow line to the suitable matrix elements in the electric dipole approximation. For the theoretical study of the photoionization process it is necessary to extend these relations to account for the fact that, while the initial state is in a discrete, bound spectral level, the final state lies in the continuous spectrum. The absorption of high energy radiation by an atom in a bound state results in the ejection of one of the outermost electrons into a free state of positive energy in the continuum, with energy $(1/2)mv^2$ and related to the energy of the absorbed photon by

$$h\nu = h\nu_i + \frac{1}{2}m_e v_e^2$$

where hν_i is the threshold energy of ionization and m$_e$ and v$_e$ are the mass and velocity of the electron, respectively. Absorption is of course possible for a continuum range of photon energies above the threshold. The photoionization cross–section associated with a particular frequency ν can be written according to [Ditchburn and Öpik 1962]

$$\sigma_\nu = \frac{8\pi^3 e^2 \nu}{3cg_i h\nu'} \cdot |M_{if}|^2 \tag{2.3}$$

where hν' is the energy of the photon in excess of the ionization threshold, g$_i$ is the statistical weight of the initial discrete state and M$_{if}$ is the matrix element defined by

$$|M_{if}|^2 = \sum_i \sum_f \left| \int \psi_f^* \sum_\mu r_\mu \psi_i d\nu \right|^2 \tag{2.4}$$

with the initial wave function ψ_i normalized in the usual way to unity and i,f denote the initial and final state of the process, respectively. The summation is carried out

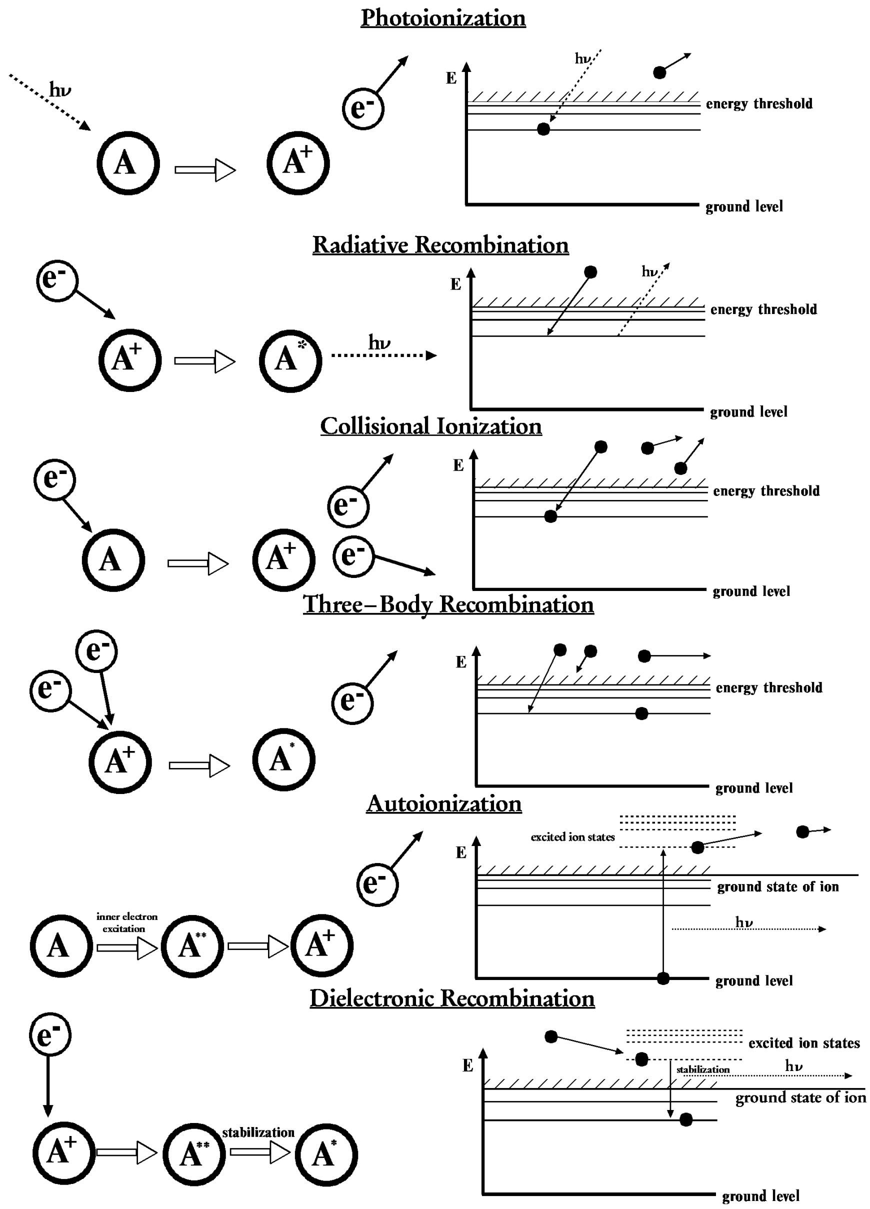

Figure 2.2: Schematic sketch of various processes of interest occuring in a plasma and contributing to the ionizational balance.

---

over the degenerate states of both levels i and f. The ψ_f represent the continuum eigenfunctions which are normalized to

$$\int \psi_f^*(E')\psi_f(E)d\nu \; = \; \delta\,(E' - E) \tag{2.5}$$

where δ is the Dirac delta function. The application of the classical electrodynamic principles outlined above lead to the calculation of the photoionization cross–section of a hydrogen like atom of charge $\mathcal{Z}$ in the theoretical work of Kramers

$$\sigma_H(n) = \frac{64\pi^4 e^{10} m \mathcal{Z}^4}{3\sqrt{3} c h^6 \nu^3 g_n n^3} \tag{2.6}$$

where n is the initial Bohr state of the atom. The quantum–mechanical treatment of this problem leads to an additional Gaunt factor G in Eq. (2.6) to account for the derivations from the classical theory. For energies not in the direct vicinity of the ionization threshold the Gaunt factor does not differ more than 10-20 % from unity and for practical purposes the use of the so called Kramers formulae (2.6) is sufficiently accurate.
The investigation of the photoionization cross-section for non–hydrogenic ions involve more elaborate computation techniques to account for the interaction forces in a many electron system (for an overview see [Marr 1967]). Generally the calculated cross-sections are given by analytic expressions, which fit the cross–section by a series of terms containing various powers of the form

$$\sigma(E) = \sigma_0 \cdot \left(\frac{E}{E_0}\right)^s \tag{2.7}$$

for specific ranges on the ν–scale ([Chapman and Henry 1971, Schmutzler 1987]). More recent explorations of the photoionization cross–sections by Yakovlev et al. [Band *et al.* 1990, Yakovlev *et al.* 1992] use a universal fit function of the form

$$F(y) = \left[(y-1)^2 + y_w^2\right] y^{-Q} \left(1 + \sqrt{\frac{y}{y_a}}\right)^{-P} \tag{2.8}$$

with

$$y = \frac{E}{E_0}, \quad Q = 5.5 + l - 0.5\,P\,, \quad \sigma(E) = \sigma_0 F(y) \tag{2.9}$$

and E_0 is the threshold energy, σ_0 the cross–section at the threshold, l an orbital quantum number of the atomic shell and y_w, y_a and P are fitting parameters.
The data used in this work are given in the Appendix.

2.2.2 Radiative Recombination

Recombination between electrons and even the simplest positive ions, those of hydrogen, normally involves a complicated series of events. Electrons and positive ions may unite by collisional–radiative recombination, a process which tends to radiative recombination in the low density plasma limit and to collisional recombination in the high density limit (see Chap. 2.2.3).
In a transition from a free state to a bounded level energy is liberated which may be radiated

$$H^+ + e^- \Longrightarrow H^* + h\nu \tag{2.10}$$

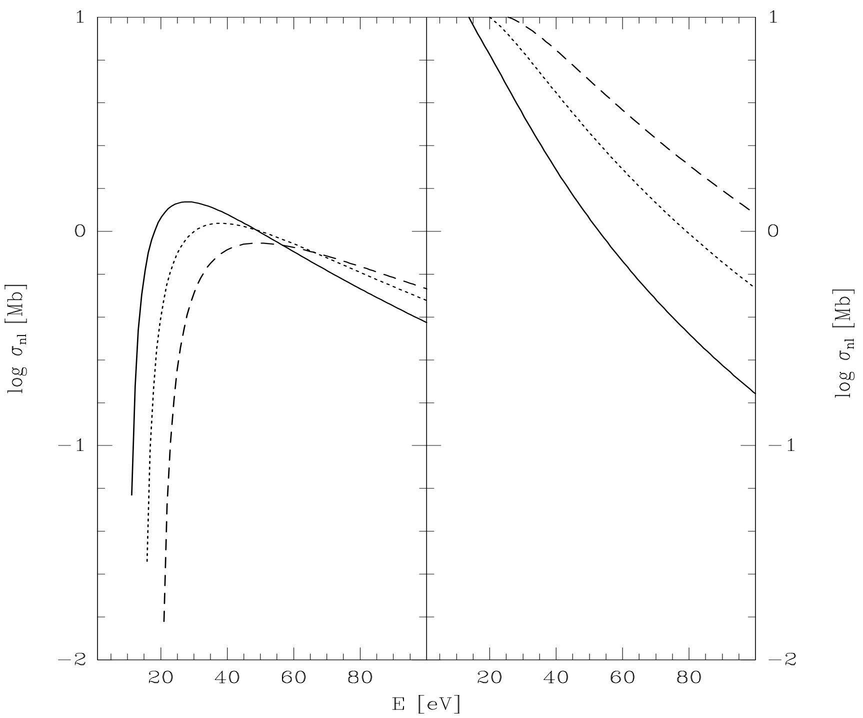

Figure 2.3: Photoionization cross–sections in Megabarn versus the energy of the incident photons in electron volts for the elements C (solid line), N (dotted line) and O (dashed line) showing the results for the quantum levels 2s (left diagram) and 2p.

where H* denotes an excited state, or it may be donated to another electron by

$$H^{+}+e^{-}+e^{-}\Longrightarrow H^{*}+e^{-}. \tag{2.11}$$

These processes cannot in general be considered in isolation. The atoms initially are in highly excited states after they have recombined and they may be re-ionized by the inverse process of (2.11)

$$H^{*}+e^{-}\Longrightarrow H^{+}+e^{-}+e^{-}. \tag{2.12}$$

Additionally they may also suffer collisional excitation

$$H(i)+e^{-}\Longrightarrow H(j)+e^{-} \qquad i<j. \tag{2.13}$$

or de-excitation

$$H(j)+e^{-}\Longrightarrow H(i)+e^{-} \qquad i<j. \tag{2.14}$$

where i, j denote the principal quantum numbers entered in the process.
If the energy or density of the plasma is too low for the collisional processes to have

an appreciable effect, the recombination coefficient α is defined by a rate equation for the two–body process (2.10):

$$\frac{dn(A^+)}{dt} = -\alpha\, n(e^-)\, n(A^+) \tag{2.15}$$

with n(A^+), n(e^-) being the number densities of the positive ions and electrons respectively. The electrons involved in this inelastic collision process have an initial energy distribution which depends on the incoming radiation field. As the elastic scattering coefficient for collisions between electrons is of the order $4\pi^2(e^2/mv^2)^2$ [Marr 1967] , these collisions tend to set up a Maxwell–Boltzmann energy distribution. Therefore all atomic processes occur at rates which are fixed by the local temperature defined by this energy distribution. Thus the recombination coefficient to a particular level characterized by the quantum numbers n,l may be written as [Massey *et al.* 1974]

$$\alpha_{nl}(A^0, T) = \int_0^\infty v\sigma_{nl}(A^0, v)\, f^{MB}(v)dv \tag{2.16}$$

and $f^{MB}(v)$ denotes the Maxwell–Boltzmann distribution function for the electrons as defined by (2.1). The total recombination coefficient is given by the sum over captures to all levels

$$\alpha = \sum_n \sum_{l=0}^{n-1} \alpha_{nl}(A^0, T) \tag{2.17}$$

For ions more complex than the hydrogenic ones the radiative recombination coefficient may be computed if the cross–section σ_{ai} of the reverse process of (2.10)is known and by using the Milne relations one obtains [Bates and Dalgarno 1962]

$$\alpha_{ia} = \frac{g_a}{g_i} \left\{ \frac{\sqrt{2} \exp \frac{h\nu_i}{kT}}{c^2 \sqrt{\pi}\, (mkT)^{\frac{3}{2}}} \right\} \int_{h\nu_a}^{\infty} (h\nu)^2 \sigma_{ai}(v) \exp\left[\frac{-h\nu}{kT}\right] d(h\nu) \tag{2.18}$$

where the subscripts denote the levels occupied and g_a, g_i are the statistical weights of A_i^+, A_a, respectively. For practical purposes the radiative recombination coefficients are fitted to expressions of the form [Aldrovandi and Péquinot 1973]

$$\alpha_{rad} = A_0 \left(\frac{T_e}{10^4}\right)^{-\eta} \tag{2.19}$$

using the parameters A_0 and η and giving α_{rad} with a good accuracy only for a specified range of temperatures $T_{min} \leq T_e \leq T_{max}$[6].

[6]The temperature ranges given by [Aldrovandi and Péquinot 1973] for the applicability of the formula (2.19) differ significantly for the species considered. For oxygen (OI) for example $T_{max} = 5 \cdot 10^4\,K$ and the critical temperature above which the dielectronic recombination gets important ($\alpha_{di} / \alpha_{rad} > 0.2$) is specified as $T_{crit} = 2.7 \cdot 10^4\,K$. The corresponding values for the single ionized carbon are: $T_{max} = 3 \cdot 10^4\,K$, $T_{crit} = 1.2 \cdot 10^4\,K$.

2.2.3 Autoionization and Dielectronic Recombination

Atoms with two or more bound electrons have doubly excited energy levels, that is, energy levels belonging to configurations with two excited electrons. If the energy of this doubly excited level p is higher than the ground state energy of the ion A^+, a radiationless transition

$$A^+ + e^- \Longrightarrow A_p \tag{2.20}$$

may take place in a plasma (see Fig.2.2). Of course also the reverse process of autoionization

$$A_p \Longrightarrow A^+ + e^- \tag{2.21}$$

is possible and under equilibrium conditions a steady but low population of the p–state is maintained. However, there is the possibility that this system can be stabilized against autoionization by means of transitions into a lower state not subjected to autoionization and denoted by the relation

$$A^+ + e^- \Longleftrightarrow A_p \longrightarrow A_b + h\nu_{pb} \tag{2.22}$$

The recombination rate for such a process than is given by

$$\frac{dn(A_p)}{dt} = n(A_p) \cdot P_{pb} \tag{2.23}$$

where P_{pb} is the spontaneous transition probability. The dielectronic recombination coefficient α_{di} depends on the population density of the autoionizing state though which is populated from the discrete bound state, so it follows that

$$n(A_p) = \frac{P_{ia}}{P_{pb} + P_i} n_s(A_p) \tag{2.24}$$

with P_i denoting the autoionizing probability and $n_s(A_p)$ is given by the Saha equation.

For a judging about the importance of the dielectronic recombination the following four parameter term to fit α_{di} is adopted from Aldrovandi and Péquinot:

$$\alpha_{di} = A_{di} T_e^{-\frac{3}{2}} \exp\left[-\frac{T_0}{T_e}\right] \left(1 + B_{di} \exp\left[-\frac{T_1}{T_0}\right]\right) \tag{2.25}$$

with A_{di}, B_{di}, T_0 and T_1 denoting the fit parameters and T_e representing the electron temperature. If we assume an electron temperature of T_e=5000 K we get by using the parameter values for single ionized carbon given in [Aldrovandi and Péquinot 1973]

$$\alpha_{di}(CI) = 1.9 \cdot 10^{-19}\, cm^3 s^{-1}. \tag{2.26}$$

This result has to be compared with the radiative recombination coefficient α defined by Eq. (2.19). For the same value of T_e one obtains

$$\alpha = 7.2 \cdot 10^{-13}\, cm^3 s^{-1}, \tag{2.27}$$

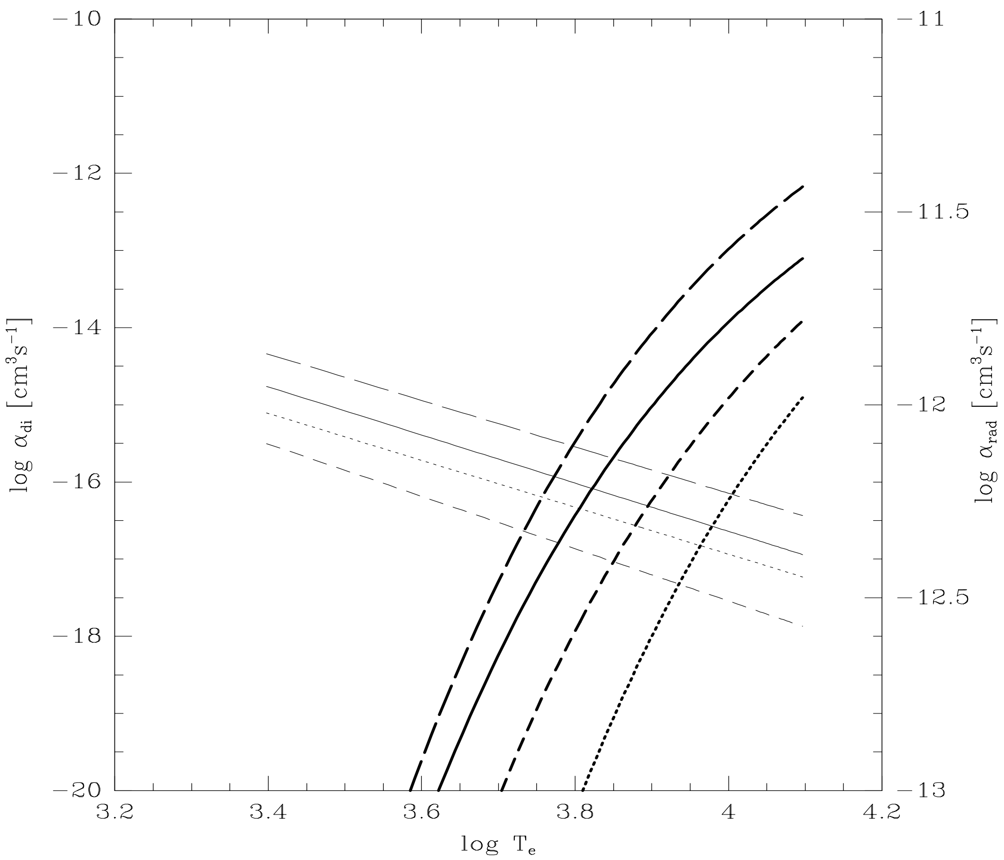

Figure 2.4: The dependence of the values for the dielectronic and the radiative recombination coefficients α_{di} (heavy lines) and α_{rad} (light lines) on the electron temperature T_e for the elements C (solid line), O (dashed line), N (dotted line) and Si (long–dashed line). Note the different scaling of the y–axis.

---

which clearly shows that for lower temperatures the process of dielectronic recombination can be neglected.
For higher electron temperatures as they are reached in typical HII zones ($T_e \approx$ 10,000 K) the corresponding values are

$$\alpha_{di}(CI) = 1.1 \cdot 10^{-14} cm^3 s^{-1}$$
$$\alpha_{rad}(CI) = 4.7 \cdot 10^{-13} cm^3 s^{-1}$$

and it is obvious that in this case the dielectronic recombination process serves a minor but not neglectable contribution to the total recombination coefficient α.

2.2.4 Collisional Ionization and Three-Body Recombination

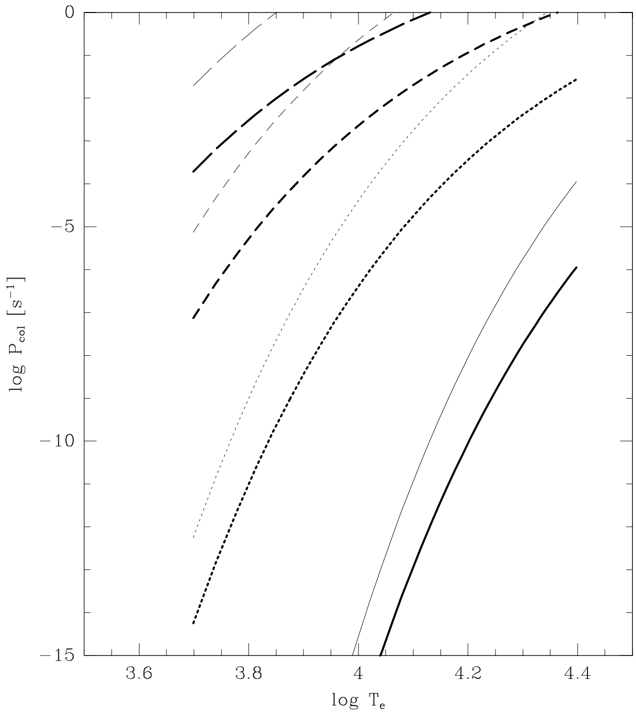

Figure 2.5: Dependence of the collisional ionization probability P_{col} for hydrogen on the electron temperature T_e for a set of quantum numbers n (n=2 (solid line), n=3 (dotted line), n=4 (dashed line), n=5 (long–dashed line)) for two different electron densities:
a) $n_e = 10^{10} cm^{-3}$ (light lines) and b) $n_e = 10^8 cm^{-3}$ (heavy lines). The data were taken from [Lang 1974] .

The process of collisional ionization and its reverse, the three–body recombination will be described not in detail but are considered for completeness. The semi-empirical formula for the probability P_{col} per unit time of a collisional induced ionization of a hydrogen–like atom is [Jeffries 1968]

$$P_{\rm col} \approx 7.8 \cdot 10^{-11} T_e^{1/2} n^3 \exp\left[-\frac{h\nu_n}{kT}\right] N_e \quad [s^{-1}] \tag{2.28}$$

with n denoting a principal quantum number and $h\nu_n$ the ionization energy of the n-th level above the ground state. If we consider a detailed balance between collisional ionization of atom A and the corresponding three–body recombination of A^+ we get

$$P_{\rm 3r} = \frac{n_e h^3}{(2\pi m_e kT)^{3/2}} \cdot n^2 \exp\left[\frac{h\nu_n}{kT}\right] \cdot P_{\rm col} \tag{2.29}$$

where the statistical weight of the n-th level is $g_n = 2n^2$. Obviously these processes do not significantly contribute to the ionization balance when the higher excitation levels are only thermally populated. In the case of optical thin nebulae it might be of importance for the calculation of the emission of radio recombination lines.

2.3 The Ionization Equation

Let f_i be the degree of ionization for atoms of species i, i.e., $n_i f_i$ is the number of ions and n_i is the particle density of species i. Then, at each point of the shell and for each species i the rate of photoionization is

$$\dot{n}_i^{ion} = n_i(1 - f_i) \int\limits_{\nu_i}^{\infty} \frac{4\pi J_\nu}{h\nu} \sigma_\nu^i \, d\nu \tag{2.30}$$

where J_ν is the mean intensity of radiation with frequency ν, σ_ν^i the ionization cross section for atoms of species i, ν_i the threshold frequency for ionization and h the Planckian constant.

Because only the stellar contribution to the radiation field inside the shell is considered and a blackbody radiation at the surface of the central nova atmosphere with photospheric radius R is assumed, one has

$$4\pi J_\nu = \left(\frac{R}{r}\right)^2 \pi B_\nu \, e^{-\tau_\nu} \tag{2.31}$$

where $r = R + V \cdot t$ is the distance of a particular point inside the shell as a function of time. The optical depth τ_ν within the shell as a function of the geometrical distance s from the inner shell boundary is defined as

$$\tau_\nu(s) = \int\limits_0^s \sum_{i=1}^{M} \sigma_\nu^i(x)(1 - f_i(x)) \, dx \ , \tag{2.32}$$

where M is the number of the species considered. Here it is assumed that $\tau = 0$ at the inner edge of the shell, i.e., the assumption is made that one has a negligible extinction by the matter between the nova photosphere and the inner edge of the shell. Then Eq.(2.30) changes into

$$\dot{n}_i^{ion} = n_i(1 - f_i) \left(\frac{R}{r}\right)^2 \int\limits_{\nu_i}^{\infty} \frac{\pi B_\nu}{h\nu} \sigma_\nu^i e^{-\tau_\nu} \, d\nu \ . \tag{2.33}$$

The recombination rate $\dot{n}_i^{rec}$ is

$$\dot{n}_i^{rec} = f_i n_i \alpha_i(T_e) n_e \tag{2.34}$$

where n_e is the electron particle density, $\alpha(T_e)$ the recombination coefficient and T_e the electron temperature.
By inserting

$$n_e = \sum_{j=1}^{M} f_j n_j \tag{2.35}$$

into (2.34), division of (2.33) and (2.34) by n_j, and equating the resulting equations, there results a system of differential equations for the time development of the ionization degree

$$\frac{df_i(\tau_{\rm M})}{dt} = a_i(\tau_{\rm M}) + b_i(\tau_{\rm M}) f_i(\tau_{\rm M}) + c_i(\tau_{\rm M}) f_i^2(\tau_{\rm M}) \tag{2.36}$$

for $i = 1, \ldots, M$. Here, the following abbreviations are used:

$$\begin{aligned} a_i(\tau_{\rm M}) &= \left(\frac{R}{r}\right)^2 \int\limits_{\nu_i}^{\infty} \frac{\pi B_\nu}{h\nu} \sigma_\nu^i e^{-\tau_\nu(\tau_{\rm M})} d\nu \\ b_i(\tau_{\rm M}) &= -\left(\frac{R}{r}\right)^2 \int\limits_{\nu_i}^{\infty} \frac{\pi B_\nu}{h\nu} \sigma_\nu^i e^{-\tau_\nu(\tau_{\rm M})} d\nu - \alpha_i \sum_{j\neq i} f_j n_j \\ c_i(\tau_{\rm M}) &= -\alpha_i n_i\,; \qquad i = 1, \ldots M\,. \end{aligned} \tag{2.37}$$

Eq.(2.37) yields a system of differential equations for the degree of ionization f_i for each species i. Its solution is described in section 2.3.2.

Numerical values required for calculating the coefficients entering into the above equations are taken from the following sources. The values for the ν_i are taken from Lang (1974) . The data for the ionization cross sections σ_i at the threshold frequencies are taken from Brown (1971) , Chapman and Henry (1971, 1972) , Henry (1970) and Osterbrock (1974). The recombination coefficients $\alpha_i(T)$ are computed by the fit formula and the data given by Aldrovandi and Péquignot (1973) and Osterbrock (1974). The effects of dielectronic recombination which are important for the heavier elements are included in the data of Aldrovandi and Péquignot (1973).

2.3.1 The Optical Depths Scale

The absorption cross sections σ_ν^i of the atoms i which are used in the calculations are fitted by power laws of the type

$$\sigma_\nu^i = \sigma(E_{A_i}) \cdot (E_{A_i}/h\nu)^{S_i}. \tag{2.38}$$

with

$$E_{A_i} \leq h\nu \leq E_{A_{i+1}} \quad ;\text{resp.} \quad E_{A_n} \leq h\nu \tag{2.39}$$

The constants $\sigma(E_{A_i})$, S_i and the appropriate division points E_{A_i} of the energy-scale are taken from Schmutzler (1987) .

Let the species i be labeled according to ascending order of the corresponding threshold frequencies

$$\nu_1 \leq ..... \leq \nu_i \leq ..... \leq \nu_M\ . \tag{2.40}$$

In all the models (see Chap. 2.5), ν_M is the threshold frequency of helium. Then the decomposition the frequency integral in Eq.(2.33) into a sum of integrals defined on the intervals defined by (2.40) leads to

$$\begin{aligned}
\int_{\nu_i}^{\infty} \frac{\pi B_\nu}{h\nu}\sigma_\nu^i e^{-\tau_\nu} d\nu &= \int_{\nu_i}^{\nu_{i+1}} \frac{\pi B_\nu}{h\nu}\sigma_\nu^i e^{-\tau_i(\nu)} d\nu \\
&+ \int_{\nu_{i+1}}^{\nu_{i+2}} \frac{\pi B_\nu}{h\nu}\sigma_\nu^i e^{-\tau_{i+1}(\nu)} d\nu + ... \\
&+ \int_{\nu_{M-1}}^{\nu_M} \frac{\pi B_\nu}{h\nu}\sigma_\nu^i e^{-\tau_{M-1}(\nu)} d\nu \\
&+ \int_{\nu_M}^{\infty} \frac{\pi B_\nu}{h\nu}\sigma_\nu^i e^{-\tau_M(\nu)} d\nu
\end{aligned} \tag{2.41}$$

$$i = 1, ...M$$

where

$$\tau_j(s) = \sum_{k=1}^{j} \sigma_\nu^k \int_0^s n_k(x)(1 - f_k(x))\, dx \tag{2.42}$$

$$j = 1, ...M$$

and s is the geometrical distance from the inner shell boundary.

As a standard optical depth scale $\tau = \tau_M$ is chosen. By differentiating Eqs.(2.42) with respect to s and dividing the resulting Eqs. by the equation for $j = M$, a set of differential equations is obtained

$$\frac{d\tau_j(\tau_\mathrm{M})}{d\tau_\mathrm{M}} = \frac{\sum_{k=1}^{j} \sigma_\nu^k n_k(\tau_\mathrm{M})\,(1 - f_k(\tau_\mathrm{M}))}{\sum_{k=1}^{M} \sigma_\nu^k n_k(\tau_\mathrm{M})\,(1 - f_k(\tau_\mathrm{M}))} \quad ; \tag{2.43}$$

$$j = 1, ...M \quad ; \quad \tau_j(0) = 0$$

which defines the optical depths $\tau_j, 1 \le j \le M - 1$ in terms of the reference scale τ_M. These equations are subject to the initial conditions $\tau_j = 0$ at $\tau_\mathrm{M} = 0$.

2.3.1.1 Calculation of the Radial Structure

The inverse of the M-th of the equations obtained by differentiating (2.42) with respect to s is used to calculate the geometrical scale s in terms of the reference scale $\tau_{\rm M}$. This differential equation

$$\frac{d\,s(\tau_{\rm M})}{d\,\tau_{\rm M}} = \left(\sum_{k=1}^{M} \sigma_\nu^k n_k(s)(1 - f_k(s)) \right)^{-1} \tag{2.44}$$

has to be solved with the initial condition $s(0) = 0$, to get the transformation of the τ_M–scale into the geometrical scale s at each time step.

If we assume an inverse square dilution form for the density, it can be seen from (2.33) that in this case f is independent of s and depends only on t. When, in addition, the variation of n_k over the shell is neglected, r can be calculated as a simple integral.

2.3.2 Solution of the Ionization Equation

From a discussion (e.g. by a semi–analytical integration of (2.36) as described by Tenorio–Tagle, 1976) of the relaxation time to a stationary solution it has been found that outside the ionization fronts, ionization equilibrium is established during a time interval of the order $1/a_i$ which is only a few seconds even for large distances ($r = 1000R$). Thus, this relaxation time is small compared to the time scale of expansion. For this reason, with very high accuracy the solution of (2.36) outside the ionization front is given by the stationary solution

$$f_i = -\frac{b_i}{2c_i} - \frac{1}{2c_i}(b_i^2 - 4a_ic_i)^{1/2} \ . \tag{2.45}$$

In principle the decrease of the ionization degree across the front has to be described by the exact solution of (2.36)

$$f_i(t + \Delta t) = \frac{f_i^o(E_iB_i - A_i) - A_iB_i + A_iE_iB_i}{f_i^o(1 - E_i) - A_iE_i + B_i} \tag{2.46}$$

where the f_i^o are the initial values of the ionization degrees at time t and Δt is the time step of integration, and

$$\begin{aligned} A_i &= \frac{b_i}{2c_i} + \frac{1}{2c_i}(b_i^2 - 4a_ic_i)^{1/2} \\ B_i &= \frac{b_i}{2c_i} - \frac{1}{2c_i}(b_i^2 - 4a_ic_i)^{1/2} \\ E_i &= \exp\left(-\Delta t(b_i^2 - 4a_ic_i)^{1/2}\right) \ . \end{aligned} \tag{2.47}$$

For the purpose of the calculations made in this work, the static approximation (2.45) suffices because the geometrical extensions of the fronts are small, as will be shown below. In the description of the dynamical evolution of the ionization front via the solution function (2.47) two particular cases are of special interest:

E=0 Inserting this value of the coefficient E into 2.47 one finds that this corresponds to a degree of ionization of f≈1. At the beginning of the expansion phase this is realized in the regions of small optical depth. At later phases of the expansion for $\Delta t \rightarrow$ inf the region of complete ionization is continuously growing.

E=1 This is true for sufficiently low radiation fields and one concludes from 2.46 that for the degree of ionization it follows $f=f_0$. For every time t a local minimum radiation field intensity and thus an optical depth is defined by E=1 determining the relation

$$b = 2\sqrt{ac} \tag{2.48}$$

for the coefficients of the ionization equation. For larger optical depths the gas will be neutral.

Basically the ionization structure of an expanding shell is described by these two borderline cases. Only in a small intermediate region of the nova envelope, which is of the dimension of the mean free path of an ionizing photon, the full solution of the ionization equation applies.

2.4 Heating and Cooling Processes in Nova Shells

From the law of conservation of energy one can derive the energy equation for the gas of the expanding nova shell. The change in the total energy per unit time in a volume element dV must equal the total flux of energy through the surface bounding of that volume. In a very general form considering the influence of thermal conductivity and viscous effects the energy balance can be written in one dimension as

$$\rho \frac{\partial}{\partial t} (c_v T) + \rho v_j \frac{\partial}{\partial x_j} (c_v T) = \frac{\partial}{\partial x_j} \left(\kappa \frac{\partial T}{\partial x_j} \right) - \rho P \frac{\partial v_j}{\partial x_j} + \varphi \tag{2.49}$$

where t is the time variable, c_v is the specific heat at constant volume, ρ the mass density, v the velocity and κ the coefficient of heat conduction. The rate φ at which energy is dissipated by viscosity is given by

$$\varphi = \frac{\mu}{2} \cdot \left(\frac{\partial v_i}{\partial x_j} + \frac{\partial v_j}{\partial x_i}^2 - \frac{4}{3} \left(\frac{\partial v_j}{\partial x_j}^2 \right) \right) \tag{2.50}$$

with μ being the coefficient of dynamic viscosity.
Whereas the effects of viscosity play an important role in the physics of accretion processes in close binary systems as nova systems are and heat conductivity must be taken into account for the description of the accretion layer on the white dwarf, these effects can be neglected in the expanding shell regions which are under consideration in this chapter. So Eq. (2.49) can be rewritten as [Field 1965]

$$n \frac{d}{dt} \left(\frac{3}{2} nkT \right) - \frac{5}{2} nkT \frac{dn}{dt} = \mathcal{G} - \mathcal{L} \tag{2.51}$$

where n is the number density of free particles and $\mathcal{G}$ and $\mathcal{L}$ denote the rate of energy gain or loss per unit volume, respectively. The first term of the left hand side of Eq. (2.51) represents the rate of increase of thermal energy of the gas whereas the second one represents the work done by the gas.
In our case the temperature[7] can be fixed by the equilibrium between photionizational heating and cooling by recombination, hydrodynamic expansion as well as radiation energy which can escape from the shell[8]. If an atom is ionized by a photon of the energy hν, a photoelectron is created carrying away the excessive photon energy above the ionization limit hν_0 of atom A, which means that

$$\frac{1}{2} m_e v_e^2 = h (\nu - \nu_0) . \tag{2.52}$$

A short estimate of the mean time $t_{\rm coll}$ between two collisions of such an electron can be obtained by using the relation

$$t_{\rm coll} \approx \frac{1}{\alpha_i n_i f_i} \tag{2.53}$$

[7]This is true in the case of the existence of an overall equilibrium temperature being valid for all species contained in the specified volume

[8]A more detailed treatment of the molecular cooling processes is given in Chap. (4.2.4)

where $n_i f_i$ is the particle density of the most abundant ion species in the zone under consideration and for the electron density we assume

$$n_e \approx n_i f_i \quad . \tag{2.54}$$

By taking the results for the electron density in Chap. (2.5) one yields:

$$t_{\text{coll}} = \begin{cases} 10^1\, s & \approx \quad \text{highly ionized region (HII zone)} \\ 10^3\, s & \approx \quad \text{moderately ionized region (CII zone)} \\ 10^5\, s & \approx \quad \text{neutral zone} \end{cases} \tag{2.55}$$

so that in the ionized zones the electrons are quickly thermalized. In the situation of ionization equilibrium the photoionizations are balanced by an equal number of recombinations. As a consequence of every recombination process a thermal electron disappears and on the average the energy quantity $\frac{1}{2} m_e \overline{v_e}^2$ is taken away from the gas. This means that the subtraction of this mean energy from the mean energy of a newly produced photoelectron leads to the net gain in energy by the electron gas per ionization process
This energy gain is balanced by the energy loss caused by radiation processes, mainly by electron collisional excitation of bounded levels of abundant species, followed by emission of photons that can escape from the nova shell.

2.4.1 Heating Mechanisms

2.4.1.1 Ionizational Heating

The gas is heated by photo-ionization of abundant elements due to the UV-radiation of the central nova atmosphere. The energy input rate to the gas is

$$\mathcal{G}(n_i) = n_i(1 - f_i) \int\limits_{\nu_i}^{\infty} \frac{4\pi J_\nu}{h\nu}\, h(\nu - \nu_i)\, \sigma_\nu^i \, d\nu \, . \tag{2.56}$$

If ionizational equilibrium is realized the neutral particles

$$n_0 \;=\; n_i(1 - f_i) \tag{2.57}$$

may be eliminated by using

$$\underbrace{n_0 \int\limits_{\nu_i}^{\infty} \frac{4\pi J_\nu}{h\nu} \sigma_v d\nu}_{ionisations} \;=\; \underbrace{n_i f_i n_e \alpha}_{recombinations} \tag{2.58}$$

and one yields

$$\mathcal{G}(n_i) \;=\; n_e n_i f_i \alpha \frac{3}{2} k T_i . \tag{2.59}$$

Basically it can be stated that the mean energy of a newly created photoelectron does not depend on the absolute strength but on the form of the ionizing radiation field, whereas the rate of the photoelectron production depends on the radiation field strength. The mean energy of an electron just produced by photoionization is represented by $\frac{3}{2}\mathrm{kT}_i$, where T_i is the initial temperature of a newly created photoelectron[9]. As the high energy photons penetrate deeper into the shell, the mean electron energy increases with increasing optical depth.

2.4.1.2 Heating by Radioactive Elements

Classical nova outbursts are known to be associated with the occurence of thermonuclear runaways proceeding in accreted hydrogen rich shells on the white dwarf component of a nova binary system[10]. In such outburst events an environment is provided in which hydrogen–burning reactions proceed on carbon, nitrogen, oxygen and heavier nuclei at high temperatures (1.5 – $4{\cdot}10^6$ K) and densities. Under these conditions the production of the radioactive isotopes ^{22}Na and ^{26}Al occurs on a detectable level [Wiescher *et al.* 1985]. Especially in the case of ONeMg novae occuring on more massive white dwarfs where abundances enrichments of elements in the range from neon to aluminium are presumed to arise as a result of the dredge–up of core matter [Truran and Livio 1986] a highly increased production of ^{22}Na and ^{26}Al occurs. Theoretical estimates of the frequency of occurence of such events [Politano *et al.* 1990] and spectroscopic analysis of the ejecta of recent novae ([Snijders *et al.* 1987], [Snijders 1990]) both indicate that such neon rich novae comprise approximately $1/4^{th}$ to $1/3^{rd}$ of all observed classical nova events [Mahoney *et al.* 1982] .
However, observations of the diffuse 1.275 MeV [Mahoney *et al.* 1982] and the 1.809 [Mahoney *et al.* 1984] emission by gamma–ray spectroscopy with the HEAO 3 have shown that there exist substantial amounts of ^{26}Al and ^{22}Na in the interstellar medium resulting from nova explosions. From the comparison with numerical simulations with the HEAO 3 observations [Higdon and Fowler 1987] an upper limit of $5.6 \cdot 10^{-7} M_\odot$ for the mean ^{22}Na yield per energetic ONeMg nova is derived. Addressing now the question of the energetical contribution of those radioactive elements to the overall energy balance in the envelope, it is clear that only the contribution of ^{22}Na, having a decay time comparable to a typical nova outburst duration, must be taken into account. By using the maximum yield for the ^{22}Na production in ONeMg–novae one can derive an upper limit for the energy input $\mathcal{G}_{\mathrm{RD}}$ by the decay of ^{22}Na of

$$\mathcal{G}_{\mathrm{RD}} \approx 2 \times 10^{-8}\, erg cm^{-3} s^{-1}\,, \tag{2.60}$$

[9]For a blackbody energy–distribution of the incident photons with $J_\nu = B_\nu(T_*)$, T_i equals the stellar temperature.

[10]The development of the thermonuclear runaway theory is due to the work of ([Gallagher and Starrfield 1978], [Starrfield *et al.* 1974a], [Starrfield 1989]).

which is in reasonable agreement with the calculations of [Livio *et al.* 1992] .
It is obvious that only a small fraction of this maximum γ–ray energy is transformed to lower energies where the optical depths are high enough for photoabsorption. Most of the γ–rays will escape from the envelope or be degraded to X–rays by multiple scattering processes[11] A more detailed treatment of the energy conversion process by [Gass 1990] has confirmed the crude estimate made above, thus we can conclude that the decay of radioactive elements does not play an important role in the energy balance in nova envelopes.

2.4.2 Cooling Processes

The gas is cooled by several processes, which are well known from gaseous nebulae: Cooling by collisionally excited forbidden line emission (usually the most efficient cooling mechanism), cooling by recombination (usually not very important) and cooling by free-free transitions (usually negligible). Additionally, one has to consider the effect of cooling by hydrodynamic expansion, which is very important for nova shells, since the gas rapidly expands. A discussion of cooling by forbidden lines is given in Sect. (2.4.2.4). The cooling rates of the other processes are discussed by (c.f. Osterbrock, 1974).

2.4.2.1 Recombination Cooling

The energy loss rate for the electron gas due to recombination processes can be written as

$$\mathcal{L}_{rec}(n_i) = f_i n_i^+ n_e \beta_i(T_e) k T_e \,. \tag{2.61}$$

The coefficient β_i for cooling by recombinations is calculated as follows. A relation between this coefficient and the recombination coefficient α_i can be derived by differentiation of the defining equation for $\alpha(T_e)$ with respect to T_e and comparing the result with the defining equation for $\beta_i(T_e)$. It follows

$$\beta_i = \frac{d\alpha_i}{dT_e} \cdot T_e + \frac{3}{2}\alpha_i \ . \tag{2.62}$$

This relation is used for computing the recombination cooling coefficients β_i from the recombination coefficients α_i.

2.4.2.2 Hydrodynamic Expansion

The cooling rate due to hydrodynamic expansion is given by the expression

$$\mathcal{L}_{exp} = kT\frac{dn}{dt} \quad . \tag{2.63}$$

[11] Even the predicted soft X–ray luminosity [Livio *et al.* 1992] produced in ONeMg–novae will be orders of magnitude lower than the γ–ray luminosity.

In the HII-part of a nova shell, all relaxation processes are fast enough that equilibrium between heating and cooling processes is rapidly established. This is not completely true in the outer HI-shell. There, the relaxation times are shorter than the characteristic timescale of hydrodynamic expansion, but not very short compared to this. Thus, in principle, the temperature has to be calculated from the time dependent energy equation. As this effect, however, is only important in the very early phases of the shell expansion, for simplicity the sum of the heating rates is equaled to the sum of all cooling rates. This yields an equation, which determines the temperature structure in the nova shell for the stationary case.

2.4.2.3 Free-Free Cooling

If a charged particle encounters an ion it is accelerated and emits continuous radiation called Bremsstrahlung. The cooling rate $\mathcal{L}_{ff}$ by this process involving ions of charge Z is

$$\mathcal{L}_{ff} = 1.42 \cdot 10^{-27} \cdot Z^2 T_e^{1/2} n_e^2 \,. \qquad (2.64)$$

Only singly ionized ions are important in our case.

2.4.2.4 Cooling by Forbidden Line Emission

Generally the principal physical processes determining the cooling by forbidden line emission in the expanding nova shell are identical with the processes in gaseous nebulae. The conditions for the formation of these lines, however, are different because

(i) the particle densities during the early phase of the shell expansion are much higher than those usually encountered in HII-regions and planetary nebulae and

(ii) the gas is expanding at extremely hypersonic velocities with the result **that the Doppler-shift of lines becomes very important for the escape probability of photons.**

Thus, this process has to be considered in some detail.

a) Optical Depth of Lines

First the Doppler-shift between two gas elements at mutual distance s is considered. For convenience, the following considerations the well known p-z coordinate system (cf. Fig. 2.6) is used. Then

$$\cos\theta_1 = \frac{z_1}{r_1} \quad , \quad \cos\theta_2 = \frac{z_2}{r_2} \qquad (2.65)$$

and we obtain for the projection of the constant radial expansion velocity v onto the ray through the two gas elements

$$v_{||1} = v \cdot \frac{z_1}{r_1} \quad , \quad v_{||2} = v \cdot \frac{z_2}{r_2} \, . \tag{2.66}$$

The gas element at *position 2* expands with respect to the gas element at *position 1* with the radial velocity

$$w = v \cdot \left(\frac{z_2}{r_2} - \frac{z_1}{r_1} \right) \, , \tag{2.67}$$

which may be written as (cf. Fig. (2.6))

$$w = v \left[\frac{s + z_1}{\sqrt{p^2 + (z_1 + s)^2}} - \frac{z_1}{\sqrt{p^2 + z_1^2}} \right] \, . \tag{2.68}$$

The frequency of a photon emitted at position 1 in the direction of the ray with

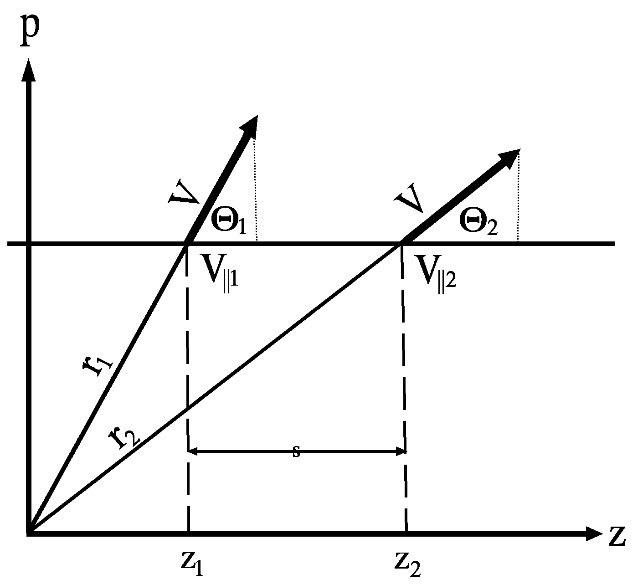

Figure 2.6: Geometry of the p-z coordinate system for calculating the frequency shift of photons due to Doppler-shift.

frequency ν_0 in the rest frame of the matter is observed at position 2 in the local frame of rest at frequency

$$\nu = \nu_0 - \frac{\nu_0}{c} \cdot w \, . \tag{2.69}$$

If ν_0 corresponds to the frequency at the line centre of an emission line the observed shift of the line centre at position 2 is given in terms of the Doppler-width of the line as

$$\frac{\Delta\nu}{\Delta\nu_{\mathrm{D}}} = -\frac{v}{v_{th}}\left[\frac{s+z_1}{\sqrt{p^2+(z_1+s)^2}} - \frac{z_1}{\sqrt{p^2+z_1^2}}\right] \tag{2.70}$$

with

$$\Delta\nu_{\mathrm{D}} = \frac{\nu_0}{c}\cdot v_{th} \quad , \quad v_{th} = \sqrt{\frac{2kT}{m}}\,. \tag{2.71}$$

Since for an expanding nova shell $v \gg v_{th}$ (typically, one has $v_{th} \approx 10$ km·s^{-1} and $v \geq 500$ km·s^{-1}), this frequency shift becomes large compared to $\Delta\nu_{\mathrm{D}}$ over a very short distance s as compared to r_1. Then, expanding (2.70) with respect to the small quantity s/r_1 yields

$$\frac{\Delta\nu}{\Delta\nu_{\mathrm{D}}} = -\frac{v}{v_{th}}\cdot\frac{s}{r_1}\cdot\left(1-(\frac{z_1}{r_1})^2\right) \tag{2.72}$$

or, in a different form,

$$\frac{s}{r_1} = -\frac{\Delta\nu}{\Delta\nu_{\mathrm{D}}}\cdot\frac{v_{th}}{v}\cdot\left(1-(\frac{z_1}{r_1})^2\right)^{-1}\,. \tag{2.73}$$

These relations are valid as long as z_1 is not extremely close to r_1. This last case corresponds to a ray with an extremely small inclination θ_1 to the radial direction, where one obviously has only a negligible radial velocity between different gas elements. Assuming the most unfavourable case that position 1 corresponds to the inner shell boundary R and s to the shell thickness Δr, one obtains by means of Eq.(2.65) and (2.73) for the inclination angle θ_{cr} of a ray for which the frequency shift at the outer boundary corresponds to just one Doppler-width

$$\theta_{cr} = \frac{v_{th}}{v}\cdot\frac{R}{\Delta r} \ll 1\,. \tag{2.74}$$

This angle defines a cone, where photons emitted in the Doppler core of a line remain within the Doppler core as seen by different observers along the ray for all rays within this cone. For rays not within this cone, the photons are rapidly Doppler shifted out of the line core for different observers along the ray in their reference frames.

Then, for rays intersecting the radial direction at angles $\theta_1 \geq \theta_{cr}$ the same simplifications can be made as by Castor (1970) in his calculation of line formation in WR-star envelopes. The optical depth at frequency ν along a ray starting at position 1 and going out of the shell is

$$\tau(\nu,p,r_1) = \int\limits_0^{\sqrt{(R+\Delta r)^2-p^2}-z_1} \kappa(\nu,p,s)\,ds \tag{2.75}$$

with

$$\kappa(\nu, p, s) = \kappa_0\,(r_1)\,\Phi(\nu + \frac{\nu_0}{c} w(s) - \nu_0) \tag{2.76}$$

where

$$\begin{aligned}\kappa_0(r_1) &= \frac{\pi e^2}{m_e c^2}\,(gf)_{\ell u}\left(\frac{N_\ell(r_1)}{g_\ell} - \frac{N_u(r_1)}{g_u}\right)\\ &= \frac{g_u A_{u\ell}\lambda^2}{8\pi}\left(\frac{N_\ell(r_1)}{g_\ell} - \frac{N_u(r_1)}{g_u}\right)\end{aligned} \tag{2.77}$$

is the absorption coefficient at the line centre, Φ the line profile function, N_ℓ and N_u the occupation numbers of the lower and upper level, respectively, and all other quantities have their usual meaning. The upper limit of the integral (2.75) is the distance between position 1 and the outer boundary of the shell in the direction of the ray.

The absorption coefficient κ_ν can be taken out of the integral (2.75) since it is at most slowly varying compared to the variation of Φ due to the Doppler shift. If position 1 is not too close to the boundary or ν not too far in the wings of the line, then Φ rapidly vanishes with increasing s and the upper limit of integration in (2.75) can be replaced by infinity. With some elementary transformations one obtains

$$\tau(\nu, p, r_1) = \kappa_0\,\frac{r_1}{\frac{\nu_0 v}{c}}\,\frac{1}{1-(\frac{z_1}{r_1})^2}\int_{-\infty}^{\Delta\nu/\Delta\nu_{\rm D}}\Phi(y)\,dy \tag{2.78}$$

which corresponds to the result of Castor (1970). At the line centre ($\Delta\nu = 0$) the optical depth along the ray is

$$\tau(\nu_0, p, r_1) = \frac{1}{2}\,\kappa_0\,\frac{r_1}{\frac{\nu_0 v}{c}}\,\frac{1}{1-(\frac{z_1}{r_1})^2}\,. \tag{2.79}$$

Typical values for an expanding nova shell are $r_1 = 10^{14}$cm, $v = 10^8$cm·s^{-1} and typical particle densities are of the order of $n \approx 10^9$cm^{-3}. With a typical wavelength $\lambda = 5000$ Å one obtains

$$\begin{aligned}\tau_0 &= \frac{1}{2}\kappa_0\frac{r_1\lambda}{v} = 6.6\cdot 10^8 (gf)_{u\ell}\left(\frac{\tilde N_\ell(r_1)}{g_\ell} - \frac{\tilde N_u(r_1)}{g_u}\right)\\ &= 4.9(g_u A_{u\ell})\left(\frac{\tilde N_\ell(r_1)}{g_\ell} - \frac{\tilde N_u(r_1)}{g_u}\right)\end{aligned} \tag{2.80}$$

where $\tilde N_u$ and $\tilde N_l$ are the occupation densities in units of 10^9cm^{-3}. **For allowed transitions the optical depth is extremely high, i.e., the probability for a photon to escape from the shell without absorption is extremely small.** Hence, allowed transitions do not contribute to the cooling of the gas. Forbidden transitions like those important for plasma cooling in gaseous nebulae have transition probabilities $A_{u\ell}$ of the order of $10^{-2}\ldots10^{-6}\mathrm{s}^{-1}$. Such lines are optically thin in the expanding nova shell and every photon emitted in such a transition immediately leaves the shell. Hence, forbidden line emission is an important cooling mechanism for the gas.

b) Level population

The mechanism of level population is different in gaseous nebulae and nova shells. Let us first consider the de-excitation of the levels. The critical electron density n_e, where de-population of the excited levels by radiative transitions and inelastic electron scattering are equally important, is

$$n_e = \frac{A_{u\ell}}{g_u q_{u\ell}} \tag{2.81}$$

[Osterbrock 1974] , where $A_{u\ell}$ is the radiative transition probability and $q_{u\ell}$ is the rate coefficient for collisional de-excitation. Using the approximation for q given in Osterbrock (1974) one gets

$$n_e = 3.7\cdot10^6\frac{A_{u\ell}g_u}{\Omega_{u\ell}}\left(\frac{T}{1000}\right)^{\frac{1}{2}}. \tag{2.82}$$

Typically one has $A_{u\ell}\approx10^{-2}\ldots10^{-6}\mathrm{s}^{-1}$ for the transitions of interest. The collision strengths $\Omega_{u\ell}$ are of the order of unity. Then, the critical electron density is at most of the order of $10^6\mathrm{cm}^{-3}$ and usually much less. The real electron density in the nova shell is of the order of the density of the abundant elements with low ionization potential, since these elements will be completely ionized by the near UV radiation of the nova atmosphere. During the first hundred days after the nova event, the electron density will not drop below $10^7\mathrm{cm}^{-3}$. Hence, de-excitation is dominated by inelastic electron scattering.

The excitation of the levels also is dominated by collisional processes. The radiative excitation rate is given by

$$N_\ell\frac{g_u A_{u\ell}}{g_\ell}\frac{c^2}{2h\nu^3}I_\nu\,, \tag{2.83}$$

while the collisional excitation rate is

$$N_\ell n_e\frac{g_u}{g_\ell}\exp(-\frac{\Delta\chi}{kT_e})q_{u\ell} \tag{2.84}$$

with T_e being the temperature of the electron gas. Assuming for I_ν a diluted black-body radiation field with temperature T_*, the critical electron density for both excitation processes becoming equally important is

$$n_e = \frac{A_{u\ell}}{q_{u\ell}}W\exp\left[\frac{\Delta\chi}{kT_e}\right]\left(\exp\left[\frac{\Delta\chi}{kT_*}\right]-1\right)^{-1}, \tag{2.85}$$

where $W = (R/r)^2$ is the dilution factor for the radiation field. One has $W \approx 10^{-2} \dots 10^{-4}$ during the first hundred days of the shell expansion. The last factor is of the order of unity for a nova temperature of $\approx 2 \times 10^4$K, an electron temperature of the order of $\approx 10^3$K and excitation energies of the order of 1eV. We conclude that this critical electron density is even less than the critical electron density in the case of de-excitation. Since we have already seen that the true electron density is much higher, the excitation is dominated by collisional processes.

Thus, both the excitation and the de-excitation of states just above the ground level is dominated by inelastic electron scattering. In this case, the levels are thermally populated with an excitation temperature equal to the temperature of the electron gas. In this respect, nova shells are different from gaseous nebulae where the level population is far from TE.

2.4.2.5 Cooling by Line Emission

From the theory of gaseous nebulae it is known, that the most important ions for cooling the region of ionized hydrogen by forbidden line emission are OII and NII. This will be the case, too, for the nova shell. In the neutral region ahead of the HII-zone, abundant ions with levels of low excitation potential are OI, CII, SII and SiII. These will be the most important coolers with respect to the process of cooling by forbidden line emission.

The cooling rate has been determined for these ions on the basis of the following two assumptions.

(i) The escape probability for photons emitted in forbidden transitions equals unity. As one has seen above, this is true for all emission directions except within a very narrow cone centred on the radial direction.

(ii) Levels of low excitation potential are thermally populated.

Then, if the lower and higher stage of excitation of an atom are denoted by the indices 1 and 2, respectively, the energy loss rate by collisionally excited line radiation of frequency ν_{21} is given by (Osterbrock, 1974)

$$\mathcal{L}_c = n_2 A_{21} h\nu_{21}, \tag{2.86}$$

where A_{21} is the line emission coefficient.
In two cases, however, the critical electron densities for collisional de-population are smaller than the true electron density, but not extremely smaller. In these cases (the ^{1}S→ ^{3}P transition in NII, critical electron density $1.8 \times 10^7\, cm^{-3}$, and the ^{1}D→ ^{3}P transition in OI, critical electron density $3 \times 10^6\, cm^{-3}$) the level population is calculated from the equilibrium between collisional excitation and collisional and radiative de-excitation in the approximation of a 2–level atom (see e.g. Hjellming, 1965) .
The final results for the cooling rates by collisionally excited line cooling are presented in the Appendix (I).

2.4.3 Calculation of the Temperature

With the aid of Eq. (2.33) and the condition of ionization equilibrium outside the fronts

$$n_i(1 - f_i)\left(\frac{R}{r}\right)^2 \int_{\nu_i}^{\infty} \frac{\pi B_\nu}{h\nu} \sigma_\nu^i e^{-\tau_\nu} d\nu = n_i f_i n_e \alpha_i(T) \tag{2.87}$$

the heating rate (2.56) can be written as

$$\mathcal{G}(n_i) = n_i f_i n_e \alpha_i(T) \frac{\int_{\nu_i}^{\infty} \frac{\pi B_\nu}{h\nu} h(\nu - \nu_i) \sigma_\nu^i e^{-\tau_\nu} d\nu}{\int_{\nu_i}^{\infty} \frac{\pi B_\nu}{h\nu} \sigma_\nu^i e^{-\tau_\nu} d\nu}. \tag{2.88}$$

Equating this to the sum of all energy loss processes, there results an equation for the electron temperature. This equation has to be solved simultaneously with the Eqs. (2.43) for the optical depth scales τ_j and (2.36) for the ionization degrees f_i.

The electron temperature enters into the Eqs. (2.43) and (2.36) through the dependence of the recombination coefficients on T_e. These coefficients depend only weakly on T_e which allows a simple iteration procedure for solving the coupled system of equations: solve (2.43) and (2.36) with an estimated temperature T_e, calculate with the resulting τ_j and f_i an improved temperature T_e, use this as a new estimate and start from the beginning. This procedure converges very rapidly.

2.5 Model Calculations of the Ionization and Temperature Structure in Novae

2.5.1 The Model

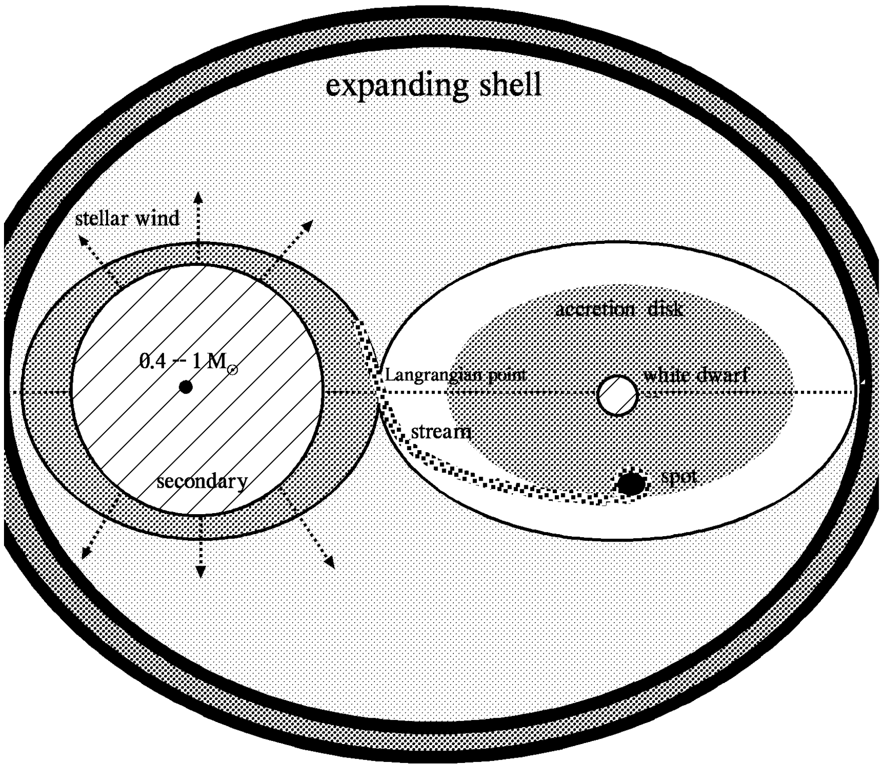

Figure 2.7: Schematic sketch of the classical nova model, including the internal close binary system ($a \approx 10^{10} cm$ between the white dwarf and the companion star), the accretion disk around the white dwarf ($d \approx 10^9 cm$), the photosphere during the outburst ($r_{\max} \approx 10^{12} cm$) and the expanding shell ($r > 10^{12} cm$).

In the following we adopt a simple model for the matter ejected in a nova event. Spectroscopic observations of the outstreaming gas indicate in most cases a complex structure of the nova outburst far away from being simply a spherically symmetric expansion [Solf 1983] , though in some specific cases rather symmetric structures have been observed (e.g.[Mustel and Boyarchuk 1970]). However, to investigate

the principal chemical and dust forming processes going on in the expanding and cooling shell, as a first approximation it suffices to consider the simplified model of a shell of constant thickness Δr, spherically expanding with constant velocity v from a central blackbody radiation source.
The variation of the total particle density n with time t within the expanding sphere then is given by

$$n(t) = n_0 \cdot \frac{(R+\Delta r)^3 - R^3}{(R+\Delta r + vt)^3 - (R+vt)^3} \tag{2.89}$$

where n_0 is the initial particle density at time $t = 0$ (corresponding to the instant where the shell detaches from the nova pseudo atmosphere), Δr is the geometrical thickness of the ejected shell and R is the radius of the nova atmosphere at $t = 0$. The initial particle density is related to the total mass M ejected in the nova event by

$$n_0 = \frac{\mathrm{M}}{\frac{4\pi}{3}\left[(R+\Delta r)^3 - R^3\right]} \,. \tag{2.90}$$

Typical expansion velocities which have been observed in nova outbursts range between 300 and 1300 km·s^{-1} (Gallagher, 1977, Gehrz et al., 1980, Harrison and Gehrz, 1988, Ney and Hatfield, 1978).

Typical mass loss rates are between some 10^{-5} and $10^{-3} M_\odot$ yr^{-1} [Bath 1978b, Bode and Evans 1983a, Gehrz *et al.* 1980b] and the typical mass ejected during the nova event is between some 10^{27}g and 10^{29}g. We choose in our model calculations for these quantities the observed values of Nova Muscae 1983 (henceforth called **case A**) and Nova Herculis 1934 (henceforth called **case B**) which can be considered as typical representatives for non dust forming novae (**case A**) and for novae with copious dust formation (**case B**). The numerical values chosen are listed in Tab. (2.1)

The shell thickness Δr in our model calculation is assumed to be 10^{13}cm. This corresponds to an assumed duration of the phase of shell ejection (i.e. the time interval during which the dominant fraction of the total mass is ejected) of approximately two days, which roughly corresponds to the duration of the nova maximum.

For the time dependence of the photospheric temperature T_* and radius R we use the semi–analytical model for a nova atmosphere given by Bath and Shaviv (1976).

This model relates R and T_* to the luminosity and the observed variation of the visual brightness during the phase where the central nova atmosphere shrinks due to decreasing mass loss while maintaining the total luminosity. The values of R vary between $R = 10^{11}$ cm [Gallagher and Starrfield 1976] and $R = 10^{13}$ cm [Bath 1978b]. For simplicity we used in the model calculation an initial radius $R = 10^{12}$cm and an initial effective temperature $T_* = 8000$K of the central object. The time dependent increase of effective temperature determined from the observed optical brightness variation for both models is shown in Fig. (2.13). The relation between abundances, mass loss and expansion velocities were computed by [Starrfield *et al.* 1978] . The calculated abundances of the CNO group elements and of other elements could be confirmed by numerous observations ([Truran 1985a] ; [Williams 1985] ;[Snijders *et al.* 1987] ; [Snijders 1990]) and the theoretical mass loss rates agree well with estimations obtained from observations. For our model calculation the element abundances for hydrogen, helium, nitrogen and oxygen were taken from Truran (1985). These numerical values are given in Tab. (2.1). Due to a lack of observational material for the metals S, Si, Fe, Mg, Na, we have assumed solar abundances for these elements, though this probably underestimates their real abundance.

	case A	**case B**
M [g]	$2.6 \cdot 10^{27}$	$1 \cdot 10^{29}$
t_3 [d]	45	100
Δr [cm]	10^{13}	10^{13}
R_0 [cm]	10^{12}	10^{12}
T_0 [K]	8000	8000
v [cm$\cdot$s^{-1}]	$6 \cdot 10^7$	$3.1 \cdot 10^7$
ϵ(H)	0.43	0.34
ϵ(He)	0.38	0.095
ϵ(C)	0.004	0.04
ϵ(O)	0.07	0.29

Table 2.1: Model parameters used in the numerical calculations. **case A** represents a typical non dust forming case, whereas **case B** is the case of a dust forming nova.

2.5.2 Blackbody Models

2.5.2.1 Time Evolution of the Ionization

The ionization fractions of the elements H, C and Si are shown in Fig. (2.8) at day 5, 15 and 25 after the outburst for models A (a nova without dust formation) and B (one with dust formation). The maximum degrees of ionization that occured for some elements during the first 75 days of the expansion are presented in Tabs. (2.5.2.1 and 2.5.2.1), the radial extent of the ionized regions within the shell are given in Tabs. (2.5.2.1) and (2.5.2.1) in units of the shell thickness $\Delta r = 10^{13}$cm for different times. The fractions > 1 correspond to the case that the ionization front would have propagated beyond the outer edge of the shell. The position of the front is defined by $f_i = 0.1$.

Element	maximum degree of ionization at day		
	5	15	75
H	0.66	0.92	0.99
He	0.00	0.00	0.99
C	0.99	0.99	0.99
N	0.44	0.84	0.99
O	0.74	0.94	0.99

Element	maximum degree of ionization at day		
	5	15	75
H	0.21	0.29	0.93
He	0.00	0.00	0.02
C	0.95	0.97	0.99
N	0.11	0.17	0.88
O	0.23	0.33	0.94

Degrees of ionization f_i in the dust forming case (B) (left) and non dust forming case (A) (right) for the elements H, He, C, N, O for the early phase (day 5 and 15) and the late phase (day 75) of the nova outburst.

For model (A), the non dust forming case, the ionization degree of helium is small during the first days after maximum visual brightness. In later phases of the expansion, however, very sharp fronts are established which coincide with each other at the outer edge of the shell. Silicon and sulfur are fully ionized all over the shell after 5 days and a region of neutral carbon exists only during the first 10 days after the outburst.

For model (B) the far UV radiation field is too weak to ionize helium. About 20% of the hydrogen and oxygen and 10% of the nitrogen are ionized in a thin layer at the inner boundary of the shell. In this model, at day 75 the carbon ionization front has reached only about 2% of the shell extension, whereas silicon and sulfur are already completely ionized. The elements Mg, Fe, Na are completely ionized already in an even shorter time interval ($t \leq 5$d).

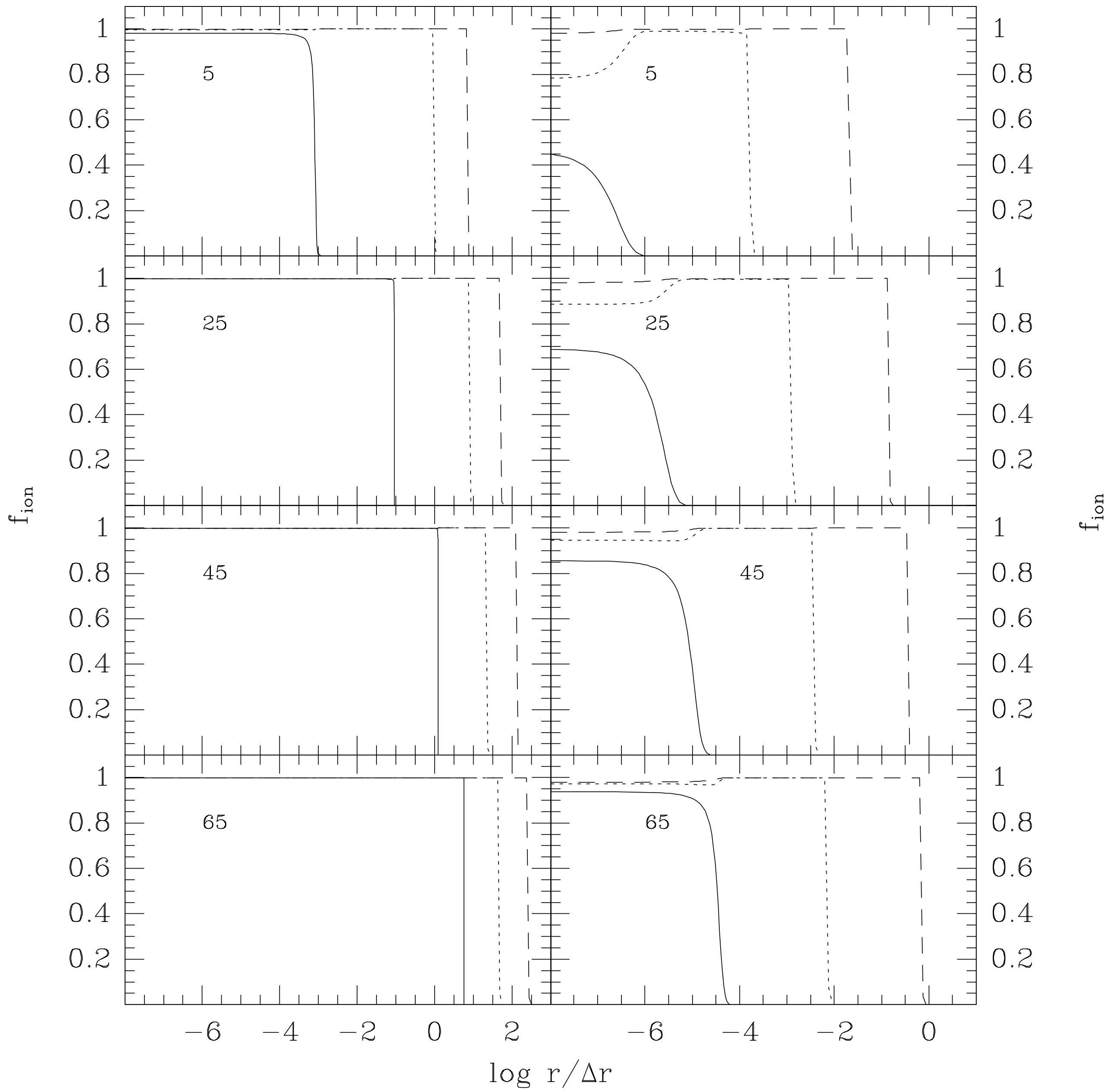

Figure 2.8: The ionization structure for the cases of a non dust forming (left) and a dust forming (right) novae are shown for the elements hydrogen (solid line), carbon (dotted line) and silicon (dashed line) for day 5, 25, 45 and 65 after the outburst. Degrees of ionization f_i are plotted versus a logarithmic scaled normalized radius scale, where Δr denotes the thickness of the expanding nova shell and r is the distance of the ionization fronts from the inner shell boundary for the elements indicated.

Element	Strömgren spheres at day 5	15	75
H	$3.7 \cdot 10^{-7}$	$5.5 \cdot 10^{-7}$	1.3
He	$< 10^{-10}$	$< 10^{-10}$	1.0
C	0.2	1.4	38
Si	1.5	10	237
S	1.3	8.6	204

Element	Strömgren spheres at day 5	15	75
H	$1.2 \cdot 10^{-7}$	$7.8 \cdot 10^{-7}$	$1.0 \cdot 10^{-4}$
He	$< 10^{-10}$	$< 10^{-10}$	$< 10^{-10}$
C	$7.4 \cdot 10^{-5}$	$4.3 \cdot 10^{-4}$	$1.7 \cdot 10^{-2}$
Si	$1.4 \cdot 10^{-2}$	$7.9 \cdot 10^{-2}$	1.6
S	$1.2 \cdot 10^{-2}$	$6.8 \cdot 10^{-2}$	1.6

Stroemgren radii for the elements H, He, C, Si and S in the non–dust forming case (A) (right) and the dust forming case (B) (left). The radius is given in units of the shell diameter.

It can be seen from Eq. (2.44) that the geometrical extensions Δr_i of the fronts essentially are determined by the particle densities of H and He. For the corresponding optical depths $\Delta\tau_i$ of the order one, during the first 100 days of expansion the Δr_i remain smaller than 5% of the shell dimension. This justifies our procedure of calculating the degree of ionization across the fronts by means of Eq.(2.45), though in principle Eq.(2.46) have to be used. The resulting error remains negligible due to the small geometrical width of the ionization fronts.

2.5.2.2 The Ionization of Carbon

The degree of ionization of carbon in the neutral HI region of a nova shell is of special importance for the type of chemistry operating in the shell. Earlier calculations (Mitchell and Evans, 1984, Rawlings, 1988) have indicated that the carbon is ionized completely throughout the shell within a few days. Our model, however, shows that the carbon ionization zone propagates much more slowly through the expanding shell. In **case A** the CII-front arrives at the outer boundary of the shell only after approximately two weeks while in **case B** even at day 75 after the outburst the CI region covers only a negligible fraction of the shell (cf. Fig. (2.9)).

This discrepancy between the results of Mitchell and Evans (1984) and Rawlings (1988) and our results can be traced back to the following reason. The former calculations treated the ionization of carbon and hydrogen as being independent of each other and calculated the extent of the region of carbon ionization from stationary Strömgren sphere theory, modified for a shell of matter. While the static assumption is completely justified, as our time dependent calculation shows, the carbon ionization is coupled to the hydrogen ionization in the following sense. In the HII-zone, the electron density is determined by the hydrogen ionization and, thus, is higher by factor $1/\epsilon_C$ (with ϵ_C being the abundance of C relative to H) than it would be in a pure region of carbon ionization. As a result, the recombination rate of carbon in this region in enhanced by the corresponding factor compared to a pure CII-zone and this means an increased abundance of neutral carbon atoms

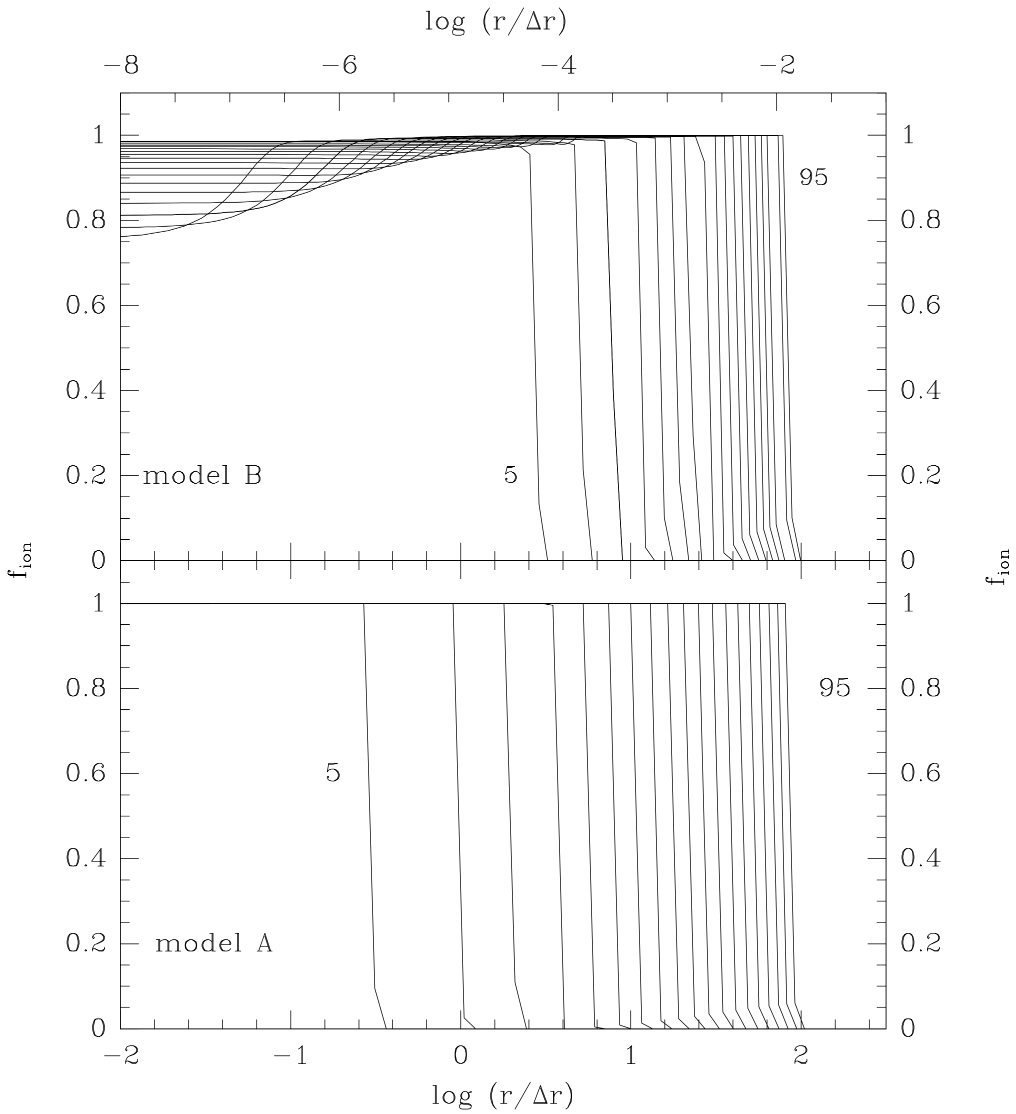

Figure 2.9: Propagation of the carbon ionization front through the nova shell. The abscissa is the logarithm of the thickness of the CII region in terms of the thickness of the nova shell. The lower part corresponds to a non dust forming nova, the upper part to nova with dust formation. Note the different scaling of the x–axis.

in the HII-zone as it would be encountered in a pure CII-zone. This can clearly be seen for the case of a dust forming nova (**case B**) in Fig. (2.8). In **case A**, this effect is less pronounced due to a lower particle density and a higher UV-flux. This increased CI abundance in the HII-zone causes an increased consumption of photons from the energy region between the carbon and hydrogen ionization edges which then are missing in the CII-region ahead of the HII-zone, where only such photons are available to ionize carbon. As a result of this enhanced consumption of such C-ionizing quanta in the HII-zone the propagation velocity of the CII-front in the outflowing shell is considerably reduced.

This has severe consequences for the chemistry of molecule and dust formation in nova shells. Since according to observations dust formation usually occurs around day 50 after the nova maximum, the abundant elements H, C, N, O are neutral in the HI-zone. The chemistry for these elements then can be expected to be dominated by neutral-neutral reactions and not by ion-neutral reactions, as has been assumed by Rawlings and Williams (1989).

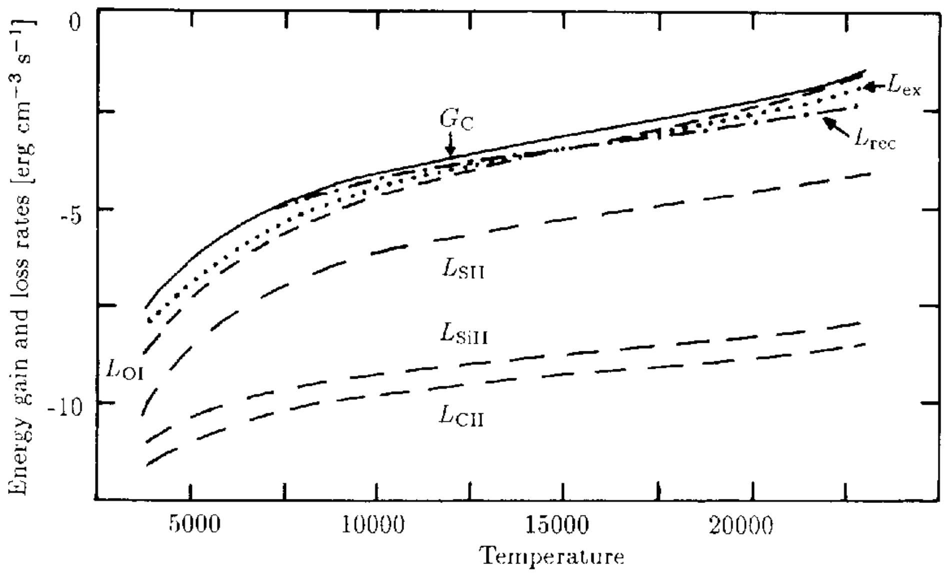

Figure 2.10: The most important energy gain and loss rates are plotted as functions of the electron temperature for the CII–region, where $L_{\mathrm{Si\,II}}$, $L_{\mathrm{S\,II}}$, $L_{\mathrm{C\,II}}$, $L_{\mathrm{O\,I}}$ and L_{rec} denote the cooling processes and G(C) the energy gain by carbon photoionization. The loss by hydrodynamic expansion is of the same order as the loss rate of electronic recombination L_{rec}.

2.5.2.3 Temperature Structure

In Fig. (2.10) the energy gain and loss processes are shown. In the HII region the main cooling processes are the recombination of ionized hydrogen, the hydrodynamic expansion and free-free radiation. Although in our models the O and N abundances are enhanced compared to solar abundances and in the later phases of the expansion both elements are completely ionized throughout the HII region, energy loss by collisional line excitation of OII and NII is not very important. This is a result of the high electron density which causes a strong depopulation of the excited states of these coolants by inelastic electron scattering and, thus, a strongly reduced cooling by radiative transitions. In the CII region the heating by photoionization is compensated essentially by the hydrodynamic expansion term. The temperature

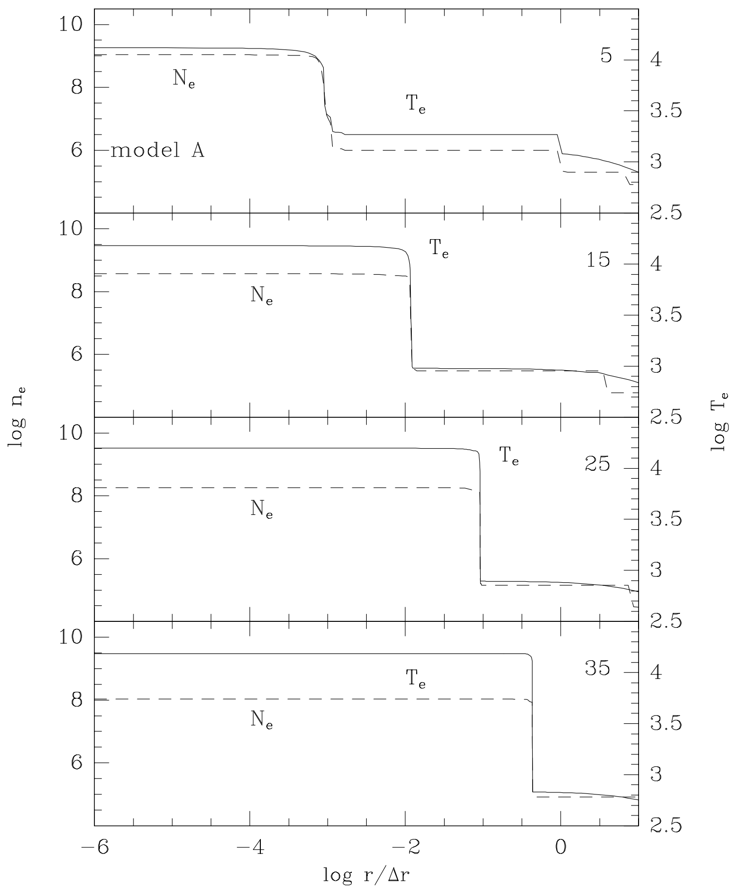

Figure 2.11: The electron density n_e (dashed line) and electron temperature T_e (solid line) at day 5, 15, 25 and 35 after outburst is plotted for a non dust forming nova (**case A**) versus a logarithmic radius scale in units of the shell thickness.

stratification and the distribution of the electron density are presented in Fig. (2.11) and Fig. (2.12) at days 5, 15, 25 and 35. At the fronts, the electron density decreases due to enhanced recombination and reflects the different ionization spheres. At the ionization fronts of H, C, N and O the electron density drops by several orders of magnitude, depending on the assumed abundances. Within the CI region, the free electrons originate from the ionized metals Fe, Mg, Si and Na. At the end of the time interval considered in the model calculations (100 days), the electron density still is $n_e = 3 \cdot 10^5 \mathrm{cm}^{-3}$ and, thus, far above the typical values $n_e = 10^2 \mathrm{cm}^{-3}$ encountered in interstellar HII regions. An increase of the temperature within the ionization fronts due to a hardening of the ionizing photons as it would be expected to occur analogous to the case of normal HII regions is not observed in our model

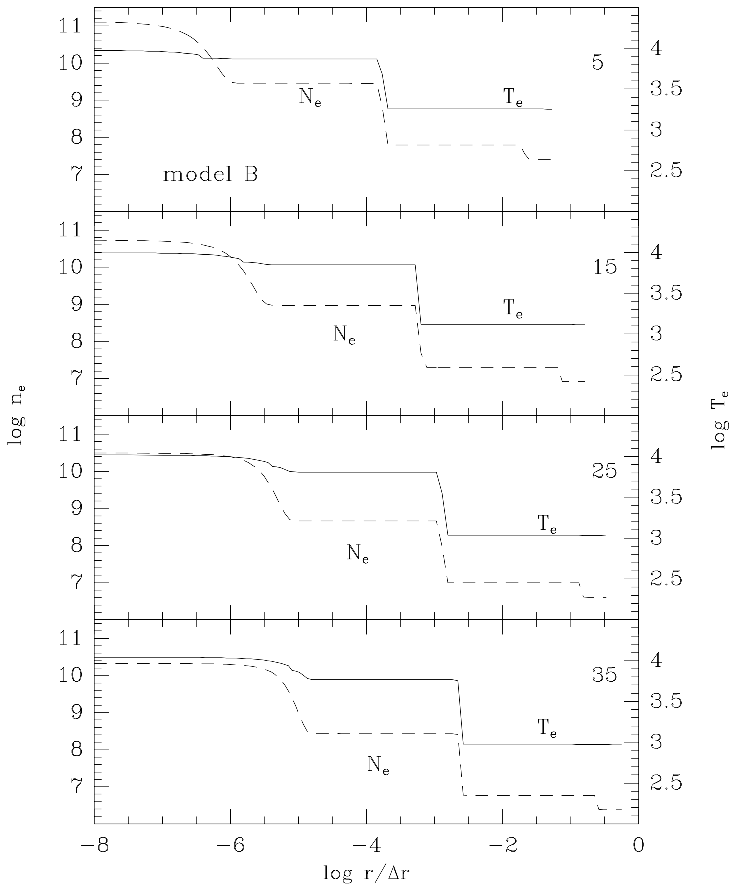

Figure 2.12: Same as Fig. (2.11), but for the case of a nova with dust formation (**case B**).

calculations. It is compensated by the strong cooling of the gas due to hydrodynamic expansion. The average temperature structure in the nova shell is shown in Fig. (2.13). The temperatures are averages of the electron temperature in the indicated ionization shell. T_* is the effective temperature of the nova atmosphere, as determined by means of the semi-quantitative theory of Bath and Shaviv (1976) from the visual brightness of Nova Muscae 1983 (**case A**, upper part of the figure) and Nova Hercules 1934 (**case B**, lower part of the figure).

The temperature $T_{\rm HII}$ in the region of hydrogen ionization is slightly below 10^4K, as is usual in gaseous nebulae. In this region, the temperature is determined by the equilibrium between heating by H-ionization and the cooling processes, especially recombination cooling and cooling by hydrodynamic expansion.

The temperature $T_{\rm CII}$ in the CII-region drops rapidly to very low values in the case of a non dust forming nova. This results from the strong adiabatic cooling of the rapidly expanding gas (cf. Fig. (2.10)) which cannot be compensated by the heating processes (mainly C-ionization). In the dust forming **case B**, the temperature in the CII-zone is much higher than in **case A** since the expansion is slower and cooling by hydrodynamic expansion not as important as in **case A**.

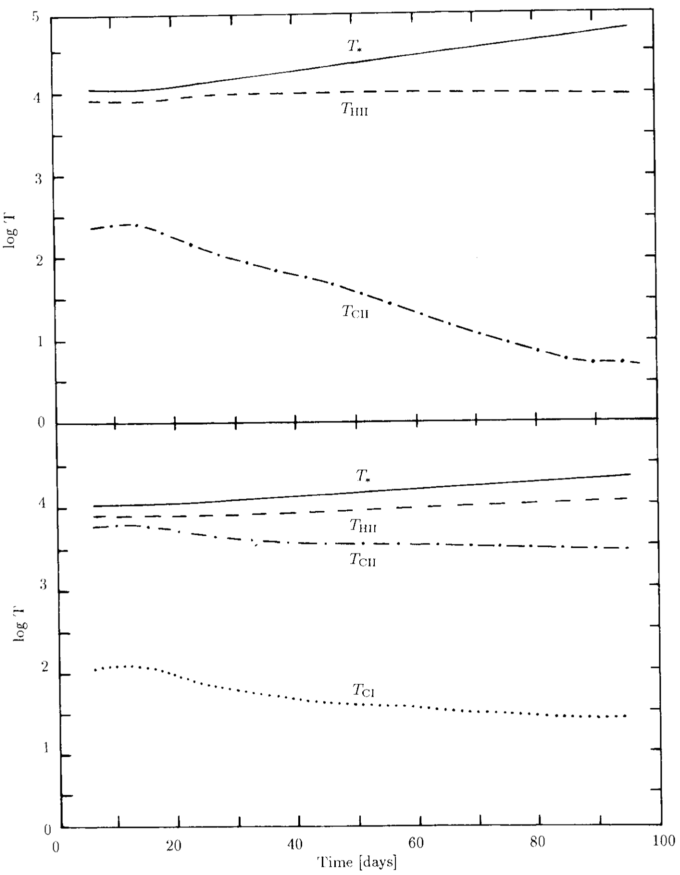

Figure 2.13: Evolution of the temperature in the nova shell with time. T_* (solid line) is the adopted temperature of the central nova atmosphere, $T_{\rm HII}$ (dashed line) the temperature in the inner HII-region etc. ($T_{\rm CII}$, dahed–dotted line; $T_{\rm CI}$, dotted line). The upper part corresponds to case A, a nova without dust formation and the lower part to **case B**, a dust forming nova.

The temperature $T_{\rm CI}$ in the CI-zone is shown only for **case B**. The temperature is very low in this region since the heating processes (mainly ionization of Si) are too inefficient to compensate the strong cooling by hydrodynamic expansion. In this region, the temperature development with time is determined mainly by adiabatic cooling.

These results show that the temperature in a nova shell in the HI-zone rapidly drops to rather low values, which is a necessary requirement for molecule and dust formation. Especially in **case B**, the absence of a significant HII-zone during the first 100 days of the shell expansion and the low temperature in the CI-zone favours molecule formation already at rather early phases of outflow.

2.5.3 Non–LTE Nova Models

2.5.3.1 Radiation Transfer in Nova Shells

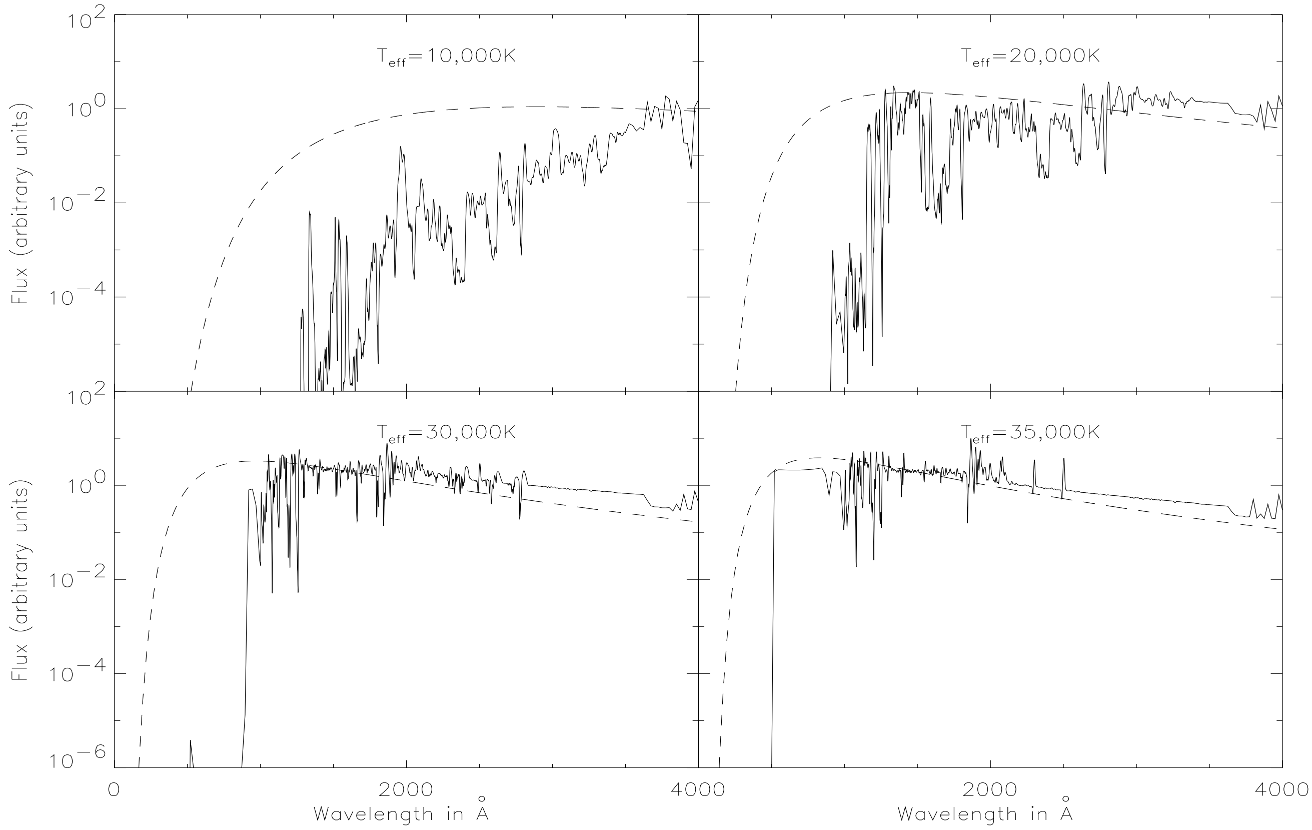

Figure 2.14: Synthetic spectra for a set of four different photospheric temperatures as indicated in the figures. For the computation of the spectra solar abundances were used. The corresponding blackbody continuum flux (dashed line) is also shown (picture is adopted with kind permission from P.H. Hauschildt).

The assumptions for modelling a nova photosphere are presented in detail in Wehrse et al. 1991, Hauschildt (1991) and Hauschildt et al. 1992, so I give here only a short description.
In the calculations an initial photospheric radius $R \approx 10^{13}$ cm is regarded, which is shrinking as the effective temperature increases following the semiempirical model given by [Bath and Shaviv 1976] . The model computations of the central atmosphere were performed for a grid of effective temperatures corresponding to several instants of time in the range $8000K \leq T_{\rm eff} \leq 30000K$ and for increments simulating fast and slow novae. For higher temperatures the stellar flux is extrapolated. The most important parameters of the photospheric model are:

1. the reference radius R, which refers to the radius where either the optical depth in absorption or extinction at $5000\mathring{A}$ is unity,
2. the effective temperature $T_{\rm eff}$, which is defined by means of the luminosity, L, and the reference radius ($T_{\rm eff} = (L/4\pi R^2\sigma)^{1/4}$ where σ is Stefan's constant),
3. the mass loss rate, $\dot{M}$,
4. the density, $\rho_{\rm out}$, at the outer edge of the envelope,
5. the element abundances.

The density within the photosphere is assumed to follow a power-law of the form

$$\rho(r) = \rho_0 \left(\frac{r}{R}\right)^{-3} \tag{2.91}$$

and the velocity field inside the photosphere is given by the condition of

$$\dot{M} = \text{const.} \tag{2.92}$$

In order to construct a model of the photosphere, one solves the equations of radiative transfer consistently for the outer radius and the energy equation. First we solve

$$\frac{dr}{d\tau} = -\frac{1}{\kappa} \tag{2.93}$$

where τ is the optical depth in absorption at some standard wavelength, r the radial coordinate and κ the absorption coefficient, with the condition $r(\tau = 1) = R$, which in turn determines the outer radius $r_{\rm out}$. Then the spherically symmetric radiative transfer equation is solved in the Lagrangian ("comoving") frame (see [Mihalas and Weibel-Mihalas 1984]

$$\begin{aligned}
\gamma(\mu+\beta)\frac{\partial I}{\partial r} \quad &+ \quad \frac{\partial}{\partial\mu}\left\{\gamma(1-\mu^2)\left[\frac{(1+\beta\mu)}{r} - \gamma^2(\mu+\beta)\frac{\partial\beta}{\partial r}\right] I\right\} \\
&- \quad \frac{\partial}{\partial\nu}\left\{\gamma\left[\frac{\beta(1-\mu^2)}{r} + \gamma^2\mu(\mu+\beta)\frac{\partial\beta}{\partial r}\right]\nu I\right\} \\
&+ \quad \gamma\left\{\frac{2\mu+\beta(3-\mu^2)}{r} + \gamma^2(1+\mu^2+2\beta\mu)\frac{\partial\beta}{\partial r}\right\} I \\
&= \eta - \chi I
\end{aligned} \tag{2.94}$$

for a prescribed set of ≈ 1700 wavelength points. In Eq. (2.94), μ is the cosine of the angle between a ray and the direction normal to the surface, ν the frequency, $I = I(r,\mu,\nu)$ denotes the specific intensity at radius r and frequency ν in direction $\arccos\mu$ in the Lagrangian frame. The matter velocity $v(r)$ is measured in units of the speed of light c, $\beta(r) = v(r)/c$, and γ is given by $\gamma = 1/\sqrt{1-\beta^2}$. The sources of radiation present in the matter are described by $\eta = \eta(r,\nu)$ and $\chi = \chi(r,\nu)$ denotes the extinction coefficient; η contains contributions from scattering terms proportional to the mean intensity J of the form $\sigma \bar{J}$ (where $\bar{J}$ is the mean intensity averaged over the line profile) which are explicitly treated in the radiative transfer. The radiation fields derived from the solution of Eq. (2.94) incorporate all relativistic effects, in particular advection and aberration. However, these effects are small in the models used in this calculations in contrast to the situation found in SN envelopes (Hauschildt et al. 1991).

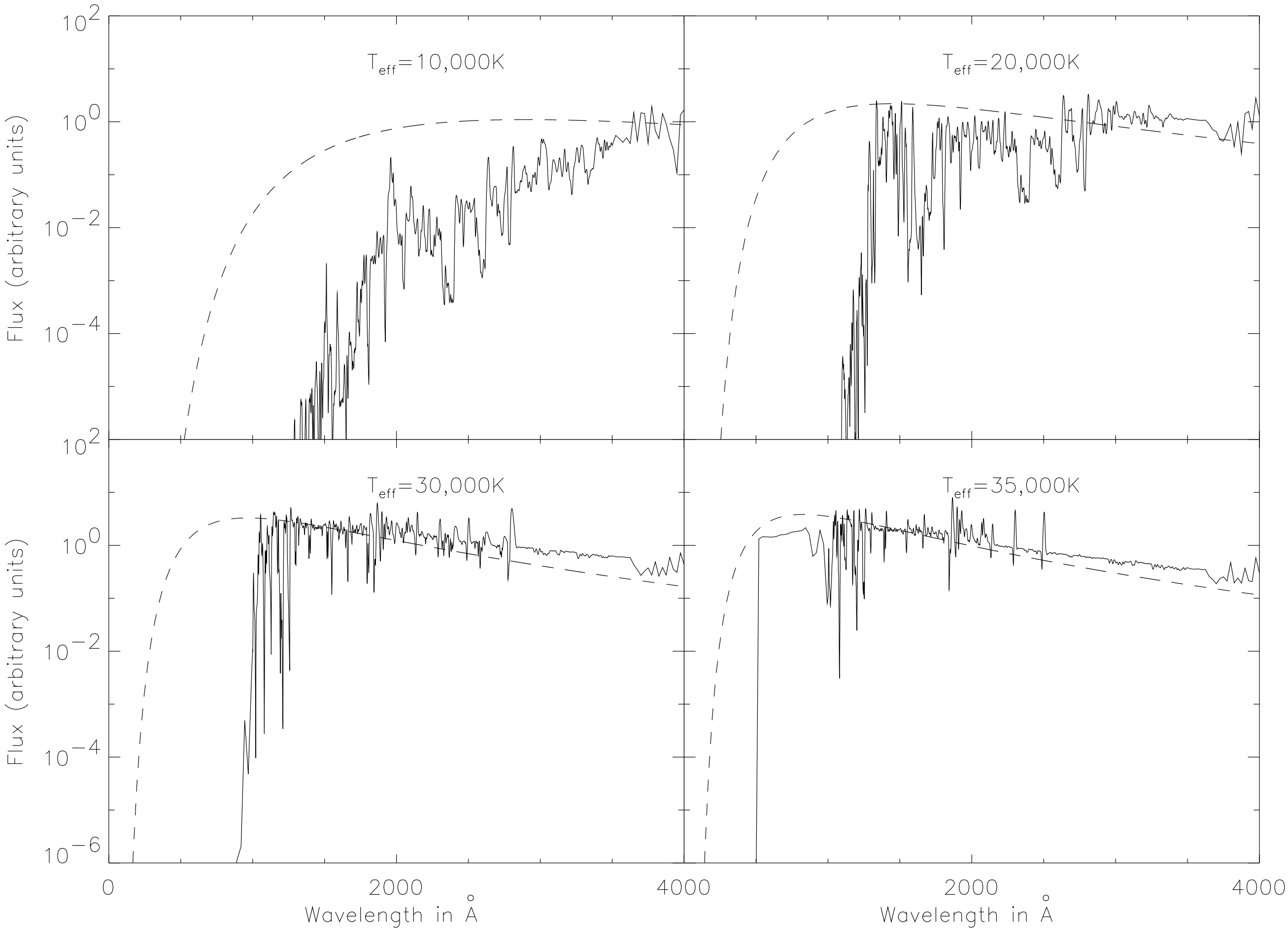

Figure 2.15: Synthetic spectra for a set of four different photospheric temperatures as indicated in the figures. For the computation of the spectra enhanced (factor 10^2) CNO abundances were used. The corresponding blackbody continuum flux (dashed line) is also shown. Picture is adapted with kind permission from P.H. Hauschildt.

The kinetic temperature distribution in the photospheres is iterated so as to fulfill the radiative equilibrium equation in the Lagrangian frame,

$$\int_0^\infty \kappa_\lambda(B_\lambda - J_\lambda)d\lambda = 0 \ , \tag{2.95}$$

where

$$J = r^2/2\int_0^\infty \int_{-1}^1 I_\lambda \, d\mu \, d\lambda \tag{2.96}$$

and B_λ denotes the Planck function scaled by r^2, or the equivalent condition for the wavelength integrated Eddington flux:

$$\frac{\partial H}{\partial r} + \beta\frac{\partial J}{\partial r} + \frac{\beta}{r}(J - K) + \gamma^2\frac{\partial \beta}{\partial r}(J + K + 2\beta H) = 0 \ , \tag{2.97}$$

where

$$H \ = \ r^2/2\int_0^\infty \int_{-1}^1 \mu I_\lambda \, d\mu \, d\lambda \tag{2.98}$$

$$K \ = \ r^2/2\int_0^\infty \int_{-1}^1 \mu^2 I_\lambda \, d\mu \, d\lambda \, . \tag{2.99}$$

The level populations for H (10 levels), Ca II (5 levels) and Mg II (3 levels) are obtained from the NLTE rate equations, whereas for the remaining levels (and other species) the Boltzmann population distribution at the local kinetic temperature is assumed. The NLTE rate equations are solved self-consistently with the radiative transfer and radiative equilibrium equations using the equivalent-two-level-atom method (e.g. [Mihalas 1978]).

All relevant absorbers are taken into account in the computation of the b-f and f-f absorption and scattering coefficients (for a complete list see Hauschildt et al. (1992)). For the calculation of the LTE line opacity the line list of Kurucz and Peytremann (1975) was used, in which a new list of Fe II lines (Kurucz, 1988) is included. The line scattering is included according to the approximation described in Hauschildt et al. (1992) .
Synthetic spectra of the photosphere for effective temperatures $T_{\rm eff} = 10000\,K$, $20000\,K$, $30000\,K$ and $35000\,K$ are presented in Fig. (2.14).

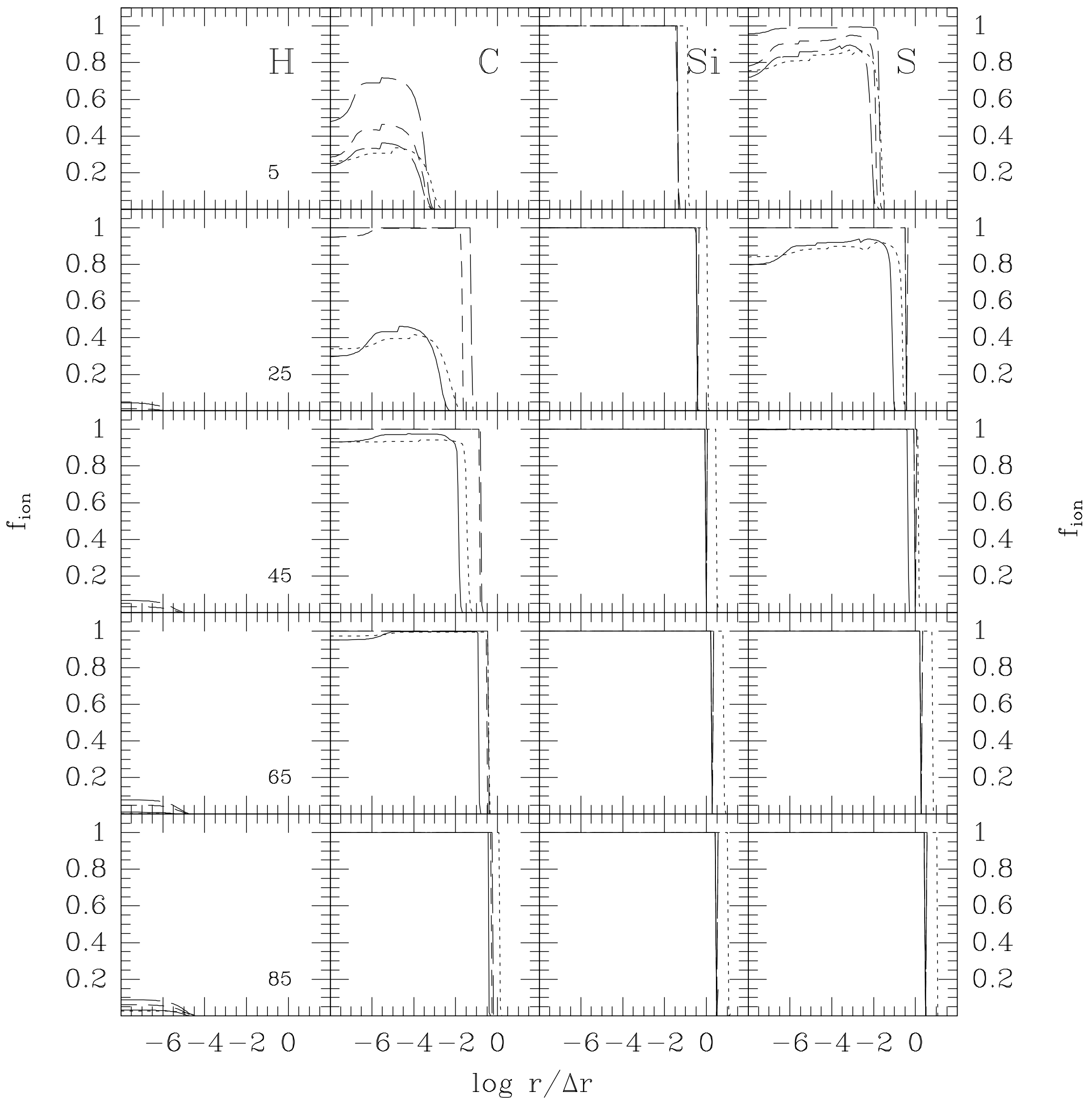

Figure 2.16: The degree of ionization is shown for the elements H, C, Si and S versus a logarithmically normalized radius scale, where Δr is the total shell diameter and r the distance measured from the inner shell boundary. We show the results for four different ionization models computed with the parameters of case (B) in Tab. (2.1), but varying the time dependence of the change in photospheric temperature (t_3-time) and the expansion velocity:
model A: (solid line), t_3= 100 days;**model B:** (dotted line), t_3= 100 days, v_{ex}= 1000km/s
model C: (short dashed line), t_3= 50 days; **model D:** (long dashed line), t_3= 25 days.
The ionization structure is depicted for t_1= 5, t_2= 25, t_3= 45 and t_4= 65 and t_5 = 65 days after the nova outburst as indicated in the figures.

2.5.3.2 Ionization and Temperature Structure

In the discussion of the results we first turn to the model structures derived for nova shells having solar abundances and a moderate to slow speed class, e.g the t_3-time is 100 days (for the other parameters cf. Tab. (2.1), resembling a case where dust formation is possible (Beck et al., 1990). In most novae where a dust shell has been observed grain formation starts long before day 100 (see Gehrz, 1989), so the chosen decline rate is not an indispensible prerequisite for the occurence of dust as the observations of V1668CYG and LW Ser have shown, both fading three magnitudes in visual brightness in 30 and 50 days respectively, but showing strong evidence for the existence of an optical thin dust shell. The degree of ionization of H always remains on a low state even after 100 days. The maximum degree of ionization of hydrogen only reaches a value of 0.02. The final Stroemgren radius is R_{st}^{H}=6.3·10^7 cm, which is only a very small fraction of the total shell diameter of d_s=10^{13} cm. The increase of the shell expansion velocity from 500 km/s (**model A**) to 1000 km/s (**model B**) is shifting the outer edge of the ionized part of the envelope by a factor of 2–5, but does not raise the maximum value of the degree of ionization.
The ionization stratification is mainly affected by the temporal development of the photospheric radiation field. In the first phase of the nova event the photospheric temperature is in the range of 10000 K to 12000 K and the UV-flux capable of ionizing the most abundant elements H, He, N and O is about four magnitudes lower than in the corresponding blackbody model. Due to the incorporation of the effects of line blanketing into the radiation transfer model for the nova photosphere there exists a "pseudocontinuum" (cf. Fig. (2.14)), which is much weaker than the corresponding continuum flux. This results in a low state of ionization for H, He, O and N. The ionization of oxygen is nearly equal to that of hydrogen and in the framework of the accuracy in this work their Stroemgren spheres coincide. The fraction of nitrogen being ionized is lower than 1% and for helium $f_{ion}^{He} \ll 1$.
So, in the starting phase of the nova expansion when the particle density is high (n $> 10^9 cm^{-3}$), the ionizing radiation is completely absorbed and the shell is optically thick building up a stratified ionization structure. This means that there exists an outer layer of predominantly neutral gas where the emission of neutral and low-ionization permitted lines is possible (see Seitter, 1990) .
For the investigation of the conditions preceding the process of grain formation in novae the study of the ionization stratification of atomic carbon is most valuable. From infrared observations it is known, that thirteen of almost 21 recent bright classical novae have produced measurable amounts of dust. Twelve of these events showed evidence for carbon based dust [Gehrz 1990] . In some cases the formation of SiC (V1370 Aql), SiO2 (V842 Cen) and/or hydrocarbons (QU Vul) is reported. Although the details of the processes of nucleation and growth remain unclear it is incontestably that at least one abundant dust forming species has to be predominantly neutral, otherwise Coulomb repulsion will prevent any nucleation process. So, it is an important result, that in the first 45 days of the nova atomic carbon predominantly remains neutral (f_{max}^{C}=0.51,t=45 days) and the region where carbon

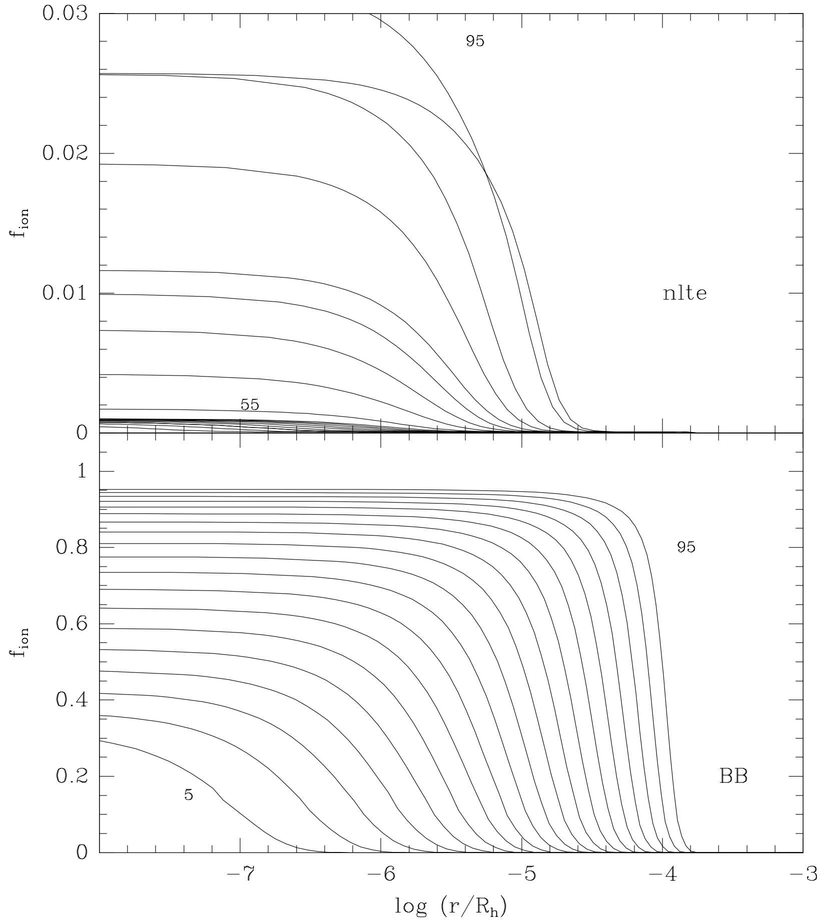

Figure 2.17: Time dependence of hydrogen ionization fronts in nova shells for model A (see Fig. (2.16). The ionization fronts are shown for the non-LTE model (top) and the corresponding black body model (bottom). The abscissa is the logarithmically normalized radius scale, where R_h is the shell diameter. The time interval between each curve is $\Delta t = 5d$. In each diagram two curves are labelled with the corresponding value of the time interval after the nova outburst.

is neutral contains more than 99% of the shell volume. At day 45, when the photospheric temperature has raised to T_*=15000 K the flux in the wavelength range shortward to λ_C=1106 Åis drastically increased. Hence the value of the maximum degree of ionization is increased too, by a factor of ≈ 2 in the time interval between day 45 and 50. After 100 days the outer edge of the carbon ionization front is located at r=0.52 d_s.

The division of the expanding envelope into distinct parts which greatly differ in their molecular composition has fundamental consequences for the chemistry preceding grain formation. In the neutral zone the production of the most stable CO molecule leads to a complete consumption of the available carbon atoms, as the CO formation can proceed at temperatures which are too high for the onset of nucleation and growth. In the partly ionized zone the consumption of carbon in CO is not complete due to the dissociation of the CO molecule by high energetic radiation from the nova photosphere. The surplus carbon is available for the formation

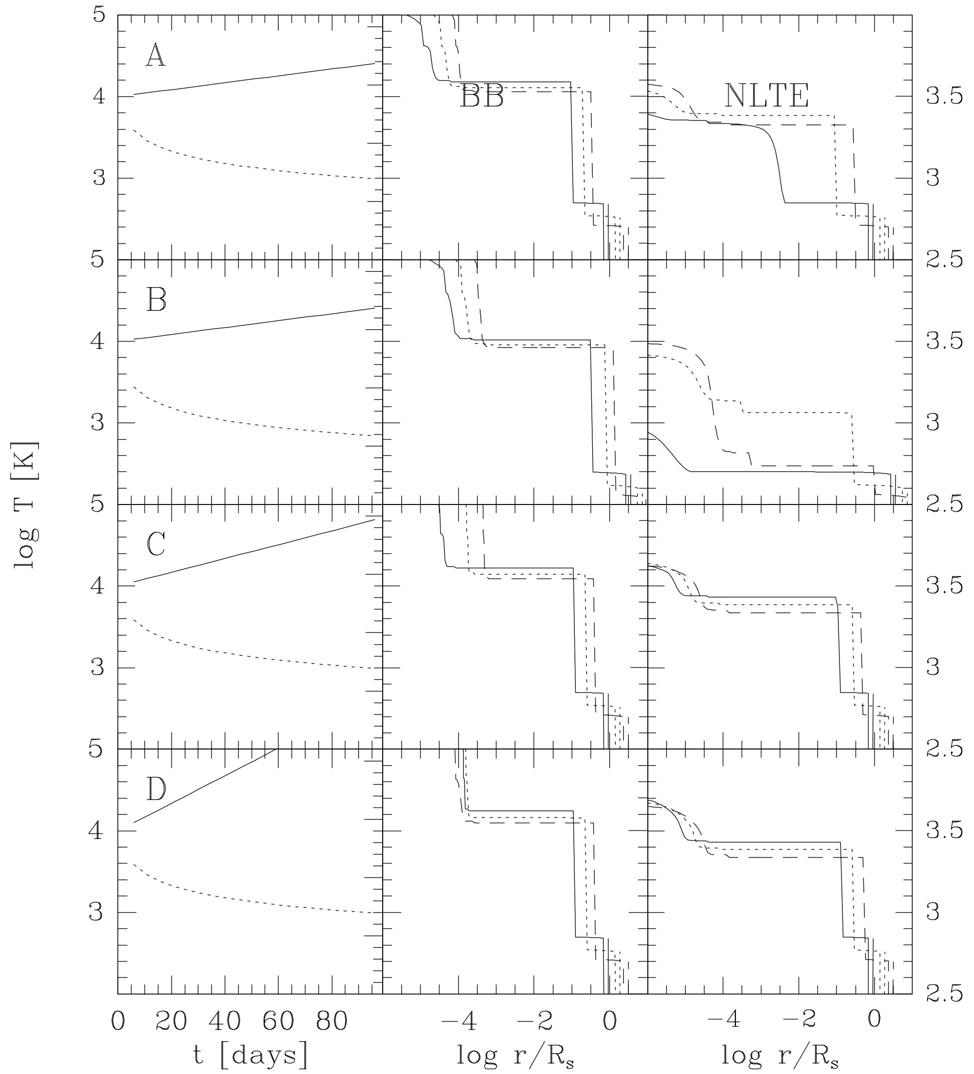

Figure 2.18: Temperature structure of four different nova models as described in Fig. (2.16). For each model the left one of the three diagrams show the time dependence of the photospheric (solid line) and the gas temperature (dotted line), where the gas temperature is given by the assumption of an exponential cooling law. The electron temperature stratification of the expanding nova shell for the case of a computed non–LTE radiation field (middle) and a given blackbody radiation field (right diagram) is depicted for $t_1 = 45$ days (solid line), $t_2 = 65$ days (dotted line) and $t_3 = 85$ days (dashed line) versus a logarithmically normalized radius scale (see Fig. (2.16).

of amorphous carbon clusters and the starting time for building of carbon clusters strongly depends on the temporal development of the temperature in this shell region (see Fig. (2.18).

The extensive observational and theoretical studies of the abundances in novae have shown that in most of the known cases the carbon abundance in the shell is lower than the abundance of oxygen ([Truran 1990] ; [Snijders 1990]). Hence, bearing in mind the commonly accepted chemical feature of the lock-uo function of carbonmonoxide, an oxygen-silicon chemistry is established which could result in the

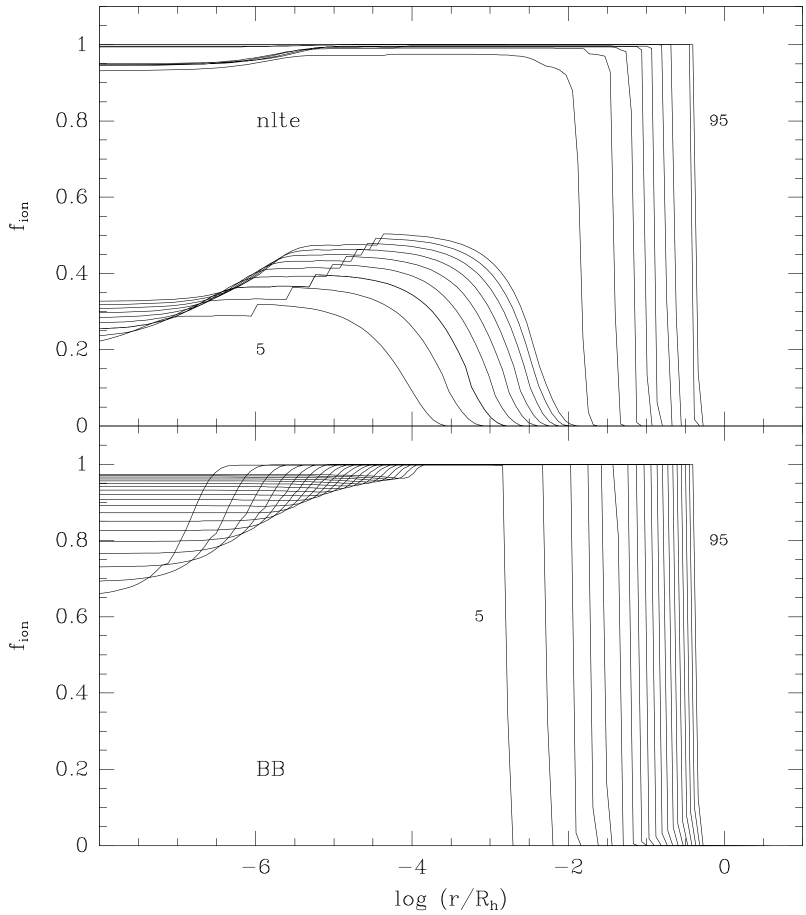

Figure 2.19: Time dependence of carbon ionization fronts in nova shells for model A (see Fig. (2.16). For detailed information see Fig. (2.17).

formation of the extreme stable SiO and SiO_2 clusters, which can either grow to macroscopic dimensions or serve as nucleation seeds for subsequent growth processes, as both species are high temperature condensates with condensation temperatures exceeding 1900 Kelvin (Weast et al., 1988). However, this requires that a substantial fraction of the silicon remains neutral to develop a silicon chemistry .
So the time dependent evolution of the ionization of atomic silicon is of special interest. Inside the Stroemgren sphere the degree of ionization is f^{Si}_{ion}=0.999 with a lower plateau in the innermost zone where the ionization is $f^{Si}_{ion} = 0.96$, which appears in the case of a blackbody radiation field (see Fig. (2.16). In all the four models depicted in Fig. (2.16) the silicon ionization front has reached the outer edge of the nova shell at day 45. The time dependence of the increase of the photospheric temperature has only a little effect on the radial ionization structure in the envelope, whereas the expansion velocity of the ejected material is mainly determining the position of the Stroemgren sphere.

The temperature of the gas in this predominantly neutral zone has cooled down to T_*= 1000 K at this time, so that there are favourable conditions for dust formation

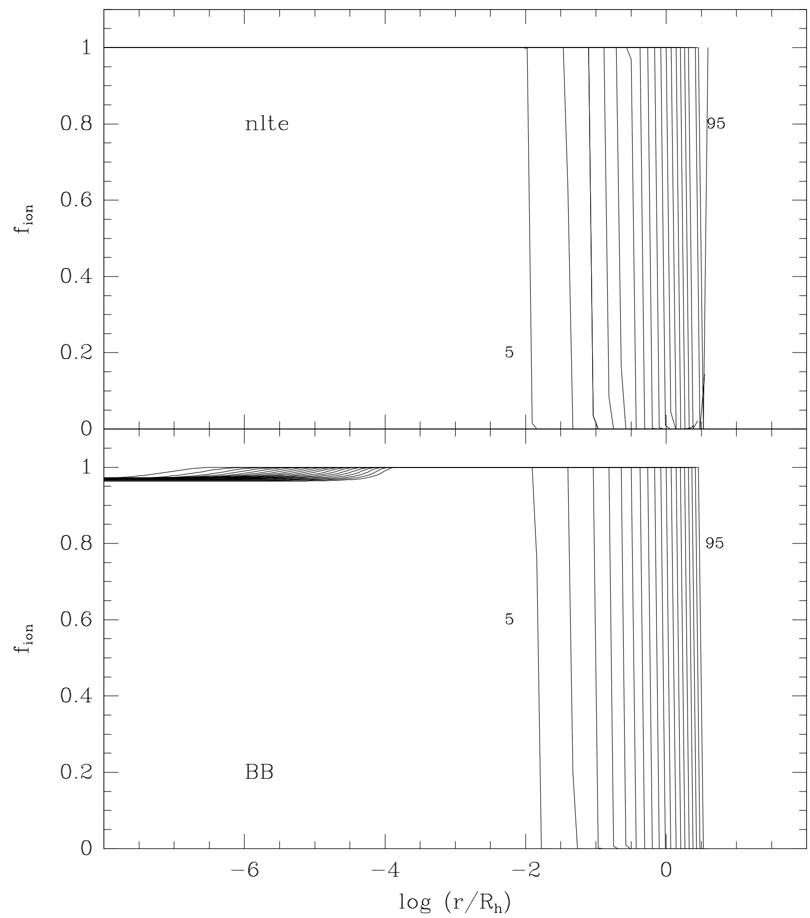

Figure 2.20: Time dependence of silicon-ionization fronts in nova shells for model A (see Fig. (2.16). For detailed information see Fig. (2.17).

to proceed. The less abundant species Fe, Na, and Mg are almost completely ionized throughout the entire shell within 2 days. In the innermost region of the shell the degree of ionization for Na is significantly reduced. This fact is due to the higher electron density in this part of the shell provided by the ionization of Si, S, C and H (cf. Fig. (2.16)). Hence the recombination of Na^+ with electrons, a process which has a high reaction coefficient α_B^{Na}, is more efficient in this zone. The contribution of this process to the lowering of the ionization for the elements Fe and Mg is moderate, decreasing the degree of ionization to f_{ion}^{Fe}=0.94 and f_{ion}^{Mg}=0.93, respectively. In the early phase of the outburst one has an ionization front for the metals Fe, Na and Mg which immediately reaches the outer boundary of the envelope thus supplying a total degree of ionization of 10^{-4}. Only a very small fraction of the elements with higher ionization potentials like H, C, N, O and He is ionized. The UV photons generated by the central nova source can penetrate only into a very thin layer of the expanding gas shell, there being absorbed.

After 10 days when the photospheric temperature has raised to T_*=12000 K, the nova envelope has expanded to a radial distance of 70 R_*. The degree of ionization

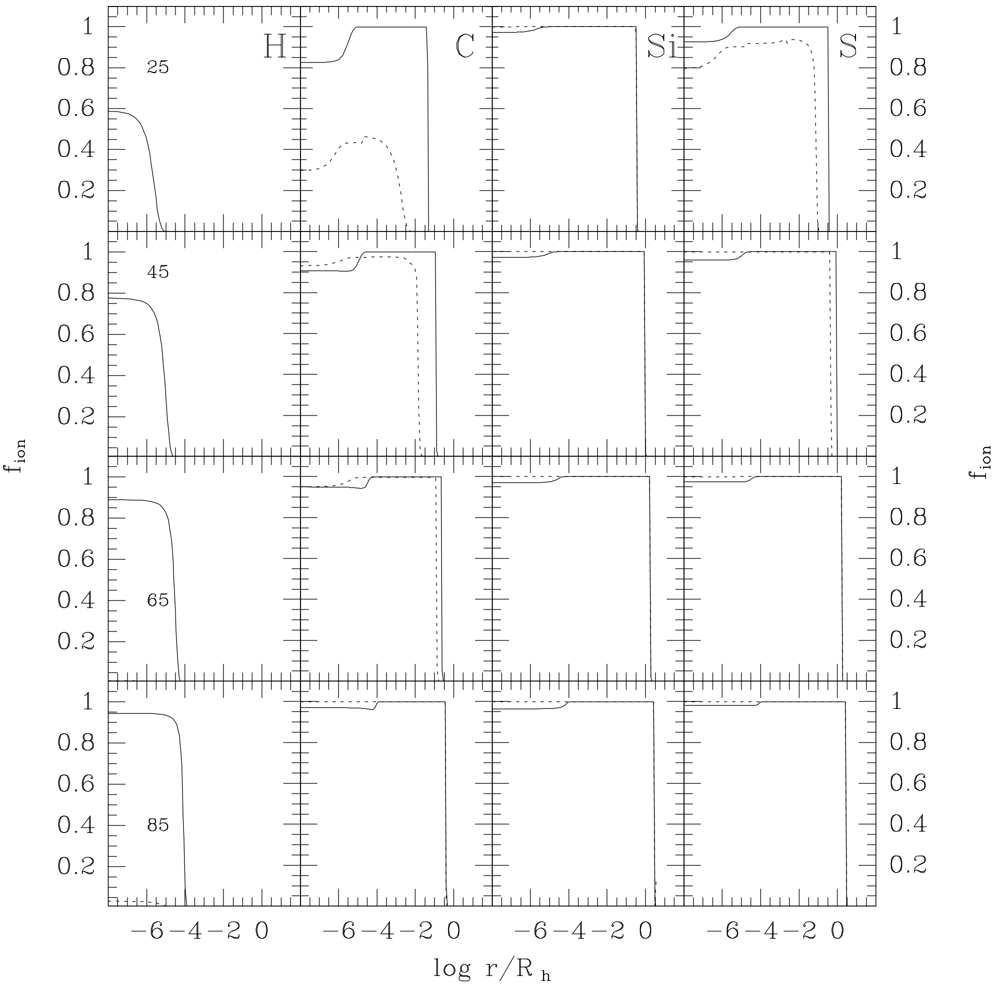

Figure 2.21: Ionization structure of a nova shell for **model A**. The degree of ionization throughout the shell is shown for the elements H, C, Si and S for a blackbody model (solid line) and the corresponding non-LTE model (broken line). The diagrams for each species are showing the state of ionization for four different times after the nova explosion: $t_1 = 25d$, $t_2 = 45$d, $t_3 = 65$d and $t_4 = 85$d. They are plotted versus a logarithmic normalized radius scale, where r is the distance of the ionization fronts from the inner shell boundary and R_h is the thickness of the moving gas shell.

has moderately grown in the case of the metals, e.g. for Na to f_{ion}^{Na}=0.54 in the inner region and to f_{ion}^{Na}=0.72 in the outer zone. Also sulfur shows a considerable response to the increase of the photospheric temperature (f_{ion}^{S}=0.1). Silicon exhibits a complete (f_{ion}^{Si} >0.99) ionization up to a distance of r=$3.2 \cdot 10^{10}$ cm, which is only a small part of the shell.

The situation dramatically changes after a time interval of 50 days has passed after the nova event. The process of carbon ionization starts to be of importance and the silicon ionization front is approaching the outer edge of the envelope, passing

it at day 54. Simultaneously the gas temperature has dropped to T_g= 1000 K, so that there are favourable conditions for the onset of nucleation processes (Gail and Sedlmayr, 1986,1987).
So our calculations show the possibility that in the neutral SiI zone massive condensation can take place before day 50. This is in agreement with the observations of DQ Her [Martin 1989].
Our value for the time when the silicon ionization front overtakes the entire envelope only gives an reliable estimate for the starting point of grain formation. The actual beginning strongly depends on the local physical and chemical conditions in the gas phase, hence this moment cannot be exactly predicted in the framework of this calculations. Nonetheless, if dust has formed before day 50, grains will survive although the environment is completely ionized. They will absorb the infalling UV radiation and transform into infrared photons. Hence the grain formation itself will obscure the outer parts of the shell thus considerably lowering the degree of ionization and creating conditions which favour the subsequent growth of the dust particles. This self amplifying property of grain formation is limited by the consumption of the condensable material.
The temperature structure of the expanding nova shell is determined by several processes. The main heating source is given by the ionization of hydrogen and carbon. For densities n< n_{crit} $\approx 10^{12}-10^{13}$cm^{-3} the contribution of collisional ionization is negligible. In the first period (50 days) all these heating processes are not sufficient to heat up the electrons in the neutral outer zones above the gas temperature, for which we assumed an adiabatic cooling law. As long as the timescales for collisions τ_c between electrons and atoms and ions are short compared to the expansion timescale τ_{ex} the system will relax immediately to an equilibrium situation where the equilibrium temperature is given by the temperature of the neutral gas outflow. Due to the large mass differences between electrons and other particles the energy exchange is approximately given by the mass ratio. Hence about 2000 impacts per electron are necessary to adjust an overall temperature. These assumptions are only valid for densities n $> 10^7 cm^{-3}$. In those phases of the expansion where collision and expansion timescale are of the same order, the complete time-dependent solution of the energy balance equation has to be calculated to account for the delay in the adjustment of the gas temperature. At day 50 the electron temperature in the innermost shell regions is about 4400 K slowly dropping to T_e=3700 K at r=10^8cm due to the simultaneous decrease in the electron density. When the carbon ionization drops below 10% no effective heating process remains, so outside the carbon Stroemgren sphere the temperature is given by the downcooled gas temperature T_g=1050 K. The internal changes in the close binary system, especially the time dependent decrease of the mass outflow change the photospheric temperature, simultaneously reducing the photospheric radius, resembling a phase of constant bolometric luminosity. The outflowing gas is penetrated by radiation which is hardening with time, heating up the inner envelope zones to T_e=5400 K at day 100. For the later phases of the nova expansion the gas will be heated to typical HII-zone temperatures of about 10000 K in the inner regions.

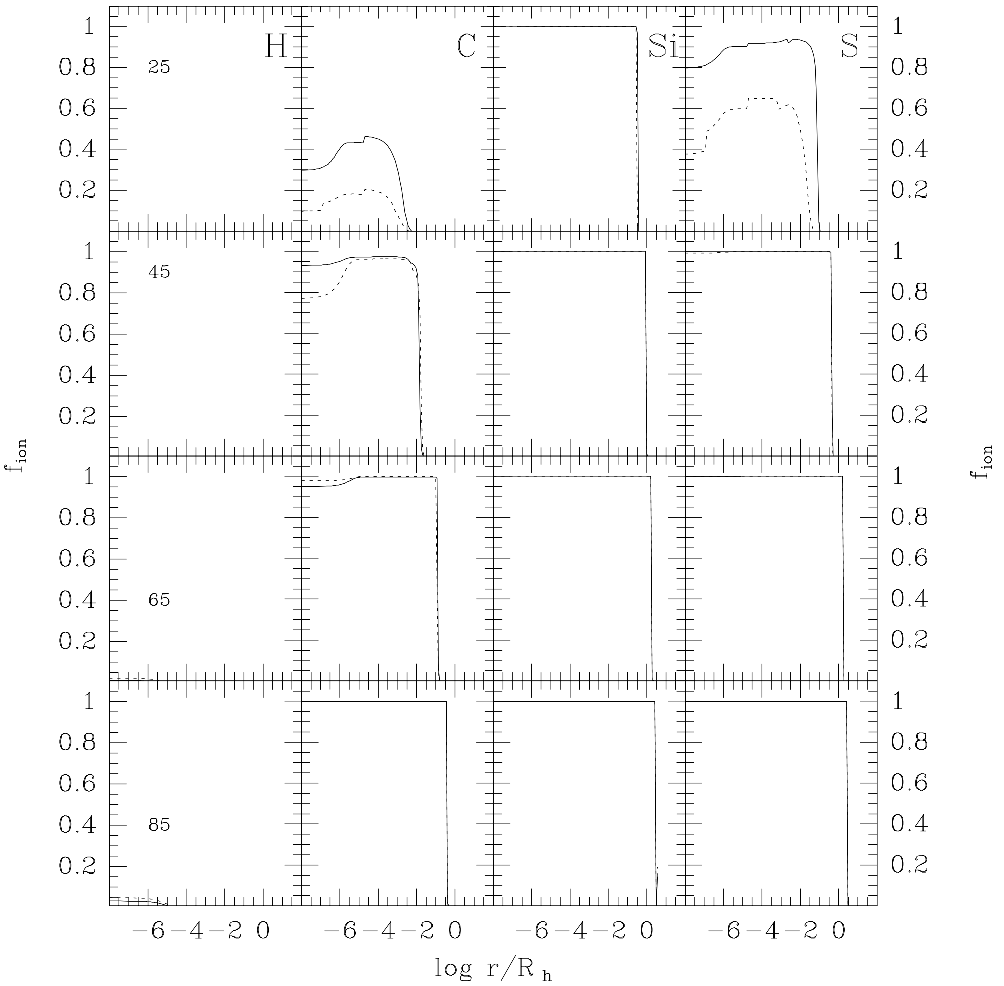

Figure 2.22: Ionization structure of a nova shell for a model with enhanced CNO abundances and a radiation field which results from radiation transfer calculations. The degree of ionization throughout the shell is shown for the elements H, C, Si and S for the enhanced abundance model (solid line) and the corresponding solar abundance model (dotted line). The diagrams for each species are showing the state of ionization for four different times after the nova explosion: $t_1 = 25d$ (top), $t_2 = 45$d, $t_3 = 65$d and $t_4 = 85$d (bottom). They are plotted versus a logarithmic normalized radius scale, where r is the distance of the ionization fronts from the inner shell boundary and R_h is the thickness of the moving gas shell.

2.5.3.3 Comparison with Blackbody Models

In the first few days of the shell expansion the ionization of all species is lower in the non-LTE model compared with a corresponding blackbody calculation. In this phase when the photospheric temperature is 10000 K the Stroemgren spheres of hydrogen and carbon in the blackbody case are more than one order of magnitude larger than in the non-LTE model. Especially hydrogen exhibits a moderate

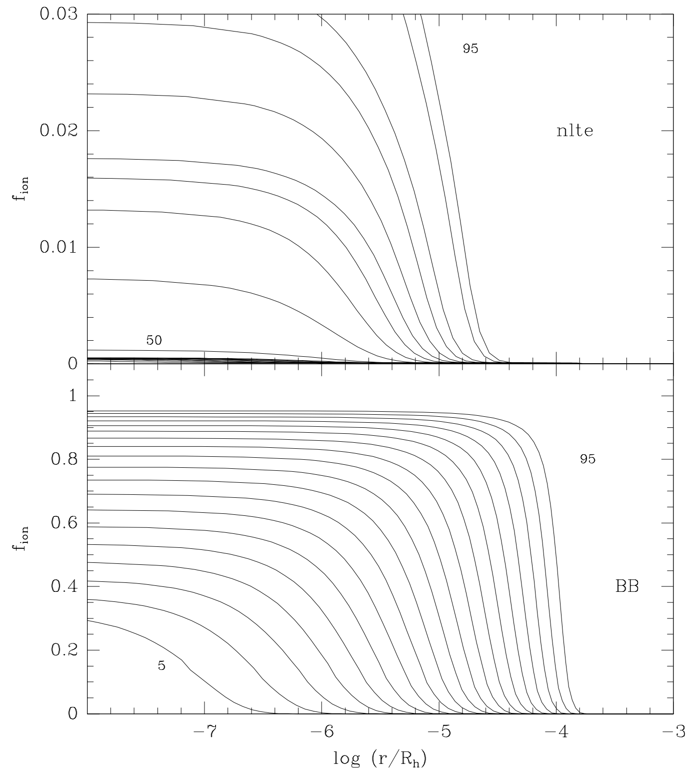

Figure 2.23: Time dependence of H-ionization fronts in nova shells for a model with enhanced CNO abundances (see Fig. (2.16). The ionization fronts of hydrogen are shown for the non-LTE model (top) and the corresponding black body model (bottom). The abscissa is the logarithmically normalized radius scale, where R_h is the shell diameter. The time interval between each curve is $\Delta t = 5d$. In each diagram two curves are labelled with the corresponding value of the time interval after the nova outburst.

ionization of f^H_{ion}=0.13, thus H^+ is the most abundant ion. This causes the electron temperature to rise to T_e=8200 K inside the zone with $\tau \leq 1$. Outside this region for $1< \tau < 10^4$ the main heating mechanism is given by carbon ionization, which still keeps the temperature as high as $6200\,K$. This condition holds until $r = 5 \cdot 10^8$ cm. The Stroemgren radius of silicon is $R^{Si}_{st} = 7.8 \cdot 10^9$cm, which is two times the non-LTE value. For later phases ($t > 50\,d$) the extension of the ionization spheres are nearly equal and for $t > 60\,d$ the non-LTE value slightly exceeds the corresponding blackbody value. The flux of photons capable of ionizing silicon increases as T_* also increases up to T_*=30000 K. For this photospheric temperature the synthetic spectra have higher UV-fluxes in the wavelength range of interest than the blackbody model. The emission line flux in this spectral region exceed the continuum flux. The influence of the line blanketing, which has led to a significant flux reduction for models with $T_* <$ 20000 K, has substantially decreased. The electron temperatures

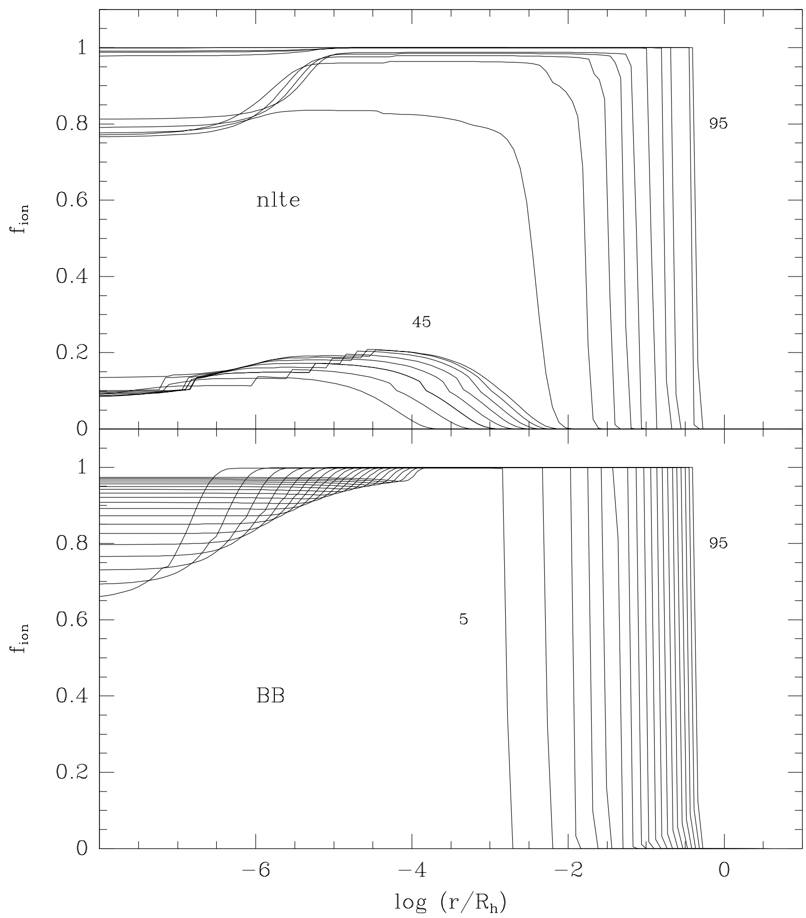

Figure 2.24: Time dependence of carbon ionization fronts in nova shells for a model with enhanced CNO abundances (see Fig. (2.16). For detailed information see Fig. (2.23).

of the blackbody model reaches typical HII region values in the innermost parts of the shell (T_e=9200 K), falling to T_e=6000 K at the outer boundary of the HII zone. In the transition region from the CII to the CI region the temperature drops further to 3700 K. At this time the temperature in the non-LTE case is only T=1100 K. This large temperature difference, due to the increased degree of ionization for the bb models holds until $t = t_{end}$. We assume that for the phase $t > t_{end}$ the temperatures of both models will approach each other, due to the steady increase of the photospheric temperature.
For models with higher abundances of C, N and O, where the abundances of all other species remain unchanged, we derive results which show that the effect of this increase on the ionization of the other atoms is small for both types of models.

2.5.3.4 Influence of Enhanced CNO Abundances

The studies of nova abundances clearly show that large overabundances of heavy elements do occur in all objects so far studied. In this work we concentrate on the CNO

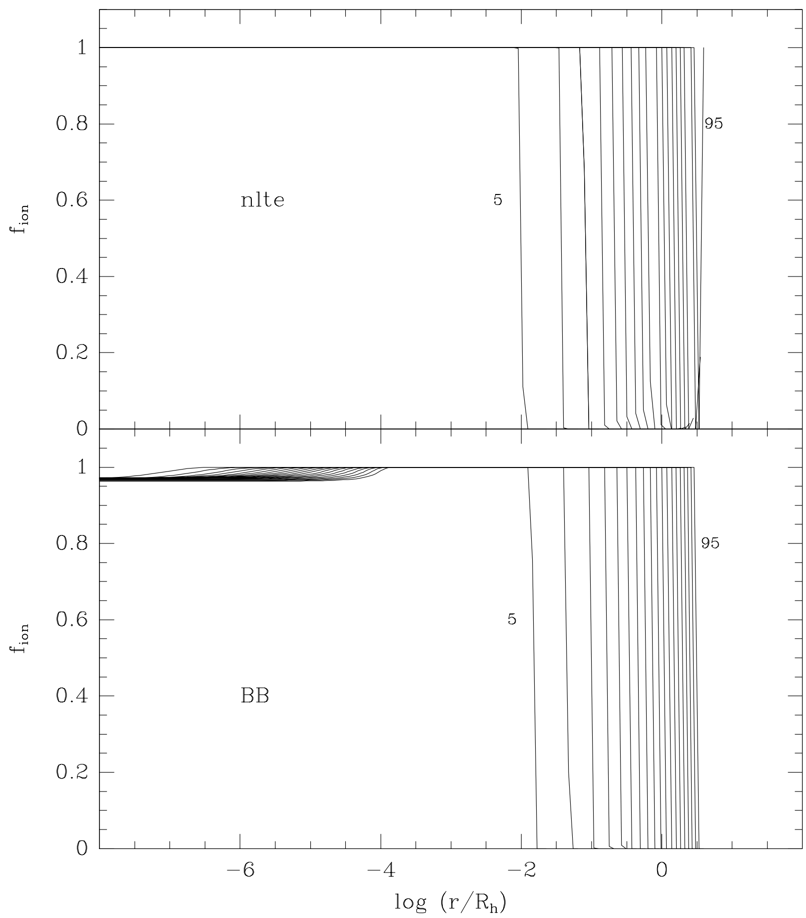

Figure 2.25: Time dependence of Si ionization fronts in nova shells for a model with enhanced CNO abundances (see Fig. (2.16). For detailed information see Fig. (2.23).

elements and do not refer to the cases of those novae having large overabundances of oxygen, neon, magnesium and heavier elements. It is now commonly accepted that the most reasonable way by which these characteristic overabundances observed in classical novae may have been generated is by mixing material from the underlying white dwarf into the newly accreted layer. Depending on the enrichment of the surface layers of the white dwarf C/O or ONeMg novae will occur. The consistently high nitrogen abundances are are a result of the explosive nuclear burning which converts carbon and oxygen preferentially into nitrogen.

The model calculations obviously show, that the general structure of the ionization is not remarkably changed by the enhancement of CNO nuclei. Hydrogen, nearly completely neutral in the considered mode, and silicon, instantaneously ionized, do not show any difference in their ionization front evolution. Carbon, the most interesting case, and sulfur do reveal a slight effect during the first epoch of the nova outburst.

Tief im menschlichen Unterbewußtsein regt sich ein drängendes Bedürfnis nach einem logischen Universum, das Sinn ergibt. Aber das wirkliche Universum ist der Logik immer einen Schritt voraus.

F. Herbert

Chapter 3

Chemistry in Circumstellar Shells

3.1 Introduction

Massive, extended circumstellar envelopes (CSEs) ejected by the red giants at the very end of their evolution are among the most interesting objects for cosmic chemistry. The study of these shells can provide significant information on the late stages of stellar evolution and the chemical reprocessing of the interstellar medium. Basic to this subject is a detailed understanding of the physical and chemical processes operating in these envelopes.
CSEs are also the most obvious location of the formation of cosmic dust grains, in which about 50% of the mass of the heavy elements in the interstellar medium are locked up. Although a lot of substantial information about circumstellar chemistry has been obtained from the detection of infrared spectral features, characteristic for the absorption and emission by macroscopic solid particles (Neugebauer and Leighton 1969, Treffers and Cohen 1974, Woolf and Ney 1969 and Soiffer et al. 1981), no comprehensive theoretical picture of the grain formation including non-equilibrium (non-LTE) chemistry has been drawn by now. In our present attempt we focus our attention on the chemical processes preceding and therefore mainly affecting the nucleation and growth of dust particles. In contrast to other investigations, which do not focus on the interdependencies of UV-field, chemistry and dust formation (Huggins 1987, Slavsky and Scalko 1984, Glassgold and Huggins 1986, Nejad and Millar 1987, Clegg et al. 1983) and Nejad and Millar 1988) this intention allows to restrict our calculations to the inner shell region. In the vicinity of the red giant the stellar radiation field, being the source of ionizing and photodissociating photons, plays a crucial role in determining the molecule concentrations. If the UV-field, especially that of a chromosphere, is strong enough the chemistry could be driven far from equilibrium. The abundances of H_2O, H_2 and SiO therefore will differ significantly from the values given by chemical equilibrium (CE) calculations (Gail and Sedlmayr 1986b, 1987a).

Observations show that the expanding circumstellar envelopes of late-type stars generally divide into carbon–rich shells defined by a C/O ratio > 1 and oxygen-rich shells defined by a C/O ratio < 1 (Zuckerman 1980, Knapp and Morris 1985 , Cernichario and Guéli 1987). Recent investigations concerning the IRAS data ([Willems and deJong 1986] , [Whitmore 1986]) have shown, that there exist a number of stars optically identified as oxygen-rich but surprisingly having a SiC dust-emission feature. This apparent contradiction is due to a C/O ratio approaching unity [Skinner *et al.* 1990] , so that the kind of dust which will be formed in their circumstellar environment critically depends on the specific physical and chemical conditions.

Model calculations of the circumstellar chemistry usually assume that, due to its strong bond, the CO-molecule locks up either all of the available oxygen (C-rich shells) or carbon (oxygen-rich shells), respectively (Tsuji 1973, 1978, , McCabe and Connon–Smith 1979, Lafont et al. 1982, Glassgold et al. 1987, and Glassgold et al. 1989). Although this is a commonly accepted feature, this assumption is based on chemical equilibrium arguments only. In many cases, however, the fundamental assumption of chemical equilibrium is not appropriate for a realistic description of circumstellar shells surrounding late-type stars. On the contrary, effects which tend to produce strong deviations from CE are common, as indicated by the observations of

- high outflow velocities up to 20 km/s (Bernat et al. 1979, Knapp et al. 1980, Honeycutt et al. 1980 and Mauron et al. 1984),
- strong chromospheric UV–radiation fields (Carpenter 1984, Brown and Carpenter 1984 and Carpenter 1985), and
- oscillations of the UV–field and the gas temperature (e.g. for α-Ori (Dupree et al. 1978).

Especially in the case, when the C/O ratio approaches unity, theories assuming chemical equilibrium are not realistic. For these reasons the non-equilibrium situation has to be accepted as the standard case of CS chemistry.

As it has been shown by Goeres et al. (1988) , the presence of a stationary UV-field as well as oscillations of the thermodynamic quantities can cause large deviations even from kinetic equilibrium (KE), so that a fully time dependent treatment of the problem is required. Earlier theoretical studies of the chemical processes in O-rich CSEs are either lacking the treatment of the stellar UV radiation (Scalo and Slavsky, 1986) or, for the purpose of simplicity, are based on the assumption of kinetical equilibrium, thus calculating only steady-state concentrations ([Clegg *et al.* 1983] , [Glassgold and Huggins 1986]).
In this work the non-LTE chemistry in the innermost regions of oxygen-rich circumstellar shells is investigated. We put the main emphasis on the study of the influence of the stellar radiation field on the chemical processes in view of the special significance of the CO-molecule and grain formation for the radial structure of these shells. In O-rich environments siliconoxide is one of the most favourable candidates for the primary dust condensation process [Gail and Sedlmayr 1986b] . The exploration of the reaction pathways leading to SiO and determining its concentration therefore is inevitable in order to obtain a more sophisticated picture of the regions inside the dust shells of mass-loosing late type stars.

Furthermore, dust grains, being macroscopic solids, have important properties which each could bear a significant influence on the physics of a system:

- the absorption of short wavelength photons and the subsequent emission at longer wavelength plays an important role for the thermal structure and for the spectral appearance of a dusty object. This energy thermalisation leads to a thermal decoupling of the dust grains from the ambient gas component and can result in a dust temperature which deviates significantly from the temperature of the surrounding gas (greenhouse effect).
- radiative momentum is absorbed by dust particles and effectively transmitted to the gas by frictional coupling. This effect can cause an efficient acceleration of the matter which dominates the hydrodynamic structure of a circumstellar envelope. In the case of luminous late-type stars substantial mass loss can be driven by this effect.
- the emerging of a dust grain in a gaseous system introduces a surface in the plasma, which allows now for a variety of chemical reactions which would not occure in the pure gas phase. In particular reactions are concerned which require a third reaction partner (H_2 formation).

In the case of late-type stars with chromospheres and mass–loss rates $\dot{M} \leq 10^{-5}\ \mathrm{M}_\odot/\mathrm{yr}$ only small to moderate amounts of dust are expected to form. As a result the back-reaction of the grains on the structure of the inner shell region will also be small and no dust driven wind can evolve. As long as the condition of a small dust to gas ratio holds, the neglect of the influence of the dust on the global structure of the circumstellar shell will have no significant effect on the results of our model calculations. On the other hand, for a late-type star without a chromosphere and a substantial mass outflow, the quantitative description of such an object would require the simultaneous treatment of radiation transfer, hydrodynamics, chemistry, and dust nucleation and growth, as all these effects are interdependent and non-linearily coupled. However, this is out of the scope of this work. Nevertheless, in this case the results of our calculation of the chemistry are reliable inside the dust condensation zone, e.g. for distances smaller than the sonic point radius. Outside this region, when the velocity of the material increases due to the radiation pressure on the dust grains, the chemistry will be affected by this acceleration.

3.2 Gas–Phase Reactions

3.2.1 Ion-Neutral Reactions

Undoubtedly the most important types of astrophysical gas-phase reactions are those between one neutral and one ionized species. The overwhelming fraction of known rate coefficients belongs to this reaction type (see Appendix). The bimolecular reactions are well studied (e.g. Prasad, 1977) by a variety of experimental techniques including ion cyclotron resonance spectroscopy, flowing afterglow and flow tubes. These experiments show that for the great majority of exothermic reactions the rate coefficients for a reaction

$$\mathrm{X}^+ + \mathrm{YZ} \Longrightarrow \mathrm{XY}^+ + \mathrm{Z} \tag{a}$$

are independent of the temperature in the range covered by the experiments (300–1000K). The typical value of a reaction coefficient for (a) is of the order of $10^{-9}cm^{-3}s^{-1}$. Apart from the fact that there exist a number of exceptions unknown rate coefficients such can be estimated with moderate confidence.
The more exact theoretical calculation of the ion–neutral rate coefficients is based on quantum mechanics. As the motion of the electrons is always fast in comparison with the heavy nuclei, the nuclei may be regarded as moving in an multidimensional potential energy hypersurface created by the moving electrons. Thus the separation of nuclei and electronic motions is possible, which means that the Born–Oppenheimer approximation is valid and affords a great simplification of the problem, but, however, the concrete solution of this problem remains rather complex and leads to an obscuration of the simple results derived from the experiments.
Thus we present the classical treatment of the process which provides some basic understanding. It is based on the fact that the charged particle induces a dipole in the previously neutral species. The interaction of a particle with charge e and a dipole with polarisability α_p can be treated as a typical orbital problem and the governing force of this interaction is described by an inverse fifth power force leading to the interaction energy

$$E_{int} = -\frac{\alpha_p e^2}{2r^4} \tag{3.1}$$

where r is the ion–molecule distance. Beyond a critical impact parameter

$$b_0 = \left(\frac{4e^2\alpha_p}{\mu v^2}\right)^{1/4} \tag{3.2}$$

with $\mu^{-1} = m_n^{-1} + m_{ion}^{-1}$ being the reduced mass, m_n and m_{ion} the mass of the neutral and the ionized particle, respectively and v the gaskinetic velocity, the path of the particle is only deflected and kinetic energy is exchanged, but the interaction does not result in a capture; if $b < b_0$ collision will occur. The geometrical cross section for a collisional event therefore is

$$\sigma = \pi b_0^2 \tag{3.3}$$

and the rate-coefficient given by

$$k = \sqrt{\frac{4e^2\pi^2\alpha_p}{\mu v^2}} \cdot v \tag{3.4}$$

does not depend on the velocity. This temperature independent rate coefficient **(Langevin–rate)** only slightly depends on the reduced mass μ and the polarisability α, which for stable molecules lies in a quite narrow range (see e.g. CRC Handbook (Weast, 1988)), thus inferring the Langevin rate coefficient to be of nearly the same order in many neutral–ion reactions.
The outlined theory proves to be only a poor approximation for those reaction involving polar molecules, as the interaction potential is incorrectly represented. The same argument applies to such systems which are not in spherically symmetric states. For these situations the average dipole orientation theory gives the rate coefficient in the parametrized form

$$k_{dipole} = \frac{2\pi e}{\sqrt{\mu}} \left[\sqrt{\alpha} + c\mu_d \sqrt{\frac{2}{\pi k T}} \right] \tag{3.5}$$

where μ_d is the dipole moment of the polar molecule, T is the kinetic temperature and c is a parameter depending on $\mu_d/\sqrt{\alpha}$. Thus compared with (3.4), a correction term is introduced which accounts for the temperature dependence of the dipole ion interaction.
Special types of ion–molecule reactions are

a)<u>Proton–transfer</u>

$$XH^+ + Y \Longrightarrow YH^+ + X \tag{b}$$

which generally occurs if the reaction is exothermic.

b) <u>H–atom abstraction</u>

$$X^+ + H_2 \Longrightarrow XH^+ + H \tag{c}$$

does not always occur with the collisional Langevin rate in exothermic cases. It is therefore difficult to make reliable predictions of the rate coefficients.

c) <u>Proton elimination reactions</u>

$$X^+ + YH \Longrightarrow XY + H^+ \tag{d}$$

This reaction type apparently does not occur.

d) <u>Condensation reactions</u>

$$CH_3^+ + NH_3 \Longrightarrow CH_2NH_2^+ + H_2 \tag{e}$$

In this type of chemical reactions new bonds between "complex" molecules are formed.

e) Charge–transfer Reactions

The charge–exchange reactions are also of indisputable importance for circumstellar chemistry. A significant example for an effective charge–exchange is the reaction:

$$H^+ + O \Longrightarrow H + O^+ \tag{f}$$

which initiates a basic part of the oxygen chemistry. In the adiabatic region of the charge–exchange interactions the energy of the collisions is too low, thus the electron can adjust to the changing environment. If the collision duration gets comparable to electron transfer time by increasing the collision energy, the probability of the electron transfer rapidly increases. Experimental analysis show that the transfer probability is inversely proportional to the difference in the ionization potentials of the interacting molecules or atoms. Additionally to the energy resonance the Franck–Condon principle must be satisfied, which means that the overlap region of the wave functions must be sufficiently large. When both criteria are met the classical approximation is valid and Eq. (3.4) is applicable. Therefore rate coefficients of $10^{-9} - 10^{-10}\, cm^3 s^{-1}$ are expected.

3.2.2 Neutral–Exchange Reactions

A more complicated situation is existing if two neutral complexes are involved in a reaction

$$X + YZ \Longrightarrow XY + Z \tag{g}$$

Measurements of the rate coefficients for such reactions have shown that very strong temperature dependence may occur. On the other hand many reactions involving carbon atoms show only little sensitivity to a change in the kinetic temperature. A crude estimation of the order of magnitude of the rate coefficient, based on the simple model that the interacting particles could be considered as hard spheres only interacting when an impact of the spheres occur thus giving a typical "geometrical"' cross section of $10^{-15}\, cm^{-2}$. The relative velocity of the reaction partners normally lies in the range of $10^4 - 10^6 cm/s$ thus the collisional approach leads to a rate coefficient of about $10^{-9} - 10^{-11}\, cm^3 s^{-1}$, a value which for example is valid for the reaction

$$O + OH \Longrightarrow O_2 + H \tag{h}$$

Anyway if the reaction is endothermic this model breaks down. In a reaction of the type (g) the electrons of species X can be in a configuration which gives rise to an instantaneous dipole moment in the *YZ* molecule and therefore an attractive potential is created which is weak and varies with intermolecular distance as r^{-6}. This attraction force is strengthened if one of the molecules is polar. When the reaction partners approach the dispersion r^{-6} interaction potential no longer adequately describes the situation, rather *X* and *YZ* form an activated complex $(XYZ)^*$ in which all atoms are closely interacting. The application of the Born-Oppenheimer approximation then allows to describe the interaction of the $(XYZ)^*$ components in terms of a function which only depends on the separation of *X*, *Y* and *Z*. The determination of this energy hypersurfaces by quantum mechanical methods and the calculation of the motion of that point representing the reaction considered on this surface by application of the classical laws of motion will make it possible to deduce a reliable rate coefficient which will be of the type

$$k = AT^{1/2} exp[-E_a/kT]. \tag{3.6}$$

If the relation $T > E_a/k$ holds the exponential term is of little effect. When $T < E_a/k$ the influence of the exponential will be dramatic. Some examples of neutral exchange reactions are shown in the following table[1]:

Reaction	A	α	E_a
$H + CH \rightarrow C + H_2$	1.71 (-11)	0.50	2200
$H + NH \rightarrow N + H_2$	1.73 (-11)	0.50	2400
$H + CO \rightarrow C + OH$	1.10 (-11)	0.50	77700
$O_2 + CH_2 \rightarrow H_2CO + O$	1.44 (-11)	0.50	3500
$OH + HCN \rightarrow H_2O + CN$	1.00 (-10)	0.60	2500

3.2.3 Radiative Association

The exemplified radiative association process

$$\mathrm{X} + \mathrm{Y} \Longrightarrow \mathrm{XY} + h\nu \tag{i}$$

can be realized by a variety of different reactions, as the reaction partners may be atoms, ions, radicals or molecules.

Based on a classical treatment and the assumption that the colliding particles are in the ground state[2] it is clear that the approach of *X* and *Y* proceeds along along a potential energy curve which is connected to the ground states of *X* and *Y*. One possibility is that the approach may go along a repulsive energy curve then there is no significant overlap of the charge clouds of *X* and *Y* and no chemical change

[1] data were taken from UMIST rate file [Millar *et al.* 1991b]

[2] This may be not true in the high temperature zones of the nova gas, but it is a useful simplification for the demonstration of some basic ideas, and however valid in the outer zones of circumstellar envelopes and naturally in the interstellar medium.

of the system will occur. But the approach may also proceed along a bound state curve and a close encounter followed by the formation of a true molecular state XY may be the result.
Generally the newly created complex XY has an excess energy E_{coll} which must be delivered e.g. by a photon of the energy $h\nu > E_{coll}$. In this way the system will get stabilized and the molecular components can no longer separate to infinity. Thus the existence of two bound states connected to the same ground state between which radiative transitions must be allowed, is a necessary prerequisite of radiative association to occur.
The estimation of the approximate size of the rate coefficient can be founded on two facts:

- The duration time of a collision is of the order of 10^{-14}s. Within this interval stabilisation must occur.
- The transition probability for a strong transition is about $10^8 s^{-1}$. Therefore the average time for a transition is 10^{-8}s and the probability for the occurence of such a transition while the collision takes place is 10^{-6} per collision.

If one takes the reaction coefficient for a neutral interaction which is $10^{-11}\, cm^3 s^{-1}$ one expects a radiative association rate coefficient[3] $k_{RA} = 10^{-17}\, cm^3 s^{-1}$.
A different situation prevails if, instead of an atom or ion, a molecule or a radical are part of the radiative association reaction. Initially this reaction will lead to a intermediate molecular complex of sufficient energy to undergo a subsequent dissociation. However, the more complex the molecule formed the more degrees of freedom are available to distribute the collisional energy and the time for the appearance of the whole dissociation energy in one single bond therefore disrupting the molecule may be sufficiently large to stabilize the excited system by either radiation or a second collisional event. If one considers a radiative de–excitation this can be represented as a two-step process:

$$1: \quad X + Y \quad \overset{k_{1f}}{\underset{k_{1r}}{\Longleftrightarrow}} \quad XY^*$$

$$2: \quad XY^* \quad \overset{k_2}{\Longrightarrow} \quad XY + h\nu$$

for which the rate coefficient of formation of XY is given by

$$k_{XY} = \frac{k_{1f} k_2}{k_2 + k_{1r}}. \tag{3.7}$$

The dissociation coefficient k_{1r} is a very steep function of the number of bonds in the XY molecule. With increasing number of degrees of freedom the k_{1r} rate coefficient decreases very rapidly as the comparison of the values of k for the dissociation reactions

[3]Various quantum mechanical calculations deriving the matrix element of the dipole moment between the free and the bound state wave functions, give about the same value.

$$\begin{array}{ll} CH_4 \longrightarrow CH_3 + H & k=6.20\cdot 10^{8} s^{-1} \\ C_4H_{10} \longrightarrow C_2H_5 + C_2H_5 & k=7.00\cdot 10^{-4} s^{-1} \end{array}$$

clearly shows.
The temperature dependence of k_{RA} is not known. Some evidence from ternary reactions is suggesting that the radiative association reactions are most effective at low temperatures. In spite of the existing theoretical methods shortly outlined above the reaction rate coefficients can differ substantially for this reaction class depending on the special reaction partners involved and their electronic configuration. Thus a reliable prediction of unknown rate coefficients seems to be not very promising and instead the data shall be deduced from laboratory experiments.

Reaction				A	α	E_a
C	+H	$\rightarrow$CH	+hν	1.00 (-17)	0.00	0.00
C	+O	$\rightarrow$CO	+hν	2.10 (-19)	0.00	0.00
CH_3	+CN	$\rightarrow CH_3CN$	+hν	1.00 (-16)	0.00	0.00
CH_3^+	$+H_2O$	$\rightarrow CH_3OH_2^+$	+hν	5.50 (-12)	-1.70	0.00
C^+	$+C_3$	$\rightarrow C_4^+$	+hν	1.00 (-13)	-1.00	0.00
C^+	$+C_4$	$\rightarrow C_5^+$	+hν	1.00 (-09)	0.00	0.00
CH_5^+	+CO	$\rightarrow C_2H_5O^+$	+hν	7.20 (-24)	-2.30	0.00

3.2.4 Dissociative Recombination

The process of dissociative recombination is realized e.g. by the fast CO formation route

$$HCO^+ + e^- \Longrightarrow CO + H \tag{j}$$

In this reaction first an intermediate state is formed

$$HCO^+ + e^- \longrightarrow HCO^*$$

through the excitation of an electron of the HCO^+ ion whereas the incident electron itself occupies a vacant orbital of the HCO. The energy brought in by the electron must correspond to the energy difference between the energy in the (HCO^* + e^-) and the HCO^* energy potential curve. If the two neutral components are formed there remains a certain probability for autoionization to occur if the separation has not become too large. Nevertheless the time scale for the separation is very short ($\approx 10^{-14}$s) since the repulsive force is too great for autoionization to prevent the dissociation process. Thus one basic requirement for an efficient dissociative recombination is that there should be at least one of the many states of HCO lying close to the initial state of HCO^+.
More advanced theoretical considerations show that the rate coefficient is in the range of 10^{-6}–10^{-7} cm^3s^{-1} and the temperature dependence is described by a $T^{-1/2}$ term.

3.2.5 Negative–Ion Reactions

Although the negative ions, even of the most abundant ions, are known to exist only on a low concentration level, the chemical processes involving these ions may be fast and effective thus often being an important intermediate reaction step in the formation of some species (e.g. H_2). Negative ions are part of various chemical processes as there are

$$\begin{array}{llll} X + e^- & \longrightarrow X^- + h\nu & \text{radiative attachment} \\ X^- + h\nu & \longrightarrow X + e^- & \text{photodetachment} \\ X^- + Y & \longrightarrow XY + e^- & \text{associative detachment} \\ X^- + Y^+ & \longrightarrow X + Y & \text{neutralisation} \end{array}$$

a) Radiative attachment
This process differs from the radiative recombination[4] in the way that the electron–neutral interaction is much weaker than the ion-electron one. Therefore one expects that the radiative attachment rate coefficient is much smaller than the radiative recombination rate coefficient.
Assuming that the typical rate coefficients for charge induced dipole collisions is of the order of $10^{-9}\,cm^3s^{-1}$, one must account for the fact that the collision time is short (10^{-14}s) compared to the radiation time (10^{-8}s), thus the probability for the emission of a photon is $10^{-6}\mathrm{s}^{-1}$ and the rate coefficient tends to be of the order $10^{-15}cm^3s^{-1}$.

b) Photodetachment
This process is fairly effective because the electron-neutral binding energy in the negative ion configuration is usually low. Therefore the electron neutral separation is large and this implies a large dipole moment present in the system and photons within a wide wavelength range are capable to detach the electron. For the case of the interstellar radiation field acting on the H^- ion a photodetachment rate coefficient of $10^{-7}\mathrm{s}^{-1}$ has been deduced. If the intensity of the radiation field is higher as for example in the presence of a chromosphere (see Chap. (3.6)) the rate for photodetachment is increased by many orders of magnitude.

c) Associative detachment
The effectivity of this reaction is controlled by a charge induced dipole interaction. This implies that the reaction rate coefficient may be of the same order as the ion–neutral collisional rate coefficient ($10^{-9}\,cm^3s^{-1}$) dependent on the probability with which every collision will lead to a reaction. The probability depends on the concrete energetic conditions of the particle approach, e.g. if the particles approach on a repulsive energy curve only an elastic scattering will occur, or if they approach on a bound state curve the reaction probability just depends on the probability for autoionization to occur which may prevent the associative detachment. Experiments

[4]Radiative recombination is not outlined in this chapter as this is described in the context of ionization structure of novae.

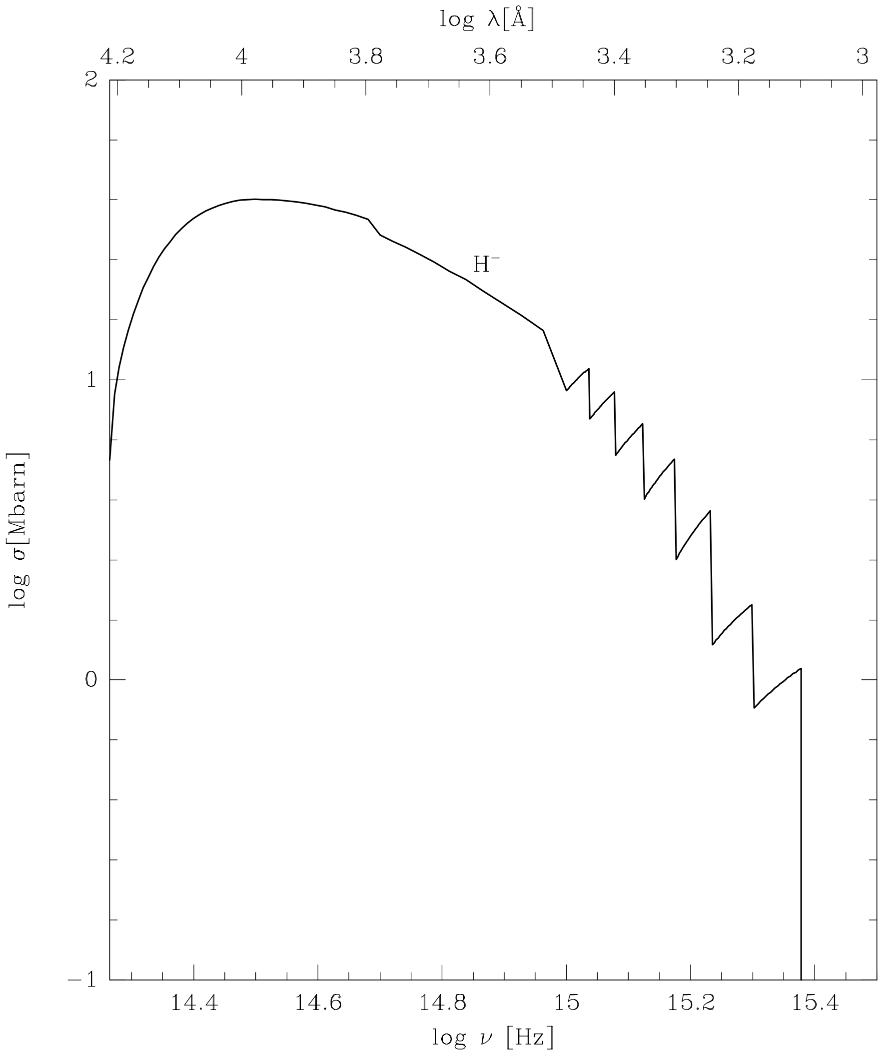

Figure 3.1: The photodetachment cross section for the H^- ion. Data were taken from Wishart *et al.* (1979).

show that these reaction will occur with a high rate or will not occur at all. Experiments also show that, if X^- and Y are atoms all exothermic associative detachments are fast. If X and Y are molecules no reliable prediction can be made. The rate coefficients for some representative reactions are shown in the table.

Reaction				A	α	E_a
H^-	$+H$	$\rightarrow H_2$	$+e^-$	1.30 (-09)	0.00	0.00
H^-	$+CO$	$\rightarrow HCO$	$+e^-$	5.00 (-11)	0.00	0.00
C^-	$+O$	$\rightarrow CO$	$+e^-$	5.00 (-10)	0.00	0.00
O^-	$+H_2$	$\rightarrow H_2O$	$+e^-$	7.00 (-10)	0.00	0.00
OH^-	$+CH_3$	$\rightarrow CH_3OH$	$+e^-$	1.00 (-09)	0.00	0.00

d) Neutralisation

In the case of mutual neutralisation the interaction is dominated by long range Coulomb forces thus a large reaction cross section will be the result. Laboratory measurements and theory agree in the fact that the temperature dependence is $T^{-1/2}$. This means that slower approaches favour the neutralisation. In the most favourable circumstances every negative ion formed might lead to the formation of a molecule, which has found to be true especially in the case of reactions with H_2. Rate coefficients for these reactions are presented in table 3.2.5

Reaction	A	α	E_a
$NH_4^+ + H^- \rightarrow NH_3 + H_2$	2.30·(-07)	-0.50	0.00
$H_3O^+ + H^- \rightarrow H_2O + H_2$	2.30·(-07)	-0.50	0.00
$Mg^+ + C^- \rightarrow Mg + C$	2.30·(-07)	-0.50	0.00

For an overview of the size and temperature dependence of the rate coefficients for the various types of reactions the rate coefficients for a set of representative reactions are drawn in Fig. (3.2). The reactions drawn and the corresponding data[5] are shown in the table[6]

Type	Reaction	A	α	E_a
CRI	$H + CR \rightarrow H^+ + e^-$	1.00·(-17)	0.00	0.00
IN	$H^+ + C_2H \rightarrow C_2^+ + H_2$	1.50·(-09)	0.00	0.00
NEx	$O + H_2 \rightarrow OH + H$	9.12·(-12)	1.00	4480
CD	$H + H_2 \rightarrow 3H$	4.67·(-07)	-1.00	55000
ChTr	$H^+ + H_2 \rightarrow H_2^+ + H$	1.00·(-10)	0.00	21200
HyAb	$C^+ + H_2 \rightarrow CH^+ + H$	1.00·(-10)	0.00	4640
PTr	$H_3^+ + O_2 \rightarrow O_2H^+ + H_2$	5.00·(-09)	0.00	150
AsDe	$H^- + H \rightarrow H_2 + e^-$	1.00·(-09)	0.00	0.00
NRAs	$N^+ + H^- \rightarrow H + N$	2.30·(-07)	-0.50	0.00
RadAs	$CH_3^+ + H_2 \rightarrow CH_5^+ + h\nu$	1.30·(-14)	-1.00	0.00
DRec	$CO^+ + e^- \rightarrow C + O$	1.80·(-07)	-0.50	0.00
PhIo	$OH + h\nu \rightarrow OH^+ + e^-$	1.60·(-12)	0.00	2.1
PhDi	$OH^+ + h\nu \rightarrow H^+ + O$	1.00·(-12)	0.00	1.8

[5]All data were taken from the UMIST rate file [Millar *et al.* 1991b]

[6]For the photoprocesses a constant interstellar radiation field is assumed [Draine 1979] .

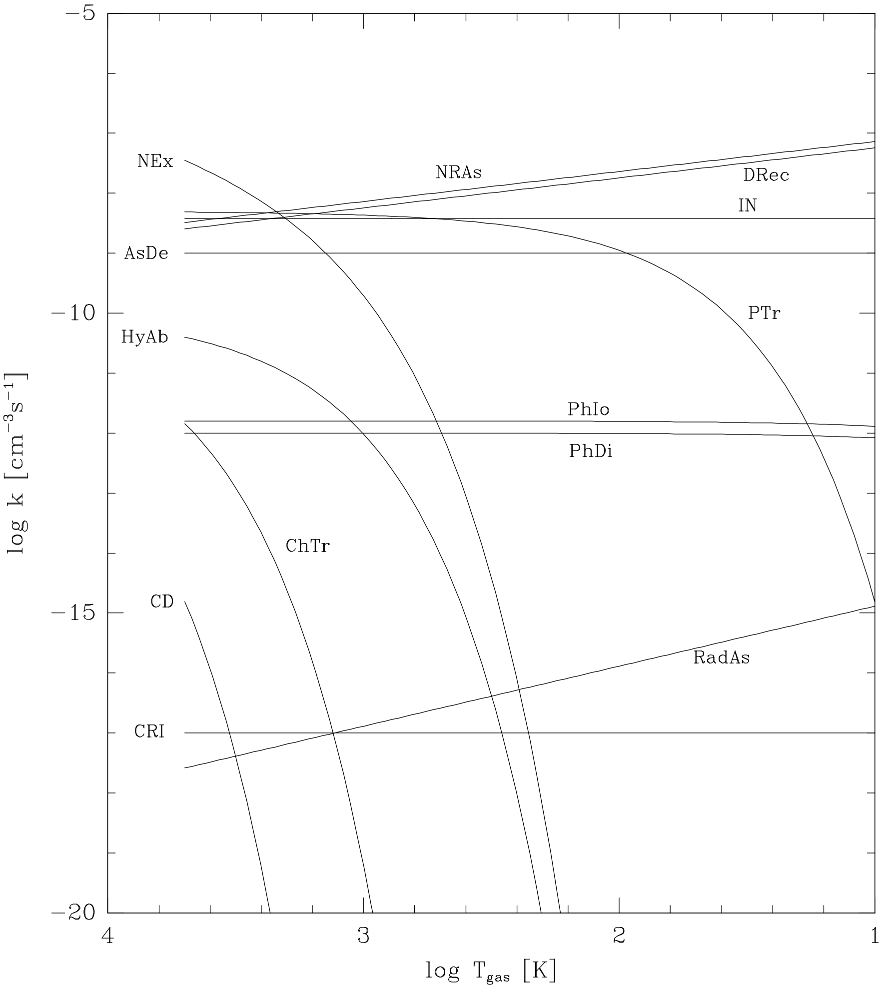

Figure 3.2: The temperature dependence of the rate coefficients for various processes including photoprocesses are presented. The following abbreviations were used: CRI: Cosmic ray ionization; IN: Ion–molecule reaction, NEx: Neutral exchange reaction; CD: Collisional dissociation; ChTr: Charge transfer; PTr: Proton transfer; HyAb: Hydrogen abstraction; AsDe: Associative detachment; NRAs: Neutral radiative association (neutralisation); RadAs: Radiative association; DRec: Dissociative Recombination; PhIo: Photoionization; PhDi: Photodissociation.

3.2.6 Basic Equations

For the description of the chemistry we consider a system of N reacting species i. With our assumption of spherical symmetry the equation of continuity can be written in comoving coordinates as

$$\frac{\partial n_i}{\partial t} = -2n_i \frac{v}{r} - n_i \frac{\partial v}{\partial r} + Q_i \quad ; \quad i = 1....N \tag{3.8}$$

where n_i is the particle density of species i and Q_i the source-term describing all chemical processes. Q_i consists of all gain and loss rates involving the species i and including kinetic- as well as photo processes. For practical purposes it is advantageous to use the concentration x_i instead of the particle densities. Therefore we introduce the particle concentration of species i according to

$$x_i = n_i/n_{<H>} \qquad \text{with} \qquad n_{<H>} = n_H + n_{H_2} \tag{3.9}$$

approximately being the total number density of H atoms in the reaction network. In our reaction network only two body reactions are taken into account. The particle densities in CSEs usually are smaller than 10^{11}cm^{-3} and, for this reason, three body collisions, which could be important for some H_2 formation reactions at densities above 10^{11}cm^{-3}, are negligible in the density regime under consideration.
The rate coefficient k_f for forward reactions and the corresponding rate coefficient for the backward rate are related by the thermodynamical expression

$$k_r = k_f \, e^{-\Delta G/RT} \tag{3.10}$$

with $\Delta G = \Delta H - T\,\Delta S$ being the change in Gibbs free enthalpy, which accounts for the enthalpies H and entropies S of all species involved in the reaction. The forward reaction coefficient k_f is parametrized by the empirical Arrhenius law

$$k_f = AT^{\beta} e^{-E_a/kT} \tag{3.11}$$

where the pre-exponential factor A, the temperature exponent β and the activation energy E_a are derived from experimental results for k_f. For the great majority of reactions only the pre-exponential factor A is non-zero. Only some special kinds of reactions deviate from this rule; particular reactions involving oxygen and hydrogen components show activation energy barriers E_a. Electronic recombinations usually have a temperature dependence with an exponent in the range $-0.3\ldots-0.9$ (Aldrovandi and Péquinot, 1973).
The photo-ionization and photo-dissociation rates are given by

$$\mathcal{R} = 4\pi \int_{\nu_{th}}^{\nu_\infty} \frac{\sigma_\nu J_\nu}{h\nu} d\nu \tag{3.12}$$

where σ_ν denotes the photo cross-section, J_ν the monochromatic mean intensity of the radiation field and ν_{th} the threshold frequency for the photoprocess. For practical purposes the upper limit of integration is given by the Lyman limit ν_{Ly}. In the case of an optically thin shell J_ν is approximately given by the geometrically diluted stellar ultraviolet flux $F_{*\nu}$

$$J_\nu = \frac{1}{4} F_{\nu *} (R_*/r)^2 \,. \tag{3.13}$$

Observations have shown that this assumption seems to be realistic for late-type stars having a chromospheric radiation field (Clegg et al., 1983). Limitations to this simplified treatment of the radiation field could probably arise from the fact that the line dominated absorption of CO leads to both, a mutual shielding of CO and H_2 and a self-shielding effect for CO (Morris and Jura, 1983; Mamon et al., 1988). The implications of this effect will be discussed in Chap. (3.4).

3.3 Description of Dust Formation

The processes of grain formation and growth are described by the following coupled system of differential equations (Gail and Sedlmayr, 1984, 1986, 1988)

$$\frac{\partial K_0}{\partial t} + \frac{1}{r^2} \frac{\partial}{\partial r} r^2 v K_0 = J_* \tag{3.14}$$

$$\frac{\partial K_i}{\partial t} + \frac{1}{r^2} \frac{\partial}{\partial r} r^2 v K_i = \frac{i}{j \tau_{gr}} K_{i-1} \qquad i = 1, 2 \ldots i_{max} \tag{3.15}$$

where J_* is the nucleation rate, τ_{gr} represents the net timescale of constructive collisions of dust particles with the condensing molecules and j indicates the spatial dimension of the type of clusters under consideration. The moments K_i of the size distribution function $f(t, N)$ are defined by

$$K_i = \sum_{N_l}^{N_u} f(t, N) N^{i/j} \tag{3.16}$$

where N_l and N_u are suitably chosen summation limits of the cluster size N. Together with the rate equations of the chemistry the problem is adequately described by a non-linear stiff system of ordinary differential equations which has to be treated numerically with a variable-step variable-order integration method to account for the different timescales entering into the system.

3.4 The Model

3.4.1 Basic Assumptions

We analyze the molecular formation and destruction processes in the comoving frame of an element of mass moving outwards which is subject to varying physical conditions of temperature, density and radiation field. We consider a stationary, spherically symmetric outflow from a late-type oxygen rich star of mass M_*, stellar radius R_* and effective temperature T_*, undergoing a phase of substantial mass loss. For the outflowing gaseous material we assume a constant hydrodynamic expansion velocity v. According to the law of mass conservation the radial dependence of the number density $n(r)$ is given by

$$n(r) = \frac{\dot{M}}{4\pi r^2 v \mu m_H} \tag{3.17}$$

where $\dot{M}$ denotes the mass loss rate and m_H the mass of a hydrogen atom. According to the composition of hydrogen-rich red giant atmospheres, the mean atomic weight μ to a good approximation is set to $\mu = 1.4$. The assumption of a r^{-2}-structure of the radial distribution of matter is consistent with studies based on quasi-thermal emission from CO and SiO [Zuckerman 1980] , infrared photometry [Sutton *et al.* 1977] , [Sutton *et al.* 1979] and polarisation measurements [McMillan and Tapia 1978] . The kinetic temperature of the gas is assumed to vary as

$$T(r) = T_0 \left(\frac{R_0}{r}\right)^{\alpha} \tag{3.18}$$

where the parameters of the initial gas temperature T_0, the initial radius R_0 and the temperature exponent α are chosen in order to fit the theoretical models of Goldreich and Scoville (1976).

3.4.2 Physical and Chemical Parameters

For the calculations we have used the basic parameters given in Table (3.4.2), which define model **(A)** and model **(B)**, with the exception of the radiation field. For model **(A)** the presence of a chromosphere is assumed. The fluxes adopted for the computation of the photoionization and photodissociation rates in the case of the standard model **(A)** are provided by the flux observed with the TD-1 (Thomson et al. . 1978) , ANS (van Duinen et al. 1975) , OAO2 (Code and Meade 1979) and IUE (Basri et al. 1981) satellites. In the wavelength range not covered by these data we use the UV-flux fit of Glassgold and Huggins (1986). This choice of parameters for a late-type M-star having substantial mass-loss is in close agreement with the values for the luminous red supergiant α Orionis. For model **(B)**, where the absence of a chromosphere is assumed, photorates are deduced using a black body radiation field characterized by the stellar temperature $T_* = 3000\,\mathrm{K}$ (see Tab. 2).

The mass loss rate of α Ori is rather uncertain and the adopted values range from 10^{-5}M$_\odot$yr^{-1} [Jura and Morris 1981] to 3×10^{-7} M$_\odot$ yr^{-1} [Knapp 1985] depending on the different observational methods used to determine the amount of outflowing material. The starting point of the calculation $r = 2R_*$ is situated well outside the

Mass loss rate	$\dot{M}$	[M$_\odot$/yr]	:	$2.0 \cdot 10^{-6}$
Start density	N_0	[cm^{-3}]	:	$3.0 \cdot 10^{9}$
Start radius	R_0	[R$_*$]	:	2
Stellar radius	R_*	[cm]	:	$6.9 \cdot 10^{13}$
Expansion velocity	v	[km/s]	:	1.0
Inner shell radius	R_0	[cm]	:	$1.4 \cdot 10^{14}$
Initial gas temperature	T_0	[K]	:	1100
Ratio of H_2/H			:	$1.6 \cdot 10^{-4}$
Abundances		$\epsilon(C)$	:	8.4
		$\epsilon(N)$	:	8.6
		$\epsilon(O)$	:	8.7
		$\epsilon(Si)$	:	7.6

Table 3.5: Model parameters assumed for models **(A)** and **(B)**.

chromospheric layer, which is assumed to be of the extent of $r_c \leq 1.4R_*$ [Cuntz 1990] but well inside the inner edge of the dust forming region.

In contrast to Honeycutt et al. (1980) and Skinner and Whitmore (1987), who deduce an outflow velocity of $10 - 20$ km/s in the wind region we adopt a value which is significantly lower. Self-consistent model calculations of dust-driven winds [Gail and Sedlmayr 1986b] show that the gas velocity for regions closer to the star than the sonic point is considerably lower than 1km/s. The acceleration of the gas due to radiation pressure on grains and close momentum coupling of dust and gas occures beyond the sonic point. The terminal velocity in the case of M-stars is in the range of $10 \ldots 20$ km/s and is reached at distances well outside the outer edge of the considered shell region. Therefore the assumption of a constant outflow velocity of 1 km/s [Clegg *et al.* 1983] is a reliable approximation.

As the published model calculations of Goldreich and Scoville (1976) are not directly applicable to α Ori due to reduced abundances of molecules and dust, we choose a different temperature exponent $\alpha = 1$ in accordance to Glassgold and Huggins (1986) for the calculation of the gas temperature in the regions $r > 5R_*$.

The presence of a chromosphere, where the gas temperature is expected to be in the range of 5000 K to 7000 K ([Basri *et al.* 1981, Hartmann and Avrett 1984, Cuntz 1990]) guarantees for a predominantly atomic state of the gaseous material. Especially the density ratio of n_{H_2}/n_H will be low. The abundances of the elements C, N, O are taken from the calculations of Lambert et al. (1984) , who has shown that the abundances in α Orionis do not deviate very much from a solar composition.

Reaction			**model A**	3500 K	**model B**	2500 K	2000 K	Ref.
H	$\longrightarrow$	H^+	1.0 (-10)	1.3 (-13)	4.3 (-16)	8.7 (-21)	1.1 (-27)	1
O	$\longrightarrow$	O^+	1.0 (-7)	2.2 (-13)	2.6 (-15)	8.9 (-20)	1.9 (-26)	1
C	$\longrightarrow$	C^+	2.0 (-6)	4.8 (-10)	6.8 (-12)	1.3 (-15)	3.9 (-21)	1
Si	$\longrightarrow$	Si^+	1.4 (-3)	1.9 (-5)	3.3 (-6)	6.0 (-9)	4.7 (-13)	4,2
S	$\longrightarrow$	S^+	2.5 (-5)	1.4 (-8)	5.0 (-10)	2.0 (-13)	1.5 (-18)	4
Mg	$\longrightarrow$	Mg^+	4.8 (-5)	8.8 (-6)	2.0 (-7)	4.4 (-10)	4.6 (-14)	4
Fe	$\longrightarrow$	Fe^+	8.0 (-5)	7.9 (-7)	1.7 (-7)	3.4 (-10)	3.1 (-14)	3
Na	$\longrightarrow$	Na^+	1.8 (-4)	5.9 (-4)	1.8 (-4)	3.0 (-6)	6.5 (-9)	2
CH^+	$\longrightarrow$	C^+	8.4 (-5)	1.9 (-7)	1.7 (-3)	6.0 (-5)	4.4 (-7)	5
CH_2^+	$\longrightarrow$	CH^+	8.0 (-4)	5.0 (-4)	6.7 (-6)	1.7 (-8)	2.3 (-12)	2
CH	$\longrightarrow$	CH^+	6.0 (-6)	1.0 (-8)	5.6 (-11)	1.5 (-14)	6.5 (-20)	6
CH	$\longrightarrow$	C	5.2 (-3)	5.1 (-1)	2.3 (-2)	1.2 (-3)	1.4 (-5)	7
C_2	$\longrightarrow$	C	2.2 (-6)	1.4 (-7)	9.3 (-13)	2.5 (-16)	1.1 (-21)	8
C_2^+	$\longrightarrow$	C^+	2.6 (-6)	6.8 (-7)	5.8 (-9)	9.5 (-12)	6.5 (-16)	9
CO	$\longrightarrow$	C	6.1 (-6)	2.5 (-10)	4.6 (-14)	6.2 (-18)	1.0 (-23)	7
C_2	$\longrightarrow$	C_2^+	4.0 (-7)	6.8 (-7)	1.6 (-13)	1.5 (-17)	1.3 (-23)	2
HCO	$\longrightarrow$	CO	8.0 (-3)	3.4 (1)	6.2 (-1)	1.7 (-1)	2.5 (-2)	10
H_2	$\longrightarrow$	H	3.0 (-12)	3.1 (-12)	7.0 (-17)	5.8 (-21)	4.6 (-27)	6
H^-	$\longrightarrow$	H	6.8 (+6)	1.3 (+4)	2.2 (+4)	1.5 (+4)	3.4 (+3)	11
O_2	$\longrightarrow$	O	6.8 (-4)	2.9 (-5)	2.3 (-8)	6.5 (-11)	8.9 (-15)	12, 13
H_2O	$\longrightarrow$	OH	1.4 (-3)	1.0 (-4)	3.2 (-7)	3.6 (-9)	1.2 (-12)	14
OH	$\longrightarrow$	O	8.4 (-4)	3.2 (-4)	6.8 (-5)	3.0 (-6)	3.0 (-8)	15
SiO_2	$\longrightarrow$	SiO	2.1 (-4)	5.6 (-6)	7.8 (-8)	2.9 (-10)	6.8 (-14)	16
SiO	$\longrightarrow$	Si	2.4 (-6)	1.1 (-9)	7.3 (-13)	2.8 (-16)	2.1 (-21)	4
SiH	$\longrightarrow$	Si	1.2 (-2)	9.9 (-2)	7.3 (-3)	4.8 (-4)	1.0 (-5)	4
SiH^+	$\longrightarrow$	Si^+	8.0 (-5)	3.4 (-6)	1.8 (-8)	6.7 (-11)	1.9 (-14)	4
SiH_2^+	$\longrightarrow$	SiH^+	8.0 (-4)	1.1 (-3)	3.1 (-5)	1.3 (-7)	3.8 (-11)	4
SiH	$\longrightarrow$	SiH^+	8.0 (-5)	6.5 (-8)	7.6 (-10)	2.0 (-13)	8.9 (-19)	4
SiO	$\longrightarrow$	SiO^+	1.2 (-6)	4.8 (-10)	2.1 (-12)	3.1 (-16)	5.7 (-22)	4
HS	$\longrightarrow$	S	6.4 (-3)	3.3 (-3)	1.4 (-4)	1.3 (-6)	1.9 (-2))	17
HS^+	$\longrightarrow$	S^+	3.6 (-7)	5.5 (-7)	1.8 (-8)	9.3 (-11)	3.8 (-6))	18
H_2S	$\longrightarrow$	HS	8.4 (-4)	8.9 (-4)	3.6 (-5)	3.1 (-7)	5.2 (-3))	19, 21
CS	$\longrightarrow$	C	2.1 (-5)	7.8 (-8)	3.9 (-11)	2.1 (-15)	9.3 (-6))	18
OCS	$\longrightarrow$	CO	2.8 (-4)	9.8 (-4)	7.3 (-5)	1.6 (-6)	6.2 (-3))	19
SO	$\longrightarrow$	S	1.1 (-3)	8.8 (-5)	8.7 (-7)	9.4 (-10)	2.1 (-3))	19
SO_2	$\longrightarrow$	SO	6.0 (-4)	5.7 (-5)	5.9 (-7)	6.9 (-10)	4.7 (-3))	19
H_2S	$\longrightarrow$	H_2S^+	4.8 (-6)	4.1 (-11)	1.0 (-14)	4.4 (-20)	1.0 (-8))	20

continued on next page

continued from previous page						
Reaction	**model A**	3500 K	**model B**	2500 K	2000 K	Ref.
$OCS \longrightarrow OCS^{+}$	2.4 (-6)	4.0 (-12)	5.8 (-16)	1.1 (-21)	9.7 (-9)	19

1: Schmutzler 1987, **2:** Prasad & Huntress 1980, **3:** Millar *et al.* 1991, **4:** Clegg *et al.* 1983, **5:** Graff & Moseley 1984, **6:** Hollenbach & McKee 1979 **7:** Viala 1988, **8:** Pouilly *et al.* 1983, **9:** Solomon & Klemperer 1973, **10:** Lee 1985, **11:** Wishart 1979, **12:** Viala 1986, **13:** Huebner *et al.* 1975, **14:** Lee 1984, **15:** van Dishoeck & Dalgarno 1984, **16:** Hudson 1971, **17:** Friedl *et al.* 1983, **18:** vanDishoeck 1987, **19:** Lee 1986, **20:** Lee *et al.* 1987a, **21:** Lee *et al.* 1987b

Table 3.6: Photorates at $r = 2R_*$. Rates are written in the form x(y) which denotes $x \cdot 10^y$. Model **(A)** indicates the presence of a chromospheric radiation field, model **(B)** indicates the corresponding case with a stellar temperature of $T_* = 3000$ K and no chromospheric radiation field.
In column 3,5 and 6 the photorates are given for the blackbody temperatures 3500 K, 2500 K and 2000 K, respectively. For the CO-photorate the unshielded values are given.

This fundamental set of parameters provides the basis for an appropriate choice of the reaction network. The chemical data include reactions of all species which either have been observed or are to be expected under the physical conditions in oxygen-rich CSEs. In order not to exclude important chemical pathways also some species which are known to have only small concentrations (e.g. $SiOH^+$, HCO^+, SiO_2 and SiO^+) were added. The complete SiO and CO chemistry does not contain nitrogen because this element is strongly blocked in the chemically inert N_2 molecules [Nercessian *et al.* 1989] . Also the elements of considerable lower cosmic abundances like Al, Cl, Ca, Ni,.. have been neglected. Altogether a system of 342 reactions, including all types of reactions of importance under these conditions have been selected, built from 54 species (see Tab. 3.7), comprising the most abundant reactive elements, their ions and electrons.
Moreover we extend this network by a comprehensive data set of 214 sulfur containing reactions including 16 new species. This enables us to study the specific effect of the sulfur chemistry on the SiO and CO formation as well as the influence on grain formation.
The chemical parameters which enter into the forward reaction rates are taken from Clegg et al. (1983) and Millar et al. (1991) . The thermodynamic quantities used to compute the backward rates were taken from the JANAF tables [Chase *et al.* 1985] .

3.4.3 Initial Conditions

For solving the system of rate equations for the particle concentrations we need initial conditions for the molecular abundances. Solely the concentrations of those

atoms	molecules	ions
H	H_2	H^+, H^-
C	CO, CH, C_2, HCO	C^+, CO^+, CH^+, CH_2^+
O	O_2, H_2O, OH	O^+
Si	SiO, SiO_2, SiH	Si^+, $SiOH^+$, SiH_2^+ SiH^+, SiO^+
S	S_2, HS, CS, SO, SO_2, OCS, SiS	S^+, S_2^+, HS^+, CS^+, SO^+ H_2S^+, HCS^+, OCS^+
Fe, Mg, Na		Fe^+, Mg^+, Na^+, e^-

Table 3.7: Species included in the chemical reaction network for αOri.

species can be affected by the initial abundances of the molecules whose determining reactions are rapidly frozen out in the innermost region of the shell. This only applies for very low mass densities in the absence of dissociating photons, a case which is not studied in this paper. Numerical experiments concerning model **(A)** and **(B)** have shown that all particle concentrations rapidly approach quasi-stationary values, irrespective of the special choice of initial conditions. For this reason we solved the equations with the simple assumption of all C and Si initially being in CO and SiO, a H_2 to H ratio of $1.6 \cdot 10^{-4}$ and all further molecule concentrations being zero.

3.5 Molecular Composition

3.5.1 General Characteristics of the Chemistry

First we discuss the results for model **(A)**. The radial course of the concentrations is typical for a stationary, optical thin flow, but deviates significantly from results derived by chemical equilibrium computations for comparable situations (e.g. [Tsuji 1987]). Both, the expanding gaseous material and the radiation field decreases like r^{-2} in density. Hence the balance of kinetical and photorates does not depend on the radial coordinate. As a consequence the concentrations of the metal ions and electrons are nearly constant. Similar to the results of Glassgold and Huggins (1986) for the outer region of CSEs we derive an electron density of $n(e^-) = 10^{-4} \cdot n_{<H>}$ which is induced by the complete ionization of the heavy elements Fe, Si, Mg and Na. The reaction coefficients for radiative electronic recombination of these species are inversely proportional to the gas temperature. Hence they increase with increasing radial distance. This results in a steady increase of the concentrations of the neutral metals for $r > 5R_*$.
The degree of ionization for the hydrogen atom is only moderate ($n_{H^+} = 10^{-3} \cdot n_H$). Most of the high energetic radiation with $\lambda \leq 912$Å is shielded just at the inner boundary of the shell of α Ori. The influence of the interstellar radiation field can be neglected in envelope regions nearer to the central star than 10^{16}cm as Mamon et al. (1988) have shown. Therefore, in the inner shell the chemistry is dominated by chromospheric UV radiation. In accordance with the results of Glassgold et al. (1989) we stress the fact, that in spite of the strong radiation field a substantial fraction of the heavy elements is processed into molecules. Molecular ions were always found to have low abundances, which is due to their large rate-coefficients for dissociative recombination, which are typically of the order of $10^{-7}\mathrm{cm}^3\mathrm{s}^{-1}$, so being roughly a factor 10^6 larger than the atomic recombination coefficients. Hence, if the UV field is strong enough to produce molecular ions, the same radiation field will generate ionized metals and the resulting photoelectrons will quickly neutralize the molecular ions.
The non-equilibrium conditions in the inner shell cause a chemical state of kinetic equilibrium for most of the molecules, indicated by high reaction rates, expressing the ability of a fast response to a change in the physical conditions, but only low net rates. For the discussion of the chemical behaviour we define the chemical timescale τ^i_{ch} for a species i by

$$\tau^i_{\mathrm{ch}} = min\{\frac{n_i}{Q^i_g}; \frac{n_i}{Q^i_l}\} \tag{3.19}$$

with Q^i_g, Q^i_l being the sum over all gain and loss rates for species i, respectively. As it can be seen in Fig. (3.5) the chemical timescale for the CO molecule lies between $\tau^{CO}_{\mathrm{ch}} = 10^{6.5}$ s and $\tau^{CO}_{\mathrm{ch}} = 10^9$ s at $r = R_0$ and $r = r_{\mathrm{end}}$ respectively. For distances $r > 10R_*$ the timescale of CO is approaching the expansion timescale τ_{ex}. This indicates that the change in the CO density is small and secondly that the influence of the chemical reactions on the CO density is of the same order as the

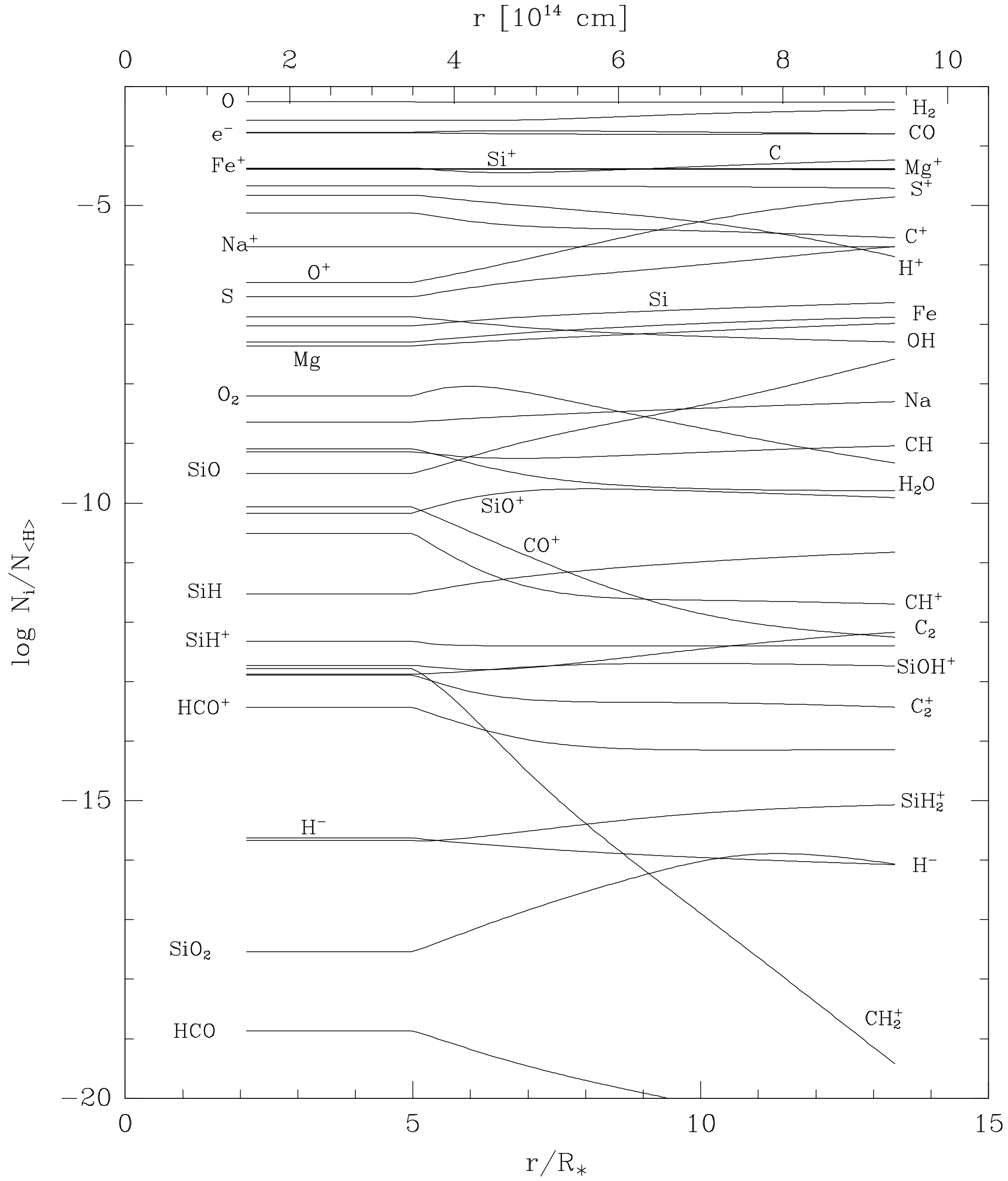

Figure 3.3: Radial distribution for the species of interest from $R = R_0$ to $R = 12R_*$ for model **(A)**. The concentrations are normalized with respect to the total hydrogen abundance $n_{<H>} = n_H + n_{H_2}$. Boldfaced lines indicate supersaturation ratios for SiO and Fe higher than 10^4.

---

change due to the expansion of the shell. On the contrary the H_2O and the SiO molecule have timescales $\tau_{\rm ch}^{H_2O} = 10^5$s and $\tau_{\rm ch}^{SiO} = 10^6$s, which are several orders of magnitude below the hydrodynamical timescale. This expresses the influence of the chromospherical radiation field in two ways. At first it dissociates H_2O with a significantly higher efficiency than the more stable CO. Secondly, due to the high

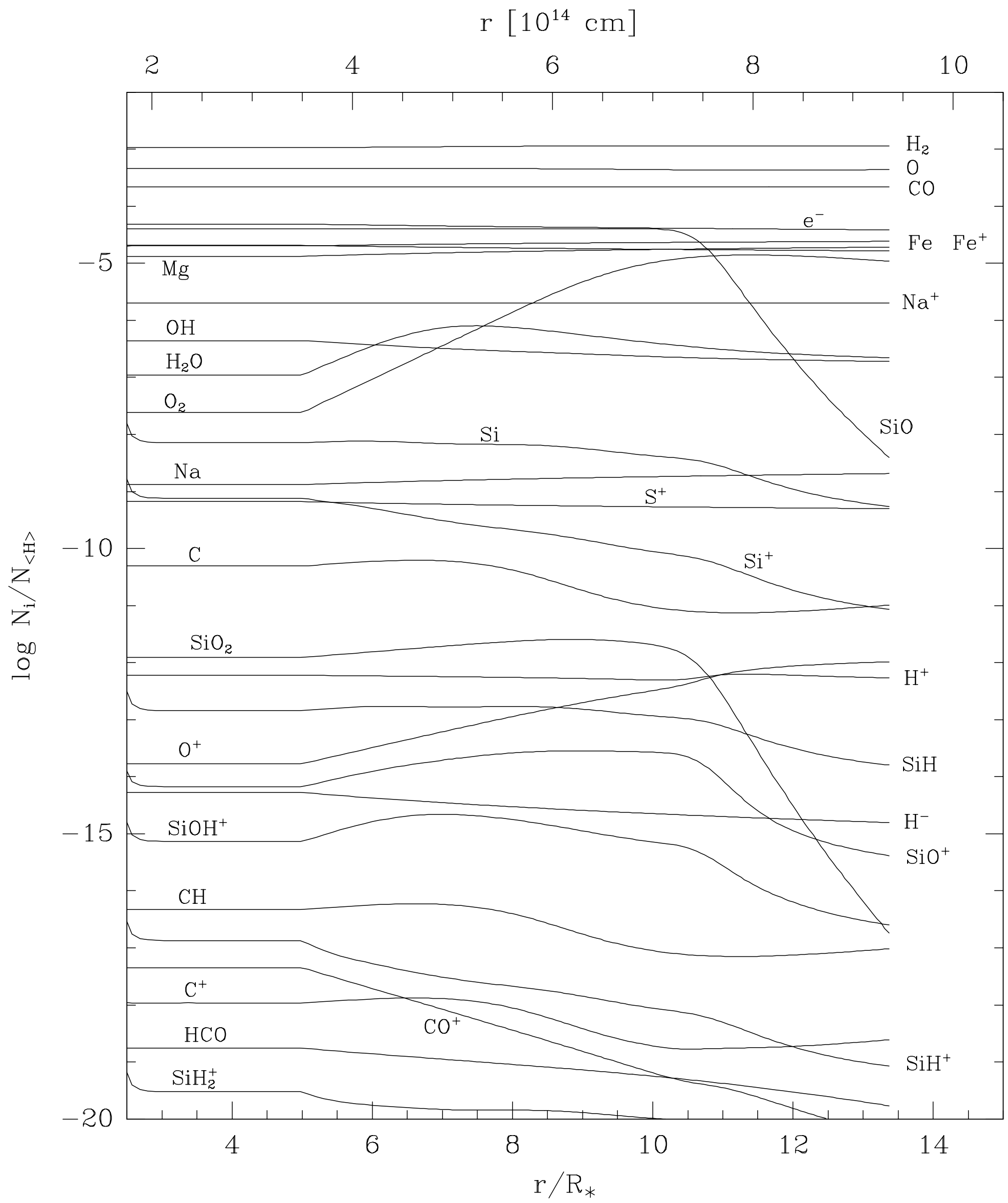

Figure 3.4: Radial distribution for the species of interest from $R = R_0$ to $R = 12R_*$ for model **(B)**. The concentrations are normalized with respect to the total hydrogen abundance $n_{<H>} = n_H + n_{H_2}$. The break in the slope of SiO and SiO_2 is due to the onset of massive dust formation.

---

ion density, neutral-ion reactions, which are faster than the neutral-neutral ones, are dominating the chemistry and convert the SiO molecules into ionized species. The H_2 molecule, however, turns from a state of kinetical equilibrium to a chemically frozen in situation at a distance $r = 9R_*$, which means $\tau_{\rm ch}^{H_2} > \tau_{\rm ex}$ for $r > 9R_*$. The same applies to atomic hydrogen for $r = 8.5R_*$.

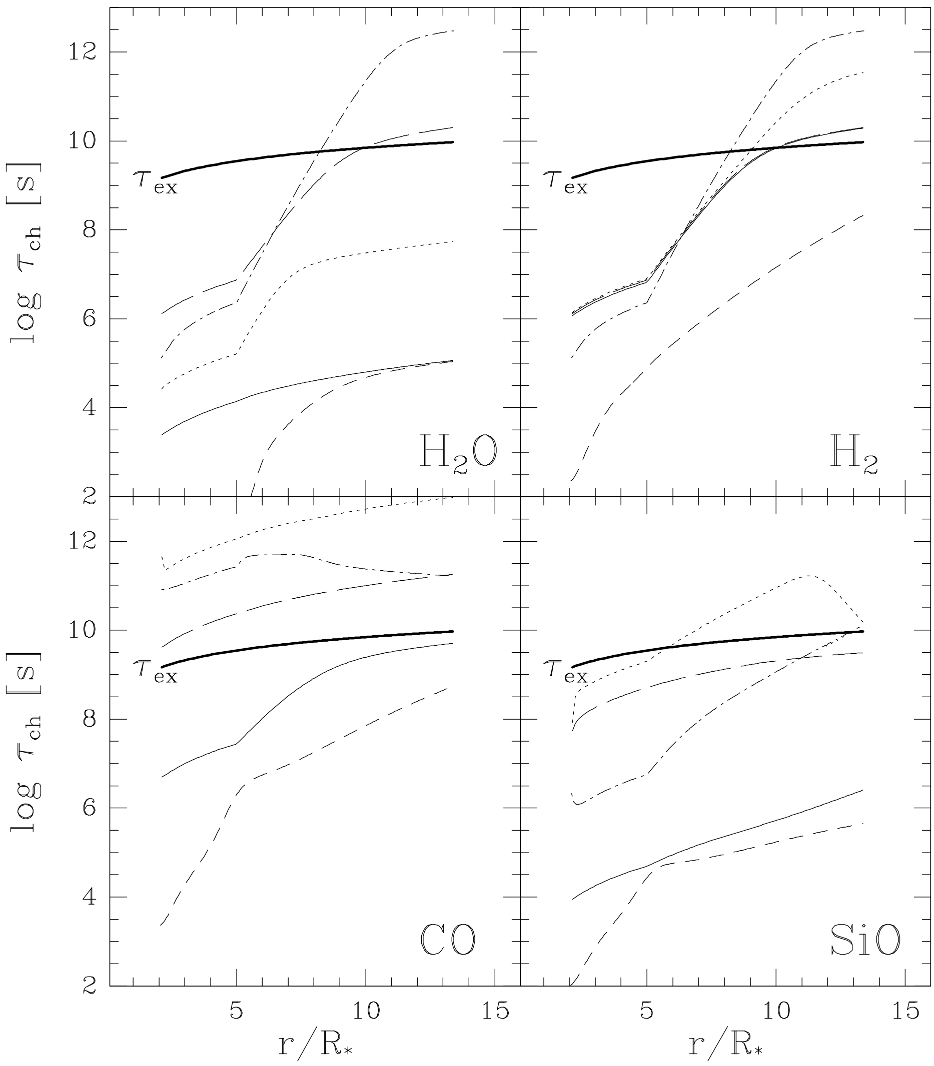

Figure 3.5: Radial course of the chemical timescales τ^i_{ch} for the species CO, H_2, SiO and H_2O. The continuous line corresponds to model **(A)**, the dotted line to model **(B)**. The short-dashed line corresponds to a model with a different temperature structure taken from Wirsich (1988) . The dashed-dotted line corresponds to a model with a higher mass-loss rate of $\dot{M} = 10\dot{M}_{\rm modelA}$. The long dashed line corresponds to a model for α Ori with a stellar blackbody temperature of $T_* = 3500\,$K [Rodgers and Glassgold 1991] . The bold line shows the hydrodynamic timescale τ_{ex}. With the exception of the above mentioned parameters the standard parameter set of Tab. (3.4.2) has been used. For all models, except for model **(A)** a blackbody radiation field was assumed. The timescales of CO for model **(B)** and the model with the increased mass loss rate were shifted by a factor of 10^{-2} in order to fit into the figure.

The computation of the chemistry up to a distance of $r = 30R_*$ for the shell of α Ori shows that the CO molecule also turns into a non-KE state at $r = 25R_*$,

indicating that the CO density is frozen in. The assumption of a chemical steady-state situation, i.e. $\tau_{\rm ch} < \tau_{\rm ex}$, therefore is highly questionable. Especially in view of the importance of the CO and the SiO molecule for chemistry and dust formation the use of a fully time-dependent model is necessary.
If we now compare these results to those of model **(B)**, it is obvious that there are some important differences to model **(A)**, due to the absence of chromospheric radiation. In this case the entire carbon is locked up in the CO molecule. The remaining free carbon atoms do have a concentration of $x_C = 10^{-10}$. Molecular hydrogen, the most abundant molecule and with $x_{H_2} = 1.1 \cdot 10^{-3}$ the second abundant species besides atomic hydrogen, reacts to the change in radiation field by doubling its concentration. Atomic oxygen, however, is reduced due to an increased consumption by the formation of CO and SiO.
The SiO contains more than 99% of the atomic silicon. The remaining Si atoms are mainly neutral, only 10% are ionized. The electron density is decreased by one order of magnitude. Hence the importance of ions and radicals for the chemistry is reduced, as the efficiency of the ion-neutral reactions is diminished. Furthermore the amount of reactive species is smaller, as carbon and silicon are extracted from the chemistry. This results in the large timescales (see Fig. 3.5):

$$\tau_{\rm ch}^{CO} = 10^{14}\,{\rm s} \quad \tau_{\rm ch}^{SiO} = 10^{10}\,{\rm s} \qquad {\rm a}t \quad r = 10R_* \tag{3.20}$$

which are significantly larger than the hydrodynamic timescale. Molecular hydrogen turns into non-KE for $r > 8.5R_*$ whereas atomic hydrogen is in a frozen state just beyond $r = 3R_*$.

The possibility of dust formation in case of model **(A)** is indicated through high supersaturation ratios attained at about $r = 8.5\,R_*$ for SiO and at $r = 7.5\,R_*$ for Fe (see Fig. (3.3). Grain formation obviously does not directly affect the chemistry in the presence of chromospheric radiation. The depletion of the SiO molecule caused by consumption due to dust forming processes is much less than the increase by chemical reactions. In this case only small amounts of dust will be formed in agreement with observations [Sutton *et al.* 1977] .
If the amount of high energetic photons is reduced by switching off the chromosphere, the onset of grain formation and the subsequent growth of dust particles dramatically reduce the concentration of the nucleating species SiO (see Fig. (3.4). Behind the condensation radius of SiO all silicon bearing species show a distinct response to the onset of this additional process of Si-consumption.

3.5.2 Chemical Pathways

One main scope of this work is a detailed analysis of the chemical reaction network in order to find out the relative importance of the various species and their formation and destruction pathways. For the discussion of the general properties of the inner shell chemistry it is advantageous to divide the entire system of species into three subsystems which comprises the essential coupling of the included species.

i. only O-H containing species (O-H system)

ii. silicon containing species (Si-system)

iii. carbon containing species (C-system)

Then the characteristics of each system can be analyzed separately. This subdivision does not include the metals Fe, Mg, S, Na and their ions. The concentrations of these species are essentially dominated by charge exchange reactions which have no activation barrier and are independent of the temperature. Therefore, these species are decoupled from the remaining network. The presence of a strong UV-radiation field increases the importance of charge exchange reactions, additionally incorporating silicon and carbon.

$$C^+ + S \Longleftrightarrow C + S^+ \quad (I)$$
$$Si^+ + Fe \Longleftrightarrow Si + Fe^+ \quad (II)$$
$$Si^+ + S \Longleftrightarrow Si + S^+ \quad (III)$$
$$Si^+ + C \Longleftrightarrow Si + C^+ \quad (IV)$$

The reactions (I) - (IV) build up a fast proceeding reaction cycle resulting in a conversion of carbon ions to neutral carbon so that with increasing distance the amount of carbon ions decreases (model **(A)**). The amount of ionized material is almost completely provided by the ions of the heavier elements whereas the degree of ionization of hydrogen and oxygen naturally remains low, even in the presence of a chromosphere.

3.5.2.1 The OH–System

This system in particular comprises the most abundant species H, H_2 and O. In contrast to the reactions of the C and the Si system all these components are closely connected by reactions in which forward and reverse rate are of the same order of magnitude, or at least balancing each other (see Fig. (3.6). Many reactions show a strong temperature dependence caused by the existence of an activation energy barrier.
In contrast to other recent LTE-computations (e.g. Tsuji, 1987) the abundance of molecular hydrogen, although having an ascending slope outwards to $r = 10R_*$, is only a fraction of 10^{-3} of the atomic hydrogen abundance. This undoubtedly confirms the assumption of Nejad and Millar (1987), who have restricted the results of their investigations concerning the chemistry of oxygen-rich shells to those cases where the UV-radiation plays only a minor role so that the crucial assumption of a dominating H_2 abundance is appropriate. Additionally it can be shown that also in the absence of a chromosphere the stellar temperature has to be below $T = 3000\,\mathrm{K}$ to yield a H_2 concentration which significantly exceeds the freeze-out value of H_2 which is $n_{H_2} = 10^{-3} n_H$ for $T_* = 3000\,\mathrm{K}$ (see Fig. 3.4).

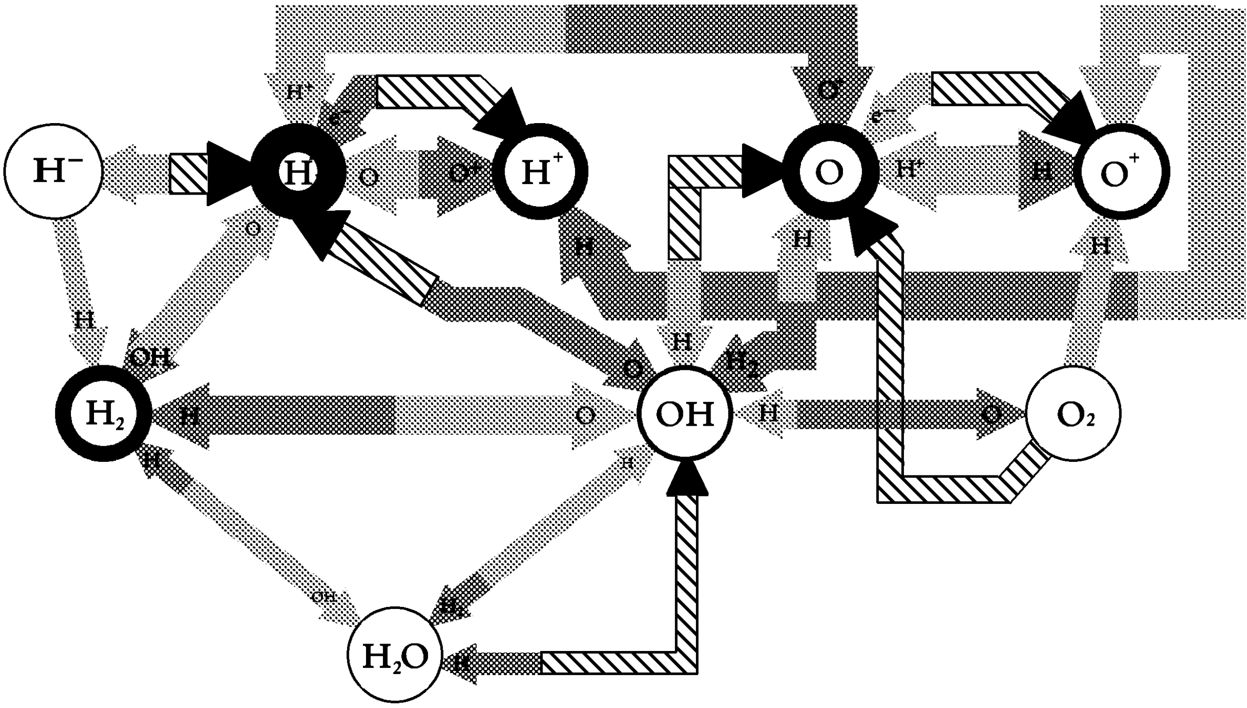

Figure 3.6: Reaction flow diagram of the O-H system for case (**A**). The thickness of the bordering wrapping the species is scaled logarithmically with respect to the concentration of atomic hydrogen. Reaction pathways are depicted as arrows with a thickness normalized on a log-scale to the reaction rate of the most efficient reaction, which for both cases (model (**A**) and (**B**)) is given by the charge exchange reaction of H^+ and O. Double arrows indicate those reaction pathways for which forward and reverse reaction are of the same order of efficiency. The ratio of forward to reverse rate is shown by a different arrow shading. Photoreactions are indicated by a hatching inside the reaction arrow. All reaction are labelled with the corresponding reaction partner.

In the innermost regions the abundances of all radicals and subordinated species are thus dominated by interactions with atomic hydrogen as long as the exponential decrease of the reaction rates due to falling gas temperature is not too large.

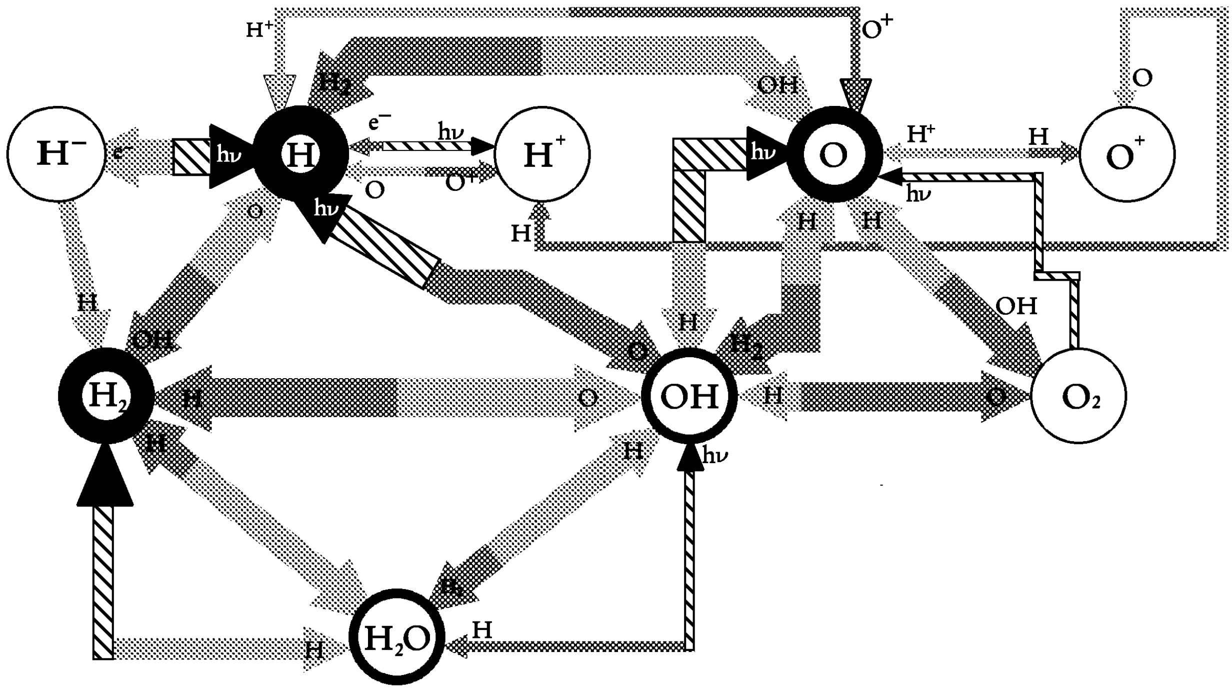

Figure 3.7: Reaction flow diagram of the O-H system for case **(B)**.

The ratio of atomic to molecular hydrogen which are coupled by the main H_2O producing hydrogen abstraction reaction:

$$\mathrm{OH} \quad + \mathrm{H_2} \quad \Longleftrightarrow \mathrm{H_2O} \quad + \mathrm{H} \qquad \text{(V)}$$

is related to the OH/H_2O ratio by

$$\frac{n_{OH}}{n_{H_2O}} = \gamma(T)e^{-E_A/kT}\frac{n_H}{n_{H_2}} \tag{3.21}$$

with $\gamma(T)$ being the ratio of the partition functions Q for the molecules OH and H_2O, respectively, and E_A the activation energy barrier. With the values corresponding to model **(A)**, i.e. $x(H) = 0.997, x(H_2) = 2.7 \cdot 10^{-4}$ and the data for reaction (V) $E_A = 1530\,\mathrm{K}$, $\gamma \approx 1$ we get a OH/H_2O ratio of $7.4 \cdot 10^2$. This is in good agreement with the computed KE concentration at $r = 5\,R_*$ (see Fig. (3.3). The fact that Eq. (3.21) is applicable shows that in spite of the non-LTE conditions the key molecules of the O-H system are in a state of kinetic equilibrium. They are closely coupled to each other by high reaction rates. At larger distances these non-LTE effects tend to depart the abundances of OH and H_2O from the KE state although the concentrations of their progenitors H and H_2 do not significantly change.
A detailed analysis of the reaction rates shows that the essential formation reaction of the H_2 molecule efficiently proceeds by two steps. The first step involves the radiative association reaction

$$Si^+ \quad + H \quad \Longrightarrow SiH^+ \quad + h\nu \tag{VI}$$

of the reactive ion Si^+ with atomic hydrogen. The second step just involves a further interaction of the SiH^+ ion with a H atom.

$$SiH^+ \quad + H \quad \Longrightarrow Si^+ \quad + H_2 \tag{VII}$$

This pathway is not very efficient. However, reaction (VII) is dominant in the presence of a chromospheric UV-field since the other two H_2 formation paths :

$$H \quad + OH \quad \Longrightarrow O \quad + H_2 \tag{VIII}$$
$$CH^+ \quad + H \quad \Longrightarrow C^+ \quad + H_2 \tag{IX}$$

are in equilibrium with their reverse rates therefore providing only a minor contribution to the H_2 concentration. With increasing distance the reactions (VIII) and (IX) are loosing their chemical significance due to a high energy barrier or a non-zero temperature exponent α, respectively. The formation rate (VII) is temperature independent whereas the backward reaction rate of (VII) strongly decreases with dropping temperature, driving the ratio of forward rate R_f and backward rate R_b to $R_f/R_b \approx 10^6$. The chemical pathways commonly assumed to apply ($H + e^- \rightarrow H^-$, $H^- + H \rightarrow H_2 + e^-$, Duley and Williams, 1984) for the H_2 molecule formation obviously do not work in the situation where an intense radiation field drives the chemistry away from chemical equilibrium.
On the other hand, if we consider the chemistry in case **(B)** with $T_* = 3000$K, where the concentration of the molecular ions are drastically reduced, the SiH^+ ion is decreased by a factor of 10^{-7}, and then, reactions (VIII) and (IX) are confirmed as the main formation routes, although (VIII) is strongly endothermic. An analysis of the characteristic timescales of chemical reactions shows that molecular hydrogen is frozen out at about $r = 8\,R_*$ and $r = 10\,R_*$ on a low concentration level of $x_{H_2} = 1.1 \cdot 10^{-3}$ in case **(B)** and $x_{H_2} = 3.4 \cdot 10^{-4}$ in case **(A)**, respectively. This situation will hold until in the outermost parts of the circumstellar shell the destruction rates

due to the influence of the interstellar radiation field will increase and dissociate the remaining molecules.
The OH radical, being involved in most reaction routes plays a crucial role in the chemistry of the O-H system. It serves as an intermediate stage for the production of the H_2O molecule as well as for molecular hydrogen. Its abundance is sensitively linked to the intensity of the UV-radiation. OH is more abundant by a factor of 10 if the chromosphere is not present (see Fig. (3.3 and (3.4).

3.5.2.2 The C–System

The most important reactions in the C-system are shown in Figs. (3.9) and (3.8). The CO molecule is assumed to be effectively self-shielded, except for the regions in the vicinity of the chromosphere which lies some 10^{12} cm inside our adopted boundary. It always locks up most of the carbon. In both cases **(A)** and **(B)**, the concentration of carbonmonoxide in the inner shell region is much larger than in the outer regions, a case discussed for α Ori by Glassgold and Huggins (1986), even if we adopt a stellar temperature of $T_* = 3500\,\mathrm{K}$ for the chemical modelling of the CS shell.
The remaining carbon not locked up in CO is strongly involved in the charge exchange reactions with S and Si. The degree of ionization of carbon $f^{C}_{\mathrm{cond}} = 0.17$ is significantly lower than for the heavy elements Fe, S and Si, for which $f^{Si}_{\mathrm{cond}} = f^{Fe}_{\mathrm{cond}} = f^{S}_{\mathrm{cond}} = 1$. This fact can be attributed to the higher ionization potential of carbon and to the very efficient radiative recombination processes (Glassgold and Huggins, 1986). The main loss process for atomic carbon is the ionization by energetic photons, but also consumption due to the formation of CO and CH is of importance. The recombination coefficient for the radiative recombination of carbon ions with electrons is inversely proportional to the the gas temperature. Hence the abundance of neutral carbon increases with increasing radial distance and the degree of ionization drops down to $f^{C}_{\mathrm{cond}} = 0.05$ at $r = r_{\mathrm{end}}$. The consumption of C^+ by the production of CO^+ via the reaction

$$C^+ \quad + OH \quad \Longleftrightarrow CO^+ \quad + H \qquad \text{(X)}$$
$$C^+ \quad + O_2 \quad \Longleftrightarrow CO^+ \quad + O \qquad \text{(XI)}$$

immediately leads to CO by the subsequent reaction

$$CO^+ \quad + H \quad \Longleftrightarrow CO \quad + H^+ \qquad \text{(XII)}$$

which due to its exceptional high bond energy of $E_{bond} = 250\,\mathrm{kcal/mol}$ collects most of the carbon. The second most abundant carbon containing species in our reaction network, which focuses on O-rich element compositions, is the CH radical. It has a concentration of $x_{CH} = 10^{-9}$, a value which is five orders of magnitude lower than of the CO molecule. As CH has a binding energy of 80 kcal/mol, less than one third of the bond strength of CO, CO is dominating the chemical structure even in the case of strong chromospheric UV-radiation influences. The formation of CH mainly proceeds via the less abundant HCO^+ ion which is formed in the reactions

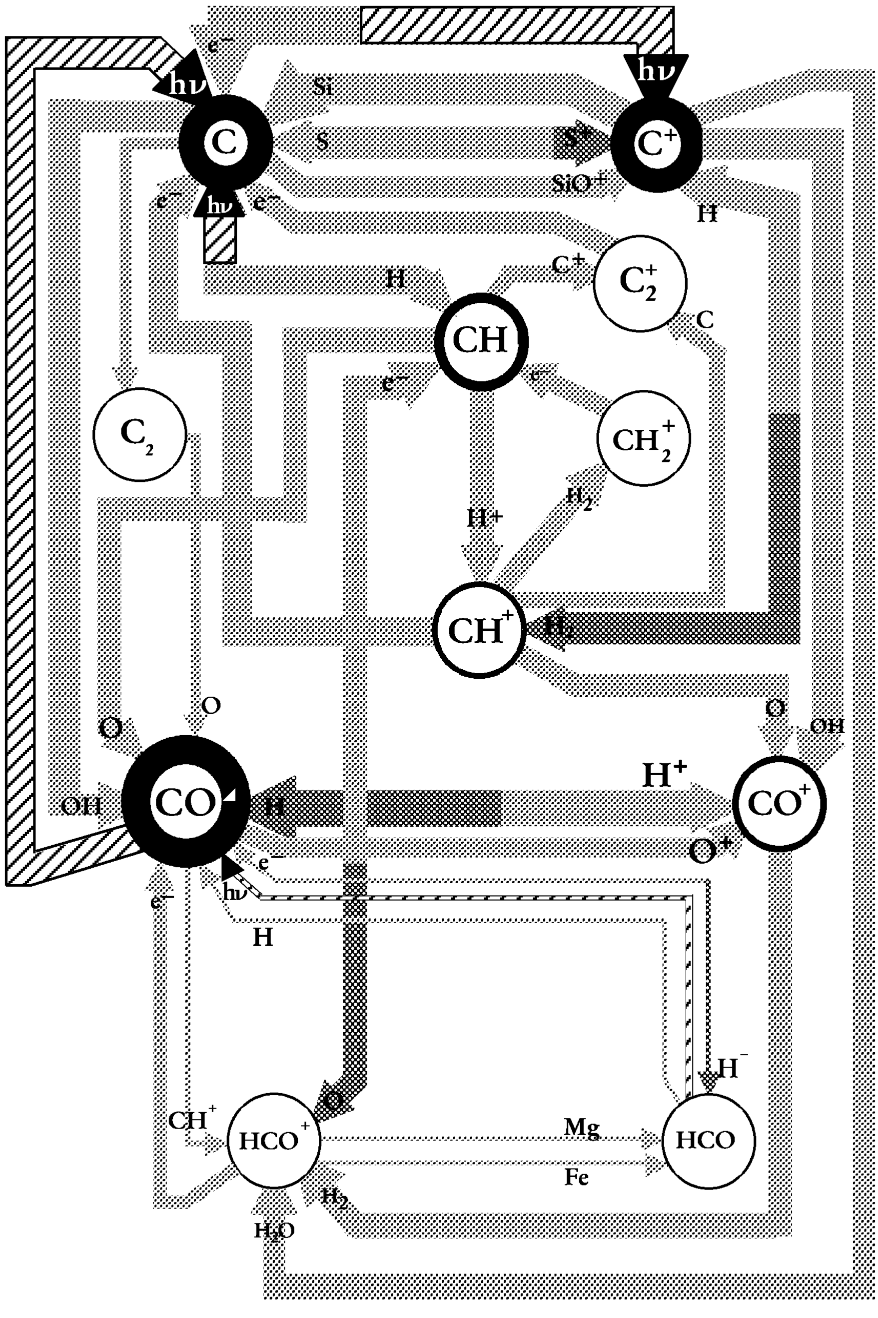

Figure 3.8: Reaction flow diagram of the C-system for model **(A)** at $r = 5R_*$. The abundances are normalized with respect to the CO molecule. For detailed instructions see Fig. (3.6).

$$CO^+ \quad + H_2 \quad \Longleftrightarrow HCO^+ \quad + H \qquad \text{(XIII)}$$
$$C^+ \quad + H_2O \quad \Longleftrightarrow HCO^+ \quad + H \qquad \text{(XIV)}$$

followed by the dissociative recombination:

$$HCO^+ + e^- \Longleftrightarrow CH + O \qquad (XV)$$

The rate of the reverse reaction of (XV) increases with increasing distance but does not compensate the forward one. Thus the pathway via the dissociative recombination of the HCO^+ ion is the main formation route of CH. The branching of HCO^+ to CO according to the dissociative recombination

$$HCO^+ + e^- \Longleftrightarrow CO + H \qquad (XVI)$$

in principle competes with the CH formation path but is less efficient for temperatures $T \geq 500\,K$. The concentration of HCO^+ in this region is low, a factor of 10^{-7} smaller than that given by Mamon et al. (1987) for the outer shell of α Ori at $r = 10^{16}$ cm. This is due to the low non-LTE concentration of the HCO^+ progenitors H_2O and OH. Other carbon bearing components like C_2, HCO or the ions CH^+ and CO^+ have very low abundances and therefore are only of minor importance. In particular, the low concentration of the CH^+ molecule in oxygen-rich compositions hinders the effective production of methane and acetylene, which are the basic constituents of the formation of PAHs ([Gail and Sedlmayr 1987a, Herbst 1988b, Herbst and Leung 1989] .

3.5.2.3 The SiO–System

In this group of silicon containing species, SiO obviously is the most important molecule. As being the basic constituent of silicate grain formation it serves as a nucleation seed, due to its exceptional high temperature stability. Most of the silicon is blocked in the SiO, although this statement only holds for such cases where the radiation field is unable to break up the Si-O bond.
If a chromosphere is present the reaction rates in the Si-system are much larger than in model **(B)**. Predominantly the chemistry proceeds on an atomic level. In this case only a small fraction of the entire silicon reservoir is converted into the SiO molecule. Its formation requires two steps

$$Si^+ + OH \Longleftrightarrow SiO^+ + H \qquad (XVII)$$
$$SiO^+ + C \Longleftrightarrow SiO + C^+ \qquad (XVIII)$$

with SiO^+ being the most abundant Si bearing molecular ion. The charge transfer process (XVIII) with atomic carbon has a temperature independent rate coefficient. These channels are the dominant production routes for siliconmonoxide in the entire radius regime under consideration. The alternative pathway due to the dissociative recombination reaction

$$SiOH^+ + e^- \Longleftrightarrow SiO + H \qquad (XIX)$$

also is of importance for the SiO formation, in accordance with Clegg et al. (1983). Its efficiency, however, is a factor of two lower than in the competing path.
The atomic components Si and Si^+ are a main part in the cycle of charge exchange reactions (II-IV). Results for a cooler star with $T_* = 2000\,K$ indicate that in the absence of dissociating UV-photons SiO is formed directly from atomic silicon and

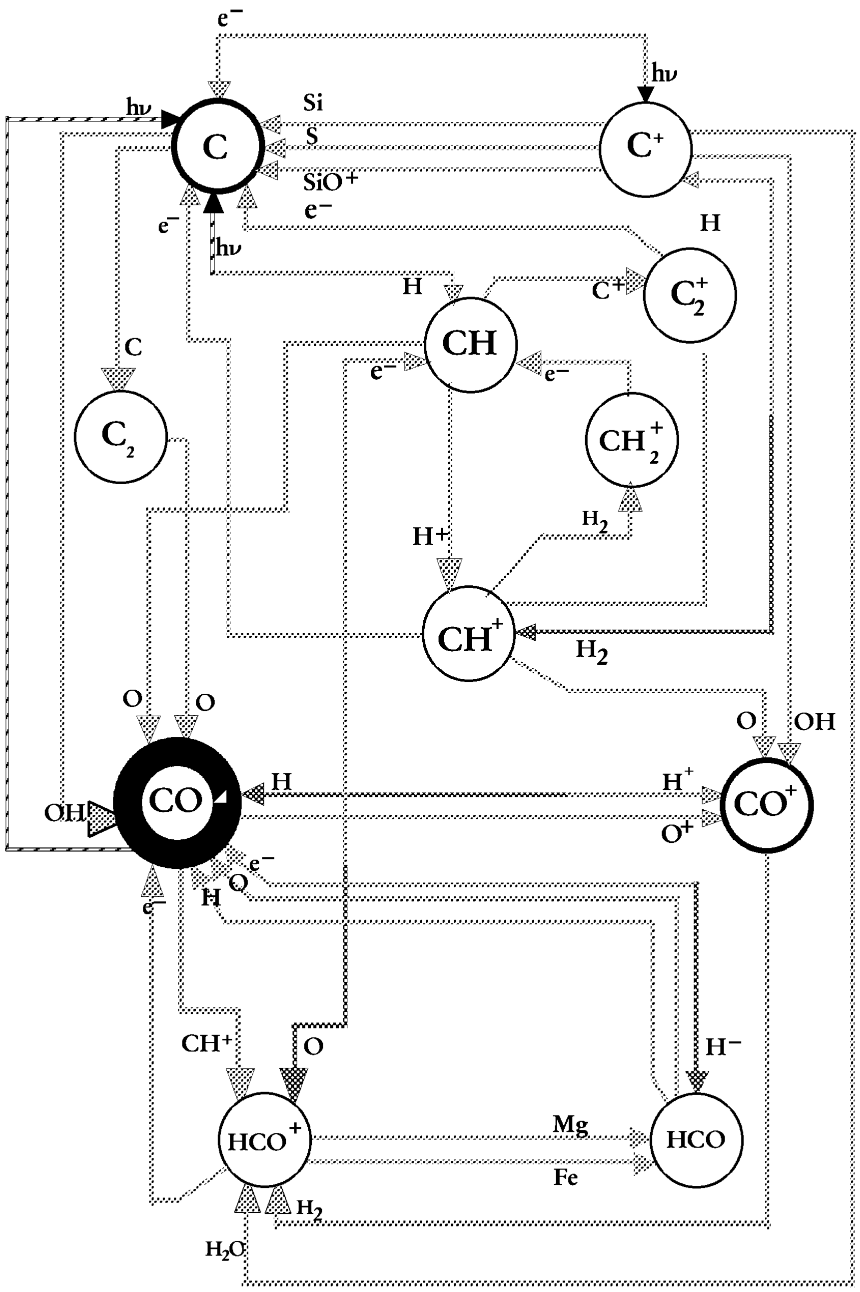

Figure 3.9: Reaction flow diagram of the C-system for model **(B)** at $r = 5R_*$. The abundances are normalized with respect to the CO molecule. For detailed instructions see Fig. (3.6).

the hydroxyl radical:

$$\mathrm{Si} \quad + \mathrm{OH} \quad \Longleftrightarrow \mathrm{SiO} \quad + \mathrm{H} \qquad \text{(XX)}.$$

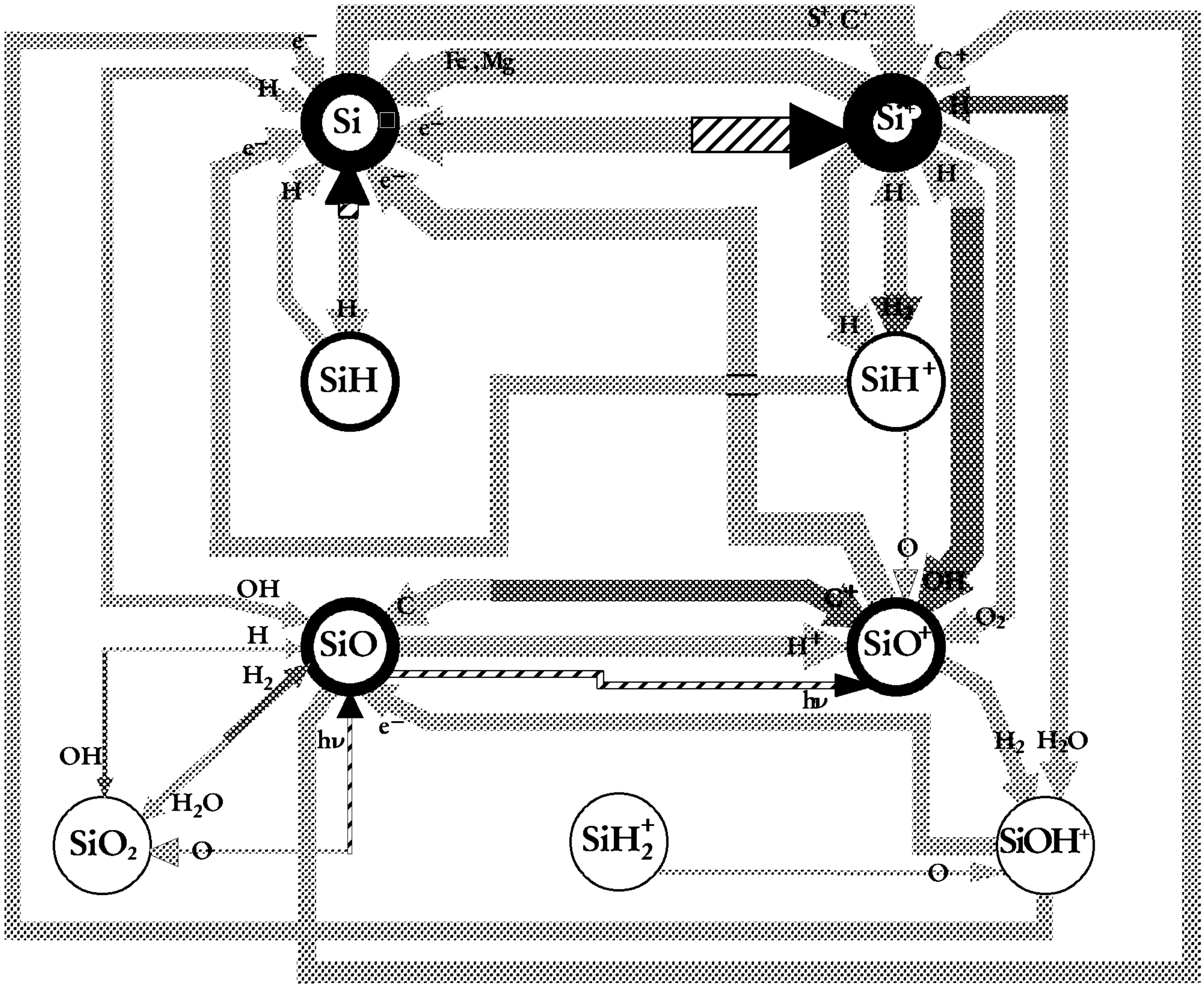

Figure 3.10: Reaction flow diagram of the Si-system for case **(A)** at $r = 5R_*$. For detailed instructions see Fig. (3.6).

In the considered temperature region this reaction proceeds on a faster level than the competing route

$$\mathrm{Si} \quad + \mathrm{O_2} \quad \Longleftrightarrow \mathrm{SiO} \quad + \mathrm{O} \qquad \text{(XXI)}$$

which according to Herbst et al. (1989) is the main building channel for SiO at low temperatures. At larger distances ($r \geq 8\,R_*$) reaction (XX) looses its importance. In this radius region SiO formation incorporates mainly the SiO_2 molecule by the reactions

$$SiO_2 + H_2 \Longleftrightarrow SiO + H_2O \qquad \text{(XXII)}$$
$$SiO_2 + H \Longleftrightarrow SiO + H_2 \qquad \text{(XXIII)}$$

The SiO and the SiO_2 molecule are closely connected, since there is no pathway of SiO_2 formation which does not incorporate SiO. For weak UV radiation fields, SiO and SiO_2 form an almost isolated subcycle in the Si-system.
The resulting concentration of SiO_2 is insufficient to allow effective dust formation based on this molecule as a nucleation species. All other components are only of minor importance as they are only intermediate states in the formation processes of the more abundant species.

3.5.2.4 Sulfur Chemistry

A reaction network for sulfur-bearing components consisting of 16 species and 242 reactions has been added to the reaction network in order to study the effects of sulfur-species on the chemistry. Generally one expects for an O-rich environment that species such as CS, OCS and HCS will be of small abundance. As the neutral hydrides of sulfur are less strongly bound than their oxygen analogues also a lower abundance of the hydride components has to be expected.
Although most of the other species are involved in reactions with sulfur containing molecules only the OH and the H_2 molecules play a crucial role in the sulfur chemistry because they are directly incorporated into the formation processes of HS, SO, SO_2, SO^+, HS^+, HCS^+, H_2S^+ and S_2^+. In all models with a substantial amount of UV radiation maintaining the dissociation of the species, the sulfur bearing molecules are less abundant compared to the results of model **(B)**. The concentrations of all other species do not change by more than 10% by invoking of the sulfur species. Particularly for model **(A)** the SiO concentration is not changed significantly by the incorporation of the sulfur bearing species. But there is a change of about 20 percent for $r > 10\,R_*$ in model **(B)**.
In order to get amounts of SO and SO_2 comparable to SiO the radiation field has to be significantly reduced. If we are approaching chemical equilibrium by increasing the mass loss rate to $\dot{M} = 10^{-5}\,\mathrm{M_\odot/yr}$ or reducing the stellar temperature to $T_* = 2000\,\mathrm{K}$, we obtain high concentrations of these molecules, as can be seen from Fig. (3.12).
The only molecule the abundance of which is significantly affected by the presence of sulfur is SiH according to the following charge exchange reaction:

$$SiS + H^+ \Longleftrightarrow S^+ + SiH. \qquad \text{(XXIV)}$$

Generally the sulfur containing molecules are very rare. Hence the bulk of the sulfur remains atomic with a high degree of ionization. The ionization of atomic sulfur and the subsequent recombination are in a state of chemical equilibrium. The charge

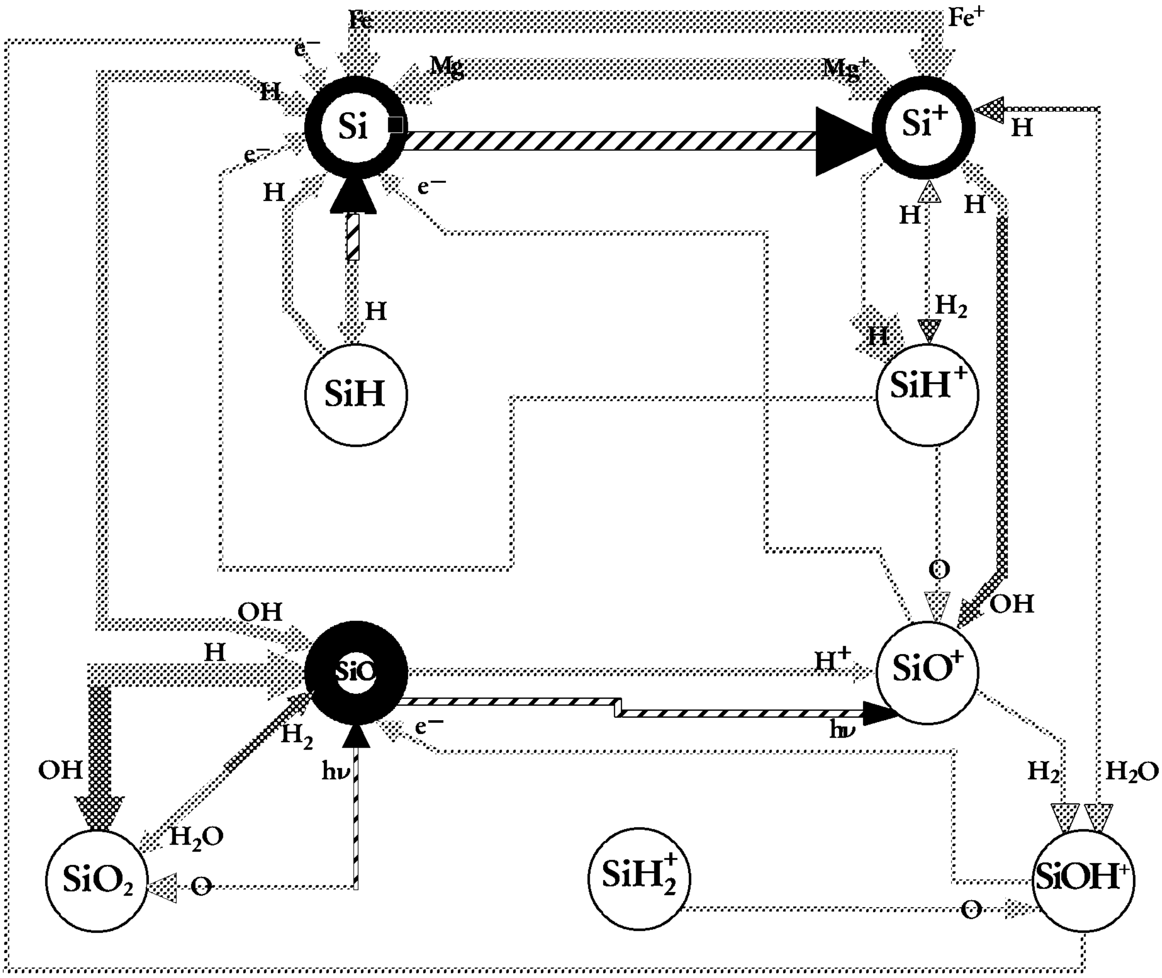

Figure 3.11: Reaction flow diagram of the Si-system for case **(B)** at $r = 5R_{*}$. For detailed instructions see Fig. (3.6)

exchange of sulfur with other species result in a loss by the reactions with H^+ and C^+

$$\mathrm{S} + \mathrm{H}^+ \Longrightarrow \mathrm{S}^+ + \mathrm{H} \qquad \mathrm{(XXV)}$$

$$\mathrm{S} + \mathrm{C}^+ \Longrightarrow \mathrm{S}^+ + \mathrm{C} \qquad \mathrm{(XXVI)}$$

and a gain by the reaction

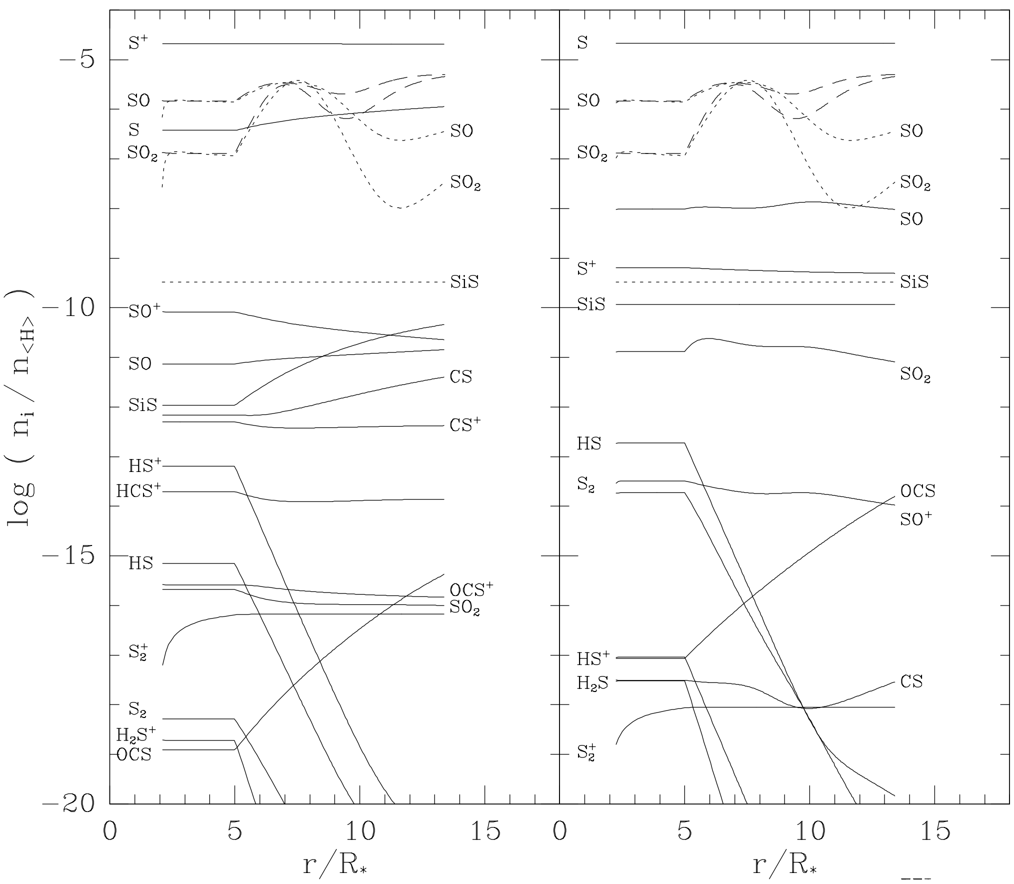

Figure 3.12: Sulfur chemistry in the inner envelope for model **(A)** (left) and model **(B)** (right). Additionally the abundances for SO, SO_2 and SiS are plotted for two different cases. Dashed lines correspond to a model with $T_* = 2000\,K$, dotted lines correspond to a model with a higher mass-loss rate of $\dot{M} = 10^2 \dot{M}_{case(\mathbf{A})}$ and a blackbody radiation field with $T_* = 3000\,K$. All other parameters remain unchanged (see Tab. (3.4.2)).

$$S^+ + Si \Longrightarrow Si^+ + S \qquad \text{(XXVII)}$$

The diatomic sulfur molecule S_2 has only a very low abundance. It is formed by the reaction

$$HS + S \Longrightarrow S_2 + H \qquad \text{(XXVIII)}$$

which has a rate dropping with decreasing temperature. It is destroyed via

$$S_2 + O \Longrightarrow SO + S \qquad \text{(XXIX)}$$

though being an intermediate in the SO formation. The formation of SO mainly proceeds along the endothermic channel

$$S + OH \Longrightarrow SO + H \qquad \text{(XXX).}$$

which has a reaction rate two orders of magnitude larger than the second effective SO producing reaction XXIX. This reaction is competing with the radiative dissociative reaction

$$\mathrm{SO} \quad + h\nu \quad \Longrightarrow \mathrm{S} \quad + \mathrm{O} \qquad \text{(XXXI)}.$$

With increasing distance, reaction (XXXI) becomes more important since a high energy barrier weakens the efficiency of reaction (XXX) with decreasing temperature. In addition the concentration of the OH radical is decreasing with increasing distance. A further loss mechanism for SO is the following reaction step leading to the production of SO_2 :

$$\mathrm{SO} \quad + \mathrm{OH} \quad \Longrightarrow \mathrm{SO_2} \quad + \mathrm{H} \qquad \text{(XXXII)},$$

whereas the destruction of SO_2 proceeds via the dissociative channel

$$\mathrm{SO_2} \quad + h\nu \quad \Longrightarrow \mathrm{SO} \quad + \mathrm{O} \qquad \text{(XXXIII)}$$

which results in a gain of SO. It is obvious that by this reaction scheme the formation of these molecules is inhibited by strong photodissociating UV fluxes.

3.6 Chromospheric Radiation and CO Formation

For the calculation of the photorates we have used the optical thin approximation. Therefore it is of special interest to examine the role of the CO molecule which is known to be a major absorber of UV radiation. The influence of these absorption effects including self-shielding has been worked out by Mamon et al. (1988) and Huggins et al. (1988) for the outer regions of circumstellar shells ($r > 10^{16}$ cm). Furthermore in their study of the SiO maser Clegg et al. (1983) have pointed out, that the envelope of α Ori will be optically thick in the wavelength range shortward of the CI threshold, whereas the optically thin approximation is valid without restriction for the longer wavelength range. From new laboratory data concerning the CO line absorption [Letzelter *et al.* 1987] some implications arise for the stellar envelopes. The consistent way to derive the interrelation between the chemistry and the radiation field would require a simultaneous treatment of the equations describing the radiation transfer problem and the chemical reaction network. However, this is far beyond the scope of this paper. Therefore we derived a more qualitative way, giving a reliable estimate of the overall role of the CO photodissociation in the frame of the entire chemistry. We computed the unshielded value of the CO photorate at $r = 2R_*$, which is $\mathcal{R}^{\mathrm{us}}_{CO} = 6.1 \cdot 10^{-6}\,\mathrm{s}^{-1}$ (model **(A)**). In order to study the influence of the CO photodissociation on the chemistry we take $\mathcal{R}^{0}_{CO} = \mathcal{R}^{\mathrm{us}}_{CO}$ as a reference value and treated the photodissociation rate $\mathcal{R}^{0}_{CO}$ as a parameter which is varied between the limits $10^{-8}\mathcal{R}^{0}_{CO}$ and $10^{+2}\mathcal{R}^{0}_{CO}$. In Fig. (3.13) the results of this investigation are plotted. In the left part of the diagram, where the chemistry is depicted in the case of small values for the CO photorate, the concentrations corresponds to a situation of total shielding of the CO molecule. From Fig. (3.13) one infers that

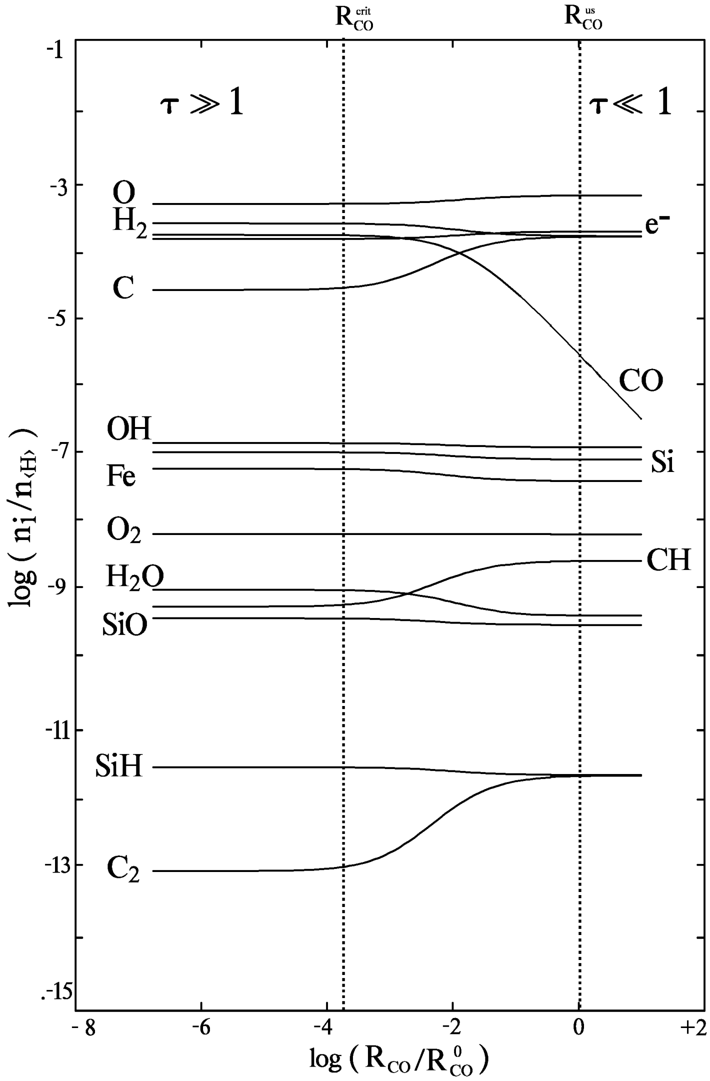

Figure 3.13: The influence of a change of the CO photodissociation rate on the chemistry for selected species at $r = 5R_*$. The photorate $\mathcal{R}_{CO}$ is normalized to the value of the unshielded rate $\mathcal{R}_{CO}^{us} = 6.1\,10^{-6}\,s^{-1}$. The values of all other rates remain constant. Model parameters are those of model (**A**).

---

the chemistry is in a full KE situation and a variation in the CO photodissociation rate over four decades does not cause any significant change in the chemical abundances. The actual CO concentration is dominated by the kinetical reactions which are of much higher efficiency than the photodestruction. When a critical value $\mathcal{R}_{CO}^{\rm crit} \approx 1.2 \cdot 10^{-10}{\rm s}^{-1}$ is reached, corresponding to an optical thickness $\tau_{CO} \approx 10$, the CO starts to be dissociated on a level comparable to the kinetic reactions, which can be seen by the increase of the abundances of all carbon bearing species. The liberated carbon remains mainly in an atomic state, due to the chromospheric UV-field which dissociates the molecules and molecular ions. In this intermediate region between $\mathcal{R}_{CO} = 10^{-1}\mathcal{R}^0_{CO}$ and $\mathcal{R}_{CO} = 10^2\mathcal{R}^0_{CO}$ the concentration of H_2 and H_2O also diminish. H_2 is destroyed by the increased reactions with the atomic oxygen injected via the channel

$$H_2 \quad + O \quad \Longrightarrow H \quad + OH \tag{XXXIV}$$

followed by photodissociation of OH. This effect also causes the decrease in H_2O which is formed by several reactions involving H_2. If we increase the photodestruction rate $\mathcal{R}_{CO}$ above $10^2 \cdot \mathcal{R}^0_{CO}$ the only effect is the additional destruction of the CO molecule without any influence on the other species. For the present model calculations we adopt a value of the photorate $\mathcal{R}_{CO} = 8.8 \cdot 10^{-10}\,\mathrm{s}^{-1}$ for model **(A)**. This choice is a reasonable approximation for the considered shell regions. It accounts for the shielding of the CO molecule, as the optical thickness for the CO molecule in the case of α Ori is large, e.g. $\tau_{CO} \gg 1$ (Clegg et al., 1983).
If we carry out the same investigations for an environment with a weak photospheric radiation field, the base value of the CO photorate is chosen to be $\mathcal{R}_{CO} = 4.6\,10^{-14}\mathrm{s}^{-1}$. Therefore it is clear that the CO concentration is saturated.

3.7 Influence of the UV Field

In order to demonstrate this influence we investigate the dependence of the molecular concentrations on a variation of the radiation field at a fixed radius $r = 5\,R_*$ (Fig.3.14). For this purpose the UV-flux F_λ is assumed as a parameter, with

$$F_\lambda = \beta \cdot F^0_\lambda \quad \text{with} \quad F^0_\lambda = F^{\mathrm{modelA}}_\lambda. \tag{3.22}$$

We varied β in the range 10^{-4} to 10^2.
Even for model **(A)**, when the flux of UV photons decreases to very low values, e.g. for $\beta < 10^{-1}$, the chemistry approaches chemical equilibrium. In this case, for $\beta < 10^{-4}$, H_2O is the most abundant oxygen containing molecule, whereas the concentrations of atomic O, C and Si become negligibly small due to the locking in H_2O, CO and SiO, respectively. In this region we have a very low state of ionization with Fe^+ to be the most abundant ion. The formation of molecules is very effective and therefore most atoms are converted to di- or polyatomic molecules. The state of the chemistry is dominated by the law of mass action. If the density is increased by a factor of 10 by choosing a larger mass loss rate at constant wind velocity the CE is already reached at $\beta = 10^{-1}$. Therefore a significantly higher UV-flux is necessary in order to produce the same departures from CE as in the case of lower densities. The SiO molecule begins to be photodissociated when $\beta > 1.8 \cdot 10^{-1}$. As a result the abundance of the Si atom also peaks about the same value of β representing that fraction of silicon stemming from the disruption of SiO which is not immediately ionized by UV photons. This plateau region of the Si concentration holds until the loss due to Si ionization is larger than the gain by SiO dissociation. The other

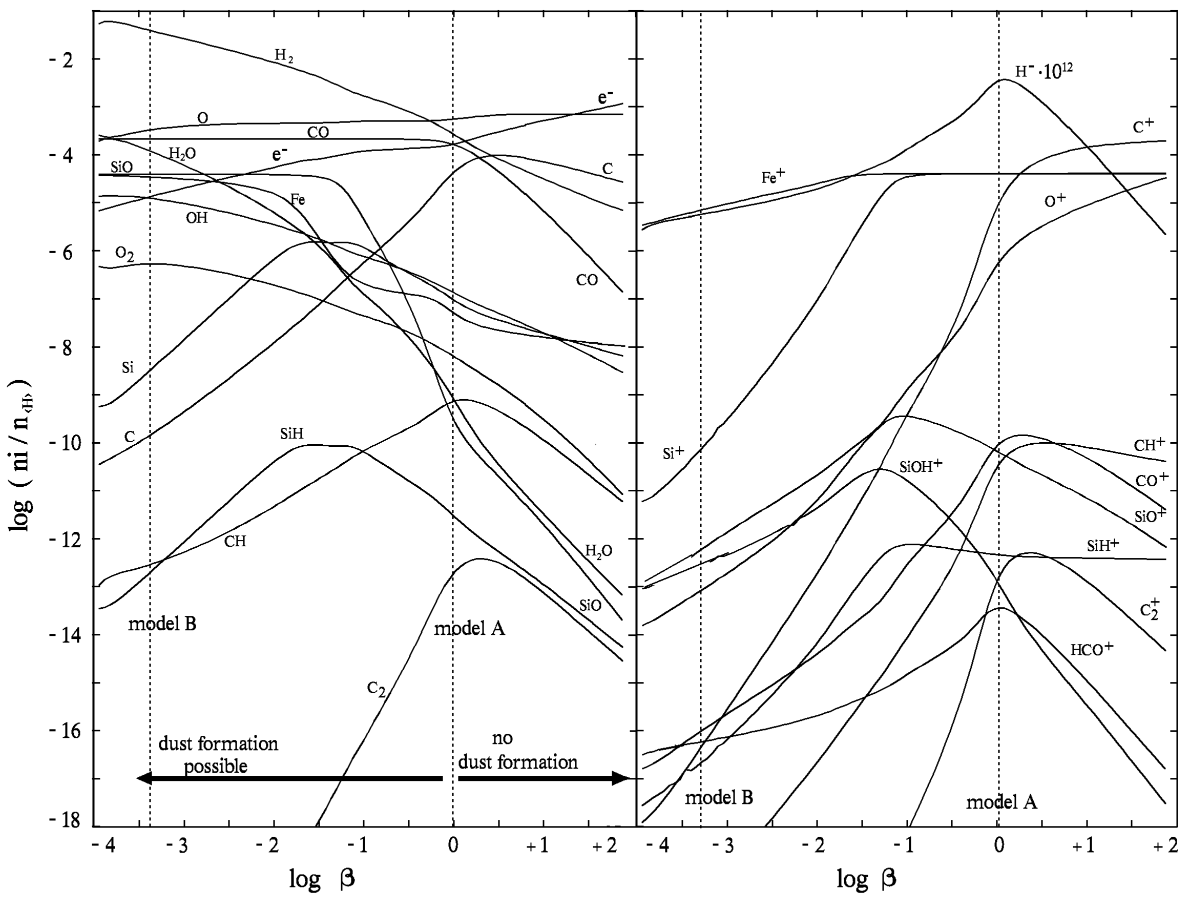

Figure 3.14: The effect of a variation of the UV-flux on the concentrations at $r = 5R_*$. The UV-flux is in units of the standard UV-flux of model (**A**).

---

heavy elements like Fe, Na and S are also fully ionized for $\beta > 0.2$ so that the neutral abundances all drop down. The carbon atom has the highest ionization potential, apart from H and O which are shielded by Lyman absorption of hydrogen, and thus the ionization of carbon requires the strongest UV-field. In the intermediate zone $10^{-1} < \beta < 10^{+0.5}$, where CO is moderately dissociated all neutral carbon species reach their maximum concentration. In contrast to SiO, the CO molecule remains stable until the strength of the UV radiation field of model (**A**) is reached, e.g. $\beta = 1$. This point also marks the transition of the chemistry from a molecule dominated to an essentially ion and atom dominated situation. The results for the modelling of the case of α Ori clearly show, that dust formation is possible up to a high level of chromospheric UV flux, as indicated by the dotted lines in Fig. (3.14)

3.8 Temperature Dependence of the Model Results

The radial temperature dependence used in our model calculations was adopted from the theoretical work of Goldreich and Scoville (1976) . They have studied the physical properties of the circumstellar envelopes of special late M-type giants. These objects are characterized by a relatively low stellar temperature ($T_* \approx 2000 - 3000\,K$), a high luminosity ($L \approx 10^4\,L_\odot$) and a chemical composition which is oxygen rich. Thus in view of the physical similarities the application of their temperature law to the case of αOri was a reasonable first approximation.
However, there are two main differences between these OH–IR stars and *Beteigeuse* (αOri):

a) as grain formation takes place almost in the inner zones of the cool envelopes of OH–IR stars, the gas is ejected by radiation pressure acting on dust grains, thus driving a massive stellar wind. In αOri dust formation does also occur, but the amount of grains formed is unsufficient to drive the continuous ejection of gaseous material from the outer atmosphere. In the case of αOri Alfven waves [Hartmann and Avrett 1984] or acoustic waves [Cuntz 1990] are proposed as driving mechanisms in recent theoretical studies.

b) In contrast to OH–IR objects, αOri has a chromosphere. This creates different conditions for the chemistry to evolve, photoreactions will play a major role in this environment. One main question which arises in this context is the extension of the chromosphere.

The role of the dust in the framework of the energy balance in the circumstellar shell mainly comprises two aspects acting in opposite ways on the energy balance.
At first dust grains effectively transfer momentum to the gas by collisions with the gas molecules. These collisions are the dominant source of heat input to the circumstellar gas in the absence of a chromosphere. Secondly dust is an efficient absorber of ultraviolet radiation and reradiates the absorbed energy in the infrared wavelength range, thus the dust is contributing a main part to the gas cooling.
The model calculations of Goldreich and Scoville do not account for this cooling contribution of the dust, but they considered the heating input by the gas–grain collisions. Except very close to the star this is the main source of energy input to the gas, so this treatment will lead to an overestimation of the kinetic temperature.
The models of Hartmann and Avrett developed for the chromospheric region of αOri lead to much higher temperatures in the inner regions. They assumed an Alfvén driven wind and the local temperature is given by the balance between wave heating, adiabatic expansion and radiative cooling terms. The temperature distribution

resulting from this model for αOri then is given in parametrized form [Wirsich 1988]
,

$$T(z) = A\,(1 - exp[1 - z]) \cdot z^{-2} + B \cdot z^{-1/2} \qquad (3.23)$$

where the parameters A and B are adjusted to give a temperature in agreement with the IUE observations of Basri, Linsky and Eriksson (1981) and the radio measurements of Newell and Hjellming (1982) . The application of the temperature law (3.23) leads to a significantly higher temperature in the regions with r$< 5\,R_*$, with a peak temperature T_{peak} of about $6000\,K$ at r$=2\,R_*$ (see Fig.(3.15). The results

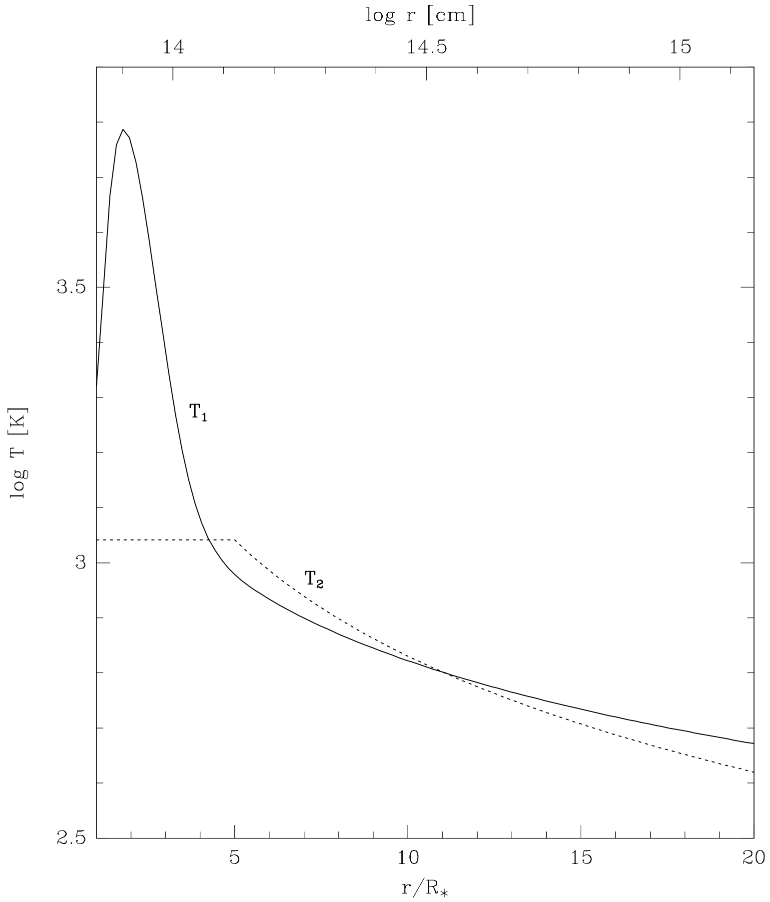

Figure 3.15: Radial temperature structure for αOri based on the models of [Hartmann and Avrett 1984] and [Cuntz 1990] (solid line) and [Goldreich and Scoville 1976] (broken line).

---

of a chemical model calculation on the basis of the chromospheric model **(A)** are presented in Fig. (3.16) Obviously there are enormous differences in the chemical abundances in the innermost region. The state of the chemistry is characterized by atomic ions, although the ionization of the elements is incomplete but substantially

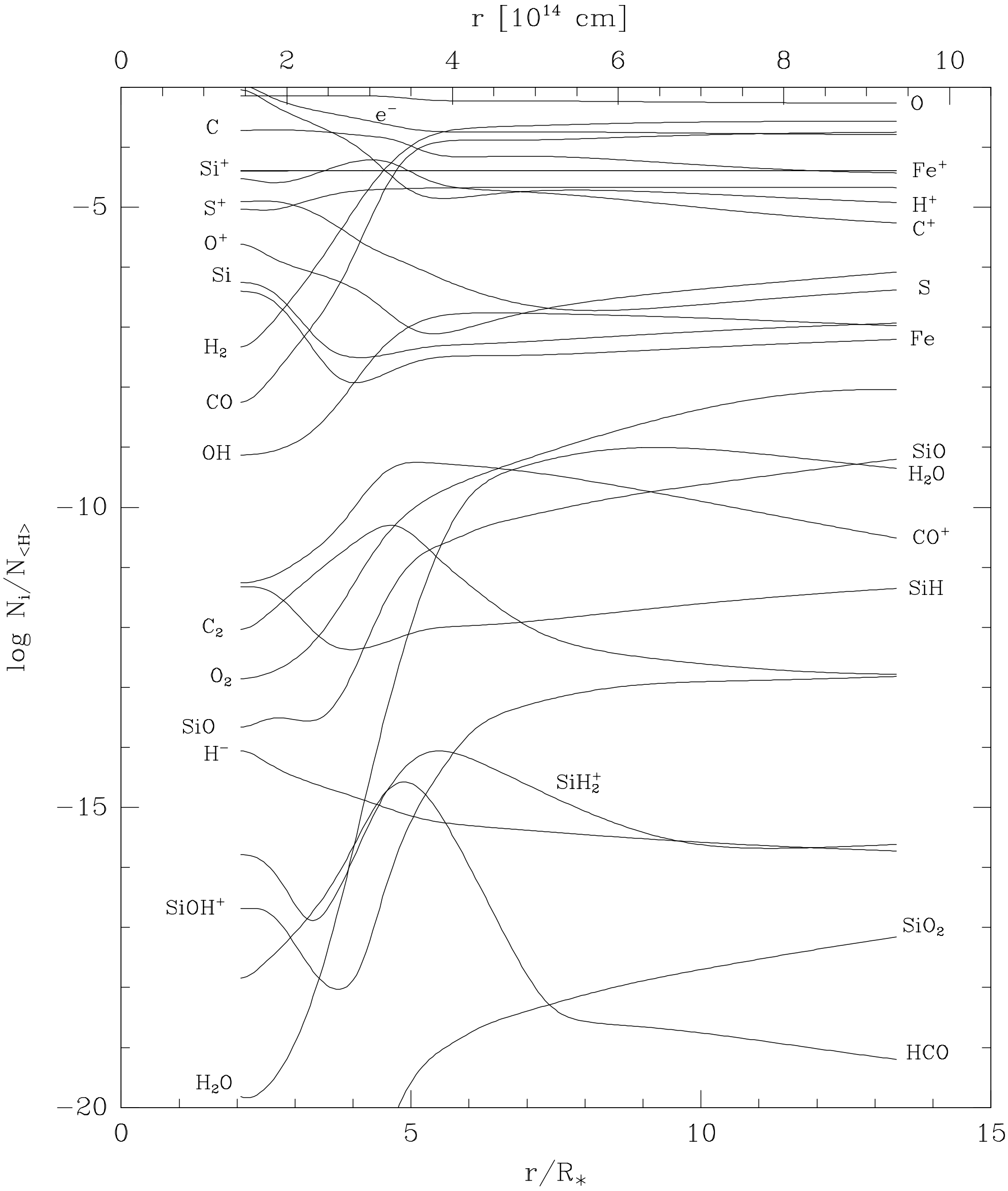

Figure 3.16: Radial distribution of the chemistry for α Ori based on the different temperature structure described in this section. The concentrations of the species are normalized to the total amount of hydrogen atoms.

---

higher than in model **(A)**. This is in agreement with the results of Hartmann and Avrett, who noted that for complete hydrogen ionization the temperature has to be larger than 9000 K. The production of molecules in this region is substantially lower and those routes of formation are favoured which require an activation energy and which under the "normal" conditions in stellar outflows, do not proceed very effectively. All the neutral molecules first show an ascending slope of their abundances, just reacting on the steep temperature decrease with increasing distance. During the high temperature phase the production of the CO molecule acts by

$$C + OH \Longrightarrow CO + H \qquad (XXXV)$$
$$CS + O \Longrightarrow CO + S \qquad (XXXVI)$$

which are not too temperature sensitive, but the low abundance of the OH molecule hinders more efficient CO formation. The water molecule, practically not present in first phase also quickly recovers to a concentration level of the standard model. Its abundance dramatically increases from $X_{H_2O} = 10^{-20}$ to $X_{H_2O} = 10^{-10}$ at r=5R$_*$. The H$_2O$ molecule and its radical are coupled by the temperature sensitive channel

$$OH + H_2 \Longrightarrow H + H_2O \qquad (XXXVII).$$

Generally it must be emphasized that the incorporation of a realistic chromospheric model for the underlying temperature structure leads to significant changes in the chemical abundances. But the high density (n$\approx 10^8 - 10^9$) in the inner zone and the resulting short collisional timescales in the hot region enables the chemistry for a fast adjustment to the changes in the physical conditions. Thus for radii larger than 5R$_*$ the resulting concentrations for both temperature structures are in reasonable agreement. In this case the possibility of dust formation, however, is probably even smaller than in the chromospheric standard model.

3.9 Dust Formation

Dust in circumstellar shells condenses in the expanding and cooling gas of the stellar wind at temperatures below 1000 K. In this temperature regime most elements are completely associated to diatomic or polyatomic molecules which possibly might condense to macroscopic solid specimens. Therefore, grain formation is one of the major problems in circumstellar chemistry. Not only it determines the properties of the emerging circumstellar dust itself but also has a decisive impact on the global shell structure (temperature structure, velocity field, IR-excess, UV shielding) and hence on the entire chemistry of the system.
A key role in determining the chemical conditions prior to dust formation is naturally attributed to the CO molecule. The blocking of CO removes either C or O from the gasphase thus determining the type of shell chemistry and of the condensable species. From our calculations one sees that even in the case of rather large UV intensities CO blocks the bulk amount of carbon and thus ensures an oxygen-rich chemistry. As a consequence of the extraordinary stability of the CO molecule even in extreme non-equilibrium situations its concentration does not deviate significantly from the corresponding CE value. Thus, we expect formation of silicate dust in an oxygen rich element mixture.

As, however, the blocking of C by CO slightly decreases with increasing UV flux of the central star (cf. Fig. (3.13), a non-negligible amount of atomic carbon exists in the gas phase in model **(A)**, which may contribute to grain formation and growth even in an oxygen rich element composition.
From observations of the IR-emission of circumstellar dust shells it is well known, that M-stars form some kind of silicate dust. Its composition is believed to be $Mg_xFe_ySiO_4$ with $x + y \approx 2$, since iron-magnesium-silicates of this type are very stable and Si, Fe and Mg have just the right abundances to form compounds of this type [Sedlmayr 1989] . It is not possible, however, to form such silicates directly from the gas phase since the nominal molecule of the condensate does not exist as a free molecule [Gail and Sedlmayr 1987a] . They can only be formed by growth processes onto the surface of some kind of seed particles. The essential problem then is to determine the nature and the formation mechanism of the primary condensate, which later changes into silicate dust by collecting the appropriate amounts of Si, Mg, Fe and O from the gas phase by surface reactions. The former investigations of Gail et al. (1984) and Gail and Sedlmayr (1986, 1988) have shown, that the exploration of the dust condensation process requires the clarification of three different steps:

a) determination of the chemical composition of the gas,

b) selection of those molecules which have a strong tendency to form large molecular aggregates at temperatures around 1000K,

c) investigation of a reasonable reaction pathway resulting in macroscopic dust grains.

In oxygen-rich compositions in chemical equilibrium (probably valid for late-type M-stars) the primary condensates should originate essentially from SiO, MgO, MgS and Fe, since these are the most abundant and reactive species in the gas phase in chemical equilibrium. The nucleation process then should proceed via clustering of SiO or MgO and MgS [Gail and Sedlmayr 1986b] .
In the case of early M-stars, where ionizing radiation is present (case **(A)**) our model calculations for the chemistry in the central parts of the circumstellar shell now provides the necessary information with respect to the molecular composition of the gas phase when the outflowing matter enters into the dust formation zone in order that we can proceed to step b). In case **(A)**, the most abundant reactive species which may form stable clusters at high temperature are Si^+, Si, Fe^+, Fe, Mg^+, Mg, C and SiO together with O and S, S^+ to form oxides or sulfides, respectively (cf. Figs. 3.3, 3.4 and 3.14). In case **(B)** these are SiO, Fe, Fe^+, Mg, Mg^+ together with O, H_2O and S. Formation of polyatomic clusters from these particles obviously requires that at least one abundant neutral species is involved, since clustering of ions is prohibited by the strong Coulomb repulsion. Formation of pure Fe- or Mg-clusters is unlikely due to the extremely low bond energy of small clusters of these elements. Although MgO and MgS also might serve as possible candidates for the primary condensate there is a complete lack of available laboratory data for the

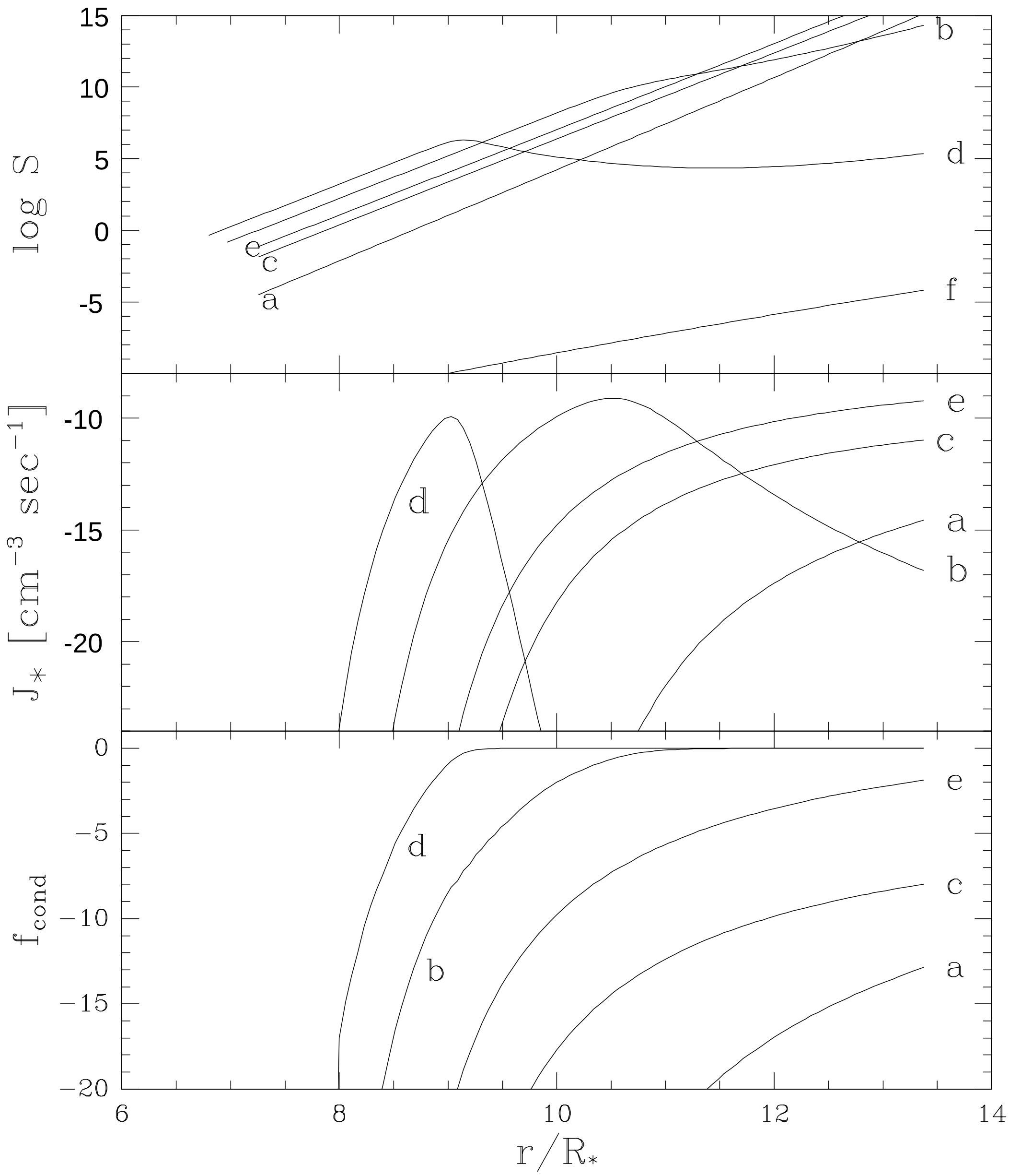

Figure 3.17: Supersaturation ratio S, nucleation rate J_* and degree of condensation f_{cond}. The labels denote the following set of models: a) case **(A)**; b) case **(B)**; c) as case **(B)**, but $v = 5km/sec$; d) as case **(B)**, but $\dot{M} = 10 \cdot \dot{M}_{case(\mathbf{A})}$; e) as case **(B)**, but $T_* = 3500\,K$; f) as case **(B)**, but temperature structure from Wirsich (1988). All other parameters remain unchanged (see Tab. (3.4.2).

---

gas phase formation reactions of these species. Hence a reliable treatment of the chemical formation of MgO and MgS in the framework of our model is not possible. Thus, in our calculations, SiO in cases **(A)** and **(B)** and possibly carbon in case **(A)** play a key role in the formation of the primary condensate. We first discuss the case of a late-type M-star which is supposed to have no chromosphere (case **(B)**). The most likely starter reaction for dust formation in this case is clustering of SiO since SiO has a high bond energy as well as a high ionization potential, thus being stable also in the presence of UV-radiation. This process has been studied in the laboratory by Nuth and Donn (1982,1983). Though we do not know the details of the reaction sequence from SiO molecules to large SiO clusters, we are in the fortunate situation that data for calculating the nucleation rate J_* are available. Nuth and Donn found that their experimental results can well be fitted by the expression for J_* resulting from classical homogeneous nucleation theory by using a fictitious "surface" tension which is derived from a fit to the experimental data for J_*. In the present calculations of J_* we adopted this value for the "surface" tension, the expression for the vapour pressure of SiO molecules over solid SiO given in Nuth and Donn (1982, 1983) and the partial pressure of SiO in the gas phase resulting from our model for the chemistry. This allows to solve the moment Eqs. (3.14) and (3.15) simultaneously with the chemical reaction network. We did not, however, include heterogeneous growth processes in our calculations which allow for growth of silicates from the SiO seed nuclei by collection of Fe and Mg from the gas phase and by oxidation processes with O and H_2O in surface reactions, since the details of this process are not known. Further, the process of subsequent growth of the silicon dust by agglomeration which has been discussed by Bloemhof et al. (1985) in order to explain the reduction of the infrared brightness as a function of radial distance has not been taken into account. As a consequence our calculations only give a lower limit for the efficiency of the formation of dust grains.

The results for the dust formation are shown in Fig. (3.17). The onset of effective dust formation of SiO takes place at a gas temperature of about $T_g < 750\,\mathrm{K}$, which corresponds to a distance of $8.5R_*$. The peak rate of nucleation occurs at approximately $T_g = 500\,\mathrm{K}$ or $r = 10.5\,R_*$. This condensation process is strongly delayed as the high supersaturation ratio at this distance indicates. The depletion of the condensable material is almost complete, which is shown by the steep decrease of the SiO concentration in the dust forming region. The degree of condensation reaches unity at about $11\,R_*$. From this one concludes that the number ratio of condensed SiO monomers to H atoms is $1.2 \cdot 10^{-5}$. The SiO grains formed have an average radius of $a = 15\,a_m$, where a_m is the hypothetical monomer radius of SiO which is assumed to be $a_m = 2.02 \cdot 10^{-8}\mathrm{cm}$. This average size shows that the average particle consists of approximately 10^4 monomers, which is very small. Certainly this size is a lower estimate for the real grain size since heterogenous grain growth is not taken into account. If the stellar temperature is increased to $T_* = 3500\,\mathrm{K}$ the onset of nucleation is shifted outwards to $r = 9.1R_*$ where the degree of condensation substantially decreases to $f_{\mathrm{cond}} = 5 \cdot 10^{-2}$. Also the amount of available siliconmonoxide is reduced and the average particle size shrinks due to the reduction of constructive collisions.

Next we consider the case of early type M-stars with a chromosphere (case A). SiO clustering is a likely starter process for dust condensation in this case, too. The high abundance of free C atoms, however, opens the possibility of a chemical pathway

from atoms to dust involving carbon. In principle, there seem to be two possibilities: (i) condensation of pure carbon dust or reactions with one of the abundant ions Si^+, Fe^+ or Mg^+ to form carbides. The second case probably can be ruled out since for instance the SiC molecule is much less stable than the SiO molecule (dissociation energies 104 and 190 kcal/mol, respectively). Since only a small fraction of the Si transforms into the more stable SiO, we expect a much less concentration of SiC molecules. Hence, a possible nucleation process involving C-Si-compounds proceeds much slower than SiO nucleation and cannot compete with this process. The same holds for other carbides. Carbon condensation, however, presently cannot be ruled out and it may well be that for early type M-stars like α Ori some amount of soot is formed additionally to the silicate dust despite of its O-rich composition due to incomplete blocking of C in CO. A sootlike dust component is not observed for these stars, but it would be difficult to detect since the PAH infrared features typical for H atoms attached to the border of fused six-rings are absent due to the extremely high abundance of monoatomic H. Hydrogen atoms then are stripped from the border by reaction wit H atoms from the gas phase. The remaining structureless continuous absorption coefficient of soot than is similar to the silicate dust continuum. Since no complete carbon chemistry is included in our reaction network, we cannot decide on the basis of our present model calculations, whether soot is formed or not. Our dust calculation, therefore, only refers to silicate dust.
In case **(A)** the efficiency of dust formation is reduced by several orders of magnitude compared to case **(B)**, as can be seen from Fig. (3.17). In model **(A)** the final degree of condensation only is 10^{-13} at the outer boundary, a value which is in agreement with the observed upper limit of the dust to gas ratio of 10^{-8} [Sopka *et al.* 1985] . Although the supersaturation ratio S is very high, mainly caused by the exponential temperature dependence of the vapour pressure, the intense UV radiation hinders the efficient production of the SiO nucleation seeds, which means that there exists only a tiny amount of condensable material. As the onset of grain formation is shifted to larger distances ($r_{\rm cond} \approx 10.5 R_*$), the density of condensable material is reduced and the conditions for nucleation and grain growth are less favourable than in model **(B)**. This result is in good agreement with the observations of Sutton et al. (1977) and Bloemhof et al. (1984), who also derived a very low grain density inside a radius $r \leq 12 R_*$.

3.10 Concluding Remarks

By means of solving the fully time dependent reaction network, we have investigated the inner shell chemistry of late-type M-stars, with special emphasis on the influence of chromospheric UV-radiation on the abundance of the molecules SiO and CO, which play a key role for the dust formation process. To demonstrate the interdependences and the essential characteristics of the chemical processes as well as their mutual coupling we have constructed a comprehensive reaction flow diagram for the main chemical systems: Si, C and O-H, respectively.

As a consequence of the significant UV flux due to the presence of a chromosphere, the total degree of ionization (defined as the ratio of the number of ions to the total number of particles without electrons) in model **(A)** ($f_{\rm ion} = 2 \cdot 10^{-4}$), where ionizing photons are abundant, is considerably higher than in model **(B)** ($f_{\rm ion} = 4 \cdot 10^{-5}$). Kinetical reactions with ions originating from photoionization and with radicals determine the chemical structure of the envelope. In this case, there is a high abundance of Si^+ and a non-negligible abundance of free C atoms due to the break up of the Si-O and C-O bonds by high energetic photons and to subsequent ionization of the Si. In the absence of chromospheric radiation nearly the entire silicon is bound up in SiO and the carbon is blocked in CO. The heavier elements Fe, Mg and Na form a closed subcycle which is essentially decoupled from the rest of the chemistry. In both cases they are completely ionized and the main electron donors. Generally the reaction rates are much lower in model **(B)**, as the ion abundance for this model is small and the fast ion-neutral reactions are only of minor importance. A comparison of the reaction flow diagrams for the Si and C systems in Figs. (3.10) and (3.8) clearly confirms this statement, also showing the important role of both, the SiO and the CO molecule.

Our investigations show that in spite of strong chromospheric UV-radiation, which favours a pronounced non-LTE situation for the formation and destruction processes in the envelope, the carbon to a large extent is blocked in CO molecules like in the TE case. This is true even up to the high level of UV flux, which is attributed to the M-type supergiant α Ori. An important result, however, is that in case **(A)** the partial pressure of free carbon atoms in the gas phase is nearly one third of the partial pressure of CO. This, in principle, opens the possibility of carbon dust formation besides the observed silicate dust around oxygen rich stars like α Ori. Future model calculations, therefore, require an inclusion of the full carbon chemistry in the chemical reaction network in order to explore this possibility.

Although our method does not consistently take into account the self shielding of CO for the computation of the photorates, our models indicate that the effect of the CO absorption on the entire chemistry is not significant for the entire radius regime considered within several orders of magnitude for the CO photorate.

Our model calculations show that even in the presence of a chromospheric UV field, nucleation and considerable growth of grains based on SiO nucleation seeds might be possible. However, in this case both the nucleation rate and the growth rate remain small. This result is in agreement with the observations of the dust shell of α Ori, which corresponds to the parameters used for model **(A)**. The comparative calculation for a late M-type giant without a chromosphere shows that in environments not exposed to high energetic photons considerable amounts of dust could be formed, even if the temperature of the central star is as high as $T_* = 3500\,\mathrm{K}$.

Zwei Gefahren bedrohen die Welt:
die Ordnung und die Unordnung.

Paul Valéry

Chapter 4

Chemistry and Dust Formation in the Shells of Classical Novae

4.1 Introduction

Galactic classical novae now are well established “astrophysical laboratories” for the study of the formation of circumstellar grains. Comparing the variety of all the dustforming objects which have been observed, novae are the most dramatic in their evolutionary manifestation of a massive dust shell obscuring the optical light emission source. Numerous infrared observations of recent classical novae have confirmed the genesis of dust grains during the evolution of the nova outflow on a timescale of 20–100 days.
Although there is now overwhelming evidence for the formation of dust during the nova explosion there has been persistent discussion about pre–existing nucleation sites functioning as condensation nuclei when they are reached by the ejected material. However, the origin of these grains predating the nova explosion remains uncertain[1]. Nevertheless the problem of getting nucleation going in a hostile and inhospitable environment of a nova is not an easy and straightforward one. Quite the reverse, the investigation of the dust formation capabilities of a nova by invoking only a single parameter like the ejected mass or the speed–class is not an appropriate approach.
Therefore the actual investigation tries to account for the fact that grains may be formed in several regions of a multi–parameter space, as preceding chemical investigations have proved (e.g. [Rawlings 1988]). The study of the chemistry in the nova outflow of course is an incontestable requirement before the question of dust formation can be addressed. For this reason the present work is mainly devoted to the study of the chemical processes which are the basis for any further and more complex course of events leading to small solid particles ejected into the interstellar space during a classical nova outburst.

Unfortunately there is only little information available about the chemical processes

[1] Two hypothesis for the formation of the pre–existing grains which are more or less conceivable have been proposed:
a) dust formation occurs already in the accretion disk of the white dwarf [Jenkins and Evans 1988] and
b) sublimation of cometary material during the nova eruption [Matese *et al.* 1989] .

in nova envelopes, especially concerning the early phases of the outburst.
For a long period the CN radical was the only molecule identified: in nova DQ Her 1934 the CN[2] violet absorption system was observed [Sanford 1935] . More recently the first detection of molecular hydrogen in the shell of a classical nova is reported by Evans (1991) , a discovery also made in nova DQ Her 1934. Ferland et al. (1979) announced the observation of the vibration–rotation bands of CO in nova NQ Vul 19 days after outburst. To summarise all this one can state that only three molecules have been identified in the gas phase of nova envelopes and from those, only CO was observed during the early outburst stage, the one we are interested in.
More information is available about the solid phase. In most nova cases where remarkable infrared emission has been reported, this emission has been assigned to amorphous carbon dust. There is, however, substantial evidence that also grains of different mineral composition like SiC (V1370 Aql), SiO (QU Vul) and also hydrocarbons (V842 Cen) can condense in nova ejecta.
As a consequence of all the facts concerning the problem of chemistry and dust formation in nova shells the present model calculations incorporate

- an extended chemical network comprising the carbon as well as the oxygen chemistry to account for the different chemical situations which may arise,
- the moment equations for nucleation and growth,
- a calculation of the energy balance by assessing the relevant heating– and cooling processes, thus having access to the actual gas temperature resulting from the current state of the gas,
- the determination of the actual photorates,
- a realistic nova radiation field supplied by the non–LTE model atmosphere calculations of Hauschildt (1991),
- a detailed treatment of the H–atom in a 3–level approximation including the continuum, added as a sub–network to the chemical equations [Beck *et al.* 1990a].

All these points will be discussed in detail in the following sections.

[2]The CN molecule is of special interest for the derivation of isotopic abundance ratios of $^{12}C/^{13}C$ and $^{14}N/^{15}N$ proving the predictions of the thermonuclear runaway theory.

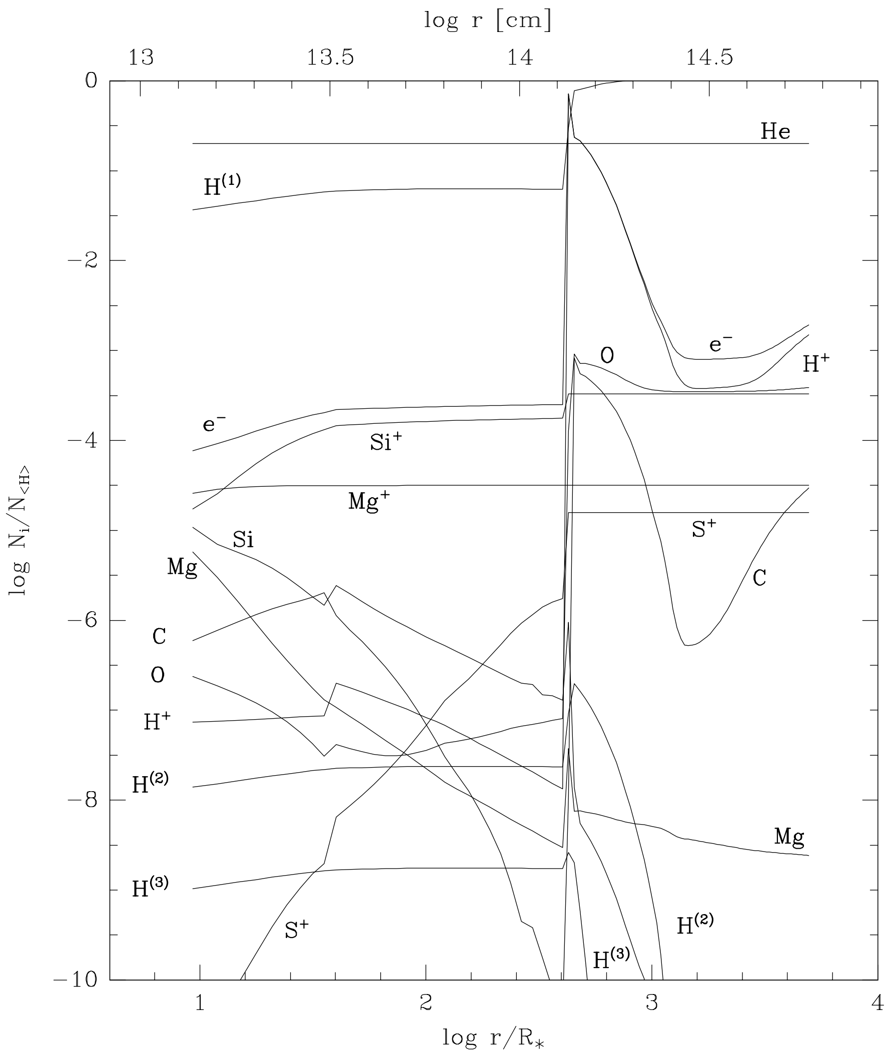

Figure 4.1: Logarithmic concentrations of atoms and their ions, normalized to the number of H-atoms over a logarithmic radius axis scaled with the stellar radius. The different excited states of hydrogen $H^{(i)}$ are also shown.

4.2 Components of Model Construction

4.2.1 The Nova

The model used for the theoretical description of the classical nova event basically is that developed for the computation of the ionization and temperature structure in Chap. (2.5.1), thus we refer to the arguments given there for the validity of the chosen model and only list up the main assumptions:

- spherical symmetry
- constant expansion velocity v
- constant shell diameter r_s
- time–dependent photospheric temperature T_*
- time– and optical depth dependent photorates

The actual parameters chosen for the calculations are shown in Tab. (4.3).
The radiation field of the nova was taken from the radiation transfer calculations of Hauschildt (1991, 1992), who has calculated various models varying the effective photospheric temperature between 8000K and 60000K (see also Sect. (2.5.3.1)). The frequency dependent flux at the surface of the photosphere then was taken as the input flux for the nova model calculation. On the basis of these data we are able to simulate the time dependence of the changing photon flux due to the increasing photospheric temperature. The space between the photospheric boundary and the inner surface of the expanding envelope is treated as an empty space, thus no photons can be absorbed between photosphere and the shell. In this way we neglect that there may be a continuous outflow of mass following the main matter ejection event, although this is not completely consistent with the assumed time dependence of the values of photospheric temperature and radius.

4.2.2 The Chemical Model

The chemical model is described in the framework of the equations presented and discussed in Sect. (3.2.6), including the equation of continuity in the comoving frame of the outflowing gas element (Eq. (3.8)), the empirical Arrhenius law (Eq. (3.11)) and the thermodynamical expression for the coupling of the forward and backward reaction rates (Eq. (3.10), Milne relation).
Dust formation is treated by the incorporation of the moment equations for nucleation and growth (see Eqs. (3.14, 3.15 and 3.16)) for the possible condensates carbon, siliconmonoxide and iron. A general reference for the chemical data is

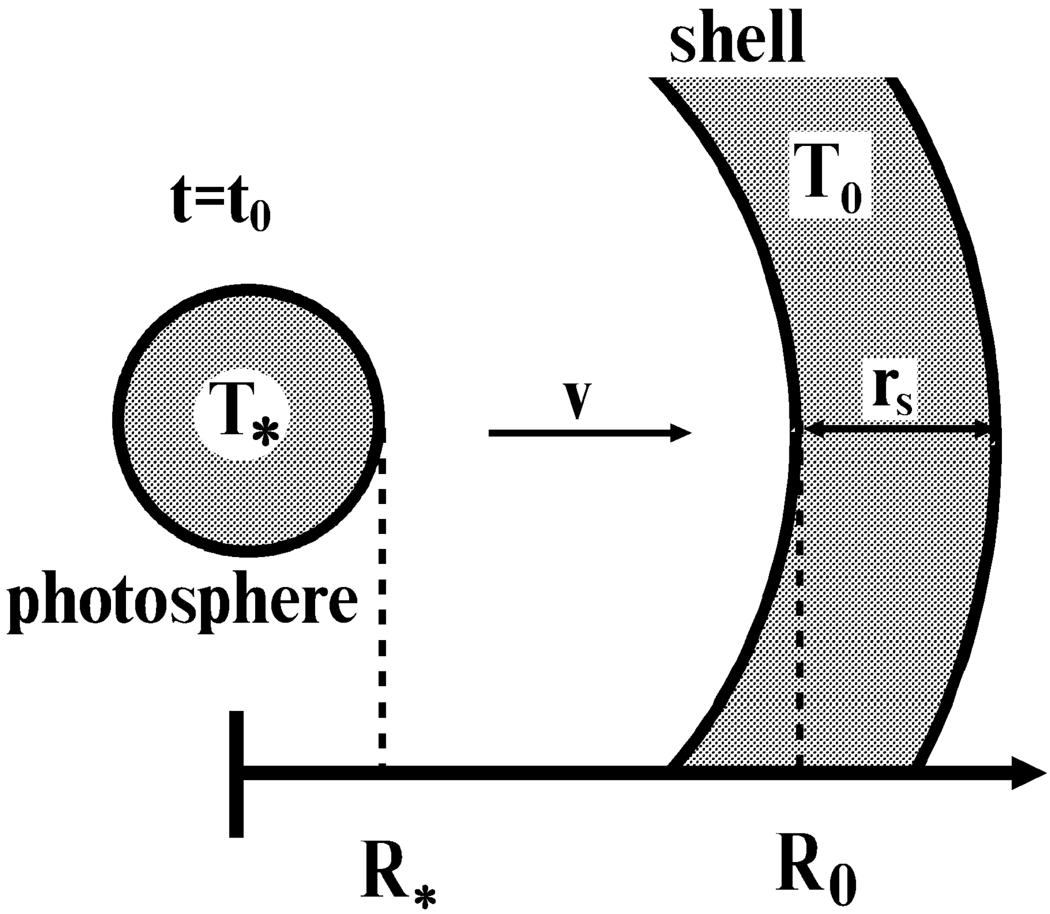

Figure 4.2: Schematic sketch of the nova model and the parameters at the start ($t=t_0$).

given in the Appendix (III.2), where the reactions and their reaction rate coefficients used for the chemical network computations are listed (Tabs. (III.2), (III.3), (III.4) and (III.5)).

For practical reasons the chemical reaction data have been divided into four groups:

A) Empirical reactions
In this class all reactions are collected for which the data are given in the empirical form

$$k = AT^{\alpha} \exp(-E_a/T). \qquad (4.1)$$

with the three parameters A, α and E_a.

B) Backward reactions

atoms	neutrals	ions
H	H, $H^{(1)}$, $H^{(2)}$, $H^{(3)}$, H_2	H^+, H^-, H_2^+, H_3^+
He	He	He^+, HeH^+
C	C, C_2 CH, CH_2, CH_3, CH_4 C_2H, C_2H_2	C^+, C^-, C_2^+, C_3^+ CH^+, CH_2^+, CH_3^+, CH_4^+, CH_5^+ C_2H^+, $C_2H_2^+$, $C_2H_3^+$ $C_2H_5^+$, C_3H^+, $C_3H_2^+$,$C_3H_3^+$
O	O, O_2 OH, H_2O CO, CO_2 HCO, H_2CO, CH_3OH	O^+, O_2^+ OH^+, OH^-, H_2O^+, H_3O^+, O_2^+ CO^+, CO_2^+ HCO^+, H_2CO^+, H_3CO^+, HCO_2^+ CH_3CO^+, C_2HO^+, $C_2H_2O^+$
N	N, N_2 NH, NH_2, NH_3 CN NO HCN, HC_3N, CH_3CN HNO OCN	N^+, N_2^+ NH^+, NH_2^+, NH_3^+, NH_4^+, N_2H^+ CN^+, CN^-, C_2N^+, C_3N^+ NO^+, NO_2^+ HCN^+, H_2CN^+, CH_4N^+, $C_2H_2N^+$ C_2NH^+, $C_2H_3N^+$, C_3HN^+ HNO^+
Na	Na	Na^+
Mg	Mg	Mg^+
Si	Si SiH SiC SiO, SiO_2	Si^+ SiH^+, SiH_2^+ SiC^+ SiO^+, $SiOH^+$ $CHSi^+$, CH_2Si^+
S	S, S_2 HS, H_2S CS, H_2CS SO, SO_2, OCS NS SiS	S^+, S^-, S_2^+ HS^+, H_2S^+, H_3S^+ CS^+, HCS^+, H_2CS^+, H_3CS^+ SO^+, HSO^+, $HOCS^+$ NS^+, HNS^+ SiS^+, $HSiS^+$
Fe	Fe	Fe^+

Table 4.1: Species included in the Nova-chemistry network. $H^{(i)}$ denotes a hydrogen atom in an excited state i. The electron has been omitted from the list as it does not fit in any of the categories.

The rate coefficient for this class of reactions is calculated by using the thermochemical data of entropy and enthalpy for the species listed in Tab. (III.6), combined with the affiliated forward rate coefficient.

C) Photoreactions

In the network 80 photoreactions are included, comprising the ionization of the elements and some molecules as well as a number of dissociations.

D) Hydrogen reactions
In spite of the sometimes peculiar element abundances in nova shells, the hydrogen atom plays a central role in evaluating the complex nova chemistry. Especially in view of the energy balance the ionization of hydrogen has to be known quite accurately. Therefore the hydrogen atom is treated in a three level approximation including the continuum to account for the Non–LTE effects in the occupation numbers of the hydrogen levels which might lead to significant changes in the time evolution of the energy balance and, as a direct consequence, in the envelope temperature.
Therefore an additional sub–network of 24 hydrogen reactions has been incorporated, comprising the various processes altering the occupation density of the hydrogen levels and including the processes of ionization and recombination. For the calculations of the reaction rate coefficients it is referred to the Appendix (II).

Altogether the chemical network comprises about 1900 reactions of 144 different species[3] (see Tab. (4.1)) built from 10 elements.
The overwhelming fraction of the reactions are of type **(A)** ($\approx$ 1550), about 250 reactions are making use of the thermochemical data (type **(B)**). The list of the species shows that we have not incorporated complex carbon molecules. The reason for this is that:

- for an accurate chemical calculation one might differentiate between the various isomers of one base–molecule, all having different thermodynamic properties and reaction rate coefficients. This would lead to an enormous amount of different species, which in practise can not be numerically treated.

- even for the small molecules the structures are highly uncertain,

- the present approach does not need to follow the chemical pathway from the small species to the complex ones, which in turn are defined as small "grains", but instead makes use of the moment method developed by Gail and Sedlmayr (1988). to investigate the problem of dust formation.

In view of the above arguments the choice of the chemical reaction network, allowing for the modelling of an O–rich as well as a C–rich composition, seems to be quite adequate.

[3]This number includes the electron, the photon and the cosmic rays.

4.2.3 Photorates

The rate for photodissociation or photoionization $\mathcal{R}_{ph}$ for the atoms or molecules in the outflowing gas can be obtained by evaluating

$$\mathcal{R}_{ph} = \int_{\nu_0}^{\infty} \frac{\pi F_\nu}{h\nu} \sigma_\nu e^{-\tau_\nu} d\nu \tag{4.2}$$

where ν_0 is the threshold frequency of the involved species undergoing the considered photoprocess, σ_ν is the absorption cross–section and τ_ν is the wavelength dependent optical depth in the shell.

The determination of the frequency dependent cross-sections σ_ν suffers from the lack of available data. Thus in cases where there is no sufficient information we use the knowledge about the threshold frequency of the photoprocess and assume an exponential decrease in the value of the absorption cross-section with increasing energy of the incident photon, or we have to go back to structural or energetical similarities to deduce the data.
In nova envelopes we are confronted with a time–increasing hardness of the radiation field emerging from the central photosphere of the remnant. For this reason we cannot make use of the integrated rates which are calculated assuming an interstellar radiation field (e.g. [van Dishoeck 1987] .
Furthermore it is necessary to recompute the actual photorates for each timestep[4]. The optical depth in the nova envelope is determined by dividing the whole shell into k distinct regions and calculating the Non-LTE chemistry in each of these regions. In the next step the τ–scale can be evaluated:

$$\tau_\nu(r_k) = \sum_{j=0}^{k} \sum_{l=1}^{n_{\rm spez}} n_l(r_j)\sigma_l(\nu)\Delta r_k \tag{4.3}$$

with $\Delta r_k = r_k - r_{k-1}$, $n_{\rm spez}$ the number of species involved in photoprocesses and $n_l(r_k)$ the particle density of the species l in the region considered.

[4]The computing time needed for this calculation is negligible compared with the time needed for the solution of the chemical system of rate equations. This is in contrary to the calculations of Rawlings and Williams (1989), who had used a parameter fit for the time dependence of their photorates.

4.2.4 Energy Balance in Nova Shells

In addition to the heating and cooling processes described in Chap. (2.4), where we have evaluated the energy balance for a more simple mixture of only atoms and their single ionized ions, we now face a more complex situation. To meet though the necessary requirements of the modelling of nova shells we now have to additionally take into account the contribution of the molecules to the energy balance.

4.2.4.1 Molecular Cooling

We have to consider the rotational and vibrational cooling of the molecules. The dominant molecular coolants which have been taken into account are CO, H_2O, OH, CH and HCl. All these molecules have the following features:

- the radiative selection rule is $\Delta J \ = \ \pm 1$
- the total inelastic cross-section σ is approximately constant and of the order of $10^{-15}\,\mathrm{cm}^2$ when $\Delta J = (E_J - E_{J-1})/kT \ll 1$ (Green and Chapman, 1978).
- In the regions under consideration for T$\geq$100 K the cooling transitions have $J \gg 1$.

For those energy levels with J$\gg$1 the spontaneous transition rates $A_J \,:\, J \longrightarrow J-1$ and the corresponding level energies E_J can be written as

$$A_J \ = \ A_0 J^3 \ \text{ and } E_J \ = \ E_0^2 \ . \tag{4.4}$$

This is also approximately valid for the molecules OH and H_2O. Following the expositions of Hollenbach and McKee (1979) one can make a simplifying assumption about the collisional cross section $\sigma_{JJ'}$ for a transition J $\rightarrow$ J$'$ in the case of the most probable collision partners H, He and H_2

$$\sigma_{JJ'}(v) \ = \ \frac{g_{J'}\,exp\,(-E_{J'}/kT)\,\sigma\,v_T}{Z} \tag{4.5}$$

with Z being the partition function, $g_{J'}$=2J$'$+1 the statistical weight of level J, v_T the thermal speed of the gas and σ the total cross section to all J. Although this assumption obeys the principle of detailed balancing, the exclusive dependence of σ on the energy of the final state $E_{J'}$ is not realistic and results in an underestimation of small ΔJ collision rates relative to large ΔJ rates. However, as the total cooling rate includes the sum over all J these details will not be very crucial.
In an optically thin medium the cooling rate L^{line} per unit volume due to a transition $u \rightarrow l$ is

$$L^{line} = n_u A_{ul} E_{ul} \tag{4.6}$$

with $E_{ul} = E_u - E_l$ being the energy of the radiated photon. If the optical depth in the lines is not negligible, the cooling rate is reduced by the escape probability ϵ_{ul}.

By assuming that the source function is constant in the line region and by the use of the line cooling coefficient Λ(ul,n,τ) the cooling rate is given (deJong, Chu and Dalgarno, 1975)

$$n \cdot n(j)\Lambda(ul, n, \tau) = n_u A_{ul} E_{ul} \tag{4.7}$$

where n is the total number density and n(j) the density of molecule j. The evaluation of the line cooling coefficient depends on the level population n_u which, in a steady state is determined by the equations of statistical equilibrium. In the case of molecular rotational levels Eq. (4.7) is rewritten as

$$n \cdot n(j)\Lambda^{rot} = \sum_{J=1}^{\infty} n_J A_J \Delta E_J \epsilon_J \tag{4.8}$$

where $\Delta E_J = E_J - E_{J-1}$ is given in terms of the vibrational ground state E_0 as $2E_0J$ and the escape probability ϵ_J is for the transition $u = J$ and $l = J - 1$.
A detailed treatment of the theory of non-LTE radiative transfer in optically thick, dusty media applied to the problem of molecular rotational cooling [Hollenbach and McKee 1979] of molecules with non-vanishing dipole moment leads to the equation for the line cooling coefficient

$$\Lambda^{rot} = \frac{2(kT)^2}{nE_0}\left[\frac{2 + y_m + \frac{3}{5}y_m^2}{1 + c_\tau + \frac{n_{cr}}{n} + 1.5\left(\frac{n_{cr}}{n}\right)^{1/2}}\right] \tag{4.9}$$

with

$$y_m = ln\left(1 + \frac{c_\tau}{1 + 10(\frac{n_{cr}}{n})}\right). \tag{4.10}$$

n_{cr} represents a critical density where the cooling states are approximately LTE populated and c_τ is an optical depth dependent parameter given as

$$c_\tau = \tau_T\left[2\pi \cdot ln\left[2.13 + \left(\frac{\tau_T}{e}\right)^2\right]\right]^{1/2} \tag{4.11}$$

with τ_T being the maximum optical depth which occurs for $J = J_T$, a level whose energy equals kT.
The molecular cooling parameters used to get the actual cooling rates for the nova shell in our model calculations are given in [Hollenbach and McKee 1979], [Tielens and Hollenbach 1985] and [Hollenbach and McKee 1989].

4.2.4.2 Cosmic Ray Heating

The ionization of atoms by highly energetic cosmic ray particles is a common physical heating process for molecular clouds and the interstellar medium. In the first phase of a nova event in the outer regions of an expanding nova shell the state of the bulk

of the material is assumed to be mainly neutral. When the envelope is optically thick most ionizing photons are absorbed in the inner layers of the envelope and the energy input in the outer gas is drastically reduced. In this situation energetic cosmic particles may be an additional heating source and the relevance of this process has to be checked.
Let us consider now the process of the ionization of an atom by a cosmic ray particle the ejected secondary electron has a kinetic energy E_0. This energy will go into new ionizational collisions, creating later–generation secondary electrons, some will go into excitation, followed by radiation and some will go directly into heating the gas through elastic collisions between the secondary electrons and the thermal electrons in the gas. If one defines ξ as the ionization rate per atom, X_e as the electron concentration, X_{H^0} as the concentration of neutral hydrogen, X_i as the concentration of atoms maintained in a single ionized state by the interstellar radiation field and α_B as the electron temperature dependent recombination coefficient to all levels except the ground state, ξ is defined by (Goldsmith *et al.*, 1969)

$$\xi = X_0 \left(\frac{X_e}{X_{H^0}} - \frac{X_0}{X_{H^0}} \right) \alpha_B(T_e) \tag{4.12}$$

and the total energy input $\mathcal{G}^{CR}$ is

$$\mathcal{G}^{CR} = \xi n_{H^0} < E > \qquad E = f\left(\frac{X_e}{X_H}\right) , \tag{4.13}$$

where $< E >$ is the mean energy per ionization process. A short estimate of this rate using the values

- $n_{H^0} = 10^{10}\, cm^{-3}$ (typical nova shell density)
- $\xi = 10^{-16} s^{-1}$ (Spitzer and Scott, 1969)
- $< E >= 3.2\, erg\, cm^{-3} s^{-1}$ (Spitzer and Scott, 1969)

results in a mean heating rate of

$$\mathcal{G}^{CR} = 3.2 \cdot 10^{-15} erg\, cm^{-3} s^{-1}. \tag{4.14}$$

A comparison with the results for the heating rate in Sect. (4.4) clearly shows that this rate will only be of minor importance for the energy balance in the outer neutral parts of the nova shell. In later phases, when the photospheric radiation field as well as the outflowing material is more diluted, the ionization by photons originating from the interstellar radiation field is of growing effectiveness, but then the hardening of the central photospheric radiation field will be the main reason for an increasing level of ionization.

4.3 Model Calculations of the Chemistry in Classical Novae

In this section we want to discuss the main features of the nova chemistry in some detail. Therefore we first present the results of a typical model calculation. The parameters of this model are shown in table (4.3).

Initial photospheric radius	R_*	: 1.0×10^{12}	cm
Initial photospheric temperature	T_*	: 8000	K
Initial gas temperature	$T_{\rm gas}$	: 8000	K
Start radius	R_0	: 5.0×10^{12}	cm
Start time	t_0	: 10	d
Start density	N_0	: 5×10^{13}	cm^{-3}
Mass ejection	M	: 2×10^{-5}	$M_\odot$
Ejecta velocity	v	: 5.0×10^{7}	cm/s
Speed of visual decline	$\dot{m}$	: 0.066	mag d^{-1}
C/O ratio	$N_{C/O}$	: 1.4	
Shell thickness	r_s	: 5.0×10^{12}	cm

Table 4.1: Basic model parameters for the calculations of the nova chemistry.

In the following the presented radial structures of the chemistry of a typical element of gas moving outwards directly correspond to the time evolution of the chemistry in this element, due to the simplified assumption of a constant outflow velocity.
Basically one can distinguish between four different chemical epochs during the evolution of the nova shell.

a) In the first epoch the molecule formation is established in a dense and cooling medium, there being shielded from the harder UV radiation. Thus the fractional ionization of the gas is only 10^{-4} and only the heavier elements are completely ionized.

b) Then, even in the early phase as well, the onset of carbon dust formation, favoured by the simultaneous existence of a gas temperature falling below 1500K and a high density in the gas flow, which still is only partially ionized, deeply changes the concentrations of a number of carbon bearing molecules forming small grains. During this time interval the intensity of the UV emission of the central photosphere steadily increases and an ionization front moves throughout the inner regions of the envelope (see Chap. (2.5) for a detailed discussion).

c) After a certain time (this time clearly depends on several parameters, as the speed class of the nova, the expansion velocity, the density structure, the elemental composition and the energy distribution of the radiation field) hydrogen gets ionized. This event dramatically changes the environment for the chemistry and a sharp break in the slope of the concentration of nearly all species occurs. The temperature of the gas shows a sudden rise from about 700K to ≈ 4500K as a reaction of the increased energy input by the photoionization of hydrogen. In addition the chemical processes are now embedded in a intensified radiation field. The instantaneous change in the density of the species is followed by a phase where the chemistry recovers from the overrun of the ionization front and adjusts to the new temperature and the changed photorates. The time needed for this adjustment marks the duration of the third period.

d) In the final phase the chemical development is mainly characterized by a steady increase in the degree of ionization and a more slowly increase in the gas temperature. Only the CO molecule and the unreactive helium atom are not affected up to the end of calculation period.

Sometimes we will even further simplify the distinction between four regions, and reduce this differentiation to the only two regions **before** Henceforth called early or first phase and **after** Henceforth called late or second phase massive ionization of hydrogen occurs. The borderline between the two zones is indicated by the unsteadiness of the radial distribution of the concentrations.

species	early phase	late phase	species	early phase	late phase
H	5.61×10^{-02}	1.0	H^+	8.50×10^{-08}	4.69×10^{-04}
H^-	4.53×10^{-15}	1.72×10^{-05}	H_2	4.77×10^{-01}	1.72×10^{-05}
H_2^+	8.14×10^{-15}	2.76×10^{-13}	H_3^+	7.33×10^{-13}	1.27×10^{-19}
He	2.00×10^{-01}	2.00×10^{-01}	He^+	6.67×10^{-18}	2.80×10^{-16}
C	1.81×10^{-06}	5.08×10^{-06}	C^+	2.11×10^{-11}	3.32×10^{-07}
C_2	2.45×10^{-07}	1.55×10^{-14}	C_2^+	2.20×10^{-10}	3.68×10^{-15}
CH	1.02×10^{-08}	6.83×10^{-12}	CH_2	1.46×10^{-09}	1.25×10^{-18}
CH_3	3.46×10^{-09}	7.29×10^{-26}	CH_4	3.23×10^{-08}	3.77×10^{-24}
CH^+	4.46×10^{-13}	1.12×10^{-10}	CH_2^+	2.34×10^{-12}	3.43×10^{-17}
CH_3^+	1.01×10^{-08}	3.77×10^{-24}	CH_4^+	2.78×10^{-13}	1.70×10^{-34}
C_2H	8.97×10^{-04}	5.10×10^{-20}	C_2H_2	3.09×10^{-06}	1.39×10^{-27}
$C_2H_2^+$	7.06×10^{-06}	2.03×10^{-25}	$C_2H_3^+$	1.29×10^{-10}	1.57×10^{-34}
N	6.07×10^{-10}	1.57×10^{-10}	N^+	3.30×10^{-21}	3.18×10^{-17}
N_2	2.08×10^{-04}	1.31×10^{-04}	NH	2.88×10^{-11}	4.97×10^{-10}
NH_2	8.75×10^{-12}	6.45×10^{-17}	NH_3	3.52×10^{-11}	5.63×10^{-25}
NH_4^+	2.35×10^{-09}	3.91×10^{-27}	CN	3.71×10^{-09}	9.97×10^{-15}
HCN	1.12×10^{-07}	1.12×10^{-19}	HC_3N	5.77×10^{-06}	5.90×10^{-06}
HCN^+	8.87×10^{-18}	7.16×10^{-18}	H_2CN^+	2.59×10^{-06}	1.34×10^{-23}

continued on next page

continued from previous page

species	early phase	late phase	species	early phase	late phase
O	4.22×10^{-08}	3.54×10^{-04}	O^+	2.73×10^{-15}	1.56×10^{-07}
O_2	2.39×10^{-13}	2.02×10^{-14}	OH	4.29×10^{-07}	1.70×10^{-11}
H_2O	1.32×10^{-04}	7.43×10^{-17}	H_3O^+	4.77×10^{-05}	3.11×10^{-18}
CO	2.94×10^{-03}	3.02×10^{-03}	CO_2	2.89×10^{-05}	1.76×10^{-12}
HCO^+	4.28×10^{-08}	1.11×10^{-13}	H_3CO^+	6.05×10^{-09}	2.85×10^{-27}
C_2HO^+	4.87×10^{-07}	2.27×10^{-27}	$C_2H_2O^+$	1.23×10^{-06}	4.24×10^{-27}
Fe	1.39×10^{-07}	3.21×10^{-10}	Fe^+	3.97×10^{-05}	3.91×10^{-05}
Si	1.83×10^{-06}	1.67×10^{-11}	Si^+	1.18×10^{-04}	3.31×10^{-04}
SiH	1.42×10^{-06}	1.02×10^{-14}	SiC	5.91×10^{-09}	1.54×10^{-18}
SiO	1.40×10^{-04}	2.75×10^{-12}	SiO_2	5.38×10^{-11}	5.33×10^{-24}
SiH^+	1.58×10^{-06}	1.29×10^{-09}	SiH_2^+	1.36×10^{-06}	6.44×10^{-15}
CH_2Si^+	1.55×10^{-06}	1.51×10^{-20}	$SiOH^+$	5.85×10^{-05}	2.34×10^{-16}
Mg	1.76×10^{-07}	2.75×10^{-09}	Mg^+	3.14×10^{-05}	3.16×10^{-05}
S	4.41×10^{-10}	5.01×10^{-12}	S^+	1.51×10^{-09}	1.58×10^{-05}
HS	9.01×10^{-07}	$2,91\times10^{-16}$	H_2S	5.84×10^{-08}	7.12×10^{-23}
CS	6.38×10^{-06}	3.17×10^{-18}	NS	4.13×10^{-10}	6.42×10^{-20}
HCS^+	2.35×10^{-06}	3.54×10^{-17}	H_2CS^+	1.10×10^{-08}	2.10×10^{-30}
SO	3.24×10^{-10}	1.38×10^{-21}	SO_2	2.56×10^{-12}	3.29×10^{-34}
OCS	1.75×10^{-08}	1.12×10^{-25}	SiS	1.85×10^{-06}	1.64×10^{-18}
$HSiS^+$	4.23×10^{-06}	2.52×10^{-23}		—	—
Na	6.70×10^{-13}	1.26×10^{-12}	Na^+	1.78×10^{-06}	1.78×10^{-06}

Table 4.2: Chemical concentrations for the early and the late phase of the nova expansion calculated for the model with the parameters given in Tab. (4.3). The early phase concentrations refer to the phase before dust formation has started.

4.3.1 The Chemistry of Carbon Bearing Molecules

4.3.1.1 The Role of CO

The primary molecule, chaining more than 90% of the entire carbon, is the carbonmonoxide, having a maximum abundance of $X_{CO} = 3.03 \cdot 10^{-3}$ at day 43 corresponding to a distance of $r = 1.6 \cdot 10^{14}$cm. Due to its extraordinary stability it can survive the critical phase when the nova radiation field overtakes most of the shell and nearly all molecules are dissociated. Different from the other species CO shows only a slight response to this dramatic change in the physical and chemical environment. The typical CO formation reactions in the first phase ($r < 10^{14.2}\,cm$) in order to their relative importance[5] with respect to the most effective formation reaction are:

C	+ O	$\Longrightarrow$ CO	+ hν	1.0	(1)
HCO^+	+ C_2H	$\Longrightarrow$ CO	+ $C_2H_2^+$	0.8	(2)
HCO^+	+ H_2O	$\Longrightarrow$ CO	+ H_3O^+	0.5	(3)
HCO^+	+ SiO	$\Longrightarrow$ CO	+ $SiOH^+$	0.1	. (4)

It is somewhat surprising, that reaction (1) is found to be the most effective CO forming path, though the rate coefficient for radiative association is known to be less efficient than other reaction types (e.g. neutral-ion or recombination), normally being of the order of $10^{-17}\text{cm}^{-3}\text{s}^{-1}$. According to the discussion of Herbst (1980) and Petuchowski *et al.* (1989) (henceforth called PDAN) the rate coefficient $k_{RA,n}$ is about 100 times smaller than the ionic radiative association coefficient $k_{RA,i}$ for the reaction

C	+ O^+	$\Longrightarrow$ CO^+	+ hν	(5)

which is given as

$$k_{RA,i} \approx 2 \times 10^{-3}\, T^{-3.08}\, exp[2114/T]. \tag{4.15}$$

This value depends on the ratio of the radiative stabilisation rate $\Gamma_{\rm rad}$ of electronically excited states of CO^+ by fluorescence to the ground-state to the two-body collisional stabilisation rate $\Gamma_{\rm coll}$, which is assumed to be of the order of the Langevin collision frequency ($\approx 10^{-9}$ s^{-1}). The process of neutral CO formation statistically favours to create CO via a metastable triplet state, which is too long-lived and therefore will be redissociated before it can be stabilized by reaching the ground–state. An alternative process, which has been proposed for Supernova shells is the charge exchange reaction

CO^+	+ O	$\Longrightarrow$ CO	+ O^+	(6)

[5]The relative strength of the reactions considered are given on a relative scale between [0...1], where the most efficient gain– or formation reaction is set to 1.

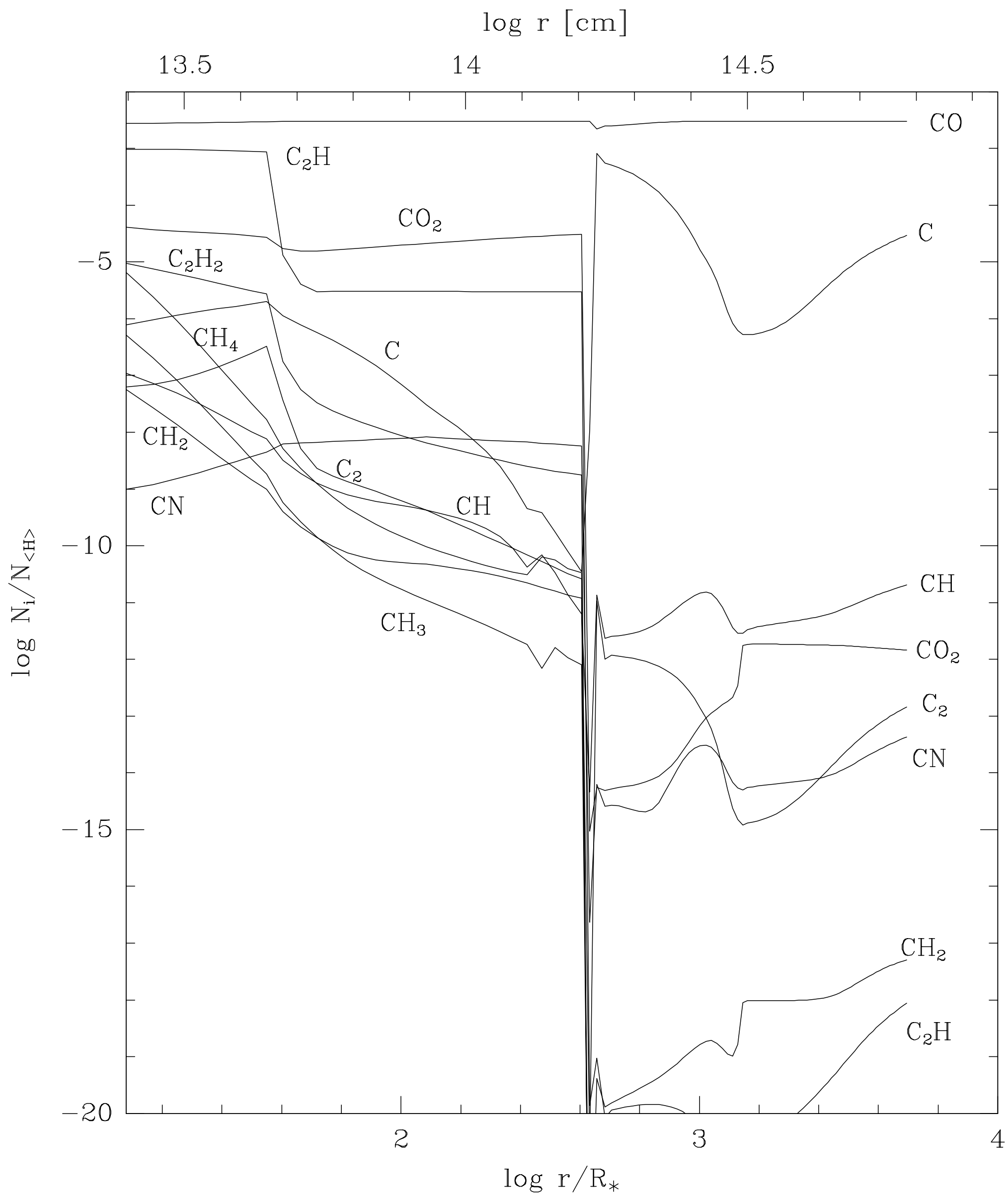

Figure 4.3: Logarithmic concentrations of the neutral C-bearing species, normalized to the number of H-atoms over a logarithmic radius axis scaled with the initial photospheric radius of the nova $R_*(t{=}t_0)$.

---

for which a rate of coefficient of

$$k_{ce} = 1.4 \cdot 10^{-10}\,(T/300)^{0.5}\,cm^{-3}s^{-1} \tag{4.16}$$

has been measured at 300 K [Fehsenfeld and Ferguson 1972]. The reverse reaction is endothermic by 0.395 eV and the reaction cross section strongly depends on the excitation state of the oxygen ion. By incorporating the observed threshold behaviour [Murad 1972] of ground-state oxygen ions and the constant reaction cross section over the temperature range of interest, the reverse reaction rate coefficient is given as (PDAN)

$$k_{ce,r} = 2 \times 10^{-11}(T/5000)^{1/2}\,exp(-4580/T)\ cm^3\,s^{-1} \tag{4.17}$$

As PDAN have shown, reaction (6) is the dominating building reaction for CO in the envelopes of Supernovae for temperatures above 2000 K. In the considered case describing the first phase of the nova expansion, this reaction does not effectively work, because the ionization fraction of oxygen f(O)= 10^{-7} is much lower than in the case of the SN1987a models calculated by PDAN (f(O)= 10^{-2}).
As a second important point the complex chemistry results clearly show that HCO^+ is a significant intermediate product of the carbonmonoxide formation ($X_{HCO^+} \approx 10^{-8}$) which, reacting with the abundant molecules SiO, H_2O and C_2H, also generates a reasonable fraction of the CO. So, in contrary to the nova-chemistry results of Rawlings (1988), the CO creation does not necessarily involve H_2 as a vital prerequisite, although its abundance is high. It should be noted that resulting from the different scientific approach the HCO^+ ion was not incorporated in the chemical network of Rawlings (1988).
Furthermore it turns out that the CO chemistry in this epoch resembles a situation closer to equilibrium, which is not the case for the other C bearing molecules.
If we now turn to the loss processes of CO one can state, that in the case of a moderate radiation field, the CO loss is governed by the interaction with magnesium ions, which are of a constantly high abundance ($X_{Mg^+} = 3 \cdot 10^{-5}$), as this heavy element is completely ionized.

CO	+ Mg^+	$\Longrightarrow$ CO^+	+ Mg	1	(7)
CO	+ SiO^+	$\Longrightarrow$ CO_2	+ Si^+	0.1	(8)
CO	+ hν	$\Longrightarrow$ C	+ O	0.05	(9)
CO	+ HS	$\Longrightarrow$ OCS	+ H	0.04	. (10)

Thus reaction (7) only proceeds towards the direction of CO destruction and therefore is completely unbalanced.

The characteristics of the "early" CO chemistry have now to be compared with the chemical routes of importance in the late phases of the nova event ($t > 70 days$), when the temperature has risen to $T \approx 5000\,K$ and the distance is $r > 10^{14.2}\,cm$. Under these conditions the main CO gain routes are

HCO	+ hν	$\Longrightarrow$ CO	+ H	1	(11)
CO^+	+ H	$\Longrightarrow$ CO	+ H^+	0.08	(12)
C	+ O	$\Longrightarrow$ CO	+ hν	0.06	(13)
HCO	+ H	$\Longrightarrow$ CO	+ H_2	10^{-5}	. (14)

The relevance of the radiative association reaction (13) has substantially decreased due to its temperature dependence. The most relevant building channel (11) needs the HCO molecule which itself is formed via

$$H_2 \quad + CO \quad \Longrightarrow HCO \quad + H \tag{15}$$

and though naturally cannot really contribute to a CO gain. The reaction channel involving CO^+ (12) is in equilibrium with the reverse reaction, a fact which does not apply to reaction (13), which mainly proceeds by the dissociation of carbonmonoxide. All other loss mechanisms are of no significance. So, after a short intermediate phase of CO destruction, when the concentration is reduced by approximately 30%, the CO recovers and returns to its original abundance. The annihilation of CO by photodestruction is reduced by the shielding of atomic carbon (see Chap. (3)).

The Carbondioxide Molecule Carbondioxide is one of those molecules which are difficult to observe for the following reasons:

- there is a substantial atmospheric fraction of CO_2, which impeds any ground based observation,
- as CO_2 has no permanent dipole moment due to ist symmetric structure it has no allowed rotational transitions thus being excluded from high-frequency radio observations.

So in general there is only rare observational information about the abundance of carbondioxide in the gas phase and even in the case of the analysis of cometary comae it has only been observed in the $4.3\mu m$ emission band for comet P/Halley[Huebner 1990] . Although the ion CO_2^+ has been observed in many comets, the lack of knowledge of the ionization processes has inhibited any attempts to deduce the abundance of the CO_2 molecule from such observations[6]. However, in the solid state (on icy grain surfaces) CO_2 is believed to be about as abundant as the CO molecule[7], a fact that is most important for grain surface chemistry. In the gas phase, however, CO_2 is believed to be only a small fraction of the carbonmonoxide, although there is neither reliable observational information nor evidence from the theoretical modelling about the mean CO_2 concentration in circumstellar environments.
Our model calculations show a high carbondioxide abundance of $X_{CO_2} \approx 3.2 \times 10^{-5}$ at the beginning, slightly decreasing at $r \approx 10^{13.6}\, cm$[8] and from there up to

[6] e.g. Huebner and Giguere (1980) only give branching ratios for several CO_2 dissociation reactions .

[7] see the observations of d'Hendecourt and Muizon (1989), who have discussed the interstellar carbon dioxide absorption feature at 15.2μm, which coincides with the bending mode of the CO_2 molecule.

[8] The minor effect of dust formation on the CO_2 concentration, in contrary to the large effects in the case of C_2H and C_2H_2, is due to the fact that CO_2 has not been incorporated in the moment equations considering the growth of the dust grains. The incorporation of CO_2 in the nucleation process by
$CO_2 \quad + \quad \text{small grain} \longrightarrow \text{small grain} + C \quad + \quad O_2$ is unlikely.

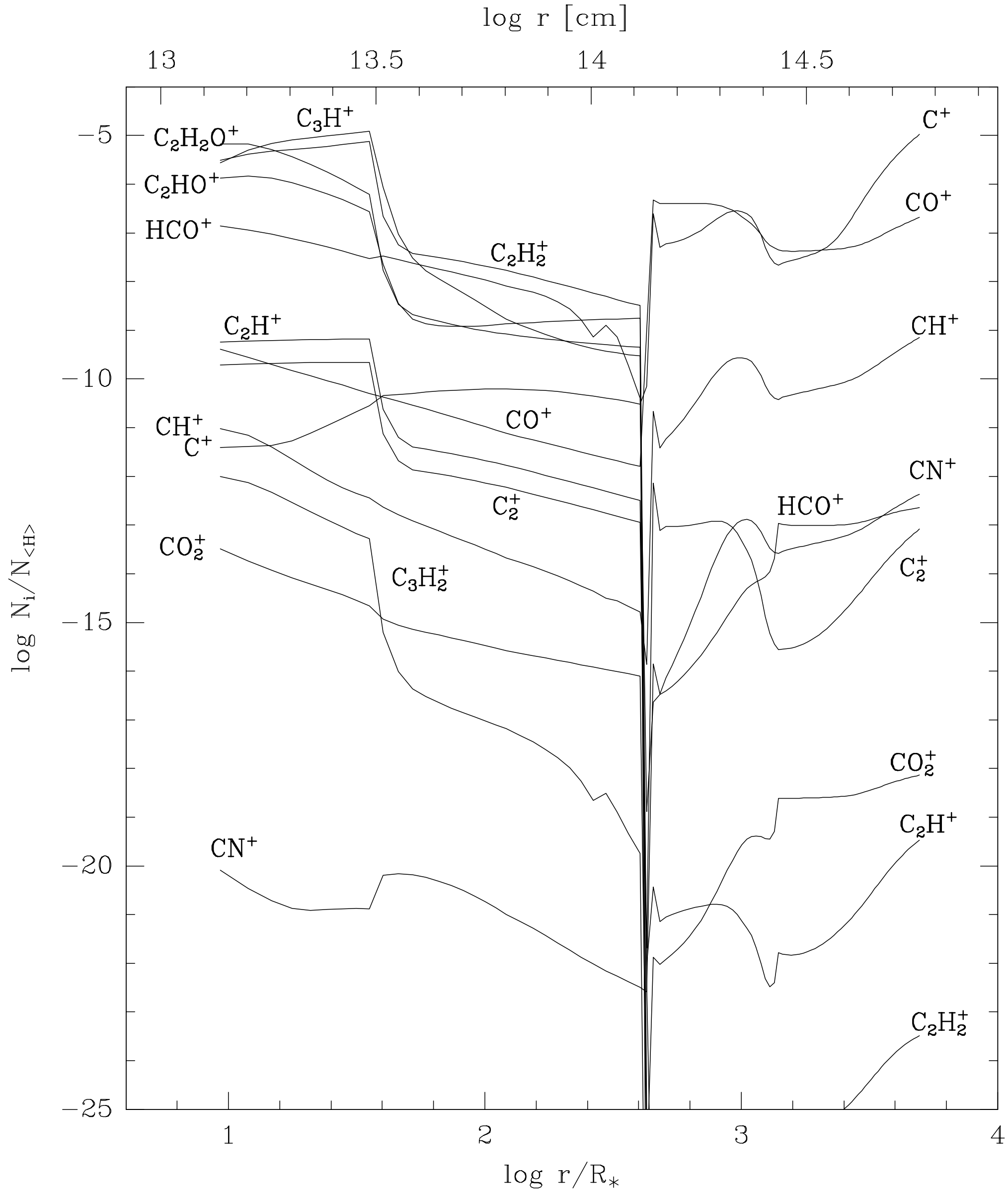

Figure 4.4: Logarithmic concentrations of the ionized C-bearing species, normalized to the number of H-atoms over a logarithmic radius axis scaled with the stellar radius.

---

the distance where the dissociation front reaches the shell CO_2 is the second most abundant C bearing molecule. Its production is closely connected with CO:

$$CO \quad + OH \quad \Longrightarrow CO_2 \quad + H \qquad 0.1 \qquad (16)$$

but also with the Si-system by

$$SiO^+ \quad + CO \quad \Longrightarrow CO_2 \quad + Si^+ \quad 1.0\ . \tag{17}$$

The loss of CO_2 generates the abundant HCO^+ ion, a route which is dominant in the scheme of CO_2 loss reactions.
For larger distances the CO_2 decouples from the constantly high CO abundance and resulting from the decrease of the precursor ion SiO^+ and the OH radical, its abundance is lowered by a factor of 10^{-7} and the formation now involves the rare O^- ion:

$$CO \quad + O^- \quad \Longrightarrow CO_2 \quad + e^- \quad . \tag{18}$$

The state of ionization of CO_2 is always low, in the second phase being the lowest of all C molecules (see Fig. (4.5). This is in fact worth mentioning but on the other hand should not been taken too serious, as the information, as already has been stated, about the photoreaction cross-sections is very incomplete.

4.3.1.2 Atomic Carbon

In the first phase of the nova expansion atomic carbon which is in excess to oxygen by a factor of 1.4 is mostly converted to neutral molecules like C_2H, CO_2 and C_2H_2. The next main change in the slope of C is due to the onset of carbon dust formation which is consuming atomic C as well as the molecules mentioned above.
Later carbon atoms are returned to the gas by the dissociation of the molecules and the carbon concentration then is maintained by

$$CO \quad + h\nu \quad \Longrightarrow C \quad + O \tag{19}$$

and the dominant loss is given by the ionization of carbon. The degree of carbon ionization constantly grows in the first chemical phase reaching a maximum of nearly complete ionization, a result of the consumption of neutral C atoms in dust, whereas the concentration of carbon ions remains constant. After the destruction of those molecules having lower dissociation potentials, neutral C is returned to the gas phase and the degree of ionization drops to $f(C) \approx 10^{-4}$. Afterwards when the strength of the radiation field increases, the amount of ionized carbon rises again.

4.3.1.3 The C_2 Molecule

Next we must draw our attention to the C_2 molecule, which is –once formed– relatively stable and plays an important role in the formation routes to complex hydrocarbons (Rawlings and Williams, (1989), henceforth called RW). The fractional abundance of C_2 is constantly growing and has a maximum value of $X_{C_2} \approx 10^{-7}$ attained just before dust formation starts. This is about three orders of magnitude higher than in the model of RW. The reason for this fact is the slightly higher abundance of free electrons in our model which promote the dissociative recombination of hydrocarbon ions resulting in the production of C_2:

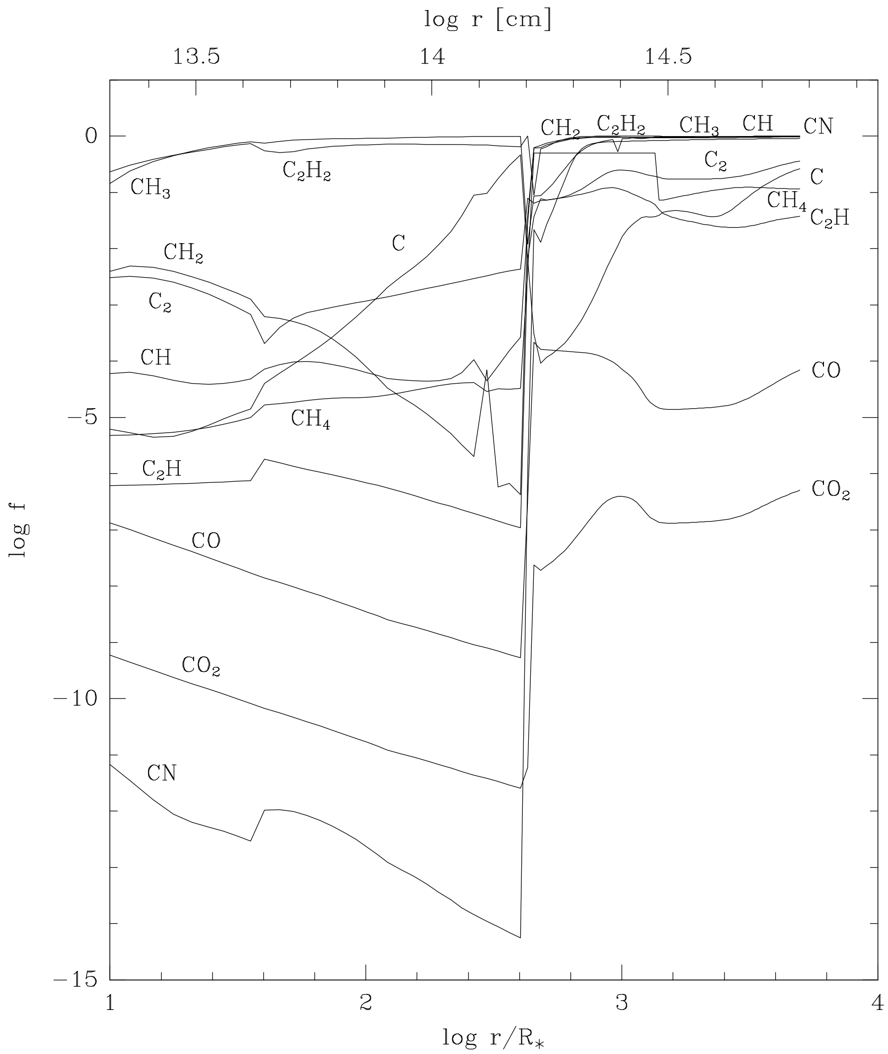

Figure 4.5: Degree of ionization on a logarithmic scale for the C-bearing species included in the nova chemistry network. The x–axis is given in logarithmic units of the radius scaled by the initial photospheric radius R_*.

C_3H^+	$+ e^-$	$\Longrightarrow C_2$	$+ CH$	1	(20)
$C_2H_2O^+$	$+ e^-$	$\Longrightarrow C_2$	$+ H_2O$	0.09	(21)
$C_2H_2^+$	$+ e^-$	$\Longrightarrow C_2$	$+ 2H$	0.83	(22)

The rare hydrocarbon ions only serve as intermediate products for the production of more complex carbon molecules via the interaction with the building block molecule C_2 (see RW).
The most significant loss routes of C_2 act by

C_2	$+ h\nu$	$\Longrightarrow C$	$+ C$	1.0	(23)
C_2	$+ H_3O^+$	$\Longrightarrow C_2H^+$	$+ H_2O$	0.66	(24)
C_2	$+ C_2H_2^+$	$\Longrightarrow C_2H^+$	$+ C_2H$	0.13 .	(25)

Most carbon bearing molecules have a complicated continuum/band structure in their photodissociation spectrum (e.g. CH_4, C_2H_2 etc.) and dissociation often occurs at wavelengths greater than ≈ 1600Å, so that these molecules can only be partially shielded against the continuum, normally absorbed by carbon. Smaller species, like C_2, have well defined pre-dissociation bands. As Pouilly *et al.* (1983) have shown, C_2 has two predissociation bands of interest: the $3^1 \prod_u \rightarrow x^1 \sum_g^+$ transition is completely shielded by carbon; the second and weaker band corresponds to the transition $2^1 \prod_u \rightarrow x^1 \sum_g^+$, which is unshielded and therefore is responsible for the residual effectiveness of C_2 photodissociation. However, C_2 is one of the more stable species and appears to be the conceivable basis of a more complex hydrocarbon chemistry[9].
The C_2 ion is closely coupled to the C_2H radical and its ion via

C_2H	$+ H^+$	$\Longleftrightarrow C_2^+$	$+ H_2$	1.0	(26)
C_2H^+	$+ h\nu$	$\Longleftrightarrow C_2^+$	$+ H$	0.0006	(27)

and has only a lower abundance of $X_{C_2^+} \approx 10^{-10} cm^{-3}$ in the beginning, reduced to $X_{C_2^+} \approx 10^{-13}$ after dust formation has taken place. Later the C_2^+ abundance is controlled by the ionization

$$C_2 \quad + h\nu \quad \Longrightarrow C_2^+ \quad + e^- \tag{28}$$

and dissociation

$$C_2^+ \quad + h\nu \quad \Longrightarrow C^+ \quad + C. \tag{29}$$

4.3.1.4 Acetylene and the Formation of Hydrocarbons

If one is interested in the topic of dust formation in nova shells one has to pay special attention to the acetylene molecule which in the case of circumstellar chemistry is discussed as most important for dust formation and is the starting point of complex

[9]The chemistry of hydrocarbons and of course of PAHs is a wide and special field of investigation. For the interstellar medium their existence is widely confirmed now and their emission features can be assigned to the so called "unidentified IR emission bands" [Léger A. 1988]. For circumstellar shells the idea of the existence of PAHs and their formation by a complex chemical pathway was first proposed by Keller (1987) . Later Frenklach and Feigelson (1989) tried to investigate the formation of PAHs by non–LTE chemical network calculations, which were recently applied by Cherchneff (1991) on the oscillating envelopes of carbon rich stars. In novae the emission of PAHs at 11.3μm was first detected by [Smith *et al.* 1990] in Nova Cen 1986, but was predicted much earlier by [Mitchell and Evans 1984]. Additional discussion on this topic is given at the end of the next section.

chemistry and soot formation to occur. ([Gail and Sedlmayr 1987b, Keller 1987]) In the calculations considering a situation of chemical equilibrium one finds that C_2H_2 is the second most abundant C bearing molecule besides the inreactive carbonmonoxide [Gail and Sedlmayr 1987a] in the region of the p-T plane which is determined by the gas pressure and temperature occuring in the first phase of nova expansion. As one can see from Fig. (4.3) the results derived by our model calculations do not supply such a high acetylene abundance for the nova situation, although the ratio of free H atoms to molecular hydrogen is only 1%. However, this seems to be sufficient to favour the creation of radical sites by

$$C_nH_m \quad + H \quad \Longrightarrow C_nH_{m-1} \quad + H_2 \tag{30}$$

thus lowering the C_2H_2 concentration significantly and preferring the production of the C_2H radical. From the reaction analysis of our network we derive the following reactions as the most effective for acetylene production:

$$\begin{array}{lllll} C_2H_2^+ & + Si & \Longrightarrow C_2H_2 & + Si^+ & 1.0 \quad (31) \\ C_2H_2^+ & + Mg & \Longrightarrow C_2H_2 & + Mg^+ & 0.17 \quad (32) \\ CH_2Si^+ & + C & \Longrightarrow C_2H_2 & + Si^+ & 0.13 \quad (33) \\ C_2H_2^+ & + Fe & \Longrightarrow C_2H_2 & + Fe^+ & 0.08 \quad . \ (34) \end{array}$$

This shows the importance of the presence of a residual fraction of non-ionized metal atoms which can take part in the charge exchange reactions(31, 32, 34). These reactions are not dependent on temperature and their relative contribution to the acetylene production should be the same, if the radiation field has a moderate to low intensity. As the investigations of Sternberg *et al.* (1987)[10], show the suppression of the interactions of the heavy metals with the C_2H_2 molecule might lead to questionable results. They found the channel

$$\begin{array}{llll} C^+ & + CH_4 & \Longrightarrow C_2H_3^+ & + H \quad (35) \\ C_2H_3^+ & + e^- & \Longrightarrow C_2H_2 & + H \quad (36) \end{array}$$

to be the most important one.
The important precursor $C_2H_2^+$ ion is created via the steps

$$\begin{array}{llll} H^+ & + C_2H & \Longrightarrow C_2^+ & + H_2 \quad (37) \\ C_2H^+ & + h\nu & \Longrightarrow C_2^+ & + H \quad (38) \end{array}$$

followed by

$$C_2^+ \quad + H_2 \quad \Longrightarrow C_2H^+ \quad + H \tag{39}$$

and

$$C_2H^+ \quad + H_2 \quad \Longrightarrow C_2H_2^+ \quad + H \quad . \tag{40}$$

[10] They have used the reaction data set included in the compilation of Anicich and Huntress (1986) to examine the chemical composition in dense molecular clouds.

The concentration of acetylene reaches a maximum of $X_{C_2H_2} \approx 10^{-5}$, then slowly decreases up to the point where the grain formation sets in. The loss of C_2H_2 is mainly due to photodissociation:

$$C_2H_2 \quad + h\nu \quad \Longrightarrow C_2H \quad + H \tag{41}$$

which is a factor of 10^3 faster than the next most effective C_2H_2 destruction path

$$C_2H_2 \quad + H^+ \quad \Longrightarrow C_2H^+ \quad + H \quad . \tag{42}$$

The photoabsorption cross section of C_2H_2 used in this work has been measured by Suto and Lee (1983). The photoabsorption spectrum of C_2H_2 shows a discrete structure with an underlying continuum (see Fig. (4.6)). The threshold wavelength for the main photodissociation channel (reaction (41)) is 2304Å. So, even in the phase of a moderate UV photon flux penetrating into the nova shell, the degree of ionization of acetylene is quite high, much higher than that for CH_2 or C_2.

At this point some remarks should be made considering the formation of more complex hydrocarbons. This particular problem has not been studied in this work, but in view of the relatively high amount of acetylene being present in the early expansion phase there is strong evidence that their formation can occur even under the conditions of a nova. Basically there are three different pathways to create hydrocarbons of increasing complexity from smaller molecules.

> The first route proceeds via carbon insertion [Millar and Freeman 1984] and leads to the production of very unsaturated species such as C_6H. In this pathway the atomic and ionized carbon play a prominent role in adding to the complexity of hydrocarbon neutrals and ions, respectively, by inserting themselves into hydrocarbon molecules and ejecting one or two hydrogen atoms. Since this mechanism results in the removal of hydrogen atoms from the hydrocarbons further hydrogenation is needed, otherwise eventually bare carbon cluster ions will be produced which will be subject of dissociative recombination reactions thus leading to smaller hydrocarbons. Having in mind the calculated results for the nova chemistry it seems to be clear that these routes are efficient, as the basic constituents are of considerable high abundance. Although there is a large evidence for such reactions involving C^+ and small hydrocarbon neutrals, there is a lack of laboratory studies of the C atom-hydrocarbon reactions.

For those hydrocarbons not produced via carbon insertion two other pathways are available, both involving reactions between hydrocarbon ions and hydrocarbon neutrals.

> In the first of these two routes these species react to form larger hydrocarbon ions and hydrogen by so called "condensation" reactions of the type

$$C_nH_m^+ \quad + C_aH_b \quad \Longrightarrow C_{n+a}H_{m+b-1}^+ \quad + H \tag{43}$$
$$C_nH_m^+ \quad + C_aH_b \quad \Longrightarrow C_{n+a}H_{m+b-2}^+ \quad + H_2 \quad . \tag{44}$$

Some of those reactions have been studied experimentally by e.g. Anicich *et al.* (1984) and Dheandhanoo *et al.* (1986) and a lot of reaction data are first contained in the compilation of Anicich and Huntress (1986) .

The other method of production of the more saturated hydrocarbons is similar to the condensation reaction path but involves reactants that are known to associate under laboratory conditions [Anicich and Huntress Jr. 1986]:

$$C_4H_2^+ \quad + C_2H_2 \quad \Longrightarrow \quad C_6H_4^+ \quad (45)$$
$$C_4H_3^+ \quad + C_2H_2 \quad \Longrightarrow \quad C_6H_5^+ \quad .(46)$$

Under typical circumstellar conditions these reactions will occur as radiative associations which are known to have a strong inverse dependence on temperature. At temperatures of about $300\,K$ these reactions proceed with rate coefficients greater than $10^{-10}\,cm^3\,s^{-1}$ [Bates and Herbst 1988].

The buildup of molecular complexity via the pathways discussed above is curtailed by reactive processes which can destroy complexity. So smaller hydrocarbons can form and more complex ones are depleted by dissociative recombination reactions with electrons. Hydrocarbon ions will also be depleted strongly by reactions with neutral oxygen and nitrogen. Reactions with atomic carbon and C_2 on the other hand tend to increase complexity and reactions with atomic nitrogen leads to the organo–nitrogen compounds, whereas reactions with atomic oxygen are a major mechanism to suppress the formation of more complex hydrocarbon species, although [Millar *et al.* 1991a] stated that by reactions with water or H_2CO the formation of also complex oxygen containing molecules such as protonated methyl formate ($H_2COOCH_3^+$), protonated acetaldehyde (CH_3CHOH^+) and protonated ethanol ($C_2H_5OH_2^+$) seems to be possible. Finally it can be mentioned, that the formation of the more complex hydrocarbons are not necessarily incorporating the processes of C^+ insertion as proposed by Millar and Freeman (1984).

4.3.1.5 Analysis of Important Radicals

The radical of acetylene is more abundant by one order of magnitude than all other C-bearing molecules except CO, until dust formation starts and reduces the C_2H concentration by a factor of about 500 from $X_{C_2H} \approx 10^{-3}$ to $X_{C_2H} \approx 3 \cdot 10^{-6}$. Naturally on one hand its abundance is closely coupled to the gain by reaction with the acetylene molecule

C_2H_2	$+ h\nu$	$\Longrightarrow C_2H$	$+ H$	1.0	(47)
$C_2H_2^+$	$+ H_2O$	$\Longrightarrow C_2H$	$+ H_3O^+$	0.61	(48)
C_3H^+	$+ e^-$	$\Longrightarrow C_2H$	$+ C$	0.01	(49)

and to the loss by conversion to C_2^+ and C_2H^+ by

C_2H	$+ H^+$	$\Longrightarrow C_2^+$	$+ H_2$	1.0	(50)
C_2H	$+ H^+$	$\Longrightarrow C_2H^+$	$+ H$	1.0	(51)
C_2H	$+ HCO^+$	$\Longrightarrow C_2H_2^+$	$+ CO$	0.2	. (52)

Later the main gain channel maintains, but the C_2H formed is quickly processed further to C_2, C_2H^+ and the abundance decreases sharply to a value of $X_{C_2H} \approx 10^{-19}$.
The comparison of the "early" abundances to the results of RW shows, that they derived a fairly similar ratio of C_2H to C_2H_2, but achieve much lower absolute abundances for both molecules, although their model is settled in a carbon neutral zone too. This fact may be due to the following reasons:

- the H_2 abundance is introduced as a free parameter in their model calculations although they stated that their results are highly sensitive to the H_2 concentration and a raise of the H_2 abundance by a factor of 500 will increase the C_2H_2 abundance by a factor of 10^8.

- the degree of ionization and as a result the electron abundance is also treated as a parameter and is only provided by the assumed total ionization of the metals.

- the gas temperature is calculated by an exponential cooling law, which does not take into account the time dependence of the heating and cooling rates in the nova shell and the close coupling between the nova photospheric radiation field, which is steadily increasing in the wavelength region most important for dissociation and ionization processes, the temperature of the envelope and the chemical evolution.

- although they have incorporated the time dependence of the photorates they have used a fit based on a blackbody spectrum of the photosphere characterized by the stellar temperature T_*. This blackbody spectrum may differ significantly from the actually emitted photospheric spectrum as the calculations of Hauschildt (1991) have shown . This effect is most pronounced in the first phase of the nova explosion, when the photospheric temperature is below 30.000 K.

In the model calculations presented here, the concentration of molecular hydrogen is a natural result of the chemical modelling, so being a straight consequence of the about 260 reactions in which the H_2 molecule is involved. In the CI-zone existing in the nova envelope studied, the resulting H_2 concentration is $X_{H_2} \approx 0.475$, strongly deviating from the results of RW. If one takes into account the high sensitivity of the chemical model to the abundance of molecular hydrogen in the shell, this difference alone may be sufficient to explain the large differences in both models in the particular case of acetylene and its radical.

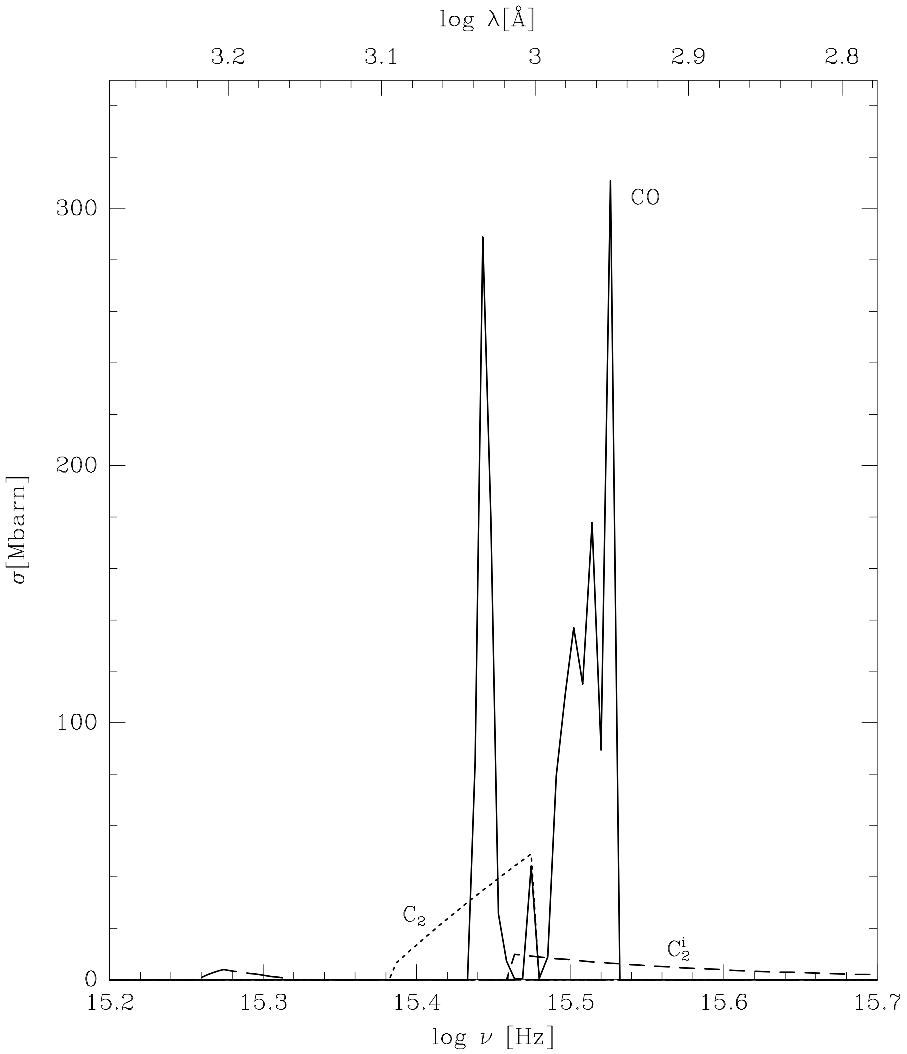

Figure 4.6: Photoionization– and Photodissociation cross–sections for selected carbon bearing molecules.

The CH molecule is also one of the basic constituents of the C–H chemistry. Although being only of a low abundance it is involved in about 120 reactions there being converted to CH_2^+ via

$$\mathrm{CH} \quad + \mathrm{H_3O^+} \quad \Longrightarrow \mathrm{CH_2^+} \quad + \mathrm{H_2O} \tag{53}$$

or for example to SiC^+ by

$$\mathrm{CH} \quad + \mathrm{Si^+} \quad \Longrightarrow \mathrm{SiC^+} \quad + \mathrm{H} \tag{54}$$

or recycled to atomic carbon:

$$\mathrm{CH} \quad + \mathrm{H} \quad \Longrightarrow \mathrm{H_2} \quad + \mathrm{C} \quad . \qquad (55)$$

The reaction (55) is an efficient channel in both directions, being 10^3 times faster than the other paths and resulting in a surplus in the direction of the H_2 formation.

4.3.1.6 Carbon Ions

The complex interactions in the system of carbon containing ions is subdivided according to the number of carbon ions contained in the species.
a) Those carbon ions containing one carbon atom are effectively coupled by reactions involving atomic and molecular hydrogen. The reactions with H_2 lead to

ion	early phase		late phase	
CH_2^+	2.3	(-12)	3.4	(-17)
CH_3^+	1.8	(-08)	3.8	(-24)
CH_4^+	2.8	(-13)	1.7	(-34)
CH_5^+	3.9	(-12)	$<$	(-34)

Table 4.3: Concentrations of carbon ions I. The values are written in the form **a(-b)**, where **(-b)** signifies 10^{-b}.

more complex ions whereas the reaction with H results in a reduction of the ion complexity (see Fig. 4.7). The abundances of CH_2^+, CH_4^+ and CH_5^+ are nearly of the same order of magnitude. The most abundant ion of this type is the CH_3^+ ion. As it can be deduced from the reaction flow analysis of this subsystem, CH_4^+ and CH_5^+ are reprocessed to CH_3^+. Also there is no efficient way to produce CH_4^+ from CH_2^+. The weakness of the radiation field due to the high optical depth is the reason for the high concentration of carbon ions. Later their abundance is decreased and the abundance hierarchy is ordered according to increasing complexity.
b) For those species containing two carbon atoms the dominating species in the first phase is the acetylene ion. As long as the shell has not been overtaken by the ionization it has a high abundance of $7.1 \cdot 10^{-7}$. It is mainly formed via the two steps

$$\mathrm{C_2^+} \quad + \mathrm{H_2} \quad \Longrightarrow \mathrm{C_2H^+} \quad + \mathrm{H} \qquad (56)$$
$$\mathrm{C_2H} \quad + \mathrm{H^+} \quad \Longrightarrow \mathrm{C_2H^+} \quad + \mathrm{H} \qquad (57)$$
$$\mathrm{C_2H^+} \quad + \mathrm{H_2} \quad \Longrightarrow \mathrm{C_2H_2^+} \quad + \mathrm{H} \quad . \qquad (58)$$

but also the route via $C_2H_3^+$ is contributing to the $C_2H_2^+$ concentration. The acetylene ion is closely connected to its neutral form by the reactions with Si and Si^+.
c) Those molecular ions comprising three carbon atoms are C_3H^+, $C_3H_2^+$ and $C_3H_3^+$.

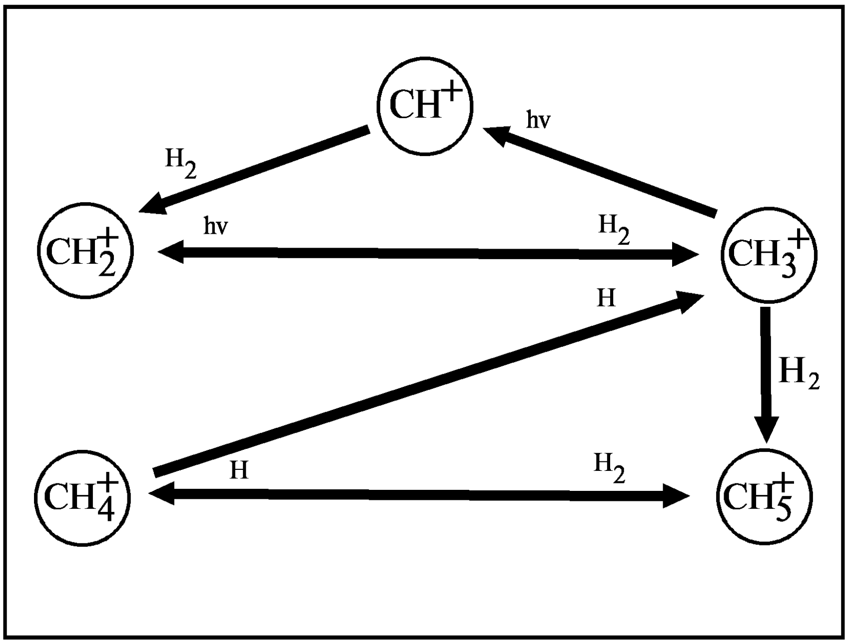

Figure 4.7: Schematic reaction flow for carbon ions for the early phase. The most effective paths for those molecular ions including one carbon atom.

ion	early phase		late phase	
C_2H^+	6.5	(-10)	1.2	(-21)
$C_2H_2^+$	7.1	(-06)	2.0	(-25)
$C_2H_3^+$	1.3	(-11)	1.6	(-34)
$C_2H_5^+$	1.7	(-10)	$<$	(-34)

Table 4.4: Concentrations of carbon ions II. The values are written in the form **a(-b)**, where **(-b)** signifies 10^{-b}.

Their abundances are shown in Tab. (4.5). In the period characterized by a temperature around 1000K the dissociative recombination channels due to the inverse temperature dependence of their reaction rate coefficients proceed very efficiently and the recombinations of C_3H^+ and $C_3H_3^+$ lead to the production of C_2H and C_2H_2, respectively. However, a substantial part of these ions remain in the ionic state. When the radiation field hardens and becomes able to break up the acetylene

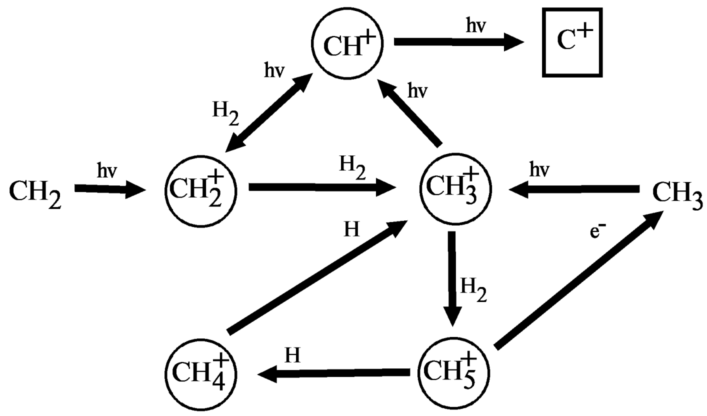

Figure 4.8: Schematic reaction flow for carbon ions. Same as Fig. (4.7) but for the late phase of the shell evolution.

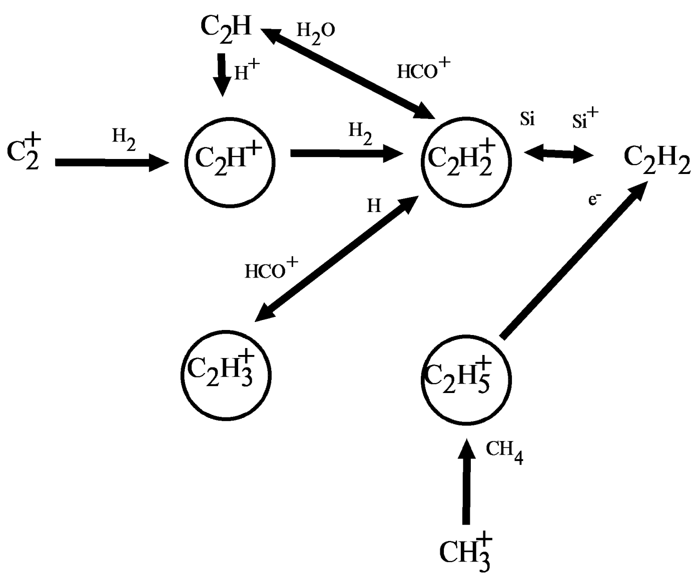

Figure 4.9: Schematic reaction flow for carbon ions III.

molecule and its radical the dissociative pathways in the carbon chemistry all lead to the level of atomic carbon.

ion	early phase		late phase	
C_3H^+	1.1	(-05)	4.0	(-29)
$C_3H_2^+$	6.7	(-14)	$<$	(-34)
$C_3H_3^+$	3.9	(-08)	$<$	(-34)

Table 4.5: Concentrations of carbon ions III. The values are written in the form **a(-b)**, where **(-b)** signifies 10^{-b}.

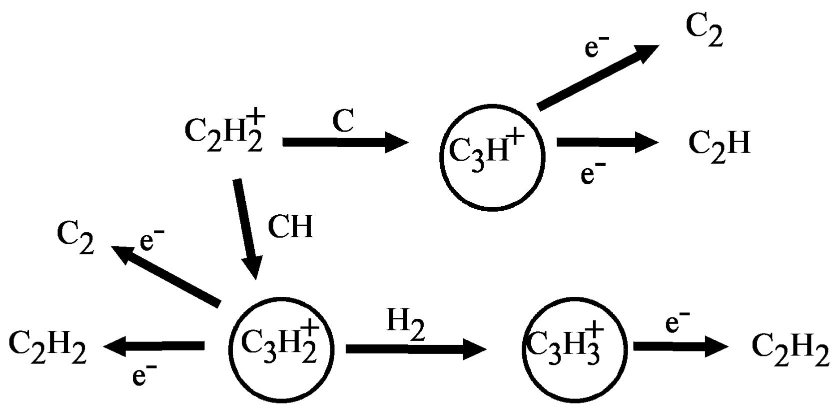

Figure 4.10: Schematic reaction flow for carbon ions IV.

4.3.2 The Role of He^+

In view of the argument of Rawlings and Williams (1989), that He^+ may be an important reduction agent for the chemistry, which could be of importance, as some novae show pronounced overabundances of helium (Roche *et al.*, 1984; Snijders *et al.*, 1987) , we analyzed the chemical network calculations for its influence. In the presented model calculations we have assumed a normal (solar) helium mass fraction of 0.24[11]. Under these conditions the formation of the helium ion can only proceed via the interaction with high energetic cosmic ray particles. The photospheric ra-

[11]The chemical abundances in novae do show large variations from 0.48 (HR Del) to 0.085 (Nova Aquilae 1982)[Truran 1990] , thus we have taken the "conservative" solar value which lies close to the mean value of helium mass fractions deduced from the observational data [Truran 1985a]

diation shortward of 1100$\AA$ is totally absorbed (see Fig. (4.17)) The most effective conversion of He^+ proceeds by

$$He^+ \quad + CO \quad \Longrightarrow He \quad + O \quad CO^+ \tag{59}$$
$$He^+ \quad + N_2 \quad \Longrightarrow He \quad + N \quad N^+ \quad . \tag{60}$$

These reactions lead to a concentration of He^+ of $X_{He^+} \approx 10^{-18}$ in the first period, increasing to $X_{He^+} \approx 10^{-16}$ at the end. The concentration of atomic helium remains totally unchanged and its influence on the concentrations of other species can be neglected.

4.3.3 Oxygen–Hydrogen Chemistry

4.3.3.1 Molecular Hydrogen – a Key Molecule in Circumnova Chemistry

The problem of the H_2 formation and its influence on the entire chemistry was primarily discussed in the context of the circumstellar chemistry of late–type stars (see Chap. (3)). The importance of the H/H_2 ratio is undisputable as it generally affects the chemical properties of the shell. Since hydrogen is by far the most abundant element it is unquestionable that the hydrogen molecule is one of the keys to the whole circumnova and circumstellar chemistry, as it is the reaction partner in many important chemical pathways.
Radical or atom reactions with closed shell molecules only have moderate activation energies, thus their reactions are quite important down to 1000K or even lower temperatures. The most abundant "radical" certainly is atomic hydrogen, though the abundance of all other radicals and subordinate species is dominated by reactions with atomic hydrogen. In the interstellar chemistry the formation of H_2 is a special problem because the typical gas phase reactions in question:

$$\begin{array}{lcllc}
H_2^+ + H & \rightarrow & H_2 + H & k \approx 10^{-18} & cm^3 s^{-1} \\
H + H^- & \rightarrow & H_2 + e^- & k \approx 10^{-9} & cm^3 s^{-1} \\
H + H & \rightarrow & H_2 + h\nu & k \approx 10^{-30} & cm^3 s^{-1} \\
3H & \rightarrow & H_2 + H & k \approx 10^{-32} & cm^6 s^{-1}
\end{array}$$

are all too slow resulting from the low concentrations of the reaction partners in the interstellar space. Under these conditions the formation of H_2 is most likely located on the surfaces of interstellar grains which act as a catalyst for the H_2[12] .
However, under the conditions prevailing in the circumnova shell the production of molecular hydrogen via one of the gas phase reactions mentioned above is possible. In the first few days of the material ejection the density in the gas shell is high enough to allow for three–body reactions and before the starting time of our calculation (day 10) H_2 can be effectively produced by such a three–body collision. Then the almost complete conversion of the atomic H into molecules will proceed and the

[12]Although this process seems to be very effective several criteria have to be met:

- A collision of a grain with an H atom must occur. This process is proportional to the geometrical cross section of the grain and the relative velocity.
- The collision must result in an adsorption, which means that the molecule must get thermally accommodated to the grain.
- Until another H atom is colliding with the grain the H atom must be retained at the surface.
- There must be a surface mobility for the adsorbed atom, thus primarily isolated H-atoms later can react.
- The reaction of two H atoms must result in the ejection of the newly formed H_2 molecule.

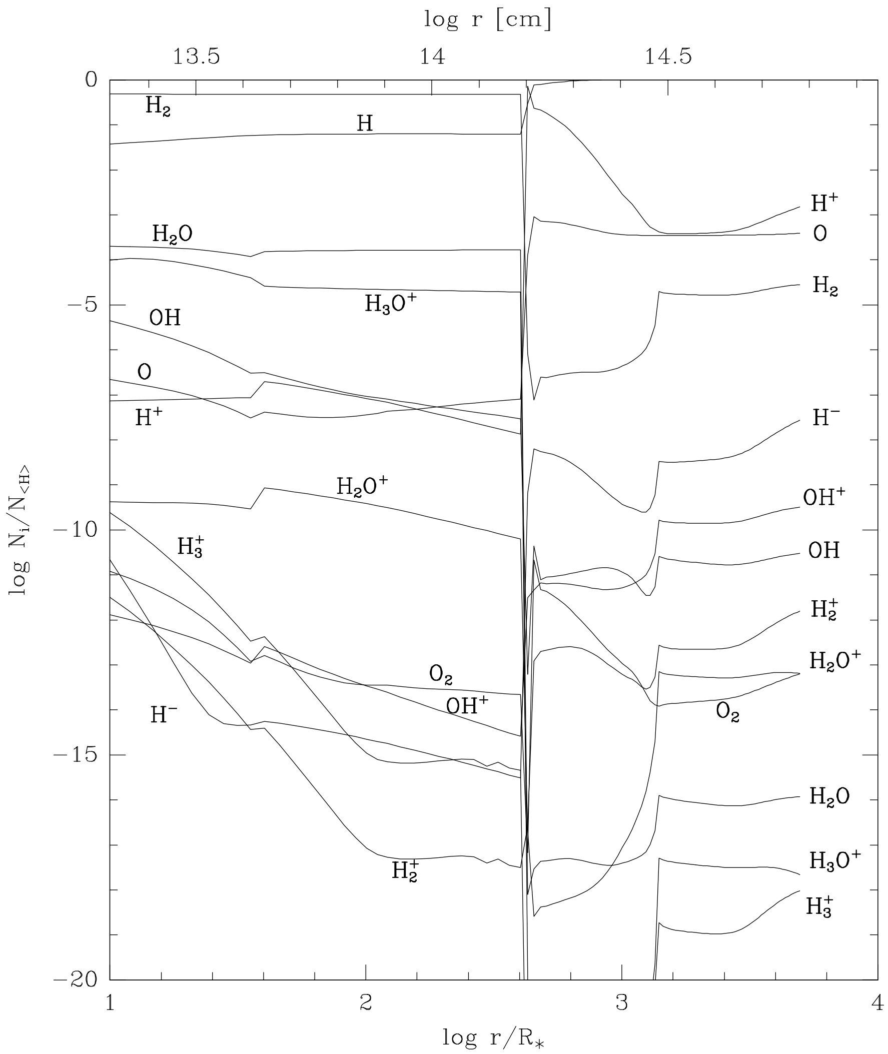

Figure 4.11: Logarithmic concentrations of the main O-H bearing species, normalized to the number of H-atoms over a logarithmic radius axis scaled with the photospheric radius of the nova $R_*(t=t_0)$.

---

concentration of H_2 nearly achieved its LTE value (see Fig. (4.11)). Up to day 44 the H_2 is the most abundant species and the most effective gain reactions are:

SiH_2^+	$+ H$	$\Longrightarrow H_2$	$+ SiH^+$	1		(61)
SiH^+	$+ H$	$\Longrightarrow H_2$	$+ Si^+$	0.5		(62)
H_2O	$+ H$	$\Longrightarrow H_2$	$+ OH$	0.01	.	(63)

The close coupling of H_2 with the abundant silicon bearing ions SiH_2^+ and SiH^+ is remarkable. Both ions have a high abundance of $X \approx 1.3 \cdot 10^{-6}$. The H_2 losses are affected mostly by the reverse reactions of (61–63). Collisional disso-

ciation reactions are of negligible influence in the temperature regime 800–3000K although the chemistry is acting all over the complete calculation period in the high density limit ($n_h > 10^5\,cm^{-3}$) of the H_2 dissociation process, so that the radiative stabilisation of collisionally excited molecular hydrogen is not efficient [Roberge and Dalgarno 1982].
The model calculations of Rawlings and Williams (1989) in comparison result in an H_2 abundance of only $X_{H_2} \approx 10^{-4}$, a value set by RW as an initial value[13]. This behaviour of the H_2 concentration in the nova shell must be seen as a natural consequence of the fact that RW neglected the O–H chemistry as well as the complete silicon network. Thus the natural routes to the formation of H_2 are suppressed. The formation reactions proposed by RW:

CH^+	$+ H$	$\Longrightarrow H_2$	$+ C^+$	(64)
H^-	$+ H$	$\Longrightarrow H_2$	$+ e^-$	(65)

are by orders of magnitudes less efficient than the reactions 61–63. The model calculations of RW are characterized by a high sensitivity of their results to the initial fraction of the H_2 abundance. If they raise the concentration of H_2 by a factor of 100 they report an increase for the hydrocarbon species by a factor up to 10^{12} for C_5H. The H_2 abundance in the model discussed in this work is a factor of 4700 higher than in the standard model of RW. The complex hydrocarbons (up to C_8H_6) therefore are expected to additionally raise in abundance, though being sufficiently present to promote effective nucleation. The treatment of a complex hydrocarbon chemistry as it has been performed by Rawlings and Williams (1989), has to take into account the time development of the chemistry from the early phases ($t \leq 30$d) up to the starting point of the calculation! Otherwise the initial conditions are highly questionable as the concentrations are depending on the chemical evolution[14].

When the radiation field has changed the chemical state of the material the H_2 abundance drops to $X_{H_2} \approx 10^{-5}$. The gain mechanism now is dominated by

H^-	$+ H$	$\Longrightarrow H_2$	$+ e^-$	1	(66)
SiH^+	$+ H$	$\Longrightarrow H_2$	$+ Si^+$	0.4	(67)
NH	$+ H$	$\Longrightarrow H_2$	$+ N$	0.2	(68)
CH^+	$+ H$	$\Longrightarrow C^+$	$+ H_2$	0.02	(69)

the route via the negative hydrogen ion. The loss is given by the reverse of reaction (67) and (66). The contribution of reaction (69) becomes more important under the conditions of more intense UV radiation.
The reactive ions H_2^+ and H_3^+ having always a low concentration of 10^{-15} or lower are making a minor contribution to the H_2 formation by

[13] Later even dropping to 10^{-7}.

[14] However, the present investigation strengthens the result of RW concerning the possibility of PAH–formation in the shells of novae.

$$H_2^+ + H \Longrightarrow H_2 + H^+ \quad (70)$$
$$H_3^+ + CO \Longrightarrow H_2 + HCO^+ \quad . \quad (71)$$

4.3.3.2 H_2O and its Radical

The water molecule is one of those molecules which can play a major role in the chemistry of circumstellar shells, either controlling the O–H chemistry and also being a major coolant. There exists a high exchange rate with the abundant $SiOH^+$ ion by

$$SiOH^+ + H \Longrightarrow H_2O + Si^+ \quad (72)$$

as forward and reverse rate for reaction (72) are in equilibrium. The exothermic hydrogen abstraction

$$OH + H_2 \Longrightarrow H_2O + H \quad (73)$$

also possesses a high activation barrier (E_a=1580 K) which is easily to be overcome in the hot nova gas outflow. For this reaction the reaction rate coefficients of Wagner and Graff (1987) are recommended, who have studied the reactions for temperatures in the range of 300K–5000K and assume vibrationally cold OH and H_2O.
The photodissociation of H_2O was calculated by using the cross section data of Lee (1984) and Kley (1984).

It turns out that the photochain makes a significant contribution to the destruction of the water molecule.
An additional building channel is provided by the dissociative recombination of the H_3O^+ ion:

$$H_3O^+ + e^- \Longrightarrow H_2O + H \quad , \quad (74)$$

an ion, which can also be dissociated in the competing channels [Herd *et al.* 1990]

$$H_3O^+ + e^- \Longrightarrow OH + H_2 \quad (75)$$
$$H_3O^+ + e^- \Longrightarrow O + H + H_2 \quad (76)$$
$$H_3O^+ + e^- \Longrightarrow OH + 2H \quad . \quad (77)$$

The predictions of the branching ratio of the four dissociative recombinations differ. Whereas Bates (1986) predicts channel (74 to be dominant the other routes to be minor, Herbst (1978, 1988) calculated that the OH formation reactions (75) (80%) and (77) (20%) are the most effective ones. In the interstellar medium and in Molecular Clouds these reactions are important in determining the OH/H_2O ratio, but none of these reactions are dominant in the circumnova gas shell. The dissociative recombination of H_3O^+ ($X_{H_3O^+} = 4.7 \cdot 10^{-5}$) is less reactive than the ion–neutral reaction of the $SiOH^+$ ion with atomic hydrogen.

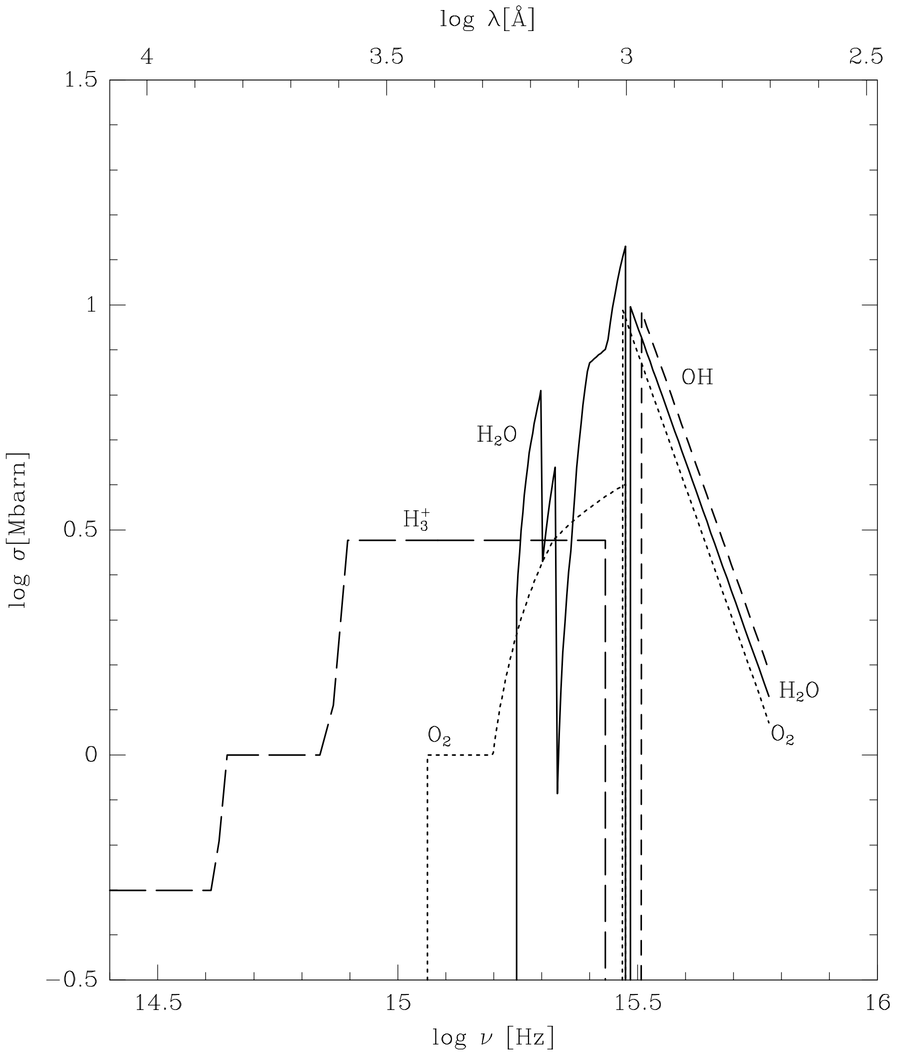

Figure 4.12: Photo cross-sections σ for O–H containing species. The logarithmically scaled cross-sections are depicted for the species OH (short–dashed), H_2O (full), O_2 (dotted) and H_3^+ (long–dashed).

For the late, high temperature phase the concentrations of H_2O drop down to $X_{H_2O} \approx 10^{-16}$. The main formation then proceeds by the slow neutral association [Clegg *et al.* 1983]

O	$+ H_2$	$\Longrightarrow H_2O$	$+ h\nu$	1.0	(78)

and the ion neutral reaction involving the HCO^+ species:

HCO^+	$+ H$	$\Longrightarrow H_2O$	$+ C^+$		(79).

Now, when the envelope has become optically thinner for photons shortward of the

H_2O dissociation threshold (1700Å) the photodissociation of H_2O is controlling the abundance of the water molecule. Thus the concentration of the OH radical is raised in comparison with the low temperature, low radiation phase and now is more than two orders of magnitude higher than the H_2O concentration.

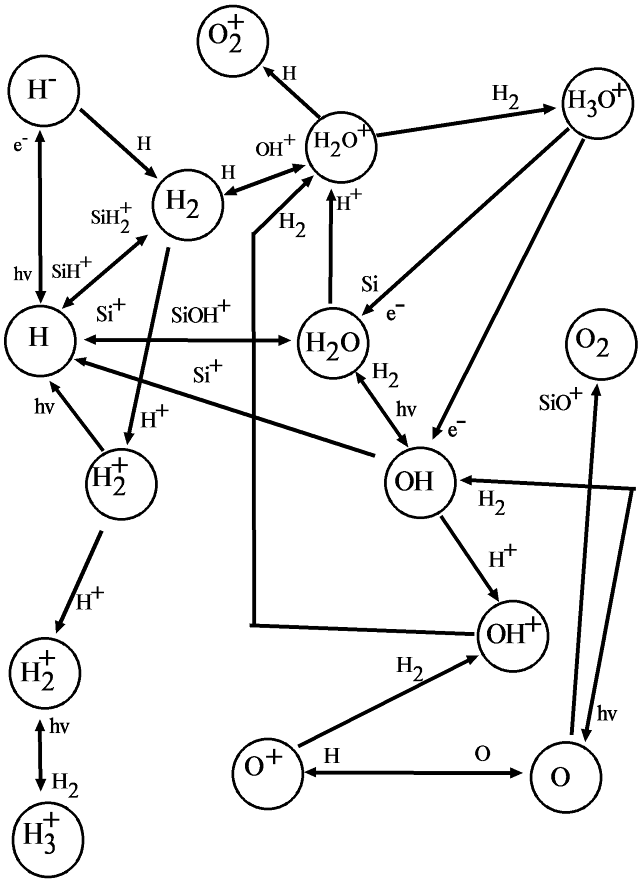

Figure 4.13: For the O–H chemistry in the case of C-rich nova outflow (standard model) the main building and destruction channels are shown for the early phase.

The Negative Hydrogen Ion The negative hydrogen ion serves as an intermediate product of the formation of molecular hydrogen. Up to day 40 it has a low abundance of $X_{H^-} \approx 10^{-15}$ and there is a large loss by

$$H^- + h\nu \Longrightarrow H + e^- \quad (80)$$
$$H^- + H \Longrightarrow H_2 + e^- \quad . \quad (81)$$

The increase of the electron concentration after day 40 and the additional increase in atomic hydrogen both are the reason for the steep rise of the H^- abundance slope.

Furthermore the H^- ion then is involved in the major H_2 production reaction.

4.3.4 Silicon Chemistry

The silicon chemistry is of special interest in view of the fact that SiO is a possible condensation nucleus in the dust formation process in circumstellar shells. Although

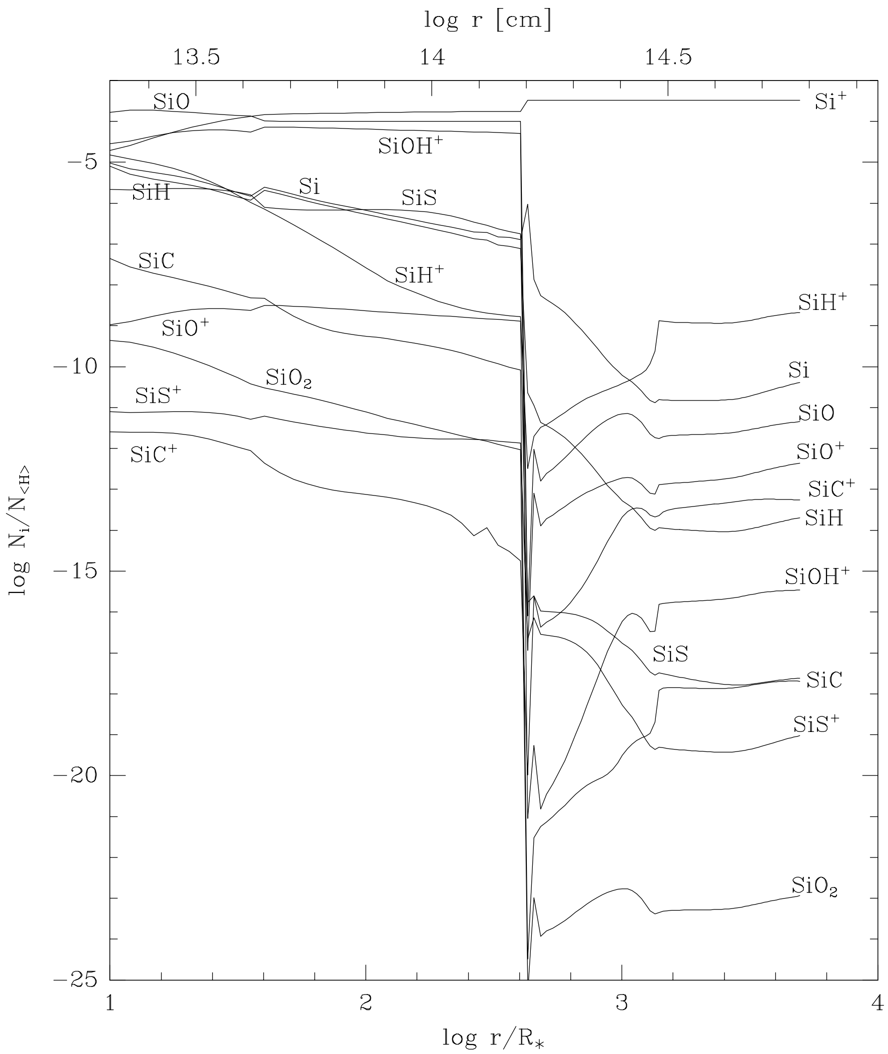

Figure 4.14: Logarithmic concentrations of the silicon bearing species, normalized to the number of H-atoms over a logarithmic radius axis scaled with the stellar radius.

---

the importance of SiO as a dust precursor molecule is more important in the case of O–rich shells an extended set of silicon bearing molecules are included in the reaction network for novae. This has been done out of the experience from the explorations of the chemistry under the influence of a moderate to strong chromospheric UV radiation field as it is present in the envelope of the late–type supergiant αOri (see Chap. (3)). The energetic UV photons penetrating in the gas lead to an incomplete blocking of either C or O in the CO molecule. Thus in the considered carbon–rich nova case not all the oxygen is removed from the chemistry and a chemical situation arises which differs from the well known and commonly applied scheme in which either carbon or oxygen is completely blocked. Instead a substantial fraction of the oxygen is injected into the chemistry and can drive and initiate several gas–phase processes. One of the straight consequences is that the stable SiO molecule can be formed. SiO has been observed in a variety of sources (Herbst *et al.*, 1989; Omont, 1991) in continuum emission as well as by maser activity (Clegg *et al.*, 1983), where the overwhelming fraction of the SiO–sources are assumed to be oxygen rich. On the basis of shock chemistry models [Hartquist *et al.* 1980, Mitchell and Deveau 1983, Ziurys *et al.* 1989] an enhanced abundance of SiO was predicted for regions characterized by a higher temperature than that in the typical interstellar clouds. The observations of Ziurys *et al.* (1989b) confirmed this assumption by comparative studies of several molecular clouds.

Despite having a cosmic abundance twice that of sulfur only two silicon bearing molecules (SiO, SiS) have been observed in the interstellar space, whereas more than 10 sulfur containing molecules have been found (for an overview see e.g. [Singh and Chaturvedi 1989, Omont 1991] . Additionally to SiO and SiS, SiC_2 and possibly $HSiC_2$ have been detected in the envelope of the famous C–rich shell of IRC+10216 [Guélin *et al.* 1986] .

Recently the gas phase chemistry of silicon has been explored by Wlodek and Bohme (Wlodek *et al.*, 1987; Bohme *et al.*, 1988) on the basis of newly derived rate coefficients and thermodynamic data from laboratory measurements. One salient feature of their explorations is that the Si^+ ion, in analogy to the C^+ and the S^+ ions can be inserted into hydrocarbon neutrals and drive a chemistry similar to that what is believed to form the organo–sulfur compounds C_2S, C_3S and C_4S, which have recently been detected in circumstellar shells [Cernichario *et al.* 1987] and also studied in laboratory by ion flow tube experiments[15] (e.g. C_4S).

In the expanding gaseous envelope of a nova, however, SiO has not been directly identified up to now. But, there is observational evidence for the presence of SiO_2 in the outflows of nova V1370 Aql (1982) [Gehrz *et al.* 1984] and QU Vul (1984) [Gehrz *et al.* 1986] . The SiC feature tentatively identified for V1370 Aql may also point to a combination of SiC and other silicate materials. Some caution of course must be paid to those identifications, as the observed features (10μ, 20μ) can only be attributed to the transitions of characteristic active functional molecular groups. For silicates the Si–O bond has a characteristic stretching mode at about 10μ, whereas the bending mode of the O–Si–O complex leads to an emission in the 20μ range.

We now turn to the analysis of the silicon chemistry in the nova gas which in this calculation has been evaluated for the C–rich case. Here one first recognizes that the SiO molecule absorbs the largest fraction of the available silicon, just in the inner regions where its abundance is as high as $X_{SiO} \approx 10^{-4}$. This is surprising as chemical equilibrium calculations for C–rich situations will not lead to any SiO in

[15]See [Wlodek *et al.* 1988] or for an overview [Bohme 1992].

this temperature zone (around $\approx 1000\,K$).
The main building channel is given by the dissociative recombination of the $SiOH^+$ ion

$SiOH^+$	$+ e^-$	$\Longrightarrow SiO$	$+ H$	1	(82)

which has a high rate coefficient and a moderate inverse temperature dependence[16]. This reactive ion is the result of

Si^+	$+ H_2O$	$\Longrightarrow SiOH^+$	$+ H$	1.0	(83)

and

SiO^+	$+ H_2$	$\Longrightarrow SiOH^+$	$+ H$	0.1	(84)

where SiO^+ is formed via:

Si^+	$+ OH$	$\Longrightarrow SiO^+$	$+ H$	.	(85)

These channels are confirmed by the reaction sequences suggested by Neufeld and Dalgarno (1989) , who have studied the molecular reformation processes behind dissociative shocks.
The other channels of relevance are the neutral exchanges

Si	$+ H_2O$	$\Longrightarrow SiO$	$+ H_2$	0.2	(86)
SiO_2	$+ H_2$	$\Longrightarrow SiO$	$+ H_2O$	0.05	(87)

together being only one fourth of the efficiency of reaction (82). Also their temperature dependence is more pronounced[17]. When the carbon begins to form dust grains there is only a little response by the silicon species. The coupling between the silicon and the carbon system is present but covered by the Si–O-H reactions. When the abundance of the SiO has dropped to $X_{SiO} = 3 \cdot 10^{-12}$ the ion–neutral reaction

Si^+	$+ CO$	$\Longrightarrow SiO$	$+ C^+$	1.0	(88)

with CO has become the most prominent reaction. The destruction of the SiO is most efficiently done by photons with energies above $E = 8.26\,eV$. The ionization of SiO on the other hand, needing energies above $10.5\,eV$ does not contribute significantly to the SiO^+.
Another ion which is surprisingly abundant is CH_2Si^+. Its abundance of $X_{CH_2Si^+} = 1.54 \cdot 10^{-6}$ is created by the reaction sequence:

[16] $k_{(82)} = 10^{-7} \cdot T^{-0.5}\ cm^3 s^{-1}$
[17] $k_{(86)} = 10^{-10} \cdot exp(-2000/T)\, cm^3 s^{-1}$

$$\begin{array}{llllr}
\mathrm{Si^+} & + \mathrm{H_2} & \Longrightarrow \mathrm{SIH^+} & + \mathrm{H} & (89)\\
\mathrm{SiH^+} & + \mathrm{H_2} & \Longrightarrow \mathrm{SiH_2^+} & + \mathrm{H} & (90)\\
\mathrm{SiH_2^+} & + \mathrm{C} & \Longrightarrow \mathrm{CHSi^+} & + \mathrm{H} & (91)\\
\mathrm{CHSi^+} & + \mathrm{H_2} & \Longrightarrow \mathrm{CH_2Si^+} & + \mathrm{H} \quad . & (92)
\end{array}$$

The CH_2Si^+ concentration is extremely sensitive to the change in the shell conditions and it drops by 20 orders of magnitude after day 44.

4.3.4.1 Silicon Carbide and Dust Formation

Besides carbon grains of different structure (graphite, diamond, amorphous carbon, fullerite), silicon carbide (SiC) is one of the most important dust species in discussion for novae [Gehrz *et al.* 1986] and late type carbon giants [Frenklach *et al.* 1989]. This has essentially two reasons:

- From a theoretical point of view, silicon carbide is one of the most refractory materials that may form under the conditions of a carbon-rich chemistry. Under these circumstances, a large fraction of the entire oxygen can be chemically blocked in the CO molecule and from the most abundant chemically active specimen, carbon and silicon carbide are the possible condensates.
- The observation of a pronounced spectral feature at 11.2μm in some novae [Gehrz 1988] and in carbon stars [Treffers and Cohen 1974] is generally interpreted as the fingerprint of SiC grains.

Since the formation of carbon grains is both theoretically and observationally established, there are two possibilities for the sequence of condensation:

1. SiC grains appear at rather high temperatures and carbon grains form later, partially as mantle structures on the SiC grains. This possibility is favoured by e.g. [Frenklach *et al.* 1989].
2. Carbon grains are the first to appear and SiC condensation takes place later with the carbon grains serving as condensation nuclei.

An important problem in the formation of SiC under the conditions in circumnova envelopes considering an equilibrium chemistry is, that the molecule SiC is very low in abundance. Therefore, the solid has to be formed by grain surface reactions. However, a large fraction of silicon is contained in rather stable molecules like SiS and SiO which have a higher bond energy than the molecule SiC. Thus, SiC condensation requires rather high temperatures, at which the activation energy for the dissociation of SiS and SiO is available from grain-gas collisions. On the other hand, at these temperatures, the solid SiC is not stable under typical circumstellar gas pressures.

This problem diminishes in the present treatment which takes into account the non-equilibrium effects always present in nova envelopes. In this case the dissociation of

molecules due to the radiation field increases the abundance of atomic Si and C and thereby enables the formation of SiC on grain surfaces.
A first attempt to evaluate these ideas for the case of the shells of late–type stars with chromospheres has been undertaken by Beck and Dominik (1992) . In this work it could be shown that under conditions typical for carbon-rich late type giant envelopes the solid compound silicon carbide is stable against evaporation only at temperatures below 1400 K. At these temperatures the deviations from chemical equilibrium support the condensation of SiC since silicon is still present in atomic form. Therefore, it seems probable that SiC may form on the surface of preexisting carbon grains instead of being the primary condensate at very high temperatures. SiC condensation at temperatures around 2800K (as suggested by Frenklach et al. , 1989) seems rather questionable since these results are obtained from experiments at much higher densities under earthlike conditions.
However, these studies are only of a preliminary character and have to be improved for the following reasons:

- In the studies mentioned above the SiC dust formation was calculated inconsistently with a given radial distribution of the chemistry which was previously derived. The consistent treatment of the formation of composite dust grains must necessarily involve the theory of heteromolecular dust formation as developed by [Gail and Sedlmayr 1988] and extended for the heterogenous case by C. Dominik (1992) .
- The calculations were based on the chemical network[18] described in Chapter (III) (see also Appendix III.1). This chemical system only includes a rudimentary set of carbon chemistry reactions, which may be unsufficient to describe the whole silicon–carbon chemistry complex.

Further investigations therefore should strive for a consistent coupling of chemistry and composite grain formation having regard to a extended Si–C reaction network as extended as possible.

The present studies examining the nova chemistry have not been worked out up to this level, but give a reliable basis as the SiC abundance in the gas–phase as well as the formation of carbon clusters, on which SiC also may form, has been calculated. The silicon carbide present in the nova envelope is built by a dissociative recombination process via the interaction with the progenitor ion CH_2Si^+:

$$CH_2Si^+ \quad + e^- \quad \Longrightarrow SiC \quad + H_2 \,. \tag{93}$$

The main loss results in the formation of the protonated siliconcarbide:

$$H_3O^+ \quad + SiC \quad \Longrightarrow CHSi^+ \quad + H_2O \tag{94}$$

[18] The network has been extended by several SiC forming and destroying reactions taken from UMIST rate file [Millar *et al.* 1991b] .

The concentration derived ($X_{SiC} = 5 \cdot 10^{-9}$) is too small for the formation of pure SiC dust by homogeneous nucleation, but would be sufficient for SiC to be the starting nuclei on which other materials can condense. The high abundance of atomic silicon and of several carbon bearing molecules also opens the other possibility of a SiC formation on the surfaces of carbon grains[19].
As most of the other molecules the SiC does react significantly to the change in the radiation field. Its abundance drops to $X_{SiC} = 1.2 \cdot 10^{-17}$ and the formation now involves the protonated ion by

$$\mathrm{CHSi^+} \quad + \mathrm{e^-} \quad \Longrightarrow \mathrm{SiC} \quad + \mathrm{H} \tag{95}$$

whereas the destruction by dissociation is dominant:

$$\mathrm{SiC} \quad + \mathrm{h}\nu \quad \Longrightarrow \mathrm{Si} \quad + \mathrm{C} \quad . \tag{96}$$

[19]It seems also possible, that both processes act in a illuminated carbon–rich environment.

4.3.5 Sulfur Chemistry

The sulfur chemistry is included in our network by 27 species covering the prominent neutral species SiS, HS, H_2S, SO, SO_2 and CS as well as some complex ions as H_3CS^+ and $HSiS^+$, all connected by several hundreds of reactions. Some sulfur components are possible candidates for dust formation[20]. [Goebel and Moseley 1985] have identified the MgS emission feature[21] by observations in the 10-50 μm range for the most prominent C–rich shell IRC+10216[22]. On the other hand the compilation of [Sahai and Wannier 1992] referring to the observations of O–rich circumstellar shells imply that sulfur is not heavily depleted into grains. In the presence of an excess of free oxygen one can predict that species like SO and SO_2 must be abundant. Furthermore the existence of MgS might be lowered by the oxidation reactions with H_2O and the OH–radical to form MgO, thus leaving free H_2S and HS molecules.
In the following we want to discuss briefly the results of the chemical nova calculations for the sulfur species. The most abundant sulfur species in the early phase is the sulfurcarbide CS with an abundance of $X_{CS} = 6.4 \cdot 10^{-6}$. Its formation requires the presence of the protonated ion HCS^+ ($X_{HCS^+} = 2.3 \cdot 10^{-6}$), thus dissociative recombination:

$$HCS^+ \quad + e^- \quad \Longrightarrow CS \quad + H \qquad 1.0 \tag{97}$$

acts very efficiently and the slightly endothermic neutral hydrogen abstraction channel[23]

$$HS \quad + C \quad \Longrightarrow CS \quad + H \qquad 0.01 \tag{98}$$

only gives a contribution in the range of 1%. The loss is performed by the ion–neutral

---

[20] Fe_2, FeS, SiS, SiS_2 and MgS have been proposed as possible first candidates for condensation (see e.g. [Gail and Sedlmayr 1986b]), which all have high melting points above 1200K and so may initiate the grain formation process as nucleation seeds. Dust formation in M–stars has been modelled by [Gail and Sedlmayr 1986b] who have taken into account especially the MgS grain component. They could show that MgS grain formation will set in first at a gas temperature of about 900 K.

[21] They compared the observed feature around 30μm with laboratory spectra measured by [Nuth *et al.* 1985] . These authors also measured other substances which had been in question (CaS, FeS, SiS_2, FeS_2 and Fe_3C). Their studies confirmed that FeS, SiS_2 and Fe_3C can be ruled out as a emission source and that CaS and FeS may only contribute but not significantly shape the feature.

[22] It might be surprising that MgS emission have been found in an envelope where carbon is more abundant than oxygen, but without oxides present the equilibrium condensation sequence running from high to low gas temperatures: carbon, SiC, Fe, MgS [Lattimer *et al.* 1978] shows that MgS might be a plausible candidate from the considerations of carbon–rich chemistry. Additionally it has been found that, based on radio measurements, the sulfur containing molecules H_2S, CS and SiS are depleted from the gas–phase in IRC+10216 [Lafont *et al.* 1982] . All this cannot rule out the additional possibility that the MgS might have formed on the surface of a previously condensed grains by e.g.:

$$Mg \quad + H_2S \quad \Longrightarrow MgS \quad + H_2$$

[23] $k = 5.1 \cdot 10^{-13} \cdot \exp(-300/T)\ cm^3 s^{-1}$

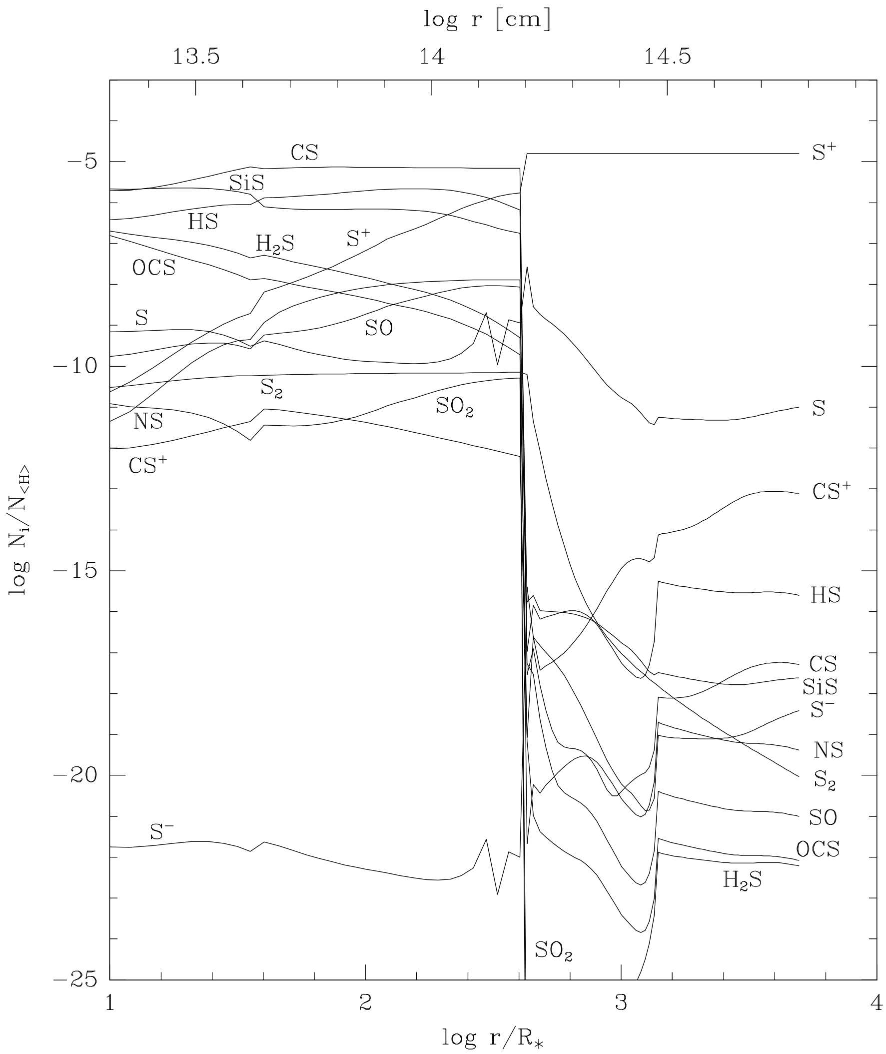

Figure 4.15: Logarithmic concentrations of the sulfur containing species, normalized to the number of H-atoms over a logarithmic radius axis scaled with the photospheric radius.

---

reaction:

$$H^+ \quad + CS \quad \Longrightarrow CS^+ \quad + H \quad 1.0 \quad . \quad (99)$$

Later the radiative dissociation destroys the CS and the dissociative recombination via (97) is reduced in its rate because of the lowered abundance of the HCS^+ ion ($X_{HCS^+} = 3.5 \cdot 10^{-17}$).
For the also stable SiS[24] the gain channel proceeds in the same way as in the case of CS:

[24] $E_{bond} = 6.46\, eV$ in comparison to $E_{bond} = 7.37\, eV$ for the CS molecule.

$$\mathrm{HSiS^+} \quad + \mathrm{e^-} \quad \Longrightarrow \mathrm{SiS} \quad + \mathrm{H} \qquad 1.0 \quad , \tag{100}$$

incorporating the protonated form of the SiS molecule, which is the most abundant sulfur containing ion ($X_{HSiS^+} = 4.2 \cdot 10^{-6}$). In the shell of IRC+10216 the situation is just the other way round: according to [Cernichario *et al.* 1987] the SiS is more abundant than the CS by a factor of 1.75.
While for the other sulfur species the degree of ionization is almost one after day 44, the CS and SiS molecule show an ionization level of 10^{-2}. Their ions are more effectively destroyed than the neutrals. The oxygen bearing sulfur species are only of minor importance: $X_{SO} = 3.2 \cdot 10^{-10}$ and $X_{SO_2} = 2.6 \cdot 10^{-12}$. The formation vitally needs the presence of atomic oxygen and the OH radical in performing the reactions

$$\mathrm{HS} \quad + \mathrm{O} \quad \Longrightarrow \mathrm{SO} \quad + \mathrm{H} \tag{101}$$
$$\mathrm{SO} \quad + \mathrm{OH} \quad \Longrightarrow \mathrm{SO_2} \quad + \mathrm{H} \quad . \tag{102}$$

At all times these molecules are subject to dissociating photons which act by

$$\mathrm{SO_2} \quad + \mathrm{h}\nu \quad \Longrightarrow \mathrm{SO} \quad + \mathrm{H} \tag{103}$$
$$\mathrm{SO} \quad + \mathrm{h}\nu \quad \Longrightarrow \mathrm{S} \quad + \mathrm{O} \tag{104}$$

and lead to the release of atomic sulfur to the gas–phase which is ionized in the next step.
The hydrogenated sulfur components HS and H_2S are formed in the sequence:

$$\mathrm{HSiS^+} \quad + \mathrm{e^-} \quad \Longrightarrow \mathrm{HS} \quad + \mathrm{Si} \tag{105}$$
$$\mathrm{HS} \quad + \mathrm{H_2} \quad \Longrightarrow \mathrm{H_2S} \quad + \mathrm{H} \tag{106}$$

and reprocessed by the interaction with energetic photons.

4.4 Energy Balance of the Nova Shell

One of the main points of the chemical modelling was to calculate the energy balance for the outflowing gas. The incorporation of the heating and cooling mechanisms guarantees for a more consistent treatment of the interdependencies between chemistry, dust formation and thermodynamics, and is an indispensible requirement in the framework of the time–dependent modelling of nova shells. The feasibility of the formation of dust grains on the basis of an elaborate chemical model thus has been investigated.
It is commonly known that

a) some reactions have a strong temperature dependence[25] which may have an important influence via the complex interactions they are involved in an extended reaction network. Different concentrations of the chemical species directly affect the energy balance, as the incorporated heating and cooling processes naturally are density dependent.

b) Dust formation also strongly depends on the gaskinetic temperature of the environment[26]. The possible onset of dust nucleation is a steep function of the gas temperature [Dominik 1992] .

The hydrodynamic structure of a nova shell fortunately is quite simple, thus the coupling of the dust to the outflow characteristics can be neglected[27].

The physics of the nova shell is not that of a gas in local thermodynamic equilibrium. In those regions where the ionization of matter is of relevance, the radiation field of the nova photosphere, roughly represented by a diluted black–body of about 10,000K with time dependent temperature increase, determines the local temperature.
The processes taken into account are given here briefly in a list as they have been outlined before (see Chap. (4.2.4) and (2.4)). As energy input processes there are:

[25]For the collisional dissociation of molecular hydrogen

$$\mathrm{H} \quad + \mathrm{H_2} \quad \Longrightarrow \mathrm{H} \quad + \mathrm{H} \quad \mathrm{H}$$

we have a rate coefficient of k= $4.67 \times 10^{-7} T^{-1} \exp(-55000/T)$.
Also the hydrogen abstraction reaction:

$$\mathrm{C^+} \quad + \mathrm{H_2} \quad \Longrightarrow \mathrm{CH^+} \quad + \mathrm{H}$$

has a temperature dependent rate coefficient of k= $1.00 \times 10^{-10} \exp(-4640/T)$.

[26]Dust formation also depends on the internal temperature of the dust grain itself. This temperature is not well defined in the case of small clusters, especially in the regime of the critical cluster, which is an intermediate phase between gas and solid and may be not in equilibrium with the radiation field. The larger the grains the better is the assumption of an energetic equilibrium between the grains and the photons.

[27]The situation is completely different for the dust formation in Red Giants or oscillating atmospheres of cool stars (Miras). In this case the complex interaction of hydrodynamics, radiation transfer and dust formation has to be treated as a coupled system (see e.g. [Fleischer *et al.* 1992]).

- Photoionization of neutral atoms in the ground state.
- Photoionization of excited hydrogen atoms.

The cooling proceeds by

- Recombination of single ionized atoms.
- Forbidden line emission.
- Emission of molecules
- Free–free emission.
- Hydrodynamic expansion.

The determination of the electron temperature then is carried out as it is outlined in Chap. (2.4.3).
For the calculation of the temperature structure of the envelope we have to face two different situations:

A. the matter is mainly neutral, then the residual electrons will accommodate to the temperature of the neutral gas, or

B. a reasonable fraction of the material is ionized, then the overall temperature will be determined by the temperature of the electrons.

For case (A) one can assume that the neutral gas can cool down and the hydrodynamic expansion is the governing cooling process. Therefore the actual gas temperature is given by an exponential cooling law, where the initial gas temperature is assumed to be equal to the initial photospheric temperature.
The relaxation time $t_{\rm rel}(e^-)$ for the electrons in the neutral gas then can be expressed as [Drawin 1971]

$$t_{rel}(e^-) = \frac{3(m_e + m_0)^2}{16 m_e m_0} \cdot \frac{1}{B n_0} \times \left[1 + \phi_2 \left(\frac{3\pi m_e}{8kT_{eff}}\right)^{1/2}\right] \tag{4.18}$$

where m_e, m_0 denote the masses of the electrons and neutrals, n_0 is the neutral particle density and T_{eff} is determined by

$$T_{eff} = \frac{(m_0 T_e + 3 m_e T_0) \cdot k}{m_0 + m_e} \tag{4.19}$$

The collisional cross-section is assumed to be dependent on the relative velocity of the colliding particles:

$$\sigma_e = \frac{B}{\phi_2 + v} \tag{4.20}$$

Inserting reasonable numerical values for the quantities needed to evaluate the relaxation time:

$$T_e = 2000K$$
$$T_0 = 500K$$
$$n_0 = 10^{10} cm^{-3}$$
$$B = 2 \times 10^{-7} cm^3 s^{-1}$$
$$\phi_2 = 2.0 \times 10^6 cms$$

yields a cross–section of

$$\sigma_e = 1.55 \times 10^{-15}\, cm^2 \tag{4.21}$$

and a relaxation time for the electrons of

$$t_{\rm rel} \approx 1.2\, s. \tag{4.22}$$

This time is negligible compared to the hydrodynamic time–scale $\tau_{\rm ex}$, which is of the order of 10^5s and therefore the assumption of a fast accommodation of the electrons to the neutral gas temperature is valid up to densities of $\approx 10^6 \rm cm^{-3}$. This validity interval is sufficient because

- a density as low as $10^6 \rm cm^{-3}$ will not be realized in the period where dust formation can take place and the chemical model thus is calculated, and
- if the matter gets less dense and the central photospheric temperature increases the gas will be radiatively dominated in the later phases and case (B) is valid.

In case (B), valid for the ionized regions of the shell, the gas temperature is given by the electron temperature.
In intermediate ionization zones this two–case model may be critical, but in view of the recent status of the nova modelling, where the temperature is set constant [Rawlings 1988] [28] or is treated by an exponential cooling law during the whole time evolution [Rawlings and Williams 1989] , this treatments seems to be one step towards a more realistic modelling of the chemistry in expanding nova shells.

4.4.1 The Temperature Structure

The time evolution of the shell temperature shows two distinct phases (see Fig. (4.16)). In the first $\approx$ 40 days of the nova event the gas of the envelope is predominantly neutral, thus the resulting electron temperature is evolving to very low temperatures of $\approx 10^2$K. This phase is characterized by an optically thick gasflow cooling down adiabatically as the expansion proceeds. The energy input to the electron gas is insufficient to determine the overall energy balance. The gas temperature decreases

[28] [Rawlings 1988] treated the nova shell as a three zone region, each zone having a constant temperature:

H^0, C^0, Fe^+, $Mg^+ \ldots$	$\rightarrow$	4000K
H^0, $C^+ \ldots$	$\rightarrow$	6000K
$H^+ \ldots$	$\rightarrow$	8000K

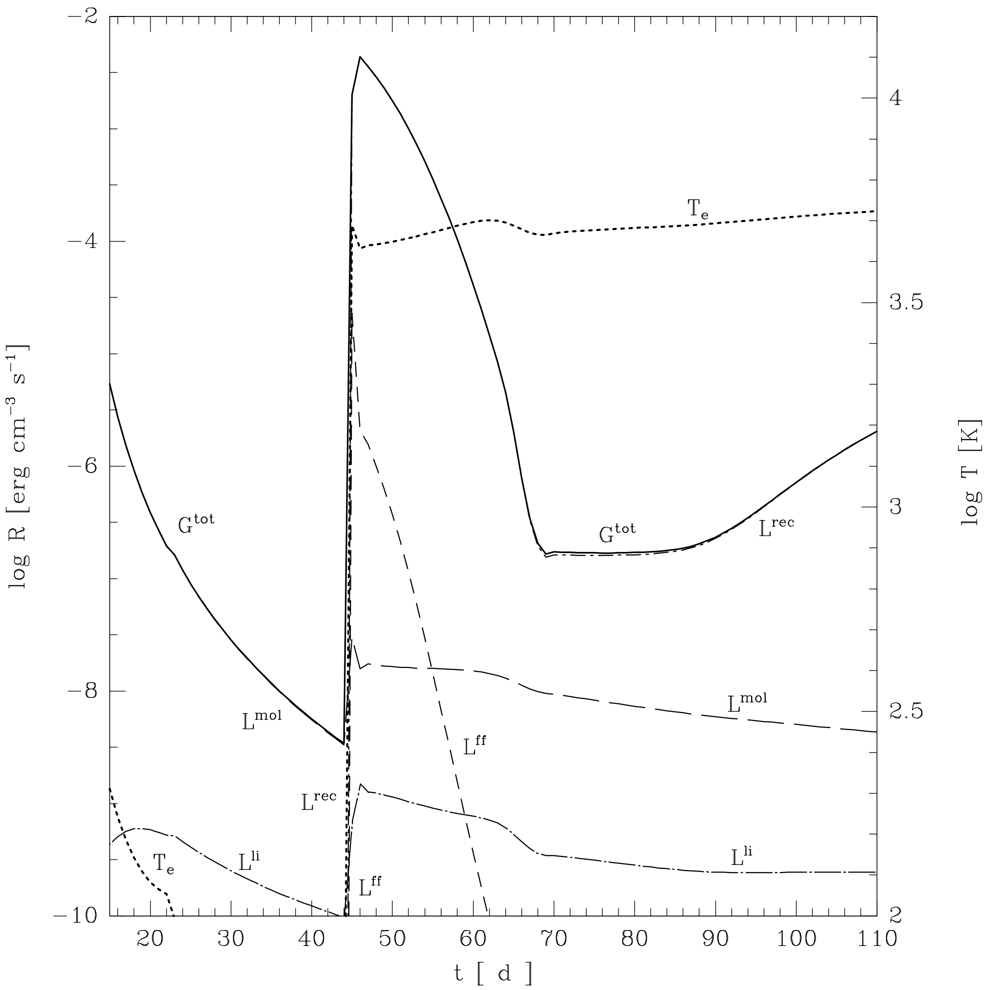

Figure 4.16: Time Evolution of the heating (**G**) and cooling rates (**L**) for nova shells. The total energy input G^{tot} (solid line) is balanced by several cooling processes: recombination cooling (L^{rec}), molecular cooling (L^{mol}), free–free cooling (L^{ff}) and line cooling (L^{li}).

---

from the initial value (8000K) to about 700K at day 40. It should be noted that the radial course of the electron temperature and the corresponding gain and loss rates up to the steep rise at day 44 is artificial, as its values are computed without taking care of the fast accommodation of the electrons to the temperature of the neutral particles. Thus in the computational procedure the coupling of the electrons and the gas is not calculated, but, depending on the ionization state of the matter, case (A) or case (B) is applied. If this low electron temperature would be realized in the envelope the molecular cooling would be the most effective process to transfer energy out of the shell and this transfer is mostly the effect of H_2O emission. The energy

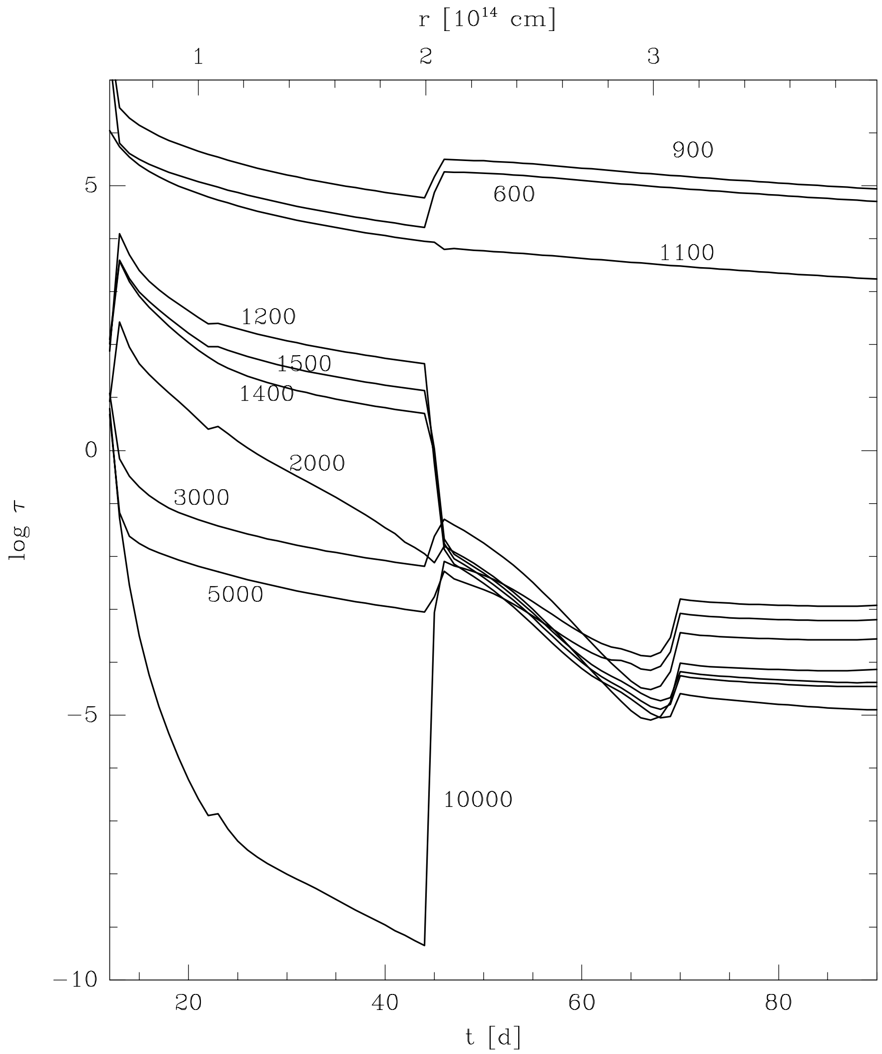

Figure 4.17: Time evolution of the optical depth in nova shells during the first 100 days. The frequencies for which the optical depth is shown is given in Ångstroems for every curve. The optical depth of the dust has not been included.

---

input for the electron gas is provided by the ionization of excited H–atoms being in the second level above the ground state. The level population of the H–levels is determined by the balance of radiative excitation and spontaneous emission which are in equilibrium[29], meaning that both reaction rates are equal and much larger than the other rates involving the hydrogen states.
The energy input dramatically rises at day 44, when the flux of ionizing photons has

[29]This does not mean that the population of the hydrogen states is governed by the conditions of local thermodynamic equilibrium; clearly they are not and thus the Boltzmann equation for the population density of the excited stages is not valid.

grown up to a critical level. Now there are sufficient high energetic photons to lift up the internal ground-state electrons of the hydrogen to the first excited level, for which photons with $\lambda \leq$ 1215Åare needed. The optical thickness for wavelength larger than 1200Åis reduced and

$$\tau_{\lambda > 1200\mathring{A}} \ll 1 \quad . \tag{4.23}$$

The radiative excitation of H–atoms proceeds very fast

$$\mathrm{H}^{(1)} + \mathrm{h}\nu_{1-2} \longleftrightarrow \mathrm{H}^{(2)} \qquad R = 2.2 \times 10^7 cm^{-3} s^{-1}$$

and is not balanced by the reverse process of spontaneous emission ($R = 1.66 \times 10^7 cm^{-3} s^{-1}$). Instead of getting de–excited the hydrogen is ionized very efficiently ($R = 5.5 \times 10^6 cm^{-3} s^{-1}$) before the excited electron can fall back to the ground state. Recombination can also not balance the ionization and is less effective by a factor of 10^5.

The mean temperature in the nova shell during the second phase of outburst evolution is about 4800K and after having a slight decrease around day 65, the gas temperature continuously rises due to the time development of the effective photospheric temperature. The nova temperature at day 65 is $\approx$ 40000 K. The energy gain by photoionization now is balanced by the recombination processes. Line cooling as well as molecular cooling are now of minor influence on the energy balance. The slope of the free-free cooling is reflecting the radial distribution of the free electrons.

4.4.1.1 Development of the Ionization

The fast ionization of the excessive excited hydrogen leads to a high degree of ionization of the gas at this instant. The maximum value of $f(H) = 0.7$ corresponding to a concentration of H^+ ions of $X_{H+} = 0.7$. The heavier elements Fe, Na, Mg and Si having lower ionization potentials have been ionized completely in the early stage of the outflow evolution on a time scale of

$$\tau_{\text{ion}} \approx 1 day \quad . \tag{4.24}$$

For the silicon one has to bear in mind that most of the silicon is bound in the stable SiO molecule and it needs about 10 days that Si^+ becomes more abundant than SiO (see Fig. (4.14)).

In the case of sulfur it also takes a period of $\approx$ 10 days until S^+ has become more abundant than the neutral atom. But it lasts already up to day 44 until the S^+ ion becomes the dominating sulfur species. Before that time the neutral molecules CS, SiS and HS are those sulfur specimen with the highest concentration.

Simultaneously to the steep rise of the hydrogen ionization also oxygen is ionized (see Fig. (4.18)) and this is not, as one may think, a direct effect of the radiation

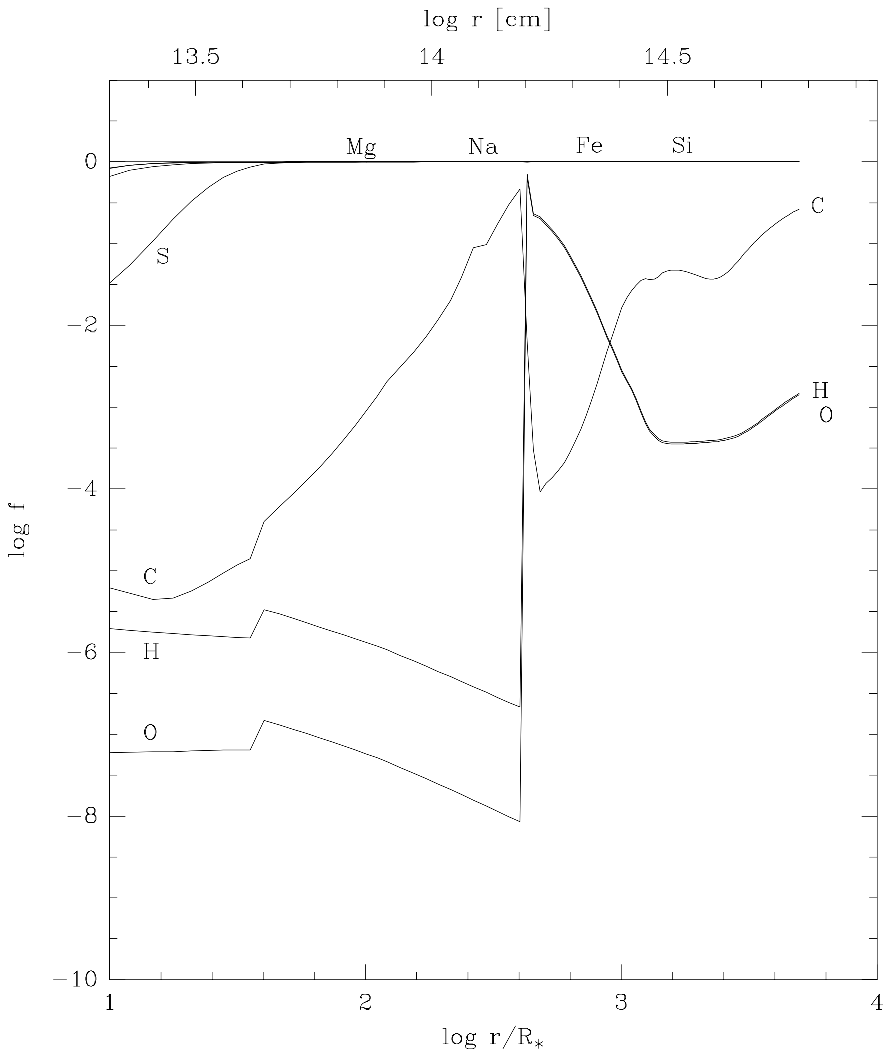

Figure 4.18: Evolution of the degree of ionization f on a logarithmic scale versus the logarithmic radial distance in units of the initial photospheric radius R_* for the elements incorporated in the model. Nitrogen and helium are not displayed as they show no ionization in the standard model.

---

field, it is rather a pure chemical effect. The charge exchange reaction of hydrogen and oxygen

$$O + H^+ \Longrightarrow H + O^+$$

results in a conversion of an originally neutral O–atom to an O^+–ion. Two arguments can be given for the effectiveness of this process:

1. there is an attractive polarization force between O and H^+, and

2. the ionization potentials of H ($E_i = 13.598 eV$) and O ($E_i = 13.618 eV$) are very nearly the same, so that the reaction is a kind of a resonance process.

Thus the cross–section for this charge exchange is very large and all the initially neutral oxygen atoms are converted. In this way the ionization state of oxygen is closely coupled to that of hydrogen. Following the radial slope of the ionization (see Fig. (4.18)) to the next phase of the ejecta evolution (t>44 days) one infers a pronounced decrease of the ionization. This is a phase where the chemistry accommodates to the instantaneous onset of the radiation field and the release of electrons. In this accommodation process some molecular ions, not being of large concentration take an important role as intermediate chemical species. These ions, once formed by ion–neutral reactions, are destroyed via dissociative recombinations, which have a large reaction cross-section and therefore transfer the ions back into the neutral state:

$$\mathrm{CO} + \mathrm{H}^+ \Longrightarrow \mathrm{CO}^+ + \mathrm{H} \quad (107)$$
$$\mathrm{CO}^+ + \mathrm{e}^- \Longrightarrow \mathrm{C} + \mathrm{O} \quad (108)$$

and

$$\mathrm{H}_2 + \mathrm{O}^+ \Longrightarrow \mathrm{OH}^+ + \mathrm{H} \quad (109)$$
$$\mathrm{OH}^+ + \mathrm{e}^- \Longrightarrow \mathrm{O} + \mathrm{H} \quad (110)$$

For hydrogen additionally the neutralization with the negative ion

$$\mathrm{H}^- + \mathrm{H}^+ \Longrightarrow \mathrm{H} + \mathrm{H}$$

adds to the decrease of the concentration of the ionized hydrogen species.
The high concentration of electrons, now available for recombination reactions with molecular ions, drastically reduces the abundance of those ions by

$$\mathrm{SiO}^+ + \mathrm{e}^- \Longrightarrow \mathrm{Si} + \mathrm{O}$$

$$\mathrm{SiOH}^+ + \mathrm{e}^- \Longrightarrow \mathrm{Si} + \mathrm{OH} \quad .$$

As a result of these dissociation reactions less complex molecules or atoms are formed. Then in a second step the atoms of the heavier elements are ionized. Especially the vanishing of the silicon ions $SiOH^+, SiH^+$ and SiO^+, involved in the most effective H_2 formation reactions in the first phase, lead to reduction of the molecular hydrogen.

Carbon, in contrary to hydrogen and oxygen, shows a significant rise from 10^{-5} to ≈ 0.3 in the degree of ionization. This is the result of the consumption of neutral carbon by the grain formation of carbon dust particles. At the critical distance, when hydrogen is ionized by the hardening radiation field, also the CO shows a response in its slope of concentration, which is mainly caused by the reactions (107) and (108). Therefore a high amount of primarily neutral carbon is released so that the carbon ionization is quickly reduced by a factor of 10^4.

After the sudden CO disruption the chemistry reacts on a larger timescale by the recovering of the CO concentration via the radiative association of C and O, thus the neutral carbon abundance is reduced and the degree of ionization decreases.

4.5 Dust in Nova Shells

The following discussion of the dust formation process in nova shells has to be embedded in the preceding investigations of the

a) ionization structure in the expanding gas [Beck *et al.* 1990b] ,

b) effects of moderate UV–fields on the envelope chemistry [Beck *et al.* 1992],

c) detailed chemistry in the nova envelope[Beck *et al.* 1993] .

In Chap. (2) and (2.5) the time development of the ionization for the elements has been recalculated. It has turned out that there exists a substantial period of time during the early phases of the nova outburst in which carbon is predominantly neutral, whereas silicon is quickly ionized. The hydrogen atom with its higher ionization potential and its dominant abundance can resist to its complete ionization within the envelope for a time which may be a few times the carbon ionization time scale. The incorporation of a realistic non–blackbody radiation field resulting from the radiative transfer calculations of Hauschildt (1991) has substantiated this picture. The ionization of the elements turns out to be even lower than in the blackbody case, especially during the first ≈ 50 days.
The facts stated above, though simplifying the achieved results, reflect the general trends inherent. The precise pattern of the ionization structure depends upon a multitude of parameters characterizing the individual nova event. One important clue that can be deduced is that there is a zone where neutral carbon is coexisting with ionized species like silicon and iron, when the trajectory of the nova shell passes the area most suitable for grain formation in the p–T plane (see Fig (4.19)). This partially ionized region allows for effective ion–neutral reactions and on the bases of the complex chemistry initiated, dust–forming species can be built and nucleate before the harsh radiation field of the nova can destroy them.

In Chap. (3) chemical models of environments exposed to moderate UV–fields generated by a chromosphere have been studied, incorporating a subset of the complete chemical network in order to describe the O–rich situation in the envelope of the late–type supergiant αOri. The choice of this middle course in chemical complexity has facilitated the study of the influence of the radiation field over a wide range of UV–intensities (see Fig. (3.14)). Thus the chemical situations range from a collisional dominated near–LTE for the absence of UV photons, to a complete non–LTE situation, where the distribution of the concentrations is governed by the chromospheric radiation field. In an intermediate intensity region it turns out that the influence of the radiation field is not only destructive. The partial release of those carbon atoms which have been locked in the unreactive CO molecule, opens the possibility of the re–participation of the carbon in the chemical processes and initiates a mixed carbon–oxygen chemistry. This also applies to the nova envelope, where the change of the radiation field coincides with the time development of the ionization

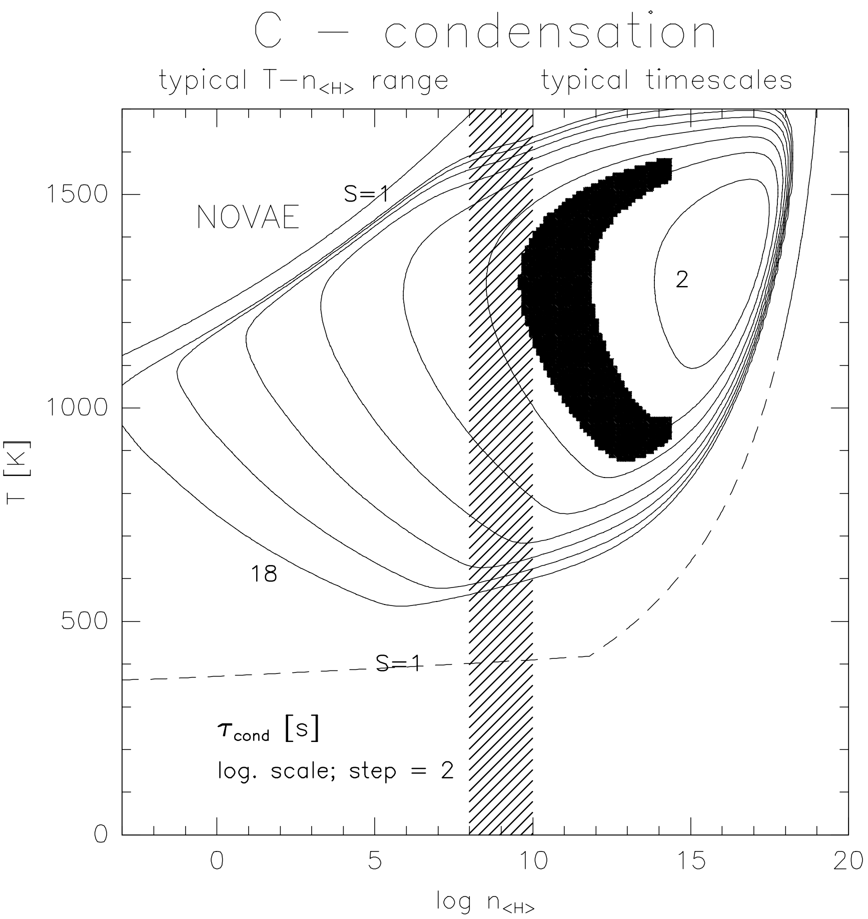

Figure 4.19: Contour plot of the condensation timescale τ_{cond}. The nucleation timescales are calculated applying homogeneous nucleation theory for carbon dust formation in a carbon–rich mixture. The shaded area marks the typical path of an element of gas in a nova shell in the p–T plane, whereas the black area represents the typical timescales for dust formation in this environment. The intersection of both areas indicates the possibility of dust formation. The figure has been adopted with kind permission from Dr˙ C˙ Dominik.

---

of the different species. One conclusion from this has to be that in any case[30] the complete chemistry containing the C–chemistry as well as the O–chemistry must be taken into account to allow for an adequate description of the relevant processes. The former investigations of the dust formation in nova shells can generally be divided into three groups, emphasizing different parts of the problem.

[30]The C–rich case for those outbursts occuring on a C/O–white dwarf and the O–rich case for explosions on ONeMg–white dwarfs, which are only about one fourth of the total nova events.

1) One type of studies tries to trace back the problem of dust formation to the competition between the timescales of ionization $\tau_{\rm ion}$ and grain nucleation $\tau_{\rm nuc}$ ([Gallagher 1977] , [Yamamoto *et al.* 1979] and [Mitchell and Evans 1984]). In the work of Gallagher (1977), later reexamined by Yamamoto et al. (1979), expressions for the timescales of dust formation and ionization have been derived based on a very simplifying model of the nova. Nevertheless, using observational results for the total luminosity (in the constant luminosity phase), the expansion velocity and the total mass ejected, the calculated values for $\tau_{\rm ion}$ and $\tau_{\rm nuc}$ are of the right magnitude and are meaningful for the question of the presence or absence of grains. However, any details of chemistry and dust formation have been omitted and even for the derivation of the ionization timescale the interaction of ionization and recombination processes of different species was neglected.

2) Clayton and Wickramasinghe (1976) and Yamamoto and Nishida (1977) put their main emphasis on the nucleation and growth of grain particles. Clayton and Wickramasinghe assumed a carbon–rich mixture[31] and developed some qualitative statements about precipitation and growth of carbon dust, in this way being able to confirm the observed typical slope of the visual nova lightcurve by their theoretical investigations.
Yamamoto and Nishida concentrated on the formation of magnesium–silicate grains (e.g. Mg_2SiO_4), assuming a solar abundance mixture for the nova gas and therefore magnesium–silicate as the primary condensate.

   A severe shortcoming of both studies is that

   – they do not treat the chemical processes preceding the phase of dust formation and,
   – that they are assuming LTE conditions for the process of nucleation and growth of the dust during the complete evolution of the nova envelope.

3) The most recent theoretical research by Rawlings and Williams (1989) on the other hand is a very chemical approach to the problem. The formation of nucleation sites is studied via a limited hydrocarbon chemistry[32], but lacking the incorporation of a realistic radiation field and temperature structure[33].

4.5.1 Carbon Dust

The model calculations presented in this work try to avoid both, the neglection of the chemical conditions in which the dust is formed and the ignoring of the radiation

[31] In fact they assumed that most of the shell material is carbon in order to achieve reasonable values for the nucleation rate. This leads to an overestimation of the dust production as even in the case of C/O–white dwarf precursors this abundance condition is not matched.

[32] The network of Rawlings and Williams (1989) includes 936 reactions with C_8H_6 to be the most complex molecule treated.

[33] For a more detailed discussion of the shortcomings see Sect. (4.3).

field and of the temperature structure determining the evolution of the shell.
In the following we concentrate the discussion on the *standard* model, which refers to the typical C–rich case.
In the following table we summarise the concentrations of the major carbon bearing species X_i and their contribution Y_i to the formation of dust:

species	X_i	Y_i
CO	2.94×10^{-3}	–
C_2	8.97×10^{-4}	99%
CO_2	2.89×10^{-5}	–
C_2H_2	3.09×10^{-6}	0.3%
C	1.80×10^{-6}	0.1%
C_2	2.46×10^{-7}	<0.1%
CH	1.02×10^{-8}	<0.1%
CH_2	1.46×10^{-9}	<0.1%

The present approach makes use of the heteromolecular homogeneous nucleation theory, as it has been worked out by Gail and Sedlmayr (1988). An important advantage of this method is the avoidance of the C_2 bottleneck by incorporating the molecules CH, C_2H, C_2H_2 and CH_2 in the nucleation procedure. In the reaction scheme of RW, C_2 is the key molecule promoting all reactions which increase the number of carbon atoms in their hydrocarbon species and therefore the efficiency of the formation of complex hydrocarbons is limited by the formation of the C_2 molecules by radiative association[34]. The consideration of the contribution to the nucleation process of carbon grains by the above mentioned species profits from the diverse and complex interactions between the various compounds in the reaction network resulting in the production of these monomers[35].

The onset of nucleation is dated at day 22 after the outburst, which seems to be very early. The corresponding radius of the material is $r = 6 \times 10^{13} cm$ and the condensation temperature is $T_{\rm cond} = 1500K$.
The temperature where the nucleation starts in principle can be obtained from photometric observations. In practice the insufficient time resolution of the data raise the necessity of extrapolating backwards the expected time of condensation. The procedure of extrapolating, however, depends on the model assumptions about the grain emission [Bode and Evans 1983b] . The temperatures deduced for the onset of condensation are in the range of $1200K \leq T_{\rm cond} \leq 2000K$, thus being not precise enough to discriminate between different possible condensates[36]. Using

[34]The reaction rate coefficient for the radiative association of C_2 is given as $k = 1.0 \times 10^{-17}\, cm^3 s^{-1}$ [Millar *et al.* 1991b] .

[35]The close coupling of these monomers to e.g. the ions $C_2H_2O^+$, C_2HO^+ or C_3H^+ can be seen from Fig. (4.4).

[36]In spite of this Lewis and Ney (1979) based their proposition about metallic iron or iron carbide cohenite (FeC_3) to be the first condensate in nova envelopes, on an observed mean condensation temperature of 900–1000K.

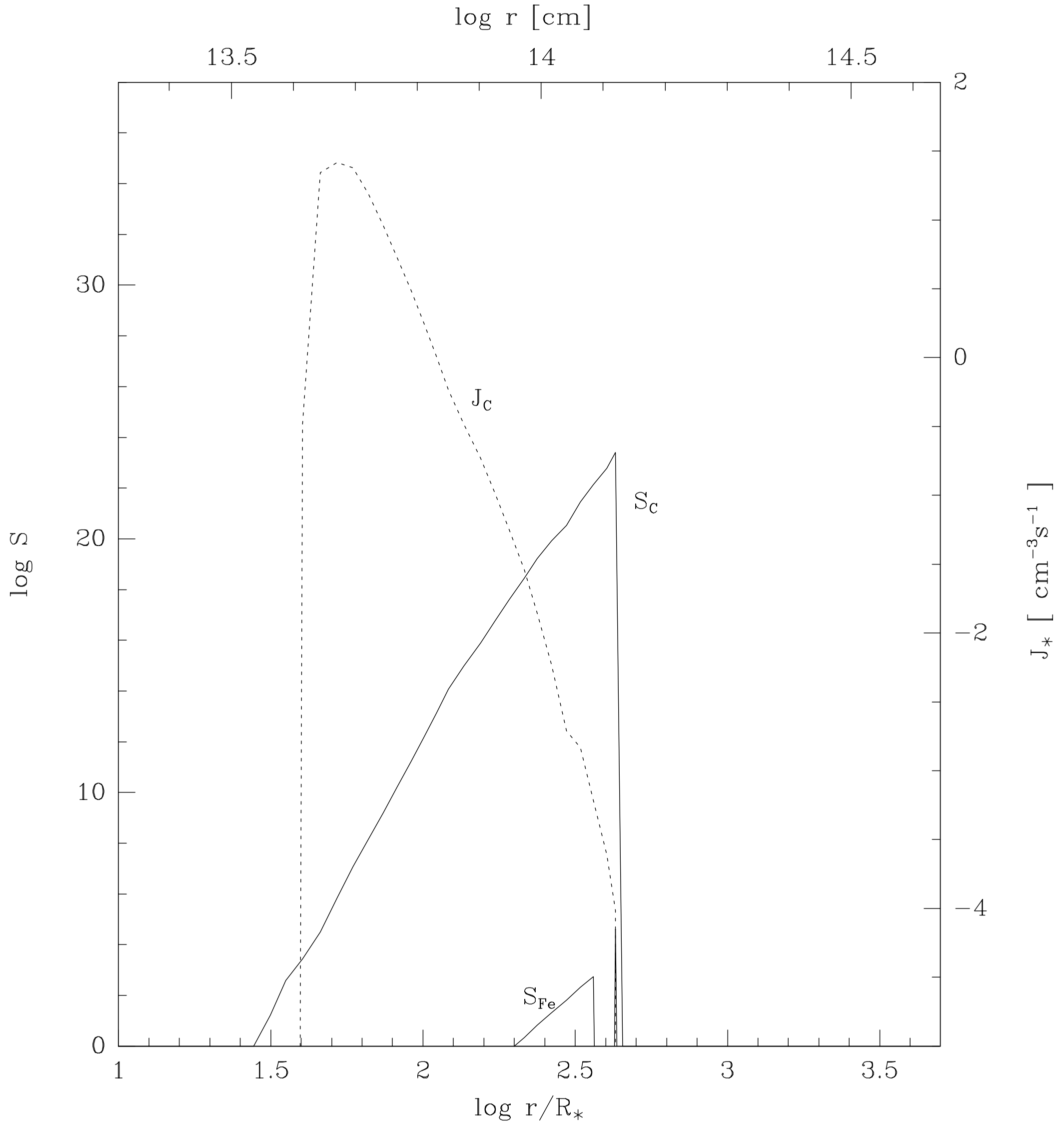

Figure 4.20: Supersaturation ratio S and nucleation rate J_* for the nucleation of carbon and iron based dust particles are plotted versus the logarithmically scaled normalized radius axis for the standard model.

---

the quantitative results of Clayton and Wickramasinghe (1976) for the radius of condensation

$$r_{\mathrm{cond}} = 7.73 \times 10^{13} \left(\frac{L_{\mathrm{CL}}}{5 \times 10^4 L_\odot}\right)^{0.5} \left(\frac{T_*}{10000}\right)^{0.825} \quad cm \qquad (4.25)$$

one gets a radius of $r_{\mathrm{cond}} = 4 \times 10^{14} cm$ corresponding to a timescale until the onset of nucleation of $\tau_{\mathrm{cond}} = 90$days by inserting the values of the model discussed. This

condensation time is larger by a factor of four, the condensation radius is larger by a factor of seven than the corresponding values in our model. Our calculations, however, give a timescale for the ionization of carbon of about 44 days, therefore a predicted onset of nucleation by Clayton and Wickramasinghe (1976), which is two times that value does not seem to be very realistic.
The average particle size $< N >$, e.g. the number of monomers per grain, defined by the ratio of the moments of the dust distribution function K_3/K_0, achieved in the nova wind is only very small: $< N > \approx 100$. The kinetical approaches of investigating the characteristics of the dust formation process in novae (e.g. [Clayton and Wickramasinghe 1976] , [Bode and Evans 1983b]), however, all suggest that the grains can grow up to very large sizes of $a \approx 3\mu m$. The chemical based calculations of RW also seem to result in a small population of large grains[37]. But already Draine (1979) has argued that the final grain size is limited to $a \approx 0.01\mu m$[38], mainly due to the effect of monomer depletion. The total consumption of all available carbon condensables also is the main reason for the small grain size in our model calculations (see Tab. (4.5.1)).
The degree of condensation $f_{\rm cond}$ quickly attains its maximum value $f_{\rm cond} = 1$. One third of all the carbon has condensed into grains, whereas the remainder is bound in CO and CO_2, in the later phases also as atomic carbon.
Unfortunately there is not sufficient observational information available to judge about the final grain size. One more detailed analysis of the infrared flux distribution in Nova Aquilae 1982 [Snijders *et al.* 1987] has shown, that the 2500Åfeature observed can be fitted well on the assumption of the presence of small soot particles with $r < 0.013\mu m$. One should bear in mind that the determination of this grain size is not straightforward[39], as it depends on

- the existence of observational data obtained from simultaneous observations in two or more wavelength bands,
- the accurate knowledge of the flux distribution emerging from the nova photosphere,
- interstellar extinction in the direction of the nova, and
- the shell geometry.

Therefore the derived mean grain sizes should be taken with some care.
The fact of an effective dust formation, however, is consistent with the observed depletion of atomic carbon from the gas phase [Snijders *et al.* 1987] .

[37]In fact RW only got a small population of small hydrocarbon clusters (C_8H_6 is the largest one) and afterwards extrapolated the for the final grain size also on the basis of a simple kinetic model.
[38]This is also confirmed by the theoretical study of Johnson et al. (1987) .
[39]Additionally the deduction of a reasonable mean size of the grains depends on the assumption of a grain size distribution which has a pronounced peak in the vicinity of the mean size. Otherwise, if a flat grain size distribution is present, the extinction peak will be smeared out.

Although the conditions for the beginning of condensation are matched very early after the expansion has begun, therefore the reactions are proceeding in a density regime of $\approx 10^{10} cm^{-3}$, the hydrodynamic velocity is large and therefore the timescales for the growth of small particles $\tau_{\rm gr} = 1.3 \times 10^6\, s$ is comparable to the expansion timescale $\tau_{\rm ex} = 1.2 \times 10^6\, s$. In spite of this unpleasant environment nearly all the free carbon available in the relevant period, which means all carbon not locked in CO, which is 30% of all the carbon, mainly present in the molecules C_2H, CO_2 and atomic carbon, is involved in the formation of small grains. The evolution of these small particles to the regime of macroscopic grains is not effective and the total dust formation process stops when the ionization of hydrogen occurs and the shell temperature flashes from 800K to about 4000K, thus suppressing any further nucleation process.
The formation of grains also results in an increase of the optical depth for the radiation emerging from the nova photosphere. Assuming that the dust grains are small compared to the wavelength of interest[40] one can apply the Mie–theory to derive the extinction coefficient $\kappa_{\rm ext}$ for the grains [Gail *et al.* 1984] :

$$\kappa_{\rm ext} = \frac{8\pi^2 r_0^3}{\lambda} Im \left\{ \frac{m^2-1}{m^2+2} \right\} \cdot K_3 \tag{4.26}$$

where r_0 is the hypothetical monomer radius and m is the complex index of refraction. Inserting the results of our model calculations for the number of condensed monomers K_3 and using the computational results of Maron (1989) and Mathis and Whippen (1989) for the index of refraction of amorphous carbon at 1μ, we get an optical depth of

$$\tau_{1\mu} \approx 5 \tag{4.27}$$

For the thickness of the dust forming region we estimated a more or less canonical value of 10^{12}cm.
The optical depth of the dust has been determined empirically for several novae by taking the ratio of the maximum values for the infrared and the optical luminosity. However, this also gives only an approximate impression of the efficiency with which nucleation and growth of grains have proceeded in the respective nova and thus allows only to distinguish between novae with optically thin and novae with optically thick dust shells. Consequently the presented model has to be classified in the category of the optical thick cases.
All the recent novae which have been identified as novae with massive dust formation show evidence for the presence of carbon, some of them additionally showing features typical for different kinds of silicates (e.g. V1370 Aql (1982)) or even hydrocarbons (e.g. V842 Cen (1986)).

[40]This condition is completely matched in the model discussed here.

Condensation radius	r_{cond}	6×10^{13}cm
Condensation time	t_{cond}	22 days
Condensation temperature	T_{cond}	1500K
Mean grain size	r_{grain}	≈ 100
Degree of condensation	f_{cond}	1
Growth timescale	τ_{gr}	1.3×10^{6}s
Optical depth at 1μ	$\tau_{1\mu}$	5
Mass of dust	M_{dust}	$2.1\times10^{-7}M_{\odot}$

Table 4.6: Quantities of carbon dust formation derived for the standard C–rich model (I).

4.5.2 Other Types of Nova Dust

In view of the existing observational material reporting infrared features significant for the presence of silicates (see e.g. Gehrz (1990)) and the proposition of Lewis and Ney (1979) of and iron compound to be the first condensate in nova envelopes we have incorporated the possibility of homogeneous homomolecular condensation of SiO as well as Fe by introducing the moment equations for these dust types in the differential equation system.
Siliconmonoxide attained a relatively high concentration of $X_{SiO} = 10^{-4}$ and thus, besides the silicon ion, is the dominating specie in the silicon chemistry. Nucleation of SiO and subsequent growth, however, does not proceed. The supersaturation ratio of SiO always remains substantially smaller than unity, which is mainly due to the gas temperature being not low enough. The same reason for the failure of SiO based dust formation can be addressed in the case of the oxygen–rich models which have been calculated.

The nucleation of iron of course is not favoured by the chemical situation present in the model. Most of the iron exists as single ionized ions and only one percent of the atoms remain neutral. Therefore the formation of iron clusters is prohibited by the nova radiation field.

4.6 Comparison with other Nova Model Calculations

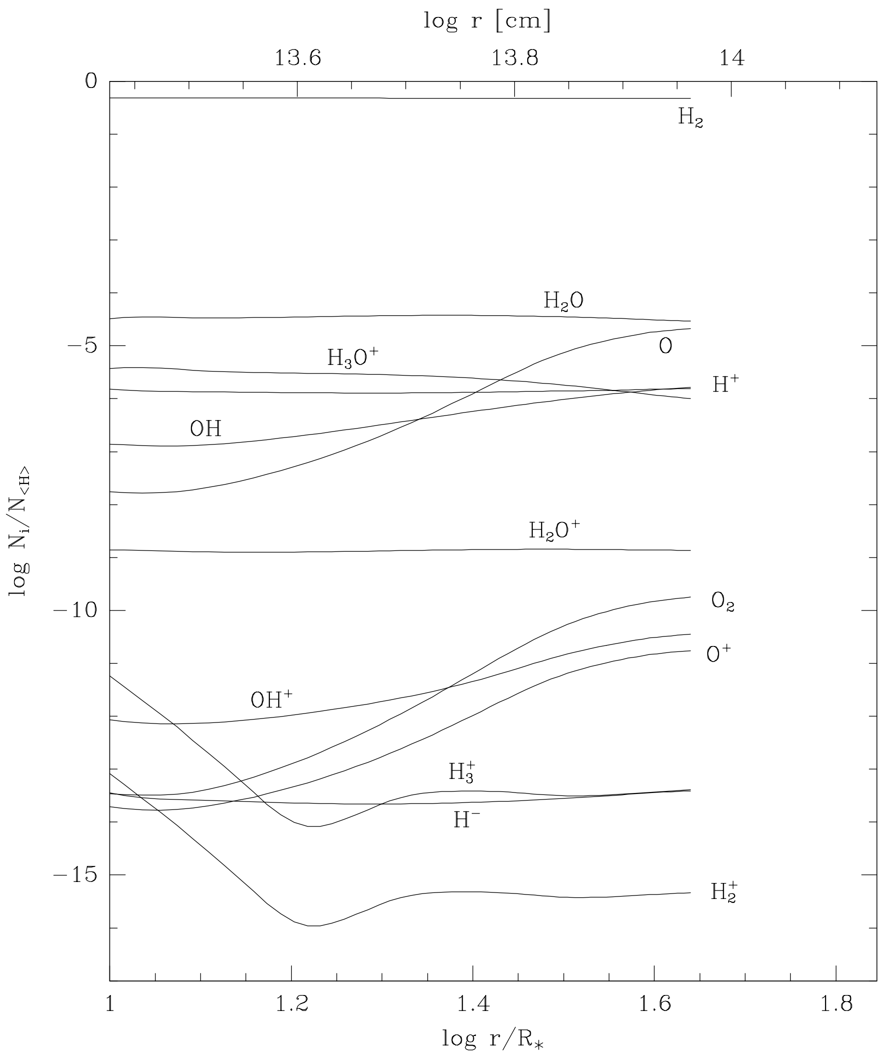

Figure 4.21: Logarithmic concentrations of the neutral OH–species, normalized to the number of H-atoms over a logarithmic radius axis scaled with the stellar radius for a model with an oxygen–rich chemistry. The radial course of the concentrations is only presented for the pre–ionization zone (t≤40 days).

A sequence of chemical model calculations based on parameter sets different from the standard model discussed in the previous sections have been performed. These models have not been analyzed in detail up to now and also the number of models calculated is not sufficient for a profound study of the multi–dimensional parameter space in which the dust formation of nova shells takes place. This work will be postponed and will be the task of the future.

Nevertheless some general statements arising from the calculations can be given. Neither a reduction of the outflow velocity nor an increase of the density in the nova shell did cause any remedy in the matter of the modelling of dust formation. All this did not change the high H/H_2 ratio of these models responsible for the significant differences in the temporal evolution of the chemistry (see next section). Calculations of O–rich envelope outflows also fail in producing dust (for a possible remedy see Sect. (4.5)).

4.7 Effects of Chemical Network Selection

In the framework of the numerical and chemical test calculations we have checked the results derived with our "standard" model (henceforth called model (I)) described in this chapter to a nova model (henceforth called model (II)) having the same parameters (see Tab. (4.3)) but using only a reduced data set for the chemical species and their reactions.
In model (II) the following species were not implemented:

HeH^+
C^-, $C_3H_3^+$, C_3N^+
CH_4N^+, C_2NH^+, $C_2H_3N^+$
HC_3N, C_3HN^+, $C_3H_2N^+$, CH_3CN
O^-, OH^-, O_2H^+, CH_3OH, CH_3CO^+, C_2HO^+, $C_2H_2O^+$
OCN, HNO, NO_2^+
SiH, SiH^+, SiH_2^+, SiC, SiC^+, $CHSi^+$, CH_2Si^+
SiO, SiO^+, SiO_2, $SiOH^+$
S^-, S_2
HS, HS^+, H_2S, H_2S^+, H_3S^+
CS, CS^+, HCS^+, H_2CS, H_2CS^+, H_3CS^+
NS, NS^+, HNS^+
SO, SO^+, SO_2, HSO^+, OCS, $HOCS^+$
SiS, SiS^+, $HSiS^+$

The whole silicon and sulfur chemistry has been omitted as well as the more complex carbon–nitrogen compounds. This way of delimiting the number of chemical species was motivated by the common prejudices coming from the study of equilibrium chemistry:

> We are studying the carbon–chemistry in the nova envelope. Therefore oxygen–bearing molecules will be of minor importance[41].

> Nitrogen is locked up in the unreactive N_2 molecule. Consequently the including of other N–bearing molecules is superfluous.

[41] Based on the argument, that CO totally blocks oxygen.

In a carbon dominated environment the silicon and sulfur containing molecules are believed to play only a minor role.

A more practical reason for this reflection lies in the strong dependence of the necessary computer time to solve the differential equation system for the considered reaction network on the number of species N_{spec} ($t \sim N_{spec}^3$) and the number of reactions N_{reac} ($t \sim N_{reac}^2$). On behalf of the above considerations we were able to reduce the number of species and the number of reactions nearly by a factor of two. One of the most obvious and also most decisive differences in the comparison of the chemical abundances is the fact that atomic and molecular hydrogen just change their roles in the first phase. While in model (I) the concentration of H_2 is 0.47 and the concentration of atomic H is 0.05, in model (II) $X_{\rm H}$ is 0.99 and $X_{\rm H_2}$ is 0.0045.

Table 4.7: Comparison of the chemical abundances for the standard model discussed (model (I)) and a model with the same parameters but a reduced set of species in the chemical network (model (II)). Abundances are compared for the early (t=15days) and the late phase (t=85days) of the nova expansion.

	early phase		late phase	
species	model (I)	model (II)	model (I)	model (II)
H	$5.61 \cdot 10^{-02}$	0.99	0.99	0.99
H^+	$8.50 \cdot 10^{-08}$	$1.00 \cdot 10^{-03}$	$4.69 \cdot 10^{-04}$	$3.61 \cdot 10^{-04}$
H^-	$4.53 \cdot 10^{-15}$	$1.79 \cdot 10^{-08}$	$1.72 \cdot 10^{-05}$	$1.56 \cdot 10^{-09}$
H_2	$4.77 \cdot 10^{-01}$	$4.54 \cdot 10^{-03}$	$1.72 \cdot 10^{-05}$	$1.13 \cdot 10^{-05}$
H_2^+	$8.14 \cdot 10^{-15}$	$6.25 \cdot 10^{-10}$	$2.76 \cdot 10^{-13}$	$5.03 \cdot 10^{-14}$
H_3^+	$7.33 \cdot 10^{-13}$	$6.97 \cdot 10^{-11}$	$1.27 \cdot 10^{-19}$	$1.52 \cdot 10^{-20}$
He	$2.00 \cdot 10^{-01}$	$2.00 \cdot 10^{-01}$	$2.00 \cdot 10^{-01}$	$2.00 \cdot 10^{-01}$
He^+	$6.67 \cdot 10^{-18}$	$< 10^{-34}$	$2.80 \cdot 10^{-16}$	$< 10^{-34}$
C	$1.81 \cdot 10^{-06}$	$1.47 \cdot 10^{-03}$	$5.08 \cdot 10^{-06}$	$1.46 \cdot 10^{-03}$
C^+	$2.11 \cdot 10^{-11}$	$5.77 \cdot 10^{-06}$	$3.32 \cdot 10^{-07}$	$1.33 \cdot 10^{-05}$
C_2	$2.45 \cdot 10^{-07}$	$3.64 \cdot 10^{-10}$	$1.55 \cdot 10^{-14}$	$2.65 \cdot 10^{-13}$
C_2^+	$2.20 \cdot 10^{-10}$	$1.87 \cdot 10^{-10}$	$3.68 \cdot 10^{-15}$	$1.99 \cdot 10^{-12}$
CH	$1.02 \cdot 10^{-08}$	$1.71 \cdot 10^{-07}$	$6.83 \cdot 10^{-12}$	$3.73 \cdot 10^{-11}$
CH_2	$1.46 \cdot 10^{-09}$	$7.56 \cdot 10^{-11}$	$1.25 \cdot 10^{-18}$	$2.31 \cdot 10^{-18}$
CH_3	$3.46 \cdot 10^{-09}$	$4.27 \cdot 10^{-13}$	$7.29 \cdot 10^{-26}$	$6.13 \cdot 10^{-26}$
CH_4	$3.23 \cdot 10^{-08}$	$1.73 \cdot 10^{-15}$	$3.77 \cdot 10^{-24}$	$< 10^{-34}$
CH^+	$4.46 \cdot 10^{-13}$	$6.53 \cdot 10^{-09}$	$1.12 \cdot 10^{-10}$	$3.46 \cdot 10^{-10}$
CH_2^+	$2.34 \cdot 10^{-12}$	$1.37 \cdot 10^{-10}$	$3.43 \cdot 10^{-17}$	$6.97 \cdot 10^{-17}$
CH_3^+	$1.01 \cdot 10^{-08}$	$3.49 \cdot 10^{-12}$	$3.77 \cdot 10^{-24}$	$5.04 \cdot 10^{-24}$
CH_4^+	$2.78 \cdot 10^{-13}$	$6.52 \cdot 10^{-18}$	$1.70 \cdot 10^{-34}$	$< 10^{-34}$
C_2H	$8.97 \cdot 10^{-04}$	$4.41 \cdot 10^{-12}$	$5.10 \cdot 10^{-20}$	$3.79 \cdot 10^{-19}$
C_2H_2	$3.09 \cdot 10^{-06}$	$1.35 \cdot 10^{-16}$	$1.39 \cdot 10^{-27}$	$1.05 \cdot 10^{-29}$
$C_2H_2^+$	$7.06 \cdot 10^{-06}$	$1.97 \cdot 10^{-13}$	$2.03 \cdot 10^{-25}$	$5.03 \cdot 10^{-26}$

continued on next page

continued from previous page				
	early phase		late phase	
species	model (I)	model (II)	model (I)	model (II)
$C_2H_3^+$	$1.29{\cdot}10^{-10}$	$5.28{\cdot}10^{-20}$	$1.57{\cdot}10^{-34}$	$6.52{\cdot}10^{-34}$
N	$6.07{\cdot}10^{-10}$	$4.37{\cdot}10^{-06}$	$1.57{\cdot}10^{-10}$	$4.59{\cdot}10^{-05}$
N^+	$3.30{\cdot}10^{-21}$	$7.26{\cdot}10^{-21}$	$3.18{\cdot}10^{-17}$	$9.28{\cdot}10^{-20}$
N_2	$2.08{\cdot}10^{-04}$	$2.10{\cdot}10^{-04}$	$1.31{\cdot}10^{-04}$	$1.89{\cdot}10^{-04}$
NH	$2.88{\cdot}10^{-11}$	$1.54{\cdot}10^{-09}$	$4.97{\cdot}10^{-10}$	$6.41{\cdot}10^{-11}$
NH_2	$8.75{\cdot}10^{-12}$	$7.46{\cdot}10^{-13}$	$6.45{\cdot}10^{-17}$	$3.44{\cdot}10^{-18}$
NH_3	$3.52{\cdot}10^{-11}$	$2.12{\cdot}10^{-15}$	$5.63{\cdot}10^{-25}$	$1.40{\cdot}10^{-26}$
NH_4^+	$2.35{\cdot}10^{-09}$	$1.45{\cdot}10^{-20}$	$3.91{\cdot}10^{-27}$	$1.15{\cdot}10^{-28}$
CN	$3.71{\cdot}10^{-09}$	$3.58{\cdot}10^{-08}$	$9.97{\cdot}10^{-15}$	$2.04{\cdot}10^{-14}$
HCN	$1.12{\cdot}10^{-07}$	$4.46{\cdot}10^{-08}$	$1.12{\cdot}10^{-19}$	$6.90{\cdot}10^{-20}$
HCN^+	$8.87{\cdot}10^{-18}$	$9.73{\cdot}10^{-15}$	$7.16{\cdot}10^{-18}$	$4.43{\cdot}10^{-18}$
H_2CN^+	$2.59{\cdot}10^{-06}$	$3.55{\cdot}10^{-16}$	$1.34{\cdot}10^{-23}$	$5.91{\cdot}10^{-21}$
O	$4.22{\cdot}10^{-08}$	$1.09{\cdot}10^{-07}$	$3.54{\cdot}10^{-04}$	$5.21{\cdot}10^{-08}$
O^+	$2.73{\cdot}10^{-15}$	$9.62{\cdot}10^{-11}$	$1.56{\cdot}10^{-07}$	$1.71{\cdot}10^{-11}$
O_2	$2.39{\cdot}10^{-13}$	$3.94{\cdot}10^{-17}$	$2.02{\cdot}10^{-14}$	$1.99{\cdot}10^{-19}$
OH	$4.29{\cdot}10^{-07}$	$7.76{\cdot}10^{-10}$	$1.70{\cdot}10^{-11}$	$8.15{\cdot}10^{-14}$
H_2O	$1.32{\cdot}10^{-04}$	$7.59{\cdot}10^{-12}$	$7.43{\cdot}10^{-17}$	$2.13{\cdot}10^{-19}$
H_3O^+	$4.77{\cdot}10^{-05}$	$1.02{\cdot}10^{-14}$	$3.11{\cdot}10^{-18}$	$1.35{\cdot}10^{-21}$
CO	$2.94{\cdot}10^{-03}$	$3.38{\cdot}10^{-03}$	$3.02{\cdot}10^{-03}$	$3.38{\cdot}10^{-03}$
CO_2	$2.89{\cdot}10^{-05}$	$5.95{\cdot}10^{-13}$	$1.76{\cdot}10^{-12}$	$1.83{\cdot}10^{-16}$
HCO^+	$4.28{\cdot}10^{-08}$	$1.15{\cdot}10^{-11}$	$1.11{\cdot}10^{-13}$	$5.12{\cdot}10^{-14}$
H_3CO^+	$6.05{\cdot}10^{-09}$	$6.21{\cdot}10^{-21}$	$2.85{\cdot}10^{-27}$	$2.91{\cdot}10^{-30}$
Fe	$1.39{\cdot}10^{-07}$	$1.54{\cdot}10^{-08}$	$3.21{\cdot}10^{-10}$	$6.37{\cdot}10^{-11}$
Fe^+	$3.97{\cdot}10^{-05}$	$3.98{\cdot}10^{-05}$	$3.91{\cdot}10^{-05}$	$3.98{\cdot}10^{-05}$
Si	$1.83{\cdot}10^{-06}$	$1.02{\cdot}10^{-06}$	$1.67{\cdot}10^{-11}$	$1.04{\cdot}10^{-11}$
Si^+	$1.18{\cdot}10^{-04}$	$3.30{\cdot}10^{-04}$	$3.31{\cdot}10^{-04}$	$3.31{\cdot}10^{-04}$
Mg	$1.76{\cdot}10^{-07}$	$2.29{\cdot}10^{-07}$	$2.75{\cdot}10^{-09}$	$2.19{\cdot}10^{-09}$
Mg^+	$3.14{\cdot}10^{-05}$	$3.14{\cdot}10^{-05}$	$3.16{\cdot}10^{-05}$	$3.16{\cdot}10^{-05}$
S	$4.41{\cdot}10^{-10}$	$3.32{\cdot}10^{-08}$	$5.01{\cdot}10^{-12}$	$1.83{\cdot}10^{-12}$
S^+	$1.51{\cdot}10^{-09}$	$1.58{\cdot}10^{-05}$	$1.58{\cdot}10^{-05}$	$1.58{\cdot}10^{-05}$
Na	$6.70{\cdot}10^{-13}$	$1.54{\cdot}10^{-09}$	$1.26{\cdot}10^{-12}$	$7.95{\cdot}10^{-13}$
Na^+	$1.78{\cdot}10^{-06}$	$1.77{\cdot}10^{-06}$	$1.78{\cdot}10^{-06}$	$1.77{\cdot}10^{-06}$

Thus a lot more free atomic hydrogen is available and can enter into fast ion–neutral reactions. One typical example is the charge exchange reaction of carbonmonoxide with hydrogen

$$CO^+ \quad + H \quad \Longrightarrow CO \quad + H^+ \tag{111}$$

and its reverse, which govern the CO, CO^+ ratio.

A second and more global consequence of the higher amount of atomic hydrogen present is that the incident UV photons, to which hydrogen is exposed, efficiently ionize those H–atoms which are in the second excited state above the ground level due to radiative excitation. This, in the first phase, by far is the most dominant energy gain for the gas and one straight consequence is, that the outflowing gas in model (II) cannot cool down to a gas temperature below 1000K, but stays hot at a temperature of about 3000K.
The close coupling of the temperature to the concentration of atomic hydrogen has an important feedback for the entire chemistry and especially for the hydrogen concentration itself: A higher amount of H–atoms simultaneously leads to more H–atoms which are in an excited state, subjected to photoionization, which will cause a higher energy input into the gas and therefore a higher temperature will be adjusted, and this in turn creates favourable conditions for a higher concentration of atomic hydrogen.
Without any exaggeration one is forced to acknowledge that the incorporation of the heating– and cooling processes in the model calculations is an indispensible prerequisite for the chemical modelling.

It is evident that the characteristics of the chemistry at the higher temperature are completely changed with respect to model (I). Analyzing the reduction of the H_2 concentration one must remember that on one hand the most efficient H_2 formation paths in model (I) did involve the silicon bearing species SiH_2^+ and SiH^+, which have been omitted in the reduced species–set of model (II), but on the other hand the concentration of these ions also would be lower under the influence of a high temperature and an increased number of free electrons present.
A more obvious fact is the more complete ability of CO to hinder the oxygen from the participation in the chemical reactions. Therefore the neutral exchange route

$$\mathrm{H} \qquad + \mathrm{H_2O} \qquad \Longrightarrow \mathrm{OH} \qquad + \mathrm{H_2} \tag{112}$$

essentially contributing to the H_2 formation in model (I), has lost its significance. Besides CO and N_2 whose role as blocking species is much more pronounced in the temperature regime of model (II), atoms and ions are dominating. The carbon atom, for example, is the second most abundant species in the complete carbon chemistry and the most abundant molecule, CH, is by four orders of magnitude lower in concentration. It is involved in the fast neutral hydrogen abstraction reaction:

$$\mathrm{C} \qquad + \mathrm{H_2} \qquad \Longrightarrow \mathrm{CH} \qquad + \mathrm{H} \tag{113}$$

which is one of the controlling mechanisms of the H/H_2 ratio[42]. All other carbon bearing molecules as C_2H, C_2H_2 and CO_2, which have revealed the carbon–chemistry in model (I) in the first phase, here they are of no importance.
The development of the nitrogen bearing species, which are already not in the focal point of our attention, for the most part is determined by the N_2 molecule and

[42]Reaction(113) is by one order of magnitude the fastest gain and loss reaction for H and H_2.

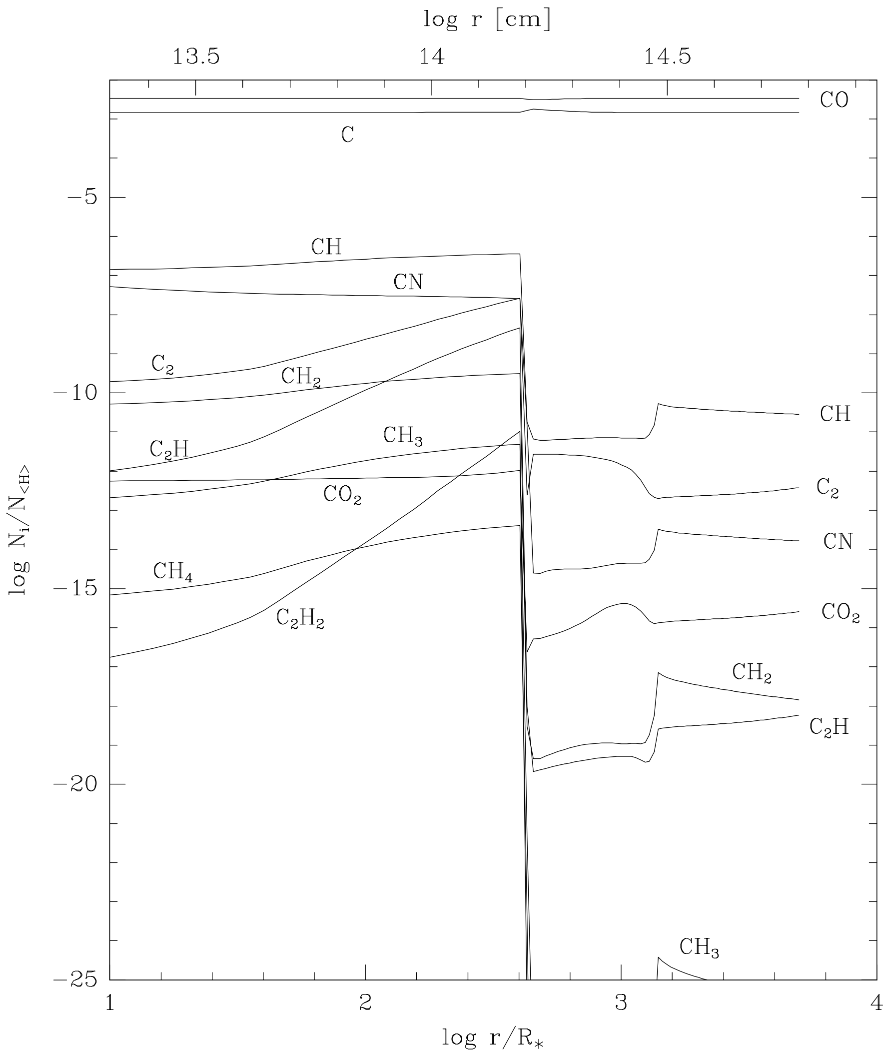

Figure 4.22: Logarithmic concentrations of the neutral C-bearing species, normalized to the number of H-atoms over a logarithmic radius axis scaled with the stellar radius for a model with a reduced set of chemical species (model (II)).

---

atomic nitrogen. While the molecular nitrogen does not change its abundance all over the whole radius range, the role of the atomic nitrogen is reinforced in the second phase.

Another important conclusion which can be drawn is that the specific moment during the time evolution of the nova envelope when the hydrogen is ionized by photoionization of those atoms which are in an excited state, does not depend on the chemical model used for the calculation. Thus the general, two–phase structure of the time evolution of the chemistry is preserved.
It must be emphasized that dust formation, one major result in model (I) and

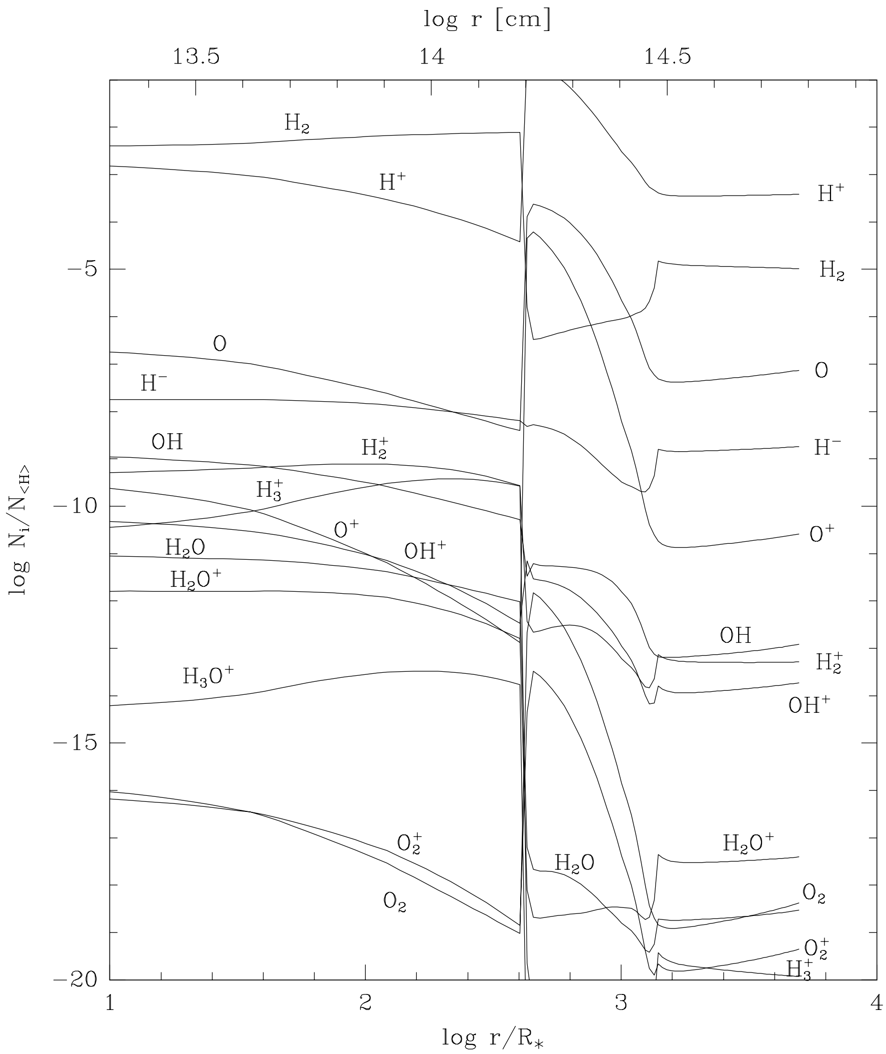

Figure 4.23: Logarithmic concentrations of the O-H species, normalized to the number of H-atoms over a logarithmic radius axis scaled with the stellar radius for a model with a reduced set of chemical species.

---

the process we are most interested in, cannot proceed under the conditions the chemistry adjusts to, on the basis of the reduced chemical network of model (II). The temperature of the gas is too high to allow for the onset of nucleation, although the number of monomers theoretically available (mainly atomic carbon) to participate in grain formation would be quite sufficient.

4.8 Conclusions

In the preceding chapter we have discussed the results for the modelling of the chemistry in the expanding shells of classical novae. Our investigation was mainly concerned with the chemical processes occuring before and during the epoch of dust formation to clarify the chemical conditions in the envelope which are favourable to allow for the onset of effective condensation processes. Two main characteristics of the classical nova outburst are the high expansion velocity of the gas and the increase in time of the strength of the UV radiation field. Obviously every promising approach of theoretical modelling must account for the important influence of the radiation field on the outflowing gas.
The present calculations therefore use the photon fluxes derived from non–LTE radiation transfer models of nova photospheres [Hauschildt 1991] as input radiation field at the inner boundary of the envelope. Furthermore the model accounts for absorption by atoms and molecules in the gas and thus enables us to derive the frequency dependent optical depth necessary to recalculate the actual rates for photoionization and photodissoziation for every time–step. In addition, the spontaneous and the induced emission of hydrogen atoms has been incorporated. The hydrogen atom therefore has been treated in a 3–level approximation including the transitions involving the continuum state.
The energy balance of the gas was determined by means of the calculation of the heating and cooling processes comprising ionization, recombination, emission of forbidden line radiation of OI, OII, CII, NII, SII and SiII, free–free radiation and molecular cooling by CO, OH, CH and H_2O.
Using an elaborate chemical model, where 145 species connected by about 1900 reactions (see Appendix), we were able to go deeply into the time evolution of the nova chemistry from the early phases of the outburst up to the time when dust formation should have occured, if possible. Nucleation and growth of dust grains has been described by homogeneous heteromolecular nucleation theory and the corresponding moment equations are solved simultaneously with the chemical network system.
Most of the nova outbursts are occuring on C/O–white dwarfs (about 75%), showing significant overabundances of the CNO elements. Infrared observations carried out during the last two decades also reveal that, based on the identifications of the measured infrared features, carbon is a major dust component in the envelopes of these novae. In view of these observational constraints, although our model also covers oxygen rich situations and the formation of silicate dust, we concentrate on the carbon–rich chemistry and its detailed analysis.

Following the radial course of a typical carbon–rich nova model obviously four distinct epochs of different stages of chemical evolution can be distinguished:

1. complex chemistry in a cooling and effectively shielded outflow,
2. nucleation and growth of small carbon solids and the simultaneous consump-

tion of the monomers,

3. sudden ionization of previously excited hydrogen atoms, coupled with an instantaneous rise in the gas temperature which is then followed by a chemical relaxation phase,

4. epoch of less complex, ion and radical dominated high temperature chemistry.

The individual appearance of the radial distribution of the chemical concentrations, especially the time of occurence of the hydrogen ionization and the associated dramatic alteration of the species' concentration, depends on a variety of nova parameters, but not on the choice of the chemical model, although other features are deeply changed due to the selection of another chemical network.
In the following we want to summarise briefly the main conclusions of this chapter:

I. The time evolution of the nova chemistry is closely connected with the local energy budget determining the temperature in the envelope and as a result the gross outlook of the temporal course of the densities of the chemical species.

II. The balance of heating and cooling processes is governed by the energy input through photoionization of excited hydrogen atoms. The level population of hydrogen has been calculated by solving the corresponding rate equations for the relevant processes of radiative and collisional ionization, radiative recombination, radiative and collisional excitation and de–excitation and induced emission. The individual timing of the onset of massive hydrogen ionization is determined by the intimate coupling of the time evolution of the nova radiation field, the optical depth, and the chemistry.

III. The temperature structure is determined by an exponential cooling in the beginning, when the material is optically thick and no efficient heating mechanism can work. Temperatures down to 700K create favourable conditions for a complex chemistry to proceed and in turn for dust formation to occur. In the second phase the temperature has grown to 4,000K and is slowly but steadily increasing, due to the growing input of energy in the UV wavelength region.

IV. The evolution of the ionization of the elements shows that Mg, Fe, Na and Si are quickly ionized ($\mathrm{f_{ion}} = 1$) on a timescale of less than a day. For sulfur $f_{\rm ion} = 1$ is realized in about ten times that period. The ionization of hydrogen is governed by photoionizations of excited H atoms and the ionization state of oxygen is intimately coupled through charge–exchange to that of hydrogen. Carbon first displays an increasing ionization due to consumption of neutral carbon in the formation of dust, then the ionization is dropping to very low values due to the release of atomic carbon from dissociated molecules.
These ionization characteristics generally confirm the results of the model calculations in Chap. (2). Furthermore, the influence of the chemistry on the ionization balance and the central role of the refined treatment of the hydrogen ionization has been demonstrated.

V. The formation of carbon dust has been successfully modelled involving homogeneous heteromolecular nucleation theory. The main molecular contributions to the carbon grains are supplied by the C_2H radical (99%). Other carbon bearing species like acetylene do not significantly contribute. In this way the C_2 bottleneck which would occur in homogeneous homomolecular nucleation is avoided, otherwise the efffiviency of dust formation would be drastically reduced.
The mean grain size has been calculated to be < 10Å in any case; further growth is limited by monomer depletion rather than by the destructive influence of the UV–field. The consumption of the available molecular and atomic material is almost complete and one third of the total amount of carbon has condensed, thus a total dust mass of $2\times10^{-7}M_\odot$ is injected into the ISM. This is in agreement with the value adapted by Gehrz (1989) for the mean dust injection rate of novae.
The modelling of the formation of silicate type– or iron grains have not yield positive results up to now. Although the concentration of the SiO molecule, the key–molecule to silicate formation, achieved high values, the corresponding temperature in the shell does not allow for the onset of dust formation.
On the other hand there is observational evidence for silicate dust formation in nova shells and a possible way out of this misagreement would be a revised treatment of the process of dust growth. The formalism for the growth of composite dust grains developed by Dominik (1992) seems to offer an attractive possibility.

VI. The role of molecular hydrogen has been worked out. High values for the H_2 concentration were achieved during the early chemical evolution due to effective reaction paths involving silicon bearing species.

VII. The dominance of the CO molecule is not decisive. Although CO is the most abundant carbon bearing specie, the excess of carbon to oxygen in the model allows for a rich carbon chemistry, where the atomic carbon or the carbon ion only play a minor role.
The C_2H radical is by one order of magnitude the most abundant molecule after CO, followed by CO_2 and C_2H_2. Compared to chemical equilibrium calculations for the carbon chemistry large deviations from chemical equilibrium are achieved.
The formation of complex hydrocarbons during the first epoch of may be also a possible way of dust formation, especially in view of the favourable conditions of a high H_2 density, a low temperature and a substantial amount of C_2H_2 present.

VIII. The silicon chemistry results in a high fraction of SiO molecules coexisting with nearly the same amount of ionized silicon atoms. But also ionized silicon bearing molecules as $SiOH^+$ and $CHSi^+$ are of a high abundance and play a vital role in a number of ion–neutral conversion paths.

IX. The sulfur chemistry is characterized by high abundances of the neutral molecules CS, SiS and HS.

X. Chemical calculations using a reduced set of chemical rate equations, where most of the silicon and sulfur bearing species as well as the more complex carbon–nitrogen components have been omitted reveal a totally different picture of the chemical evolution: During the entire period under consideration (10 days$< t <$100 days) the chemistry proceeds under high temperature conditions and dust formation is completely supressed.

Concluding Remarks

In this thesis the chemistry and dust formation in the outflows of novae and late–type M stars has been investigated.

Oxygen–rich giants are a main source of the mass return from the stars to the interstellar matter. Therefore the detailed study of the circumstellar shells of these objects is providing significant information about the late stages of stellar evolution and the chemical reprocessing of the interstellar medium.
In Chap. (3) the non–LTE chemistry in the inner, dust forming zones of the late–type supergiant αOri is studied by solving the time dependent chemical rate equations in an outflowing element of gas. A special feature of this object is the presence of a chromosphere emitting substantial amounts of ultraviolet radiation. Thus photoprocesses cause significant departures of the derived chemical concentrations from chemical equilibrium. Nevertheless, it is shown that the CO molecule is blocking the available carbon to a large extent. However, the blocking is not complete. Under the dissociative influence of the UV field, the partial pressure of free carbon achieves nearly one third of the partial pressure of CO. This, in principle, opens the possibility of a participation of the carbon in the process of nucleation and growth of dust particles. If carbon as well as silicon can contribute to grain formation, an extended concept of dust formation, allowing for the growth of composite grains with variable, non–stoichiometric composition [Dominik 1992], will be an attractive alternative, which should be explored.
The present model calculations show that even in the presence of chromospheric UV radiation nucleation and reasonable growth of grains based on SiO alone is possible. The small, but non–negligible rates in both, nucleation and growth, are in agreement with the observations of the dust shell of αOri.
Since observational information about the inner zones of αOri is not available, a comparison of our results concerning the radial course of concentrations is unfortunately not possible. For this reason a chemical model can only be linked to observations if the calculation follows the evolution of the chemistry from the innermost parts of the wind, where molecules are primarily formed and dust formation occurs, to the outer observable zones. Thereby the considered gas element passes the region in which the kinetic reaction rates decrease and the concentrations freeze out on certain levels. These levels characteristically depend on the chemical model used. At the outer edge of the envelope the interstellar UV field penetrates into the shell and totally dissociates the molecules at certain distances from the central source[43].

[43] As a further complication, such calculations have to account for the combined effects of mutual– and self–shielding and should also take into account the role of the dust.

On one hand this distance will be determined by the amounts of molecules produced in the inner shell, on the other hand this quantity can be derived from observations.

The second part of this thesis is devoted to the study of classical novae, with special emphasis on the topics of ionization, chemistry, and dust formation in their outflowing gaseous shells. The work concerning these subjects is splitted into three parts, each of which is directing its attention on different aspects of the problem.

The first chapter deals with the main properties of classical novae, reviewing the present state of our knowledge about this class of objects. Classical novae are interpreted as a subclass of the cataclysmic variables (CVs), relations existing between the different types of CVs are briefly discussed, giving hints for a possible interchange of different classes of CVs. The nova system is then discussed in terms of the commonly accepted close binary system model and the parameter space of basic quantities, such as orbital periods, component masses and elemental abundances is examined. Attention is also directed to the thermonuclear runaway model, which explains the nova event as a nuclear explosion occuring in an accreted hydrogen shell on top of a degenerate white dwarf. This model naturally accounts for the observed anomalous isotopic ratios and the large overabundances of ^{22}Na and ^{26}Al in nova shells as a result of the nuclear burning process. These anomalies are an individual fingerprint which is preserved by the subsequent trapping of these atoms in dust particles injected into the ISM. Later these distinctive isotopes (or their decay products) can be recovered in primitive solar system bodies, which allows for tracing back from solar system dust to the original birth place of the grains.

Dust formation of very different kinds has been observed in many novae. Amorphous carbon as well as silicates, siliconcarbide and also PAHs are reported to be identified in the expanding outflows. However, an even larger fraction of novae seem to display no sign of dust formation in their lightcurves. One key to the understanding of *why and under what circumstances the nucleation and growth of small solids can occur* surely is the investigation of the time dependent ionization structure. The second chapter is dedicated to this problem, presenting studies of the time evolution of nova shell ionization based on a generalisation of the methods first used by Bosma (1972) for a mixture of the elements H, He, C, N, O, Mg, Fe, Na, Si and S.
It turns out that:
For a timescale sufficient for the onset of dust formation, carbon is not completely ionized throughout the shell.
The heavy elements are quickly ionized, thus an efficient chemistry can develop and molecules serving as nucleating species can form.
This result is confirmed by the fact that the gas temperature, determined by balancing the relevant heating and cooling processes for the gas, gets low enough to favour high supersaturation ratios and, thereby, effective dust production.
A replacement of the blackbody radiation field by a radiation field resulting from radiative transfer calculations supports the previous results. Significant lower values of carbon ionization during the first 50 days of the outburst evolution were achieved.
The enhancement of the CNO elements as it is commonly observed in nova outflows

did not remarkably change the ionization characteristics.

In the last part of the thesis the investigations are focussed on the study of the chemical processes in nova envelopes, determining the initial conditions for the formation of grains.
Based on the preceding parts of the work this complex problem is attacked with a treatment going beyond previous approaches in some essential points:

- the incorporation of a very complex chemical network accounting for O–rich as well as C–rich situations,
- a refined treatment of the photoprocesses based on a simplified radiation transfer throughout the shell including the absorption of atoms and molecules and the emission of hydrogen, where hydrogen is treated as a 3–level atom with continuum, and
- a calculation of the gas temperature also including the molecular cooling contributions.

As a first result it is demonstrated that in carbon–rich nova shells massive dust formation can occur during the first 30 days of the outburst evolution. Complete consumption of the available carbon material, mainly involving C_2H radicals, leads to a conversion of 30% of the carbon into grains. Thus a total dust mass of $2\times10^{-7}M_\odot$ is injected into the ISM. This is in agreement with the value adapted by Gehrz (1989) for the mean dust injection rate of novae.
However, it remains uncertain in which way the primarily condensed material is processed further during the later stages of the nova outburst. Although grain size reduction is reported [Mitchell *et al.* 1985] for the phases when the photospheric temperature of the central remnant is 100,000K or more, the opposite effect might also be possible. When the degree of ionization increases, the grains can get negatively charged due to the increased number of collisions with free electrons, and particle growth would speed up due to the attractive force between the grain and the positively charged carbon monomers[44].
If hydrogen is completely ionized it can become attached to surface sites of the grain and subsequently energetic photons can excite emission caused by the oscillation of the C–H bonds on the grain surface.
In the earlier phases of nova evolution growth processes due to ionized species also would significantly increase the mean particle size. This could be of special importance in the case of silicate grains, as it has turned out that most of the silicon is already ionized in the earlier phases of the nova expansion.

[44]However, the development of the grain charge in the nova outflow has to be determined in detail by taking into account the collisions of the grain with electrons and ions, the photoeffect, injecting a grain electron to the gas and charge exchange reactions. Investigations of Augustin (1990) referring to the situation of the late–type M supergiant αOri indicate the presence of negatively charged grains even in the case of very strong ultraviolet radiation fields.

As a second major result it has been clarified that the time evolution of the chemistry is mainly determined by the photoionization of excited hydrogen atoms. The energy input by this process governs the heating and cooling balance.
It seems to be appropriate to treat at least the most important heavier atoms in a similar way, although this would cause heavy burden for the model calculations due to their much more complex electronic structure. However, the ionization state of these heavy elements might be changed and thus the initial conditions for nucleation of dust may become worse.
Up to now our model does not incorporate the backaction of the dust on the thermodynamic structure of the envelope. Dust may serve as an important cooling agent and thus may cause deviations from the energy balance as it is presented. Especially the second epoch of high temperature chemistry may change.

In the spectra of two novae (V842 Cen and QV Vul) hydrocarbon emission is reported. At first sight it seems to be unprobable to realize the formation of these polyaromatic species in the hostile environment of a nova. Nevertheless the chemical modelling of Rawlings and Williams (1989) concerning the formation of hydrocarbons in novae, has claimed for enhanced evidence of the existence of hydrocarbons. A shortcoming of this approach surely is the very low abundance of the more complex hydrocarbon molecules, which seems to be hardly sufficient for relevant dust formation. Key parameters of their model are the H_2 abundance and the temperature structure, both have been treated inconsistently. Compared to their model, in our calculations the environmental conditions for the formation of hydrocarbons are much more favourable since the molecular hydrogen abundance is substantially higher (X_{H_2}), and the gas temperature is significantly lower during the first epoch[45]. This clearly demonstrates the necessity of a consistent treatment of hydrogen chemistry and energy balance.
A further extension of the present chemical reaction network by an appropriate set of reactions will enable us to proof the hydrocarbon hypothesis for classical novae.

Silicon carbide is another possible candidate for dust formation possessing two possible identifications in nova events (V1370 Aql and QV Vul). However, molecular SiC is found to be not very abundant according to our model calculations. Therefore the direct formation of pure SiC grains seems to be not very reasonable. A possible solution would be the formation of SiC from *atomic* silicon and carbon on the surface of previously formed small carbon grains. It is, in any case, a matter of fact that SiC has formed in nova outflows. A special feature of the nova TNR is the extensive production of characteristic isotopes, like ^{22}Na. This isotope decays with a half–life of 2.6 years. If such an atom is incorporated in the interior of a newly formed SiC cluster its decay product ^{22}Ne will still be trapped, although neon as a noble gas would never have been bound by a grain. During the injection of the SiC cluster to the interstellar space it retains the neon as a memory about its nova birth site.

[45]The amount of C_2H_2, a key molecule of their reaction sequence, is also raised.

Billion years later the cluster may be discovered as a part of a carbonaceous chondrite or a comet, and a detailed chemical analysis will show: this grain formed in a classical nova.

Die Erkenntnis der Wahrheit ist herrlich, aber als Führerin ist sie so ohnmächtig, daß sie nicht einmal die Berechtigung und den Wert unseres Strebens nach Wahrheit zu begründen vermag.

A. Einstein

Appendix I

Cooling Rates for Collisionally Excited Line Emission

Here the cooling rates due to collisionally excited forbidden line emission as they are used in the model calculations of Chap. (2.5). Atomic data are taken from Aller (1984) .

a) Cooling by OI
The transitions between the excited level $^1\mathrm{D}_2$ and the ground states $^3\mathrm{P}_2$, $^3\mathrm{P}_1$ and $^3\mathrm{P}_0$ are considered. The critical electron density for collisional deexcitation to dominate over radiative transitions is $3.24 \cdot 10^6$ for transitions between $^1\mathrm{D}_2$ and lower levels. The level population in this case is calculated for a two-level model atom. The result for the cooling rate is

$$\begin{aligned} L_{\mathrm{OI}} &= 1.33 \cdot 10^{-13} e^{-22830/T} \\ &\cdot \left(9 + 5e^{-22830/T} + \frac{3.24 \cdot 10^6}{n_e}\right)^{-1} n_{\mathrm{OI}} \,. \end{aligned} \tag{I.1}$$

The cooling rate for the ^{3}P-levels is calculated for a TE level population. The result is

$$\begin{aligned} L_{\mathrm{OI}} &= \left(8.40 \cdot 10^{-18} e^{-228/T} + 2.37 \cdot 10^{-19} e^{-327/T}\right) \\ &\cdot \left(5 + 3e^{-228/T} + e^{-327/T}\right)^{-1} n_{\mathrm{OI}} \,. \end{aligned} \tag{I.2}$$

b) Cooling by OII
The transitions between the lowest exited levels $^2\mathrm{D}_{3/2}$ and $^2\mathrm{D}_{5/2}$ and the $^4\mathrm{S}_{3/2}$ ground state are considered. The cooling rate is calculated for a TE level population. The result is

$$L_{\mathrm{OII}} = 4.70 \cdot 10^{-15}\, e^{-38600/T} \cdot \left(4 + 10e^{-38600/T}\right)^{-1} n_{\mathrm{OII}} \,. \tag{I.3}$$

c) Cooling by NII

The transitions between the excited levels $^1\mathrm{D}_2$ and $^1\mathrm{S}_0$ and the ground states $^3\mathrm{P}_2$, $^3\mathrm{P}_1$ and $^3\mathrm{P}_0$ are considered. The critical electron density for collisional depopulation of the $^1\mathrm{S}_0$ level is $1.75 \cdot 10^7$. The population of this level is calculated in non-TE for a three-level model atom. The population of all other levels is assumed to be in TE.

The result for the cooling rate is

$$L_{\mathrm{NII}} = \left(6.08 \cdot 10^{-14} e^{-22020/T} + 4.08 \cdot 10^{-12} e^{-46910/T} \cdot X\right) \cdot \left(9 + 5e^{-22020/T} + e^{-46910/T} \cdot X\right)^{-1} n_{\mathrm{NII}} . \tag{I.4}$$

with

$$X = \frac{n_e}{n_e + 1.75 \cdot 10^7} . \tag{I.5}$$

Transitions between the ^{3}P-states are not considered since NII is an important cooler only in the HII-region and, then, these low energy transitions are inefficient compared to transition from higher excited levels.

d) Cooling by CII

Only transitions between the $^2\mathrm{P}_{3/2}$ and the $^2\mathrm{P}_{1/2}$ levels are considered. The excited level is assumed to be thermally populated. The cooling rate is

$$L_{\mathrm{CII}} = 1.15 \cdot 10^{-19} e^{-91.3/T} \cdot \left(2 + 4e^{-91.3/T}\right)^{-1} n_{\mathrm{CII}} . \tag{I.6}$$

e) Cooling by SII

Transitions between the levels $^2\mathrm{D}_{3/2}$, $^2\mathrm{D}_{5/2}$, $^2\mathrm{P}_{3/2}$ and $^2\mathrm{P}_{1/2}$ and the ground level $^4\mathrm{S}_{3/2}$ are considered. The levels are assumed to be thermally populated. The cooling rate is

$$L_{\mathrm{SII}} = \left(1.50 \cdot 10^{-14} e^{-21370/T} + 3.33 \cdot 10^{-12} e^{-35330/T}\right) \cdot \left(4 + 10e^{-21370/T} + 6e^{-35330/T}\right)^{-1} n_{\mathrm{SII}} . \tag{I.7}$$

f) Cooling by SiII

Only transitions between the levels $^2\mathrm{P}_{3/2}$ and $^2\mathrm{P}_{1/2}$ are considered. The cooling rate is

$$L_{\mathrm{SiII}} = 4.95 \cdot 10^{-17} e^{-413/T} \cdot \left(2 + 4e^{-413/T}\right)^{-1} n_{\mathrm{SiII}} . \tag{I.8}$$

Appendix II

The 3–level Hydrogen Atom

In the framework of the nova model it turns out to be an indispensible ingredients for the calculation of the time dependent energy balance to use the statistical rate equations for the description of the population of the hydrogen levels. Therefore we take the first three hydrogen levels and the continuum state and computed the different processes which populate or de–populate the considered energy states.

A: Photoionization

For the calculation of the ionization rates caused by photospheric photons we need the ionization energy E_i in the considered levels

level	E_i [eV]	ν_i [10^{14}Hz]
1	13.61	32.60
2	3.40	7.95
3	1.51	3.63

and the absorption cross–sections $\sigma_i(\nu)$:

$$\begin{aligned}
\sigma_1(\nu) &= \frac{2.81 \times 10^{29}}{\nu^3} \left[0.9916 + \left(2.72 \times 10^{13} - 2.26 \times 10^{30}/\nu\right) \cdot \frac{1}{\nu}\right] && \text{(II.1)} \\
\sigma_2(\nu) &= \frac{8.797 \times 10^{27}}{\nu^3} \left[1.105 + \left(-2.375 \times 10^{14} + 4.07 \times 10^{21}/\nu\right) \cdot \frac{1}{\nu}\right] && \text{(II.2)} \\
\sigma_3(\nu) &= \frac{1.158 \times 10^{27}}{\nu^3} \left[1.101 + \left(-9.863 \times 10^{13} + 1.03 \times 10^{30}/\nu\right) \cdot \frac{1}{\nu}\right] && \text{(II.3)} \\
& && \text{(II.4)}
\end{aligned}$$

B: Radiative Recombination

The recombination of ionized hydrogen with a free electron results in a neutral atom with an electron being in one of the three energy states under consideration and an emitted photon. The recombination rate coefficients were taken from [Osterbrock 1974]

$$\begin{aligned}
\alpha_1 &= 2.28\times10^{-13} \qquad \mathrm{cm}^3\, s^{-1} \\
\alpha_2 &= 1.17\times10^{-13} \qquad \mathrm{cm}^3\, s^{-1} \\
\alpha_3 &= 7.33\times10^{-14} \qquad \mathrm{cm}^3\, s^{-1}
\end{aligned}$$

assuming an electron temperature of 5000K. The temperature variation is taken into account by a factor of $1/\sqrt{T}$. As the typical velocities are of the order of 10^7–10^8 cm/s the cross–section for recombination is of the order of 10^{-20}–10^{-21} cm^2, which is much smaller than the geometrical cross–section of a hydrogen atom.

C: Collisional Ionization

The rate coefficient for the collisional ionization of electrons being at level i can be written as

$$k_i^{CI} \;=\; 1.10\times 10^{-8}\sqrt{T_e}\frac{1}{E_i^2}\;\times 10^{-\frac{5040\cdot E_i}{T_e}} \tag{II.5}$$

where the ionization energy E_i must be inserted in electron volts. Usually the contribution of the ionization by collision with electrons is negligible.

D: Collisional Excitation and De–excitation

The collisional rates are of the general form

$$\mathcal{R_C} \;=\; n_e n_H\, f_{ij}(T_e) \tag{II.6}$$

and the temperature dependent function $f_{i-j}(T)$ for an excitation from level i to level j is given as

$$f_{1-2} \;=\; 4.12\times 10^{-6}\,T^{-1/2}\exp\left(-118300/T\right) \tag{II.7}$$
$$f_{1-3} \;=\; 4.31\times 10^{-6}\,T^{-1/2}\exp\left(-140200/T\right) \tag{II.8}$$
$$f_{2-3} \;=\; 1.08\times 10^{-6}\,T^{-1/2}\exp\left(-21920/T\right) \tag{II.9}$$

For a de–excitation process f_{j-i} from level j to level i is defined as

$$f_{3-1}, = \;4.79\times 10^{-7}\,T^{-1/2} \tag{II.10}$$
$$f_{3-2}, = \;4.79\times 10^{-7}\,T^{-1/2} \tag{II.11}$$
$$f_{3-1}, = \;1.03\times 10^{-6}\,T^{-1/2}. \tag{II.12}$$
$$\tag{II.13}$$

E: Spontaneous Emission, induced Emission and Absorption

The rate coefficient for the spontaneous emission of a photon with the energy $h\nu = h\nu_i - h\nu_j$ and $i > j$ is provided by the Einstein rate coefficient A_{ij}. The rate coefficient for absorption and induced emission is given by the product of the Einstein B_{ij} coefficient with the integral of the mean intensity weighted with a suitably chosen profile function ψ. The values of the coefficients are presented in the following table

	A_{i-j}	B_{i-j}	B_{j-i}
2–1	4.7×10^{8}	5.07×10^{18}	2.03×10^{19}
3–1	5.5×10^{7}	3.62×10^{17}	3.26×10^{18}
3–2	4.4×10^{7}	7.50×10^{19}	1.69×10^{20}

Appendix III

Chemical Data

III.1 Data for Circumstellar Chemistry

Table III.1: Chemical Network for α Ori

Nr.	Reaction				A	E_a	α	R_{ph}
1	SiH^+	$+ e^-$	$\longleftrightarrow$ Si	+ H	1.0×10^{-7}	0	0	0
2	SiO_2	+ O	$\longleftrightarrow$ O_2	+ SiO	5.0×10^{-12}	2.5×10^{3}	0	0
3	SiO	+ H_2O	$\longleftrightarrow$ SiO_2	+ H_2	5.0×10^{-13}	3.0×10^{3}	0	0
4	SiO	+ OH	$\longleftrightarrow$ SiO_2	+ H	2.0×10^{-11}	2.0×10^{3}	0	0
5	SiH	+ O	$\longleftrightarrow$ SiO	+ H	1.0×10^{-11}	2.0×10^{3}	0	0
6	H_2	+ O	$\longleftrightarrow$ H_2O	+ hν	1.0×10^{-16}	0	0	0
7	Si	+ OH	$\longleftrightarrow$ SiO	+ H	2.0×10^{-10}	2.0×10^{3}	0	0
8	Si	+ O_2	$\longleftrightarrow$ SiO	+ O	1.0×10^{-10}	2.0×10^{3}	0	0
9	Si	+ H_2O	$\longleftrightarrow$ SiO	+ H_2	1.0×10^{-10}	2.0×10^{3}	0	0
10	$SiOH^+$	$+ e^-$	$\longleftrightarrow$ SiO	+ H	4.0×10^{-7}	0	0	0
11	SiH	+ O_2	$\longleftrightarrow$ SiO_2	+ H	1.0×10^{-11}	2.0×10^{3}	0	0
12	SiH	+ O	$\longleftrightarrow$ Si	+ OH	3.0×10^{-12}	2.0×10^{3}	0	0
13	SiH	+ H	$\longleftrightarrow$ Si	+ H_2	1.0×10^{-11}	2.0×10^{3}	0	0
14	OH	+ O	$\longleftrightarrow$ O_2	+ H	2.0×10^{-7}	2.8×10^{3}	-9.1×10^{-1}	0
15	OH	+ OH	$\longleftrightarrow$ O	+ H_2O	9.1×10^{-11}	3.49×10^{3}	0	0
16	SiO^+	+ H_2	$\longleftrightarrow$ $SiOH^+$	+ H	3.2×10^{-10}	0	0	0
17	$SiH_2{}^+$	$+ e^-$	$\longleftrightarrow$ SiH	+ H	5.0×10^{-7}	0	0	0
18	OH	+ OH	$\longleftrightarrow$ O_2	+ H_2	2.8×10^{-11}	1.84×10^{4}	0	0
19	SiO^+	+ O	$\longleftrightarrow$ Si^+	+ O_2	2.0×10^{-10}	0	0	0
20	Si^+	+ O	$\longleftrightarrow$ SiO^+	+ hν	1.0×10^{-17}	0	0	0
21	$SiOH^+$	$+ e^-$	$\longleftrightarrow$ Si	+ OH	2.0×10^{-7}	0	0	0
22	H	+ OH	$\longleftrightarrow$ O	+ H_2	3.7×10^{-10}	6.66×10^{3}	0	0
23	SiH^+	+ H	$\longleftrightarrow$ Si^+	+ H_2	1.0×10^{-9}	0	0	0
24	OH	+ H_2	$\longleftrightarrow$ H	+ H_2O	5.3×10^{-17}	1.53×10^{3}	$1.8 \times 10^{+0}$	0
25	H^-	+ H	$\longleftrightarrow$ H_2	$+ e^-$	1.3×10^{-9}	0	0	0
26	SiO^+	$+ e^-$	$\longleftrightarrow$ Si	+ O	1.0×10^{-7}	0	0	0
27	Si^+	+ OH	$\longleftrightarrow$ SiO^+	+ H	1.0×10^{-9}	0	0	0
28	Si^+	+ H_2O	$\longleftrightarrow$ $SiOH^+$	+ H	2.3×10^{-10}	0	0	0

continued on next page

continued from previous page

Nr.	Reaction				A	E_a	α	R_{ph}
29	CH^+	$+ e^-$	$\longleftrightarrow C$	$+ H$	1.73×10^{-6}	0	-5.0×10^{-1}	0
30	$CH_2{}^+$	$+ e^-$	$\longleftrightarrow C$	$+ H_2$	2.6×10^{-6}	0	-5.0×10^{-1}	0
31	$CH_2{}^+$	$+ e^-$	$\longleftrightarrow CH$	$+ H$	2.6×10^{-6}	0	-5.0×10^{-1}	0
32	CH^+	$+ H$	$\longleftrightarrow C^+$	$+ H_2$	7.53×10^{-15}	0	$1.25 \times 10^{+0}$	0
33	C^+	$+ O_2$	$\longleftrightarrow CO^+$	$+ O$	7.5×10^{-10}	0	0	0
34	C^+	$+ O_2$	$\longleftrightarrow O^+$	$+ CO$	4.1×10^{-10}	0	0	0
35	CO^+	$+ O$	$\longleftrightarrow O^+$	$+ CO$	1.4×10^{-10}	0	0	0
36	CO^+	$+ H$	$\longleftrightarrow H^+$	$+ CO$	1.9×10^{-10}	0	0	0
37	C^+	$+ OH$	$\longleftrightarrow CO^+$	$+ H$	7.7×10^{-10}	0	0	0
38	C^+	$+ CH$	$\longleftrightarrow C_2{}^+$	$+ H$	3.8×10^{-10}	0	0	0
39	C^+	$+ CH$	$\longleftrightarrow CH^+$	$+ C$	3.8×10^{-10}	0	0	0
40	CH^+	$+ C$	$\longleftrightarrow C_2{}^+$	$+ H$	1.2×10^{-10}	0	0	0
41	CO^+	$+ e^-$	$\longleftrightarrow O$	$+ C$	3.12×10^{-6}	0	-5.0×10^{-1}	0
42	$C_2{}^+$	$+ e^-$	$\longleftrightarrow C$	$+ C$	3.46×10^{-6}	0	-5.0×10^{-1}	0
43	H^+	$+ O$	$\longleftrightarrow O^+$	$+ H$	7.0×10^{-10}	2.32×10^{2}	0	0
44	H^+	$+ Si$	$\longleftrightarrow Si^+$	$+ H$	9.9×10^{-10}	0	0	0
45	H^+	$+ S$	$\longleftrightarrow S^+$	$+ H$	1.3×10^{-9}	0	0	0
46	H^+	$+ Fe$	$\longleftrightarrow Fe^+$	$+ H$	7.4×10^{-9}	0	0	0
47	H^+	$+ Na$	$\longleftrightarrow Na^+$	$+ H$	1.2×10^{-9}	0	0	0
48	H^+	$+ Mg$	$\longleftrightarrow Mg^+$	$+ H$	1.1×10^{-9}	0	0	0
49	H^+	$+ C_2$	$\longleftrightarrow C_2{}^+$	$+ H$	3.1×10^{-9}	0	0	0
50	H^+	$+ CH$	$\longleftrightarrow CH^+$	$+ H$	1.9×10^{-9}	0	0	0
51	H^+	$+ SiO$	$\longleftrightarrow SiO^+$	$+ H$	3.3×10^{-9}	0	0	0
52	H^+	$+ SiH$	$\longleftrightarrow Si^+$	$+ H_2$	1.7×10^{-9}	0	0	0
53	H^+	$+ HCO$	$\longleftrightarrow CO^+$	$+ H_2$	9.4×10^{-10}	0	0	0
54	H^+	$+ HCO$	$\longleftrightarrow HCO^+$	$+ H$	9.4×10^{-10}	0	0	0
55	H^+	$+ SiH$	$\longleftrightarrow SiH^+$	$+ H$	1.7×10^{-9}	0	0	0
56	C^+	$+ Si$	$\longleftrightarrow Si^+$	$+ C$	2.1×10^{-9}	0	0	0
57	C^+	$+ S$	$\longleftrightarrow S^+$	$+ C$	1.5×10^{-9}	0	0	0
58	C^+	$+ Fe$	$\longleftrightarrow Fe^+$	$+ C$	2.6×10^{-9}	0	0	0
59	C^+	$+ Na$	$\longleftrightarrow Na^+$	$+ C$	1.1×10^{-9}	0	0	0
60	C^+	$+ Mg$	$\longleftrightarrow Mg^+$	$+ C$	1.1×10^{-9}	0	0	0
61	C^+	$+ SiO$	$\longleftrightarrow SiO^+$	$+ C$	5.4×10^{-10}	0	0	0
62	C^+	$+ SiO$	$\longleftrightarrow Si^+$	$+ CO$	5.4×10^{-10}	0	0	0
63	C^+	$+ H_2O$	$\longleftrightarrow HCO^+$	$+ H$	2.7×10^{-9}	0	0	0
64	C^+	$+ HCO$	$\longleftrightarrow HCO^+$	$+ C$	4.8×10^{-10}	0	0	0
65	C^+	$+ HCO$	$\longleftrightarrow CH^+$	$+ CO$	4.8×10^{-10}	0	0	0
66	O^+	$+ Fe$	$\longleftrightarrow Fe^+$	$+ O$	2.9×10^{-9}	0	0	0
67	O^+	$+ C_2$	$\longleftrightarrow C_2{}^+$	$+ O$	4.8×10^{-10}	0	0	0
68	O^+	$+ C_2$	$\longleftrightarrow CO^+$	$+ C$	4.8×10^{-10}	0	0	0

continued on next page

continued from previous page

Nr.	Reaction					A	E_a	α	R_{ph}
69	O^+	$+ CH$	$\longleftrightarrow$	CH^+	$+ O$	3.5×10^{-10}	0	0	0
70	O^+	$+ CH$	$\longleftrightarrow$	CO^+	$+ H$	3.5×10^{-10}	0	0	0
71	O^+	$+ HCO$	$\longleftrightarrow$	HCO^+	$+ O$	4.3×10^{-10}	0	0	0
72	Si^+	$+ Fe$	$\longleftrightarrow$	Fe^+	$+ Si$	1.9×10^{-9}	0	0	0
73	Si^+	$+ Na$	$\longleftrightarrow$	Na^+	$+ Si$	2.7×10^{-9}	0	0	0
74	Si^+	$+ Mg$	$\longleftrightarrow$	Mg^+	$+ Si$	2.9×10^{-9}	0	0	0
75	Fe^+	$+ Na$	$\longleftrightarrow$	Na^+	$+ Fe$	1.0×10^{-11}	0	0	0
76	Mg^+	$+ Na$	$\longleftrightarrow$	Na^+	$+ Mg$	1.0×10^{-11}	0	0	0
77	SiH^+	$+ H_2$	$\longleftrightarrow$	$SiH_2{}^+$	$+ H$	4.5×10^{-10}	0	0	0
78	SiH^+	$+ O$	$\longleftrightarrow$	SiO^+	$+ H$	6.1×10^{-10}	0	0	0
79	SiH^+	$+ CH$	$\longleftrightarrow$	$CH_2{}^+$	$+ Si$	6.0×10^{-10}	0	0	0
80	$C_2{}^+$	$+ C$	$\longleftrightarrow$	C^+	$+ C_2$	1.1×10^{-10}	0	0	0
81	$C_2{}^+$	$+ O$	$\longleftrightarrow$	CO^+	$+ C$	6.6×10^{-11}	0	0	0
82	$C_2{}^+$	$+ O_2$	$\longleftrightarrow$	CO^+	$+ CO$	8.0×10^{-10}	0	0	0
83	$C_2{}^+$	$+ CH$	$\longleftrightarrow$	CH^+	$+ C_2$	3.2×10^{-10}	0	0	0
84	HCO^+	$+ H^-$	$\longleftrightarrow$	CO	$+ H_2$	3.98×10^{-6}	0	-5.0×10^{-1}	0
85	CH^+	$+ O$	$\longleftrightarrow$	CO^+	$+ H$	7.6×10^{-10}	0	0	0
86	CH^+	$+ Si$	$\longleftrightarrow$	Si^+	$+ CH$	2.0×10^{-10}	0	0	0
87	CH^+	$+ Fe$	$\longleftrightarrow$	Fe^+	$+ CH$	2.6×10^{-10}	0	0	0
88	CH^+	$+ Na$	$\longleftrightarrow$	Na^+	$+ CH$	3.5×10^{-10}	0	0	0
89	CH^+	$+ Mg$	$\longleftrightarrow$	Mg^+	$+ CH$	3.6×10^{-10}	0	0	0
90	CH^+	$+ H_2$	$\longleftrightarrow$	$CH_2{}^+$	$+ H$	1.0×10^{-9}	0	0	0
91	CH^+	$+ O_2$	$\longleftrightarrow$	HCO^+	$+ O$	4.8×10^{-10}	0	0	0
92	CH^+	$+ CH$	$\longleftrightarrow$	$C_2{}^+$	$+ H_2$	7.4×10^{-10}	0	0	0
93	CH^+	$+ OH$	$\longleftrightarrow$	CO^+	$+ H_2$	7.5×10^{-10}	0	0	0
94	CH^+	$+ H_2O$	$\longleftrightarrow$	HCO^+	$+ H_2$	1.0×10^{-9}	0	0	0
95	CH^+	$+ HCO$	$\longleftrightarrow$	$CH_2{}^+$	$+ CO$	4.6×10^{-10}	0	0	0
96	CH^+	$+ HCO$	$\longleftrightarrow$	HCO^+	$+ CH$	4.6×10^{-10}	0	0	0
97	CO^+	$+ C$	$\longleftrightarrow$	C^+	$+ CO$	1.1×10^{-10}	0	0	0
98	CO^+	$+ H_2$	$\longleftrightarrow$	HCO^+	$+ H$	2.0×10^{-9}	0	0	0
99	CO^+	$+ C_2$	$\longleftrightarrow$	$C_2{}^+$	$+ CO$	8.4×10^{-10}	0	0	0
10	CH^+	$+ S$	$\longleftrightarrow$	S^+	$+ CH$	4.7×10^{-10}	0	0	0
101	CO^+	$+ CH$	$\longleftrightarrow$	CH^+	$+ CO$	3.2×10^{-10}	0	0	0
102	CO^+	$+ CH$	$\longleftrightarrow$	HCO^+	$+ C$	3.2×10^{-10}	0	0	0
103	S^+	$+ Si$	$\longleftrightarrow$	Si^+	$+ S$	1.6×10^{-9}	0	0	0
104	S^+	$+ Fe$	$\longleftrightarrow$	Fe^+	$+ S$	1.8×10^{-10}	0	0	0
105	CO^+	$+ H_2O$	$\longleftrightarrow$	HCO^+	$+ OH$	4.2×10^{-10}	0	0	0
106	CO^+	$+ HCO$	$\longleftrightarrow$	HCO^+	$+ CO$	7.4×10^{-10}	0	0	0
107	SiO^+	$+ C$	$\longleftrightarrow$	Si^+	$+ CO$	1.0×10^{-9}	0	0	0
108	SiO^+	$+ CH$	$\longleftrightarrow$	HCO^+	$+ Si$	5.9×10^{-10}	0	0	0

continued on next page

continued from previous page

Nr.	Reaction				A	E_a	α	R_{ph}
109	SiO^+	+ HCO	$\longleftrightarrow$ HCO^+	+ SiO	6.6×10^{-10}	0	0	0
110	$CH_2{}^+$	+ O	$\longleftrightarrow$ HCO^+	+ H	7.5×10^{-10}	0	0	0
111	$CH_2{}^+$	+ O_2	$\longleftrightarrow$ HCO^+	+ OH	4.7×10^{-10}	0	0	0
112	CO^+	+ OH	$\longleftrightarrow$ HCO^+	+ O	3.1×10^{-10}	0	0	0
113	HCO^+	+ C	$\longleftrightarrow$ CH^+	+ CO	1.1×10^{-9}	0	0	0
114	HCO^+	+ Si	$\longleftrightarrow$ SiH^+	+ CO	1.6×10^{-9}	0	0	0
115	HCO^+	+ Fe	$\longleftrightarrow$ Fe^+	+ HCO	1.9×10^{-9}	0	0	0
116	HCO^+	+ Na	$\longleftrightarrow$ Na^+	+ HCO	2.6×10^{-9}	0	0	0
117	HCO^+	+ Mg	$\longleftrightarrow$ Mg^+	+ HCO	2.9×10^{-9}	0	0	0
118	HCO^+	+ CH	$\longleftrightarrow$ $CH_2{}^+$	+ CO	6.3×10^{-10}	0	0	0
119	HCO^+	+ SiO	$\longleftrightarrow$ $SiOH^+$	+ CO	7.9×10^{-10}	0	0	0
120	HCO^+	+ SiH	$\longleftrightarrow$ $SiH_2{}^+$	+ CO	8.7×10^{-10}	0	0	0
121	$SiH_2{}^+$	+ O	$\longleftrightarrow$ $SiOH^+$	+ H	6.3×10^{-10}	0	0	0
122	H^-	+ C	$\longleftrightarrow$ CH	+ e^-	1.0×10^{-9}	0	0	0
123	H^-	+ O	$\longleftrightarrow$ OH	+ e^-	1.0×10^{-9}	0	0	0
124	S^+	+ Na	$\longleftrightarrow$ Na^+	+ S	2.6×10^{-10}	0	0	0
125	H^-	+ OH	$\longleftrightarrow$ H_2O	+ e^-	1.0×10^{-10}	0	0	0
126	H^-	+ CO	$\longleftrightarrow$ HCO	+ e^-	5.0×10^{-11}	0	0	0
127	C	+ OH	$\longleftrightarrow$ CO	+ H	6.35×10^{-12}	0	5.0×10^{-1}	0
128	C	+ O_2	$\longleftrightarrow$ CO	+ O	1.91×10^{-12}	0	5.0×10^{-1}	0
129	O	+ CH	$\longleftrightarrow$ CO	+ H	2.31×10^{-12}	0	5.0×10^{-1}	0
130	O	+ CH	$\longleftrightarrow$ HCO^+	+ e^-	1.63×10^{-12}	0	4.4×10^{-1}	0
131	C_2	+ O	$\longleftrightarrow$ CO	+ C	2.89×10^{-12}	0	5.0×10^{-1}	0
132	HCO	+ H	$\longleftrightarrow$ H_2	+ CO	1.15×10^{-12}	0	5.0×10^{-1}	0
133	HCO	+ O	$\longleftrightarrow$ OH	+ CO	6.93×10^{-12}	0	5.0×10^{-1}	0
134	S^+	+ Mg	$\longleftrightarrow$ Mg^+	+ S	2.8×10^{-10}	0	0	0
135	HCO^+	+ e^-	$\longleftrightarrow$ CO	+ H	1.44×10^{-5}	0	-7.5×10^{-1}	0
136	H^+	+ H^-	$\longleftrightarrow$ H	+ H	3.98×10^{-6}	0	-5.0×10^{-1}	0
137	C^+	+ H^-	$\longleftrightarrow$ H	+ C	3.98×10^{-6}	0	-5.0×10^{-1}	0
138	O^+	+ H^-	$\longleftrightarrow$ H	+ O	3.98×10^{-6}	0	-5.0×10^{-1}	0
139	Si^+	+ H^-	$\longleftrightarrow$ Si	+ H	3.98×10^{-6}	0	-5.0×10^{-1}	0
140	S^+	+ H^-	$\longleftrightarrow$ S	+ H	3.98×10^{-6}	0	-5.0×10^{-1}	0
141	Fe^+	+ H^-	$\longleftrightarrow$ Fe	+ H	3.98×10^{-6}	0	-5.0×10^{-1}	0
142	Na^+	+ H^-	$\longleftrightarrow$ Na	+ H	3.98×10^{-6}	0	-5.0×10^{-1}	0
143	Mg^+	+ H^-	$\longleftrightarrow$ Mg	+ H	3.98×10^{-6}	0	-5.0×10^{-1}	0
144	S^+	+ SiH	$\longleftrightarrow$ SiH^+	+ S	4.2×10^{-10}	0	0	0
145	S^+	+ HCO	$\longleftrightarrow$ HCO^+	+ S	3.6×10^{-10}	0	0	0
146	S^+	+ SiH	$\longleftrightarrow$ SiS	+ H^+	5.0×10^{-10}	0	0	0
147	C^+	+ SiS	$\longleftrightarrow$ Si^+	+ CS	5.0×10^{-10}	0	0	0
148	S^+	+ SiH	$\longleftrightarrow$ SiH^+	+ S	4.2×10^{-10}	0	0	0

continued on next page

continued from previous page

Nr.	Reaction				A	E_a	α	R_{ph}
149	HS^+	+ Si	$\longleftrightarrow$ Si^+	+ HS	1.4×10^{-9}	0	0	0
150	SiO^+	+ S	$\longleftrightarrow$ Si^+	+ SO	1.0×10^{-9}	0	0	0
151	CS^+	+ Si	$\longleftrightarrow$ Si^+	+ CS	1.5×10^{-10}	0	0	0
152	H_2S^+	+ Si	$\longleftrightarrow$ Si^+	+ H_2S	1.6×10^{-9}	0	0	0
153	S	+ H_2	$\longleftrightarrow$ HS	+ H	9.3×10^{-11}	1.0×10^{4}	4.2×10^{-2}	0
154	HS	+ H_2	$\longleftrightarrow$ H_2S	+ H	2.5×10^{-11}	7.2×10^{3}	-1.9×10^{-1}	0
155	HS	+ HS	$\longleftrightarrow$ H_2S	+ S	1.5×10^{-11}	0	0	0
156	HS	+ S	$\longleftrightarrow$ S_2	+ H	1.0×10^{-12}	0	5.0×10^{-1}	0
157	S^+	+ H_2	$\longleftrightarrow$ HS^+	+ H	2.2×10^{-10}	$9.86\times{}^{3}$	0	0
158	HS^+	+ H_2	$\longleftrightarrow$ H_2S^+	+ H	1.9×10^{-10}	6.38×10^{3}	0	0
159	H^+	+ HS	$\longleftrightarrow$ HS^+	+ H	1.6×10^{-9}	0	0	0
160	H^+	+ HS	$\longleftrightarrow$ S^+	+ H_2	1.6×10^{-9}	0	0	0
161	H^+	+ H_2S	$\longleftrightarrow$ H_2S^+	+ H	7.6×10^{-9}	0	0	0
162	S^+	+ HS	$\longleftrightarrow$ HS^+	+ S	9.7×10^{-10}	5.5×10^{2}	0	0
163	HS^+	+ H_2S	$\longleftrightarrow$ H_2S^+	+ HS	4.5×10^{-10}	6.2×10^{2}	0	0
164	S^+	+ H_2S	$\longleftrightarrow$ $S_2{}^+$	+ H_2	2.5×10^{-10}	0	0	0
165	S^+	+ H_2S	$\longleftrightarrow$ H_2S^+	+ S	2.1×10^{-10}	0	0	0
166	HS^+	+ Mg	$\longleftrightarrow$ HS	+ Mg^+	2.6×10^{-9}	0	0	0
167	HS^+	+ Fe	$\longleftrightarrow$ HS	+ Fe^+	1.6×10^{-9}	0	0	0
168	HS^+	+ Na	$\longleftrightarrow$ HS	+ Na^+	2.2×10^{-9}	0	0	0
169	H_2S^+	+ Mg	$\longleftrightarrow$ H_2S	+ Mg^+	2.8×10^{-9}	0	0	0
170	H_2S^+	+ Fe	$\longleftrightarrow$ H_2S	+ Fe^+	1.8×10^{-9}	0	0	0
171	H_2S^+	+ Na	$\longleftrightarrow$ H_2S	+ Na^+	2.5×10^{-9}	0	0	0
172	HS^+	+ e^-	$\longleftrightarrow$ H	+ S	3.5×10^{-6}	0	-5.0×10^{-1}	0
173	H_2S^+	+ e^-	$\longleftrightarrow$ HS	+ H	2.6×10^{-6}	0	-5.0×10^{-1}	0
174	S	+ CH	$\longleftrightarrow$ CS	+ H	2.9×10^{-12}	0	5.0×10^{-1}	0
175	HS	+ C	$\longleftrightarrow$ CS	+ H	9.2×10^{-12}	0	5.0×10^{-1}	0
176	CS	+ C	$\longleftrightarrow$ S	+ C_2	8.3×10^{-13}	2.04×10^{4}	5.0×10^{-1}	0
177	S	+ CH	$\longleftrightarrow$ HS	+ C	1.0×10^{-12}	4.0×10^{3}	5.0×10^{-1}	0
178	S_2	+ C	$\longleftrightarrow$ S	+ CS	1.0×10^{-12}	0	5.0×10^{-1}	0
179	C^+	+ HS	$\longleftrightarrow$ CS^+	+ H	1.1×10^{-9}	0	0	0
180	C^+	+ H_2S	$\longleftrightarrow$ HCS^+	+ H	1.4×10^{-9}	0	0	0
181	C^+	+ H_2S	$\longleftrightarrow$ H_2S^+	+ C	6.0×10^{-10}	0	0	0
182	C^+	+ CS	$\longleftrightarrow$ CS^+	+ C	1.6×10^{-9}	0	0	0
183	H^+	+ CS	$\longleftrightarrow$ CS^+	+ H	4.9×10^{-9}	0	0	0
184	S^+	+ CH	$\longleftrightarrow$ CS^+	+ H	6.2×10^{-10}	0	0	0
185	HS	+ O	$\longleftrightarrow$ S	+ OH	3.7×10^{-13}	9.5×10^{2}	6.7×10^{-1}	0
186	CS^+	+ H_2	$\longleftrightarrow$ HCS^+	+ H	7.3×10^{-10}	0	0	0
187	CH^+	+ S	$\longleftrightarrow$ HS^+	+ C	4.7×10^{-10}	0	0	0
188	CH^+	+ S	$\longleftrightarrow$ CS^+	+ H	4.7×10^{-10}	0	0	0

continued on next page

continued from previous page

Nr.	Reaction				A	E_a	α	R_{ph}
189	CH_2^+	+ S	$\longleftrightarrow$ HCS^+	+ H	1.4×10^{-9}	0	0	0
190	CH_2^+	+ S	$\longleftrightarrow$ HS^+	+ CH	5.8×10^{-10}	7.8×10^{3}	0	0
191	HS^+	+ C	$\longleftrightarrow$ CS^+	+ H	9.9×10^{-10}	0	0	0
192	S^+	+ C_2	$\longleftrightarrow$ CS^+	+ C	8.1×10^{-10}	0	0	0
193	CH^+	+ H_2S	$\longleftrightarrow$ HCS^+	+ H_2	1.5×10^{-9}	0	0	0
194	CS^+	+ Mg	$\longleftrightarrow$ CS	+ Mg^+	2.7×10^{-10}	0	0	0
195	CS^+	+ Fe	$\longleftrightarrow$ CS	+ Fe^+	1.7×10^{-10}	0	0	0
196	CS^+	+ Na	$\longleftrightarrow$ CS	+ Na^+	2.3×10^{-10}	0	0	0
197	CS^+	+ e^-	$\longleftrightarrow$ S	+ C	3.5×10^{-6}	0	-5.0×10^{-1}	0
198	HCS^+	+ e^-	$\longleftrightarrow$ CS	+ H	3.6×10^{-6}	0	-7.5×10^{-1}	0
199	SO	+ H	$\longleftrightarrow$ S	+ OH	2.0×10^{-10}	1.07×10^{4}	0	0
20	HS	+ O	$\longleftrightarrow$ SO	+ H	9.2×10^{-12}	0	5.0×10^{-1}	0
201	H_2S	+ OH	$\longleftrightarrow$ H_2O	+ HS	2.3×10^{-11}	4.5×10^{2}	0	0
202	SO	+ OH	$\longleftrightarrow$ SO_2	+ H	5.8×10^{-12}	0	5.0×10^{-1}	0
203	HS	+ O	$\longleftrightarrow$ S	+ OH	2.0×10^{-11}	0	0	0
204	SO	+ O_2	$\longleftrightarrow$ SO_2	+ O	7.5×10^{-13}	3.25×10^{3}	0	0
205	S	+ O_2	$\longleftrightarrow$ SO	+ O	2.0×10^{-12}	0	0	0
206	S	+ SO_2	$\longleftrightarrow$ SO	+ SO	3.0×10^{-14}	0	0	0
207	HS	+ OH	$\longleftrightarrow$ S	+ H_2O	7.2×10^{-12}	0	0	0
208	S_2	+ O	$\longleftrightarrow$ SO	+ S	1.0×10^{-12}	0	5.0×10^{-1}	0
209	H_2S	+ O	$\longleftrightarrow$ HS	+ OH	1.0×10^{-11}	1.81×10^{3}	0	0
210	S^+	+ OH	$\longleftrightarrow$ SO^+	+ H	6.1×10^{-10}	0	0	0
211	S^+	+ OH	$\longleftrightarrow$ HS^+	+ O	2.9×10^{-10}	9.43×10^{3}	0	0
212	HS^+	+ O	$\longleftrightarrow$ SO^+	+ H	2.9×10^{-10}	0	0	0
213	H_2S^+	+ O	$\longleftrightarrow$ HS^+	+ OH	3.1×10^{-10}	0	0	0
214	H_2S^+	+ O	$\longleftrightarrow$ SO^+	+ H_2	3.1×10^{-10}	0	0	0
215	O^+	+ H_2S	$\longleftrightarrow$ H_2S^+	+ O	1.8×10^{-9}	0	0	0
216	S^+	+ O_2	$\longleftrightarrow$ SO^+	+ O	1.6×10^{-11}	0	0	0
217	SO^+	+ H_2S	$\longleftrightarrow$ S_2^+	+ H_2O	1.1×10^{-10}	0	0	0
218	SO^+	+ Mg	$\longleftrightarrow$ SO	+ Mg^+	1.0×10^{-10}	0	0	0
219	SO^+	+ Fe	$\longleftrightarrow$ SO	+ Fe^+	1.6×10^{-9}	0	0	0
220	SO^+	+ Na	$\longleftrightarrow$ SO	+ Na^+	2.3×10^{-9}	0	0	0
221	SO^+	+ e^-	$\longleftrightarrow$ S	+ O	3.5×10^{-6}	0	-5.0×10^{-1}	0
222	CS	+ O	$\longleftrightarrow$ CO	+ S	2.6×10^{-10}	7.6×10^{2}	0	0
223	HS	+ CO	$\longleftrightarrow$ OCS	+ H	3.0×10^{-11}	5.36×10^{3}	0	0
224	CS	+ O	$\longleftrightarrow$ SO	+ C	2.7×10^{-12}	2.89×10^{4}	5.0×10^{-1}	0
225	OCS	+ O	$\longleftrightarrow$ SO	+ CO	2.1×10^{-11}	2.2×10^{3}	0	0
226	CS^+	+ O	$\longleftrightarrow$ CO^+	+ S	6.0×10^{-11}	0	0	0
227	HCS^+	+ O	$\longleftrightarrow$ HCO^+	+ S	1.0×10^{-9}	0	0	0
228	C^+	+ SO	$\longleftrightarrow$ S^+	+ CO	1.0×10^{-9}	0	0	0

continued on next page

continued from previous page

Nr.	Reaction	A	E_a	α	R_{ph}
229	$C^+ + SO \longleftrightarrow CO^+ + S$	1.0×10^{-9}	0	0	0
230	$C^+ + SO \longleftrightarrow CS^+ + O$	2.6×10^{-10}	0	0	0
231	$C^+ + SO \longleftrightarrow SO^+ + C$	2.6×10^{-10}	0	0	0
232	$CH_2{}^+ + SO \longleftrightarrow H_2S^+ + CO$	1.0×10^{-9}	0	0	0
233	$CH^+ + SO \longleftrightarrow HS^+ + CO$	1.0×10^{-9}	0	0	0
234	$C^+ + SO_2 \longleftrightarrow SO^+ + CO$	2.3×10^{-9}	0	0	0
235	$C^+ + OCS \longleftrightarrow CS^+ + CO$	9.3×10^{-10}	0	0	0
236	$C^+ + OCS \longleftrightarrow OCS^+ + C$	4.0×10^{-10}	0	0	0
237	$S^+ + HCO \longleftrightarrow HS^+ + CO$	3.6×10^{-10}	0	0	0
238	$CH^+ + OCS \longleftrightarrow HCS^+ + CO$	1.1×10^{-9}	0	0	0
239	$CH_2{}^+ + OCS \longleftrightarrow HCS^+ + HCO$	1.1×10^{-9}	0	0	0
240	$HCS^+ + O \longleftrightarrow OCS^+ + H$	5.0×10^{-10}	0	0	0
241	$HCO^+ + S \longleftrightarrow HS^+ + CO$	3.3×10^{-10}	0	0	0
242	$HCO^+ + CS \longleftrightarrow HCS^+ + CO$	1.2×10^{-9}	0	0	0
243	$HCO^+ + HS \longleftrightarrow H_2S^+ + CO$	8.2×10^{-10}	0	0	0
244	$OCS^+ + e^- \longleftrightarrow S + CO$	2.6×10^{-6}	0	-5.0×10^{-1}	0
245	$OCS^+ + e^- \longleftrightarrow CS + O$	2.6×10^{-6}	0	-5.0×10^{-1}	0
246	$C_2{}^+ + S \longleftrightarrow CS^+ + C$	5.8×10^{-10}	0	0	0
247	$C^+ + OCS \longleftrightarrow CO^+ + CS$	9.3×10^{-10}	0	0	0
248	$H^+ + OCS \longleftrightarrow HS^+ + CO$	5.9×10^{-9}	0	0	0
249	$CO + S \longleftrightarrow OCS + h\nu$	1.35×10^{-9}	0	$-3.2 \times 10^{+0}$	2.4×10^{-3}
250	$SO + O \longleftrightarrow SO_2 + h\nu$	2.9×10^{-12}	0	$-1.6 \times 10^{+0}$	1.2×10^{-3}
251	$H_2S^+ + e^- \longleftrightarrow H_2S + h\nu$	6.0×10^{-9}	0	-7.0×10^{-1}	1.2×10^{-6}
252	$S + H \longleftrightarrow HS + h\nu$	0	0	0	4.3×10^{-3}
253	$S^+ + H \longleftrightarrow HS^+ + h\nu$	0	0	0	2.5×10^{-7}
254	$HS + H \longleftrightarrow H_2S + h\nu$	0	0	0	2.7×10^{-4}
255	$C + S \longleftrightarrow CS + h\nu$	0	0	0	1.1×10^{-4}
256	$S + O \longleftrightarrow SO + h\nu$	0	0	0	6.3×10^{-4}
257	$OCS^+ + e^- \longleftrightarrow OCS + h\nu$	0	0	0	6.0×10^{-7}
258	$O^+ + e^- \longleftrightarrow O + h\nu$	1.24×10^{-10}	0	-6.3×10^{-1}	2.5×10^{-8}
259	$SiO + O \longleftrightarrow SiO_2 + h\nu$	1.0×10^{-17}	2.5×10^{3}	0	5.3×10^{-5}
260	$Mg^+ + e^- \longleftrightarrow Mg + h\nu$	3.7×10^{-10}	0	-8.6×10^{-1}	1.2×10^{-5}
261	$Si + O \longleftrightarrow SiO + h\nu$	1.0×10^{-17}	0	0	6.1×10^{-7}
262	$OH + H \longleftrightarrow H_2O + h\nu$	1.0×10^{-16}	0	0	3.5×10^{-4}
263	$O + O \longleftrightarrow O_2 + h\nu$	1.0×10^{-18}	0	0	1.7×10^{-4}
264	$Si + H \longleftrightarrow SiH + h\nu$	1.0×10^{-16}	0	0	3.2×10^{-3}
265	$Na^+ + e^- \longleftrightarrow Na + h\nu$	1.4×10^{-10}	0	-6.9×10^{-1}	4.6×10^{-5}
266	$Fe^+ + e^- \longleftrightarrow Fe + h\nu$	1.5×10^{-10}	0	-6.5×10^{-1}	2.0×10^{-5}
267	$O + H \longleftrightarrow OH + h\nu$	1.1×10^{-19}	0	8.0×10^{-1}	2.1×10^{-4}
268	$Si^+ + H \longleftrightarrow SiH^+ + h\nu$	1.0×10^{-17}	0	0	2.0×10^{-5}

continued on next page

continued from previous page

Nr.	Reaction	A	E_a	α	R_{ph}
269	$SiH^+ + H \longrightarrow SiH_2{}^+ + h\nu$	1.0×10^{-15}	0	0	2.0×10^{-4}
270	$Si^+ + e^- \longrightarrow Si + h\nu$	1.5×10^{-10}	0	-6.4×10^{-1}	3.4×10^{-4}
271	$S^+ + e^- \longrightarrow S + h\nu$	1.4×10^{-10}	0	-6.3×10^{-1}	6.2×10^{-6}
272	$H + e^- \longrightarrow H^- + h\nu$	1.0×10^{-18}	0	$1.0 \times 10^{+0}$	1.7×10^{4}
273	$SiH^+ + e^- \longrightarrow SiH + h\nu$	0	0	0	2.0×10^{-5}
274	$SiO^+ + e^- \longrightarrow SiO + h\nu$	0	0	0	3.0×10^{-7}
275	$C^+ + H \longrightarrow CH^+ + h\nu$	1.7×10^{-17}	0	0	2.1×10^{-5}
276	$CH^+ + H \longrightarrow CH_2{}^+ + h\nu$	6.0×10^{-16}	0	0	2.0×10^{-4}
277	$CH^+ + e^- \longrightarrow CH + h\nu$	0	0	0	1.5×10^{-6}
278	$C + H \longrightarrow CH + h\nu$	1.0×10^{-17}	0	0	1.3×10^{-3}
279	$C + C \longrightarrow C_2 + h\nu$	1.0×10^{-17}	0	0	5.5×10^{-7}
280	$C^+ + C \longrightarrow C_2{}^+ + h\nu$	0	0	0	6.5×10^{-7}
281	$C + O \longrightarrow CO + h\nu$	0	0	0	8.8×10^{-9}
282	$H + H \longrightarrow H_2 + h\nu$	0	0	0	7.5×10^{-13}
283	$H^+ + e^- \longrightarrow H + h\nu$	1.9×10^{-10}	0	-7.0×10^{-1}	2.5×10^{-11}
284	$C^+ + e^- \longrightarrow C + h\nu$	1.43×10^{-10}	0	-6.1×10^{-1}	5.0×10^{-7}
285	$C_2{}^+ + e^- \longrightarrow C_2 + h\nu$	0	0	0	1.0×10^{-7}
286	$CO + H \longrightarrow HCO + h\nu$	0	0	0	2.0×10^{-3}

III.2 Chemical Data for Nova Chemistry

Table III.2: Chemical Network for Novae I

Nr.	Reaction	A	E_a	α	Ref.
1	$H + \gamma \Longrightarrow H^+ + e^-$	4.6×10^{-01}	0	0	1
2	$He + \gamma \Longrightarrow He^+ + e^-$	5.0×10^{-01}	0	0	1
3	$C + \gamma \Longrightarrow C^+ + e^-$	$1.8 \times 10^{+00}$	0	0	1
4	$N + \gamma \Longrightarrow N^+ + e^-$	$2.1 \times 10^{+00}$	0	0	1
5	$O + \gamma \Longrightarrow O^+ + e^-$	$2.8 \times 10^{+00}$	0	0	1
6	$H_2 + \gamma \Longrightarrow H^+ + H + e^-$	2.2×10^{-02}	0	0	1
7	$H_2 + \gamma \Longrightarrow H_2{}^+ + e^-$	9.3×10^{-01}	0	0	1
8	$H_2 + \gamma \Longrightarrow H + H$	1.0×10^{-01}	0	0	1
9	$H_2 + \gamma \Longrightarrow H^+ +$ H-	3.0×10^{-04}	0	0	1
10	$CO + \gamma \Longrightarrow CO^+ + e^-$	$3.0 \times 10^{+00}$	0	0	1
11	$H + H + H \Longrightarrow H_2 + H$	5.0×10^{-32}	0	0	1
12	$H^+ + O \Longrightarrow O^+ + H$	7.0×10^{-10}	0	$2.3 \times 10^{+02}$	1
13	$H^+ + Si \Longrightarrow Si^+ + H$	9.9×10^{-10}	0	0	1
14	$H^+ + S \Longrightarrow S^+ + H$	1.3×10^{-09}	0	0	1
15	$H^+ + Fe \Longrightarrow Fe^+ + H$	7.4×10^{-09}	0	0	1
16	$H^+ + Na \Longrightarrow Na^+ + H$	1.2×10^{-09}	0	0	1
17	$H^+ + Mg \Longrightarrow Mg^+ + H$	1.1×10^{-09}	0	0	1
18	$H^+ + C_2 \Longrightarrow C_2{}^+ + H$	3.1×10^{-09}	0	0	1
19	$H^+ + O_2 \Longrightarrow O_2{}^+ + H$	1.2×10^{-09}	0	0	1
20	$H^+ + CH \Longrightarrow CH^+ + H$	1.9×10^{-09}	0	0	1
21	$H^+ + NH \Longrightarrow NH^+ + H$	2.1×10^{-09}	0	0	1
22	$H^+ + OH \Longrightarrow OH^+ + H$	2.1×10^{-09}	0	0	1
23	$H^+ + NO \Longrightarrow NO^+ + H$	1.9×10^{-09}	0	0	1
24	$H^+ + SiC \Longrightarrow SiC^+ + H$	1.6×10^{-08}	0	0	1
25	$H^+ + SiS \Longrightarrow SiS^+ + H$	1.5×10^{-08}	0	0	1
26	$H^+ + SiO \Longrightarrow SiO^+ + H$	3.3×10^{-09}	0	0	1
27	$H^+ + SiH \Longrightarrow Si^+ + H_2$	1.7×10^{-09}	0	0	1
28	$H^+ + SiH \Longrightarrow SiH^+ + H$	1.7×10^{-09}	0	0	1
29	$H^+ + HS \Longrightarrow HS^+ + H$	1.6×10^{-09}	0	0	1
30	$H^+ + HS \Longrightarrow S^+ + H_2$	1.6×10^{-09}	0	0	1
31	$H^+ + CS \Longrightarrow CS^+ + H$	4.9×10^{-09}	0	0	1
32	$H^+ + NS \Longrightarrow NS^+ + H$	4.7×10^{-09}	0	0	1
33	$H^+ + SO \Longrightarrow SO^+ + H$	3.2×10^{-09}	0	0	1
34	$H^+ + CH_2 \Longrightarrow CH^+ + H_2$	1.4×10^{-09}	0	0	1
35	$H^+ + CH_2 \Longrightarrow CH_2{}^+ + H$	1.4×10^{-09}	0	0	1
36	$H^+ + H_2 \Longrightarrow H_2{}^+ + H$	1.0×10^{-10}	0	$2.1 \times 10^{+04}$	4
37	$H^+ + NH_2 \Longrightarrow NH_2{}^+ + H$	2.9×10^{-09}	0	0	1
38	$H^+ + H2O \Longrightarrow H_2O^+ + H$	8.2×10^{-09}	0	0	1
39	$H^+ + HCO \Longrightarrow CO^+ + H_2$	9.4×10^{-10}	0	0	1
40	$H^+ + HCO \Longrightarrow H_2{}^+ + CO$	9.4×10^{-10}	0	0	1
41	$H^+ + HCO \Longrightarrow HCO^+ + H$	9.4×10^{-10}	0	0	1
42	$H^+ + C_2H \Longrightarrow C_2H^+ + H$	1.5×10^{-09}	0	0	1
43	$H^+ + C_2H \Longrightarrow C_2{}^+ + H_2$	1.5×10^{-09}	0	0	1
44	$H^+ + CO_2 \Longrightarrow HCO^+ + O$	3.0×10^{-09}	0	0	1

continued on next page

continued from previous page

Nr.	Reaction	A	E_a	α	Ref.
45	$H^+ + H_2S \Longrightarrow H_2S^+ + H$	7.6×10^{-09}	0	0	1
46	$H^+ + OCS \Longrightarrow HS^+ + CO$	5.9×10^{-09}	0	0	1
47	$H^+ + H_2CO \Longrightarrow H_2CO^+ + H$	2.0×10^{-09}	0	0	1
48	$H^+ + H_2CO \Longrightarrow HCO^+ + H_2$	2.0×10^{-09}	0	0	1
49	$H^+ + NH_3 \Longrightarrow NH_3{}^+ + H$	5.2×10^{-09}	0	0	1
50	$H^+ + C_2H2 \Longrightarrow C_2H^+ + H_2$	4.3×10^{-09}	0	0	1
51	$H^+ + CH_3 \Longrightarrow CH_3{}^+ + H$	3.4×10^{-09}	0	0	1
52	$H^+ + CH_4 \Longrightarrow CH_3{}^+ + H_2$	2.3×10^{-09}	0	0	1
53	$H^+ + CH_4 \Longrightarrow CH_4{}^+ + H$	1.5×10^{-09}	0	0	1
54	$H^+ + H_2CS \Longrightarrow H_2CS^+ + H$	4.7×10^{-09}	0	0	1
55	$He^+ + H \Longrightarrow H^+ + He + h\nu$	1.9×10^{-15}	0	0	1
56	$He^+ + Si \Longrightarrow Si^+ + He$	3.3×10^{-09}	0	0	1
57	$He^+ + H_2 \Longrightarrow H^+ + H + He$	1.5×10^{-13}	0	0	1
58	$He^+ + C_2 \Longrightarrow C^+ + C + He$	1.6×10^{-09}	0	0	1
59	$He^+ + N_2 \Longrightarrow N_2{}^+ + He$	4.0×10^{-10}	0	0	1
60	$He^+ + N_2 \Longrightarrow N^+ + N + He$	8.0×10^{-10}	0	0	1
61	$He^+ + O_2 \Longrightarrow O^+ + O + He$	1.0×10^{-09}	0	0	1
62	$He^+ + CH \Longrightarrow C^+ + H + He$	1.1×10^{-09}	0	0	1
63	$He^+ + NH \Longrightarrow N^+ + H + He$	1.1×10^{-09}	0	0	1
64	$He^+ + OH \Longrightarrow O^+ + H + He$	1.1×10^{-09}	0	0	1
65	$He^+ + CO \Longrightarrow C^+ + O + He$	1.6×10^{-09}	0	0	1
66	$He^+ + CN \Longrightarrow C^+ + N + He$	8.8×10^{-10}	0	0	1
67	$He^+ + CN \Longrightarrow N^+ + C + He$	8.8×10^{-10}	0	0	1
68	$He^+ + NO \Longrightarrow O^+ + N + He$	2.0×10^{-10}	0	0	1
69	$He^+ + NO \Longrightarrow N^+ + O + He$	1.4×10^{-09}	0	0	1
70	$He^+ + SiC \Longrightarrow C^+ + Si + He$	4.0×10^{-09}	0	0	1
71	$He^+ + SiC \Longrightarrow Si^+ + C + He$	4.0×10^{-09}	0	0	1
72	$He^+ + SiS \Longrightarrow Si^+ + S + He$	3.8×10^{-09}	0	0	1
73	$He^+ + SiS \Longrightarrow S^+ + Si + He$	3.8×10^{-09}	0	0	1
74	$He^+ + SiO \Longrightarrow Si^+ + O + He$	8.6×10^{-10}	0	0	1
75	$He^+ + SiO \Longrightarrow O^+ + Si + He$	8.6×10^{-10}	0	0	1
76	$He^+ + SiH \Longrightarrow Si^+ + H + He$	1.8×10^{-09}	0	0	1
77	$He^+ + HS \Longrightarrow S^+ + H + He$	1.7×10^{-09}	0	0	1
78	$He^+ + CS \Longrightarrow S^+ + C + He$	1.3×10^{-09}	0	0	1
79	$He^+ + CS \Longrightarrow C^+ + S + He$	1.3×10^{-09}	0	0	1
80	$He^+ + NS \Longrightarrow N^+ + S + He$	1.2×10^{-09}	0	0	1
81	$He^+ + NS \Longrightarrow S^+ + N + He$	1.2×10^{-09}	0	0	1
82	$He^+ + SO \Longrightarrow O^+ + S + He$	8.3×10^{-10}	0	0	1
83	$He^+ + SO \Longrightarrow S^+ + O + He$	8.3×10^{-10}	0	0	1
84	$He^+ + CH_2 \Longrightarrow CH^+ + H + He$	7.5×10^{-10}	0	0	1
85	$He^+ + CH_2 \Longrightarrow C^+ + H_2 + He$	7.5×10^{-10}	0	0	1
86	$He^+ + NH_2 \Longrightarrow NH^+ + H + He$	8.0×10^{-10}	0	0	1
87	$He^+ + NH_2 \Longrightarrow N^+ + H_2 + He$	8.0×10^{-10}	0	0	1
88	$He^+ + H_2O \Longrightarrow OH^+ + H + He$	3.7×10^{-10}	0	0	1
89	$He^+ + H_2O \Longrightarrow H_2O^+ + He$	7.0×10^{-11}	0	0	1
90	$He^+ + HCN \Longrightarrow CN^+ + H + He$	1.6×10^{-09}	0	0	1

continued on next page

continued from previous page

Nr.	Reaction					A	E_a	α	Ref.
91	He^+ +	HCN	$\Longrightarrow CH^+$	+ N	+ He	6.0×10^{-10}	0	0	1
92	He^+ +	HCN	$\Longrightarrow N^+$	+ CH	+ He	2.0×10^{-10}	0	0	1
93	He^+ +	HCN	$\Longrightarrow C^+$	+ N	+ H + He	7.0×10^{-10}	0	0	1
94	He^+ +	HCO	$\Longrightarrow CO^+$	+ H	+ He	4.9×10^{-10}	0	0	1
95	He^+ +	HCO	$\Longrightarrow CH^+$	+ O	+ He	4.9×10^{-10}	0	0	1
96	He^+ +	HCO	$\Longrightarrow HeH^+$	+ CO		3.0×10^{-10}	0	0	1
97	He^+ +	C_2H	$\Longrightarrow CH^+$	+ C	+ He	5.1×10^{-10}	0	0	1
98	He^+ +	C_2H	$\Longrightarrow C_2{}^+$	+ H	+ He	5.1×10^{-10}	0	0	1
99	He^+ +	C_2H	$\Longrightarrow C^+$	+ CH	+ He	5.1×10^{-10}	0	0	1
100	He^+ +	CO_2	$\Longrightarrow O^+$	+ CO	+ He	2.0×10^{-10}	0	0	1
101	He^+ +	CO_2	$\Longrightarrow CO^+$	+ O	+ He	8.0×10^{-10}	0	0	1
102	He^+ +	CO_2	$\Longrightarrow C^+$	+ O_2	+ He	4.0×10^{-11}	0	0	1
103	He^+ +	OCN	$\Longrightarrow O^+$	+ CN	+ He	3.0×10^{-09}	0	0	1
104	He^+ +	OCN	$\Longrightarrow CN^+$	+ O	+ He	3.0×10^{-09}	0	0	1
105	He^+ +	H_2S	$\Longrightarrow H_2S^+$	+ He		3.1×10^{-10}	0	0	1
106	He^+ +	H_2S	$\Longrightarrow S^+$	+ H_2	+ He	3.6×10^{-09}	0	0	1
107	He^+ +	H_2S	$\Longrightarrow HS^+$	+ H	+ He	4.8×10^{-10}	0	0	1
108	He^+ +	OCS	$\Longrightarrow CS^+$	+ O	+ He	7.6×10^{-10}	0	0	1
109	He^+ +	OCS	$\Longrightarrow S^+$	+ CO	+ He	7.6×10^{-10}	0	0	1
110	He^+ +	OCS	$\Longrightarrow CO^+$	+ S	+ He	7.6×10^{-10}	0	0	1
111	He^+ +	OCS	$\Longrightarrow O^+$	+ CS	+ He	7.6×10^{-11}	0	0	1
112	He^+ +	SO_2	$\Longrightarrow O_2{}^+$	+ S	+ He	7.9×10^{-10}	0	0	1
113	He^+ +	SO_2	$\Longrightarrow S^+$	+ O_2	+ He	7.9×10^{-10}	0	0	1
114	He^+ +	SO_2	$\Longrightarrow SO^+$	+ O	+ He	7.9×10^{-10}	0	0	1
115	He^+ +	H_2CO	$\Longrightarrow CO^+$	+ H_2	+ He	1.0×10^{-09}	0	0	1
116	He^+ +	H_2CO	$\Longrightarrow HCO^+$	+ H	+ He	1.0×10^{-09}	0	0	1
117	He^+ +	NH_3	$\Longrightarrow NH_3{}^+$	+ He		2.6×10^{-10}	0	0	1
118	He^+ +	NH_3	$\Longrightarrow NH^+$	+ H_2	+ He	2.0×10^{-10}	0	0	1
119	He^+ +	NH_3	$\Longrightarrow NH_2{}^+$	+ H	+ He	1.8×10^{-09}	0	0	1
120	He^+ +	C_2H2	$\Longrightarrow C_2{}^+$	+ H_2	+ He	1.6×10^{-09}	0	0	1
121	He^+ +	C_2H2	$\Longrightarrow C_2H2^+$	+ He		2.5×10^{-10}	0	0	1
122	He^+ +	C_2H2	$\Longrightarrow C_2H^+$	+ H	+ He	8.8×10^{-10}	0	0	1
123	He^+ +	C_2H2	$\Longrightarrow CH^+$	+ CH	+ He	7.7×10^{-10}	0	0	1
124	He^+ +	CH_3	$\Longrightarrow CH^+$	+ H_2	+ He	1.8×10^{-09}	0	0	1
125	He^+ +	CH_4	$\Longrightarrow CH_2{}^+$	+ H_2	+ He	9.3×10^{-10}	0	0	1
126	He^+ +	CH_4	$\Longrightarrow CH_3{}^+$	+ H	+ He	6.3×10^{-11}	0	0	1
127	He^+ +	CH_4	$\Longrightarrow CH_4{}^+$	+ He		3.8×10^{-11}	0	0	1
128	He^+ +	HC_3N	$\Longrightarrow C_2H^+$	+ CN	+ He	1.0×10^{-10}	0	0	1
129	He^+ +	H_2CS	$\Longrightarrow CS^+$	+ H_2	+ He	8.1×10^{-10}	0	0	1
130	He^+ +	H_2CS	$\Longrightarrow CH_2{}^+$	+ S	+ He	8.1×10^{-10}	0	0	1
131	He^+ +	H_2CS	$\Longrightarrow S^+$	+ CH_2	+ He	8.1×10^{-10}	0	0	1
132	He^+ +	CH_3CN	$\Longrightarrow CH_3{}^+$	+ CN	+ He	1.2×10^{-09}	0	0	1
133	He^+ +	CH_3CN	$\Longrightarrow CN^+$	+ CH_3	+ He	1.2×10^{-09}	0	0	1
134	He^+ +	CH_3OH	$\Longrightarrow OH^+$	+ CH_3	+ He	1.1×10^{-09}	0	0	1
135	He^+ +	CH_3OH	$\Longrightarrow CH_3{}^+$	+ OH	+ He	1.1×10^{-09}	0	0	1
136	C^+ +	Si	$\Longrightarrow Si^+$	+ C		2.1×10^{-09}	0	0	1

continued on next page

continued from previous page

Nr.	Reaction					A	E_a	α	Ref.
137	C^+ +	S	$\Longrightarrow$ S^+	+	C	1.5×10^{-09}	0	0	1
138	C^+ +	Fe	$\Longrightarrow$ Fe^+	+	C	2.6×10^{-09}	0	0	1
139	C^+ +	Na	$\Longrightarrow$ Na^+	+	C	1.1×10^{-09}	0	0	1
140	C^+ +	Mg	$\Longrightarrow$ Mg^+	+	C	1.1×10^{-09}	0	0	1
141	C^+ +	O_2	$\Longrightarrow$ CO^+	+	O	7.5×10^{-10}	0	0	1
142	C^+ +	O_2	$\Longrightarrow$ O^+	+	CO	4.1×10^{-10}	0	0	1
143	C^+ +	CH	$\Longrightarrow$ $C_2{}^+$	+	H	1.0×10^{-09}	0	0	1
144	C^+ +	CH	$\Longrightarrow$ CH^+	+	C	1.0×10^{-09}	0	0	1
145	C^+ +	NH	$\Longrightarrow$ CN^+	+	H	7.8×10^{-10}	0	0	1
146	C^+ +	OH	$\Longrightarrow$ CO^+	+	H	7.7×10^{-10}	0	0	1
147	C^+ +	NO	$\Longrightarrow$ NO^+	+	C	8.5×10^{-10}	0	0	1
148	C^+ +	SiC	$\Longrightarrow$ Si^+	+	C_2	2.5×10^{-09}	0	0	1
149	C^+ +	SiC	$\Longrightarrow$ SiC^+	+	C	2.5×10^{-09}	0	0	1
150	C^+ +	SiS	$\Longrightarrow$ SiC^+	+	S	2.3×10^{-09}	0	0	1
151	C^+ +	SiS	$\Longrightarrow$ SiS^+	+	C	2.3×10^{-09}	0	0	1
152	C^+ +	SiO	$\Longrightarrow$ SiO^+	+	C	5.4×10^{-10}	0	0	1
153	C^+ +	SiO	$\Longrightarrow$ Si^+	+	CO	5.4×10^{-10}	0	0	1
154	C^+ +	SiH	$\Longrightarrow$ SiC^+	+	H	1.1×10^{-09}	0	0	1
155	C^+ +	HS	$\Longrightarrow$ CS^+	+	H	1.1×10^{-09}	0	0	1
156	C^+ +	CS	$\Longrightarrow$ CS^+	+	C	1.6×10^{-09}	0	0	1
157	C^+ +	NS	$\Longrightarrow$ NS^+	+	C	7.6×10^{-10}	0	0	1
158	C^+ +	NS	$\Longrightarrow$ CS^+	+	N	7.6×10^{-10}	0	0	1
159	C^+ +	SO	$\Longrightarrow$ S^+	+	CO	2.6×10^{-10}	0	0	1
160	C^+ +	SO	$\Longrightarrow$ CS^+	+	O	2.6×10^{-10}	0	0	1
161	C^+ +	SO	$\Longrightarrow$ SO^+	+	C	2.6×10^{-10}	0	0	1
162	C^+ +	SO	$\Longrightarrow$ CO^+	+	S	2.6×10^{-10}	0	0	1
163	C^+ +	CH_2	$\Longrightarrow$ $CH_2{}^+$	+	C	5.2×10^{-10}	0	0	1
164	C^+ +	CH_2	$\Longrightarrow$ C_2H^+	+	H	5.2×10^{-10}	0	0	1
165	C^+ +	NH_2	$\Longrightarrow$ HCN^+	+	H	5.5×10^{-10}	0	0	1
166	C^+ +	H_2O	$\Longrightarrow$ HCO^+	+	H	2.7×10^{-09}	0	0	1
167	C^+ +	HCN	$\Longrightarrow$ C_2N^+	+	H	3.2×10^{-09}	0	0	1
168	C^+ +	HCO	$\Longrightarrow$ HCO^+	+	C	4.8×10^{-10}	0	0	1
169	C^+ +	HCO	$\Longrightarrow$ CH^+	+	CO	4.8×10^{-10}	0	0	1
170	C^+ +	C_2H	$\Longrightarrow$ $C_3{}^+$	+	H	1.0×10^{-09}	0	0	1
171	C^+ +	CO_2	$\Longrightarrow$ CO^+	+	CO	1.1×10^{-09}	0	0	1
172	C^+ +	OCN	$\Longrightarrow$ CO^+	+	CN	3.8×10^{-09}	0	0	1
173	C^+ +	H_2S	$\Longrightarrow$ HCS^+	+	H	1.4×10^{-09}	0	0	1
174	C^+ +	H_2S	$\Longrightarrow$ H_2S^+	+	C	6.0×10^{-10}	0	0	1
175	C^+ +	OCS	$\Longrightarrow$ CO^+	+	CS	9.3×10^{-10}	0	0	1
176	C^+ +	OCS	$\Longrightarrow$ CS^+	+	CO	9.3×10^{-10}	0	0	1
177	C^+ +	SO_2	$\Longrightarrow$ SO^+	+	CO	2.3×10^{-09}	0	0	1
178	C^+ +	H_2CO	$\Longrightarrow$ $CH_2{}^+$	+	CO	2.1×10^{-09}	0	0	1
179	C^+ +	H_2CO	$\Longrightarrow$ HCO^+	+	CH	9.2×10^{-10}	0	0	1
180	C^+ +	H_2CO	$\Longrightarrow$ H_2CO^+	+	C	1.4×10^{-09}	0	0	1
181	C^+ +	NH_3	$\Longrightarrow$ H_2CN^+	+	H	1.1×10^{-09}	0	0	1
182	C^+ +	NH_3	$\Longrightarrow$ $NH_3{}^+$	+	C	1.2×10^{-09}	0	0	1

continued on next page

continued from previous page

Nr.	Reaction	A	E_a	α	Ref.
183	$C^+ + NH_3 \Longrightarrow HCN^+ + H_2$	7.0×10^{-11}	0	0	1
184	$C^+ + C_2H2 \Longrightarrow C_3H^+ + H$	1.5×10^{-09}	0	0	1
185	$C^+ + CH_3 \Longrightarrow C_2H2^+ + H$	1.3×10^{-09}	0	0	1
186	$C^+ + CH_4 \Longrightarrow C_2H3^+ + H$	1.0×10^{-09}	0	0	1
187	$C^+ + CH_4 \Longrightarrow C_2H2^+ + H_2$	5.0×10^{-10}	0	0	1
188	$C^+ + H_2CS \Longrightarrow CH_2{}^+ + CS$	1.5×10^{-09}	0	0	1
189	$N^+ + Fe \Longrightarrow Fe^+ + N$	1.5×10^{-09}	0	0	1
190	$N^+ + Mg \Longrightarrow Mg^+ + N$	1.2×10^{-09}	0	0	1
191	$N^+ + H_2 \Longrightarrow NH^+ + H$	7.0×10^{-10}	0	0	1
192	$N^+ + C_2 \Longrightarrow C_2{}^+ + N$	1.0×10^{-09}	0	0	1
193	$N^+ + O_2 \Longrightarrow O^+ + NO$	3.6×10^{-11}	0	0	1
194	$N^+ + O_2 \Longrightarrow NO^+ + O$	1.7×10^{-10}	0	0	1
195	$N^+ + O_2 \Longrightarrow O_2{}^+ + N$	4.0×10^{-10}	0	0	1
196	$N^+ + CH \Longrightarrow CN^+ + H$	3.6×10^{-10}	0	0	1
197	$N^+ + CH \Longrightarrow CH^+ + N$	3.6×10^{-10}	0	0	1
198	$N^+ + NH \Longrightarrow N_2{}^+ + H$	3.7×10^{-10}	0	0	1
199	$N^+ + NH \Longrightarrow NH^+ + N$	3.7×10^{-10}	0	0	1
200	$N^+ + OH \Longrightarrow OH^+ + N$	3.7×10^{-10}	0	0	1
201	$N^+ + OH \Longrightarrow NO^+ + H$	3.7×10^{-10}	0	0	1
202	$N^+ + CO \Longrightarrow CO^+ + N$	4.9×10^{-10}	0	0	1
203	$N^+ + CO \Longrightarrow C^+ + NO$	1.0×10^{-11}	0	0	1
204	$N^+ + CO \Longrightarrow NO^+ + C$	6.0×10^{-11}	0	0	1
205	$N^+ + CN \Longrightarrow CN^+ + N$	1.1×10^{-09}	0	0	1
206	$N^+ + NO \Longrightarrow NO^+ + N$	5.1×10^{-10}	0	0	1
207	$N^+ + NO \Longrightarrow N_2{}^+ + O$	5.0×10^{-11}	0	0	1
208	$N^+ + CH_2 \Longrightarrow CH_2{}^+ + N$	1.0×10^{-09}	0	0	1
209	$N^+ + NH_2 \Longrightarrow NH_2{}^+ + N$	1.0×10^{-09}	0	0	1
210	$N^+ + H_2O \Longrightarrow H_2O^+ + N$	2.6×10^{-09}	0	0	1
211	$N^+ + HCN \Longrightarrow HCN^+ + N$	1.2×10^{-09}	0	0	1
212	$N^+ + HCO \Longrightarrow NH^+ + CO$	4.5×10^{-10}	0	0	1
213	$N^+ + HCO \Longrightarrow HCO^+ + N$	4.5×10^{-10}	0	0	1
214	$N^+ + C_2H \Longrightarrow C_2H^+ + N$	9.5×10^{-10}	0	0	1
215	$N^+ + CO_2 \Longrightarrow CO_2{}^+ + N$	1.3×10^{-09}	0	0	1
216	$N^+ + H_2CO \Longrightarrow NH_2{}^+ + CO$	1.3×10^{-09}	0	0	1
217	$O^+ + H \Longrightarrow H^+ + O$	7.0×10^{-10}	0	0	1
218	$O^+ + Fe \Longrightarrow Fe^+ + O$	2.9×10^{-09}	0	0	1
219	$O^+ + H_2 \Longrightarrow OH^+ + H$	1.6×10^{-09}	0	0	1
220	$O^+ + C_2 \Longrightarrow C_2{}^+ + O$	4.8×10^{-10}	0	0	1
221	$O^+ + C_2 \Longrightarrow CO^+ + C$	4.8×10^{-10}	0	0	1
222	$O^+ + N_2 \Longrightarrow NO^+ + N$	1.2×10^{-12}	0	0	1
223	$O^+ + O_2 \Longrightarrow O_2{}^+ + O$	2.0×10^{-11}	0	0	1
224	$O^+ + CH \Longrightarrow CH^+ + O$	3.5×10^{-10}	0	0	1
225	$O^+ + CH \Longrightarrow CO^+ + H$	3.5×10^{-10}	0	0	1
226	$O^+ + NH \Longrightarrow NH^+ + O$	3.6×10^{-10}	0	0	1
227	$O^+ + NH \Longrightarrow NO^+ + H$	3.6×10^{-10}	0	0	1
228	$O^+ + OH \Longrightarrow OH^+ + O$	3.6×10^{-10}	0	0	1

continued on next page

continued from previous page

Nr.	Reaction					A	E_a	α	Ref.
229	O^+ +	OH	$\Longrightarrow$ $O_2{}^+$	+	H	3.6×10^{-10}	0	0	1
230	O^+ +	NO	$\Longrightarrow$ NO^+	+	O	1.0×10^{-12}	0	0	1
231	O^+ +	CH_2	$\Longrightarrow$ $CH_2{}^+$	+	O	9.7×10^{-10}	0	0	1
232	O^+ +	NH_2	$\Longrightarrow$ $NH_2{}^+$	+	O	1.0×10^{-09}	0	0	1
233	O^+ +	H_2O	$\Longrightarrow$ H_2O^+	+	O	2.3×10^{-09}	0	0	1
234	O^+ +	HCO	$\Longrightarrow$ OH^+	+	CO	4.3×10^{-10}	0	0	1
235	O^+ +	HCO	$\Longrightarrow$ HCO^+	+	O	4.3×10^{-10}	0	0	1
236	O^+ +	C_2H	$\Longrightarrow$ C_2H^+	+	O	4.6×10^{-10}	0	0	1
237	O^+ +	C_2H	$\Longrightarrow$ CO^+	+	CH	4.6×10^{-10}	0	0	1
238	O^+ +	CO_2	$\Longrightarrow$ $O_2{}^+$	+	CO	1.1×10^{-09}	0	0	1
239	O^+ +	H_2S	$\Longrightarrow$ H_2S^+	+	O	1.8×10^{-09}	0	0	1
240	O^+ +	H_2CO	$\Longrightarrow$ CO^+	+	H_2O	4.0×10^{-10}	0	0	1
241	O^+ +	H_2CO	$\Longrightarrow$ H_2CO^+	+	O	4.0×10^{-10}	0	0	1
242	O^+ +	H_2CO	$\Longrightarrow$ H_2O^+	+	CO	4.0×10^{-10}	0	0	1
243	Si^+ +	Fe	$\Longrightarrow$ Fe^+	+	Si	1.9×10^{-09}	0	0	1
244	Si^+ +	Na	$\Longrightarrow$ Na^+	+	Si	2.7×10^{-09}	0	0	1
245	Si^+ +	Mg	$\Longrightarrow$ Mg^+	+	Si	2.9×10^{-09}	0	0	1
246	Si^+ +	O_2	$\Longrightarrow$ SiO^+	+	O	7.6×10^{-10}	0	0	1
247	Si^+ +	CH	$\Longrightarrow$ SiC^+	+	H	6.3×10^{-10}	0	0	1
248	Si^+ +	OH	$\Longrightarrow$ SiO^+	+	H	6.3×10^{-10}	0	0	1
249	Si^+ +	CH_2	$\Longrightarrow$ $CHSi^+$	+	H	8.7×10^{-10}	0	0	1
250	Si^+ +	H_2O	$\Longrightarrow$ $SiOH^+$	+	H	8.5×10^{-10}	0	0	1
251	Si^+ +	OCS	$\Longrightarrow$ SiS^+	+	CO	1.3×10^{-09}	0	0	1
252	Si^+ +	CH_3	$\Longrightarrow$ CH_2Si^+	+	H	1.0×10^{-09}	0	0	1
253	S^+ +	Si	$\Longrightarrow$ Si^+	+	S	1.6×10^{-09}	0	0	1
254	S^+ +	Fe	$\Longrightarrow$ Fe^+	+	S	1.8×10^{-10}	0	0	1
255	S^+ +	Na	$\Longrightarrow$ Na^+	+	S	2.6×10^{-10}	0	0	1
256	S^+ +	Mg	$\Longrightarrow$ Mg^+	+	S	2.8×10^{-10}	0	0	1
257	S^+ +	C_2	$\Longrightarrow$ CS^+	+	C	8.1×10^{-10}	0	0	1
258	S^+ +	CH	$\Longrightarrow$ CS^+	+	H	6.2×10^{-10}	0	0	1
259	S^+ +	NH	$\Longrightarrow$ NS^+	+	H	6.3×10^{-10}	0	0	1
260	S^+ +	OH	$\Longrightarrow$ SO^+	+	H	6.1×10^{-10}	0	0	1
261	S^+ +	NO	$\Longrightarrow$ NO^+	+	S	4.2×10^{-10}	0	0	1
262	S^+ +	SiC	$\Longrightarrow$ SiC^+	+	S	3.7×10^{-09}	0	0	1
263	S^+ +	SiS	$\Longrightarrow$ SiS^+	+	S	3.2×10^{-09}	0	0	1
264	S^+ +	SiH	$\Longrightarrow$ SiS^+	+	H	4.2×10^{-10}	0	0	1
265	S^+ +	SiH	$\Longrightarrow$ SiH^+	+	S	4.2×10^{-10}	0	0	1
266	S^+ +	CH_2	$\Longrightarrow$ HCS^+	+	H	1.0×10^{-11}	0	0	1
267	S^+ +	HCO	$\Longrightarrow$ HS^+	+	CO	3.6×10^{-10}	0	0	1
268	S^+ +	HCO	$\Longrightarrow$ HCO^+	+	S	3.6×10^{-10}	0	0	1
269	S^+ +	H_2CO	$\Longrightarrow$ H_2S^+	+	CO	8.9×10^{-10}	0	0	1
270	S^+ +	NH_3	$\Longrightarrow$ $NH_2{}^+$	+	HS	7.0×10^{-11}	0	0	1
271	S^+ +	NH_3	$\Longrightarrow$ $NH_3{}^+$	+	S	1.2×10^{-09}	0	0	1
272	S^+ +	CH_3	$\Longrightarrow$ H_2CS^+	+	H	1.0×10^{-11}	0	0	1
273	S^+ +	CH_4	$\Longrightarrow$ H_3CS^+	+	H	1.4×10^{-10}	0	0	1
274	Fe^+ +	Na	$\Longrightarrow$ Na^+	+	Fe	1.0×10^{-11}	0	0	1

continued on next page

continued from previous page

Nr.	Reaction	A	E_a	α	Ref.
275	$Mg^+ + Na \Longrightarrow Na^+ + Mg$	1.0×10^{-11}	0	0	1
276	$SiH^+ + H \Longrightarrow Si^+ + H_2$	1.9×10^{-09}	0	0	1
277	$SiH^+ + O \Longrightarrow SiO^+ + H$	6.1×10^{-10}	0	0	1
278	$SiH^+ + H_2 \Longrightarrow SiH_2{}^+ + H$	4.5×10^{-10}	0	0	1
279	$SiH^+ + CH \Longrightarrow CH_2{}^+ + Si$	6.0×10^{-10}	0	0	1
280	$SiH^+ + H_2O \Longrightarrow H_3O^+ + Si$	8.0×10^{-10}	0	0	1
281	$SiH^+ + HCN \Longrightarrow H_2CN^+ + Si$	9.4×10^{-10}	0	0	1
282	$SiH^+ + HCO \Longrightarrow H_2CO^+ + Si$	6.8×10^{-10}	0	0	1
283	$SiH^+ + NH_3 \Longrightarrow NH_4{}^+ + Si$	1.0×10^{-09}	0	0	1
284	$H_2{}^+ + H \Longrightarrow H^+ + H_2$	1.0×10^{-10}	0	0	1
285	$H_2{}^+ + C \Longrightarrow CH^+ + H$	2.4×10^{-09}	0	0	1
286	$H_2{}^+ + N \Longrightarrow NH^+ + H$	1.9×10^{-09}	0	0	1
287	$H_2{}^+ + O \Longrightarrow OH^+ + H$	1.5×10^{-09}	0	0	1
288	$H_2{}^+ + H_2 \Longrightarrow H_3{}^+ + H$	2.1×10^{-09}	0	0	1
289	$H_2{}^+ + C_2 \Longrightarrow C_2H^+ + H$	1.1×10^{-09}	0	0	1
290	$H_2{}^+ + C_2 \Longrightarrow C_2{}^+ + H_2$	1.1×10^{-09}	0	0	1
291	$H_2{}^+ + N_2 \Longrightarrow N_2H^+ + H$	2.0×10^{-09}	0	0	1
292	$H_2{}^+ + O_2 \Longrightarrow O_2H^+ + H$	1.9×10^{-09}	0	0	1
293	$H_2{}^+ + O_2 \Longrightarrow O_2{}^+ + H_2$	8.0×10^{-10}	0	0	1
294	$H_2{}^+ + CH \Longrightarrow CH^+ + H_2$	7.1×10^{-10}	0	0	1
295	$H_2{}^+ + CH \Longrightarrow CH_2{}^+ + H$	7.1×10^{-10}	0	0	1
296	$H_2{}^+ + NH \Longrightarrow NH_2{}^+ + H$	7.6×10^{-10}	0	0	1
297	$H_2{}^+ + NH \Longrightarrow NH^+ + H_2$	7.6×10^{-10}	0	0	1
298	$H_2{}^+ + OH \Longrightarrow OH^+ + H_2$	7.6×10^{-10}	0	0	1
299	$H_2{}^+ + OH \Longrightarrow H_2O^+ + H$	7.6×10^{-10}	0	0	1
300	$H_2{}^+ + CO \Longrightarrow CO^+ + H_2$	6.0×10^{-10}	0	0	1
301	$H_2{}^+ + CO \Longrightarrow HCO^+ + H$	2.2×10^{-09}	0	0	1
302	$H_2{}^+ + CN \Longrightarrow HCN^+ + H$	1.2×10^{-09}	0	0	1
303	$H_2{}^+ + CN \Longrightarrow CN^+ + H_2$	1.2×10^{-09}	0	0	1
304	$H_2{}^+ + NO \Longrightarrow HNO^+ + H$	1.1×10^{-09}	0	0	1
305	$H_2{}^+ + NO \Longrightarrow NO^+ + H_2$	1.1×10^{-09}	0	0	1
306	$H_2{}^+ + CH_2 \Longrightarrow CH_3{}^+ + H$	1.0×10^{-09}	0	0	1
307	$H_2{}^+ + CH_2 \Longrightarrow CH_2{}^+ + H_2$	1.0×10^{-09}	0	0	1
308	$H_2{}^+ + NH_2 \Longrightarrow NH_2{}^+ + H_2$	2.1×10^{-09}	0	0	1
309	$H_2{}^+ + H_2O \Longrightarrow H_2O^+ + H_2$	3.9×10^{-09}	0	0	1
310	$H_2{}^+ + H_2O \Longrightarrow H_3O^+ + H$	3.4×10^{-09}	0	0	1
311	$H_2{}^+ + HCN \Longrightarrow HCN^+ + H_2$	2.7×10^{-09}	0	0	1
312	$H_2{}^+ + HCO \Longrightarrow H_3{}^+ + CO$	1.0×10^{-09}	0	0	1
313	$H_2{}^+ + HCO \Longrightarrow HCO^+ + H_2$	1.0×10^{-09}	0	0	1
314	$H_2{}^+ + C_2H \Longrightarrow C_2H^+ + H_2$	1.0×10^{-09}	0	0	1
315	$H_2{}^+ + C_2H \Longrightarrow C_2H2^+ + H$	1.0×10^{-09}	0	0	1
316	$H_2{}^+ + CO_2 \Longrightarrow CO_2{}^+ + H_2$	1.4×10^{-09}	0	0	1
317	$H_2{}^+ + CO_2 \Longrightarrow CO^+ + H_2O$	1.4×10^{-09}	0	0	1
318	$H_2{}^+ + H_2S \Longrightarrow HS^+ + H + H_2$	8.6×10^{-10}	0	0	1
319	$H_2{}^+ + H_2S \Longrightarrow H_2S^+ + H_2$	2.7×10^{-09}	0	0	1
320	$H_2{}^+ + H_2S \Longrightarrow S^+ + H_2 + H_2$	7.7×10^{-10}	0	0	1

continued on next page

continued from previous page

Nr.	Reaction	A	E_a	α	Ref.
321	$H_2^+ + H_2CO \Longrightarrow H_2CO^+ + H_2$	1.4×10^{-09}	0	0	1
322	$H_2^+ + H_2CO \Longrightarrow HCO^+ + H + H_2$	1.4×10^{-09}	0	0	1
323	$H_2^+ + NH_3 \Longrightarrow NH_3^+ + H_2$	5.7×10^{-09}	0	0	1
324	$H_2^+ + C_2H2 \Longrightarrow C_2H2^+ + H_2$	4.8×10^{-09}	0	0	1
325	$H_2^+ + C_2H2 \Longrightarrow C_2H3^+ + H$	4.8×10^{-10}	0	0	1
326	$H_2^+ + CH_4 \Longrightarrow CH_4^+ + H_2$	1.4×10^{-09}	0	0	1
327	$H_2^+ + CH_4 \Longrightarrow CH_5^+ + H$	1.1×10^{-10}	0	0	1
328	$H_2^+ + CH_4 \Longrightarrow CH_3^+ + H + H_2$	2.3×10^{-09}	0	0	1
329	$C_2^+ + C \Longrightarrow C^+ + C_2$	1.1×10^{-10}	0	0	1
330	$C_2^+ + N \Longrightarrow C^+ + CN$	8.3×10^{-11}	0	0	1
331	$C_2^+ + O \Longrightarrow CO^+ + C$	6.6×10^{-11}	0	0	1
332	$C_2^+ + S \Longrightarrow CS^+ + C$	5.8×10^{-10}	0	0	1
333	$C_2^+ + S \Longrightarrow S^+ + C_2$	5.8×10^{-10}	0	0	1
334	$C_2^+ + H_2 \Longrightarrow C_2H^+ + H$	1.1×10^{-09}	0	0	1
335	$C_2^+ + C_2 \Longrightarrow C_3^+ + C$	8.7×10^{-10}	0	0	1
336	$C_2^+ + O_2 \Longrightarrow CO^+ + CO$	8.0×10^{-10}	0	0	1
337	$C_2^+ + CH \Longrightarrow C_3^+ + H$	3.2×10^{-10}	0	0	1
338	$C_2^+ + CH \Longrightarrow CH^+ + C_2$	3.2×10^{-10}	0	0	1
339	$C_2^+ + NH \Longrightarrow C_2N^+ + H$	3.3×10^{-10}	0	0	1
340	$C_2^+ + NH \Longrightarrow C_2H^+ + N$	3.3×10^{-10}	0	0	1
341	$C_2^+ + OH \Longrightarrow OH^+ + C_2$	6.5×10^{-10}	0	0	1
342	$C_2^+ + NO \Longrightarrow NO^+ + C_2$	8.3×10^{-10}	0	0	1
343	$C_2^+ + CH_2 \Longrightarrow C_3H^+ + H$	4.5×10^{-10}	0	0	1
344	$C_2^+ + CH_2 \Longrightarrow CH_2^+ + C_2$	4.5×10^{-10}	0	0	1
345	$C_2^+ + NH_2 \Longrightarrow C_2NH^+ + H$	4.6×10^{-10}	0	0	1
346	$C_2^+ + NH_2 \Longrightarrow NH_2^+ + C_2$	4.6×10^{-10}	0	0	1
347	$C_2^+ + H_2O \Longrightarrow C_2HO^+ + H$	4.4×10^{-10}	0	0	1
348	$C_2^+ + H_2O \Longrightarrow C_2H^+ + OH$	4.4×10^{-10}	0	0	1
349	$C_2^+ + HCN \Longrightarrow C_3N^+ + H$	5.3×10^{-10}	0	0	1
350	$C_2^+ + HCN \Longrightarrow C_2H^+ + CN$	5.3×10^{-10}	0	0	1
351	$C_2^+ + HCO \Longrightarrow C_2H^+ + CO$	3.8×10^{-10}	0	0	1
352	$C_2^+ + HCO \Longrightarrow HCO^+ + C_2$	3.8×10^{-10}	0	0	1
353	$N_2^+ + H \Longrightarrow H^+ + N_2$	1.9×10^{-10}	0	0	1
354	$N_2^+ + C \Longrightarrow C^+ + N_2$	1.1×10^{-10}	0	0	1
355	$N_2^+ + N \Longrightarrow N^+ + N_2$	1.0×10^{-11}	0	0	1
356	$N_2^+ + O \Longrightarrow NO^+ + N$	1.4×10^{-10}	0	0	1
357	$N_2^+ + S \Longrightarrow S^+ + N_2$	1.1×10^{-09}	0	0	1
358	$N_2^+ + Fe \Longrightarrow Fe^+ + N_2$	4.3×10^{-10}	0	0	1
359	$N_2^+ + Na \Longrightarrow Na^+ + N_2$	1.9×10^{-09}	0	0	1
360	$N_2^+ + Mg \Longrightarrow Mg^+ + N_2$	7.0×10^{-10}	0	0	1
361	$N_2^+ + H_2 \Longrightarrow N_2H^+ + H$	1.7×10^{-09}	0	0	1
362	$N_2^+ + C_2 \Longrightarrow C_2^+ + N_2$	8.4×10^{-10}	0	0	1
363	$N_2^+ + O_2 \Longrightarrow O_2^+ + N_2$	5.0×10^{-11}	0	0	1
364	$N_2^+ + CH \Longrightarrow CH^+ + N_2$	6.3×10^{-10}	0	0	1
365	$N_2^+ + NH \Longrightarrow NH^+ + N_2$	6.5×10^{-10}	0	0	1
366	$N_2^+ + OH \Longrightarrow OH^+ + N_2$	6.3×10^{-10}	0	0	1

continued on next page

continued from previous page

Nr.	Reaction						A	E_a	α	Ref.
367	N_2^+	+	CO	$\Longrightarrow$	CO^+	+ N_2	7.0×10^{-11}	0	0	1
368	N_2^+	+	CN	$\Longrightarrow$	CN^+	+ N_2	1.0×10^{-10}	0	0	1
369	N_2^+	+	NO	$\Longrightarrow$	NO^+	+ N_2	3.3×10^{-10}	0	0	1
370	N_2^+	+	CH_2	$\Longrightarrow$	CH_2^+	+ N_2	8.7×10^{-10}	0	0	1
371	N_2^+	+	NH_2	$\Longrightarrow$	NH_2^+	+ N_2	8.9×10^{-10}	0	0	1
372	N_2^+	+	H_2O	$\Longrightarrow$	N_2H^+	+ OH	2.0×10^{-09}	0	0	1
373	N_2^+	+	H_2O	$\Longrightarrow$	H_2O^+	+ N_2	2.2×10^{-09}	0	0	1
374	N_2^+	+	HCN	$\Longrightarrow$	HCN^+	+ N_2	1.0×10^{-09}	0	0	1
375	N_2^+	+	HCO	$\Longrightarrow$	HCO^+	+ N_2	3.7×10^{-10}	0	0	1
376	N_2^+	+	HCO	$\Longrightarrow$	N_2H^+	+ CO	3.7×10^{-10}	0	0	1
377	N_2^+	+	C_2H	$\Longrightarrow$	C_2H^+	+ N_2	7.9×10^{-10}	0	0	1
378	N_2^+	+	CO_2	$\Longrightarrow$	CO_2^+	+ N_2	9.0×10^{-10}	0	0	1
379	N_2^+	+	H_2CO	$\Longrightarrow$	H_2CO^+	+ N_2	1.0×10^{-09}	0	0	1
380	O_2^+	+	C	$\Longrightarrow$	CO^+	+ O	5.2×10^{-11}	0	0	1
381	O_2^+	+	C	$\Longrightarrow$	C^+	+ O_2	5.2×10^{-11}	0	0	1
382	O_2^+	+	N	$\Longrightarrow$	NO^+	+ O	1.8×10^{-10}	0	0	1
383	O_2^+	+	Si	$\Longrightarrow$	Si^+	+ O_2	1.6×10^{-09}	0	0	1
384	O_2^+	+	S	$\Longrightarrow$	SO^+	+ O	5.4×10^{-10}	0	0	1
385	O_2^+	+	S	$\Longrightarrow$	S^+	+ O_2	5.4×10^{-10}	0	0	1
386	O_2^+	+	Fe	$\Longrightarrow$	Fe^+	+ O_2	1.1×10^{-09}	0	0	1
387	O_2^+	+	Na	$\Longrightarrow$	Na^+	+ O_2	2.0×10^{-09}	0	0	1
388	O_2^+	+	Mg	$\Longrightarrow$	Mg^+	+ O_2	1.2×10^{-09}	0	0	1
389	O_2^+	+	C_2	$\Longrightarrow$	CO^+	+ CO	4.1×10^{-10}	0	0	1
390	O_2^+	+	C_2	$\Longrightarrow$	C_2^+	+ O_2	4.1×10^{-10}	0	0	1
391	O_2^+	+	CH	$\Longrightarrow$	CH^+	+ O_2	3.1×10^{-10}	0	0	1
392	O_2^+	+	CH	$\Longrightarrow$	HCO^+	+ O	3.1×10^{-10}	0	0	1
393	O_2^+	+	NH	$\Longrightarrow$	NO_2^+	+ H	3.2×10^{-10}	0	0	1
394	O_2^+	+	NH	$\Longrightarrow$	HNO^+	+ O	3.2×10^{-10}	0	0	1
395	O_2^+	+	NO	$\Longrightarrow$	NO^+	+ O_2	6.3×10^{-10}	0	0	1
396	O_2^+	+	CH_2	$\Longrightarrow$	H_2CO^+	+ O	4.3×10^{-10}	0	0	1
397	O_2^+	+	CH_2	$\Longrightarrow$	CH_2^+	+ O_2	4.3×10^{-10}	0	0	1
398	O_2^+	+	NH_2	$\Longrightarrow$	NH_2^+	+ O_2	8.7×10^{-10}	0	0	1
399	O_2^+	+	HCO	$\Longrightarrow$	O_2H^+	+ CO	3.6×10^{-10}	0	0	1
400	O_2^+	+	HCO	$\Longrightarrow$	HCO^+	+ O_2	3.6×10^{-10}	0	0	1
401	O_2^+	+	H_2S	$\Longrightarrow$	H_2S^+	+ O_2	1.4×10^{-09}	0	0	1
402	O_2^+	+	H_2CO	$\Longrightarrow$	H_2CO^+	+ O_2	9.9×10^{-10}	0	0	1
403	O_2^+	+	NH_3	$\Longrightarrow$	NH_3^+	+ O_2	2.4×10^{-09}	0	0	1
404	HeH^+	+	H	$\Longrightarrow$	H_2^+	+ He	9.0×10^{-10}	0	0	1
405	HeH^+	+	H_2	$\Longrightarrow$	H_3^+	+ He	1.8×10^{-09}	0	0	1
406	CH^+	+	H	$\Longrightarrow$	C^+	+ H_2	9.4×10^{-12}	$1.2\times10^{+00}$	0	1
407	CH^+	+	C	$\Longrightarrow$	C_2^+	+ H	1.2×10^{-09}	0	0	1
408	CH^+	+	N	$\Longrightarrow$	CN^+	+ H	9.5×10^{-10}	0	0	1
409	CH^+	+	O	$\Longrightarrow$	CO^+	+ H	7.6×10^{-10}	0	0	1
410	CH^+	+	Si	$\Longrightarrow$	Si^+	+ CH	2.0×10^{-10}	0	0	1
411	CH^+	+	S	$\Longrightarrow$	S^+	+ CH	4.7×10^{-10}	0	0	1
412	CH^+	+	S	$\Longrightarrow$	HS^+	+ C	4.7×10^{-10}	0	0	1

continued on next page

continued from previous page

Nr.	Reaction					A	E_a	α	Ref.
413	CH^+ +	S	$\Longrightarrow$ CS^+	+ H		4.7×10^{-10}	0	0	1
414	CH^+ +	Fe	$\Longrightarrow$ Fe^+	+ CH		2.6×10^{-10}	0	0	1
415	CH^+ +	Na	$\Longrightarrow$ Na^+	+ CH		3.5×10^{-10}	0	0	1
416	CH^+ +	Mg	$\Longrightarrow$ Mg^+	+ CH		3.6×10^{-10}	0	0	1
417	CH^+ +	H_2	$\Longrightarrow$ $CH_2{}^+$	+ H		1.0×10^{-09}	0	0	1
418	CH^+ +	C_2	$\Longrightarrow$ $C_3{}^+$	+ H		1.0×10^{-09}	0	0	1
419	CH^+ +	O_2	$\Longrightarrow$ $CO_2{}^+$	+ H		4.8×10^{-10}	0	0	1
420	CH^+ +	O_2	$\Longrightarrow$ HCO^+	+ O		9.7×10^{-10}	0	0	1
421	CH^+ +	CH	$\Longrightarrow$ $C_2{}^+$	+ H_2		7.4×10^{-10}	0	0	1
422	CH^+ +	NH	$\Longrightarrow$ CN^+	+ H_2		7.6×10^{-10}	0	0	1
423	CH^+ +	OH	$\Longrightarrow$ CO^+	+ H_2		7.5×10^{-10}	0	0	1
424	CH^+ +	CN	$\Longrightarrow$ C_2N^+	+ H		1.1×10^{-09}	0	0	1
425	CH^+ +	NO	$\Longrightarrow$ NO^+	+ CH		1.0×10^{-09}	0	0	1
426	CH^+ +	CH_2	$\Longrightarrow$ C_2H^+	+ H_2		1.0×10^{-09}	0	0	1
427	CH^+ +	NH_2	$\Longrightarrow$ HCN^+	+ H_2		1.1×10^{-09}	0	0	1
428	CH^+ +	H_2O	$\Longrightarrow$ HCO^+	+ H_2		1.0×10^{-09}	0	0	1
429	CH^+ +	HCN	$\Longrightarrow$ C_2N^+	+ H_2		1.3×10^{-09}	0	0	1
430	CH^+ +	HCO	$\Longrightarrow$ $CH_2{}^+$	+ CO		4.6×10^{-10}	0	0	1
431	CH^+ +	HCO	$\Longrightarrow$ HCO^+	+ CH		4.6×10^{-10}	0	0	1
432	CH^+ +	C_2H	$\Longrightarrow$ $C_3{}^+$	+ H_2		9.8×10^{-10}	0	0	1
433	CH^+ +	CO_2	$\Longrightarrow$ HCO^+	+ CO		1.2×10^{-09}	0	0	1
434	CH^+ +	H_2S	$\Longrightarrow$ HCS^+	+ H_2		6.6×10^{-10}	0	0	1
435	CH^+ +	H_2CO	$\Longrightarrow$ C_2H2O^+	+ H		1.3×10^{-09}	0	0	1
436	CH^+ +	CH_4	$\Longrightarrow$ C_2H2^+	+ H_2 +	H	1.6×10^{-10}	0	0	1
437	CH^+ +	CH_4	$\Longrightarrow$ C_2H3^+	+ H_2		1.1×10^{-10}	0	0	1
438	NH^+ +	C	$\Longrightarrow$ CH^+	+ N		1.6×10^{-09}	0	0	1
439	NH^+ +	N	$\Longrightarrow$ $N_2{}^+$	+ H		1.3×10^{-09}	0	0	1
440	NH^+ +	O	$\Longrightarrow$ OH^+	+ N		1.0×10^{-09}	0	0	1
441	NH^+ +	S	$\Longrightarrow$ NS^+	+ H		6.9×10^{-10}	0	0	1
442	NH^+ +	S	$\Longrightarrow$ HS^+	+ N		6.9×10^{-10}	0	0	1
443	NH^+ +	S	$\Longrightarrow$ S^+	+ NH		6.9×10^{-10}	0	0	1
444	NH^+ +	H_2	$\Longrightarrow$ $NH_2{}^+$	+ H		1.0×10^{-09}	0	0	1
445	NH^+ +	C_2	$\Longrightarrow$ C_2N^+	+ H		4.9×10^{-10}	0	0	1
446	NH^+ +	C_2	$\Longrightarrow$ HCN^+	+ C		4.9×10^{-10}	0	0	1
447	NH^+ +	C_2	$\Longrightarrow$ C_2H^+	+ N		4.9×10^{-10}	0	0	1
448	NH^+ +	N_2	$\Longrightarrow$ N_2H^+	+ N		1.5×10^{-09}	0	0	1
449	NH^+ +	O_2	$\Longrightarrow$ $NO_2{}^+$	+ H		7.1×10^{-10}	0	0	1
450	NH^+ +	O_2	$\Longrightarrow$ O_2H^+	+ N		7.1×10^{-10}	0	0	1
451	NH^+ +	CH	$\Longrightarrow$ $CH_2{}^+$	+ N		9.9×10^{-09}	0	0	1
452	NH^+ +	NH	$\Longrightarrow$ $NH_2{}^+$	+ N		1.0×10^{-09}	0	0	1
453	NH^+ +	OH	$\Longrightarrow$ H_2O^+	+ N		1.0×10^{-09}	0	0	1
454	NH^+ +	CO	$\Longrightarrow$ HCO^+	+ N		1.6×10^{-09}	0	0	1
455	NH^+ +	CN	$\Longrightarrow$ HCN^+	+ N		1.6×10^{-09}	0	0	1
456	NH^+ +	NO	$\Longrightarrow$ HNO^+	+ N		1.5×10^{-09}	0	0	1
457	NH^+ +	CH_2	$\Longrightarrow$ $CH_3{}^+$	+ N		1.4×10^{-09}	0	0	1
458	NH^+ +	NH_2	$\Longrightarrow$ $NH_3{}^+$	+ N		1.5×10^{-09}	0	0	1

continued on next page

continued from previous page

Nr.	Reaction					A	E_a	α	Ref.
459	NH^+ +	H_2O	$\Longrightarrow$	H_3O^+ +	N	1.4×10^{-09}	0	0	1
460	NH^+ +	HCN	$\Longrightarrow$	H_2CN^+ +	N	1.8×10^{-09}	0	0	1
461	NH^+ +	HCO	$\Longrightarrow$	H_2CO^+ +	N	1.3×10^{-09}	0	0	1
462	NH^+ +	C_2H	$\Longrightarrow$	C_2H2^+ +	N	1.4×10^{-09}	0	0	1
463	NH^+ +	CO_2	$\Longrightarrow$	$HCO_2{}^+$ +	N	1.0×10^{-09}	0	0	1
464	NH^+ +	H_2CO	$\Longrightarrow$	H_3CO^+ +	N	1.9×10^{-09}	0	0	1
465	OH^+ +	C	$\Longrightarrow$	CH^+ +	O	1.2×10^{-09}	0	0	1
466	OH^+ +	N	$\Longrightarrow$	NO^+ +	H	8.9×10^{-10}	0	0	1
467	OH^+ +	O	$\Longrightarrow$	$O_2{}^+$ +	H	7.1×10^{-10}	0	0	1
468	OH^+ +	Si	$\Longrightarrow$	SiH^+ +	O	1.9×10^{-09}	0	0	1
469	OH^+ +	S	$\Longrightarrow$	S^+ +	OH	4.3×10^{-10}	0	0	1
470	OH^+ +	S	$\Longrightarrow$	SO^+ +	H	4.3×10^{-10}	0	0	1
471	OH^+ +	S	$\Longrightarrow$	HS^+ +	O	4.3×10^{-10}	0	0	1
472	OH^+ +	H_2	$\Longrightarrow$	H_2O^+ +	H	1.1×10^{-09}	0	0	1
473	OH^+ +	C_2	$\Longrightarrow$	C_2H^+ +	O	4.8×10^{-10}	0	0	1
474	OH^+ +	C_2	$\Longrightarrow$	$C_2{}^+$ +	OH	4.8×10^{-10}	0	0	1
475	OH^+ +	N_2	$\Longrightarrow$	N_2H^+ +	O	9.5×10^{-10}	0	0	1
476	OH^+ +	O_2	$\Longrightarrow$	$O_2{}^+$ +	OH	2.0×10^{-10}	0	0	1
477	OH^+ +	CH	$\Longrightarrow$	CH^+ +	OH	3.5×10^{-10}	0	0	1
478	OH^+ +	CH	$\Longrightarrow$	$CH_2{}^+$ +	O	3.5×10^{-10}	0	0	1
479	OH^+ +	NH	$\Longrightarrow$	NH^+ +	OH	3.6×10^{-10}	0	0	1
480	OH^+ +	NH	$\Longrightarrow$	$NH_2{}^+$ +	O	3.6×10^{-10}	0	0	1
481	OH^+ +	OH	$\Longrightarrow$	H_2O^+ +	O	7.0×10^{-10}	0	0	1
482	OH^+ +	CO	$\Longrightarrow$	HCO^+ +	O	2.0×10^{-11}	0	0	1
483	OH^+ +	CN	$\Longrightarrow$	HCN^+ +	O	1.0×10^{-09}	0	0	1
484	OH^+ +	NO	$\Longrightarrow$	NO^+ +	OH	4.6×10^{-10}	0	0	1
485	OH^+ +	NO	$\Longrightarrow$	HNO^+ +	O	4.6×10^{-10}	0	0	1
486	OH^+ +	SiC	$\Longrightarrow$	$CHSi^+$ +	O	4.5×10^{-09}	0	0	1
487	OH^+ +	SiO	$\Longrightarrow$	$SiOH^+$ +	O	9.4×10^{-10}	0	0	1
488	OH^+ +	SiH	$\Longrightarrow$	$SiH_2{}^+$ +	O	1.0×10^{-09}	0	0	1
489	OH^+ +	CH_2	$\Longrightarrow$	$CH_2{}^+$ +	OH	4.8×10^{-10}	0	0	1
490	OH^+ +	CH_2	$\Longrightarrow$	$CH_3{}^+$ +	O	4.8×10^{-10}	0	0	1
491	OH^+ +	NH_2	$\Longrightarrow$	$NH_3{}^+$ +	O	5.0×10^{-10}	0	0	1
492	OH^+ +	NH_2	$\Longrightarrow$	$NH_2{}^+$ +	OH	5.0×10^{-10}	0	0	1
493	OH^+ +	H_2O	$\Longrightarrow$	H_2O^+ +	OH	1.5×10^{-09}	0	0	1
494	OH^+ +	H_2O	$\Longrightarrow$	H_3O^+ +	O	1.3×10^{-09}	0	0	1
495	OH^+ +	HCN	$\Longrightarrow$	H_2CN^+ +	O	1.2×10^{-09}	0	0	1
496	OH^+ +	HCO	$\Longrightarrow$	H_2O^+ +	CO	2.8×10^{-10}	0	0	1
497	OH^+ +	HCO	$\Longrightarrow$	HCO^+ +	OH	2.8×10^{-10}	0	0	1
498	OH^+ +	HCO	$\Longrightarrow$	H_2CO^+ +	O	2.8×10^{-10}	0	0	1
499	OH^+ +	C_2H	$\Longrightarrow$	C_2H2^+ +	O	4.5×10^{-10}	0	0	1
500	OH^+ +	C_2H	$\Longrightarrow$	C_2H^+ +	OH	4.5×10^{-10}	0	0	1
501	OH^+ +	CO_2	$\Longrightarrow$	HCO^+ +	O_2	5.4×10^{-10}	0	0	1
502	OH^+ +	CO_2	$\Longrightarrow$	$HCO_2{}^+$ +	O	5.4×10^{-10}	0	0	1
503	OH^+ +	H_2S	$\Longrightarrow$	H_3S^+ +	O	9.1×10^{-10}	0	0	1
504	OH^+ +	H_2CO	$\Longrightarrow$	H_3CO^+ +	O	5.9×10^{-10}	0	0	1

continued on next page

continued from previous page

Nr.	Reaction					A	E_a	α	Ref.
505	OH^+ +	H_2CO	$\Longrightarrow$ H_2CO^+	+	OH	5.9×10^{-10}	0	0	1
506	OH^+ +	NH_3	$\Longrightarrow$ $NH_3{}^+$	+	OH	1.2×10^{-09}	0	0	1
507	OH^+ +	NH_3	$\Longrightarrow$ $NH_4{}^+$	+	O	1.2×10^{-09}	0	0	1
508	OH^+ +	CH_4	$\Longrightarrow$ H_3O^+	+	CH_2	1.3×10^{-09}	0	0	1
509	CO^+ +	H	$\Longrightarrow$ H^+	+	CO	1.9×10^{-10}	0	0	1
510	CO^+ +	C	$\Longrightarrow$ C^+	+	CO	1.1×10^{-10}	0	0	1
511	CO^+ +	N	$\Longrightarrow$ NO^+	+	C	8.1×10^{-11}	0	0	1
512	CO^+ +	O	$\Longrightarrow$ O^+	+	CO	1.4×10^{-10}	0	0	1
513	CO^+ +	S	$\Longrightarrow$ S^+	+	CO	1.1×10^{-09}	0	0	1
514	CO^+ +	H_2	$\Longrightarrow$ HCO^+	+	H	2.0×10^{-09}	0	0	1
515	CO^+ +	C_2	$\Longrightarrow$ $C_2{}^+$	+	CO	8.4×10^{-10}	0	0	1
516	CO^+ +	O_2	$\Longrightarrow$ $O_2{}^+$	+	CO	7.6×10^{-10}	0	0	1
517	CO^+ +	CH	$\Longrightarrow$ CH^+	+	CO	3.2×10^{-10}	0	0	1
518	CO^+ +	CH	$\Longrightarrow$ HCO^+	+	C	3.2×10^{-10}	0	0	1
519	CO^+ +	NH	$\Longrightarrow$ NH^+	+	CO	3.2×10^{-10}	0	0	1
520	CO^+ +	NH	$\Longrightarrow$ HCO^+	+	N	3.2×10^{-10}	0	0	1
521	CO^+ +	OH	$\Longrightarrow$ OH^+	+	CO	3.1×10^{-10}	0	0	1
522	CO^+ +	OH	$\Longrightarrow$ HCO^+	+	O	3.1×10^{-10}	0	0	1
523	CO^+ +	NO	$\Longrightarrow$ NO^+	+	CO	3.3×10^{-10}	0	0	1
524	CO^+ +	CH_2	$\Longrightarrow$ $CH_2{}^+$	+	CO	4.3×10^{-10}	0	0	1
525	CO^+ +	CH_2	$\Longrightarrow$ HCO^+	+	CH	4.3×10^{-10}	0	0	1
526	CO^+ +	NH_2	$\Longrightarrow$ HCO^+	+	NH	4.5×10^{-10}	0	0	1
527	CO^+ +	NH_2	$\Longrightarrow$ $NH_2{}^+$	+	CO	4.5×10^{-10}	0	0	1
528	CO^+ +	H_2O	$\Longrightarrow$ H_2O^+	+	CO	1.7×10^{-09}	0	0	1
529	CO^+ +	H_2O	$\Longrightarrow$ HCO^+	+	OH	8.8×10^{-10}	0	0	1
530	CO^+ +	HCN	$\Longrightarrow$ HCN^+	+	CO	5.1×10^{-10}	0	0	1
531	CO^+ +	HCN	$\Longrightarrow$ HCO^+	+	CN	5.1×10^{-10}	0	0	1
532	CO^+ +	HCO	$\Longrightarrow$ HCO^+	+	CO	7.4×10^{-10}	0	0	1
533	CO^+ +	C_2H	$\Longrightarrow$ HCO^+	+	C_2	3.9×10^{-10}	0	0	1
534	CO^+ +	C_2H	$\Longrightarrow$ C_2H^+	+	CO	3.9×10^{-10}	0	0	1
535	CO^+ +	CO_2	$\Longrightarrow$ $CO_2{}^+$	+	CO	1.1×10^{-09}	0	0	1
536	CO^+ +	SO_2	$\Longrightarrow$ SO^+	+	CO_2	1.5×10^{-09}	0	0	1
537	CO^+ +	H_2CO	$\Longrightarrow$ HCO^+	+	HCO	5.1×10^{-10}	0	0	1
538	CO^+ +	H_2CO	$\Longrightarrow$ H_2CO^+	+	CO	5.1×10^{-10}	0	0	1
539	CN^+ +	H	$\Longrightarrow$ H^+	+	CN	1.9×10^{-10}	0	0	1
540	CN^+ +	C	$\Longrightarrow$ C^+	+	CN	1.1×10^{-10}	0	0	1
541	CN^+ +	O	$\Longrightarrow$ O^+	+	CN	6.5×10^{-11}	0	0	1
542	CN^+ +	S	$\Longrightarrow$ S^+	+	CN	1.1×10^{-09}	0	0	1
543	CN^+ +	H_2	$\Longrightarrow$ HCN^+	+	H	1.2×10^{-09}	0	0	1
544	CN^+ +	C_2	$\Longrightarrow$ $C_2{}^+$	+	CN	8.5×10^{-10}	0	0	1
545	CN^+ +	O_2	$\Longrightarrow$ $O_2{}^+$	+	CN	7.8×10^{-10}	0	0	1
546	CN^+ +	CH	$\Longrightarrow$ CH^+	+	CN	6.4×10^{-10}	0	0	1
547	CN^+ +	NH	$\Longrightarrow$ NH^+	+	CN	6.5×10^{-10}	0	0	1
548	CN^+ +	OH	$\Longrightarrow$ OH^+	+	CN	6.4×10^{-10}	0	0	1
549	CN^+ +	CO	$\Longrightarrow$ CO^+	+	CN	8.9×10^{-10}	0	0	1
550	CN^+ +	NO	$\Longrightarrow$ NO^+	+	CN	8.1×10^{-10}	0	0	1

continued on next page

continued from previous page

Nr.	Reaction					A	E_a	α	Ref.
551	CN^+ +	CH_2	$\Longrightarrow CH_2{}^+$	+	CN	8.8×10^{-10}	0	0	1
552	CN^+ +	NH_2	$\Longrightarrow NH_2{}^+$	+	CN	9.1×10^{-10}	0	0	1
553	CN^+ +	H_2O	$\Longrightarrow H_2O^+$	+	CN	8.6×10^{-10}	0	0	1
554	CN^+ +	HCN	$\Longrightarrow HCN^+$	+	CN	1.0×10^{-09}	0	0	1
555	CN^+ +	HCO	$\Longrightarrow HCN^+$	+	CO	3.7×10^{-10}	0	0	1
556	CN^+ +	HCO	$\Longrightarrow HCO^+$	+	CN	3.7×10^{-10}	0	0	1
557	CN^+ +	C_2H	$\Longrightarrow C_2H^+$	+	CN	8.0×10^{-10}	0	0	1
558	CN^+ +	CO_2	$\Longrightarrow CO_2{}^+$	+	CN	9.3×10^{-10}	0	0	1
559	CN^+ +	H_2CO	$\Longrightarrow HCO^+$	+	HCN	5.2×10^{-10}	0	0	1
560	CN^+ +	H_2CO	$\Longrightarrow H_2CO^+$	+	CN	5.2×10^{-10}	0	0	1
561	NO^+ +	Si	$\Longrightarrow Si^+$	+	NO	1.6×10^{-09}	0	0	1
562	NO^+ +	Fe	$\Longrightarrow Fe^+$	+	NO	9.2×10^{-10}	0	0	1
563	NO^+ +	Na	$\Longrightarrow Na^+$	+	NO	7.0×10^{-11}	0	0	1
564	NO^+ +	Mg	$\Longrightarrow Mg^+$	+	NO	8.1×10^{-10}	0	0	1
565	SiS^+ +	H	$\Longrightarrow Si^+$	+	HS	1.9×10^{-09}	0	0	1
566	SiS^+ +	H_2	$\Longrightarrow HSiS^+$	+	H	1.5×10^{-09}	0	0	1
567	SiC^+ +	N	$\Longrightarrow Si^+$	+	CN	7.7×10^{-10}	0	0	1
568	SiC^+ +	O	$\Longrightarrow SiO^+$	+	C	6.0×10^{-10}	0	0	1
569	SiC^+ +	H_2	$\Longrightarrow CHSi^+$	+	H	1.5×10^{-09}	0	0	1
570	HS^+ +	C	$\Longrightarrow CS^+$	+	H	9.9×10^{-10}	0	0	1
571	HS^+ +	N	$\Longrightarrow NS^+$	+	H	7.4×10^{-10}	0	0	1
572	HS^+ +	O	$\Longrightarrow SO^+$	+	H	2.9×10^{-10}	0	0	1
573	HS^+ +	O	$\Longrightarrow S^+$	+	OH	2.9×10^{-10}	0	0	1
574	HS^+ +	Si	$\Longrightarrow Si^+$	+	HS	1.4×10^{-09}	0	0	1
575	HS^+ +	S	$\Longrightarrow S^+$	+	HS	9.7×10^{-10}	0	0	1
576	HS^+ +	Fe	$\Longrightarrow Fe^+$	+	HS	1.6×10^{-09}	0	0	1
577	HS^+ +	Na	$\Longrightarrow Na^+$	+	HS	2.2×10^{-09}	0	0	1
578	HS^+ +	Mg	$\Longrightarrow Mg^+$	+	HS	2.6×10^{-09}	0	0	1
579	HS^+ +	CH	$\Longrightarrow CH_2{}^+$	+	S	5.8×10^{-10}	0	0	1
580	HS^+ +	H_2O	$\Longrightarrow H_3O^+$	+	S	3.2×10^{-10}	0	0	1
581	HS^+ +	HCN	$\Longrightarrow H_2CN^+$	+	S	8.9×10^{-10}	0	0	1
582	HS^+ +	H_2S	$\Longrightarrow H_3S^+$	+	S	2.9×10^{-10}	0	0	1
583	HS^+ +	H_2S	$\Longrightarrow H_2S^+$	+	HS	4.5×10^{-10}	0	0	1
584	HS^+ +	NH_3	$\Longrightarrow NH_3{}^+$	+	HS	8.4×10^{-10}	0	0	1
585	HS^+ +	NH_3	$\Longrightarrow NH_4{}^+$	+	S	7.7×10^{-10}	0	0	1
586	HS^+ +	CH_4	$\Longrightarrow H_3CS^+$	+	H_2	1.0×10^{-10}	0	0	1
587	SiO^+ +	C	$\Longrightarrow Si^+$	+	CO	1.0×10^{-09}	0	0	1
588	SiO^+ +	N	$\Longrightarrow NO^+$	+	Si	2.0×10^{-10}	0	0	1
589	SiO^+ +	N	$\Longrightarrow Si^+$	+	NO	2.0×10^{-10}	0	0	1
590	SiO^+ +	O	$\Longrightarrow Si^+$	+	O_2	2.0×10^{-10}	0	0	1
591	SiO^+ +	S	$\Longrightarrow Si^+$	+	SO	1.0×10^{-09}	0	0	1
592	SiO^+ +	H_2	$\Longrightarrow SiOH^+$	+	H	1.5×10^{-09}	0	0	1
593	SiO^+ +	C_2	$\Longrightarrow SiC^+$	+	CO	7.6×10^{-10}	0	0	1
594	SiO^+ +	CH	$\Longrightarrow HCO^+$	+	Si	5.9×10^{-10}	0	0	1
595	SiO^+ +	CO	$\Longrightarrow Si^+$	+	CO_2	7.9×10^{-10}	0	0	1
596	SiO^+ +	NO	$\Longrightarrow NO^+$	+	SiO	7.2×10^{-10}	0	0	1

continued on next page

continued from previous page

Nr.	Reaction	A	E_a	α	Ref.
597	$SiO^+ + CH_2 \Longrightarrow Si^+ + H_2CO$	8.2×10^{-10}	0	0	1
598	$SiO^+ + HCO \Longrightarrow HCO^+ + SiO$	6.6×10^{-10}	0	0	1
599	$CS^+ + O \Longrightarrow CO^+ + S$	6.0×10^{-11}	0	0	1
600	$CS^+ + Si \Longrightarrow Si^+ + CS$	1.5×10^{-10}	0	0	1
601	$CS^+ + Fe \Longrightarrow Fe^+ + CS$	1.7×10^{-10}	0	0	1
602	$CS^+ + Na \Longrightarrow Na^+ + CS$	2.3×10^{-10}	0	0	1
603	$CS^+ + Mg \Longrightarrow Mg^+ + CS$	2.7×10^{-10}	0	0	1
604	$CS^+ + H_2 \Longrightarrow HCS^+ + H$	1.5×10^{-09}	0	0	1
605	$SO^+ + N \Longrightarrow NS^+ + O$	5.0×10^{-11}	0	0	1
606	$SO^+ + Fe \Longrightarrow Fe^+ + SO$	1.6×10^{-09}	0	0	1
607	$SO^+ + Na \Longrightarrow Na^+ + SO$	2.3×10^{-09}	0	0	1
608	$SO^+ + Mg \Longrightarrow Mg^+ + SO$	1.0×10^{-10}	0	0	1
609	$SO^+ + NH_3 \Longrightarrow NH_3{}^+ + SO$	1.3×10^{-09}	0	0	1
610	$NS^+ + O \Longrightarrow NO^+ + S$	6.1×10^{-10}	0	0	1
611	$H_3{}^+ + C \Longrightarrow CH^+ + H_2$	2.0×10^{-09}	0	0	1
612	$H_3{}^+ + N \Longrightarrow NH_2{}^+ + H$	1.0×10^{-09}	0	0	1
613	$H_3{}^+ + O \Longrightarrow OH^+ + H_2$	8.0×10^{-10}	0	0	1
614	$H_3{}^+ + Si \Longrightarrow SiH^+ + H_2$	3.7×10^{-09}	0	0	1
615	$H_3{}^+ + S \Longrightarrow HS^+ + H_2$	2.6×10^{-09}	0	0	1
616	$H_3{}^+ + Fe \Longrightarrow Fe^+ + H + H_2$	4.9×10^{-09}	0	0	1
617	$H_3{}^+ + Na \Longrightarrow Na^+ + H + H_2$	1.1×10^{-09}	0	0	1
618	$H_3{}^+ + Mg \Longrightarrow Mg^+ + H + H_2$	1.0×10^{-09}	0	0	1
619	$H_3{}^+ + C_2 \Longrightarrow C_2H^+ + H_2$	1.8×10^{-09}	0	0	1
620	$H_3{}^+ + N_2 \Longrightarrow N_2H^+ + H_2$	1.7×10^{-09}	0	0	1
621	$H_3{}^+ + O_2 \Longrightarrow O_2H^+ + H_2$	6.4×10^{-10}	0	0	1
622	$H_3{}^+ + CH \Longrightarrow CH_2{}^+ + H_2$	1.2×10^{-09}	0	0	1
623	$H_3{}^+ + NH \Longrightarrow NH_2{}^+ + H_2$	1.3×10^{-09}	0	0	1
624	$H_3{}^+ + OH \Longrightarrow H_2O^+ + H_2$	1.3×10^{-09}	0	0	1
625	$H_3{}^+ + CO \Longrightarrow HCO^+ + H_2$	1.7×10^{-09}	0	0	1
626	$H_3{}^+ + CN \Longrightarrow HCN^+ + H_2$	2.0×10^{-09}	0	0	1
627	$H_3{}^+ + NO \Longrightarrow HNO^+ + H_2$	1.4×10^{-09}	0	0	1
628	$H_3{}^+ + SiC \Longrightarrow CHSi^+ + H_2$	9.2×10^{-09}	0	0	1
629	$H_3{}^+ + SiS \Longrightarrow HSiS^+ + H_2$	8.7×10^{-09}	0	0	1
630	$H_3{}^+ + SiO \Longrightarrow SiOH^+ + H_2$	2.0×10^{-09}	0	0	1
631	$H_3{}^+ + SiH \Longrightarrow SiH_2{}^+ + H_2$	2.0×10^{-09}	0	0	1
632	$H_3{}^+ + HS \Longrightarrow H_2S^+ + H_2$	1.9×10^{-09}	0	0	1
633	$H_3{}^+ + CS \Longrightarrow HCS^+ + H_2$	2.9×10^{-09}	0	0	1
634	$H_3{}^+ + NS \Longrightarrow HNS^+ + H_2$	2.8×10^{-09}	0	0	1
635	$H_3{}^+ + SO \Longrightarrow HSO^+ + H_2$	1.9×10^{-09}	0	0	1
636	$H_3{}^+ + CH_2 \Longrightarrow CH_3{}^+ + H_2$	1.7×10^{-09}	0	0	1
637	$H_3{}^+ + NH_2 \Longrightarrow NH_3{}^+ + H_2$	1.8×10^{-09}	0	0	1
638	$H_3{}^+ + H_2O \Longrightarrow H_3O^+ + H_2$	5.9×10^{-09}	0	0	1
639	$H_3{}^+ + HCN \Longrightarrow H_2CN^+ + H_2$	8.0×10^{-09}	0	0	1
640	$H_3{}^+ + HCO \Longrightarrow H_2CO^+ + H_2$	1.7×10^{-09}	0	0	1
641	$H_3{}^+ + C_2H \Longrightarrow C_2H2^+ + H_2$	1.7×10^{-09}	0	0	1
642	$H_3{}^+ + CO_2 \Longrightarrow HCO_2{}^+ + H_2$	1.9×10^{-09}	0	0	1

continued on next page

continued from previous page

Nr.	Reaction						A	E_a	α	Ref.
643	H_3^+	+	H_2S	$\Longrightarrow$	H_3S^+	+ H_2	3.7×10^{-09}	0	0	1
644	H_3^+	+	OCS	$\Longrightarrow$	$HOCS^+$	+ H_2	3.5×10^{-09}	0	0	1
645	H_3^+	+	H_2CO	$\Longrightarrow$	H_3CO^+	+ H_2	2.4×10^{-09}	0	0	1
646	H_3^+	+	NH_3	$\Longrightarrow$	NH_4^+	+ H_2	4.7×10^{-09}	0	0	1
647	H_3^+	+	C_2H2	$\Longrightarrow$	C_2H3^+	+ H_2	2.6×10^{-09}	0	0	1
648	H_3^+	+	CH_3	$\Longrightarrow$	CH_4^+	+ H_2	2.1×10^{-09}	0	0	1
649	H_3^+	+	CH_4	$\Longrightarrow$	CH_5^+	+ H_2	2.4×10^{-09}	0	0	1
650	H_3^+	+	H_2CS	$\Longrightarrow$	H_3CS^+	+ H_2	2.8×10^{-09}	0	0	1
651	CH_2^+	+	C	$\Longrightarrow$	C_2H^+	+ H	1.2×10^{-09}	0	0	1
652	CH_2^+	+	N	$\Longrightarrow$	HCN^+	+ H	9.4×10^{-10}	0	0	1
653	CH_2^+	+	O	$\Longrightarrow$	HCO^+	+ H	7.5×10^{-10}	0	0	1
654	CH_2^+	+	S	$\Longrightarrow$	HCS^+	+ H	1.4×10^{-09}	0	0	1
655	CH_2^+	+	H_2	$\Longrightarrow$	CH_3^+	+ H	7.2×10^{-10}	0	0	1
656	CH_2^+	+	C_2	$\Longrightarrow$	C_3H^+	+ H	1.0×10^{-09}	0	0	1
657	CH_2^+	+	O_2	$\Longrightarrow$	HCO_2^+	+ H	4.7×10^{-10}	0	0	1
658	CH_2^+	+	O_2	$\Longrightarrow$	HCO^+	+ OH	9.1×10^{-10}	0	0	1
659	CH_2^+	+	CH	$\Longrightarrow$	C_2H2^+	+ H	7.2×10^{-10}	0	0	1
660	CH_2^+	+	NH	$\Longrightarrow$	H_2CN^+	+ H	7.5×10^{-10}	0	0	1
661	CH_2^+	+	OH	$\Longrightarrow$	H_2CO^+	+ H	7.4×10^{-10}	0	0	1
662	CH_2^+	+	NO	$\Longrightarrow$	NO^+	+ CH_2	9.8×10^{-10}	0	0	1
663	CH_2^+	+	CH_2	$\Longrightarrow$	C_2H3^+	+ H	1.0×10^{-09}	0	0	1
664	CH_2^+	+	NH_2	$\Longrightarrow$	H_2CN^+	+ H_2	1.0×10^{-09}	0	0	1
665	CH_2^+	+	H_2O	$\Longrightarrow$	H_3CO^+	+ H	1.2×10^{-09}	0	0	1
666	CH_2^+	+	HCN	$\Longrightarrow$	C_2H2N^+	+ H	1.2×10^{-09}	0	0	1
667	CH_2^+	+	HCO	$\Longrightarrow$	C_2H2O^+	+ H	4.5×10^{-10}	0	0	1
668	CH_2^+	+	HCO	$\Longrightarrow$	CH_3^+	+ CO	4.5×10^{-10}	0	0	1
669	CH_2^+	+	C_2H	$\Longrightarrow$	C_3H2^+	+ H	9.5×10^{-10}	0	0	1
670	CH_2^+	+	CO_2	$\Longrightarrow$	H_2CO^+	+ CO	1.2×10^{-09}	0	0	1
671	CH_2^+	+	H_2S	$\Longrightarrow$	H_3CS^+	+ H	3.9×10^{-10}	0	0	1
672	CH_2^+	+	H_2S	$\Longrightarrow$	HCS^+	+ H_2 + H	2.0×10^{-10}	0	0	1
673	CH_2^+	+	H_2CO	$\Longrightarrow$	CH_3CO^+	+ H	1.3×10^{-09}	0	0	1
674	CH_2^+	+	NH_3	$\Longrightarrow$	CH_4N^+	+ H	3.1×10^{-10}	0	0	1
675	CH_2^+	+	NH_3	$\Longrightarrow$	NH_4^+	+ CH	1.2×10^{-09}	0	0	1
676	CH_2^+	+	CH_4	$\Longrightarrow$	C_2H5^+	+ H	2.9×10^{-10}	0	0	1
677	CH_2^+	+	CH_4	$\Longrightarrow$	C_2H2^+	+ H_2 + H_2	1.4×10^{-10}	0	0	1
678	CH_2^+	+	CH_4	$\Longrightarrow$	C_2H3^+	+ H_2 + H	2.6×10^{-10}	0	0	1
679	NH_2^+	+	C	$\Longrightarrow$	CH^+	+ NH	1.2×10^{-09}	0	0	1
680	NH_2^+	+	N	$\Longrightarrow$	N_2H^+	+ H	9.1×10^{-11}	0	0	1
681	NH_2^+	+	O	$\Longrightarrow$	HNO^+	+ H	7.2×10^{-11}	0	0	1
682	NH_2^+	+	S	$\Longrightarrow$	HNS^+	+ H	4.4×10^{-10}	0	0	1
683	NH_2^+	+	S	$\Longrightarrow$	HS^+	+ NH	4.4×10^{-10}	0	0	1
684	NH_2^+	+	S	$\Longrightarrow$	S^+	+ NH_2	4.4×10^{-10}	0	0	1
685	NH_2^+	+	H_2	$\Longrightarrow$	NH_3^+	+ H	1.2×10^{-10}	0	0	1
686	NH_2^+	+	C_2	$\Longrightarrow$	C_2H^+	+ NH	9.7×10^{-10}	0	0	1
687	NH_2^+	+	O_2	$\Longrightarrow$	NO^+	+ H_2O	1.0×10^{-10}	0	0	1
688	NH_2^+	+	CH	$\Longrightarrow$	CH^+	+ NH_2	3.5×10^{-10}	0	0	1

continued on next page

continued from previous page

Nr.	Reaction	A	E_a	α	Ref.
689	NH_2^+ + CH ⟹ CH_2^+ + NH	3.5×10^{-10}	0	0	1
690	NH_2^+ + NH ⟹ NH_3^+ + N	7.3×10^{-10}	0	0	1
691	NH_2^+ + OH ⟹ H_2O^+ + NH	7.1×10^{-10}	0	0	1
692	NH_2^+ + CN ⟹ H_2CN^+ + N	1.0×10^{-10}	0	0	1
693	NH_2^+ + NO ⟹ NO^+ + NH_2	9.4×10^{-10}	0	0	1
694	NH_2^+ + CH_2 ⟹ CH_2^+ + NH_2	4.9×10^{-10}	0	0	1
695	NH_2^+ + CH_2 ⟹ CH_3^+ + NH	4.9×10^{-10}	0	0	1
696	NH_2^+ + NH_2 ⟹ NH_3^+ + NH	1.0×10^{-09}	0	0	1
697	NH_2^+ + H_2O ⟹ NH_3^+ + OH	1.0×10^{-10}	0	0	1
698	NH_2^+ + H_2O ⟹ H_3O^+ + NH	1.6×10^{-09}	0	0	1
699	NH_2^+ + H_2O ⟹ NH_4^+ + O	3.0×10^{-11}	0	0	1
700	NH_2^+ + HCN ⟹ H_2CN^+ + NH	1.2×10^{-09}	0	0	1
701	NH_2^+ + HCO ⟹ H_2CO^+ + NH	4.3×10^{-10}	0	0	1
702	NH_2^+ + HCO ⟹ HCO^+ + NH_2	4.3×10^{-10}	0	0	1
703	NH_2^+ + C_2H ⟹ C_2H2^+ + NH	9.1×10^{-10}	0	0	1
704	NH_2^+ + H_2S ⟹ H_2S^+ + NH_2	3.4×10^{-10}	0	0	1
705	NH_2^+ + H_2S ⟹ H_3S^+ + NH	2.4×10^{-10}	0	0	1
706	NH_2^+ + H_2CO ⟹ H_3CO^+ + NH	6.0×10^{-10}	0	0	1
707	NH_2^+ + H_2CO ⟹ H_2CO^+ + NH_2	6.0×10^{-10}	0	0	1
708	NH_2^+ + NH_3 ⟹ NH_4^+ + NH	1.0×10^{-09}	0	0	1
709	NH_2^+ + NH_3 ⟹ NH_3^+ + NH_2	1.5×10^{-09}	0	0	1
710	H_2O^+ + C ⟹ CH^+ + OH	1.1×10^{-09}	0	0	1
711	H_2O^+ + N ⟹ HNO^+ + H	8.8×10^{-11}	0	0	1
712	H_2O^+ + O ⟹ O_2^+ + H_2	7.0×10^{-11}	0	0	1
713	H_2O^+ + S ⟹ S^+ + H_2O	4.3×10^{-10}	0	0	1
714	H_2O^+ + S ⟹ HSO^+ + H	4.3×10^{-10}	0	0	1
715	H_2O^+ + S ⟹ HS^+ + OH	4.3×10^{-10}	0	0	1
716	H_2O^+ + Fe ⟹ Fe^+ + H_2O	1.5×10^{-09}	0	0	1
717	H_2O^+ + Na ⟹ Na^+ + H_2O	2.7×10^{-09}	0	0	1
718	H_2O^+ + Mg ⟹ Mg^+ + H_2O	2.2×10^{-09}	0	0	1
719	H_2O^+ + H_2 ⟹ H_3O^+ + H	6.1×10^{-10}	0	0	1
720	H_2O^+ + C_2 ⟹ C_2^+ + H_2O	4.7×10^{-10}	0	0	1
721	H_2O^+ + C_2 ⟹ C_2H^+ + OH	4.7×10^{-10}	0	0	1
722	H_2O^+ + O_2 ⟹ O_2^+ + H_2O	2.0×10^{-10}	0	0	1
723	H_2O^+ + CH ⟹ CH^+ + H_2O	3.4×10^{-10}	0	0	1
724	H_2O^+ + CH ⟹ CH_2^+ + OH	3.4×10^{-10}	0	0	1
725	H_2O^+ + NH ⟹ H_3O^+ + N	7.1×10^{-10}	0	0	1
726	H_2O^+ + OH ⟹ H_3O^+ + O	6.9×10^{-10}	0	0	1
727	H_2O^+ + NO ⟹ NO^+ + H_2O	9.1×10^{-10}	0	0	1
728	H_2O^+ + CH_2 ⟹ CH_3^+ + OH	4.7×10^{-10}	0	0	1
729	H_2O^+ + CH_2 ⟹ CH_2^+ + H_2O	4.7×10^{-10}	0	0	1
730	H_2O^+ + NH_2 ⟹ NH_3^+ + OH	4.9×10^{-10}	0	0	1
731	H_2O^+ + NH_2 ⟹ NH_2^+ + H_2O	4.9×10^{-10}	0	0	1
732	H_2O^+ + H_2O ⟹ H_3O^+ + OH	2.1×10^{-09}	0	0	1
733	H_2O^+ + HCN ⟹ H_2CN^+ + OH	1.1×10^{-09}	0	0	1
734	H_2O^+ + HCO ⟹ H_3O^+ + CO	2.8×10^{-10}	0	0	1

continued on next page

continued from previous page

Nr.	Reaction					A	E_a	α	Ref.
735	H_2O^+ +	HCO	⟹ HCO^+	+	H_2O	2.8×10^{-10}	0	0	1
736	H_2O^+ +	HCO	⟹ H_2CO^+	+	OH	2.8×10^{-10}	0	0	1
737	H_2O^+ +	C_2H	⟹ C_2H^+	+	H_2O	4.4×10^{-10}	0	0	1
738	H_2O^+ +	C_2H	⟹ C_2H2^+	+	OH	4.4×10^{-10}	0	0	1
739	H_2O^+ +	H_2S	⟹ H_2S^+	+	H_2O	8.9×10^{-10}	0	0	1
740	H_2O^+ +	H_2S	⟹ H_3S^+	+	OH	7.0×10^{-10}	0	0	1
741	H_2O^+ +	H_2S	⟹ H_3O^+	+	HS	5.9×10^{-10}	0	0	1
742	H_2O^+ +	H_2CO	⟹ H_2CO^+	+	H_2O	5.8×10^{-10}	0	0	1
743	H_2O^+ +	H_2CO	⟹ H_3CO^+	+	OH	5.8×10^{-10}	0	0	1
744	H_2O^+ +	NH_3	⟹ $NH_3{}^+$	+	H_2O	2.2×10^{-09}	0	0	1
745	H_2O^+ +	NH_3	⟹ $NH_4{}^+$	+	OH	9.0×10^{-10}	0	0	1
746	H_2O^+ +	CH_4	⟹ H_3O^+	+	CH_3	1.3×10^{-09}	0	0	1
747	HCO^+ +	C	⟹ CH^+	+	CO	1.1×10^{-09}	0	0	1
748	HCO^+ +	Si	⟹ SiH^+	+	CO	1.6×10^{-09}	0	0	1
749	HCO^+ +	S	⟹ HS^+	+	CO	3.3×10^{-10}	0	0	1
750	HCO^+ +	Fe	⟹ Fe^+	+	HCO	1.9×10^{-09}	0	0	1
751	HCO^+ +	Na	⟹ Na^+	+	HCO	2.6×10^{-09}	0	0	1
752	HCO^+ +	Mg	⟹ Mg^+	+	HCO	2.9×10^{-09}	0	0	1
753	HCO^+ +	C_2	⟹ C_2H^+	+	CO	8.3×10^{-10}	0	0	1
754	HCO^+ +	CH	⟹ $CH_2{}^+$	+	CO	6.3×10^{-10}	0	0	1
755	HCO^+ +	NH	⟹ $NH_2{}^+$	+	CO	6.4×10^{-10}	0	0	1
756	HCO^+ +	OH	⟹ H_2O^+	+	CO	6.2×10^{-10}	0	0	1
757	HCO^+ +	SiC	⟹ $CHSi^+$	+	CO	3.8×10^{-09}	0	0	1
758	HCO^+ +	SiS	⟹ $HSiS^+$	+	CO	3.3×10^{-09}	0	0	1
759	HCO^+ +	SiO	⟹ $SiOH^+$	+	CO	7.9×10^{-10}	0	0	1
760	HCO^+ +	SiH	⟹ $SiH_2{}^+$	+	CO	8.7×10^{-10}	0	0	1
761	HCO^+ +	HS	⟹ H_2S^+	+	CO	8.2×10^{-10}	0	0	1
762	HCO^+ +	CS	⟹ HCS^+	+	CO	1.2×10^{-09}	0	0	1
763	HCO^+ +	NS	⟹ HNS^+	+	CO	1.1×10^{-09}	0	0	1
764	HCO^+ +	SO	⟹ HSO^+	+	CO	7.5×10^{-10}	0	0	1
765	HCO^+ +	CH_2	⟹ $CH_3{}^+$	+	CO	8.6×10^{-10}	0	0	1
766	HCO^+ +	NH_2	⟹ $NH_3{}^+$	+	CO	8.9×10^{-10}	0	0	1
767	HCO^+ +	H_2O	⟹ H_3O^+	+	CO	3.2×10^{-09}	0	0	1
768	HCO^+ +	HCN	⟹ H_2CN^+	+	CO	1.1×10^{-09}	0	0	1
769	HCO^+ +	HCO	⟹ H_2CO^+	+	CO	7.3×10^{-10}	0	0	1
770	HCO^+ +	C_2H	⟹ C_2H2^+	+	CO	7.8×10^{-10}	0	0	1
771	HCO^+ +	H_2S	⟹ H_3S^+	+	CO	1.1×10^{-09}	0	0	1
772	HCO^+ +	OCS	⟹ $HOCS^+$	+	CO	1.3×10^{-09}	0	0	1
773	HCO^+ +	H_2CO	⟹ H_3CO^+	+	CO	1.0×10^{-09}	0	0	1
774	HCO^+ +	NH_3	⟹ $NH_4{}^+$	+	CO	2.6×10^{-09}	0	0	1
775	HCO^+ +	C_2H2	⟹ C_2H3^+	+	CO	1.1×10^{-09}	0	0	1
776	HCO^+ +	H_2CS	⟹ H_3CS^+	+	CO	1.1×10^{-09}	0	0	1
777	HCN^+ +	H	⟹ H^+	+	HCN	1.9×10^{-10}	0	0	1
778	HCN^+ +	C	⟹ CH^+	+	CN	1.1×10^{-09}	0	0	1
779	HCN^+ +	O	⟹ O^+	+	HCN	6.5×10^{-11}	0	0	1
780	HCN^+ +	S	⟹ S^+	+	HCN	5.7×10^{-10}	0	0	1

continued on next page

continued from previous page

Nr.	Reaction	A	E_a	α	Ref.
781	$HCN^+ + S \Longrightarrow HS^+ + CN$	5.7×10^{-10}	0	0	1
782	$HCN^+ + H_2 \Longrightarrow H_2CN^+ + H$	9.0×10^{-10}	0	0	1
783	$HCN^+ + C_2 \Longrightarrow C_2H^+ + CN$	8.4×10^{-10}	0	0	1
784	$HCN^+ + O_2 \Longrightarrow O_2{}^+ + HCN$	7.7×10^{-10}	0	0	1
785	$HCN^+ + CH \Longrightarrow CH_2{}^+ + CN$	6.3×10^{-10}	0	0	1
786	$HCN^+ + NH \Longrightarrow NH_2{}^+ + CN$	6.5×10^{-10}	0	0	1
787	$HCN^+ + OH \Longrightarrow H_2O^+ + CN$	6.3×10^{-10}	0	0	1
788	$HCN^+ + CO \Longrightarrow HCO^+ + CN$	8.8×10^{-10}	0	0	1
789	$HCN^+ + NO \Longrightarrow NO^+ + HCN$	8.1×10^{-10}	0	0	1
790	$HCN^+ + CH_2 \Longrightarrow CH_3{}^+ + CN$	8.7×10^{-10}	0	0	1
791	$HCN^+ + NH_2 \Longrightarrow NH_3{}^+ + CN$	9.0×10^{-10}	0	0	1
792	$HCN^+ + H_2O \Longrightarrow H_3O^+ + CN$	8.5×10^{-10}	0	0	1
793	$HCN^+ + HCN \Longrightarrow H_2CN^+ + CN$	1.0×10^{-09}	0	0	1
794	$HCN^+ + HCO \Longrightarrow H_2CO^+ + CN$	3.7×10^{-10}	0	0	1
795	$HCN^+ + HCO \Longrightarrow H_2CN^+ + CO$	3.7×10^{-10}	0	0	1
796	$HCN^+ + C_2H \Longrightarrow C_2H2^+ + CN$	7.9×10^{-10}	0	0	1
797	$HCN^+ + CO_2 \Longrightarrow HCO_2{}^+ + CN$	9.2×10^{-10}	0	0	1
798	$HCN^+ + H_2CO \Longrightarrow H_3CO^+ + CN$	1.0×10^{-09}	0	0	1
799	$HCN^+ + NH_3 \Longrightarrow NH_4{}^+ + CN$	1.1×10^{-09}	0	0	1
800	$HNO^+ + C \Longrightarrow CH^+ + NO$	1.0×10^{-09}	0	0	1
801	$HNO^+ + O \Longrightarrow NO_2{}^+ + H$	1.0×10^{-12}	0	0	1
802	$HNO^+ + S \Longrightarrow HS^+ + NO$	1.1×10^{-09}	0	0	1
803	$HNO^+ + C_2 \Longrightarrow C_2H^+ + NO$	8.2×10^{-10}	0	0	1
804	$HNO^+ + N_2 \Longrightarrow N_2H^+ + NO$	8.1×10^{-10}	0	0	1
805	$HNO^+ + CH \Longrightarrow CH_2{}^+ + NO$	6.2×10^{-10}	0	0	1
806	$HNO^+ + NH \Longrightarrow NH_2{}^+ + NO$	6.3×10^{-10}	0	0	1
807	$HNO^+ + OH \Longrightarrow H_2O^+ + NO$	6.2×10^{-10}	0	0	1
808	$HNO^+ + CO \Longrightarrow HCO^+ + NO$	8.5×10^{-10}	0	0	1
809	$HNO^+ + CN \Longrightarrow HCN^+ + NO$	8.7×10^{-10}	0	0	1
810	$HNO^+ + CH_2 \Longrightarrow CH_3{}^+ + NO$	8.6×10^{-10}	0	0	1
811	$HNO^+ + NH_2 \Longrightarrow NH_3{}^+ + NO$	8.8×10^{-10}	0	0	1
812	$HNO^+ + H_2O \Longrightarrow H_3O^+ + NO$	8.3×10^{-10}	0	0	1
813	$HNO^+ + HCN \Longrightarrow H_2CN^+ + NO$	9.9×10^{-10}	0	0	1
814	$HNO^+ + HCO \Longrightarrow H_2CO^+ + NO$	7.2×10^{-10}	0	0	1
815	$HNO^+ + C_2H \Longrightarrow C_2H2^+ + NO$	7.7×10^{-10}	0	0	1
816	$HNO^+ + CO_2 \Longrightarrow HCO_2{}^+ + NO$	8.8×10^{-10}	0	0	1
817	$HNO^+ + H_2CO \Longrightarrow H_3CO^+ + NO$	1.0×10^{-09}	0	0	1
818	$HNO^+ + NH_3 \Longrightarrow NH_4{}^+ + NO$	1.1×10^{-09}	0	0	1
819	$C_2H^+ + C \Longrightarrow C_3{}^+ + H$	1.1×10^{-09}	0	0	1
820	$C_2H^+ + N \Longrightarrow C_2N^+ + H$	8.3×10^{-10}	0	0	1
821	$C_2H^+ + O \Longrightarrow HCO^+ + C$	1.0×10^{-11}	0	0	1
822	$C_2H^+ + S \Longrightarrow S^+ + C_2H$	1.2×10^{-09}	0	0	1
823	$C_2H^+ + H_2 \Longrightarrow C_2H2^+ + H$	7.8×10^{-10}	0	0	1
824	$C_2H^+ + CH \Longrightarrow C_3H^+ + H$	3.2×10^{-10}	0	0	1
825	$C_2H^+ + CH \Longrightarrow CH_2{}^+ + C_2$	3.2×10^{-10}	0	0	1
826	$C_2H^+ + CN \Longrightarrow C_3N^+ + H$	9.1×10^{-10}	0	0	1

continued on next page

continued from previous page

Nr.	Reaction					A	E$_a$	α	Ref.
827	C_2H^+ +	CH_2	$\Longrightarrow CH_3{}^+$	+	C_2	4.4×10^{-10}	0	0	1
828	C_2H^+ +	CH_2	$\Longrightarrow C_3H2^+$	+	H	4.4×10^{-10}	0	0	1
829	C_2H^+ +	NH_2	$\Longrightarrow NH_3{}^+$	+	C_2	4.6×10^{-10}	0	0	1
830	C_2H^+ +	NH_2	$\Longrightarrow C_2H2N^+$	+	H	4.6×10^{-10}	0	0	1
831	C_2H^+ +	H_2O	$\Longrightarrow C_2H2O^+$	+	H	8.7×10^{-10}	0	0	1
832	C_2H^+ +	HCN	$\Longrightarrow H_2CN^+$	+	C_2	5.2×10^{-10}	0	0	1
833	C_2H^+ +	HCN	$\Longrightarrow C_3HN^+$	+	H	5.2×10^{-10}	0	0	1
834	C_2H^+ +	HCO	$\Longrightarrow C_2H2^+$	+	CO	7.6×10^{-10}	0	0	1
835	C_2H^+ +	CO_2	$\Longrightarrow C_2HO^+$	+	CO	9.4×10^{-10}	0	0	1
836	C_2H^+ +	H_2CO	$\Longrightarrow H_3CO^+$	+	C_2	1.1×10^{-09}	0	0	1
837	C_2H^+ +	NH_3	$\Longrightarrow C_2H2N^+$	+	H_2	5.5×10^{-10}	0	0	1
838	C_2H^+ +	NH_3	$\Longrightarrow NH_4{}^+$	+	C_2	5.5×10^{-10}	0	0	1
839	N_2H^+ +	C	$\Longrightarrow CH^+$	+	N_2	1.1×10^{-09}	0	0	1
840	N_2H^+ +	S	$\Longrightarrow HS^+$	+	N_2	1.1×10^{-09}	0	0	1
841	N_2H^+ +	C_2	$\Longrightarrow C_2H^+$	+	N_2	8.3×10^{-10}	0	0	1
842	N_2H^+ +	CH	$\Longrightarrow CH_2{}^+$	+	N_2	6.3×10^{-10}	0	0	1
843	N_2H^+ +	NH	$\Longrightarrow NH_2{}^+$	+	N_2	6.4×10^{-10}	0	0	1
844	N_2H^+ +	OH	$\Longrightarrow H_2O^+$	+	N_2	6.2×10^{-10}	0	0	1
845	N_2H^+ +	CO	$\Longrightarrow HCO^+$	+	N_2	8.6×10^{-10}	0	0	1
846	N_2H^+ +	CH_2	$\Longrightarrow CH_3{}^+$	+	N_2	8.6×10^{-10}	0	0	1
847	N_2H^+ +	NH_2	$\Longrightarrow NH_3{}^+$	+	N_2	8.9×10^{-10}	0	0	1
848	N_2H^+ +	H_2O	$\Longrightarrow H_3O^+$	+	N_2	2.6×10^{-09}	0	0	1
849	N_2H^+ +	HCN	$\Longrightarrow H_2CN^+$	+	N_2	1.0×10^{-09}	0	0	1
850	N_2H^+ +	HCO	$\Longrightarrow H_2CO^+$	+	N_2	7.3×10^{-10}	0	0	1
851	N_2H^+ +	C_2H	$\Longrightarrow C_2H2^+$	+	N_2	7.8×10^{-10}	0	0	1
852	N_2H^+ +	CO_2	$\Longrightarrow HCO_2{}^+$	+	N_2	9.2×10^{-10}	0	0	1
853	N_2H^+ +	H_2CO	$\Longrightarrow H_3CO^+$	+	N_2	1.0×10^{-09}	0	0	1
854	N_2H^+ +	NH_3	$\Longrightarrow NH_4{}^+$	+	N_2	1.1×10^{-09}	0	0	1
855	N_2H^+ +	CH_4	$\Longrightarrow CH_5{}^+$	+	N_2	9.0×10^{-10}	0	0	1
856	O_2H^+ +	C	$\Longrightarrow CH^+$	+	O_2	1.0×10^{-09}	0	0	1
857	O_2H^+ +	N	$\Longrightarrow NO_2{}^+$	+	H	1.0×10^{-12}	0	0	1
858	O_2H^+ +	O	$\Longrightarrow OH^+$	+	O_2	6.2×10^{-10}	0	0	1
859	O_2H^+ +	S	$\Longrightarrow HS^+$	+	O_2	1.1×10^{-09}	0	0	1
860	O_2H^+ +	H_2	$\Longrightarrow H_3{}^+$	+	O_2	3.2×10^{-10}	0	0	1
861	O_2H^+ +	C_2	$\Longrightarrow C_2H^+$	+	O_2	8.1×10^{-10}	0	0	1
862	O_2H^+ +	N_2	$\Longrightarrow N_2H^+$	+	O_2	7.9×10^{-10}	0	0	1
863	O_2H^+ +	CH	$\Longrightarrow CH_2{}^+$	+	O_2	6.2×10^{-10}	0	0	1
864	O_2H^+ +	NH	$\Longrightarrow NH_2{}^+$	+	O_2	6.3×10^{-10}	0	0	1
865	O_2H^+ +	OH	$\Longrightarrow H_2O^+$	+	O_2	6.1×10^{-10}	0	0	1
866	O_2H^+ +	CO	$\Longrightarrow HCO^+$	+	O_2	8.4×10^{-10}	0	0	1
867	O_2H^+ +	CN	$\Longrightarrow HCN^+$	+	O_2	8.6×10^{-10}	0	0	1
868	O_2H^+ +	NO	$\Longrightarrow HNO^+$	+	O_2	7.7×10^{-10}	0	0	1
869	O_2H^+ +	CH_2	$\Longrightarrow CH_3{}^+$	+	O_2	8.5×10^{-10}	0	0	1
870	O_2H^+ +	NH_2	$\Longrightarrow NH_3{}^+$	+	O_2	8.7×10^{-10}	0	0	1
871	O_2H^+ +	H_2O	$\Longrightarrow H_3O^+$	+	O_2	8.2×10^{-10}	0	0	1
872	O_2H^+ +	HCN	$\Longrightarrow H_2CN^+$	+	O_2	9.7×10^{-10}	0	0	1

continued on next page

continued from previous page

Nr.	Reaction					A	E_a	α	Ref.
873	O_2H^+ +	HCO	$\Longrightarrow$	H_2CO^+ +	O_2	7.1×10^{-10}	0	0	1
874	O_2H^+ +	C_2H	$\Longrightarrow$	C_2H2^+ +	O_2	7.6×10^{-10}	0	0	1
875	O_2H^+ +	CO_2	$\Longrightarrow$	$HCO_2{}^+$ +	O_2	8.6×10^{-10}	0	0	1
876	O_2H^+ +	H_2CO	$\Longrightarrow$	H_3CO^+ +	O_2	9.8×10^{-10}	0	0	1
877	O_2H^+ +	NH_3	$\Longrightarrow$	$NH_4{}^+$ +	O_2	1.0×10^{-09}	0	0	1
878	$CO_2{}^+$ +	H	$\Longrightarrow$	HCO^+ +	O	3.0×10^{-10}	0	0	1
879	$CO_2{}^+$ +	H_2	$\Longrightarrow$	$HCO_2{}^+$ +	H	1.4×10^{-09}	0	0	1
880	$CO_2{}^+$ +	O_2	$\Longrightarrow$	$O_2{}^+$ +	CO_2	5.0×10^{-11}	0	0	1
881	$CO_2{}^+$ +	NO	$\Longrightarrow$	NO^+ +	CO_2	1.2×10^{-10}	0	0	1
882	$NO_2{}^+$ +	H	$\Longrightarrow$	NO^+ +	OH	1.9×10^{-10}	0	0	1
883	$NO_2{}^+$ +	H_2	$\Longrightarrow$	NO^+ +	H_2O	1.5×10^{-10}	0	0	1
884	$SiH_2{}^+$ +	C	$\Longrightarrow$	$CHSi^+$ +	H	1.1×10^{-09}	0	0	1
885	$SiH_2{}^+$ +	O	$\Longrightarrow$	$SiOH^+$ +	H	6.3×10^{-10}	0	0	1
886	$SiH_2{}^+$ +	S	$\Longrightarrow$	$HSiS^+$ +	H	1.1×10^{-09}	0	0	1
887	H_2S^+ +	C	$\Longrightarrow$	HCS^+ +	H	1.0×10^{-09}	0	0	1
888	H_2S^+ +	N	$\Longrightarrow$	NS^+ +	H_2	7.9×10^{-10}	0	0	1
889	H_2S^+ +	O	$\Longrightarrow$	HS^+ +	OH	3.1×10^{-10}	0	0	1
890	H_2S^+ +	O	$\Longrightarrow$	SO^+ +	H_2	3.1×10^{-10}	0	0	1
891	H_2S^+ +	Si	$\Longrightarrow$	Si^+ +	H_2S	1.6×10^{-09}	0	0	1
892	H_2S^+ +	S	$\Longrightarrow$	S^+ +	H_2S	1.1×10^{-09}	0	0	1
893	H_2S^+ +	Fe	$\Longrightarrow$	Fe^+ +	H_2S	1.8×10^{-09}	0	0	1
894	H_2S^+ +	Na	$\Longrightarrow$	Na^+ +	H_2S	2.5×10^{-09}	0	0	1
895	H_2S^+ +	Mg	$\Longrightarrow$	Mg^+ +	H_2S	2.8×10^{-09}	0	0	1
896	H_2S^+ +	NO	$\Longrightarrow$	NO^+ +	H_2S	7.6×10^{-10}	0	0	1
897	H_2S^+ +	H_2O	$\Longrightarrow$	H_3O^+ +	HS	7.0×10^{-10}	0	0	1
898	H_2S^+ +	HCO	$\Longrightarrow$	HCO^+ +	H_2S	7.0×10^{-10}	0	0	1
899	H_2S^+ +	H_2S	$\Longrightarrow$	H_3S^+ +	HS	5.8×10^{-10}	0	0	1
900	H_2S^+ +	NH_3	$\Longrightarrow$	$NH_4{}^+$ +	HS	1.3×10^{-09}	0	0	1
901	H_2S^+ +	NH_3	$\Longrightarrow$	$NH_3{}^+$ +	H_2S	5.6×10^{-10}	0	0	1
902	$NH_3{}^+$ +	C	$\Longrightarrow$	$CH_2{}^+$ +	NH	1.0×10^{-11}	0	0	1
903	$NH_3{}^+$ +	O	$\Longrightarrow$	HNO^+ +	H_2	1.0×10^{-11}	0	0	1
904	$NH_3{}^+$ +	Si	$\Longrightarrow$	Si^+ +	NH_3	1.9×10^{-09}	0	0	1
905	$NH_3{}^+$ +	Fe	$\Longrightarrow$	Fe^+ +	NH_3	2.3×10^{-09}	0	0	1
906	$NH_3{}^+$ +	Na	$\Longrightarrow$	Na^+ +	NH_3	3.2×10^{-09}	0	0	1
907	$NH_3{}^+$ +	Mg	$\Longrightarrow$	Mg^+ +	NH_3	3.3×10^{-09}	0	0	1
908	$NH_3{}^+$ +	H_2	$\Longrightarrow$	$NH_4{}^+$ +	H	1.0×10^{-13}	0	0	1
909	$NH_3{}^+$ +	C_2	$\Longrightarrow$	C_2H2^+ +	NH	1.0×10^{-11}	0	0	1
910	$NH_3{}^+$ +	CH	$\Longrightarrow$	$NH_4{}^+$ +	C	6.9×10^{-10}	0	0	1
911	$NH_3{}^+$ +	NH	$\Longrightarrow$	$NH_4{}^+$ +	N	7.1×10^{-10}	0	0	1
912	$NH_3{}^+$ +	OH	$\Longrightarrow$	$NH_4{}^+$ +	O	7.0×10^{-10}	0	0	1
913	$NH_3{}^+$ +	NO	$\Longrightarrow$	NO^+ +	NH_3	9.2×10^{-10}	0	0	1
914	$NH_3{}^+$ +	CH_2	$\Longrightarrow$	$CH_3{}^+$ +	NH_2	9.6×10^{-10}	0	0	1
915	$NH_3{}^+$ +	NH_2	$\Longrightarrow$	$NH_4{}^+$ +	NH	1.0×10^{-11}	0	0	1
916	$NH_3{}^+$ +	H_2O	$\Longrightarrow$	$NH_4{}^+$ +	OH	1.1×10^{-10}	0	0	1
917	$NH_3{}^+$ +	HCO	$\Longrightarrow$	$NH_4{}^+$ +	CO	4.2×10^{-10}	0	0	1
918	$NH_3{}^+$ +	HCO	$\Longrightarrow$	HCO^+ +	NH_3	4.2×10^{-10}	0	0	1

continued on next page

continued from previous page

Nr.	Reaction					A	E_a	α	Ref.
919	NH_3^+	+	H_2S	$\Longrightarrow$ NH_4^+	+ HS	6.5×10^{-10}	0	0	1
920	NH_3^+	+	H_2S	$\Longrightarrow$ H_3S^+	+ NH_2	1.1×10^{-10}	0	0	1
921	NH_3^+	+	H_2CO	$\Longrightarrow$ NH_4^+	+ HCO	5.0×10^{-10}	0	0	1
922	NH_3^+	+	NH_3	$\Longrightarrow$ NH_4^+	+ NH_2	2.3×10^{-09}	0	0	1
923	NH_3^+	+	CH_4	$\Longrightarrow$ NH_4^+	+ CH_3	3.9×10^{-10}	0	0	1
924	H_2CO^+	+	Si	$\Longrightarrow$ Si^+	+ H_2CO	1.6×10^{-09}	0	0	1
925	H_2CO^+	+	S	$\Longrightarrow$ HS^+	+ HCO	5.5×10^{-10}	0	0	1
926	H_2CO^+	+	S	$\Longrightarrow$ S^+	+ H_2CO	5.5×10^{-10}	0	0	1
927	H_2CO^+	+	Fe	$\Longrightarrow$ Fe^+	+ H_2CO	1.9×10^{-09}	0	0	1
928	H_2CO^+	+	Na	$\Longrightarrow$ Na^+	+ H_2CO	2.6×10^{-09}	0	0	1
929	H_2CO^+	+	Mg	$\Longrightarrow$ Mg^+	+ H_2CO	2.9×10^{-09}	0	0	1
930	H_2CO^+	+	C_2	$\Longrightarrow$ C_2H^+	+ HCO	8.2×10^{-10}	0	0	1
931	H_2CO^+	+	CH	$\Longrightarrow$ CH^+	+ H_2CO	3.1×10^{-10}	0	0	1
932	H_2CO^+	+	CH	$\Longrightarrow$ CH_2^+	+ HCO	3.1×10^{-10}	0	0	1
933	H_2CO^+	+	NH	$\Longrightarrow$ H_3CO^+	+ N	6.4×10^{-10}	0	0	1
934	H_2CO^+	+	NO	$\Longrightarrow$ NO^+	+ H_2CO	7.8×10^{-10}	0	0	1
935	H_2CO^+	+	CH_2	$\Longrightarrow$ CH_3^+	+ HCO	4.3×10^{-10}	0	0	1
936	H_2CO^+	+	CH_2	$\Longrightarrow$ CH_2^+	+ H_2CO	4.3×10^{-10}	0	0	1
937	H_2CO^+	+	NH_2	$\Longrightarrow$ NH_3^+	+ HCO	8.8×10^{-10}	0	0	1
938	H_2CO^+	+	H_2O	$\Longrightarrow$ H_3O^+	+ HCO	8.4×10^{-10}	0	0	1
939	H_2CO^+	+	HCN	$\Longrightarrow$ H_2CN^+	+ HCO	1.4×10^{-09}	0	0	1
940	H_2CO^+	+	HCO	$\Longrightarrow$ HCO^+	+ H_2CO	3.6×10^{-10}	0	0	1
941	H_2CO^+	+	HCO	$\Longrightarrow$ H_3CO^+	+ CO	3.6×10^{-10}	0	0	1
942	H_2CO^+	+	C_2H	$\Longrightarrow$ C_2H2^+	+ HCO	7.7×10^{-10}	0	0	1
943	H_2CO^+	+	H_2CO	$\Longrightarrow$ H_3CO^+	+ HCO	1.0×10^{-09}	0	0	1
944	H_2CO^+	+	NH_3	$\Longrightarrow$ NH_4^+	+ HCO	1.1×10^{-09}	0	0	1
945	H_2CO^+	+	NH_3	$\Longrightarrow$ NH_3^+	+ H_2CO	1.1×10^{-09}	0	0	1
946	CH_3^+	+	C	$\Longrightarrow$ C_2H^+	+ H_2	5.0×10^{-10}	0	0	1
947	CH_3^+	+	N	$\Longrightarrow$ HCN^+	+ H_2	6.7×10^{-11}	0	0	1
948	CH_3^+	+	O	$\Longrightarrow$ HCO^+	+ H_2	4.4×10^{-10}	0	0	1
949	CH_3^+	+	Si	$\Longrightarrow$ Si^+	+ CH_3	9.7×10^{-10}	0	0	1
950	CH_3^+	+	Si	$\Longrightarrow$ CH_2Si^+	+ H	9.7×10^{-10}	0	0	1
951	CH_3^+	+	S	$\Longrightarrow$ HCS^+	+ H_2	1.4×10^{-09}	0	0	1
952	CH_3^+	+	Fe	$\Longrightarrow$ Fe^+	+ CH_3	2.4×10^{-09}	0	0	1
953	CH_3^+	+	Na	$\Longrightarrow$ Na^+	+ CH_3	3.4×10^{-09}	0	0	1
954	CH_3^+	+	Mg	$\Longrightarrow$ Mg^+	+ CH_3	3.5×10^{-09}	0	0	1
955	CH_3^+	+	C_2	$\Longrightarrow$ C_3H^+	+ H_2	9.9×10^{-10}	0	0	1
956	CH_3^+	+	O_2	$\Longrightarrow$ HCO^+	+ H_2O	4.3×10^{-11}	0	0	1
957	CH_3^+	+	CH	$\Longrightarrow$ C_2H2^+	+ H_2	7.1×10^{-10}	0	0	1
958	CH_3^+	+	NH	$\Longrightarrow$ H_2CN^+	+ H_2	7.4×10^{-10}	0	0	1
959	CH_3^+	+	OH	$\Longrightarrow$ H_2CO^+	+ H_2	7.2×10^{-10}	0	0	1
960	CH_3^+	+	CN	$\Longrightarrow$ C_2H2N^+	+ H	1.1×10^{-09}	0	0	1
961	CH_3^+	+	NO	$\Longrightarrow$ NO^+	+ CH_3	9.4×10^{-10}	0	0	1
962	CH_3^+	+	SiH	$\Longrightarrow$ CH_2Si^+	+ H_2	1.0×10^{-09}	0	0	1
963	CH_3^+	+	HS	$\Longrightarrow$ H_2CS^+	+ H_2	1.0×10^{-09}	0	0	1
964	CH_3^+	+	SO	$\Longrightarrow$ $HOCS^+$	+ H_2	9.5×10^{-10}	0	0	1

continued on next page

continued from previous page

Nr.	Reaction	A	E_a	α	Ref.
965	$CH_3^+ + CH_2 \Longrightarrow C_2H3^+ + H_2$	9.9×10^{-10}	0	0	1
966	$CH_3^+ + NH_2 \Longrightarrow CH_4N^+ + H$	1.0×10^{-09}	0	0	1
967	$CH_3^+ + HCO \Longrightarrow CH_4^+ + CO$	4.4×10^{-10}	0	0	1
968	$CH_3^+ + HCO \Longrightarrow HCO^+ + CH_3$	4.4×10^{-10}	0	0	1
969	$CH_3^+ + H_2S \Longrightarrow H_3CS^+ + H_2$	1.4×10^{-09}	0	0	1
970	$CH_3^+ + H_2CO \Longrightarrow HCO^+ + CH_4$	1.0×10^{-09}	0	0	1
971	$CH_3^+ + NH_3 \Longrightarrow NH_4^+ + CH_2$	2.0×10^{-10}	0	0	1
972	$CH_3^+ + NH_3 \Longrightarrow CH_4N^+ + H_2$	7.0×10^{-10}	0	0	1
973	$CH_3^+ + C_2H2 \Longrightarrow C_3H3^+ + H_2$	1.2×10^{-09}	0	0	1
974	$CH_3^+ + CH_4 \Longrightarrow C_2H5^+ + H_2$	9.6×10^{-10}	0	0	1
975	$H_3O^+ + C \Longrightarrow HCO^+ + H_2$	1.0×10^{-11}	0	0	1
976	$H_3O^+ + Si \Longrightarrow SiH^+ + H_2O$	1.8×10^{-09}	0	0	1
977	$H_3O^+ + Na \Longrightarrow Na^+ + H_2O + H$	3.1×10^{-09}	0	0	1
978	$H_3O^+ + C_2 \Longrightarrow C_2H^+ + H_2O$	9.2×10^{-10}	0	0	1
979	$H_3O^+ + CH \Longrightarrow CH_2^+ + H_2O$	6.8×10^{-10}	0	0	1
980	$H_3O^+ + SiC \Longrightarrow CHSi^+ + H_2O$	4.3×10^{-09}	0	0	1
981	$H_3O^+ + SiH \Longrightarrow SiH_2^+ + H_2O$	9.7×10^{-10}	0	0	1
982	$H_3O^+ + CH_2 \Longrightarrow CH_3^+ + H_2O$	9.4×10^{-10}	0	0	1
983	$H_3O^+ + NH_2 \Longrightarrow NH_3^+ + H_2O$	9.7×10^{-10}	0	0	1
984	$H_3O^+ + HCN \Longrightarrow H_2CN^+ + H_2O$	1.1×10^{-09}	0	0	1
985	$H_3O^+ + H_2CO \Longrightarrow H_3CO^+ + H_2O$	1.1×10^{-09}	0	0	1
986	$H_3O^+ + NH_3 \Longrightarrow NH_4^+ + H_2O$	2.2×10^{-09}	0	0	1
987	$H_2CN^+ + Na \Longrightarrow Na^+ + HCN + H$	2.7×10^{-09}	0	0	1
988	$H_2CN^+ + CH \Longrightarrow CH_2^+ + HCN$	6.3×10^{-10}	0	0	1
989	$H_2CN^+ + CH_2 \Longrightarrow CH_3^+ + HCN$	8.7×10^{-10}	0	0	1
990	$H_2CN^+ + NH_2 \Longrightarrow NH_3^+ + HCN$	8.9×10^{-10}	0	0	1
991	$H_2CN^+ + NH_3 \Longrightarrow NH_4^+ + HCN$	2.2×10^{-09}	0	0	1
992	$C_2H2^+ + C \Longrightarrow C_3H^+ + H$	1.1×10^{-09}	0	0	1
993	$C_2H2^+ + N \Longrightarrow C_2N^+ + H_2$	8.2×10^{-10}	0	0	1
994	$C_2H2^+ + O \Longrightarrow C_2HO^+ + H$	1.3×10^{-09}	0	0	1
995	$C_2H2^+ + Si \Longrightarrow Si^+ + C_2H2$	1.7×10^{-09}	0	0	1
996	$C_2H2^+ + Fe \Longrightarrow Fe^+ + C_2H2$	2.0×10^{-09}	0	0	1
997	$C_2H2^+ + Na \Longrightarrow Na^+ + C_2H2$	2.7×10^{-09}	0	0	1
998	$C_2H2^+ + Mg \Longrightarrow Mg^+ + C_2H2$	3.0×10^{-09}	0	0	1
999	$C_2H2^+ + C_2 \Longrightarrow C_2H^+ + C_2H$	8.5×10^{-10}	0	0	1
1000	$C_2H2^+ + CH \Longrightarrow C_3H2^+ + H$	6.4×10^{-10}	0	0	1
1001	$C_2H2^+ + NH \Longrightarrow C_2H2N^+ + H$	6.5×10^{-10}	0	0	1
1002	$C_2H2^+ + OH \Longrightarrow C_2H2O^+ + H$	6.4×10^{-10}	0	0	1
1003	$C_2H2^+ + CN \Longrightarrow C_3HN^+ + H$	9.0×10^{-10}	0	0	1
1004	$C_2H2^+ + NO \Longrightarrow NO^+ + C_2H2$	8.1×10^{-10}	0	0	1
1005	$C_2H2^+ + CH_2 \Longrightarrow C_3H3^+ + H$	8.8×10^{-10}	0	0	1
1006	$C_2H2^+ + NH_2 \Longrightarrow C_2H3N^+ + H$	4.5×10^{-10}	0	0	1
1007	$C_2H2^+ + NH_2 \Longrightarrow NH_3^+ + C_2H$	4.5×10^{-10}	0	0	1
1008	$C_2H2^+ + H_2O \Longrightarrow H_3O^+ + C_2H$	2.2×10^{-10}	0	0	1
1009	$C_2H2^+ + HCN \Longrightarrow C_3H2N^+ + H$	7.0×10^{-11}	0	0	1
1010	$C_2H2^+ + HCN \Longrightarrow H_2CN^+ + C_2H$	3.0×10^{-11}	0	0	1

continued on next page

continued from previous page

Nr.	Reaction	A	E_a	α	Ref.
1011	C_2H2^+ + HCO $\Longrightarrow$ HCO^+ + C_2H2	5.0×10^{-10}	0	0	1
1012	C_2H2^+ + HCO $\Longrightarrow$ C_2H3^+ + CO	3.7×10^{-10}	0	0	1
1013	C_2H2^+ + H_2S $\Longrightarrow$ C_2H3^+ + HS	4.6×10^{-11}	0	0	1
1014	C_2H2^+ + H_2S $\Longrightarrow$ H_3S^+ + C_2H	4.6×10^{-11}	0	0	1
1015	C_2H2^+ + H_2S $\Longrightarrow$ H_2S^+ + C_2H2	2.2×10^{-09}	0	0	1
1016	C_2H2^+ + H_2CO $\Longrightarrow$ H_3CO^+ + C_2H	4.1×10^{-10}	0	0	1
1017	C_2H2^+ + H_2CO $\Longrightarrow$ H_2CO^+ + C_2H2	8.6×10^{-10}	0	0	1
1018	C_2H2^+ + NH_3 $\Longrightarrow$ ${NH_4}^+$ + C_2H	1.1×10^{-09}	0	0	1
1019	C_2H2^+ + NH_3 $\Longrightarrow$ ${NH_3}^+$ + C_2H2	2.1×10^{-09}	0	0	1
1020	C_3N^+ + H_2 $\Longrightarrow$ C_3HN^+ + H	1.5×10^{-09}	0	0	1
1021	${HCO_2}^+$ + C $\Longrightarrow$ CH^+ + CO_2	1.0×10^{-09}	0	0	1
1022	${HCO_2}^+$ + CO $\Longrightarrow$ HCO^+ + CO_2	7.8×10^{-10}	0	0	1
1023	${HCO_2}^+$ + H_2O $\Longrightarrow$ H_3O^+ + CO_2	7.8×10^{-10}	0	0	1
1024	H_3CO^+ + Na $\Longrightarrow$ Na^+ + H_2CO + H	2.6×10^{-09}	0	0	1
1025	H_3CO^+ + CH $\Longrightarrow$ ${CH_2}^+$ + H_2CO	6.2×10^{-10}	0	0	1
1026	H_3CO^+ + NH_2 $\Longrightarrow$ ${NH_3}^+$ + H_2CO	8.8×10^{-10}	0	0	1
1027	H_3CO^+ + HCN $\Longrightarrow$ H_2CN^+ + H_2CO	9.9×10^{-10}	0	0	1
1028	H_3CO^+ + H_2S $\Longrightarrow$ H_3S^+ + H_2CO	1.1×10^{-09}	0	0	1
1029	H_3CO^+ + NH_3 $\Longrightarrow$ ${NH_4}^+$ + H_2CO	2.3×10^{-09}	0	0	1
1030	${NH_4}^+$ + C $\Longrightarrow$ H_2CN^+ + H_2	1.0×10^{-11}	0	0	1
1031	C_2H3^+ + H $\Longrightarrow$ C_2H2^+ + H_2	1.9×10^{-10}	0	0	1
1032	C_2H3^+ + H_2O $\Longrightarrow$ H_3O^+ + C_2H2	8.5×10^{-10}	0	0	1
1033	C_2H3^+ + H_2S $\Longrightarrow$ H_3S^+ + C_2H2	8.4×10^{-10}	0	0	1
1034	C_2H3^+ + NH_3 $\Longrightarrow$ ${NH_4}^+$ + C_2H2	2.5×10^{-09}	0	0	1
1035	C_3H2^+ + H_2 $\Longrightarrow$ C_3H3^+ + H	1.5×10^{-09}	0	0	1
1036	$CHSi^+$ + H_2 $\Longrightarrow$ CH_2Si^+ + H	1.5×10^{-09}	0	0	1
1037	C_3HN^+ + H_2 $\Longrightarrow$ C_3H2N^+ + H	1.0×10^{-09}	0	0	1
1038	${CH_4}^+$ + H $\Longrightarrow$ ${CH_3}^+$ + H_2	2.0×10^{-10}	0	0	1
1039	${CH_4}^+$ + H_2 $\Longrightarrow$ ${CH_5}^+$ + H	4.1×10^{-11}	0	0	1
1040	${CH_4}^+$ + H_2O $\Longrightarrow$ H_3O^+ + CH_3	1.5×10^{-09}	0	0	1
1041	${CH_4}^+$ + H_2S $\Longrightarrow$ ${CH_5}^+$ + HS	9.0×10^{-11}	0	0	1
1042	${CH_4}^+$ + H_2S $\Longrightarrow$ H_2S^+ + CH_4	5.9×10^{-10}	0	0	1
1043	${CH_4}^+$ + H_2S $\Longrightarrow$ H_3S^+ + CH_3	7.2×10^{-10}	0	0	1
1044	${CH_4}^+$ + NH_3 $\Longrightarrow$ ${CH_5}^+$ + NH_2	3.0×10^{-11}	0	0	1
1045	${CH_4}^+$ + NH_3 $\Longrightarrow$ ${NH_3}^+$ + CH_4	6.9×10^{-10}	0	0	1
1046	${CH_4}^+$ + NH_3 $\Longrightarrow$ ${NH_4}^+$ + CH_3	6.6×10^{-10}	0	0	1
1047	${CH_4}^+$ + C_2H2 $\Longrightarrow$ C_2H2^+ + CH_4	1.1×10^{-09}	0	0	1
1048	${CH_4}^+$ + CH_4 $\Longrightarrow$ ${CH_5}^+$ + CH_3	1.2×10^{-09}	0	0	1
1049	CH_2Si^+ + C $\Longrightarrow$ Si^+ + C_2H2	1.0×10^{-09}	0	0	1
1050	CH_2Si^+ + N $\Longrightarrow$ Si^+ + HCN + H	7.6×10^{-10}	0	0	1
1051	CH_2Si^+ + O $\Longrightarrow$ Si^+ + H_2CO	6.0×10^{-10}	0	0	1
1052	CH_2Si^+ + S $\Longrightarrow$ Si^+ + H_2CS	1.0×10^{-09}	0	0	1
1053	${CH_5}^+$ + H $\Longrightarrow$ ${CH_4}^+$ + H_2	2.0×10^{-11}	0	0	1
1054	${CH_5}^+$ + C $\Longrightarrow$ CH^+ + CH_4	1.2×10^{-09}	0	0	1
1055	${CH_5}^+$ + S $\Longrightarrow$ HS^+ + CH_4	1.3×10^{-09}	0	0	1
1056	${CH_5}^+$ + C_2 $\Longrightarrow$ C_2H^+ + CH_4	9.5×10^{-10}	0	0	1

continued on next page

continued from previous page

Nr.	Reaction							A	E_a	α	Ref.
1057	CH_5^+	+	CH	$\Longrightarrow$	CH_2^+	+	CH_4	6.9×10^{-10}	0	0	1
1058	CH_5^+	+	NH	$\Longrightarrow$	NH_2^+	+	CH_4	7.1×10^{-10}	0	0	1
1059	CH_5^+	+	OH	$\Longrightarrow$	H_2O^+	+	CH_4	7.0×10^{-10}	0	0	1
1060	CH_5^+	+	CO	$\Longrightarrow$	HCO^+	+	CH_4	1.0×10^{-09}	0	0	1
1061	CH_5^+	+	CH_2	$\Longrightarrow$	CH_3^+	+	CH_4	9.6×10^{-10}	0	0	1
1062	CH_5^+	+	NH_2	$\Longrightarrow$	NH_3^+	+	CH_4	9.9×10^{-10}	0	0	1
1063	CH_5^+	+	H_2O	$\Longrightarrow$	H_3O^+	+	CH_4	9.5×10^{-10}	0	0	1
1064	CH_5^+	+	HCN	$\Longrightarrow$	H_2CN^+	+	CH_4	1.2×10^{-09}	0	0	1
1065	CH_5^+	+	HCO	$\Longrightarrow$	H_2CO^+	+	CH_4	8.5×10^{-10}	0	0	1
1066	CH_5^+	+	C_2H	$\Longrightarrow$	C_2H2^+	+	CH_4	9.0×10^{-10}	0	0	1
1067	CH_5^+	+	H_2CO	$\Longrightarrow$	H_3CO^+	+	CH_4	1.2×10^{-09}	0	0	1
1068	CH_5^+	+	NH_3	$\Longrightarrow$	NH_4^+	+	CH_4	1.2×10^{-09}	0	0	1
1069	CH_5^+	+	C_2H2	$\Longrightarrow$	C_2H3^+	+	CH_4	1.3×10^{-09}	0	0	1
1070	C_2H5^+	+	C_2H2	$\Longrightarrow$	C_3H3^+	+	CH_4	6.8×10^{-11}	0	0	1
1071	H^-	+	H_2O	$\Longrightarrow$	OH^-	+	H_2	3.8×10^{-09}	0	0	1
1072	H^-	+	HCN	$\Longrightarrow$	CN^-	+	H_2	3.8×10^{-09}	0	0	1
1073	C^-	+	O_2	$\Longrightarrow$	O^-	+	CO	4.0×10^{-10}	0	0	1
1074	C^-	+	NO	$\Longrightarrow$	CN^-	+	O	1.0×10^{-09}	0	0	1
1075	C^-	+	CO_2	$\Longrightarrow$	CO	+	CO + e^-	4.7×10^{-11}	0	0	1
1076	O^-	+	H_2	$\Longrightarrow$	OH^-	+	H	3.0×10^{-11}	0	0	1
1077	O^-	+	CN	$\Longrightarrow$	CN^-	+	O	1.0×10^{-09}	0	0	1
1078	O^-	+	H_2O	$\Longrightarrow$	OH^-	+	OH	1.4×10^{-09}	0	0	1
1079	O^-	+	HCN	$\Longrightarrow$	CN^-	+	OH	1.2×10^{-09}	0	0	1
1080	O^-	+	CH_4	$\Longrightarrow$	OH^-	+	CH_3	1.0×10^{-10}	0	0	1
1081	OH^-	+	CN	$\Longrightarrow$	CN^-	+	OH	1.0×10^{-09}	0	0	1
1082	OH^-	+	HCN	$\Longrightarrow$	CN^-	+	H_2O	1.2×10^{-09}	0	0	1
1083	C^+	+	H	$\Longrightarrow$	CH^+	+	$h\nu$	1.7×10^{-17}	0	0	1
1084	C^+	+	H_2	$\Longrightarrow$	CH_2^+	+	$h\nu$	1.0×10^{-16}	0	0	1
1085	Si^+	+	O	$\Longrightarrow$	SiO^+	+	$h\nu$	1.0×10^{-17}	0	0	1
1086	Si^+	+	H	$\Longrightarrow$	SiH^+	+	$h\nu$	1.0×10^{-17}	0	0	1
1087	Si^+	+	H_2	$\Longrightarrow$	SiH_2^+	+	$h\nu$	1.0×10^{-15}	0	0	1
1088	CH_3^+	+	H_2	$\Longrightarrow$	CH_5^+	+	$h\nu$	3.0×10^{-15}	0	0	1
1089	H^-	+	H	$\Longrightarrow$	H_2	+	e^-	1.3×10^{-09}	0	0	1
1090	H^-	+	C	$\Longrightarrow$	CH	+	e^-	1.0×10^{-09}	0	0	1
1091	H^-	+	N	$\Longrightarrow$	NH	+	e^-	1.0×10^{-09}	0	0	1
1092	H^-	+	O	$\Longrightarrow$	OH	+	e^-	1.0×10^{-09}	0	0	1
1093	H^-	+	C_2	$\Longrightarrow$	C_2H	+	e^-	1.0×10^{-09}	0	0	1
1094	H^-	+	CH	$\Longrightarrow$	CH_2	+	e^-	1.0×10^{-10}	0	0	1
1095	H^-	+	NH	$\Longrightarrow$	NH_2	+	e^-	1.0×10^{-10}	0	0	1
1096	H^-	+	OH	$\Longrightarrow$	H_2O	+	e^-	1.0×10^{-10}	0	0	1
1097	H^-	+	CO	$\Longrightarrow$	HCO	+	e^-	5.0×10^{-11}	0	0	1
1098	H^-	+	CN	$\Longrightarrow$	HCN	+	e^-	1.0×10^{-10}	0	0	1
1099	H^-	+	CH_2	$\Longrightarrow$	CH_3	+	e^-	1.0×10^{-09}	0	0	1
1100	H^-	+	NH_2	$\Longrightarrow$	NH_3	+	e^-	1.0×10^{-09}	0	0	1
1101	H^-	+	HCO	$\Longrightarrow$	H_2CO	+	e^-	1.0×10^{-09}	0	0	1
1102	H^-	+	C_2H	$\Longrightarrow$	C_2H2	+	e^-	1.0×10^{-09}	0	0	1

continued on next page

continued from previous page

Nr.	Reaction	A	E_a	α	Ref.
1103	$H^- + CH_3 \Longrightarrow CH_4 + e^-$	1.0×10^{-09}	0	0	1
1104	$C^- + H \Longrightarrow CH + e^-$	5.0×10^{-10}	0	0	1
1105	$C^- + C \Longrightarrow C_2 + e^-$	5.0×10^{-10}	0	0	1
1106	$C^- + N \Longrightarrow CN + e^-$	5.0×10^{-10}	0	0	1
1107	$C^- + O \Longrightarrow CO + e^-$	5.0×10^{-10}	0	0	1
1108	$C^- + H_2 \Longrightarrow CH_2 + e^-$	1.0×10^{-13}	0	0	1
1109	$C^- + O_2 \Longrightarrow CO_2 + e^-$	5.0×10^{-11}	0	0	1
1110	$C^- + CH \Longrightarrow C_2H + e^-$	5.0×10^{-10}	0	0	1
1111	$C^- + NH \Longrightarrow HCN + e^-$	5.0×10^{-10}	0	0	1
1112	$C^- + OH \Longrightarrow HCO + e^-$	5.0×10^{-10}	0	0	1
1113	$C^- + CH_2 \Longrightarrow C_2H2 + e^-$	5.0×10^{-10}	0	0	1
1114	$C^- + H_2O \Longrightarrow H_2CO + e^-$	5.0×10^{-10}	0	0	1
1115	$O^- + H \Longrightarrow OH + e^-$	5.0×10^{-10}	0	0	1
1116	$O^- + C \Longrightarrow CO + e^-$	5.0×10^{-10}	0	0	1
1117	$O^- + N \Longrightarrow NO + e^-$	2.2×10^{-10}	0	0	1
1118	$O^- + O \Longrightarrow O_2 + e^-$	1.9×10^{-10}	0	0	1
1119	$O^- + H_2 \Longrightarrow H_2O + e^-$	7.0×10^{-10}	0	0	1
1120	$O^- + CH \Longrightarrow HCO + e^-$	5.0×10^{-10}	0	0	1
1121	$O^- + CO \Longrightarrow CO_2 + e^-$	6.5×10^{-10}	0	0	1
1122	$O^- + CH_2 \Longrightarrow H_2CO + e^-$	5.0×10^{-10}	0	0	1
1123	$S^- + H \Longrightarrow HS + e^-$	1.0×10^{-10}	0	0	1
1124	$S^- + C \Longrightarrow CS + e^-$	1.0×10^{-10}	0	0	1
1125	$S^- + N \Longrightarrow NS + e^-$	1.0×10^{-10}	0	0	1
1126	$S^- + O \Longrightarrow SO + e^-$	1.0×10^{-10}	0	0	1
1127	$S^- + O_2 \Longrightarrow SO_2 + e^-$	3.0×10^{-11}	0	0	1
1128	$S^- + CO \Longrightarrow OCS + e^-$	3.0×10^{-10}	0	0	1
1129	$OH^- + H \Longrightarrow H_2O + e^-$	1.4×10^{-09}	0	0	1
1130	$OH^- + C \Longrightarrow HCO + e^-$	5.0×10^{-10}	0	0	1
1131	$OH^- + CH \Longrightarrow H_2CO + e^-$	5.0×10^{-10}	0	0	1
1132	$OH^- + CH_3 \Longrightarrow CH_3OH + e^-$	1.0×10^{-09}	0	0	1
1133	$CN^- + H \Longrightarrow HCN + e^-$	1.3×10^{-09}	0	0	1
1134	$CN^- + CH_3 \Longrightarrow CH_3CN + e^-$	1.0×10^{-09}	0	0	1
1135	$O + CH \Longrightarrow HCO^+ + e^-$	2.0×10^{-11}	4.4×10^{-01}	0	1
1136	$C + OH \Longrightarrow CO + H$	1.1×10^{-10}	5.0×10^{-01}	0	1
1137	$C + NO \Longrightarrow CN + O$	1.1×10^{-10}	5.0×10^{-01}	0	1
1138	$C + NH \Longrightarrow CN + H$	5.0×10^{-11}	5.0×10^{-01}	0	1
1139	$C + OCN \Longrightarrow CO + CN$	4.0×10^{-11}	5.0×10^{-01}	0	1
1140	$C + O_2 \Longrightarrow CO + O$	3.3×10^{-11}	5.0×10^{-01}	0	1
1141	$N + OH \Longrightarrow NO + H$	5.0×10^{-11}	5.0×10^{-01}	0	1
1142	$N + NO \Longrightarrow N_2 + O$	8.2×10^{-11}	0	$4.1 \times 10^{+02}$	1
1143	$N + CH \Longrightarrow CN + H$	2.5×10^{-11}	5.0×10^{-01}	0	1
1144	$N + CN \Longrightarrow C + N_2$	1.5×10^{-13}	5.0×10^{-01}	0	1
1145	$N + NH \Longrightarrow N_2 + H$	5.0×10^{-11}	5.0×10^{-01}	0	1
1146	$O + CH \Longrightarrow CO + H$	4.0×10^{-11}	5.0×10^{-01}	0	1
1147	$O + OH \Longrightarrow O_2 + H$	3.0×10^{-11}	-3.6×10^{-01}	0	1
1148	$O + NH \Longrightarrow OH + N$	2.9×10^{-11}	5.0×10^{-01}	0	1

continued on next page

continued from previous page

Nr.	Reaction	A	E_a	α	Ref.
1149	$O + CH_3 \Longrightarrow H_2CO + H$	1.8×10^{-10}	5.0×10^{-01}	0	1
1150	$O + CN \Longrightarrow CO + N$	1.8×10^{-11}	5.0×10^{-01}	0	1
1151	$O + SiH \Longrightarrow SiO + H$	4.0×10^{-11}	5.0×10^{-01}	0	1
1152	$O + OCN \Longrightarrow NO + CO$	5.0×10^{-11}	0	$2.0\times10^{+02}$	1
1153	$S + O_2 \Longrightarrow SO + O$	2.4×10^{-12}	5.0×10^{-01}	0	1
1154	$C_2 + N \Longrightarrow CN + C$	5.0×10^{-11}	5.0×10^{-01}	0	1
1155	$C_2 + O \Longrightarrow CO + C$	5.0×10^{-11}	5.0×10^{-01}	0	1
1156	$CH + S \Longrightarrow CS + H$	5.0×10^{-11}	5.0×10^{-01}	0	1
1157	$OH + CO \Longrightarrow CO_2 + H$	2.2×10^{-13}	0	$8.0\times10^{+01}$	1
1158	$OH + H_2CO \Longrightarrow HCO + H_2O$	3.0×10^{-11}	0	$2.5\times10^{+02}$	1
1159	$OH + Si \Longrightarrow SiO + H$	2.0×10^{-11}	5.0×10^{-01}	0	1
1160	$OH + S \Longrightarrow SO + H$	2.0×10^{-11}	5.0×10^{-01}	0	1
1161	$CN + O_2 \Longrightarrow O + OCN$	7.0×10^{-12}	5.0×10^{-01}	0	1
1162	$NO + NH_2 \Longrightarrow N_2 + H_2O$	1.6×10^{-10}	0	0	1
1163	$NO + NH \Longrightarrow O + N_2 + H$	4.7×10^{-11}	5.0×10^{-01}	0	1
1164	$HS + O \Longrightarrow SO + H$	1.6×10^{-10}	5.0×10^{-01}	0	1
1165	$NO + N \Longrightarrow N_2 + O$	8.2×10^{-11}	0	$4.1\times10^{+02}$	4
1166	$HS + N \Longrightarrow NS + H$	1.6×10^{-10}	5.0×10^{-01}	0	1
1167	$CS + O \Longrightarrow CO + S$	2.6×10^{-10}	0	$7.5\times10^{+02}$	1
1168	$SO + N \Longrightarrow NO + S$	1.0×10^{-11}	0	$7.5\times10^{+02}$	1
1169	$SO + OH \Longrightarrow SO_2 + H$	1.0×10^{-10}	5.0×10^{-01}	0	1
1170	$CH_2 + OH \Longrightarrow H_2CO + H$	1.0×10^{-10}	0	$2.5\times10^{+02}$	1
1171	$CH_2 + O \Longrightarrow CO + H + H$	2.0×10^{-11}	5.0×10^{-01}	0	1
1172	$CH_2 + O \Longrightarrow HCO + H$	5.0×10^{-12}	5.0×10^{-01}	0	1
1173	$CH_2 + N \Longrightarrow HCN + H$	1.0×10^{-11}	5.0×10^{-01}	0	1
1174	$NH_2 + O \Longrightarrow NH + OH$	3.5×10^{-12}	5.0×10^{-01}	0	1
1175	$HCO + H \Longrightarrow H_2 + CO$	2.0×10^{-10}	5.0×10^{-01}	0	1
1176	$O_2 + H_2 \Longrightarrow OH + OH$	1.0×10^{-10}	0	$9.3\times10^{+03}$	4
1177	$OCN + O \Longrightarrow NO + CO$	5.0×10^{-11}	0	$2.0\times10^{+02}$	4
1178	$OH + H_2 \Longrightarrow H_2O + H$	3.6×10^{-11}	0	$2.5\times10^{+03}$	4
1179	$HCO + O \Longrightarrow OH + CO$	1.2×10^{-10}	5.0×10^{-01}	0	1
1180	$HCO + O \Longrightarrow H + CO_2$	8.9×10^{-11}	5.0×10^{-01}	0	1
1181	$C_2H + O \Longrightarrow CO + CH$	1.0×10^{-10}	0	$2.5\times10^{+02}$	1
1182	$CH_3 + S \Longrightarrow H_2CS + H$	2.0×10^{-11}	5.0×10^{-01}	0	1
1183	$CH_3 + N \Longrightarrow HCN + H + H$	2.0×10^{-11}	5.0×10^{-01}	0	1
1184	$C + H \Longrightarrow CH + h\nu$	1.0×10^{-17}	0	0	1
1185	$C + N \Longrightarrow CN + h\nu$	1.0×10^{-17}	0	0	1
1186	$C + C \Longrightarrow C_2 + h\nu$	1.0×10^{-17}	0	0	1
1187	$O + O \Longrightarrow O_2 + h\nu$	4.9×10^{-20}	$1.5\times10^{+00}$	0	1
1188	$CO + S \Longrightarrow OCS + h\nu$	1.6×10^{-17}	$-3.2\times10^{+00}$	0	1
1189	$SO + O \Longrightarrow SO_2 + h\nu$	3.2×10^{-16}	$-1.6\times10^{+00}$	0	1
1190	$C_2H + CN \Longrightarrow HC_3N + h\nu$	1.0×10^{-16}	0	0	1
1191	$CH_3 + CN \Longrightarrow CH_3CN + h\nu$	1.0×10^{-16}	0	0	1
1192	$SiH^+ + e^- \Longrightarrow Si + H$	2.0×10^{-07}	-5.0×10^{-01}	0	1
1193	$C_2^+ + e^- \Longrightarrow C + C$	2.0×10^{-07}	-5.0×10^{-01}	0	1
1194	$N_2^+ + e^- \Longrightarrow N + N$	1.8×10^{-07}	-3.9×10^{-01}	0	1

continued on next page

continued from previous page

Nr.	Reaction	A	E_a	α	Ref.
1195	O_2^+ + e^- ⟹ O + O	2.0×10^{-07}	-5.0×10^{-01}	0	1
1196	HeH^+ + e^- ⟹ H + He	2.0×10^{-07}	-5.0×10^{-01}	0	1
1197	CH^+ + e^- ⟹ C + H	1.0×10^{-07}	-5.0×10^{-01}	0	1
1198	NH^+ + e^- ⟹ N + H	2.0×10^{-07}	-5.0×10^{-01}	0	1
1199	OH^+ + e^- ⟹ O + H	2.0×10^{-07}	-5.0×10^{-01}	0	1
1200	CO^+ + e^- ⟹ O + C	1.8×10^{-07}	-5.0×10^{-01}	0	1
1201	CN^+ + e^- ⟹ C + N	1.8×10^{-07}	-5.0×10^{-01}	0	1
1202	NO^+ + e^- ⟹ N + O	4.1×10^{-07}	$-1.0\times10^{+00}$	0	1
1203	SiS^+ + e^- ⟹ Si + S	2.0×10^{-07}	-5.0×10^{-01}	0	1
1204	SiC^+ + e^- ⟹ Si + C	2.0×10^{-07}	-5.0×10^{-01}	0	1
1205	HS^+ + e^- ⟹ S + H	2.0×10^{-07}	-5.0×10^{-01}	0	1
1206	SiO^+ + e^- ⟹ Si + O	2.0×10^{-07}	-5.0×10^{-01}	0	1
1207	CS^+ + e^- ⟹ C + S	2.0×10^{-07}	-5.0×10^{-01}	0	1
1208	SO^+ + e^- ⟹ S + O	2.0×10^{-07}	-5.0×10^{-01}	0	1
1209	NS^+ + e^- ⟹ N + S	2.0×10^{-07}	-5.0×10^{-01}	0	1
1210	H_3^+ + e^- ⟹ H_2 + H	1.1×10^{-07}	-5.0×10^{-01}	0	1
1211	H_3^+ + e^- ⟹ H + H + H	1.1×10^{-07}	-5.0×10^{-01}	0	1
1212	CH_2^+ + e^- ⟹ C + H_2	1.5×10^{-07}	-5.0×10^{-01}	0	1
1213	CH_2^+ + e^- ⟹ CH + H	1.5×10^{-07}	-5.0×10^{-01}	0	1
1214	NH_2^+ + e^- ⟹ N + H + H	1.5×10^{-07}	-5.0×10^{-01}	0	1
1215	NH_2^+ + e^- ⟹ NH + H	1.5×10^{-07}	-5.0×10^{-01}	0	1
1216	H_2O^+ + e^- ⟹ OH + H	2.0×10^{-07}	-5.0×10^{-01}	0	1
1217	H_2O^+ + e^- ⟹ O + H_2	2.0×10^{-07}	-5.0×10^{-01}	0	1
1218	HCO^+ + e^- ⟹ CO + H	2.0×10^{-07}	-7.5×10^{-01}	0	1
1219	HCN^+ + e^- ⟹ CN + H	2.0×10^{-07}	-5.0×10^{-01}	0	1
1220	HNO^+ + e^- ⟹ NO + H	3.0×10^{-07}	-5.0×10^{-01}	0	1
1221	C_2H^+ + e^- ⟹ C_2 + H	1.5×10^{-07}	-5.0×10^{-01}	0	1
1222	C_2H^+ + e^- ⟹ CH + C	1.5×10^{-07}	-5.0×10^{-01}	0	1
1223	N_2H^+ + e^- ⟹ N_2 + H	3.0×10^{-07}	-5.0×10^{-01}	0	1
1224	O_2H^+ + e^- ⟹ O_2 + H	3.0×10^{-07}	-5.0×10^{-01}	0	1
1225	C_2N^+ + e^- ⟹ C + CN	1.5×10^{-07}	-5.0×10^{-01}	0	1
1226	C_2N^+ + e^- ⟹ C_2 + N	1.5×10^{-07}	-5.0×10^{-01}	0	1
1227	C_3^+ + e^- ⟹ C_2 + C	3.0×10^{-07}	-5.0×10^{-01}	0	1
1228	CO_2^+ + e^- ⟹ O + CO	4.0×10^{-07}	-5.0×10^{-01}	0	1
1229	NO_2^+ + e^- ⟹ O + NO	3.0×10^{-07}	-5.0×10^{-01}	0	1
1230	$SiOH^+$ + e^- ⟹ SiO + H	1.5×10^{-07}	-5.0×10^{-01}	0	1
1231	$SiOH^+$ + e^- ⟹ Si + OH	1.5×10^{-07}	-5.0×10^{-01}	0	1
1232	SiH_2^+ + e^- ⟹ SiH + H	2.0×10^{-07}	-5.0×10^{-01}	0	1
1233	SiH_2^+ + e^- ⟹ Si + H + H	2.0×10^{-07}	-5.0×10^{-01}	0	1
1234	H_2S^+ + e^- ⟹ S + H + H	1.5×10^{-07}	-5.0×10^{-01}	0	1
1235	H_2S^+ + e^- ⟹ HS + H	1.5×10^{-07}	-5.0×10^{-01}	0	1
1236	HCS^+ + e^- ⟹ CS + H	3.0×10^{-07}	-5.0×10^{-01}	0	1
1237	HSO^+ + e^- ⟹ SO + H	2.0×10^{-07}	-5.0×10^{-01}	0	1
1238	HNS^+ + e^- ⟹ NS + H	3.0×10^{-07}	-5.0×10^{-01}	0	1
1239	NH_3^+ + e^- ⟹ NH_2 + H	3.0×10^{-07}	-5.0×10^{-01}	0	1
1240	NH_3^+ + e^- ⟹ NH + H + H	3.0×10^{-07}	-5.0×10^{-01}	0	1

continued on next page

continued from previous page

Nr.	Reaction	A	E_a	α	Ref.
1241	$H_2CO^+ + e^- \Longrightarrow HCO + H$	1.0×10^{-07}	-5.0×10^{-01}	0	1
1242	$H_2CO^+ + e^- \Longrightarrow CO + H + H$	5.0×10^{-07}	-5.0×10^{-01}	0	1
1243	$CH_3{}^+ + e^- \Longrightarrow CH_2 + H$	1.5×10^{-07}	-5.0×10^{-01}	0	1
1244	$CH_3{}^+ + e^- \Longrightarrow CH + H + H$	1.5×10^{-07}	-5.0×10^{-01}	0	1
1245	$H_3O^+ + e^- \Longrightarrow H_2O + H$	6.5×10^{-07}	-5.0×10^{-01}	0	1
1246	$H_3O^+ + e^- \Longrightarrow OH + H + H$	6.5×10^{-07}	-5.0×10^{-01}	0	1
1247	$H_2CN^+ + e^- \Longrightarrow CN + H + H$	3.0×10^{-07}	-5.0×10^{-01}	0	1
1248	$H_2CN^+ + e^- \Longrightarrow HCN + H$	3.0×10^{-07}	-5.0×10^{-01}	0	1
1249	$C_2H2^+ + e^- \Longrightarrow C_2H + H$	2.0×10^{-07}	-5.0×10^{-01}	0	1
1250	$C_2H2^+ + e^- \Longrightarrow CH + CH$	2.0×10^{-07}	-5.0×10^{-01}	0	1
1251	$C_2H2^+ + e^- \Longrightarrow C_2 + H + H$	2.0×10^{-07}	-5.0×10^{-01}	0	1
1252	$C_2HO^+ + e^- \Longrightarrow CO + C + H$	1.5×10^{-07}	-5.0×10^{-01}	0	1
1253	$C_2HO^+ + e^- \Longrightarrow C_2H + O$	1.5×10^{-07}	-5.0×10^{-01}	0	1
1254	$C_3H^+ + e^- \Longrightarrow C_2 + CH$	1.5×10^{-07}	-5.0×10^{-01}	0	1
1255	$C_3H^+ + e^- \Longrightarrow C_2H + C$	1.5×10^{-07}	-5.0×10^{-01}	0	1
1256	$C_2NH^+ + e^- \Longrightarrow HCN + C$	1.5×10^{-07}	-5.0×10^{-01}	0	1
1257	$C_2NH^+ + e^- \Longrightarrow CH + CN$	1.5×10^{-07}	-5.0×10^{-01}	0	1
1258	$C_3N^+ + e^- \Longrightarrow C_2 + CN$	3.0×10^{-07}	-5.0×10^{-01}	0	1
1259	$C_2H2O^+ + e^- \Longrightarrow C_2 + H_2O$	2.0×10^{-07}	-5.0×10^{-01}	0	1
1260	$C_2H2O^+ + e^- \Longrightarrow C_2H2 + O$	2.0×10^{-07}	-5.0×10^{-01}	0	1
1261	$C_2H2O^+ + e^- \Longrightarrow CH_2 + CO$	2.0×10^{-07}	-5.0×10^{-01}	0	1
1262	$HCO_2{}^+ + e^- \Longrightarrow CO_2 + H$	5.0×10^{-07}	-5.0×10^{-01}	0	1
1263	$HCO_2{}^+ + e^- \Longrightarrow CO + H + O$	1.0×10^{-07}	-5.0×10^{-01}	0	1
1264	$H_3CO^+ + e^- \Longrightarrow CO + H + H_2$	2.0×10^{-07}	-5.0×10^{-01}	0	1
1265	$H_3CO^+ + e^- \Longrightarrow HCO + H + H$	2.0×10^{-07}	-5.0×10^{-01}	0	1
1266	$H_3CO^+ + e^- \Longrightarrow H_2CO + H$	2.0×10^{-07}	-5.0×10^{-01}	0	1
1267	$NH_4{}^+ + e^- \Longrightarrow NH_3 + H$	3.0×10^{-07}	-5.0×10^{-01}	0	1
1268	$NH_4{}^+ + e^- \Longrightarrow NH_2 + H + H$	3.0×10^{-07}	-5.0×10^{-01}	0	1
1269	$C_2H3^+ + e^- \Longrightarrow C_2H2 + H$	6.0×10^{-07}	-5.0×10^{-01}	0	1
1270	$C_2H2N^+ + e^- \Longrightarrow CN + CH_2$	3.0×10^{-07}	-5.0×10^{-01}	0	1
1271	$C_2H2N^+ + e^- \Longrightarrow CH + HCN$	3.0×10^{-07}	-5.0×10^{-01}	0	1
1272	$C_3H2^+ + e^- \Longrightarrow C_2H2 + C$	3.0×10^{-07}	-5.0×10^{-01}	0	1
1273	$C_3H2^+ + e^- \Longrightarrow C_2 + CH_2$	3.0×10^{-07}	-5.0×10^{-01}	0	1
1274	$CH_3CO^+ + e^- \Longrightarrow CH_3 + CO$	3.0×10^{-07}	-5.0×10^{-01}	0	1
1275	$CH_4N^+ + e^- \Longrightarrow CN + H_2 + H_2$	3.0×10^{-08}	-5.0×10^{-01}	0	1
1276	$CH_4N^+ + e^- \Longrightarrow HCN + H + H_2$	3.0×10^{-07}	-5.0×10^{-01}	0	1
1277	$CHSi^+ + e^- \Longrightarrow Si + CH$	1.5×10^{-07}	-5.0×10^{-01}	0	1
1278	$CHSi^+ + e^- \Longrightarrow SiC + H$	1.5×10^{-07}	-5.0×10^{-01}	0	1
1279	$HSiS^+ + e^- \Longrightarrow SiS + H$	1.5×10^{-07}	-5.0×10^{-01}	0	1
1280	$SiH + S^+ \Longrightarrow SiS + H^+$	5.0×10^{-09}	0	0	1
1281	$HSiS^+ + e^- \Longrightarrow Si + HS$	1.5×10^{-07}	-5.0×10^{-01}	0	1
1282	$C_3H3^+ + e^- \Longrightarrow C_2H2 + CH$	6.0×10^{-07}	-5.0×10^{-01}	0	1
1283	$C_3HN^+ + e^- \Longrightarrow C_2 + HCN$	3.0×10^{-07}	-5.0×10^{-01}	0	1
1284	$C_3HN^+ + e^- \Longrightarrow C_2H + CN$	3.0×10^{-07}	-5.0×10^{-01}	0	1
1285	$CH_4{}^+ + e^- \Longrightarrow CH_3 + H$	3.0×10^{-07}	-5.0×10^{-01}	0	1
1286	$CH_4{}^+ + e^- \Longrightarrow CH_2 + H + H$	3.0×10^{-07}	-5.0×10^{-01}	0	1

continued on next page

continued from previous page

Nr.	Reaction							A	E_a	α	Ref.
1287	C_2H3N$^+$	+	e^-	$\Longrightarrow$	CH_3	+	CN	6.0×10^{-07}	-5.0 $\times 10^{-01}$	0	1
1288	C_3H2N$^+$	+	e^-	$\Longrightarrow$	C_2H2	+	CN	3.0×10^{-07}	-5.0 $\times 10^{-01}$	0	1
1289	C_3H2N$^+$	+	e^-	$\Longrightarrow$	HC_3N	+	H	3.0×10^{-07}	-5.0 $\times 10^{-01}$	0	1
1290	H_3S^+	+	e^-	$\Longrightarrow$	H_2S	+	H	3.0×10^{-07}	-5.0 $\times 10^{-01}$	0	1
1291	H_3S^+	+	e^-	$\Longrightarrow$	HS	+ H +	H	1.0×10^{-07}	-5.0 $\times 10^{-01}$	0	1
1292	$HOCS^+$	+	e^-	$\Longrightarrow$	OH	+	CS	2.0×10^{-07}	-5.0 $\times 10^{-01}$	0	1
1293	$HOCS^+$	+	e^-	$\Longrightarrow$	OCS	+	H	2.0×10^{-07}	-5.0 $\times 10^{-01}$	0	1
1294	CH_2Si^+	+	e^-	$\Longrightarrow$	SiC	+	H_2	2.0×10^{-07}	-5.0 $\times 10^{-01}$	0	1
1295	CH_2Si^+	+	e^-	$\Longrightarrow$	Si	+	CH_2	2.0×10^{-07}	-5.0 $\times 10^{-01}$	0	1
1296	H_2CS^+	+	e^-	$\Longrightarrow$	CS	+ H +	H	3.0×10^{-07}	-5.0 $\times 10^{-01}$	0	1
1297	H_3CS^+	+	e^-	$\Longrightarrow$	CS	+ H +	H_2	3.0×10^{-07}	-5.0 $\times 10^{-01}$	0	1
1298	H_3CS^+	+	e^-	$\Longrightarrow$	H_2CS	+	H	3.0×10^{-07}	-5.0 $\times 10^{-01}$	0	1
1299	$CH_5{}^+$	+	e^-	$\Longrightarrow$	CH_4	+	H	3.0×10^{-07}	-5.0 $\times 10^{-01}$	0	1
1300	$CH_5{}^+$	+	e^-	$\Longrightarrow$	CH_3	+	H_2	3.0×10^{-07}	-5.0 $\times 10^{-01}$	0	1
1301	C_2H5$^+$	+	e^-	$\Longrightarrow$	C_2H2	+ H_2 +	H	3.0×10^{-07}	-5.0 $\times 10^{-01}$	0	1
1302	C_2H5$^+$	+	e^-	$\Longrightarrow$	C_2H	+ H_2 +	H_2	1.5×10^{-07}	-5.0 $\times 10^{-01}$	0	1
1303	He^+	+	e^-	$\Longrightarrow$	He	+	hν	4.5×10^{-12}	-6.7 $\times 10^{-01}$	0	1
1304	C^+	+	e^-	$\Longrightarrow$	C	+	hν	4.4×10^{-12}	-6.1 $\times 10^{-01}$	0	1
1305	N^+	+	e^-	$\Longrightarrow$	N	+	hν	3.8×10^{-12}	-6.2 $\times 10^{-01}$	0	1
1306	O^+	+	e^-	$\Longrightarrow$	O	+	hν	3.4×10^{-12}	-6.3 $\times 10^{-01}$	0	1
1307	Si^+	+	e^-	$\Longrightarrow$	Si	+	hν	4.9×10^{-12}	-6.0 $\times 10^{-01}$	0	1
1308	S^+	+	e^-	$\Longrightarrow$	S	+	hν	3.9×10^{-12}	-6.3 $\times 10^{-01}$	0	1
1309	Fe^+	+	e^-	$\Longrightarrow$	Fe	+	hν	3.7×10^{-12}	-6.5 $\times 10^{-01}$	0	1
1310	Na^+	+	e^-	$\Longrightarrow$	Na	+	hν	2.7×10^{-12}	-6.9 $\times 10^{-01}$	0	1
1311	Mg^+	+	e^-	$\Longrightarrow$	Mg	+	hν	2.8×10^{-12}	-8.6 $\times 10^{-01}$	0	1
1312	H_2S^+	+	e^-	$\Longrightarrow$	H_2S	+	hν	1.1×10^{-10}	-7.0 $\times 10^{-01}$	0	1
1313	H_2CO^+	+	e^-	$\Longrightarrow$	H_2CO	+	hν	1.1×10^{-10}	-7.0 $\times 10^{-01}$	0	1
1314	$CH_3{}^+$	+	e^-	$\Longrightarrow$	CH_3	+	hν	1.1×10^{-10}	-7.0 $\times 10^{-01}$	0	1
1315	H_2CS^+	+	e^-	$\Longrightarrow$	H_2CS	+	hν	1.1×10^{-10}	-7.0 $\times 10^{-01}$	0	1
1316	H^+	+	H-	$\Longrightarrow$	H	+	H	2.3×10^{-07}	-5.0 $\times 10^{-01}$	0	1
1317	H^+	+	C-	$\Longrightarrow$	H	+	C	2.3×10^{-07}	-5.0 $\times 10^{-01}$	0	1
1318	H^+	+	S-	$\Longrightarrow$	H	+	S	2.3×10^{-07}	-5.0 $\times 10^{-01}$	0	1
1319	He^+	+	H-	$\Longrightarrow$	H	+	He	2.3×10^{-07}	-5.0 $\times 10^{-01}$	0	1
1320	He^+	+	C-	$\Longrightarrow$	He	+	C	2.3×10^{-07}	-5.0 $\times 10^{-01}$	0	1
1321	He^+	+	S-	$\Longrightarrow$	He	+	S	2.3×10^{-07}	-5.0 $\times 10^{-01}$	0	1
1322	C^+	+	H-	$\Longrightarrow$	H	+	C	2.3×10^{-07}	-5.0 $\times 10^{-01}$	0	1
1323	C^+	+	C-	$\Longrightarrow$	C	+	C	2.3×10^{-07}	-5.0 $\times 10^{-01}$	0	1
1324	C^+	+	S-	$\Longrightarrow$	C	+	S	2.3×10^{-07}	-5.0 $\times 10^{-01}$	0	1
1325	N^+	+	H-	$\Longrightarrow$	H	+	N	2.3×10^{-07}	-5.0 $\times 10^{-01}$	0	1
1326	N^+	+	C-	$\Longrightarrow$	N	+	C	2.3×10^{-07}	-5.0 $\times 10^{-01}$	0	1
1327	N^+	+	S-	$\Longrightarrow$	N	+	S	2.3×10^{-07}	-5.0 $\times 10^{-01}$	0	1
1328	O^+	+	H-	$\Longrightarrow$	H	+	O	2.3×10^{-07}	-5.0 $\times 10^{-01}$	0	1
1329	O^+	+	C-	$\Longrightarrow$	O	+	C	2.3×10^{-07}	-5.0 $\times 10^{-01}$	0	1
1330	O^+	+	S-	$\Longrightarrow$	O	+	S	2.3×10^{-07}	-5.0 $\times 10^{-01}$	0	1
1331	Si^+	+	H-	$\Longrightarrow$	Si	+	H	2.3×10^{-07}	-5.0 $\times 10^{-01}$	0	1
1332	Si^+	+	C-	$\Longrightarrow$	Si	+	C	2.3×10^{-07}	-5.0 $\times 10^{-01}$	0	1

continued on next page

continued from previous page

Nr.	Reaction	A	E_a	α	Ref.
1333	Si^+ + S- $\Longrightarrow$ Si + S	2.3×10^{-07}	-5.0×10^{-01}	0	1
1334	S^+ + H- $\Longrightarrow$ S + H	2.3×10^{-07}	-5.0×10^{-01}	0	1
1335	S^+ + C- $\Longrightarrow$ S + C	2.3×10^{-07}	-5.0×10^{-01}	0	1
1336	S^+ + S- $\Longrightarrow$ S + S	2.3×10^{-07}	-5.0×10^{-01}	0	1
1337	Fe^+ + H- $\Longrightarrow$ Fe + H	2.3×10^{-07}	-5.0×10^{-01}	0	1
1338	Fe^+ + C- $\Longrightarrow$ Fe + C	2.3×10^{-07}	-5.0×10^{-01}	0	1
1339	Fe^+ + S- $\Longrightarrow$ Fe + S	2.3×10^{-07}	-5.0×10^{-01}	0	1
1340	Na^+ + H- $\Longrightarrow$ Na + H	2.3×10^{-07}	-5.0×10^{-01}	0	1
1341	Na^+ + C- $\Longrightarrow$ Na + C	2.3×10^{-07}	-5.0×10^{-01}	0	1
1342	Na^+ + S- $\Longrightarrow$ Na + S	2.3×10^{-07}	-5.0×10^{-01}	0	1
1343	Mg^+ + H- $\Longrightarrow$ Mg + H	2.3×10^{-07}	-5.0×10^{-01}	0	1
1344	Mg^+ + C- $\Longrightarrow$ Mg + C	2.3×10^{-07}	-5.0×10^{-01}	0	1
1345	Mg^+ + S- $\Longrightarrow$ Mg + S	2.3×10^{-07}	-5.0×10^{-01}	0	1
1346	H_2^+ + H- $\Longrightarrow$ H + H_2	2.3×10^{-07}	-5.0×10^{-01}	0	1
1347	H_3^+ + H- $\Longrightarrow$ H_2 + H_2	2.3×10^{-07}	-5.0×10^{-01}	0	1
1348	HCO^+ + H- $\Longrightarrow$ CO + H_2	2.3×10^{-07}	-5.0×10^{-01}	0	1
1349	H_3O^+ + H- $\Longrightarrow$ OH + H_2 + H	2.3×10^{-07}	-5.0×10^{-01}	0	1
1350	H_3O^+ + H- $\Longrightarrow$ H_2O + H_2	2.3×10^{-07}	-5.0×10^{-01}	0	1
1351	NH_4^+ + H- $\Longrightarrow$ NH_3 + H_2	2.3×10^{-07}	-5.0×10^{-01}	0	1
1352	H + e^- $\Longrightarrow$ H^- + $h\nu$	3.0×10^{-16}	$1.0 \times 10^{+00}$	0	1
1353	C + e^- $\Longrightarrow$ C^- + $h\nu$	3.0×10^{-15}	0	0	1
1354	O + e^- $\Longrightarrow$ O^- + $h\nu$	1.5×10^{-15}	0	0	1
1355	S + e^- $\Longrightarrow$ S^- + $h\nu$	5.0×10^{-15}	0	0	1
1356	HCS^+ + O $\Longrightarrow$ HCO^+ + S	1.0×10^{-09}	0	0	3
1357	HCS^+ + O $\Longrightarrow$ OCS^+ + H	1.0×10^{-09}	0	0	3
1358	SO + C $\Longrightarrow$ CO + S	2.0×10^{-11}	5.0×10^{-01}	0	3
1359	SO + C $\Longrightarrow$ CS + O	2.0×10^{-13}	5.0×10^{-01}	0	3
1360	C^+ + H_2 $\Longrightarrow$ CH^+ + H	9.3×10^{-12}	$1.2 \times 10^{+00}$	$4.7 \times 10^{+03}$	4
1361	CH_2^+ + H $\Longrightarrow$ CH^+ + H_2	1.0×10^{-09}	0	$7.0 \times 10^{+03}$	4
1362	CH_3^+ + H $\Longrightarrow$ CH_2^+ + H_2	7.0×10^{-10}	0	$1.0 \times 10^{+04}$	4
1363	C + H_2 $\Longrightarrow$ CH + H	1.1×10^{-09}	5.0×10^{-01}	$1.4 \times 10^{+04}$	4
1364	N + H_2 $\Longrightarrow$ NH + H	8.6×10^{-10}	5.0×10^{-01}	$1.0 \times 10^{+04}$	4
1365	S + H_2 $\Longrightarrow$ HS + H	1.1×10^{-10}	4.2×10^{-02}	$1.0 \times 10^{+04}$	4
1366	CH + H $\Longrightarrow$ H_2 + C	1.1×10^{-09}	5.0×10^{-01}	$2.2 \times 10^{+03}$	4
1367	CH + H_2 $\Longrightarrow$ CH_2 + H	2.2×10^{-11}	6.7×10^{-01}	$8.8 \times 10^{+03}$	4
1368	CN + N $\Longrightarrow$ N_2 + C	7.3×10^{-10}	0	$4.5 \times 10^{+03}$	4
1369	CN + H_2 $\Longrightarrow$ HCN + H	1.7×10^{-11}	0	$3.5 \times 10^{+03}$	4
1370	CO + OH $\Longrightarrow$ H + CO_2	5.1×10^{-13}	0	$3.0 \times 10^{+02}$	4
1371	HS + C $\Longrightarrow$ CS + H	1.6×10^{-10}	5.0×10^{-01}	0	4
1372	HS + CO $\Longrightarrow$ OCS + H	3.0×10^{-11}	0	$5.3 \times 10^{+03}$	4
1373	HS + H_2 $\Longrightarrow$ H_2S + H	8.6×10^{-12}	-1.8×10^{-01}	$7.2 \times 10^{+03}$	4
1374	NH + H $\Longrightarrow$ N + H_2	8.6×10^{-10}	5.0×10^{-01}	$2.4 \times 10^{+03}$	4
1375	NH + H_2 $\Longrightarrow$ NH_2 + H	3.1×10^{-12}	7.0×10^{-01}	$6.7 \times 10^{+03}$	4
1376	NO + O $\Longrightarrow$ N + O_2	7.5×10^{-13}	$1.0 \times 10^{+00}$	$1.9 \times 10^{+03}$	4
1377	NS + C $\Longrightarrow$ CN + S	1.9×10^{-11}	5.0×10^{-01}	0	4
1378	NS + O $\Longrightarrow$ NO + S	5.0×10^{-12}	5.0×10^{-01}	0	4

continued on next page

continued from previous page

Nr.	Reaction					A	E_a	α	Ref.
1379	O_2	+ H	$\Longrightarrow$ OH	+	O	3.7×10^{-10}	0	$8.4\times10^{+00}$	4
1380	O_2	+ N	$\Longrightarrow$ NO	+	O	3.3×10^{-12}	$1.0\times10^{+00}$	$3.1\times10^{+00}$	4
1381	SO	+ H	$\Longrightarrow$ S	+	OH	2.0×10^{-10}	0	$1.0\times10^{+04}$	4
1382	SO	+ O	$\Longrightarrow$ S	+	O_2	5.0×10^{-11}	0	$2.7\times10^{+03}$	4
1383	CH_2	+ H	$\Longrightarrow$ CH	+	H_2	2.2×10^{-11}	6.7×10^{-01}	$1.2\times10^{+03}$	4
1384	CH_2	+ H_2	$\Longrightarrow$ CH_3	+	H	5.1×10^{-11}	1.6×10^{-01}	$6.4\times10^{+03}$	4
1385	CH_3	+ H	$\Longrightarrow$ CH_2	+	H_2	2.0×10^{-11}	1.6×10^{-01}	$5.6\times10^{+03}$	4
1386	CH_3	+ H_2	$\Longrightarrow$ CH_4	+	H	1.0×10^{-10}	0	$5.5\times10^{+03}$	4
1387	CH_4	+ H	$\Longrightarrow$ H_2	+	CH_3	1.0×10^{-10}	0	$5.8\times10^{+03}$	4
1388	H_2S	+ H	$\Longrightarrow$ HS	+	H_2	1.5×10^{-11}	0	$8.5\times10^{+02}$	4
1389	HCN	+ O	$\Longrightarrow$ OH	+	CN	8.7×10^{-12}	0	$4.1\times10^{+03}$	4
1390	HNO	+ H	$\Longrightarrow$ NO	+	H_2	1.5×10^{-11}	0	$1.5\times10^{+03}$	4
1391	NO	+ HCO	$\Longrightarrow$ HNO	+	CO	5.7×10^{-12}	5.0×10^{-01}	$1.0\times10^{+03}$	22
1392	NH_2	+ H	$\Longrightarrow$ NH	+	H_2	5.2×10^{-12}	7.9×10^{-01}	$2.2\times10^{+03}$	4
1393	NH_2	+ H_2	$\Longrightarrow$ NH_3	+	H	6.2×10^{-11}	1.6×10^{-01}	$6.3\times10^{+03}$	4
1394	NH_3	+ H	$\Longrightarrow$ NH_2	+	H_2	6.2×10^{-11}	1.6×10^{-01}	$5.7\times10^{+03}$	4
1395	NH_3	+ O	$\Longrightarrow$ OH	+	NH_2	2.5×10^{-12}	0	$3.0\times10^{+03}$	4
1396	NH_3	+ OH	$\Longrightarrow$ NH_2	+	H_2O	2.3×10^{-12}	0	$8.0\times10^{+02}$	4
1397	H_2CO	+ H	$\Longrightarrow$ HCO	+	H_2	2.2×10^{-11}	0	$1.8\times10^{+03}$	4
1400	SiO_2	+ O	$\Longrightarrow$ O_2	+	SiO	5.0×10^{-12}	0	$2.5\times10^{+03}$	5
1401	SiO	+ H_2O	$\Longrightarrow$ SiO_2	+	H_2	5.0×10^{-13}	0	$3.0\times10^{+03}$	5
1402	SiO	+ OH	$\Longrightarrow$ SiO_2	+	H	2.0×10^{-11}	0	$2.0\times10^{+03}$	5
1403	SiH	+ O	$\Longrightarrow$ SiO	+	H	1.0×10^{-11}	0	$2.0\times10^{+03}$	5
1405	Si	+ O_2	$\Longrightarrow$ SiO	+	O	1.0×10^{-10}	0	$2.0\times10^{+03}$	5
1406	Si	+ H_2O	$\Longrightarrow$ SiO	+	H_2	1.0×10^{-10}	0	$2.0\times10^{+03}$	5
1407	SiH	+ O_2	$\Longrightarrow$ SiO_2	+	H	1.0×10^{-11}	0	$2.0\times10^{+03}$	5
1408	SiH	+ O	$\Longrightarrow$ Si	+	OH	3.0×10^{-12}	0	$2.0\times10^{+03}$	5
1409	SiH	+ H	$\Longrightarrow$ Si	+	H_2	1.0×10^{-11}	0	$2.0\times10^{+03}$	5
1416	OH	+ OH	$\Longrightarrow$ O	+	H_2O	9.1×10^{-11}	0	$3.4\times10^{+03}$	5
1417	OH	+ O	$\Longrightarrow$ O_2	+	H	4.0×10^{-10}	0	$6.0\times10^{+02}$	4
1418	OH	+ OH	$\Longrightarrow$ O_2	+	H_2	2.8×10^{-11}	0	$1.8\times10^{+04}$	5
1420	H	+ OH	$\Longrightarrow$ O	+	H_2	3.7×10^{-10}	0	$6.6\times10^{+03}$	5
1421	OH	+ H_2	$\Longrightarrow$ H	+	H_2O	1.5×10^{-12}	$1.8\times10^{+00}$	$1.5\times10^{+03}$	5
1422	C	+ O + H	$\Longrightarrow$ CO	+	H	9.1×10^{-22}	$-3.0\times10^{+00}$	$-2.1\times10^{+03}$	6
1423	C	+ O + He	$\Longrightarrow$ CO	+	He	9.1×10^{-22}	$-3.0\times10^{+00}$	$-2.1\times10^{+03}$	6
1424	C	+ O + C	$\Longrightarrow$ CO	+	C	9.1×10^{-22}	$-3.0\times10^{+00}$	$-2.1\times10^{+03}$	6
1425	C	+ O + N	$\Longrightarrow$ CO	+	N	9.1×10^{-22}	$-3.0\times10^{+00}$	$-2.1\times10^{+03}$	6
1426	C	+ O + O	$\Longrightarrow$ CO	+	O	9.1×10^{-22}	$-3.0\times10^{+00}$	$-2.1\times10^{+03}$	6
1427	C	+ O + Fe	$\Longrightarrow$ CO	+	Fe	9.1×10^{-22}	$-3.0\times10^{+00}$	$-2.1\times10^{+03}$	6
1428	C	+ O + Mg	$\Longrightarrow$ CO	+	Mg	9.1×10^{-22}	$-3.0\times10^{+00}$	$-2.1\times10^{+03}$	6
1429	C	+ O + Si	$\Longrightarrow$ CO	+	Si	9.1×10^{-22}	$-3.0\times10^{+00}$	$-2.1\times10^{+03}$	6
1430	C	+ O + Na	$\Longrightarrow$ CO	+	Na	9.1×10^{-22}	$-3.0\times10^{+00}$	$-2.1\times10^{+03}$	6
1431	C	+ O + S	$\Longrightarrow$ CO	+	S	9.1×10^{-22}	$-3.0\times10^{+00}$	$-2.1\times10^{+03}$	6
1432	C^+	+ O + H	$\Longrightarrow$ CO^+	+	H	1.1×10^{-19}	$-3.0\times10^{+00}$	$-2.1\times10^{+03}$	6
1433	C^+	+ O + He	$\Longrightarrow$ CO^+	+	He	1.1×10^{-19}	$-3.0\times10^{+00}$	$-2.1\times10^{+03}$	6
1434	C^+	+ O + C	$\Longrightarrow$ CO^+	+	C	1.1×10^{-19}	$-3.0\times10^{+00}$	$-2.1\times10^{+03}$	6

continued on next page

continued from previous page

Nr.	Reaction	A	E_a	α	Ref.
1435	$C^+ + O + N \Longrightarrow CO^+ + N$	1.1×10^{-19}	$-3.0 \times 10^{+00}$	$-2.1 \times 10^{+03}$	6
1436	$C^+ + O + O \Longrightarrow CO^+ + O$	1.1×10^{-19}	$-3.0 \times 10^{+00}$	$-2.1 \times 10^{+03}$	6
1437	$C^+ + O + Fe \Longrightarrow CO^+ + Fe$	1.1×10^{-19}	$-3.0 \times 10^{+00}$	$-2.1 \times 10^{+03}$	6
1438	$C^+ + O + Mg \Longrightarrow CO^+ + Mg$	1.1×10^{-19}	$-3.0 \times 10^{+00}$	$-2.1 \times 10^{+03}$	6
1439	$C^+ + O + Si \Longrightarrow CO^+ + Si$	1.1×10^{-19}	$-3.0 \times 10^{+00}$	$-2.1 \times 10^{+03}$	6
1440	$C^+ + O + Na \Longrightarrow CO^+ + Na$	1.1×10^{-19}	$-3.0 \times 10^{+00}$	$-2.1 \times 10^{+03}$	6
1441	$C^+ + O + S \Longrightarrow CO^+ + S$	1.1×10^{-19}	$-3.0 \times 10^{+00}$	$-2.1 \times 10^{+03}$	6
1442	$C + O^+ + H \Longrightarrow CO^+ + H$	1.1×10^{-19}	$-3.0 \times 10^{+00}$	$-2.1 \times 10^{+03}$	6
1443	$C + O^+ + He \Longrightarrow CO^+ + He$	1.1×10^{-19}	$-3.0 \times 10^{+00}$	$-2.1 \times 10^{+03}$	6
1444	$C + O^+ + C \Longrightarrow CO^+ + C$	1.1×10^{-19}	$-3.0 \times 10^{+00}$	$-2.1 \times 10^{+03}$	6
1445	$C + O^+ + N \Longrightarrow CO^+ + N$	1.1×10^{-19}	$-3.0 \times 10^{+00}$	$-2.1 \times 10^{+03}$	6
1446	$C + O^+ + O \Longrightarrow CO^+ + O$	1.1×10^{-19}	$-3.0 \times 10^{+00}$	$-2.1 \times 10^{+03}$	6
1447	$C + O^+ + Fe \Longrightarrow CO^+ + Fe$	1.1×10^{-19}	$-3.0 \times 10^{+00}$	$-2.1 \times 10^{+03}$	6
1448	$C + O^+ + Mg \Longrightarrow CO^+ + Mg$	1.1×10^{-19}	$-3.0 \times 10^{+00}$	$-2.1 \times 10^{+03}$	6
1449	$C + O^+ + Si \Longrightarrow CO^+ + Si$	1.1×10^{-19}	$-3.0 \times 10^{+00}$	$-2.1 \times 10^{+03}$	6
1450	$C + O^+ + Na \Longrightarrow CO^+ + Na$	1.1×10^{-19}	$-3.0 \times 10^{+00}$	$-2.1 \times 10^{+03}$	6
1451	$C + O^+ + S \Longrightarrow CO^+ + S$	1.1×10^{-19}	$-3.0 \times 10^{+00}$	$-2.1 \times 10^{+03}$	6
1452	$C + O \Longrightarrow CO + h\nu$	1.8×10^{-05}	$-3.0 \times 10^{+00}$	$-2.1 \times 10^{+03}$	6
1453	$C + O^+ \Longrightarrow CO^+ + h\nu$	1.8×10^{-05}	$-3.0 \times 10^{+00}$	$-2.1 \times 10^{+03}$	6
1454	$C^+ + O \Longrightarrow CO^+ + h\nu$	1.8×10^{-05}	$-3.0 \times 10^{+00}$	$-2.1 \times 10^{+03}$	6
1455	$CO + H \Longrightarrow C + O + H$	1.5×10^{-06}	$-3.5 \times 10^{+00}$	$1.1 \times 10^{+05}$	6
1456	$CO + He \Longrightarrow C + O + He$	1.5×10^{-06}	$-3.5 \times 10^{+00}$	$1.1 \times 10^{+05}$	6
1457	$CO + C \Longrightarrow C + O + C$	1.5×10^{-06}	$-3.5 \times 10^{+00}$	$1.1 \times 10^{+05}$	6
1458	$CO + N \Longrightarrow C + O + N$	1.5×10^{-06}	$-3.5 \times 10^{+00}$	$1.1 \times 10^{+05}$	6
1459	$CO + O \Longrightarrow C + O + O$	1.5×10^{-06}	$-3.5 \times 10^{+00}$	$1.1 \times 10^{+05}$	6
1460	$CO + Mg \Longrightarrow C + O + Mg$	1.5×10^{-06}	$-3.5 \times 10^{+00}$	$1.1 \times 10^{+05}$	6
1461	$CO + Si \Longrightarrow C + O + Si$	1.5×10^{-06}	$-3.5 \times 10^{+00}$	$1.1 \times 10^{+05}$	6
1462	$CO + Fe \Longrightarrow C + O + Fe$	1.5×10^{-06}	$-3.5 \times 10^{+00}$	$1.1 \times 10^{+05}$	6
1463	$CO + Na \Longrightarrow C + O + Na$	1.5×10^{-06}	$-3.5 \times 10^{+00}$	$1.1 \times 10^{+05}$	6
1464	$CO + S \Longrightarrow C + O + S$	1.5×10^{-06}	$-3.5 \times 10^{+00}$	$1.1 \times 10^{+05}$	6
1465	$CO + H^+ \Longrightarrow C^+ + O + H$	1.4×10^{-16}	-5.0×10^{-01}	0	6
1466	$CO + He^+ \Longrightarrow C^+ + O + He$	1.4×10^{-16}	-5.0×10^{-01}	0	6
1467	$CO + C^+ \Longrightarrow C^+ + O + C$	1.4×10^{-16}	-5.0×10^{-01}	0	6
1468	$CO + N^+ \Longrightarrow C^+ + O + N$	1.4×10^{-16}	-5.0×10^{-01}	0	6
1469	$CO + O^+ \Longrightarrow C^+ + O + O$	1.4×10^{-16}	-5.0×10^{-01}	0	6
1470	$CO + Mg^+ \Longrightarrow C^+ + O + Mg$	1.4×10^{-16}	-5.0×10^{-01}	0	6
1471	$CO + Si^+ \Longrightarrow C^+ + O + Si$	1.4×10^{-16}	-5.0×10^{-01}	0	6
1472	$CO + Fe^+ \Longrightarrow C^+ + O + Fe$	1.4×10^{-16}	-5.0×10^{-01}	0	6
1473	$CO + Na^+ \Longrightarrow C^+ + O + Na$	1.4×10^{-16}	-5.0×10^{-01}	0	6
1474	$CO + S^+ \Longrightarrow C^+ + O + S$	1.4×10^{-16}	-5.0×10^{-01}	0	6
1475	$CO + H^+ \Longrightarrow CO^+ + H$	4.8×10^{-12}	5.0×10^{-01}	$4.5 \times 10^{+03}$	6
1476	$CO + He^+ \Longrightarrow CO^+ + He$	4.8×10^{-12}	5.0×10^{-01}	$4.5 \times 10^{+03}$	6
1477	$CO + N^+ \Longrightarrow CO^+ + N$	4.8×10^{-12}	5.0×10^{-01}	$4.5 \times 10^{+03}$	6
1478	$CO + O^+ \Longrightarrow CO^+ + O$	4.8×10^{-12}	5.0×10^{-01}	$4.5 \times 10^{+03}$	6
1479	$CO + C^+ \Longrightarrow CO^+ + C$	4.8×10^{-12}	5.0×10^{-01}	$4.5 \times 10^{+03}$	6
1480	$CO + Mg^+ \Longrightarrow CO^+ + Mg$	4.8×10^{-12}	5.0×10^{-01}	$4.5 \times 10^{+03}$	6

continued on next page

continued from previous page

Nr.	Reaction					A	E_a	α	Ref.
1481	CO	+ H	$\Longrightarrow$ C	+ OH		5.1×10^{-13}	0	$7.7 \times 10^{+04}$	4
1482	C^+	+ SiS	$\Longrightarrow$ CS	+ Si^+		5.0×10^{-10}	0	0	7
1483	HS	+ HS	$\Longrightarrow$ H_2S	+ S		1.5×10^{-11}	0	0	7
1484	HS	+ S	$\Longrightarrow$ S_2	+ H		1.0×10^{-12}	5.0×10^{-01}	0	3
1485	S^+	+ H_2	$\Longrightarrow$ HS^+	+ H		2.2×10^{-10}	0	$9.8 \times 10^{+03}$	8
1486	S^+	+ HS	$\Longrightarrow$ HS^+	+ S		9.7×10^{-10}	0	0	8
1487	S^+	+ H_2S	$\Longrightarrow$ H_2S^+	+ S		2.1×10^{-10}	0	0	3
1488	HS^+	+ H_2	$\Longrightarrow$ H_2S^+	+ H		1.9×10^{-10}	0	$6.3 \times 10^{+03}$	8
1489	S^+	+ H_2S	$\Longrightarrow$ $S_2{}^+$	+ H_2		2.5×10^{-10}	0	0	3
1490	CS	+ C	$\Longrightarrow$ S	+ C_2		8.3×10^{-13}	5.0×10^{-01}	$2.0 \times 10^{+04}$	3
1491	S	+ CH	$\Longrightarrow$ HS	+ C		1.0×10^{-12}	5.0×10^{-01}	$4.0 \times 10^{+03}$	3
1492	S_2	+ C	$\Longrightarrow$ S	+ CS		1.0×10^{-12}	5.0×10^{-01}	0	3
1493	S	+ $CH_2{}^+$	$\Longrightarrow$ HS^+	+ CH		5.8×10^{-10}	0	$7.8 \times 10^{+03}$	8
1494	HS	+ O	$\Longrightarrow$ S	+ OH		3.7×10^{-13}	6.7×10^{-01}	$9.5 \times 10^{+02}$	8
1495	H_2S	+ OH	$\Longrightarrow$ H_2O	+ HS		2.3×10^{-11}	0	$4.5 \times 10^{+02}$	7
1496	SO	+ O_2	$\Longrightarrow$ SO_2	+ O		7.5×10^{-13}	0	$3.2 \times 10^{+03}$	7
1497	S	+ SO_2	$\Longrightarrow$ SO	+ SO		3.0×10^{-14}	0	0	7
1498	HS	+ OH	$\Longrightarrow$ S	+ H_2O		7.2×10^{-12}	0	0	7
1499	S_2	+ O	$\Longrightarrow$ SO	+ S		1.0×10^{-12}	5.0×10^{-01}	0	3
1500	H_2S	+ O	$\Longrightarrow$ HS	+ OH		1.0×10^{-11}	0	$1.8 \times 10^{+03}$	3
1501	S^+	+ OH	$\Longrightarrow$ HS^+	+ O		2.9×10^{-10}	0	$9.4 \times 10^{+03}$	8
1502	S^+	+ O_2	$\Longrightarrow$ SO^+	+ O		1.6×10^{-11}	0	0	3
1503	SO^+	+ H_2S	$\Longrightarrow$ $S_2{}^+$	+ H_2O		1.1×10^{-09}	0	0	3
1504	CS	+ O	$\Longrightarrow$ SO	+ C		2.7×10^{-12}	5.0×10^{-01}	$2.8 \times 10^{+04}$	3
1505	OCS	+ O	$\Longrightarrow$ SO	+ CO		2.1×10^{-11}	0	$2.2 \times 10^{+03}$	3
1506	$CH_2{}^+$	+ SO	$\Longrightarrow$ H_2S^+	+ CO		1.1×10^{-09}	0	0	8
1507	CH^+	+ SO	$\Longrightarrow$ HS^+	+ CO		1.0×10^{-09}	0	0	8
1508	CH^+	+ OCS	$\Longrightarrow$ HCS^+	+ CO		1.1×10^{-09}	0	0	3
1509	$CH_2{}^+$	+ OCS	$\Longrightarrow$ HCS^+	+ HCO		1.1×10^{-09}	0	0	3
1510	H_2	+ CO	$\Longrightarrow$ H_2	+ C	+ O	6.0×10^{-09}	0	$1.2 \times 10^{+05}$	15

References			
1	[Prasad and Huntress Jr. 1980]	3	[Mitchell 1984]
4	[Mitchell and Deveau 1983]	5	[Clegg *et al.* 1983]
6	[Petuchowski *et al.* 1988]	7	[Slavsky and Scalo 1984]
8	[Pineau des Forêts *et al.* 1986]	15	[Roberge and Dalgarno 1982]

Table III.3: Chemical Network for Novae II: Explicit backward Reactions

Nr.	Reaction	Nr.	Reaction
1511	$O_2 + SiO \longrightarrow SiO_2 + O$	1512	$SiO_2 + H_2 \longrightarrow SiO + H_2O$
1513	$SiO_2 + H \longrightarrow SiO + OH$	1514	$SiO + H \longrightarrow SiH + O$
1515	$SiO + O \longrightarrow Si + O_2$	1516	$SiO + H_2 \longrightarrow Si + H_2O$
1517	$SiO + H \longrightarrow SiOH^+ + e^-$	1518	$SiO_2 + H \longrightarrow SiH + O_2$
1519	$Si + OH \longrightarrow SiH + O$	1520	$Si + H_2 \longrightarrow SiH + H$
1521	$O + H_2O \longrightarrow OH + OH$	1522	$O + H_2 \longrightarrow H + OH$
1523	$H + H_2O \longrightarrow OH + H_2$	1524	$CS + Si^+ \longrightarrow C^+ + SiS$
1525	$H_2S + S \longrightarrow HS + HS$	1526	$S_2 + H \longrightarrow HS + S$
1527	$H_2S^+ + H \longrightarrow H_2 + HS^+$	1528	$S_2{}^+ + H_2 \longrightarrow S^+ + H_2S$
1529	$S + C_2 \longrightarrow CS + C$	1530	$HS + C \longrightarrow S + CH$
1531	$CS + S \longrightarrow S_2 + C$	1532	$S + OH \longrightarrow HS + O$
1533	$HS + H_2O \longrightarrow OH + H_2S$	1534	$SO_2 + O \longrightarrow SO + O_2$
1535	$SO + SO \longrightarrow S + SO_2$	1536	$S + H_2O \longrightarrow HS + OH$
1537	$SO + S \longrightarrow S_2 + O$	1538	$HS + OH \longrightarrow H_2S + O$
1539	$SO^+ + O \longrightarrow S^+ + O_2$	1540	$S_2{}^+ + H_2O \longrightarrow SO^+ + H_2S$
1541	$SO + CO \longrightarrow OCS + O$	1542	$H_2S^+ + CO \longrightarrow CH_2{}^+ + SO$
1543	$HS^+ + CO \longrightarrow CH^+ + SO$	1544	$HCS^+ + CO \longrightarrow CH^+ + OCS$
1545	$HCO + HCS^+ \longrightarrow CH_2{}^+ + OCS$	1546	$H_2 + H \longrightarrow H + H + H$
1547	$Si^+ + H \longrightarrow H^+ + Si$	1548	$S^+ + H \longrightarrow H^+ + S$
1549	$Fe^+ + H \longrightarrow H^+ + Fe$	1550	$Na^+ + H \longrightarrow H^+ + Na$
1551	$Mg^+ + H \longrightarrow H^+ + Mg$	1552	$C_2{}^+ + H \longrightarrow H^+ + C_2$
1553	$CH^+ + H \longrightarrow H^+ + CH$	1554	$SiS^+ + H \longrightarrow H^+ + SiS$
1555	$SiO^+ + H \longrightarrow H^+ + SiO$	1556	$Si^+ + H_2 \longrightarrow H^+ + SiH$
1557	$SiH^+ + H \longrightarrow H^+ + SiH$	1558	$HS^+ + H \longrightarrow H^+ + HS$
1559	$S^+ + H_2 \longrightarrow H^+ + HS$	1560	$CS^+ + H \longrightarrow H^+ + CS$
1561	$SO^+ + H \longrightarrow H^+ + SO$	1562	$CO^+ + H_2 \longrightarrow H^+ + HCO$
1563	$HCO^+ + H \longrightarrow H^+ + HCO$	1564	$H_2S^+ + H \longrightarrow H^+ + H_2S$
1565	$HS^+ + CO \longrightarrow H^+ + OCS$	1566	$Si^+ + C \longrightarrow C^+ + Si$
1567	$S^+ + C \longrightarrow C^+ + S$	1568	$Fe^+ + C \longrightarrow C^+ + Fe$
1569	$Na^+ + C \longrightarrow C^+ + Na$	1570	$Mg^+ + C \longrightarrow C^+ + Mg$
1571	$CO^+ + O \longrightarrow C^+ + O_2$	1572	$O^+ + CO \longrightarrow C^+ + O_2$
1573	$C_2{}^+ + H \longrightarrow C^+ + CH$	1574	$CH^+ + C \longrightarrow C^+ + CH$
1575	$CO^+ + H \longrightarrow C^+ + OH$	1576	$SiS^+ + C \longrightarrow C^+ + SiS$
1577	$SiO^+ + C \longrightarrow C^+ + SiO$	1578	$Si^+ + CO \longrightarrow C^+ + SiO$
1579	$CS^+ + H \longrightarrow C^+ + HS$	1580	$CS^+ + C \longrightarrow C^+ + CS$
1581	$S^+ + CO \longrightarrow C^+ + SO$	1582	$CS^+ + O \longrightarrow C^+ + SO$
1583	$SO^+ + C \longrightarrow C^+ + SO$	1584	$CO^+ + S \longrightarrow C^+ + SO$
1585	$HCO^+ + H \longrightarrow C^+ + H_2O$	1586	$HCO^+ + C \longrightarrow C^+ + HCO$
1587	$CH^+ + CO \longrightarrow C^+ + HCO$	1588	$HCS^+ + H \longrightarrow C^+ + H_2S$
1589	$H_2S^+ + C \longrightarrow C^+ + H_2S$	1590	$CO^+ + CS \longrightarrow C^+ + OCS$
1591	$CS^+ + CO \longrightarrow C^+ + OCS$	1592	$SO^+ + CO \longrightarrow C^+ + SO_2$
1593	$Fe^+ + O \longrightarrow O^+ + Fe$	1594	$C_2{}^+ + O \longrightarrow O^+ + C_2$
1595	$CO^+ + C \longrightarrow O^+ + C_2$	1596	$CH^+ + O \longrightarrow O^+ + CH$
1597	$CO^+ + H \longrightarrow O^+ + CH$	1598	$HCO^+ + O \longrightarrow O^+ + HCO$

continued on next page

continued from previous page

Nr.	Reaction	Nr.	Reaction
1599	$H_2S^+ + O \longrightarrow O^+ + H_2S$	1600	$Fe^+ + Si \longrightarrow Si^+ + Fe$
1601	$Na^+ + Si \longrightarrow Si^+ + Na$	1602	$Mg^+ + Si \longrightarrow Si^+ + Mg$
1603	$SiO^+ + H \longrightarrow Si^+ + OH$	1604	$SiOH^+ + H \longrightarrow Si^+ + H_2O$
1605	$SiS^+ + CO \longrightarrow Si^+ + OCS$	1606	$Si^+ + S \longrightarrow S^+ + Si$
1607	$Fe^+ + S \longrightarrow S^+ + Fe$	1608	$Na^+ + S \longrightarrow S^+ + Na$
1609	$Mg^+ + S \longrightarrow S^+ + Mg$	1610	$CS^+ + C \longrightarrow S^+ + C_2$
1611	$CS^+ + H \longrightarrow S^+ + CH$	1612	$SO^+ + H \longrightarrow S^+ + OH$
1613	$SiS^+ + S \longrightarrow S^+ + SiS$	1614	$SiS^+ + H \longrightarrow S^+ + SiH$
1615	$SiH^+ + S \longrightarrow S^+ + SiH$	1616	$HS^+ + CO \longrightarrow S^+ + HCO$
1617	$HCO^+ + S \longrightarrow S^+ + HCO$	1618	$Na^+ + Fe \longrightarrow Fe^+ + Na$
1619	$Na^+ + Mg \longrightarrow Mg^+ + Na$	1620	$Si^+ + H_2 \longrightarrow SiH^+ + H$
1621	$SiO^+ + H \longrightarrow SiH^+ + O$	1622	$SiH_2{}^+ + H \longrightarrow SiH^+ + H_2$
1623	$CH_2{}^+ + Si \longrightarrow SiH^+ + CH$	1624	$C^+ + C_2 \longrightarrow C_2{}^+ + C$
1625	$CO^+ + C \longrightarrow C_2{}^+ + O$	1626	$CS^+ + C \longrightarrow C_2{}^+ + S$
1627	$S^+ + C_2 \longrightarrow C_2{}^+ + S$	1628	$CO^+ + CO \longrightarrow C_2{}^+ + O_2$
1629	$CH^+ + C_2 \longrightarrow C_2{}^+ + CH$	1630	$HCO^+ + C_2 \longrightarrow C_2{}^+ + HCO$
1631	$C_2{}^+ + H \longrightarrow CH^+ + C$	1632	$CO^+ + H \longrightarrow CH^+ + O$
1633	$Si^+ + CH \longrightarrow CH^+ + Si$	1634	$S^+ + CH \longrightarrow CH^+ + S$
1635	$HS^+ + C \longrightarrow CH^+ + S$	1636	$CS^+ + H \longrightarrow CH^+ + S$
1637	$Fe^+ + CH \longrightarrow CH^+ + Fe$	1638	$Na^+ + CH \longrightarrow CH^+ + Na$
1639	$Mg^+ + CH \longrightarrow CH^+ + Mg$	1640	$HCO^+ + O \longrightarrow CH^+ + O_2$
1641	$C_2{}^+ + H_2 \longrightarrow CH^+ + CH$	1642	$CO^+ + H_2 \longrightarrow CH^+ + OH$
1643	$HCO^+ + H_2 \longrightarrow CH^+ + H_2O$	1644	$CH_2{}^+ + CO \longrightarrow CH^+ + HCO$
1645	$HCO^+ + CH \longrightarrow CH^+ + HCO$	1646	$HCS^+ + H_2 \longrightarrow CH^+ + H_2S$
1647	$HCO^+ + H \longrightarrow CO^+ + H_2$	1648	$C_2{}^+ + CO \longrightarrow CO^+ + C_2$
1649	$CH^+ + CO \longrightarrow CO^+ + CH$	1650	$HCO^+ + C \longrightarrow CO^+ + CH$
1651	$HCO^+ + O \longrightarrow CO^+ + OH$	1652	$HCO^+ + OH \longrightarrow CO^+ + H_2O$
1653	$HCO^+ + CO \longrightarrow CO^+ + HCO$	1654	$HSiS^+ + H \longrightarrow SiS^+ + H_2$
1655	$CS^+ + H \longrightarrow HS^+ + C$	1656	$SO^+ + H \longrightarrow HS^+ + O$
1657	$Si^+ + HS \longrightarrow HS^+ + Si$	1658	$Fe^+ + HS \longrightarrow HS^+ + Fe$
1659	$Na^+ + HS \longrightarrow HS^+ + Na$	1660	$Mg^+ + HS \longrightarrow HS^+ + Mg$
1661	$H_2S^+ + HS \longrightarrow HS^+ + H_2S$	1662	$Si^+ + CO \longrightarrow SiO^+ + C$
1663	$Si^+ + SO \longrightarrow SiO^+ + S$	1664	$SiOH^+ + H \longrightarrow SiO^+ + H_2$
1665	$HCO^+ + Si \longrightarrow SiO^+ + CH$	1666	$HCO^+ + SiO \longrightarrow SiO^+ + HCO$
1667	$CO^+ + S \longrightarrow CS^+ + O$	1668	$Si^+ + CS \longrightarrow CS^+ + Si$
1669	$Fe^+ + CS \longrightarrow CS^+ + Fe$	1670	$Na^+ + CS \longrightarrow CS^+ + Na$
1671	$Mg^+ + CS \longrightarrow CS^+ + Mg$	1672	$HCS^+ + H \longrightarrow CS^+ + H_2$
1673	$Fe^+ + SO \longrightarrow SO^+ + Fe$	1674	$Na^+ + SO \longrightarrow SO^+ + Na$
1675	$Mg^+ + SO \longrightarrow SO^+ + Mg$	1676	$HCO^+ + H \longrightarrow CH_2{}^+ + O$
1677	$HCS^+ + H \longrightarrow CH_2{}^+ + S$	1678	$HCO^+ + OH \longrightarrow CH_2{}^+ + O_2$
1679	$CH^+ + CO \longrightarrow HCO^+ + C$	1680	$SiH^+ + CO \longrightarrow HCO^+ + Si$
1681	$HS^+ + CO \longrightarrow HCO^+ + S$	1682	$Fe^+ + HCO \longrightarrow HCO^+ + Fe$
1683	$Na^+ + HCO \longrightarrow HCO^+ + Na$	1684	$Mg^+ + HCO \longrightarrow HCO^+ + Mg$
1685	$CH_2{}^+ + CO \longrightarrow HCO^+ + CH$	1686	$HSiS^+ + CO \longrightarrow HCO^+ + SiS$
1687	$SiOH^+ + CO \longrightarrow HCO^+ + SiO$	1688	$SiH_2{}^+ + CO \longrightarrow HCO^+ + SiH$
1689	$H_2S^+ + CO \longrightarrow HCO^+ + HS$	1690	$HCS^+ + CO \longrightarrow HCO^+ + CS$

continued on next page

continued from previous page

Nr.	Reaction	Nr.	Reaction
1691	$SiOH^+ + H \longrightarrow SiH_2^+ + O$	1692	$HSiS^+ + H \longrightarrow SiH_2^+ + S$
1693	$HCS^+ + H \longrightarrow H_2S^+ + C$	1694	$HS^+ + OH \longrightarrow H_2S^+ + O$
1695	$SO^+ + H_2 \longrightarrow H_2S^+ + O$	1696	$Si^+ + H_2S \longrightarrow H_2S^+ + Si$
1697	$Fe^+ + H_2S \longrightarrow H_2S^+ + Fe$	1698	$Na^+ + H_2S \longrightarrow H_2S^+ + Na$
1699	$Mg^+ + H_2S \longrightarrow H_2S^+ + Mg$	1700	$HCO^+ + H_2S \longrightarrow H_2S^+ + HCO$
1701	$H_2 + e^- \longrightarrow H^- + H$	1702	$CH + e^- \longrightarrow H^- + C$
1703	$OH + e^- \longrightarrow H^- + O$	1704	$H_2O + e^- \longrightarrow H^- + OH$
1705	$HCO + e^- \longrightarrow H^- + CO$	1706	$HCO^+ + e^- \longrightarrow O + CH$
1707	$CO + O \longrightarrow C + O_2$	1708	$CO + H \longrightarrow O + CH$
1709	$CO + C \longrightarrow C_2 + O$	1710	$CS + H \longrightarrow CH + S$
1711	$SiO + H \longrightarrow OH + Si$	1712	$SO + H \longrightarrow HS + O$
1713	$CO + S \longrightarrow CS + O$	1714	$SO_2 + H \longrightarrow SO + OH$
1715	$H_2 + CO \longrightarrow HCO + H$	1716	$OH + CO \longrightarrow HCO + O$
1717	$Si + H \longrightarrow SiH^+ + e^-$	1718	$C + C \longrightarrow C_2^+ + e^-$
1719	$C + H \longrightarrow CH^+ + e^-$	1720	$O + C \longrightarrow CO^+ + e^-$
1721	$Si + S \longrightarrow SiS^+ + e^-$	1722	$S + H \longrightarrow HS^+ + e^-$
1723	$Si + O \longrightarrow SiO^+ + e^-$	1724	$C + S \longrightarrow CS^+ + e^-$
1725	$S + O \longrightarrow SO^+ + e^-$	1726	$C + H_2 \longrightarrow CH_2^+ + e^-$
1727	$CH + H \longrightarrow CH_2^+ + e^-$	1728	$CO + H \longrightarrow HCO^+ + e^-$
1729	$Si + OH \longrightarrow SiOH^+ + e^-$	1730	$SiH + H \longrightarrow SiH_2^+ + e^-$
1731	$HS + H \longrightarrow H_2S^+ + e^-$	1732	$CS + H \longrightarrow HCS^+ + e^-$
1733	$SiS + H \longrightarrow HSiS^+ + e^-$	1734	$Si + HS \longrightarrow HSiS^+ + e^-$
1735	$H + H \longrightarrow H^+ + H\text{-}$	1736	$H + C \longrightarrow C^+ + H\text{-}$
1737	$H + O \longrightarrow O^+ + H\text{-}$	1738	$Si + H \longrightarrow Si^+ + H\text{-}$
1739	$S + H \longrightarrow S^+ + H\text{-}$	1740	$Fe + H \longrightarrow Fe^+ + H\text{-}$
1741	$Na + H \longrightarrow Na^+ + H\text{-}$	1742	$Mg + H \longrightarrow Mg^+ + H\text{-}$
1743	$CO + H_2 \longrightarrow HCO^+ + H\text{-}$	1744	$HCO^+ + S \longrightarrow HCS^+ + O$
1745	$OCS^+ + H \longrightarrow HCS^+ + O$	1746	$CO + S \longrightarrow SO + C$
1747	$HS + H \longrightarrow S + H_2$	1748	$CS + H \longrightarrow HS + C$
1749	$OCS + H \longrightarrow HS + CO$	1750	$SiO^+ \longrightarrow Si^+ + O$
1751	$H_2O \longrightarrow H_2 + O$	1752	$O_2 + H \longrightarrow OH + O$
1753	$CO^+ + H \longrightarrow C^+ + O + H$	1754	$CO^+ + C \longrightarrow C^+ + O + C$
1755	$CO^+ + O \longrightarrow C^+ + O + O$	1756	$CO^+ + Fe \longrightarrow C^+ + O + Fe$
1757	$CO^+ + Mg \longrightarrow C^+ + O + Mg$	1758	$CO^+ + Si \longrightarrow C^+ + O + Si$
1759	$CO^+ + Na \longrightarrow C^+ + O + Na$	1760	$CO^+ + S \longrightarrow C^+ + O + S$
1761	$CO^+ + H \longrightarrow C + O^+ + H$	1762	$CO^+ + C \longrightarrow C + O^+ + C$
1763	$CO^+ + O \longrightarrow C + O^+ + O$	1764	$CO^+ + Fe \longrightarrow C + O^+ + Fe$
1765	$CO^+ + Mg \longrightarrow C + O^+ + Mg$	1766	$CO^+ + Si \longrightarrow C + O^+ + Si$
1767	$CO^+ + Na \longrightarrow C + O^+ + Na$	1768	$CO^+ + S \longrightarrow C + O^+ + S$

Table III.4: Chemical Network for Novae III: Photo–Reactions

Nr.	Reaction	Nr.	Reaction
1769	$H + h\nu \longrightarrow H^+ + e^-$	1770	$He + h\nu \longrightarrow He^+ + e^-$
1771	$O + h\nu \longrightarrow O^+ + e^-$	1772	$N + h\nu \longrightarrow N^+ + e^-$
1773	$C + h\nu \longrightarrow C^+ + e^-$	1774	$Si + h\nu \longrightarrow Si^+ + e^-$
1775	$S + h\nu \longrightarrow S^+ + e^-$	1776	$Fe + h\nu \longrightarrow Fe^+ + e^-$
1777	$Na + h\nu \longrightarrow Na^+ + e^-$	1778	$Mg + h\nu \longrightarrow Mg^+ + e^-$
1779	$C_2 + h\nu \longrightarrow C_2{}^+ + e^-$	1780	$O_2 + h\nu \longrightarrow O_2{}^+ + e^-$
1781	$CH + h\nu \longrightarrow CH^+ + e^-$	1782	$NH + h\nu \longrightarrow NH^+ + e^-$
1783	$OH + h\nu \longrightarrow OH^+ + e^-$	1784	$NO + h\nu \longrightarrow NO^+ + e^-$
1785	$CH_2 + h\nu \longrightarrow CH_2{}^+ + e^-$	1786	$H_2O + h\nu \longrightarrow H_2O^+ + e^-$
1787	$H^- + h\nu \longrightarrow H + e^-$	1788	$C^- + h\nu \longrightarrow C + e^-$
1789	$O^- + h\nu \longrightarrow O + e^-$	1790	$S^- + h\nu \longrightarrow S + e^-$
1791	$OH^- + h\nu \longrightarrow OH + e^-$	1792	$C_2H + h\nu \longrightarrow C_2H^+ + e^-$
1793	$CH_3 + h\nu \longrightarrow CH_3{}^+ + e^-$	1794	$H_2CO + h\nu \longrightarrow H_2CO^+ + e^-$
1795	$CN^- + h\nu \longrightarrow CN + e^-$	1796	$C_2 + h\nu \longrightarrow C + C$
1797	$O_2 + h\nu \longrightarrow O + O$	1798	$CH + h\nu \longrightarrow C + H$
1799	$NH + h\nu \longrightarrow H + N$	1800	$OH + h\nu \longrightarrow O + H$
1801	$CO + h\nu \longrightarrow C + O$	1802	$CN + h\nu \longrightarrow C + N$
1803	$NO + h\nu \longrightarrow N + O$	1804	$SiC + h\nu \longrightarrow Si + C$
1805	$SiS + h\nu \longrightarrow Si + S$	1806	$SiO + h\nu \longrightarrow Si + O$
1807	$SiH + h\nu \longrightarrow Si + H$	1808	$HS + h\nu \longrightarrow H + S$
1809	$CS + h\nu \longrightarrow C + S$	1810	$NS + h\nu \longrightarrow N + S$
1811	$SO + h\nu \longrightarrow O + S$	1812	$CH_2 + h\nu \longrightarrow CH + H$
1813	$NH_2 + h\nu \longrightarrow NH + H$	1814	$H_2O + h\nu \longrightarrow OH + H$
1815	$HCN + h\nu \longrightarrow CN + H$	1816	$HCO + h\nu \longrightarrow H + CO$
1817	$C_2H + h\nu \longrightarrow C_2 + H$	1818	$OCN + h\nu \longrightarrow O + CN$
1819	$H_2S + h\nu \longrightarrow HS + H$	1820	$OCS + h\nu \longrightarrow CO + S$
1821	$SO_2 + h\nu \longrightarrow SO + O$	1822	$H_2CO + h\nu \longrightarrow CO + H_2$
1823	$H_2CO + h\nu \longrightarrow CO + H + H$	1824	$H_2CO + h\nu \longrightarrow HCO^+ + H + e^-$
1825	$NH_3 + h\nu \longrightarrow NH_2 + H$	1826	$NH_3 + h\nu \longrightarrow NH + H_2$
1827	$CH_3 + h\nu \longrightarrow CH + H_2$	1828	$CH_3 + h\nu \longrightarrow CH_2 + H$
1829	$CH_4 + h\nu \longrightarrow CH_3 + H$	1830	$CH_4 + h\nu \longrightarrow CH_2 + H_2$
1831	$CH_4 + h\nu \longrightarrow CH + H + H_2$	1832	$H_2CS + h\nu \longrightarrow CS + H_2$
1833	$H_2{}^+ + h\nu \longrightarrow H^+ + H$	1834	$C_2{}^+ + h\nu \longrightarrow C^+ + C$
1835	$CH^+ + h\nu \longrightarrow C^+ + H$	1836	$OH^+ + h\nu \longrightarrow H^+ + O$
1837	$H_3{}^+ + h\nu \longrightarrow H_2{}^+ + H$	1838	$H_3{}^+ + h\nu \longrightarrow H^+ + H_2$
1839	$CH_2{}^+ + h\nu \longrightarrow CH^+ + H$	1840	$C_2H^+ + h\nu \longrightarrow C_2{}^+ + H$
1841	$CH_3{}^+ + h\nu \longrightarrow CH_2{}^+ + H$	1842	$CH_3{}^+ + h\nu \longrightarrow CH^+ + H_2$
1843	$SiH^+ + h\nu \longrightarrow Si^+ + H$	1844	$SiH_2{}^+ + h\nu \longrightarrow Si^+ + H_2$
1845	$SiO_2 + h\nu \longrightarrow SiO + O$	1846	$C_2H2 + h\nu \longrightarrow C_2H + H$
1847	$H_2 + h\nu \longrightarrow H + H$		

Table III.5: Chemical Network for Novae IV: Hydrogen–Reactions

Nr.	Reaction	Nr.	Reaction
1848	$H^{(1)} + h\nu \longrightarrow H^{+} + e^{-}$	1849	$H^{(2)} + h\nu \longrightarrow H^{+} + e^{-}$
1850	$H^{(3)} + h\nu \longrightarrow H^{+} + e^{-}$	1851	$H^{(1)} + e^{-} \longrightarrow H^{+} + e^{-} + e^{-}$
1852	$H^{(2)} + e^{-} \longrightarrow H^{+} + e^{-} + e^{-}$	1853	$H^{(3)} + e^{-} \longrightarrow H^{+} + e^{-} + e^{-}$
1854	$H^{+} + e^{-} \longrightarrow H^{(1)} + h\nu$	1855	$H^{+} + e^{-} \longrightarrow H^{(2)} + h\nu$
1856	$H^{+} + e^{-} \longrightarrow H^{(3)} + h\nu$	1857	$H^{(1)} \longrightarrow H^{(2)} + h\nu$
1858	$H^{(1)} \longrightarrow H^{(3)} + h\nu$	1859	$H^{(2)} \longrightarrow H^{(3)} + h\nu$
1860	$H^{(2)} + h\nu \longrightarrow H^{(1)} + h\nu$	1861	$H^{(3)} + h\nu \longrightarrow H^{(1)} + h\nu$
1862	$H^{(3)} + h\nu \longrightarrow H^{(2)} + h\nu$	1863	$H^{(1)} + e^{-} \longrightarrow H^{(2)} + e^{-}$
1864	$H^{(2)} + e^{-} \longrightarrow H^{(1)} + e^{-}$	1865	$H^{(1)} + e^{-} \longrightarrow H^{(3)} + e^{-}$
1866	$H^{(3)} + e^{-} \longrightarrow H^{(1)} + e^{-}$	1867	$H^{(2)} + e^{-} \longrightarrow H^{(3)} + e^{-}$
1868	$H^{(3)} + e^{-} \longrightarrow H^{(2)} + e^{-}$	1869	$H^{(2)} \longrightarrow H^{(1)} + h\nu$
1870	$H^{(3)} \longrightarrow H^{(1)} + h\nu$	1871	$H^{(3)} \longrightarrow H^{(2)} + h\nu$

III.3 Enthalpy and Entropy Data

Table III.6: Thermodynamic Data for Various Species

specie	$\Delta S \left[\frac{cal}{mol}\right]$	$\Delta H \left[\frac{kcal}{mol}\right]$	specie	$\Delta S \left[\frac{cal}{mol}\right]$	$\Delta H \left[\frac{kcal}{mol}\right]$
C	44.278	171.931	C^+	43.471	437.098
C^-	42.667	137.260	CH	53.173	141.695
CH^+	50.413	388.455	HCN	61.787	31.800
HCN^+	61.783	350.881	HCO	66.466	9.254
HCO^+	62.192	202.424	HCS^+	65.000	232.000
CH_2	58.673	91.161	CH_2^+	58.676	336.400
H_2CO	67.316	-30.012	CH_3	61.484	32.699
$CH_3{}^+$	61.472	265.075	CH_4	60.844	-21.690
$CH_4{}^+$	60.851	272.256	CN	58.062	96.000
CN^+	61.135	434.917	CN^-	56.377	10.168
OCN	70.716	38.356	CO	56.818	-26.909
CO^+	56.812	301.717	OCS	71.057	-48.385
OCS^+	71.056	214.800	CO_2	65.614	-94.369
$CO_2{}^+$	65.607	228.702	CS	60.589	51.287
CS^+	60.588	318.100	SiC	64.262	172.109
C_2	59.387	200.610	$C_2{}^+$	59.393	485.300
C_2H	63.447	113.299	C_2H_2	65.916	47.670
$C_2H_2{}^+$	65.918	316.019	C_2N^+	71.989	416.144
$C_3{}^+$	69.240	478.350	e^-	11.500	0.000
Fe	50.709	96.705	Fe^+	51.546	284.072
H	33.903	53.252	H^+	32.524	372.304
H^-	32.528	30.395	NH	52.609	89.963
NH^+	52.605	406.507	HNO	65.577	23.061
HNO^+	65.583	261.432	OH	53.222	9.093
OH^+	53.013	318.606	OH^-	50.430	-38.581
O_2H^+	67.663	266.818	HS	56.688	27.180
HS^+	56.692	271.800	SiH	57.149	88.638
SiH^+	54.284	276.795	H_2	40.419	0.000
$H_2{}^+$	43.710	361.611	NH_2	58.163	44.230
$NH_2{}^+$	58.174	306.583	H_2O	56.580	-59.383
H_2S	61.427	-21.578	H_2S^+	61.424	225.000
$SiH_2{}^+$	60.342	218.000	NH_3	60.225	-13.253
$NH_3{}^+$	60.229	226.501	H_3O^+	59.761	140.180
HE	36.637	0.000	HE^+	38.014	572.464
Mg	42.013	31.421	Mg^+	43.391	213.212
N	43.125	113.999	N^+	44.732	454.874

continued on next page

continued from previous page

specie	ΔS $\left[\frac{cal}{mol}\right]$	ΔH $\left[\frac{kcal}{mol}\right]$	specie	ΔS $\left[\frac{cal}{mol}\right]$	ΔH $\left[\frac{kcal}{mol}\right]$
NO	60.181	21.620	NO^+	56.859	240.466
$NO_2{}^+$	71.439	237.974	NS	63.659	47.833
NS^+	63.671	257.841	N_2	55.285	0.000
$N_2{}^+$	56.804	364.817	Na	43.213	23.335
Na^+	41.847	147.309	O	45.120	60.473
O^+	43.522	379.783	O^-	44.316	21.266
SO	63.482	-14.203	SO^+	63.480	229.300
SiO	60.882	-25.349	SiO^+	60.875	243.700
$SiOH^+$	81.200	185.000	O_2	59.016	0.000
$O_2{}^+$	59.024	283.666	SO_2	74.330	-86.481
SiO_2	71.061	-73.608	S	47.128	51.651
S^+	45.593	295.634	S^-	46.326	-1.809
S_2	65.577	0.000	$S_2{}^+$	65.583	250.000
SiS	64.481	8.676	SiS^+	64.480	218.000
$HSiS^+$	81.200	285.000	Si	46.801	106.932
Si^+	45.971	300.450			

Bibliography

[Aldrovandi and Péquinot 1973] S.M.V. Aldrovandi and D. Péquinot, 1973. Radiative and Dielectronic Recombination Coefficients for Complex Ions. *Astron. & Astrophys.*, **25**, 137.

[Alksne and Platais 1975] Z. Alksne and I. Platais, 1975. Nova Cygni 1975. IAU Circ. 2839.

[Allen 1954] C.W. Allen, 1954. . *Mon. Not. R. Astron. Soc.*, **114**, 387.

[Aller 1984] L.H. Aller, 1984. *Physics of thermal Gaseous Nebulae.* Reidel Publishing Company, Dordrecht.

[Anders *et al.* 1989] E. Anders, R.S. Lewis, T. Ming, and E. Zinner, 1989. Interstellar Grains in Meteorites: Diamond and Silicon Carbide. In *Interstellar Dust*, page 389.

[Andreä *et al.* 1991] J. Andreä, H. Drechsel, M.A.J. Snijders, and A. Cassatella, 1991. The Nebular Stage of Nova PW Vulpeculae. *Astron. & Astrophys.*, **244**, 111–119.

[Anicich and Huntress Jr. 1986] V.G. Anicich and W.T. Huntress Jr., 1986. A Survey of Bimolecular Ion–Molecule Reactions for Use in Modelling the Chemistry of Planetary Atmospheres, Cometary Comae and Interstellar Clouds. *Astrophys. J. Suppl. Ser.*, **62**, 553–672.

[Anicich *et al.* 1984] V.G. Anicich, G.A. Blake, J.K. Kim, M.J. McEwan, and W.T. Huntress Jr., 1984. . *J. Phys. Chem.*, **88**, 4608.

[Augustin 1990] K. Augustin, 1990. Einfluš von Ladungsprozessen auf das Staubwachstum in zirkumstellaren Hüllen. Master's thesis, TU Berlin, Berlin, Germany.

[Balm and Kroto 1991] S.P. Balm and H.W. Kroto, 1991. Possible Assignment of the $11.3\mu m$ UIR Feature To Emission From Soot-Like Microparticles With Internal Hydrogen. In *Chemistry in Space*, pages 439–440, Kluwer Academics Publisher, Dordrecht, Netherlands.

[Band *et al.* 1990] I.M. Band, M.B. Trzhaskovskaya, D.A. Verner, and D.G. Yakovlev, 1990. K-shell Photoionization Cross Sections: calculations and simple Fitting formulae. *Astron. & Astrophys.*, **237**, 267.

[Basri *et al.* 1981] G.S. Basri, J.L. Linsky, and K. Erikson, 1981. Outer Atmospheres of Cool Stars VIII. IUE Observations And Chromospheric Models for Supergiant Stars β Draconis, ϵ Geminorum and α Orionis. *Astrophys. J.*, **251**, 162.

[Bates 1986] D.R. Bates, 1986. Products of Dissociative Recombination of polyatomic Ions. *Astrophys. J. (Letters)*, **306**, L45.

[Bates and Dalgarno 1962] D.R. Bates and A. Dalgarno, 1962. *Atomic and Molecular Processes*, volume 13 of *Pure and applied Physics*, chapter Electronic Recombination, page 245. Academic Press, New York, London.

[Bates and Herbst 1988] D.R. Bates and E. Herbst, 1988. Radiative Association. In *Rate Coefficients in Astrochemistry*, pages 17–40, Kluwer Academics Publisher, Dordrecht, Netherlands.

[Bath 1976] G.T. Bath, 1976. Theory of Dwarf Novae. In P. Eggleton, S. Mitton, and J. Whelan, editors, *Structure and Evolution of Close Binary Systems*, page 173. D. Reidel.

[Bath 1978a] G.T. Bath, 1978. Optically thick Winds in Classical Novae. *Mon. Not. R. Astron. Soc.*, **182**, 35.

[Bath 1978b] G.T. Bath, 1978. The Explosions of Novae. *Q. Jl. R. astr. Soc.*, **19**, 442–455.

[Bath and Shaviv 1976] G.T. Bath and G. Shaviv, 1976. Classical Novae - a Steady State Constant Luminosity, Continous Ejection Model. *Mon. Not. R. Astron. Soc.*, **175**, 305.

[Beck and Dominik 1992] H. Beck and C. Dominik, 1992. Formation of Silicon/silicon-carbide Mixed Dust under Non-equilibrium Conditions in the Circumstellar Shells of C-stars. *Abstract Ser. Astron. Ges.*, **7**, 104.

[Beck *et al.* 1990a] H. Beck, H.-P. Gail, H. Gass, M. Köhler, and E. Sedlmayr, 1990. The Effects of Non–LTE Occupation in the Hydrogen Atom for Dust Formation in Nova Shells. *Abstract Ser. Astron. Soc. Germany*, **5**, 73.

[Beck *et al.* 1990b] H. Beck, H.-P. Gail, H. Gass, and E. Sedlmayr, 1990. Ionization and Temperature Structure in Nova Shells. *Astron. & Astrophys.*, **238**, 283–295.

[Beck *et al.* 1992] H. Beck, H.-P. Gail, R. Henkel, and E. Sedlmayr, 1992. Chemistry in Circumstellar Shells. I: Chromospheric Radiation Fields and Dust Formation in the Optically thin Shells of M–giants. *Astron. & Astrophys.*, **265**, 626.

[Beck *et al.* 1993] H. Beck, H.P. Gail, and E. Sedlmayr, 1993. Chemistry in Nova Shells. Astronomy and Astrophysics, in preparation.

[Bernat *et al.* 1979] A.P. Bernat, D.N.B. Hall, K.H. Hinkle, and S.T. Ridgway, 1979. Observations of CO Circumstellar Absorption in The 4.6μ Spectrum of Alpha Orionis. *Astrophys. J. (Letters)*, **233**, L135.

[Bianchini 1980] A. Bianchini, 1980. Photometric and Spectroscopic Observations of the old Nova T Aur. *Mon. Not. R. Astron. Soc.*, **192**, 127.

[Bloemhof *et al.* 1985] E.E. Bloemhof, W.C. Danchi, and C.H. Townes, 1985. Rapid Variation in the Circumstellar $10\,\mu$ emission of α Orionis. *Astrophys. J. (Letters)*, **299**, L37.

[Bode and Evans 1981] M.F. Bode and A. Evans, 1981. Transition and the Infrared Development of Novae. *Mon. Not. R. Astron. Soc.*, **197**, 1055.

[Bode and Evans 1983a] M.F. Bode and A. Evans, 1983. Dust in Nova Systems - Thoughts in Transition. *Q. Jl. R. astr. Soc.*, **24**, 83–105.

[Bode and Evans 1983b] M.F. Bode and A. Evans, 1983. Time Dependence of the Infrared Spectra of Nova Dust Shells. *Mon. Not. R. Astron. Soc.*, **203**, 285.

[Bode *et al.* 1984] M.F. Bode, A. Evans, D.C.B. Whittet, D.K. Aitken, P.F. Roche, and B. Whitmore, 1984. Infrared Photometry and Spectroscopy of Nova Aquilae 1982. *Mon. Not. R. Astron. Soc.*, **207**, 897.

[Bohme 1992] D.K. Bohme, 1992. *Advances in Gas Phase Chemistry*, volume 1, chapter Chemistry Initiated by Atomic Silicon Ions, pages 225–270. JAI Press Inc.

[Bohme *et al.* 1988] D.K. Bohme, S. Wlodek, and A. Fox, 1988. Chemical Pathways from Atomic Silicon to Silicon Carbides and Oxides . In *Rate Coefficients in Astrochemistry*, pages 193–200, Kluwer Academics Publisher, Dordrecht, Netherlands.

[Bosma 1972] P.B. Bosma, 1972. The State of Ionization in Nova Shells I. the Ionization Equation for Hydrogen Shells. *Astron. & Astrophys.*, **21**, 223.

[Bosma 1975a] P.B. Bosma, 1975. The State of Ionization in Nova Shells II. the Interpretation of the Ionization Equation for Optically thick Shells. *Astron. & Astrophys.*, **40**, 175.

[Bosma 1975b] P.B. Bosma, 1975. The State of Ionization in Nova Shells. III. A new Explanation for the Light Curve of Nova Herculis 1934. *Astron. & Astrophys.*, **40**, 185.

[Boyarchuk and Antipova 1990] A.A. Boyarchuk and L.I. Antipova, 1990. Chemistry of Nova Envelopes. In A. Cassatella and R. Viotti, editors, *Physics of Classical Novae*, pages 97–114, Springer Verlag, Heidelberg.

[Brown 1971] R.L. Brown, 1971. On the Photoionization of Hydrogen and Helium. *Astrophys. J.*, **164**, 387.

[Brown and Carpenter 1984] A. Brown and K.G. Carpenter, 1984. The Temperature of CII Emission–Line Formation Regions in Cool Stars'. *Astrophys. J. (Letters)*, **287**, L43.

[Brownlee and Kissel 1990] D.E. Brownlee and J. Kissel, 1990. *Comet Halley: Investigations, Results, Interpretations Volume 2: Dust, Nucleus, Evolution*, chapter The Composition of Dust Particles in the Environment of Comet Halley, page 89. Library of Space Science and Space Technology. Ellis Horwood, New York.

[Buscombe and De Vaucouleurs 1955] W. Buscombe and G. De Vaucouleurs, 1955. . *Observatory*, **75**, 170.

[Cameron 1982] A.G.W. Cameron, 1982. . In C.A. Barnes, D.D. Clayton, and D.N. Schramm, editors, *Essays in Nuclear Astrophysics*, page 23, Cambridge University Press, Cambridge.

[Cameron and Iben Jr. 1986] A.G.W. Cameron and I. Iben Jr., 1986. On the Behaviour of Double Degenerate Binaries associated with Type I Supernovae. *Astrophys. J.*, **305**, 228.

[Cardelli and Savage 1988] J.A. Cardelli and B.D. Savage, 1988. Two Lines of Sight with Exceedingly Anomalous Interstellar Extinction. *Astrophys. J.*, **325**, 864.

[Carpenter 1984] K.G. Carpenter, 1984. *Astrophys. J.*, **285**, 181.

[Carpenter *et al.* 1985] K.G. Carpenter, A. Brown, and R.E. Stencel, 1985. In M. Morris and B. Zuckerman, editors, *Mass Loss from Red Giants*, page 55, D. Reidel, Dordrecht.

[Castor 1970] J.I. Castor, 1970. Spectral Line Formation in Wolf-Rayet Envelopes. *Mon. Not. R. Astron. Soc.*, **149**, 111–127.

[Cernicharo and Guélin 1987] J. Cernicharo and M. Guélin, 1987. Metals in IRC +10216: Detection of NaCl, AlCl and KCl, and Tentative Detection of AlF. *Astron. & Astrophys.*, **183**, L10.

[Cernicharo *et al.* 1987] J. Cernicharo, M. Guélin, H. Hein, and C. Kahane, 1987. Sulfur in IRC+10216. *Astron. & Astrophys.*, **181**, L9.

[Chapman and Henry 1971] R.D. Chapman and R.J.W. Henry, 1971. Photoionization Cross Sections of atoms and Ions of Sulfur. *Astrophys. J.*, **168**, 169.

[Chapman and Henry 1972] R.D. Chapman and R.J.W. Henry, 1972. Photoionization Cross Sections for atoms and Ions of aluminium , Silicon and argon. *Astrophys. J.*, **173**, 242.

[Chase *et al.* 1985] M.W. Chase, C.A. Davies, J.R. Downey, D.J. Frurip, R.A. McDonald, and A.N. Syverup, 1985. *JANAF Thermochemical Tables*, 14$^{\mathrm{th}}$ edition.

[Cherchneff *et al.* 1992] I. Cherchneff, J.R. Barker, and A.G.G.M. Tielens, 1992. Polycyclic Aromatic Hydrocarbon Formation in Carbon Rich Stellar Envelopes. APJ, in press.

[Chincarini and Walker 1981] G. Chincarini and M.F. Walker, 1981. Image Tube Spectroscopic Studies of Rapid Variables. *Astron. & Astrophys.*, **104**, 24.

[Clayton and Wickramasinghe 1976] D.D. Clayton and W.C. Wickramasinghe, 1976. On the Development of Infrared Radiation from an Expanding Nova Shell. *Astrophys. Space Sci.*, **42**, 463.

[Clegg *et al.* 1983] R.E.S. Clegg, L.A. Allamandola, and L.J. van IJzendoorn, 1983. Circumstellar Silicon Chemistry and the *SiO* Maser. *Mon. Not. R. Astron. Soc.*, **203**, 125.

[Code and Meade 1979] A.D. Code and M.R. Meade, 1979. Ultraviolett Photometry from the orbiting Astronomical Observatory. XXXII. An Atlas of Ultraviolett Stellar Spectra. *Astrophys. J. Suppl. Ser.*, **39**, 195.

[Cohen 1985] J.G. Cohen, 1985. Nova Shells II: Calibration of the Distance Scale using Novae. *Astrophys. J.*, **292**, 90.

[Cohen and Rosenthal 1983] J.G. Cohen and J. Rosenthal, 1983. Nova Shells. *Astrophys. J.*, **268**, 689.

[Cuntz 1990] M. Cuntz, 1990. Chromospheric Extents Predicted by Time Depndent Acoustic Wave Models. *Astrophys. J.*, **349**, 141–149.

[De Vaucouleurs 1978] G. De Vaucouleurs, 1978. The Extragalactic Distance Scale. I. A Review of Distance Indicators: Zero Point Errors of Primary Indicators. *Astrophys. J.*, **223**, 351.

[deJong *et al.* 1975] T. deJong, S.I. Chu, and A. Dalgarno, 1975. Carbon Monoxide in Collapsing Interstellar Clouds. *Astrophys. J.*, **199**, 69.

[DellaValle and Claudi 1990] M. DellaValle and R. Claudi, 1990. The Galactic Nova Rate. In A. Cassatella and R. Viotti, editors, *Physics of Classical Novae*, pages 53–54, Springer Verlag, Heidelberg.

[Dheandhanoo *et al.* 1986] S. Dheandhanoo, L. Forte, A. Fox, and D.K. Bohme, 1986. . *Canadian J. Chem.*, **64**, 641.

[d'Hendecourt and Jourdain de Muizon 1989] L.B. d'Hendecourt and M. Jourdain de Muizon, 1989. The Discovery of Interstellar Carbon Dioxide. *Astron. & Astrophys.*, **223**, L5.

[Diaz and Steiner 1989] M.P. Diaz and J.E. Steiner, 1989. The Photometric Period of Nova Muscae 1983. *Astrophys. J. (Letters)*, **339**, L41.

[Ditchburn and Öpik 1962] R.W. Ditchburn and U. Öpik, 1962. *Atomic and Molecular Processes*, volume 13 of *Pure and applied Physics*, chapter Photoionization Processes, page 79. Academic Press, New York, London.

[Dominik 1992] C. Dominik, 1992. *Formation of Dust Grains in the Winds of Cool Giants.* PhD thesis, TU Berlin.

[Donn *et al.* 1989] B.D. Donn, J.E. Allen, and R.K. Khanna, 1989. A critical assessment to the pah hypothesis. In *Interstellar Dust*, page 181, Kluwer Academics Publisher, Dordrecht.

[Downes 1986] R.A. Downes, 1986. The Space Density of Classical Novae. *Astrophys. J.*, **307**, 170.

[Draine 1979] B.T. Draine, 1979. Time Dependent Nucleation Theory and the Formation of Interstellar Grains. *Astrophys. Space Sci.*, **65**, 313.

[Draine 1989] B.T. Draine, 1989. Interpretation of the 2175ÅFeature. In *Interstellar Dust*, page 313.

[Drawin 1971] H.W. Drawin, 1971. *Reactions under Plasma Conditions*, volume 1, chapter Thermodynamic Properties of the Equilibrium and Nonequilibrium States of Plasmas, page 53. Wiley, New York.

[Duerbeck 1987] H.W. Duerbeck, 1987. A Reference Catalogue and Atlas of Galactic Novae. *Space Sci. Rev.*, **46**(1), 1.

[Duerbeck 1990] H.W. Duerbeck, 1990. Galactic Distribution and Frequency of Classsical Novae. In A. Cassatella and R. Viotti, editors, *Physics of Classical Novae*, pages 34–41, Springer Verlag, Heidelberg.

[Duley and Williams 1981] W.W. Duley and D.A. Williams, 1981. The Infrared Spectrum Interstellar Dust: Surface Functional Groups on Carbon. *Mon. Not. R. Astron. Soc.*, **196**, 196.

[Duley and Williams 1983] W.W. Duley and D.A. Williams, 1983. A $3.4\mu m$ absorption band in amorphous carbon. *Mon. Not. R. Astron. Soc.*, **205**, 67P.

[Duley and Williams 1984] W.W. Duley and D.A. Williams, 1984. *Interstellar Chemistry.* Academic Press, London.

[Duley and Williams 1986] W.W. Duley and D.A. Williams, 1986. PAH Molecules and Carbon Dust in Interstellar Clouds. *Mon. Not. R. Astron. Soc.*, **219**, 859.

[Duley and Williams 1988] W.W. Duley and D.A. Williams, 1988. Excess Infrared Emission from Large Interstellar Carbon Grains. *Mon. Not. R. Astron. Soc.*, **231**, 969.

[Dupree *et al.* 1987] A.K. Dupree, S.L. Baliumas, E.F. Guinan, L. Hartmann, G.E. Nassipoulos, and G. Sonneborn, 1987. Periodic Photospheric and Chromospheric Modulation in Alpha Orionis (Beteigeuse). *Astrophys. J. (Letters)*, **317**, L85.

[Eggleton 1983] P.P. Eggleton, 1983. Approximations to the Radii of Roche Lobes. *Astrophys. J.*, **268**, 368.

[Ennis *et al.* 1977] D. Ennis, E.E. Becklin, S. Beckwith, J. Elias, I. Gatley, K. Mathews, G. Neugebauer, and S.P. Willner, 1977. Infrared Observations of Nova Cygni 1975. *Astrophys. J.*, **214**, 478.

[Evans 1991] A. Evans, 1991. Detection of Molecular Hydrogen in the Shell of the Old Nova DQ Her. *Mon. Not. R. Astron. Soc.*, **251**, 54P–56P.

[Fehsenfeld and Ferguson 1972] F.C. Fehsenfeld and E.E. Ferguson, 1972. . *J. Chem. Phys.*, **56**, 3055.

[Ferland and Shields 1978] G.J. Ferland and G.A. Shields, 1978. Heavy Element Abundances in Nova Cygni 1975. *Astrophys. J.*, **226**, 172.

[Ferland *et al.* 1986] G.J. Ferland, D.L. Lambert, and J.H. Woodman, 1986. Spectroscopic Observations of Nova Cygni 1975: The Coronal Line Region Revisited. *Astrophys. J. Suppl. Ser.*, **60**, 375.

[Field 1965] G.B. Field, 1965. Thermal Instability. *Astrophys. J.*, **142**, 531.

[Fitzpatrick and Massa 1986] E.L. Fitzpatrick and D. Massa, 1986. An Analysis of the Shapes of Ultraviolett Extinction Curves. I. The 2175ÅBump. *Astrophys. J.*, **307**, 286.

[Fleischer *et al.* 1992] A.J. Fleischer, A. Gauger, and E. Sedlmayr, 1992. Circumstellar Dust Shells around Long–period variables I. Dynamical Models of C–stars Including Dust Formation, Evaporation and Growth. *Astron. & Astrophys.*, **266**, 321.

[Frenklach and Feigelson 1989] M. Frenklach and E.D. Feigelson, 1989. Formation of Polycyclic Aromatic Hydrocarbons In Circumstellar Envelopes. *Astrophys. J.*, **341**, 372–384.

[Frenklach *et al.* 1989] M. Frenklach, C.S. Carmer, and E.D. Feigelson, 1989. Silicon Carbide and the Origin of Interstellar Carbon Grains. *Penn State Astronomy Preprint*, .

[Gail and Sedlmayr 1984] H.P. Gail and E. Sedlmayr, 1984. Formation of Crystalline and Amorphous Carbon Grains. *Astron. & Astrophys.*, **132**, 163–167.

[Gail and Sedlmayr 1986a] H.P. Gail and E. Sedlmayr, 1986. The Maximum Possible Mass Loss Rate in a Dust Driven Wind. *Astron. & Astrophys.*, **161**, 201–202.

[Gail and Sedlmayr 1986b] H.P. Gail and E. Sedlmayr, 1986. The Primary Condensation Process for Dust Around Late M-type Stars. *Astron. & Astrophys.*, **166**, 225–236.

[Gail and Sedlmayr 1987a] H.P. Gail and E. Sedlmayr, 1987. Dust Formation in Stellar Winds. In G.E. Morfill and M. Scholer, editors, *Physical Processes in Interstellar Clouds*, pages 275–303, Reidel, Dordrecht.

[Gail and Sedlmayr 1987b] H.P. Gail and E. Sedlmayr, 1987. Dust Formation in Stellar Winds III. Self-consistent Models for Dust Driven Winds Around C-Stars. *Astron. & Astrophys.*, **171**, 197–204.

[Gail and Sedlmayr 1987c] H.P. Gail and E. Sedlmayr, 1987. Dust Formation in Stellar Winds V. the Minimum Possible Mass Loss Rate for Dust Driven Winds. *Astron. & Astrophys.*, **177**, 186–192.

[Gail and Sedlmayr 1988] H.P. Gail and E. Sedlmayr, 1988. Dust Formation in Stellar Winds IV. Heteromolecular Carbon Grain Formation and Growth. *Astron. & Astrophys.*, **206**, 153–168.

[Gail *et al.* 1984] H.P. Gail, R. Keller, and E. Sedlmayr, 1984. Dust Formation in Stellar Winds I. A Rapid Computational Method and Application to Graphite Condensation. *Astron. & Astrophys.*, **133**, 320–332.

[Gallagher 1977] J.S. Gallagher, 1977. Dust Formation in Novae. *Astrophys. J.*, **82**(3), 209.

[Gallagher and Code 1974] J.S. Gallagher and G. Code, 1974. Ultraviolett Photometry from the Orbiting astronomical Observatory X. Nova FH Serpentis 1970. *Astrophys. J.*, **189**, 303f.

[Gallagher and Ney 1976] J.S. Gallagher and E.P. Ney, 1976. The Early Infrared Development of Nova Cygni 1975. *Astrophys. J. (Letters)*, **204**, L35–L39.

[Gallagher and Starrfield 1976] J.S. Gallagher and S. Starrfield, 1976. On the Total Energy Output of the Nova Outburst. *Mon. Not. R. Astron. Soc.*, **176**, 53–61.

[Gallagher and Starrfield 1978] J.S. Gallagher and S. Starrfield, 1978. Theory and Observations of Classical Novae. *Ann. Rev. Astron. Astrophys.*, **16**, 171–214.

[Gass 1990] H. Gass, 1990. Contribution of the Decay of ^{22}Na to the Energy Balance in Nova Shells. private communication.

[Gehrz 1988] R.D. Gehrz, 1988. The Infrared Temporal Development of Classical Novae. *Ann. Rev. Astron. Astrophys.*, **26**, 377–412.

[Gehrz 1989] R.D. Gehrz, 1989. Sources of Stardust in the Galaxy. In *Interstellar Dust*, page 445.

[Gehrz 1990] R.D. Gehrz, 1990. New Infrared Results for Classical Novae. In A. Cassatella and R. Viotti, editors, *Physics of Classical Novae*, pages 138–147, Springer Verlag, Heidelberg.

[Gehrz and Jones 1987] R.D. Gehrz and T.J. Jones, 1987. Nova Herculis 1987. *IAU Circular*, **4371**.

[Gehrz *et al.* 1980a] R.D. Gehrz, G.L Grasdalen, J.A. Hackwell, and E.P. Ney, 1980. The Evolution of the Dust Shell of Nova Serpentis 1978. *Astrophys. J.*, **237**, 855.

[Gehrz *et al.* 1980b] R.D. Gehrz, J.A. Hackwell, G.L. Grasdalen, E.P. Ney, G. Neugebauer, and K. Sellgren, 1980. The Optically thin Dust Shell of Nova Cygni 1978. *Astrophys. J.*, **239**, 570–580.

[Gehrz *et al.* 1984] R.D. Gehrz, E.P. Ney, G.L. Grasdalen, J.P. Hackwell, and H.A Thronson Jr., 1984. The Mysterious 10 Micron Emission Feature in the spectrum of Nova Aquilae 1982. *Astrophys. J.*, **281**, 303.

[Gehrz *et al.* 1985a] R.D. Gehrz, G.L. Grasdalen, and J.A. Hackwell, 1985. A Neon Nova: Discovery of a Remarkable 12.8 μ [NeII] Emission Line in Nova Vulpeculae 1984 No. 2. *Astrophys. J. (Letters)*, **298**, L47.

[Gehrz *et al.* 1985b] R.D. Gehrz, G.L. Grasdalen, and J.A. Hackwell, 1985. Nova Vulpeculae 1984 No. 2. *IAU Circular*, **4111**.

[Gehrz *et al.* 1985c] R.D. Gehrz, G.L. Grasdalen, and J.A. Hackwell, 1985. PW Vulpeculae 1984 No. 1. *IAU Circular*, **4065**.

[Gehrz *et al.* 1986] R.D. Gehrz, G.L. Grasdalen, M. Greenhouse, J.S. Hackwell, T. Hayward, and A.F. Bentley, 1986. The Neon Nova. II. Condensation of Silicate Grains in the Ejecta of Nova Vulpeculae 1984 Number 2. *Astrophys. J. (Letters)*, **308**, L63–L66.

[Gehrz *et al.* 1988] R.D. Gehrz, T.E. Harrison, E.P. Ney, K. Mathews, G. Neugebauer, J. Elias, G.L: Grasdalen, and J.A. Hackwell, 1988. PW Vulpeculae: a Dust–poor DQ Herculis ? *Astrophys. J.*, **329**, 894.

[Geisel *et al.* 1970] S.L. Geisel, D.E. Kleinman, and F.J. Low, 1970. Infrared Emission of Novae. *Astrophys. J. (Letters)*, **161**, L101–104.

[Glassgold and Huggins 1986] A.E. Glassgold and P.J. Huggins, 1986. The Ionization Structure of the Circumstellar Envelope of Alpha Orionis. *Astrophys. J.*, **306**, 605.

[Glassgold *et al.* 1987] A.E. Glassgold, G.A. Mamon, A. Omont, and R. Lucas, 1987. Photochemistry and Molecular Ions in Carbon-rich Circumstellar Envelopes. *Astron. & Astrophys.*, **180**, 183.

[Glassgold *et al.* 1989] A.E. Glassgold, G.A. Mamon, and P.J. Huggins, 1989. Molecule Formation in Fast Neutral Winds From Protostars. *Astrophys. J. (Letters)*, **336**, L29.

[Goebel and Moseley 1985] J.H. Goebel and S.H. Moseley, 1985. MgS Grain Component in Circumstellar Shells. *Astrophys. J. (Letters)*, **290**, L35–L39.

[Goeres *et al.* 1988] A. Goeres, R. Henkel, E. Sedlmayr, and H.-P. Gail, 1988. Nonequilibrium Chemistry in Circumstellar Shells. *Ann. Rev. Astron. Astrophys.*, **1**, 231.

[Goldreich and Scoville 1976] P. Goldreich and N.Z. Scoville, 1976. OH-IR Stars I. Physical Properties of Circumstellar Envelopes . *Astrophys. J.*, **205**, 144.

[Goldsmith *et al.* 1969] D.W. Goldsmith, H.J. Habing, and G.B. Field, 1969. Thermal Properties of Interstellar Gas Heated by Cosmic Rays. *Astrophys. J.*, **158**(173).

[Green and Chapman 1978] S. Green and S. Chapman, 1978. Collisional Excitation of Interstellar Molecules: Linear Molecules: CO, CS, OCS and HC_3N. *Astrophys. J. Suppl. Ser.*, **37**, 169–194.

[Greenberg 1986] J.M. Greenberg, 1986. Dust in Diffuse Clouds: One Stage in a Cycle. In F.P. Israel, editor, *Light on Dark Matter*, D. Reidel Publishing Company, Dordrecht.

[Greenberg and Hage 1990] J. M. Greenberg and J. I. Hage, 1990. From Interstellar Dust to Comets: A Unification of Observational Constraints. *Astrophys. J.*, **361**, 260.

[Greenhouse *et al.* 1987] M.A. Greenhouse, R.D. Gehrz, and T.J. Jones, 1987. Nova Herculis 1987. *IAU Circular*, **4398**.

[Greenhouse *et al.* 1988] M.A. Greenhouse, G.L. Grasdalen, T.L Hayward, R.D. Gehrz, and T.J. Jones, 1988. The Infrared Coronal Lines of Nova Vulpeculae 1984 No. 2. *Astronom. J.*, **95**, 172.

[Grotrian 1937] W. Grotrian, 1937. Zur physikalischen Bedeutung der Lichtkurve der Nova Herculis 1934. *Zeitschrift fuer Astrophysik*, **13**, 213.

[Guélin *et al.* 1986] M. Guélin, J. Cernichario, J. Kahane, and J. Gomez-Gonzales, 1986. A new free Radical in IRC+10216. *Astron. & Astrophys.*, **157**, L17.

[Harrison and Gehrz 1988] T.E. Harrison and R.D. Gehrz, 1988. A Survey of IRAS Data on 41 Classical Novae. *Astronom. J.*, **96**(3), 1001.

[Hartmann and Avrett 1984] L. Hartmann and E.H. Avrett, 1984. On the Extended Chromosphere of Alpha Orionis. *Astrophys. J.*, **284**, 238.

[Hartquist *et al.* 1980] T.W. Hartquist, M. Oppenheimer, and A. Dalgarno, 1980. . *Astrophys. J.*, **236**, 182.

[Hassall *et al.* 1989] B.J.M. Hassall, M.A.J. Snijders, A.W. Harris, A. Cassatella, M. Dennefeld, M. Friedjung, M. Bode, D. Whittet, P. Whitelock, J. Menzies, T. Lloyd Evans, and G.T. Bath, 1989. Measurements of Outburst Characteristics, Temperatures, Densities and Abundances in the Ejecta of Nova Muscae 1983. In A. Cassatella and R. Viotti, editors, *Physica of Classical Novae*, page 202.

[Hatfield and Brodzik 1977] B.F. Hatfield and D. Brodzik, 1977. Nova Sagittarii 1977. *IAU Circular*, **3082**.

[Hauschildt 1991] P.H. Hauschildt, 1991. *Non-LTE Modellatmosphaeren fuer Novae und Supernovae.* PhD thesis, Ruprecht-Karls-Universitaet, Heidelberg, Germany.

[Hauschildt *et al.* 1992] P.H. Hauschildt, S. Starrfield, and R. Wehrse, 1992. . in preparation.

[Henry 1970] R.J.W. Henry, 1970. Photoionization Cross Sections for atoms and Ions of Carbon, Nitrogen, Oxygen and Neon. *Astrophys. J.*, **161**, 1153.

[Herbst 1978] E. Herbst, 1978. What are the Products of Polyatomic Ion–Electron Dissociative Recombination Reactions ? *Astrophys. J.*, **222**, 508.

[Herbst 1980] E. Herbst, 1980. A new Look at Radiative Association in Dense Interstellar Clouds. *Astrophys. J.*, **237**, 462.

[Herbst 1988a] E. Herbst, 1988. Dense Interstellar Cloud Chemistry . In *Rate Coefficients in Astrochemistry*, pages 239–262, Kluwer Academics Publisher, Dordrecht, Netherlands.

[Herbst 1988b] E. Herbst, 1988. Interstellar molecule formation processes. *Rev. in Mod. Astron.*, **1**, 114.

[Herbst and Leung 1989] E. Herbst and C.L. Leung, 1989. Gas-Phase Production of Complex Hydrocarbons, Cyanopolyynes, and Related Compounds in Dense Interstellar Clouds. *Astrophys. J. Suppl. Ser.*, **69**, 271–300.

[Herbst *et al.* 1989] E. Herbst, T.J. Millar, S. Wlodek, and D.K. Bohme, 1989. The Chemistry of Silicon in Dense Interstellar Clouds. *Astron. & Astrophys.*, **222**, 205.

[Herd *et al.* 1990] C.R. Herd, N.G. Adams, and D. Smith, 1990. OH-Production in the Dissociative Recombination of H_3O^+ and HCO_2^+ and N_2OH^+. Comparison with theory and Interstellar Implications. *Astrophys. J.*, **349**, 388.

[Higdon and Fowler 1987] J.C. Higdon and W.A. Fowler, 1987. Gamma-Ray Constrants on ^{22}Na Yields in Nova Explosions. *Astrophys. J.*, **317**, 710–716.

[Hjellming 1965] R.M. Hjellming, 1965. Physical Processes in HII Regions. *Mon. Not. R. Astron. Soc.*, **143**, 420.

[Hollenbach and McKee 1979] D.J. Hollenbach and C.F. McKee, 1979. Molecule Formation and Infrared Emission in Fast Interstellar Shocks. 1. Physical Processes. *Astrophys. J. Suppl. Ser.*, **41**, 555.

[Hollenbach and McKee 1989] D.J. Hollenbach and C.F. McKee, 1989. Molecule Formation and Infrared Emission in Fast Interstellar Shocks. *Astrophys. J.*, **342**, 306.

[Honeycutt *et al.* 1980] R.K. Honeycutt, A.P. Bernat, J.E. Kephart, C.E. Gow, M.T. Sandford II, and D.L. Lambert, 1980. The Size and Surface Brightness of the Circumstellar Gas Shell Surrounding Beteigeuse. *Astrophys. J.*, **239**, 565.

[Horne 1980] K. Horne, 1980. Stepanyans Star: A new Eclipsing Cataclysmic Variable. *Astrophys. J. (Letters)*, **242**, L167.

[Huebner 1990] W.F. Huebner, 1990. *Physics and Chemistry of Comets.* Astronomy and Astrophysics Library. Springer Verlag, Heidelberg.

[Huebner and Giguere 1980] W.F. Huebner and P.T. Giguere, 1980. A Model of Comae II. Effects of Solar Photodissociative Ionization. *Astrophys. J.*, **238**, 753.

[Huggins 1987] P.J. Huggins, 1987. CO in the Circumstellar Envelope of Alpha Orionis. *Astrophys. J.*, **313**, 400.

[Huggins *et al.* 1988] P.J. Huggins, H. Oloffson, and L.E.B. Johansson, 1988. The CO Envelope of IRC +10216. *Astrophys. J.*, **332**, 1009.

[Hutchings *et al.* 1981] J.B. Hutchings, D. Crampton, and A. Cowley, 1981. . *Astrophys. J.*, **232**, 500.

[Hyland and MacGregor 1989] A.R. Hyland and P.J. MacGregor, 1989. . In *Interstellar Dust: Contributed Papers (NASA CP-3036)*, page 101.

[I. Iben Jr. *et al.* 1992] I. Iben Jr., M.Y. Fujimoto, and J. MacDonald, 1992. On Mass Transfer Rates in Classical Nova Precursors. *Astrophys. J.*, **384**, 580–586.

[Jeffries 1968] J.T. Jeffries, 1968. *Spectral Line Formation.* Waltham, Mass., Blaisdell.

[Jenkins and Evans 1988] R.N. Jenkins and A. Evans, 1988. . In M.E. Bailey and D.A. Williams, editors, *Dust in the Universe*, page 373, Cambridge University Press, Cambridge.

[Johnson *et al.* 1987] D. Johnson, M.W. Friedlander, and J.I. Katz, 1987. Dust Formation in Novae. *Bull. Amer. Astron. Soc.*, **19**, 724.

[Jura and Morris 1981] M. Jura and M. Morris, 1981. Model for the Circumstellar Gas around α Orionis. *Astrophys. J.*, **251**, 181.

[Keller 1987] R. Keller, 1987. Polyaromatic Hydrocarbons and the Condensation of Carbon in Stellar Winds. In *Polycyclic Aromatic Hydrocarbons and Astrophysics*, pages 387–397, Reidel, Dordrecht.

[Keller and Sedlmayr 1983] R. Keller and E. Sedlmayr, 1983. Entstehung von Kohlenstoffstaub in Sternhüllen. *Mitt. d. Astr. Ges.*, **60**, 312.

[Kerridge 1990] J.F. Kerridge, 1990. Carbon in Primitive Meteorites. In J.C. Tarter, S. Chang, and D.J. DeFrees, editors, *Carbon in the Galaxy: Studies from Earth and Space*, page 3, NASA, Ames Research Center, Moffett Field.

[King 1989] A.R. King, 1989. *Classical Novae*, chapter Mass TRansfer in Cataclysmic Binary Systems, page 17. John Wiley & Sons, Chichester.

[Klare *et al.* 1980] G. Klare, B. Wolf, and J. Krautter, 1980. Spectral Evolution of Nova Cygni 1978. *Astron. & Astrophys.*, **89**, 282.

[Kley 1984] D. Kley, 1984. . *J. Atmos. Chem.*, **2**, 203.

[Knapp 1985] G.R. Knapp, 1985. Mass Loss From Evolved Stars IV. Dust-To-Gas Ratios. *Astrophys. J.*, **293**, 273.

[Knapp and Morris 1985] G.R. Knapp and M. Morris, 1985. Mass Loss From Evolved Stars III. Mass Loss Rates for 50 Stars. *Astrophys. J.*, **292**, 640.

[Knapp *et al.* 1980] G.R. Knapp, T.G. Phillips, and P.J. Huggins, 1980. Detection of CO Emission at 1.3 Millimeters from the Beteigeuse Circumstellar Shell. *Astrophys. J. (Letters)*, **242**, L25.

[Kraft 1962a] R.P. Kraft, 1962. Binary Stars among Cataclysmic Variables I. U Geminorum Stars (Dwarf Novae). *Astrophys. J.*, **135**, 408.

[Kraft 1962b] R.P. Kraft, 1962. Binary Stars among Cataclysmic Variables II. Nova WZ Sagittae: A Possible Radiator of Gravitational Waves. *Astrophys. J. (Letters)*, **136**, 312.

[Kraft 1964] R.P. Kraft, 1964. Binary Stars among Cataclysmic Variables III. Ten old Novae. *Astrophys. J.*, **139**, 457.

[Krautter *et al.* 1984] J. Krautter, K. Beuermann, C. Leitherer, E. Oliva, A.F.M. Moorwood, E. Deul, W. Wargau, G. Klare, L. Kohoutek, J. van Paradijs, and B. Wolf, 1984. Observations of Nova Muscae 1983 from 1200 Å to 12 μm During its Early Decline Stage. *Astron. & Astrophys.*, **137**, 307.

[Kroto 1990] H.W. Kroto, 1990. The Formation and Structure of Circumstellar and Interstellar Dust. In J.C. Tarter, S. Chang, and D.J. DeFrees, editors, *Carbon in the Galaxy: Studies from Earth and Space*, page 275, NASA, Ames Research Center, Moffett Field.

[Kroto and Jura 1992] H.W. Kroto and M. Jura, 1992. Circumstellar and Interstellar Fullerenes and their analogues. *Astron. & Astrophys.*, **263**, 275.

[Kurucz and Peytremann 1975] R.L. Kurucz and E. Peytremann, 1975. *A Table of Semiempirical gf Values*, volume Special Report of *62*. Smithsonian Astrophysical Observatory.

[Léger A. 1988] Léger A., 1988. PAH's, the State of the Art. In E. Bussoletti, C. Fusco, and G. Longo, editors, *Experiments on Cosmic Dust Analogues*, page 75, Kluwer Academic Publishers, Dordrecht.

[Léger 1989] A. Léger, 1989. The pah hypothesis and the extinction curve. In *Interstellar Dust*, page 173, Kluwer Academics Publisher, Dordrecht.

[Lafont *et al.* 1982] S. Lafont, R. Lucas, and A. Omont, 1982. Molecular Abundances in IRC+10216. *Astron. & Astrophys.*, **106**, 201.

[Lambert *et al.* 1984] D.L. Lambert, J.A. Brown, K.H. Hinkle, and H.B. Johnson, 1984. Carbon, Nitrogen and Oxygen Abundances in Beteigeuse. *Astrophys. J.*, **284**, 223–237.

[Lance *et al.* 1988] C.M. Lance, M.L. McCall, and A.K. Uomoto, 1988. Portrait of a Novel Nova: V1500 Cygni. *Astrophys. J. Suppl. Ser.*, **66**, 151.

[Lang 1974] K.R. Lang, 1974. *Astrophysical Formulae.* Springer–Verlag, Heidelberg.

[Lattimer *et al.* 1978] J.M. Lattimer, D.N. Schramm, and L. Grossman, 1978. Condensation in Supernovae Ejecta and Isotopic Anomalies in Meteorites. *Astrophys. J.*, **219**, 230.

[Lee 1984] L.C. Lee, 1984. Photodissociation Rates of Molecules in the Interstellar Radiation Field. *Astrophys. J.*, **282**, 172.

[Letzelter *et al.* 1987] C. Letzelter, M. Eidelsberg, F. Rostas, J. Breton, and T. Thieblemont, 1987. . *J. Chem. Phys.*, **114**, 273.

[Lewis and Ney 1979] J.S. Lewis and E.P. Ney, 1979. Iron and the Formation of Astrophysical Dust Grains. *Astrophys. J.*, **234**, 154.

[Liller and Mayer 1987] W. Liller and B. Mayer, 1987. . *Publ. Astron. Soc. Pac.*, **99**, 606.

[Liller *et al.* 1975] W. Liller, C.Y. Shao, B. Mayer, and P. Garnavich, 1975. Nova Cygni 1975. IAU Circ. 2848.

[Livio and Soker 1984] M. Livio and N. Soker, 1984. . *Mon. Not. R. Astron. Soc.*, **208**, 783.

[Livio *et al.* 1986] M. Livio, N. Soker, and R. Dgani, 1986. On the Stream–Disk Interaction in Accreting Compact Objects. *Astrophys. J.*, **305**, 267.

[Livio *et al.* 1991] M. Livio, A. Govarie, and H. Ritter, 1991. Changes in the Binary System Parameters from Nova Explosions. *Astron. & Astrophys.*, **246**, 84–90.

[Livio *et al.* 1992] M. Livio, A. Mastichiadis, H. Ögelman, and J.W. Truran, 1992. On the Role of Radioactive Decays in Powering Gamma-Rays and X-Rays from Novae. *Astrophys. J.*, **394**, 217.

[Lundmark 1921] K. Lundmark, 1921. Suspected New Stars Recorded in old Chronicles and among Recent Meridian Observations. *Publ. Astron. Soc. Pac.*, **33**, 225.

[MacDonald 1986] J. MacDonald, 1986. Postthermonuclear Runaway Angular Momentum Loss in Cataclysmic Binaries. *Astrophys. J.*, **305**, 251.

[MacDonald *et al.* 1985] J. MacDonald, M.Y. Fujimoto, and J.W. Truran, 1985. The Decline and Fall of Classical Novae. *Astrophys. J.*, **294**, 263.

[Mahoney *et al.* 1982] W.A. Mahoney, J.C. Ling, A.S. Jacobson, and R.E. Lingenfelter, 1982. Diffuse Galactic Gamma–Ray Line Emission from Nucleosynthetic ^{60}Fe, ^{26}Al and ^{22}Na: Preliminary Limits from HEAO 3 . *Astrophys. J.*, **262**, 742.

[Mahoney *et al.* 1984] W.A. Mahoney, J.C. Ling, and A.S. Jacobsen, 1984. HEAO Discovery of ^{26}Al in the Interstellar Medium. *Astrophys. J.*, **286**, 578.

[Mamon *et al.* 1988] G.A. Mamon, A.E. Glassgold, and P.J. Huggins, 1988. The Photodissociation of CO in Circumstellar Envelopes. *Astrophys. J.*, **328**, 797.

[Marr 1967] G.V. Marr, 1967. *Photoionization Processes in Gases.* Pure and Applied Physics. Academic Press, London.

[Marr 1968] G.V. Marr, 1968. *Plasma Spectroscopy.* Elsevier Publishhing Company, Amsterdam.

[Marsh *et al.* 1983] T.R. Marsh, R.A. Wade, and J. Oke, 1983. A Nebulae around Nova BT Monocerotis. *Mon. Not. R. Astron. Soc.*, **205**, 39P.

[Martin 1989] P.G. Martin, 1989. *Classical Novae*, chapter Photoionization Models of the Evolution of DQ Her 1934, page 113. John Wiley & Sons, Chichester.

[Massa and Savage 1989] D. Massa and B.D. Savage, 1989. Measurements of interstellar extinction. In *Interstellar Dust*, page 3, Kluwer Academics Publisher, Dordrecht.

[Massey *et al.* 1974] H.S.W. Massey, E.H.S. Burshop, and H.B. Gilbody, 1974. *Electronic and Ionic Impact Phenomena IV: Recombination and Fast Collisions of Heavy Particles*, volume IV of *The International Series of Monographs on Physics.* Clarendon Press, Oxford, 2 edition.

[Matese *et al.* 1989] J.J. Matese, D.P. Whitmire, and R.T. Reynolds, 1989. Sublimating Icy Comets as the Source of Nucleation Seeds for Grain Condensation in Classical Nova. In L.J. Allamandola and A.G.G.M. Tielens, editors, *Interstellar Dust*, page 502, Kluwer Academic Publishers, Boston.

[Mathis 1989] J.S. Mathis, 1989. Bare Carbon/Silicate Theories. In *Interstellar Dust*, page 357.

[Mauron *et al.* 1984] N. Mauron, B. Fort, F. Querci, M. Dreux, T. Fauconnier, and P. Lamy, 1984. *Astron. & Astrophys.*, **130**, 341.

[McCabe and Connon-Smith 1979] E.M. McCabe and R.C. Connon-Smith, 1979. *Nature*, **281**, 263.

[McDermott and Taam 1989] P.N. McDermott and R.E. Taam, 1989. On the Disrupted Magnetic Braking Model for the Period Gap of Cataclysmic Variables. *Astrophys. J.*, **342**, 1019.

[McLaughlin 1960] D.B. McLaughlin, 1960. The Spectra of Novae. In J.L. Greenstein, editor, *Stars and Stellar Systems VI Stellar Atmospheres*, chapter 17, pages 585–652. University of Chicago Press, Chicago.

[McMillan and Tapia 1978] R.S. McMillan and S. Tapia, 1978. Discovery of Polarized Light Scattered by Dust around Alpha Orionis. *Astrophys. J. (Letters)*, **226**, L87.

[Mestel and Spruit 1987] L. Mestel and H.C. Spruit, 1987. On Magnetic Braking of Late–Type Stars. *Mon. Not. R. Astron. Soc.*, **226**, 57.

[Mihalas 1978] D. Mihalas, 1978. *Stellar Atmospheres.* W.H. Freeman, San Francisco.

[Mihalas and Weibel-Mihalas 1984] D. Mihalas and B. Weibel-Mihalas, 1984. *Foundations of Radiation Hydrodynamics.* The University Press, London.

[Millar and Freeman 1984] T.J. Millar and A. Freeman, 1984. Chemical Modelling of Molecular Sources – I. TMC–1. *Mon. Not. R. Astron. Soc.*, **207**, 405.

[Millar *et al.* 1991a] T.J. Millar, E. Herbst, and S.B. Charnley, 1991. The Formation of Oxygen-containing Organic Molecules in the Orion Compact Ridge. *Astrophys. J.*, **369**, 147–156.

[Millar *et al.* 1991b] T.J. Millar, J.M.C. Rawlings, A. Bennett, P.D. Brown, and S.B. Charnley, 1991. Gas Phase Reactions and Rate Coefficients for Use in Astrophysics. *Astron. & Astrophys. Suppl. Ser.*, **87**, 585–619.

[Mitchell 1984] G.F. Mitchell, 1984. Effects of Shocks on the Sulfur Chemistry of a Dense Interstellar Cloud. *Astrophys. J.*, **287**, 665.

[Mitchell and Deveau 1983] G.F. Mitchell and T.J. Deveau, 1983. Effects of a Shock on the Molecular Composition of a Diffuse Interstellar Cloud. *Astrophys. J.*, **266**, 646–661.

[Mitchell and Evans 1984] R.M. Mitchell and A. Evans, 1984. Grain Growth and Destruction in Novae. *Mon. Not. R. Astron. Soc.*, **209**, 945–954.

[Mitchell *et al.* 1985] R.M. Mitchell, G. Robinson, A.R. Hyland, and G. Neugebauer, 1985. The Late Infrared Development of Nova Serpentis 1970. *Mon. Not. R. Astron. Soc.*, **216**, 1057–1071.

[Murad 1972] E. Murad, 1972. . *J. Chem. Phys.*, **58**, 4374.

[Mustel 1956] E.R. Mustel, 1956. The Mechanism of Ejection of Matter from Novae. *Vistas in Astronomy*, **2**, 1486.

[Mustel and Boyarchuk 1970] E.R. Mustel and A.A. Boyarchuk, 1970. Structure of Envelopes Ejected by Novae. *Astrophys. Space Sci.*, **6**, 183.

[Nejad and Millar 1987] L.A.M. Nejad and T.J. Millar, 1987. Chemical modelling of molecular sources v. irc+10216. *Astron. & Astrophys.*, **183**, 279.

[Nejad and Millar 1988] L.A.M. Nejad and T.J. Millar, 1988. Chemical Modelling of Molecular Sources - VI. Carbon Bearing Molecules in Oxygen-Rich Circumstellar Envelopes. *Mon. Not. R. Astron. Soc.*, **230**, 79.

[Nercessian *et al.* 1989] E. Nercessian, S. Guilloteau, A. Omont, and J.J. Bunayoun, 1989. HCN Emission and Nitrogen-Bearing Molecules in Oxygen-Rich Circumstellar Envelopes. *Astron. & Astrophys.*, **210**, 225.

[Neufeld and Dalgarno 1989] D.A. Neufeld and A. Dalgarno, 1989. Fast Molecular Shocks. I. Refomation of Molecules Behind a Dissociative Shock. *Astrophys. J.*, **340**, 869–893.

[Neugebauer and Leighton 1969] G. Neugebauer and R.B. Leighton, 1969. *NASA Sp*, **3047**.

[Newell and Hjellming 1982] R.T. Newell and R.M. Hjellming, 1982. Radio Emission from the Extende Chromosphere of Alpha Orionis. *Astrophys. J. (Letters)*, **263**, L85.

[Ney and Hatfield 1978] E. Ney and A. Hatfield, 1978. The Isothermal Dust Condensation of Nova Vulpeculae 1976. *Astrophys. J. (Letters)*, **219**(L111-L115).

[Nofar *et al.* 1991] I. Nofar, G. Shaviv, and S. Starrfield, 1991. The Formation of ^{26}Al in Nova Envelopes. *Astrophys. J.*, **369**, 440–450.

[Nuth and Donn 1982] J.A. Nuth and B.D. Donn, 1982. . *J. Chem. Phys.*, **77**, 2639.

[Nuth and Donn 1983] J.A. Nuth and B.D. Donn, 1983. . *J. Chem. Phys.*, **78**, 1618.

[Nuth *et al.* 1985] J.A. Nuth, S.H. Moseley, R.F. Silverberg, J.H. Goebel, and W.J. Moore, 1985. Laboratory Infrared Spectra of Predicted Condensates in Carbon-rich Stars. *Astrophys. J. (Letters)*, **290**, L41–L43.

[Ögelmann *et al.* 1984] H. Ögelmann, K. Beuermann, and J. Krautter, 1984. The Detection of X–Rays from Nova Muscae 1983 with the EXOSAT Satellite. *Astrophys. J. (Letters)*, **287**, L31.

[Ögelmann *et al.* 1987] H. Ögelmann, J. Krautter, and K. Beuermann, 1987. EXOSAT Observations of X–rays from Classical Novae. *Astron. & Astrophys.*, **177**, 110.

[Omont 1991] A. Omont, 1991. Circumstellar Chemistry . In *Chemistry in Space*, pages 171–198, Kluwer Academics Publisher, Dordrecht, Netherlands.

[Osterbrock 1974] D.E. Osterbrock, 1974. *Astrophysics of Gaseous Nebulae.* A Series of Books in Astronomy and Astrophysics. W.H. Freeman and Company, San Francisco, 1 edition.

[Patterson 1979] J. Patterson, 1979. The Stabilization of the 3 Hour Period of Nova Cygni 1975. *Astrophys. J.*, **231**, 789.

[Patterson 1984] J. Patterson, 1984. The Evolution of Cataclysmic and Low–Mass X–Ray Binaries. *Astrophys. J. Suppl. Ser.*, **54**, 443.

[Payne–Gaposchkin 1957] C. Payne–Gaposchkin, 1957. *The Galactic Novae.* Dover Books on Astronomy and Astrophysics. Dover Publ., New York.

[Petuchowski *et al.* 1988] S.J. Petuchowski, E. Dwek, J.E. Allen, and J.A. Nuth, 1988. CO Formation in the Metal-Rich Ejecta of SN 1987 A. *Astrophys. J.*, **342**, 406–415.

[Pfau 1976] W. Pfau, 1976. Recalibration of the Absolute Magnitudes of Novae and Application to Nova Cygni 1975. *Astron. & Astrophys.*, **50**, 113.

[Phillips and Selby 1977] J.P. Phillips and M.J. Selby, 1977. The Inception of Novae Transition Zone Oscillations. *Astrophys. Space Sci.*, **49**, 339.

[Pineau des Forêts *et al.* 1986] G. Pineau des Forêts, D.R. Flower, T.W. Hartquist, and A. Dalgarno, 1986. Theoretical Studies of Imterstellar Molecular Shocks – III.: The Formation of CH^+ in Diffuse Clouds. *Mon. Not. R. Astron. Soc.*, **220**, 801.

[Politano and Webbink 1990] M. Politano and R.F. Webbink, 1990. The White Dwarf Mass and Orbital Period Distributions in Zero–Age Cataclysmic Variables. In A. Cassatella and R. Viotti, editors, *Physics of Classical Novae*, page 392, Springer Verlag, Heidelberg.

[Politano *et al.* 1990] M. Politano, M. Livio, J.W. Truran, and R.F. Webbimk, 1990. The Theoretical Frequency of Classical Nova Outbursts as a Function of White Dwarf Mass. In A. Cassatella and R. Viotti, editors, *Physics of Classical Novae*, page 386, Springer-Verlag, Heidelberg.

[Pouilly *et al.* 1983] B. Pouilly, J.M. Robbe, J.M. Schamps, and E. Roueff, 1983. *J.Phys. B*, **16**, 437.

[Prasad and Huntress Jr. 1980] S.S. Prasad and W.T. Huntress Jr., 1980. A Model for Gas Phase Chemistry in Interstellar Clouds. II. Nonequilibrium Effects and Effects of Temperature and Activation Energies. *Astrophys. J.*, **239**, 151–165.

[Prialnik 1989] D. Prialnik, 1989. The Cyclic Evolution of Classical Novae. In A. Casatella and R. Viotti, editors, *Physics of Classical Novae*, page 351, Springer Verlag, Heidelberg.

[Prialnik and Shara 1986] D. Prialnik and M.M. Shara, 1986. Rapid Accretion and Hibernation in the Preoutburst History of Classical Novae. *Astrophys. J.*, **311**, 172.

[Pringle 1975] J.E. Pringle, 1975. Period Changes in Eruptive Binaries. *Mon. Not. R. Astron. Soc.*, **170**, 633.

[Rawlings 1988] J.M.C. Rawlings, 1988. Chemistry in the Ejecta of Novae. *Mon. Not. R. Astron. Soc.*, **232**, 507.

[Rawlings and Williams 1987] J.M.C. Rawlings and D.A. Williams, 1987. Chemistry in Novae. In M.F. Bode, editor, *RS Opiuchi and the Recurrent Nova Phenomenen*, VNU Science Press, Utrecht, Netherlands.

[Rawlings and Williams 1989] J.M.C. Rawlings and D.A. Williams, 1989. Chemical Routes to Dust Formation in the Ejecta of Novae. *Mon. Not. R. Astron. Soc.*, **240**, 729–740.

[Rees 1976] M.J. Rees, 1976. Accretion Processes in Close Binaries. In P. Eggleton, S. Mitton, and J. Whelan, editors, *Structure and Evolution of Close Binary Systems*, page 225. D. Reidel.

[Ritter 1990] H. Ritter, 1990. Catalogue of Cataclysmic Variables, Low–Mass X–Ray Binaries and Related Objects. Preprint.

[Ritter and Burkert 1986] H. Ritter and A. Burkert, 1986. The Mass–Spectrum of White Dwarfs in Cataclysmic Binaries. *Astron. & Astrophys.*, **158**, 161.

[Roberge and Dalgarno 1982] W. Roberge and A. Dalgarno, 1982. Collision Induced Dissociaton of H_2. *Astrophys. J.*, **255**, 176f.

[Robinson 1975] E.L: Robinson, 1975. Preeruption Light Curves of Novae. *Astronom. J.*, **80**(7), 515.

[Robinson 1976] E.L. Robinson, 1976. The Structure of Cataclysmic Variables. *Ann. Rev. Astron. Astrophys.*, , 119f.

[Robinson 1983] E.L. Robinson, 1983. The Periods of Cataclysmic Variables. In M. Livio and G. Shaviv, editors, *Cataclysmic Variables and Related Objects*, page 1, D. Reidel, Dordrecht.

[Robinson *et al.* 1982] E.L. Robinson, R.E. Nather, and S.O. Kepler, 1982. BT Monocerotis: An Eclipsing Nova. *Astrophys. J.*, **254**, 337.

[Roche *et al.* 1984] P.F. Roche, D.K. Aitken, and B. Whitmore, 1984. The Development of the 8-13 μm Spectra of Nova Aquilae 1982. *Mon. Not. R. Astron. Soc.*, **211**, 535.

[Rodgers and Glassgold 1991] B. Rodgers and A.E. Glassgold, 1991. The Temperature of the Circumstellar Envelope Of Alpha Orionis. *Astrophys. J.*, **382**, 606–616.

[Rosino *et al.* 1983] L. Rosino, T. Iijima, and S. Ortolani, 1983. Light Curve and Spectral Evolution of Nova Aquilae 1982. *Mon. Not. R. Astron. Soc.*, **205**, 1069.

[Rosino *et al.* 1986] L. Rosino, F. Ciatti, and M. Delle Valle, 1986. Researches on Novae and Related Objects I.: The Spectral Evolution of Nova FH Ser (1970). *Astron. & Astrophys.*, **158**, 34.

[Sahai and Wannier 1992] R. Sahai and P.G. Wannier, 1992. SO and SO_2 in Mass-Loss Envelopes of Red Giants: Probes of Nonequilibrium Circumstellar Chemistry and Mass-Loss Rates. *Astrophys. J.*, **394**, 320.

[Sakata *et al.* 1984] A. Sakata, S. Wada, and T. Tanabe amd T. Onaka, 1984. . *Astrophys. J. (Letters)*, **287**, L51.

[Samus 1975] N.N. Samus, 1975. Nova Cygni1975. IAU Circ. 2839.

[Sandford 1989] S.A. Sandford, 1989. Interstellar Dust in Collected IDPs. In *Interstellar Dust*, page 412.

[Sanford 1935] R.F. Sanford, 1935. . *Publ. Astron. Soc. Pac.*, **47**, 209.

[Sanyal 1974] A. Sanyal, 1974. Nova Delphini 1967. I. Spectroscopic Observations. *Astrophys. J. Suppl. Ser.*, **28**, 115.

[Schaeffer and Patterson 1983] B.E. Schaeffer and J. Patterson, 1983. Orbital Periods of Novae Before Eruption. *Astrophys. J.*, **268**, 710–717.

[Schmutzler 1987] E. Schmutzler, 1987. *Zum thermischen Zusatnd dünner Plasmen unter Einfluš beliebiger Photnenspektren.* PhD thesis, Universität Bonn, Bonn.

[Schwarzenberg–Czerny and Udalski 1990] A. Schwarzenberg–Czerny and A. Udalski, 1990. On V603 Aql and Magnetic Novae. In A. Cassatella and R. Viotti, editors, *Physics of Classical Novae*, page 73, Springer–Verlag, Heidelberg.

[Sedlmayr 1989] E. Sedlmayr, 1989. Dust formation in stellar outflows. In *Interstellar Dust*, page 400, Kluwer Academics Publisher, Dordrecht.

[Seitter 1990] W.C. Seitter, 1990. Optical Studies of Classical Novae in Outburst. In A. Cassatella and R. Viotti, editors, *Physics of Classical Novae*, pages 79–96, Springer Verlag, Heidelberg.

[Shankar *et al.* 1991] A. Shankar, M. Livio, and J.W. Truran, 1991. The Common Envelope Phase in Classical Novae: One-Dimensional Models. *Astrophys. J.*, **374**, 623–630.

[Shara 1981a] M. Shara, 1981. A Theoretical Explanation of the Absolutes Magnitude Decline Time (M_b–t_3) Relationship for Classical Nova. *Astrophys. J.*, **243**, 926.

[Shara 1981b] M. Shara, 1981. On the Constancy of the Absolute Magnitude $M_b(15)$ of a Classical Nova 15 Days after Maximum Light. *Astrophys. J.*, **243**, 268.

[Shara *et al.* 1984] M.M. Shara, A.F.J. Moffat, J. McGraw, D.S. Dearborn, H.E. Bond, E. Kemper, and R. Lamontagne, 1984. WY Sagittae (Nova 1783): A Transition between Classical Novae and Dwarf Novae? . *Astrophys. J.*, **282**, 763.

[Shara *et al.* 1985] M.M. Shara, A.F.J. Moffat, and R.F. Webbink, 1985. Unraveling the Oldest and Faintest Recovered Nova: CK Vulpeculae (1670). *Astrophys. J.*, **294**, 271.

[Shara *et al.* 1986] M.M. Shara, M. Livio, A.F.J. Moffat, and M. Orio, 1986. Do Novae Hibernate most of the Milennia between Eruptions? Links between Dwarf and Classical Novae, and Implications for the Space Densities and Evolution of Cataclysmic Binaries. *Astrophys. J.*, **311**, 163.

[Sharov 1972] A.S. Sharov, 1972. Estimate for the Frequency of Novae in the Andromeda Nebula and our Galaxy. *Soviet Astron.*, **16**, 41.

[Shima *et al.* 1985] E. Shima, T. Matsuda, H. Takeda, and K. Sawade, 1985. Hydrodynamic Calculations of Axissymmetric Accretion Flow. *Mon. Not. R. Astron. Soc.*, **217**, 367.

[Singh and Chaturvedi 1989] M. Singh and J.P. Chaturvedi, 1989. Polyatomic Molecules, Molecular Ions and Radicals of astrophysical Interest I. and II. . *Astrophys. Space Sci.*, **162**, 251f.

[Skinner and Whitmore 1987] C.J. Skinner and B. Whitmore, 1987. The Circumstellar Environment of α Orionis. *Mon. Not. R. Astron. Soc.*, **224**, 335.

[Skinner *et al.* 1990] C.J. Skinner, I. Griffin, and B. Whitmore, 1990. Red Giants with Unusual Dust Shells - I. the Database. *Mon. Not. R. Astron. Soc.*, **243**, 78.

[Slavsky and Scalo 1984] D.B. Slavsky and J.M. Scalo, 1984. Chemistry in oxygen–rich circumstellar shells. Preprint.

[Smith *et al.* 1990] C.H. Smith, D.K. Aitken, and P.F. Roche, 1990. PAH's and Silicate Emision in Nova Cen 1986. In A. Cassatella and R. Viotti, editors, *Physics of Classical Novae*, pages 197–198, Springer Verlag, Heidelberg.

[Snijders 1990] M.A.J. Snijders, 1990. Physical Properties and Abundances of Novae in the Nebular Phase. In A. Cassatella and R. Viotti, editors, *Physics of Classical Novae*, pages 188–194, Springer Verlag, Heidelberg.

[Snijders *et al.* 1984] M.A.J. Snijders, , T.J. Batt, M.J. Seaton, J.C. Blades, and D.C. Morton, 1984. Nova Aquilae 1982 — A Short Report. *Mon. Not. R. Astron. Soc.*, **211**, 7P.

[Snijders *et al.* 1987] M.A.J. Snijders, T.J. Batt, P.F. Roche, M.J. Seaton, D.C. Morton, T.A.T. Spoelstra, and J.C. Blades, 1987. Nova Aquilae 1982. *Mon. Not. R. Astron. Soc.*, **228**, 329f.

[Soifer *et al.* 1981] B.T. Soifer, S.P. Willner, R.W Capps, and R.J. Rudy, 1981. 4–8 Micron Spectrophotometry of OH 0739–14. *Astrophys. J.*, **250**, 631.

[Solf 1983] J. Solf, 1983. On the Geometrical and Kinematical Structure of the Postnova Shell of HR Delphini. *Astrophys. J.*, **273**, 647.

[Sopka *et al.* 1985] R.J. Sopka, R. Hidebrand, D.T. Jaffe, D.T. Gatley, T. Roellig, M. Werner, M. Jura, and B. Zuckerman, 1985. Submillimeter Observations of Evolved Stars. *Astrophys. J.*, **294**, 242.

[Sparks *et al.* 1990] W.M. Sparks, G.S. Kutter, S. Starrfield, and J.W. Truran, 1990. Thermonuclear Runaway Model. In A. Cassatella and R. Viotti, editors, *Physics of Classical Novae*, page 361, Springer Verlag, Heidelberg.

[Spitzer and Scott 1969] L.Jr. Spitzer and E.H. Scott, 1969. Heating of HI Regions by Energetic Particles. *Astrophys. J.*, **158**, 161f.

[Starrfield 1989] S. Starrfield, 1989. *Classical Novae*, chapter Thermonuclear Processes in the Classical Novae Outburst, pages 39–57. Wiley, Chichester.

[Starrfield *et al.* 1972] S. Starrfield, W.M. Sparks, and G. Kutter, 1972. CNO abundances and Hydrodynamic Models of the Nova Outburst. *Astrophys. J.*, **176**, 169–176.

[Starrfield *et al.* 1974a] S. Starrfield, W.M. Sparks, and J.W. Truran, 1974. CNO abundances and Hydrodynamic Models of the Nova Outburst. II. $1.00 M_{\odot}$ Models with Enhanced Carbon and Oxygen. *Astrophys. J. Suppl. Ser.*, **261**(28), 247–270.

[Starrfield *et al.* 1974b] S. Starrfield, W.M. Sparks, and J.W. Truran, 1974. CNO abundances and Hydrodynamic Models of the Nova Outburst. *Astrophys. J.*, **192**, 647–655.

[Starrfield *et al.* 1974c] S. Starrfield, W.M. Sparks, and J.W. Truran, 1974. CNO abundances and Hydrodynamic Models of the Nova Outburst. III. $0.5 M_\odot$ Models with Enhanced Carbon and Oxygen. *Astrophys. J.*, **192**, 647–655.

[Starrfield *et al.* 1976] S. Starrfield, W.M. Sparks, and J.W. Truran, 1976. CNO abundances and Hydrodynamic Models of the Nova Outburst. IV. Comparison with Observations. *Astrophys. J.*, **208**, 819–825.

[Starrfield *et al.* 1978] S. Starrfield, J.W. Truran, and W.M. Sparks, 1978. CNO abundances and Hydrodynamic Studies of the Nova Outburst. V. 1.00 $M_\odot$ Models with Small Mass Envelopes. *Astrophys. J.*, **226**, 186–202.

[Starrfield *et al.* 1987] S. Starrfield, W.M. Sparks, and J.W. Truran, 1987. Nova Outburst and its Application to the Recurrent Nova Phenomenon. In M.F. Bode, editor, *RS Opiuchi and the Recurrent Nova Phenomenen*, VNU Science Press, Utrecht, Netherlands.

[Stephenson 1967] C.B. Stephenson, 1967. The Pre–outburst Spectrum of Nova Delphini 1967. *Publ. Astron. Soc. Pac.*, **79**, 584.

[Stephenson and Herr 1963] C.B. Stephenson and R.B. Herr, 1963. Pre–Outburst Spectrum of Nova Herculis 1963. *Publ. Astron. Soc. Pac.*, **75**, 253.

[Sternberg *et al.* 1987] A. Sternberg, A. Dalgarno, and S. Lepp, 1987. Cosmic-Ray Induced Photodestruction of Interstellar Molecules in Dense Clouds. *Astrophys. J.*, **320**, 676.

[Stickland *et al.* 1981] D.J. Stickland, C.J. Penn, M.J. Seaton, M.A.J. Snijders, , and P.J. Storey, 1981. Nova Cygni 1978 – I. The Nebular Phase. *Mon. Not. R. Astron. Soc.*, **197**, 107.

[Stockman *et al.* 1988] H.S. Stockman, G.D. Schmidt, and D.Q. Lamb, 1988. V 1500 Cygni: Discovery of a Magnetic Nova. *Astrophys. J.*, **332**, 282–286.

[Suto and Lee 1983] M. Suto and L.C. Lee, 1983. . *J. Chem. Phys.*, **78**, 4515.

[Sutton *et al.* 1977] E.C. Sutton, J.W.V. Storey, A.L. Betz, C.H. Townes, and D.L. Spears, 1977. Spatial Heterodyne Interferometry of VY Canis Majoris, Alpha Orionis, Alpha Scorpii and R Leonis at 11μ. *Astrophys. J. (Letters)*, **217**, L95.

[Sutton *et al.* 1979] E.C. Sutton, A.L. Betz, J.W.V. Storey, and D.L. Spears, 1979. The Brightness Distribution of IRC+10216 at 11 Microns. *Astrophys. J. (Letters)*, **230**, L105.

[Taylor *et al.* 1987] A.R. Taylor, E.R. Seaquist, J.M. Hollis, and S.R. Pottasch, 1987. The Unusual Radio Outburst of Nova Vulpeculae No. 2. *Astron. & Astrophys.*, **183**, 38.

[Tenorio–Tagle 1976] G. Tenorio–Tagle, 1976. The Time Evolution of an Ionization Front. *Astron. & Astrophys.*, **53**, 411.

[Thompson *et al.* 1978] G.I. Thompson, K. Nandy, C. Jamar, A. Monfils, L.Houziaux, D.J. Carnochan, and R. Wilson, 1978. In *Catalogue of Stellar UV Fluxes*, page 1234.

[Tielens and Hollenbach 1985] A.G.G.M. Tielens and D.J. Hollenbach, 1985. Photodissociation Regions: I. Basic Model. *Astrophys. J.*, **291**, 722f.

[Treffers and Cohen 1974] R. Treffers and M. Cohen, 1974. High-Resolution Spectra of Cool Stars in the 10 μ and 20μ Regions. *Astrophys. J.*, **188**, 545.

[Truran 1985a] J.W. Truran, 1985. CNO-Nuclei and the Classical Nova Outburst. In *Production and Distribution of the C,N,O Elements*, page 211.

[Truran 1985b] J.W. Truran, 1985. Nucleosynthesis accompanying Classical Nova Outburst. In *Nucleosynthesis and its Implicationson Nuclear and Particle Physics*, page 97. D. reidel.

[Truran 1990] J.W. Truran, 1990. Theoretical Implications of Nova Abundances. In A. Cassatella and R. Viotti, editors, *Physics of Classical Novae*, page 373, Springer Verlag, Heidelberg.

[Truran and Livio 1986] J.W. Truran and M. Livio, 1986. On the Freuency of occurence of Oxygen-neon Magnesium White Dwarfs in Classical Nova Systems. *Astrophys. J.*, **308**, 721f.

[Tsuji 1973] T. Tsuji, 1973. Molecular Abundances in Stellar Atmospheres II. *Astron. & Astrophys.*, **23**, 411.

[Tsuji 1978] T. Tsuji, 1978. Spectral Energy Distributions and Effective Temperature Scale of M-giant Stars. *Astron. & Astrophys.*, **62**, 29.

[Tsuji 1987] T. Tsuji, 1987. In M.S. Varyda and S.P. Taradfar, editors, *Astrochemistry*, page 409, D. Reidel, Dordrecht.

[van den Bergh 1975] S. van den Bergh, 1975. . In A. Sandage, M. Sandage, and J. Kristian, editors, *Galaxies in the Universe*, page 509, Univ. Chicago Press, Chicago.

[van den Bergh and Younger 1987] S. van den Bergh and P.F. Younger, 1987. UBV Photometry of Novae. *Astron. & Astrophys. Suppl. Ser.*, **70**, 125.

[van Dishoeck 1987] E.F. van Dishoeck, 1987. Photodissociation and photoionization processes. In T.J. Millar and D.A. Williams, editors, *Rate Coefficients in Astrochemistry*, page 49, Kluwer Academics Publisher, Dordrecht.

[van Duinen *et al.* 1975] R.J. van Duinen, J.W.G. Aalders, P.W.P. Wesselius, K.J. Wildemann, C.C. Wu, W. Luinge, and D. Snel, 1975. The Ultraviolett Experiment onboard the Astronomical Netherlands Satellite – ANS. *Astron. & Astrophys.*, **39**, 159.

[Vogt 1989] N. Vogt, 1989. *Classical Novae*, chapter Relationship of Classical Novae to other Eruptive Variables, page 225. John Wiley & Sons, Chichester.

[Vrba *et al.* 1977] J. Vrba, G.D. Schmidt, and E.W. Burke Jr., 1977. The Infrared Development of Nova Aquilae 1975. *Astrophys. J.*, **211**, 480–485.

[Wagner and Graff 1987] A.F Wagner and M.M. Graff, 1987. Oxygen Chemistry of Shocked Interstellar Clouds. *Astrophys. J.*, **317**, 423f.

[Walker 1963] M.F. Walker, 1963. Nova T Aurigae 1891 : A new Short–Period Eclipsing Binary. *Astrophys. J.*, **138**, 313.

[Warner 1976] B. Warner, 1976. Observations of Dwarf Novae. In P. Eggleton, S. Mitton, and J. Whelan, editors, *Structure and Evolution of Close Binary Systems*, page 85. D. Reidel.

[Warner 1990] B. Warner, 1990. Classical Novae: Properties between Outbursts. In A. Cassatella and R. Viotti, editors, *Physics of Classical Novae*, pages 24–33, Springer Verlag, Heidelberg.

[Wehrse *et al.* 1991] R. Wehrse, P.H. Hauschildt, G. Shaviv, and S. Starrfield, 1991. Model atmospheres for Novae During the Early Stages. In *Lecture notes in Physics: Physics of Classical Novae.* Springer Verlag Heidelberg.

[Weiss and Truran 1990] A. Weiss and J.W. Truran, 1990. ^{22}Na and ^{26}Al Production and Nucleosynthesis in Novae Explosions. *Astron. & Astrophys.*, **238**, 178–186.

[Whitelock *et al.* 1984] P.A. Whitelock, B.S. Carter, M.W. Feast, I.S. Glass, D. Laney, J.W. Menzies, J. Walsh, and P.M. Williams, 1984. Infrared and Optical Observations of Nova Muscae 1983. *Mon. Not. R. Astron. Soc.*, **2111**, 421f.

[Whitmore 1986] B. Whitmore, 1986. . PhD thesis, University of London, London.

[Wiescher *et al.* 1985] M. Wiescher, J.Görres, F.-K. Thielemann, and H. Ritter, 1985. Reaction Rates in the RP-Process and Nucleosynthesis in Novae. In J. Audouze and N. Mathieu, editors, *Nucleosythesis and its Implications on Nuclear and Particle Physics*, page 105, D. Reidel, Dordrecht.

[Wiescher *et al.* 1986] M. Wiescher, J. Görres, F.-K. Thielemann, and H. Ritter, 1986. Explosive Hydrogen Burning in Novae. *Astron. & Astrophys.*, **160**, 56–72.

[Willems and deJong 1986] F.J. Willems and T. deJong, 1986. . *Astrophys. J. (Letters)*, **309**, L39.

[Williams 1983] G. Williams, 1983. Spectroscopy od Cataclysmic Variables I. Observations. *Astrophys. J. Suppl. Ser.*, **53**, 523.

[Williams 1985] R.E. Williams, 1985. CNO Abundances in Nova Ejecta. In *ESO Workshop Proceedings.*

[Williams 1990] R.E. Williams, 1990. The Ionization of Nova Ejecta. In A. Cassatella and R. Viotti, editors, *Physics of Classical Novae*, pages 215–227, Springer Verlag, Heidelberg.

[Williams and Ferguson 1982] R.E. Williams and D.H. Ferguson, 1982. . *Astrophys. J.*, **257**, 672.

[Williams and Longmore 1984] P.M. Williams and A.J. Longmore, 1984. Nova Aquilae 1982: New or Pre Existing Dust. *Mon. Not. R. Astron. Soc.*, **207**, 139f.

[Williams *et al.* 1981] R.E. Williams, W.M. Sparks, J.S. Gallagher, E.P. Ney, S.G. Starrfield, and J.W. Truran, 1981. Ultraviolett Spectroscopy of the Recurrent Nova U Scorpii During Outburst. *Astrophys. J.*, **251**, 221.

[Williams *et al.* 1985] R.E. Williams, E.P. Ney, W.M. Sparks, S.G. Starrfield, S. Wyckoff, and J.W. Truran, 1985. Ultraviolett Spectral Evolution and Heavy Element abundances in Nova Coronae Austrinae 1981. *Mon. Not. R. Astron. Soc.*, **212**, 753f.

[Wirsich 1988] J. Wirsich, 1988. Photodestruction Rates in the Circumstellar Shell of Alpha Orionis by Chromospheric Radiation. *Astrophys. J.*, **331**, 463.

[Wishart 1979] A.W. Wishart, 1979. The Bound–free Detachment Cross-section of H^-. *Mon. Not. R. Astron. Soc.*, **187**, 59P.

[Witt *et al.* 1986] A.N. Witt, R.C. Bohlina, and T.P. Stecher, 1986. Detection of Scattering in the 2175ÅInterstellar Band. *Astrophys. J. (Letters)*, **305**, L23.

[Wlodek *et al.* 1987] S. Wlodek, A. Fox, and D.K. Bohme, 1987. . *J. Am. Chem. Soc.*, **109**, 6663.

[Wlodek *et al.* 1988] S. Wlodek, D.K. Bohme, and E. Herbst, 1988. A Synthesis of Interstellar C_4S. *Mon. Not. R. Astron. Soc.*, **235**, 493.

[Wolf 1977] B. Wolf, 1977. . In R. Kippenhahn, J. Rahe, and W. Strohmeier, editors, *The Interaction of Variable Stars with their Environment*, page 187, Bamberg.

[Woolf and Ney 1969] N.J. Woolf and E.P. Ney, 1969. Circumstellar infrared emission from cool stars. *Astrophys. J. (Letters)*, **155**, L181.

[Wu and Kester 1977] C.C. Wu and D. Kester, 1977. Ultraviolett Photometry of Nova Cagni 1975. *Astron. & Astrophys.*, **58**, 331.

[Yakovlev *et al.* 1992] D.G. Yakovlev, I.M. Band, M.B. Trzhaskovskaya, and D.A. Verner, 1992. Photoionisation Cross Sections of Atoms and Ions from He to Zn. *Astron. & Astrophys.*, **preprint**.

[Yamamoto and Nishida 1977] T. Yamamoto and E. Nishida, 1977. Grain Formation in Nova Envelopes. *Progress of Theoretical Physics*, **57**(6).

[Yamamoto *et al.* 1979] T. Yamamoto, S. Sato, and K. Nariai, 1979. Dust Formation and Ionization in Novae. *Publ. Astr. Soc. Japan*, **31**, 691–696.

[Yoke 1962] H.P. Yoke, 1962. Ancient and Mediaeval Observations of Comets and Novae in Chinese Sources. *Vistas in Astronomy*, **5**, 127.

[Young and Schneider 1980] P. Young and D.P. Schneider, 1980. Emission Line Eclipse Phenomena In Nova Herculis 1934. *Astrophys. J.*, **238**, 955.

[Young and Schneider 1981] P. Young and D.P. Schneider, 1981. . *Astrophys. J.*, **247**, 960.

[Young *et al.* 1981] P. Young, D.P. Schneider, and S.A. Schectman, 1981. The Voracous Vortex in HT Cassipeiae. *Astrophys. J.*, **245**, 1035.

[Ziurys *et al.* 1989] L.M. Ziurys, R.L. Snell, and R.L. Dickman, 1989. Shock Chemistry in the Molecular Clouds associated with SNR IC 443. *Astrophys. J.*, **341**, 857.

[Zuckerman 1980] B. Zuckerman, 1980. Envelopes around Late–Type Stars. *Ann. Rev. Astron. Astrophys.*, **18**, 263.

Index

Danksagung

Zunächst möchte ich mich ganz besonders bei Prof. Dr. Erwin Sedlmayr bedanken, dem ich die Auseinandersetzung mit diesem interessanten Thema zu verdanken habe und der meine Promotion betreut hat. Er war es auch, der durch seine visionäre Kraft und seine besondere Art Zusammenhänge zu sehen und zu formulieren, mein Interesse für die Astrophysik wiedererweckt, und über die Jahre erhalten unf vertieft hat.

Des weiteren danke ich Herrn Priv. Doz. J.P. Kaufmann für seine Bereitschaft die Erstellung des Zweitgutachtens zu übernehmen.

Herrn Prof. Dr. P. Zimmermann danke ich für die Übernahme des Amtes des Prüfungsvorsitzenden.

Priv. Doz. Dr. H. –P. Gail danke ich für die wichtigen Hinweise und Anregungen die er mir gegeben hat, und für seine Großzügigkeit, die es überhaupt erst ermöglichte, ein für mich angenehmes Arbeitsklima zu schaffen.

Mein Freund Carsten Dominik hat viel zur Entstehung der vorliegenden Arbeit beigetragen. Seine schnelle Auffassungsgabe und seine stete Hilfsbereitschaft, auch in Detailfragen, waren für mich sehr wertvoll. Da er wichtige Lebensstationen[1] jeweils etwas eher als ich erreicht hat, konnte ich von den dabei gewonnene Erkenntnissen stets profitieren.

Hans Gass war für mich insbesondere in den Anfangsjahren immer ein wichtiger Ansprech– und Arbeitspartner, dessen stets offenes Ohr, gerade in schwierigen Phasen, mir oft geholfen hat.

Robert Henkel verdanke ich neben vielen interessanten Einsichten in die philosophischen Zusammenhänge des Lebens auch die Möglichkeit, den verschlungenen Pfaden der Erkenntnis zu folgen, wie sie die tiefe Analyse der Resultate chemischer Netzwerkrechnungen liefert.

Beate Patzer war mir oft eine hilfsbereite Quelle thermodynamischer und chemischer Daten.

Uwe Bolick hat mir sein unentbehrliches Expertenwissen stets freundlich und mit Geduld zur Verfügung gestellt.

P. H. Hauschildt danke ich herzlich für die Zurverfügungstellung der Ergebnisse seiner Strahlungstransportrechnungen für Novaphotosphären.

Allen Mitgliedern des Instituts bin ich für die angenehme Arbeitsatmosphäre zu Dank verpflichtet. Ein solches Klima läßt den Arbeitscharakter des Forschens in den Hintergrund treten, und die montägliche Aussicht auf den intitutionalisierten Wochenausklang im Rahmen einer anständigen Bierrunde erweist sich als äußerst antriebsstark.

[1] Abgesehen von familienplanerischen Aspekten

Lebenslauf

Name	Holger Beck
Geburtsdatum	27. April 1959
Geburtsort	Bad Homburg v.d.H.
Eltern	Ingeborg Brieschke geb. Kirsch (Hausfrau)
	Alfred Beck (Tennislehrer)
Staatsanghörigkeit	deutsch
Familienstand	ledig
	3 Kinder

Schulbesuch

1966–1969	Friedrich-Ebert-Grundschule in Bad Homburg
1969–1972	Kaiser-Friedrich Gymnasium in Bad Homburg
1972–1978	Droste-Hülshoff Gymansium in Berlin-Zehlendorf
Dezember 1978	Abitur (Allgemeine Hochschulreife)

Studium

1979–1980	Studium des Wirtschaftsingenieurwesens am Fachbereich 18 der Technischen Universiät Berlin
1980–1988	Studium der Physik am Fachbereich 4 der Technischen Universität Berlin
Mai 1983	Abschluß der Diplomvorprüfung
Dezember 1988	Abschluß der Diplomhauptprüfung
April 1985 – März 1988	Tutor im Projektlabor am Fachbereich Physik
Oktober 1988	Abschluß der Diplomarbeit am Institut für Astronomie und Astrophysik über das Thema: *Chemische Struktur und Staubbildung in Novahüllen.*
seit 1. 12. 1988	Wissenschaftlicher Mitarbeiter bei Priv.-Doz. Dr. H.-P. Gail (Inst. für Theoretische Astrophysik, Ruprecht-Karls Universität, Heidelberg

Berlin, den 2. März 1996

Um umzuschaffen das Geschaffne,
Damit sichs nicht zum Starren waffne,
Wirkt ewiges, lebendges Tun.
Und was nicht war, nun will es werden,
Zu reinen Sonnen, farbigen Erden,
In keinem Falle darf es ruhn.

Es muß sich regen, schaffend handeln,
Erst sich gestalten, dann verwandeln,
Nur scheinbar stehts Momente still.
Das Ewige regt sich dort in allem,
Denn Alles muß in Nichts zerfallen,
Wenn es im Sein beharren will.

Goethe